SECURITY CLASSIFICATION OF THIS PAGE (When Data Entered)

AD A125249

REPORT DOCUMENTATION PAGE		READ INSTRUCTIONS BEFORE COMPLETING FORM
1. REPORT NUMBER AFIT/CI/NR 82-75D	2. GOVT ACCESSION NO. AD-A125249	3. RECIPIENT'S CATALOG NUMBER
4. TITLE (and Subtitle) Experimental Investigation of the Mixing of Highly Swirling Flows		5. TYPE OF REPORT & PERIOD COVERED THESIS/DISSERTATION
		6. PERFORMING ORG. REPORT NUMBER
7. AUTHOR(s) Jack Denton Mattingly		8. CONTRACT OR GRANT NUMBER(s)
9. PERFORMING ORGANIZATION NAME AND ADDRESS AFIT STUDENT AT: University of Washington		10. PROGRAM ELEMENT, PROJECT, TASK AREA & WORK UNIT NUMBERS
11. CONTROLLING OFFICE NAME AND ADDRESS AFIT/NR WPAFB OH 45433		12. REPORT DATE May 82
		13. NUMBER OF PAGES 463
14. MONITORING AGENCY NAME & ADDRESS(if different from Controlling Office)		15. SECURITY CLASS. (of this report) UNCLASS
		15a. DECLASSIFICATION/DOWNGRADING SCHEDULE

16. DISTRIBUTION STATEMENT (of this Report)

APPROVED FOR PUBLIC RELEASE; DISTRIBUTION UNLIMITED

DTIC
MAR 4 1983
H

17. DISTRIBUTION STATEMENT (of the abstract entered in Block 20, if different from Report)

18. SUPPLEMENTARY NOTES

APPROVED FOR PUBLIC RELEASE: IAW AFR 190-17

Lynn E. Wolaver

LYNN E. WOLAVER
Dean for Research and
Professional Development
AFIT, Wright-Patterson AFB OH

17 Feb 83

19. KEY WORDS (Continue on reverse side if necessary and identify by block number)

20. ABSTRACT (Continue on reverse side if necessary and identify by block number)

ATTACHED

DTIC FILE COPY

DD FORM 1 JAN 73 1473 EDITION OF 1 NOV 65 IS OBSOLETE

UNCLASS

SECURITY CLASSIFICATION OF THIS PAGE (When Data Entered)

83 03 03 042

University of Washington

Abstract

EXPERIMENTAL INVESTIGATION OF THE MIXING OF HIGHLY SWIRLING FLOWS

By Jack Denton Mattingly

Chairperson of the Supervisory Committee: Professor Gordon C. Oates, Department of Aeronautics and Astronautics

An extensive experimental investigation has been performed of the mixing behavior of incompressible co-annular air streams with substantial swirl present in the inner stream. Four sets of experiments were performed and each set corresponded to a different configuration of the test section. The test section configuration of each of the four sets of experiments were: free annular swirling jet, annular swirling jet with a centerbody, co-annular streams with swirl present in the inner stream and with a centerbody, and co-annular streams with swirl present in the inner stream and with a constant-area annular duct test section. The experimental investigation determined the behavior of the mean flow profiles at several axial locations for the four sets of tests with the most extensive investigation performed in the fourth

P-1

set of tests. Five-hole probes were used to determine the flow property variations, and their development and calibration are described in detail. The variation of the axial velocity, tangential velocity, total pressure, and static pressure profiles and their behavior are presented. The measurements reveal the highly complex flowfield and the influence of the swirl on the mixing behavior. A short analytical model of an ideal mixer with swirl is presented to estimate the effects of swirl on "ideal" mixing.

AFIT RESEARCH ASSESSMENT

The purpose of this questionnaire is to ascertain the value and/or contribution of research accomplished by students or faculty of the Air Force Institute of Technology (ATC). It would be greatly appreciated if you would complete the following questionnaire and return it to:

AFIT/NR
Wright-Patterson AFB OH 45433

RESEARCH TITLE: Experimental Investigation of the Mixing of HIghly Swirling Flows

AUTHOR: Jack Denton Mattingly

RESEARCH ASSESSMENT QUESTIONS:

1. Did this research contribute to a current Air Force project?

( ) a. YES ( ) b. NO

2. Do you believe this research topic is significant enough that it would have been researched (or contracted) by your organization or another agency if AFIT had not?

( ) a. YES ( ) b. NO

3. The benefits of AFIT research can often be expressed by the equivalent value that your agency achieved/received by virtue of AFIT performing the research. Can you estimate what this research would have cost if it had been accomplished under contract or if it had been done in-house in terms of manpower and/or dollars?

( ) a. MAN-YEARS _________ ( ) b. $_________

4. Often it is not possible to attach equivalent dollar values to research, although the results of the research may, in fact, be important. Whether or not you were able to establish an equivalent value for this research (3. above), what is your estimate of its significance?

( ) a. HIGHLY SIGNIFICANT ( ) b. SIGNIFICANT ( ) c. SLIGHTLY SIGNIFICANT ( ) d. OF NO SIGNIFICANCE

5. AFIT welcomes any further comments you may have on the above questions, or any additional details concerning the current application, future potential, or other value of this research. Please use the bottom part of this questionnaire for your statement(s).

NAME GRADE POSITION

ORGANIZATION LOCATION

STATEMENT(s):

University of Washington

Abstract

EXPERIMENTAL INVESTIGATION OF THE MIXING OF HIGHLY SWIRLING FLOWS

By Jack Denton Mattingly

Chairperson of the Supervisory Committee: Professor Gordon C. Oates, Department of Aeronautics and Astronautics

An extensive experimental investigation has been performed of the mixing behavior of incompressible co-annular air streams with substantial swirl present in the inner stream. Four sets of experiments were performed and each set corresponded to a different configuration of the test section. The test section configuration of each of the four sets of experiments were: free annular swirling jet, annular swirling jet with a centerbody, co-annular streams with swirl present in the inner stream and with a centerbody, and co-annular streams with swirl present in the inner stream and with a constant-area annular duct test section. The experimental investigation determined the behavior of the mean flow profiles at several axial locations for the four sets of tests with the most extensive investigation performed in the fourth

set of tests. Five-hole probes were used to determine the flow property variations, and their development and calibration are described in detail. The variation of the axial velocity, tangential velocity, total pressure, and static pressure profiles and their behavior are presented. The measurements reveal the highly complex flowfield and the influence of the swirl on the mixing behavior. A short analytical model of an ideal mixer with swirl is presented to estimate the effects of swirl on "ideal" mixing.

Experimental Investigation of the

Mixing of Highly Swirling Flows

by

Jack Denton Mattingly

A dissertation submitted in partial fulfillment
of the requirements for the degree of

Doctor of Philosophy

University of Washington

1982

Approved by ______________________
(Chairperson of Supervisory Committee)

Program Authorized
to Offer Degree Department of Aeronautics and Astronautics

Date May 28, 1982

Doctoral Dissertation

In presenting this dissertation in partial fulfillment of the requirements for the Doctoral degree at the University of Washington, I agree that the Library shall make its copies freely available for inspection. I further agree that extensive copying of this dissertation is allowable only for scholarly purposes, consistent with "fair use" as prescribed in the U.S. Copyright Law. Requests for copying or reproduction of this dissertation may be referred to University Microfilms, 300 North Zeeb Road, Ann Arbor, Michigan 48106, tq whom the author has granted "the right to reproduce and sell (a) copies of the manuscript in microform and/or (b) printed copies of the manuscript made from microform."

Signature ____________________

Date ____________________

TABLE OF CONTENTS

Page

Page

LIST OF FIGURES

Page

Page

Page

Page

Page

Page

Page

Page

Page

Page

LIST OF TABLES

Page

SYMBOLS

A	Area; dummy variable (= u/V, v/V, C_o or C_q)
A^*	Choked Area
b	Half-radius of velocity, location where velocity is one half its maximum
C_o	Total pressure coefficient
C_q	Dynamic pressure coefficient
C_α	Angle of attack pressure coefficient
C_β	Angle of sideslip pressure coefficient
c	Chord
c_f	Coefficient of friction
$[D]$	Calibration matrix composed of pressure coefficients C_α and C_β
D	Diameter
d	Diameter
F	Force
f	Friction factor; tip to hub ratio of inner annulus, (= r_t / r_h)
G_z	Axial momentum, defined by Eqn. G-18
G_θ	Tangential momentum, defined by Eqn. G-12
g	Overall tip to hub ratio, (= R_t / r_h)
H	Stagnation enthalpy
H_{12}	Shape factor, ratio of displacement thickness to momentum thickness

H_{32}	Shape factor, ratio of energy thickness to momentum thickness
h	Overall hub to tip ratio,(= 1/g)
$[K_A]$	Calibration coefficients
L	Length
M'	Momentum
M_z	Axial momentum flux, defined by Eqn. 5-23
M_z'	Axial momentum flux, defined by Eqn. 5-24
M_θ	Tangential momentum flux, defined by Eqn 5-25
$\dot{m}$	Mass flow rate
O1	Orifice plate #1
O2	Orifice plate #2
P	Pressure
R	Gas constant per unit mass, radius
R_t	Radius of tip
r	Radius
S	Swirl number, standard deviation
S_t	Tip swirl ratio,(= v_t /w_t)
T	Temperature
t	Time
u	Radial velocity
V	Total velocity; voltage
v	Tangential velocity
W	Axial momentum, defined by Eqn. G-13
w	Axial velocity

$\left.\begin{matrix} x \\ y \\ z \end{matrix}\right\}$ Space co-ordinates

GREEK LETTERS

α	Angle of attack; mass flow ratio ($= \dot{m}_2 / \dot{m}_0$)
β	Angle of sideslip; flow angle
Γ	$\sqrt{\gamma}\left(\frac{2}{\gamma+1}\right)^{\frac{\gamma+1}{2(\gamma-1)}}$
γ	Ratio of specific heats; angle
Δ	Change in
δ	Leaving angle relative to stator, $(=\beta_2-\gamma_2)$
δ_1	Displacement thickness
δ_2	Momentum thickness
θ	Angle in cylindrical co-ordinate system
θ^*	Change across stator row of stager angle, $(=\gamma_1-\gamma_2)$
ν	Viscosity
ρ	Density
σ	Solidity of stator row, standard deviation
τ	Shear stress
Φ	Turning angle, modified stream function
ψ	Incompressible stream function

SPECIAL NOTATION

[A]	Vector or matrix A

SUBSCRIPTS

A	Dummy variable (= u/V, v/V, C_o or C_q)
C_o	Total pressure coefficient
C_q	Dynamic pressure coefficient
C_α	Angle of attack pressure coefficient
C_β	Angle of sideslip pressure coefficient
c	Corrected
d	Outer wall of inner stream
e	Exit
f	Final
H	High
h	Hub
i	Initial; inside
L	Low; line
N	Incompressible nozzle
NC	Isentropic nozzle
o	Reference state; outside
p	Probe
r	Relative
S	Static
SW	Swirl with incompressible nozzle
SWC	Swirl with isentropic nozzle
ST	Straight with incompressible nozzle

STC Straight with isentropic nozzle

T Total or stagnation property; tank

t Tip

UM Unmixed with incompressible nozzles

UMC Unmixed with isentropic nozzles

x Variable subscript where x stands for 1 through 74

z Axial

α Angle of attack

β Angle of sideslip

θ Tangential

Σ Sum

$\left.\begin{array}{l}\emptyset\\1\\2\\3\\4\\5\end{array}\right\}$ Referring to different locations in space

SUPERSCRIPTS

T Transpose of matrix or vector

' Instantaneous variation

— Time average

-1 Inverse of matrix or vector

ACKNOWLEDGEMENTS

The author wishes to express sincere appreciation to Professor Gordon C. Oates for his assistance in the preparation of this manuscript. In addition, special thanks to my wife, Sheila, for her inspiration and her help in typing this manuscript. Finally, a special acknowledgement to Mr. Robert Skimming for his support and hard work in the construction of the experimental apparatus.

CHAPTER 1

INTRODUCTION

The turbulent mixing of two concentric incompressible streams with swirl present in the inner stream has received an increasing amount of attention during recent years. The primary motivations for this have been the application to combustion and the swirling wake behind a propller for propulsion or a windmill (Reference 1). Swirling flows have been classified by King, Rothfus, and Kermode (Reference 2) according to the wall boundary conditions in the following fashion:

1. Unconfined swirling flows - where the wall effects are negligible.

2. Small L/D, confined swirling flows - in short, large-diameter chambers where sidewall effects strongly interact with the swirl to produce significant secondary flows.

3. Large L/D, confined swirling flows - in tubes where circumferential wall effects interact strongly with the swirl flow.

To date, most investigations of confined mixing with swirl present have considered the mixing of fuels and air in cylindrical combustors where a secondary reverse flow

provides the necessary flame stability and greatly influences the mixing process (References 3, 4, 5, 6 and 7). Turbulent mixing with swirl has many engineering applications where a centerbody may be present and the secondary reverse flow is absent. Such an application is present in modern turbofan engines where mixing of the engine core stream and the fan stream is utilized to improve the engine thrust and/or to reduce the nozzle exhaust noise.

Experimental data and analytical methods are available for unconfined swirling flows and small L/D swirling flows in combustion chambers (References 1 through 8). A limited amount of experimental data is available for the turbulent mixing of two concentric incompressible streams in a constant cross-sectional area channel, with swirl present in the inner stream. The only work in this area known to the author was done by Launder and Morse (Reference 9) and was concerned with a swirling jet with and without an external coaxial stream. No known work has been done with a centerbody present.

The focal point of this study was experimentally obtaining the variation of mean flow properties for the turbulent mixing of two concentric incompressible air

streams, with swirl present in the inner stream, flowing through a constant area annulus. In addition, experimental data was obtained for the turbulent mixing without an outside wall and with/without a centerbody. Data was also obtained for turbulent mixing of a swirling annular jet. Four sets of experiments were performed with a swirl ratio (tangential to axial velocity ratio) of 0.8 in the inner stream. The test configuration for each test is listed in Table 1-1. The most extensive experiment was performed for test #4, the focal point of this study.

TABLE 1-1

EXPERIMENTS

Test	Flow Present in Outer Annulus	Center-Body in Place	Outer Wall in Place	α ($\dot{m}_o/\dot{m}_i$)
1	No	No	No	0.00
2	Yes	No	No	1.00
3	Yes	Yes	No	1.00
4	Yes	Yes	Yes	0.00
4	Yes	Yes	Yes	0.47
4	Yes	Yes	Yes	1.00
4	Yes	Yes	Yes	2.13
4	Yes	Yes	Yes	3.91

where $\dot{m}_i$ is the inner stream's mass flow rate
and $\dot{m}_o$ is the outer stream's mass flow rate

A five-hole probe was used for mean flow measurements. The experimental measurements, test apparatus, five-hole probe, data reduction, and discussion of results are

contained in Chapters 3, 4, 5, 6 and 7, respectively.

A one-dimensional analytical model of a constant area ideal incompressible mixer with swirl was developed and compared to a mixer without swirl. This analytical work is presented in Chapter 2.

REFERENCES

1. Schetz, J.A., Injection and Mixing in Turbulent Flow, Progress in Astronautics and Aeronautics, Volume 68, American Institute of Aeronautics and Astronautics, New York, 1980.

2. King, M.K., Rothfus, R.R., and Kermode, R.I., "Static Pressure and Velocity Profiles in Swirling Incompressible Tube Flow", A.I.ChE. Journal, Vol. 15, No. 6, Nov. 1969, pp. 837-842.

3. Lilley, D.G., "Swirl Flows in Combustion: A Review", AIAA Journal, Vol. 15, No. 8, August 1977, pp. 1063-1078.

4. Chigier, N.A. and Beer, J.M., "Velocity and Static-Pressure Distributions in Swirling Air Jets Issuing From Annular and Divergent Nozzles", Journal of Basic Engineering, Trans. ASME, Dec. 1964, pp. 788-796.

5. Chigier, N.A. and Chervinsky, A., "Experimental Investigation of Swirling Vortex Motion in Jets", Journal of Applied Mechanics, Trans. ASME, June 1967, pp. 443-451.

6. Fujii, S., Eguchi, K., and Gomi, M., "Swirling Jets With and Without Combustion", AIAA Journal, Vol. 19, No. 11, Nov. 1981, pp. 1438-1442.

7. Habib, M. A. and Whitelaw, J. H., "Velocity Characteristics of Confined Coaxial Jets With and Without Swirl". Journal of Fluid Mechanics, Vol. 102, March 1980, pp. 47-53.

8. Ribeiro, M. M. and Whitelaw, J. H., "Coaxial Jets With and Without Swirl", Journal of Fluid Mechanics, Vol. 96, Part 4, 1980, pp. 769-795.

9. Launder, B. E. and Morse, A., "Some Experiments on the Turbulent Swirling Jet With and Without an External Stream", Unpuplished Paper.

CHAPTER 2

ANALYSIS OF AN IDEAL SWIRL MIXER

I. INTRODUCTION

Turbulent mixing of two concentric incompressible streams with swirl present in the inner stream is of interest in several engineering applications. Research is presently being conducted to obtain a better understanding of the mixing process. To date, most investigations of mixing with swirl present have considered the mixing of fuels and air in combustors where a secondary reverse flow provides the necessary flame stability and greatly influences the mixing process (References 1 and 2). Turbulent mixing with swirl has many engineering applications where a centerbody may be present and the secondary reverse flow is absent. Such an application is present in modern turbofan engines where mixing of the engine core stream and the fan stream is utilized to improve the engine thrust and/or to reduce the nozzle exhaust noise. Present day turbofan engines remove most of the swirl from the engine core stream with the turbine exit nozzle row and then mix the two concentric parallel jets in a mixer which contains devices (e.g. paddle mixers) to enhance the mixing process. These forced

mixing devices also reduce the total pressure of the mixed stream and thus reduce the available thrust from the turbofan engine. It is possible that the mixing losses of the engine core stream and the fan stream can be reduced by leaving off the turbine exit nozzle row so that the engine core stream enters the mixer with swirl. The swirl of the combined stream would subsequently be removed by guide vanes at the exit to the mixer. The presence of swirl in the inner stream entering the mixer makes the boundary between the inner and outer streams unstable because the fluid angular momentum decreases in the radial direction (Reference 3). This instability in the radial direction enhances the turbulent mixing of the two streams.

In the following section, an ideal incompressible constant area mixer with swirl is modeled and its performance determined. The swirl velocity profile of the inner stream entering the mixer is assumed to be that of a free vortex. The swirl velocity profile of the mixed stream is assumed to be that of a solid body rotation. Both streams entering the mixer and the departing stream are assumed to have uniform axial velocity.

The performance of an ideal incompressible constant area

mixer without swirl is also determined so that the effects of swirl can be determined by comparison of the two solutions.

II. CONSTANT AREA MIXER WITH SWIRL

In this section, the ideal incompressible constant area mixer with swirl is considered. The performance equations are developed in Appendix B. The configuration of this ideal mixer with swirl is shown in Figure 2-1. The following conditions are prescribed:

a. An incompressible stream enters the annular channel "Ø", formed between the outer radius of r_t and the inner radius of r_h, with uniform density (ρ_0), uniform total pressure (P_{T_0}), uniform axil velocity (w_0) and no radial or swirl velocity.

b. An incompressible stream enters the annular channel "2", formed between the outer radius of R_t and the inner radius of r_t with uniform density (ρ_2), uniform total pressure (P_{T_2}), uniform axial velocity (w_2) and no radial or swirl velocity.

c. The incompressible stream in annular channel "Ø" passes through stator-1, an ideal free vortex stator, and departs with a free vortex swirl velocity profile and no radial velocity at station "1". The total pressure of the

inner stream, P_{T_0} , and the cross-sectional area are unchanged through stator-1.

d. The ratio of the static pressure of the inner stream with swirl at its outer wall, P_d, to the static pressure of the outer stream without swirl, P_2, meets a modified Kutta condition at the end of the cylindrical wall of radius r_t dividing the two incompressible streams. This modified Kutta condition is specified by the ratio P_d/P_2.

e. The inner stream with swirl, "1", and the outer stream without swirl, "2", enter a constant area mixing region in which the two incompressible streams mix. The mixing process is assumed to occur with no wall friction. As a result, the total angular momentum of the flow and the total "stream thrust" are conserved (Appendix G). The stream departing the mixing region is assumed to have uniform axial velocity, w_3 , and a solid body rotation swirl velocity profile.

f. The mixed incompressible stream, "3", passes through stator-2, an ideal stator that removes the swirl velocity component. The total pressure is assumed to be constant along streamlines through this ideal stator.

g. The mixed stream without swirl, stream "4", passes through an ideal nozzle to the exit, "e", which exhausts to uniform static pressure of P_e. Analysis is performed

for both incompressible flow through the nozzle and isentropic flow of a perfect gas through the nozzle.

Special attention was used in the selection of input variables for calculation of the performance of the ideal incompressible constant area mixer with swirl so that the same input variables could be used for calculation of the performance of the mixer without swirl. The input variables chosen are $P_{T_0}, \rho_0, w_0, P_{T_2}, \rho_2, \alpha, R_t/r_h, P_e, P_d/P_2$, γ (for isentropic nozzle calculations) and, S_t, the tip swirl ratio departing stator-1 ($S_t = v_{t_1}/w_0$). This choice of input variables fixes the axial velocity stream "2" and the tip to hub ratio of the inner annulus, f, as given by the following equations:

$$w_2 = \left\{ \frac{2}{\rho_2}\left[P_{T_2} - \frac{P_{T_0}}{P_d/P_2} \right] + \frac{\rho_0 \; \rho_2}{P_d/P_2} w_0^2 \;\; (1+S_t^2) \right\}^{1/2} \qquad (2\text{-}1)$$

$$f = \frac{r_t}{r_h} = \left[\frac{\dfrac{R_t^2}{r_h^2} + \dfrac{\rho_0 w_0}{\rho_2 w_2} \alpha}{1 + \dfrac{\rho_0 w_0}{\rho_2 w_2} \alpha} \right]^{1/2} \qquad (2\text{-}2)$$

Equations 2-1 and 2-2 show that for increases in the magnitude of the tip swirl ratio departing stator-1, S_t, with all other input variables constant, the value of

axial velocity of stream "2", w_2, increases and the value of the tip to hub ratio of the inner annulus, f, increases. w_2 increases with increasing $|S_t|$ (P_d decreases as S_t increases) in order to satisfy the modified Kutta condition (ratio of P_d/P_2) at the end of the splitter plate by decreasing P_2. The value of the tip to hub ratio of the inner annulus, f, increases with increasing magnitude of S_t to give the ratio of outer annulus area to inner annulus area required for the densities, ρ_0 and ρ_2, the axial velocities, w_0 and w_2, and the mass flow ratio, α.

The tip swirl ratio of the mixed stream departing the mixer, v_{t_3}/w_3, is fixed by the conservation of angular momentum. The relationship between the two tip swirl ratios is:

$$\frac{v_{t_3}}{w_3} = S_t \frac{2 g f (g^2 - 1)}{(1+\alpha)(1+\alpha \rho_0/\rho_2)(g^2+1)(f^2-1)} \qquad (2\text{-}3)$$

where "g" is the overall tip to hub ratio, R_t/r_h

Equation 2-3 shows that v_{t_3}/w_3 increases with increasing S_t for constant value of all other variables. Equations 2-1 and 2-2 show that f increases with increasing S_t , however, this change is small, resulting in the quantity

$(f^2-1)/f$ increasing less than the increase in S_t.

The axial force on stator-1, F_1, divided by the total mass flow rate and the axial velocity of the inner stream (see Appendix B) is

$$\frac{F_1}{(\dot{m}_0+\dot{m}_2)\,w_0} = -\,S_t^2\,\frac{f^2\,\ln(f)}{(1+\alpha)\,(f^2-1)} \qquad (2\text{-}4)$$

A plot of the variation of F_1 with S_t is shown in Figure 2-2 for typical input values. The axial force on stator-2, F_2, divided by the total mass flow rate and the axial velocity of the inner stream (see Appendix B) is

$$\frac{F_2}{(m_0+m_2)\,w_0} = \frac{v_{t_3}^2}{w_3^2}\,\frac{1+\alpha\rho_0/\rho_2}{24\left(1+\dfrac{\rho_0 w_0}{\rho_2 w_2}\alpha\right)}\left[6\left(1+\frac{1}{g^2}\right)-\frac{v_{t_3}^2}{w_3^2}\left(1-\frac{1}{g^2}\right)^2\right] \qquad (2\text{-}5)$$

The thrust on stator-2 increases with an increase in magnitude of S_t, however, the increase in the thrust of stator-2 is less than the increase in the magnitude of the thrust of stator-1 and the combined thrust on the stators, $F_1 + F_2$, is negative and its magnitude increases with increases in the magnitude of S_t. Plots of the variations of F_2 and $F_1 + F_2$ with S_t are shown in Figure 2-2 for the same input values as used for the calculation of F_1.

The variations of the static pressure at stations "Ø", "1", "2", "3" and "4" across the annulus for values of S_t equal to Ø.48 and Ø.68 are shown in Figures 2-3 and 2-5, respectively. Also, the corresponding variations of the axial velocity and swirl velocity at these same stations are shown in Figures 2-4 and 2-6, for S_t equal to Ø.48 and Ø.68, respectively. Input variables utilized in Figures 2-2 through 2-6 are:

P_{T_0} = 101,ØØØ Pa	P_{T_0}/P_{T_2} = 1.ØØ3
$\rho_0 = \rho_2$ = 1.23 kg/m	R_t/r_h = 2.Ø
w_0 = 3Ø m/sec	P_2/P_d = 1.Ø
α = 1	

Comparison of Figures 2-3 and 2-5 and Figures 2-4 and 2-6 show that an increase in S_t results in:

a) v_1 increases with a resultant decrease in P_1

b) P_2 decreases with a resultant increase in w_2

c) w_3 increases, v_3 increases and P_3 decreases

d) w_4 increases and P_4 decreases

The total pressure profiles for station "4", P_{T_4}, for both values of S_t, Ø.48 and Ø.68, are plotted in Figure 2-7. This figure shows that as S_t increases, then P_{T_4}

decreases and the change in P_{T_4}, with respect to the dimensionless radius, r/r_h, increases.

The exhaust velocity, w_e, resulting from flow through an incompressible nozzle to uniform static pressure, P_e, is given by the following equation:

$$w_e = \sqrt{2}\left\{\frac{P_3}{\rho_3}\left[1 - \frac{P_e}{P_4}\right] + \frac{w_3^2}{2}\left[1 + \frac{v_{t_3}^2}{2\,w_3^2}(1-h^2)\right] - \phi\right\}^{1/2} \qquad (2\text{-}6)$$

where $\phi = 2\,\dfrac{\psi\, v_{t_3}^2}{w_3 R_t^2}$

and ψ is the incompressible stream function which is related to the dimensionless radius, r/r_h, at station "4" by the equation

$$\psi = \frac{w_3 R_t^2}{2}\left\{\left[1 - \frac{v_{t_3}^2}{2w_3^2}(1+h^2)\right]\left[1-h^2\,\frac{r^2}{r_h^2}\right] + \frac{v_{t_3}^2}{2w_3^2}\left[1-h^4\,\frac{r^4}{r_h^4}\right]\right\} \qquad (2\text{-}7)$$

The axial velocity at station "4", w_4, is plotted in Figure 2-8 versus the dimensionless radius, r/r_h, for the two values of S_t, 0.48 and 0.68. The exhaust velocity, w_e, is also plotted in Figure 2-8 versus the dimensionless radius at station "4", r/r_h, for the two values of S and for the two values of P_e/P_T, 0.9 and 0.99. Although w_4 is higher for the higher value of S_t, w_e is reduced for increased S_t for either value of P_e/P_{T_0}

because the total pressure at station "4", P_{T_4}, decreases as S_t increases.

The axial thrust of this nozzle, F_N, is given by the following relationship for incompressible flow:

$$\frac{F_N}{(\dot{m}_0+\dot{m}_2)\,w_0} = \frac{w_{e_t}^3 - w_{e_h}^3}{3\; w_0\, v_{t_3}^2 (1-h^2)} \tag{2-8}$$

where w_{e_t} is the exhaust velocity at the tip, $\phi = 0$

and w_{e_h} is the exhaust velocity at the hub, $\phi = (1-h)\,v_t$

Figure 2-8 shows that as S_t increases, so does the difference between the exhaust velocity at the tip, w_{e_t}, and the exhaust velocity at the hub, w_{e_h}.

The net thrust of the incompressible swirl mixer and nozzle, F_{SW}, is the sum of the thrust of stator-1, stator-2 and the nozzle.

$$F_{SW} = F_1 + F_2 + F_N \tag{2-9}$$

As described above, the sum of the thrust of both stators, $F_1 + F_2$, decreases as S_t increases, as does the thrust of the nozzle, F_N. Thus, the net thrust of the incompressible swirl mixer and nozzle, F_{SW}, decreases as the swirl is increased with the other input varialbes

held constant.

The exhaust velocity, w_e, for isentropic flow of a compressible (perfect) gas to uniform static pressure, P_e, is given by the following equation:

$$w_e = \sqrt{\frac{2\gamma}{\gamma-1}} \left\{ \frac{P_4}{\rho_3}\left[1 - \frac{\rho_3 P_e}{\rho_e P_4}\right] + \frac{1}{2} w_3^2 \left[1 + \frac{1}{2}\frac{v_{t_3}^2}{w_3^2}(1-h^2)\right]^2 - \phi \right\}^{1/2} \quad (2\text{-}10)$$

where $\phi = \dfrac{2\,\psi\,v_{t_3}^2}{w_3\,R_t^2}$, $\rho_e = \rho_3 \left[\dfrac{P_e}{P_4}\right]^{1/\gamma}$

and the stream function, ψ, is related to the dimensionless radius, r/r_h, at station "4" by Equation 2-7.

The exhaust velocity for compressible isentropic flow through a nozzle is greater than that for incompressible isentropic flow through a nozzle operating with the same inlet conditions and the same exhaust pressure. The energy required for the higher exhaust velocity of the compressible flow comes from the internal energy of the gas. Comparison of Equations 2-6 and 2-10 reveals the different velocities calculated for the two cases. For the isentropic flow, the quantity within the large brackets is increased by the quantity $(P_e/P_4)\left[1-(P_4/P_e)^{1/\gamma}\right]$ and the quantity within the small square root symbol is

multiplied by the quantity $(\gamma/(\gamma-1))$, both increasing the numerical value of the exhaust velocity.

The axial thrust of the nozzle alone, with compressible flow, F_{NC}, is given by

$$\frac{F_{NC}}{(\dot{m}_0+\dot{m}_2)\,w_0} = \frac{\gamma-1}{3\gamma}\;\frac{w_{e_t}^3 - w_{e_h}^3}{w_0\,v_{t_3}^2\,(1-h^2)} \tag{2-11}$$

where w_{e_t} is the exhaust velocity at the tip, $\phi = 0$ and w_{e_h} is the exhaust velocity at the hub, $\phi = (1-h^2)\,v_{t_3}^2$

This nozzle thrust increases slightly with increasing S_t for some values of the input variables, decreases for some others and shows a maximum for others. The upstream interactions are complex, indeed, for variations in swirl parameter, so it is not simple to explain such results. The results for the overall performance follow intuitive reasoning, however, as evidenced in Figures 2-10 through 2-13 and the following discussion.

The nozzle thrust is plotted in Figure 2-9 versus S_t for different values of the total pressure ratio, P_{T_0}/P_{T_2} and the following values of the other input variables:

$P_{T_0} = 101{,}000$ Pa	$P_e/P_{T_0} = 0.8$	$\alpha = 1$
$\rho_0 = \rho_2 = 1.23$ kg/m	$P_2/P_d = 1.0$	$\gamma = 1.4$
$w_0 = 30$ m/sec	$R_t/r_h = 5.0$	

Although the nozzle thrust varies slightly as S_t increases, the net thrust of the swirl mixer plus nozzle decreases with increasing S_t. This decrease in the net thrust with increase in S_t is due to the dominance of change in the net thrust of the two stators, stator-1 and stator-2, over the slight variation in the thrust of the nozzle.

III. CONSTANT AREA MIXER WITHOUT SWIRL

The analysis of an ideal incompressible constant area mixer without swirl is contained in Appendix B. The physical configuration of this mixer is the same as shown in Figure 2-1 with the two stators removed. Without stator-1 and stator-2, states "0" and "1" are the same and states "3" and "4" are the same. The Kutta condition at the end of the splitter plate requires that the static pressures of both entering streams, "0" and "2", must be equal. Using the same input variables as are used for the mixer with swirl (P_{T_0}, ρ_0, w_0, P_{T_2}, ρ_2, α, R_t/r_h, P_e and γ),

the axial velocity of stream "2" and the tip to hub radius ratio are given by the following relationships:

$$w_2 = \left\{ \frac{2}{\rho_2} \left[P_{T_2} - P_{T_0} \right] + \frac{\rho_0}{\rho_2} w_0^2 \right\}^{1/2} \tag{2-12}$$

$$f = \frac{r_t}{r_h} = \left[\frac{\dfrac{R_t^2}{r_h^2} + \dfrac{\rho_0 w_0}{\rho_2 w_2} \alpha}{1 + \dfrac{\rho_0 w_0}{\rho_2 w_2} \alpha} \right]^{1/2} \tag{2-13}$$

The total pressure at station "3" is given by the following relationship:

$$P_{T_3} = P_{T_0} - \frac{\rho_0 w_0^2}{2} \left[\frac{(1+\alpha)(1+\alpha \rho_0/\rho_2)}{\left(1 + \dfrac{\rho_0 w_0}{\rho_2 w_2} \alpha\right)^2} - 1 \right] - \left[\frac{2 \dfrac{\rho_0 w_0}{\rho_2 w_2} \alpha}{1 + \dfrac{\rho_0 w_0}{\rho_2 w_2} \alpha} \right] (P_{T_0} - P_{T_2}) \tag{2-14}$$

The thrust for incompressible flow, F_{ST}, is given by

$$F_{ST} = (\dot{m}_0 + \dot{m}_2)\, w_e \tag{2-15}$$

where $w_e = \left[2(P_{T_3} - P_e)/\rho_3 \right]^{1/2}$

and $\rho_3 = \rho_0(1+\alpha)/(1+\alpha\rho_0/\rho_2)$

The thrust for compressible flow, F_{STC}, is given by Equation 2-15, above, but with the exhaust velocity, w_e, given by the following relationship:

$$w_e = \left\{ \frac{2\gamma}{\gamma-1} \frac{P_{T_3}}{\rho_3} \left[1 - \frac{P_e}{P_{T_3}} \left(\frac{P_3}{P_e} \right)^{1/\gamma} \right] \right\}^{1/2} \tag{2-16}$$

where ρ_3 is given above and

$$P_3 = P_{T_3} - \frac{1}{2}\rho_0 w_0^2 \frac{(1+\alpha)(1+\alpha\rho_0/\rho_2)}{(1+\alpha\rho_0 w_0/(\rho_2 w_2))}$$

The exhaust velocity and the thrust of the compressible flow are higher than those for incompressible flow. Higher nozzle thrusts are obtained with the highest value of the total pressure of the mixed stream, P_{T_3}. Equations 2-12, 2-13 and 2-14, above, show that for a fixed value of P_{T_0}, w_0, ρ_0, ρ_2 and α, P_{T_3} increases with increasing values of P_{T_2}.

IV. COMPARISON OF CONSTANT AREA MIXERS

This section compares the performance of an ideal incompressible constant area mixer with swirl to one without swirl. The ratio of the thrust of the mixer with swirl, F_{SW}, to one without swirl, F_{ST}, was calculated for different values of S with the same values of the input variables (P_{T_0}, ρ_0, w_0, P_{T_2}, ρ_2, α, R_t/r_h and P_e).

The working equations listed in Section XI of Appendix B were programmed on the University of Washington's CDC computer. The results for several examples are plotted in Figures 2-10 through 2-13 for the following constant values of input variables:

P_{T_0} = 101,000 Pa P_e/P_{T_0} = 0.8 ρ = 1.23 kg/m

w_0 = 30 m/sec R_t/r_h = 2.0 P_2/P_d = 1.0

Figures 2-10 and 2-12 are for alpha (α) equal to one and Figures 2-11 and 2-13 are for alpha (α) equal to five. Figures 2-10 and 2-11 are for ρ_0 equal to 1.23 kg/m (ρ_0/ρ_2 =1) and Figures 2-12 and 2-13 are for ρ_0 equal to 0.615 kg/m (ρ_0/ρ_2 =0.5). Each figure contains a plot of the thrust ratio of the swirl mixer to a straight mixer (F_{SW} F_{ST}) versus the tip swirl ratio ($S_t = v_{t_1}/w_0$), a plot of the tip to hub ratio of the inner channel ($f = r_t/r_h$) versus S_t and a plot of the axial velocity at station "2" (w_2) versus S_t. Each plot has curves plotted for different values of the total pressure ratio, P_{T_0}/P_{T_2}. Any of these four figures shows that an increase in S_t reduces the thrust ratio and increases w_2, resulting in an increase of f. These figures also show that an increase in the total pressure ratio, P_{T_0}/P_{T_2}, will increase the thrust ratio and decrease w , with resulting decrease in f.

This comparison of the ideal incompressible constant area mixer with swirl with the ideal incompressible constant area mixer without swirl shows that the introduction of swirl in the inner stream and its subsequent removal

reduces the available thrust. Figures 2-10 through 2-13 show that the penalty for introduction of swirl to the inner stream can be reduced by decreasing the total pressure of stream "2", P_{T_2}, toward its minimum ($w_2 = 0$). The change in the cross-section of the entrance (for mixers having the same mass flow rates) resulting from a decrease in P_{T_2} with all other input variables fixed is shown below. The flow cross-sectional area for the inner stream is the same in both cases, but the area for the outer stream increases with decreasing P_{T_2} because w_2 decreases.

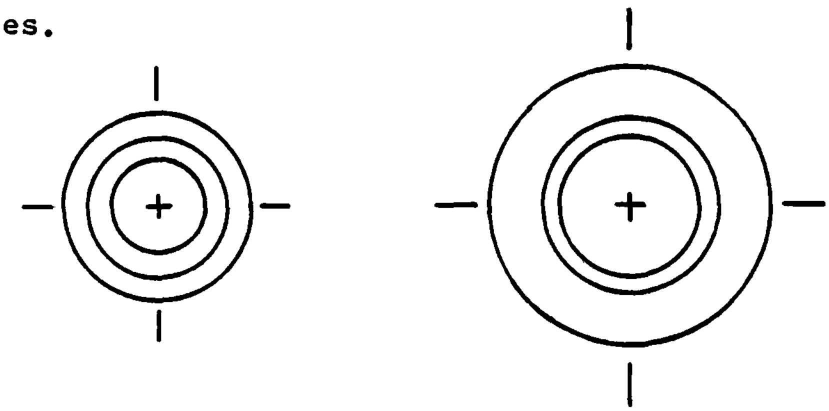

The hub radius of the mixer increases with decreasing P_{T_2} to maintain the same overall hub to tip ratio and the swirl velocity (v_{t_3}) of the mixed stream decreases. The swirl velocity (v_{t_3}) of the mixed stream is expressed analytically below. It is clear that v_{t_3} decreases with increasing hub radius because f (tip to hub ratio of the inner stream) decreases as indicated in the drawings above and in Figures 2-10 through 2-13. The lower value

of v_{t_3} reduces the difference between the tip and hub total pressures at station "4". Further, as a result, the nozzle thrust is penalized less because of the reduced variation of stagnation enthalpy across streamlines.

$$\frac{v_{t_3}}{v_{t_1}} = \frac{2}{1+\alpha} \frac{g\ f}{g^2+1}$$

Comparison of Figures 2-1Ø and 2-11 or Figures 2-12 and 2-13 shows that an increase in the mass ratio, α $(=\dot{m}_2/\dot{m}_0)$, reduces the loss in thrust of the mixer with swirl as compared to the mixer without swirl. This is as expected because an increase in the mass ratio reduces the portion of the total mass flow to which swirl is added.

Comparison of Figures 2-1Ø and 2-12 or Figures 2-11 and 2-13 shows that the density ratio, ρ_0/ρ_2 , of Ø.5 has less loss in thrust than does the density ratio of 1.Ø. This again is expected because the portion of the total mass flow to which swirl is added is lower for the density ratio of Ø.5.

An analysis was also performed for overall tip to hub ratios other than 2.Ø and this analysis shows that an increase in tip to hub ratio decreases the thrust the thrust ratio of the swirl mixer to a straight mixer. This

decrease in thrust ratio is mainly due to the increase in magnitude of the thrust of stator-1 with an increase in overall tip to hub ratio.

REFERENCES

1. Lilley, D. G., "Swirl Flows in Combustion: A Review", AIAA Journal, Vol. 15, No. 8, August 1977, pp. 1063-1078

2. Habib, M. A. and Whitelaw, J. H., "Velocity Characteristics of Confined Coaxial Jets With and Without Swirl," Journal of Fluids Engineering, Vol. 102, March 1980, pp. 47-53

3. White, F. M., "Viscous Fluid Flow", McGraw-Hill, New York (1974)

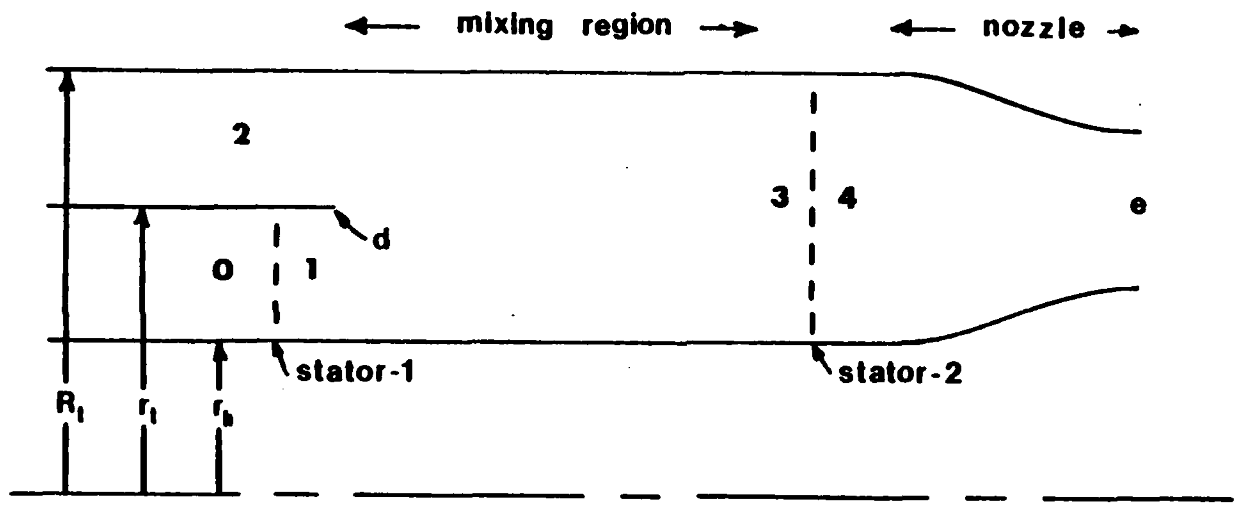

CONSTANT AREA MIXER
WITH SWIRL

Figure 2-1

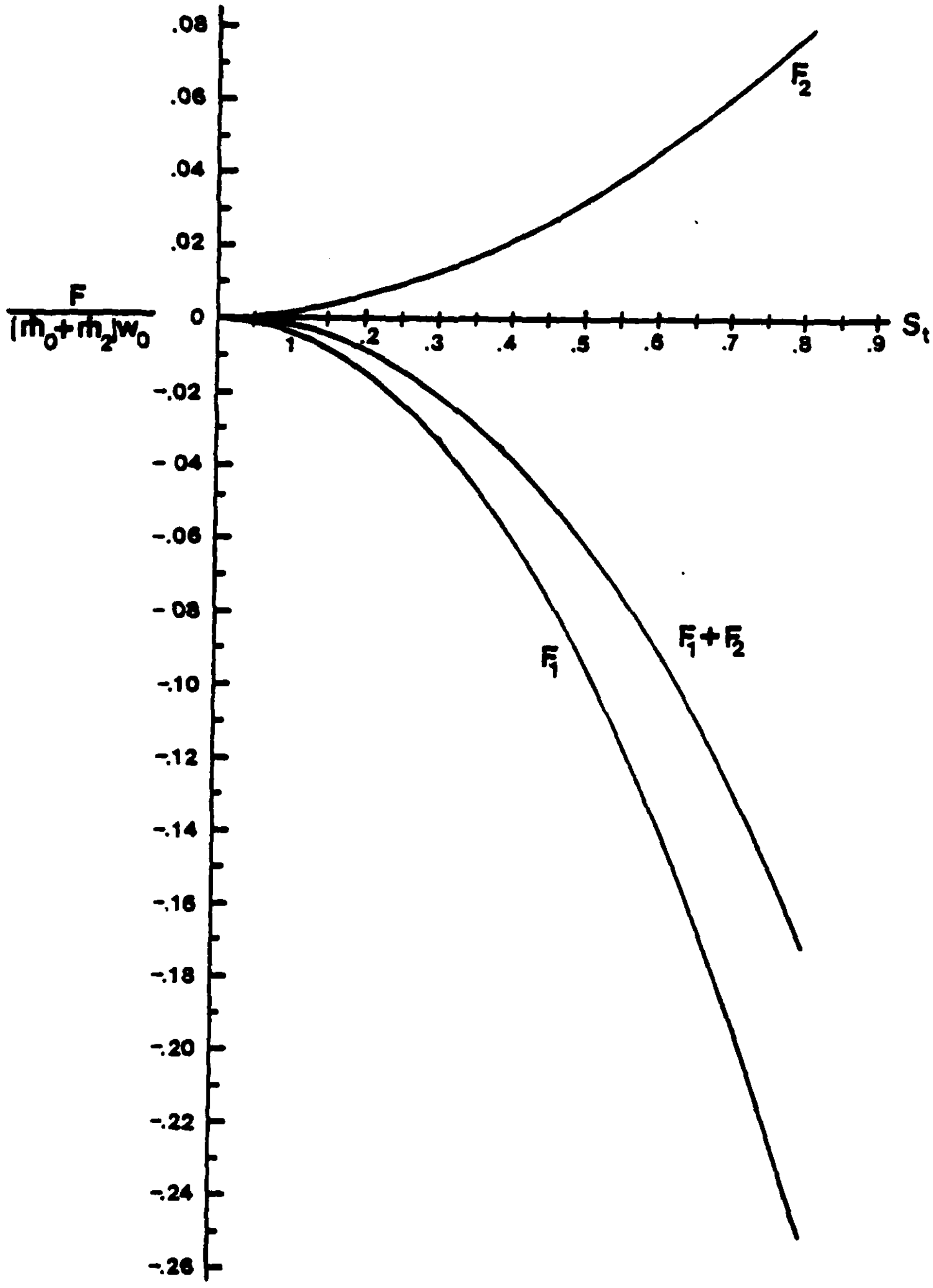

Figure 2-2 Thrust on Stators 1 and 2 versus Tip Swirl Ratio

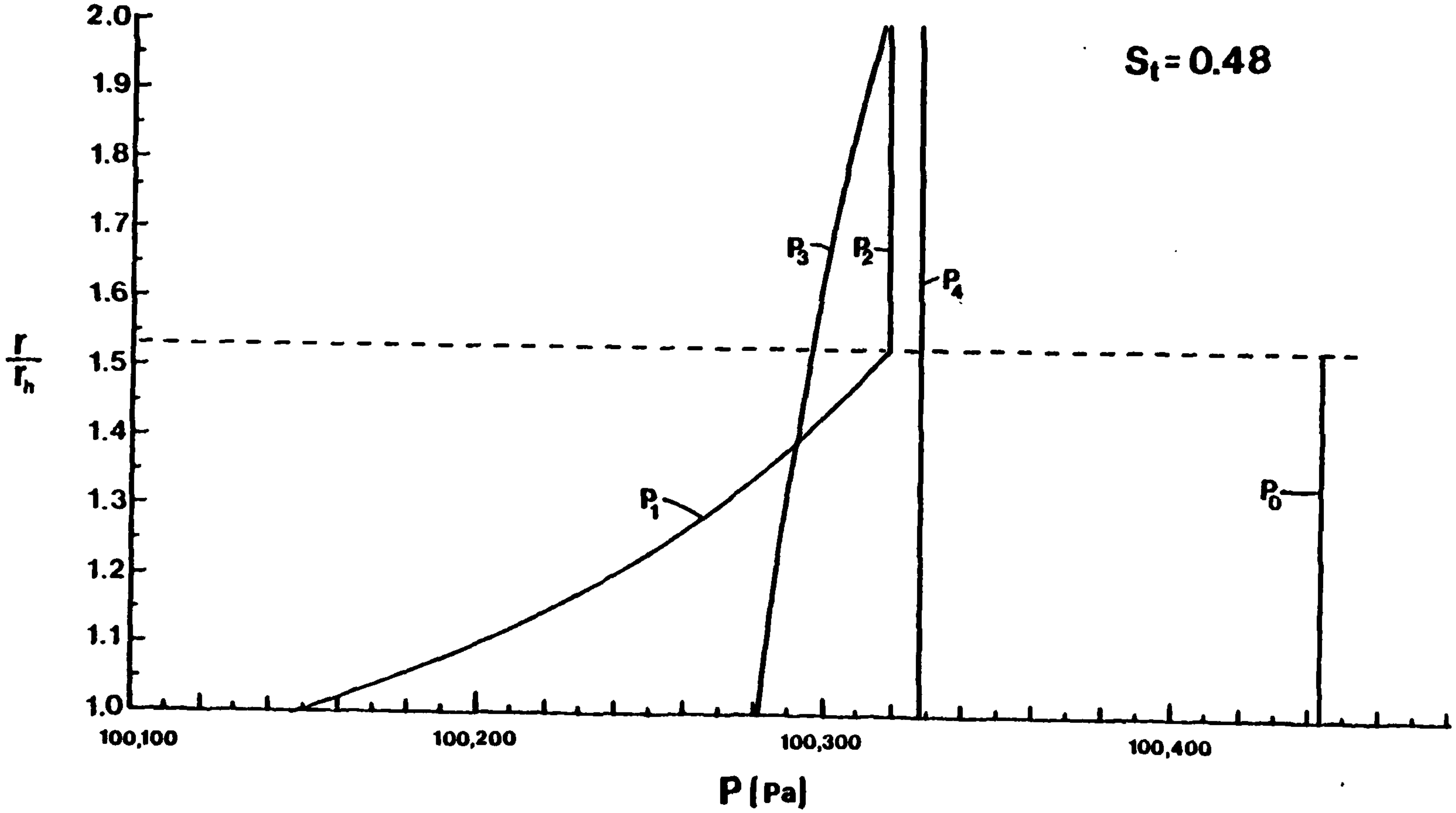

Figure 2-3 Pressures in Ideal Swirl Mixer, S_t = Ø.48

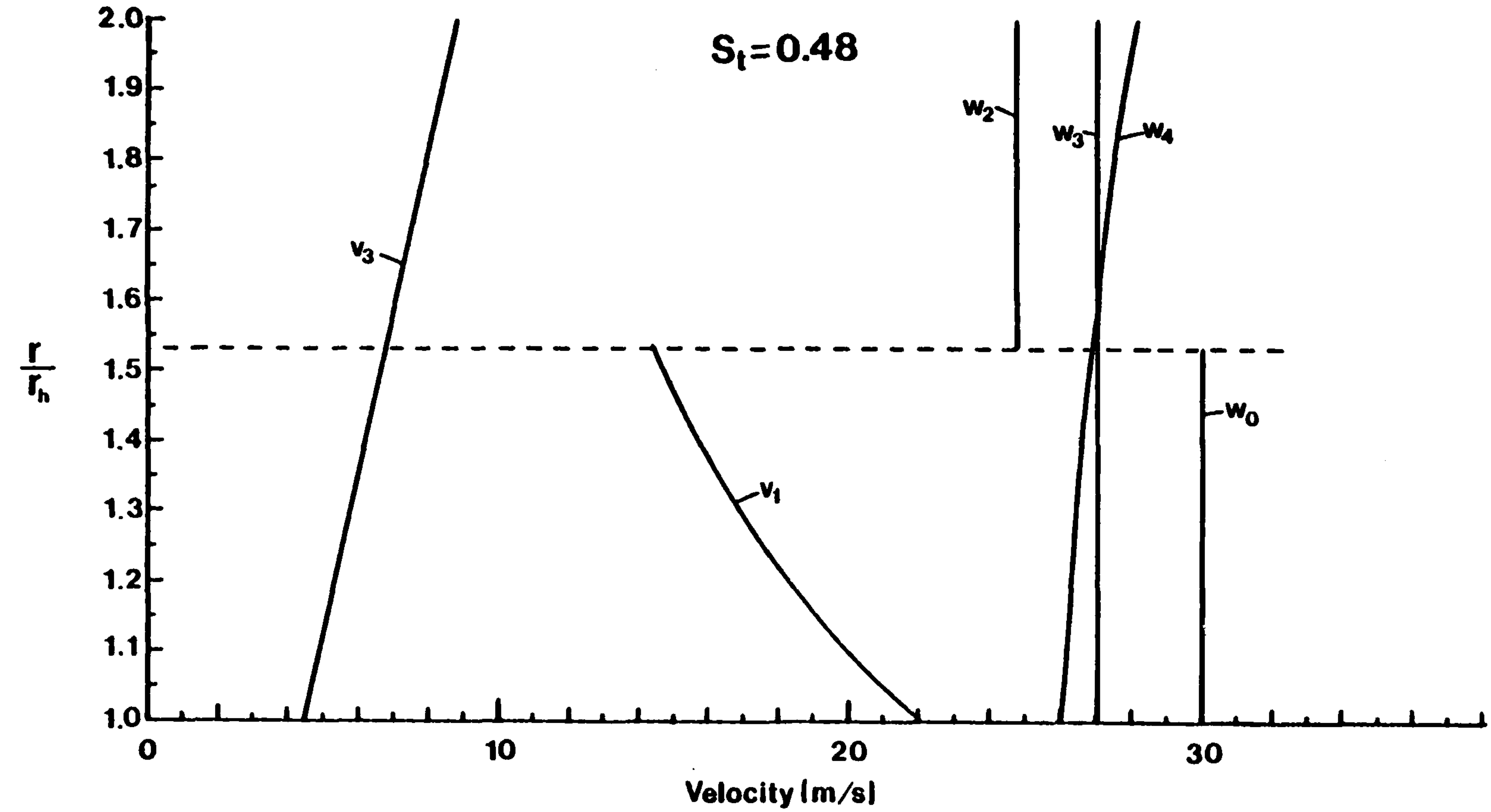

Figure 2-4 Velocities in Ideal Swirl Mixer, S_t = Ø.48

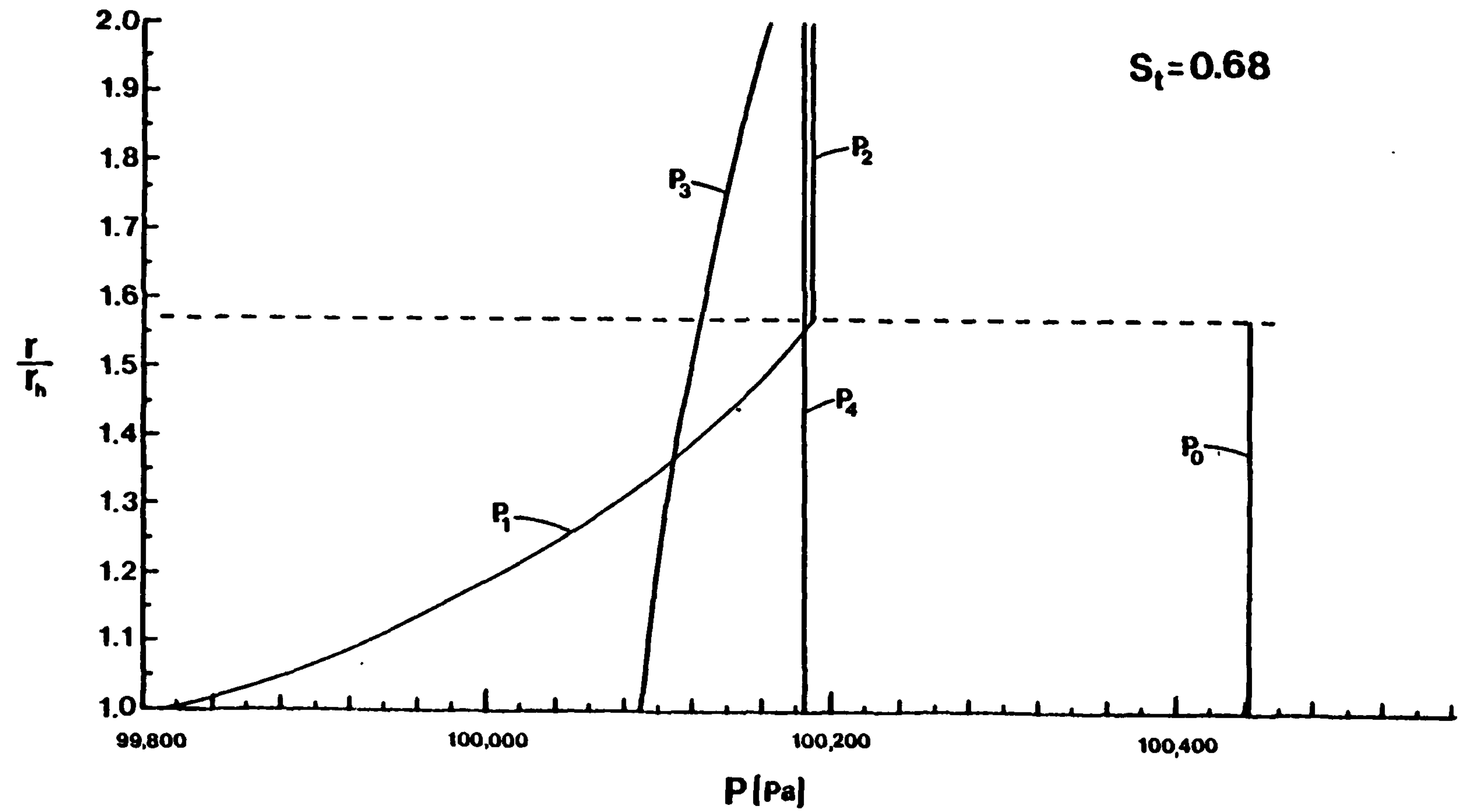

Figure 2-5 Pressures in Ideal Swirl Mixer, $S_t = 0.68$

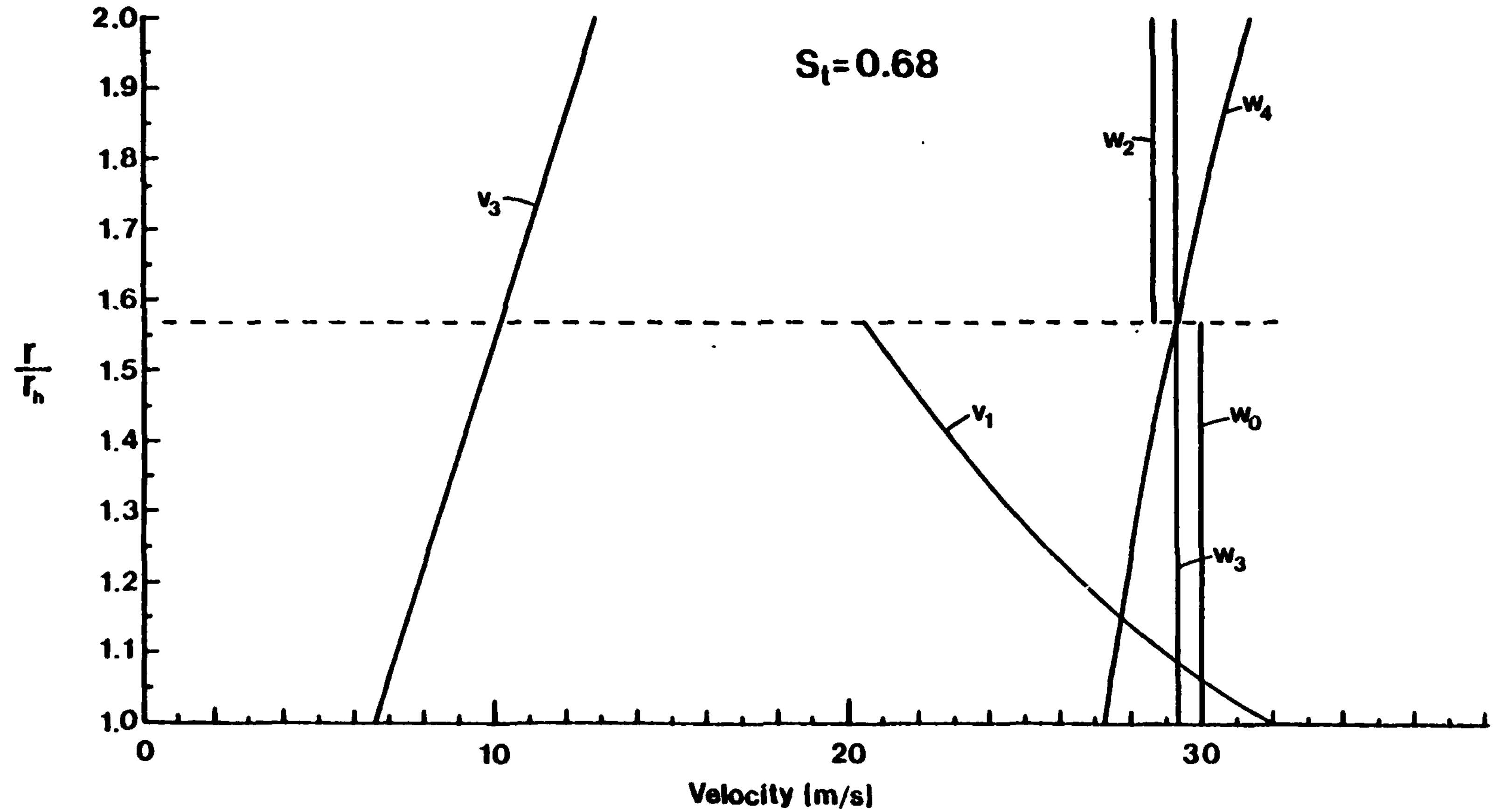

Figure 2-6 Velocities in Ideal Swirl Mixer, S_t = Ø.68

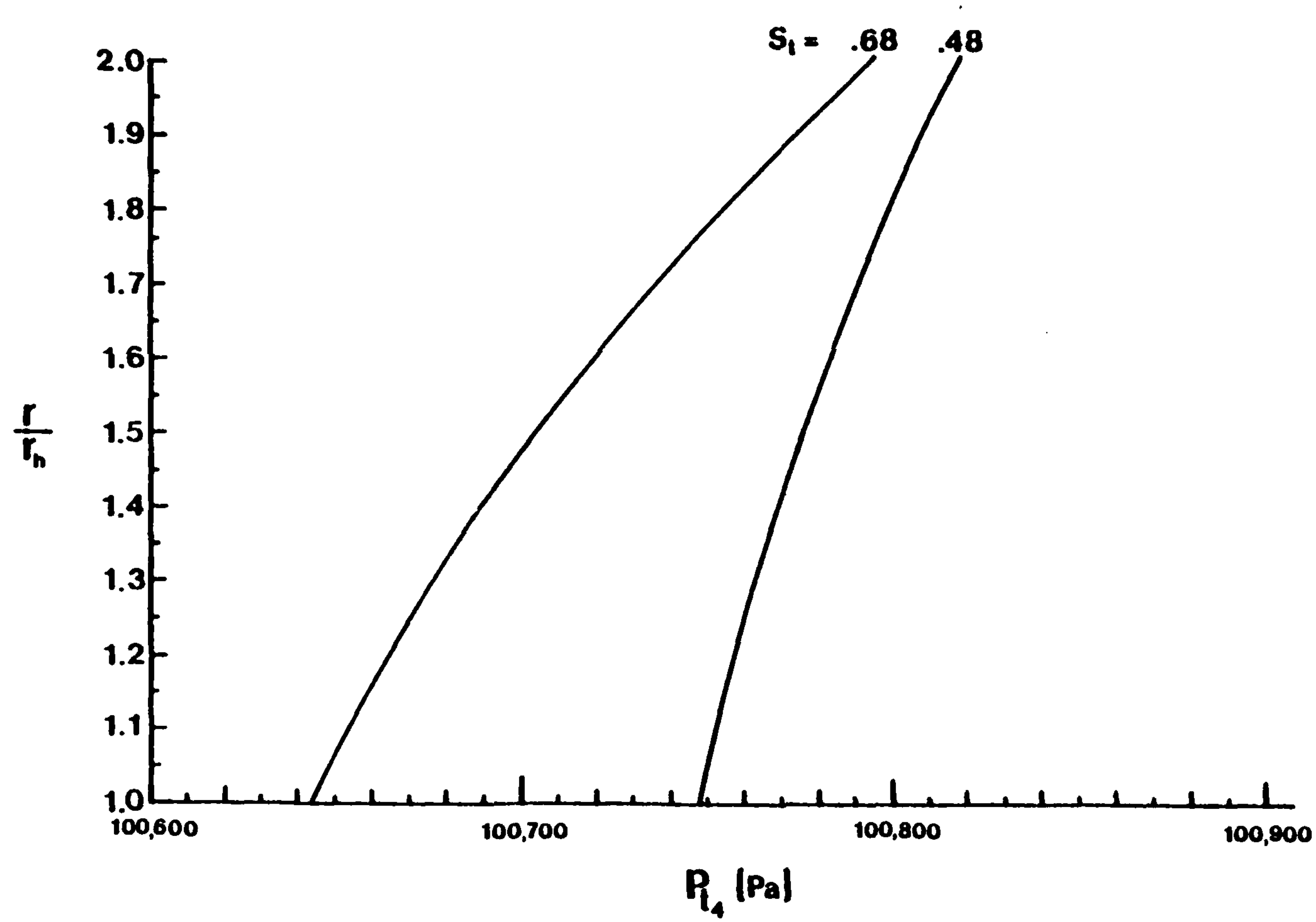

Figure 2-7 Total Pressure at Exit of Stator 2

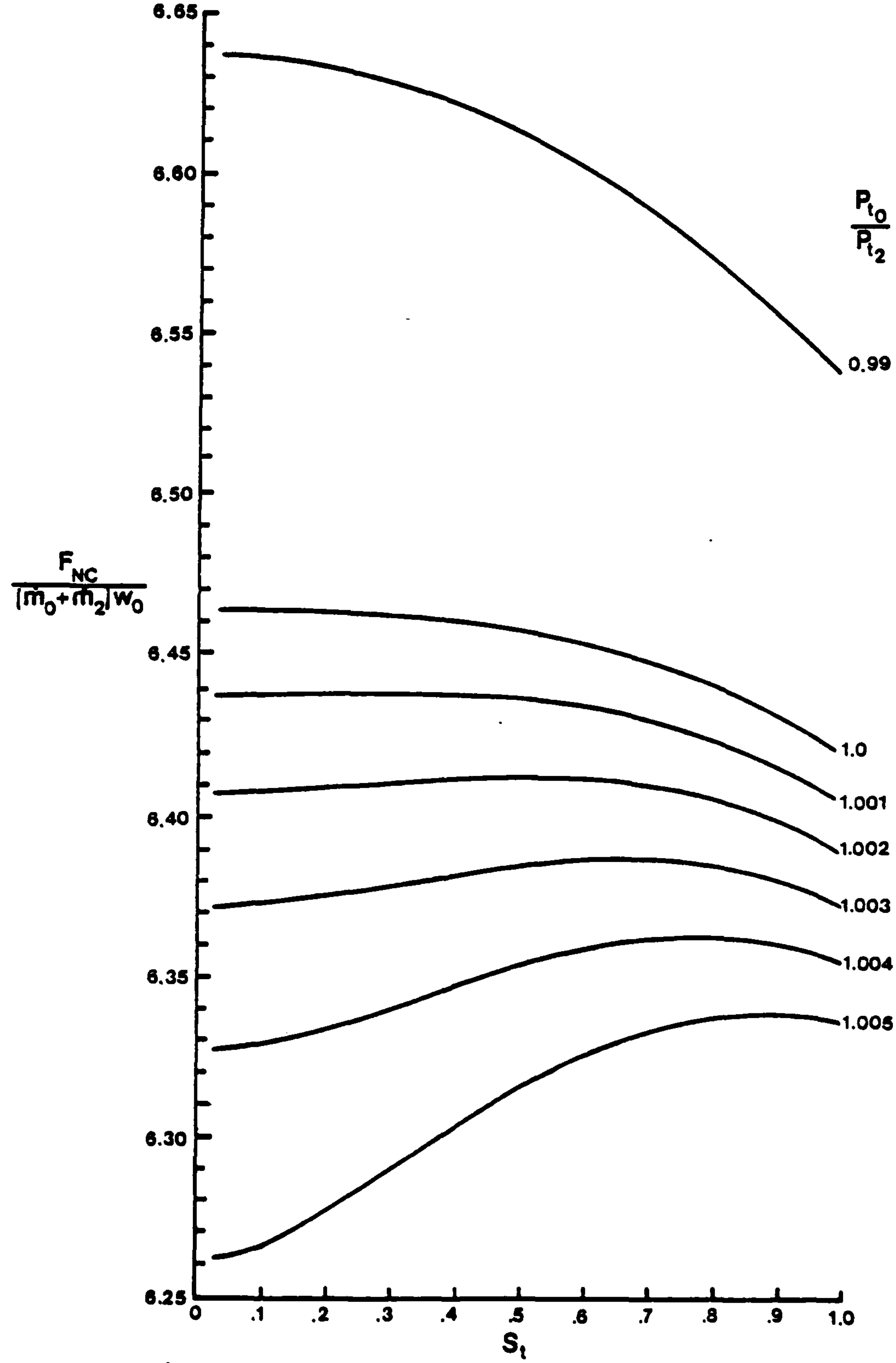

Figure 2-8 Axial Velocity at Exit of Stator 2 and at Exhaust

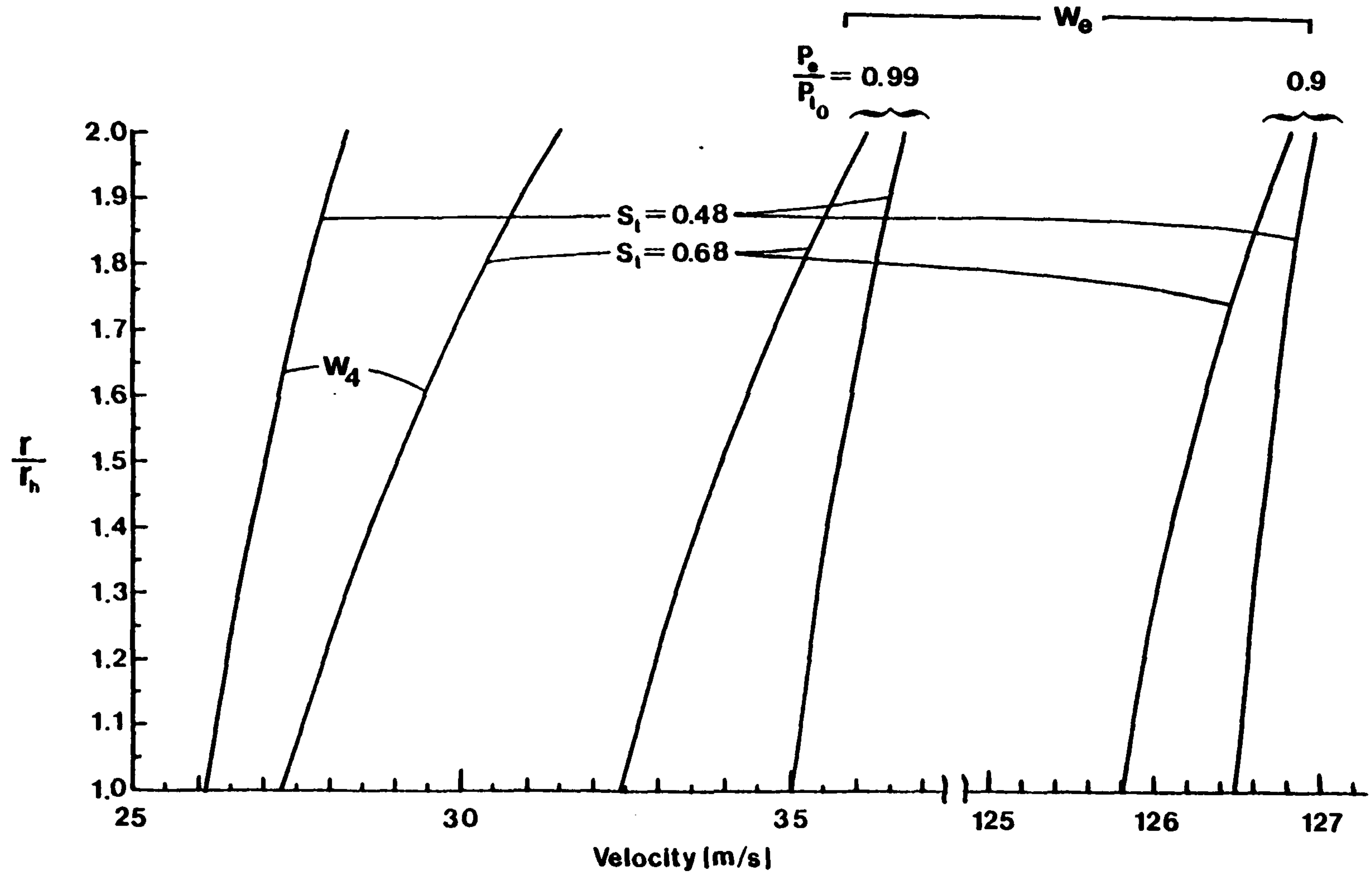

Figure 2-9 Ideal Swirl Mixer Nozzle Thrust

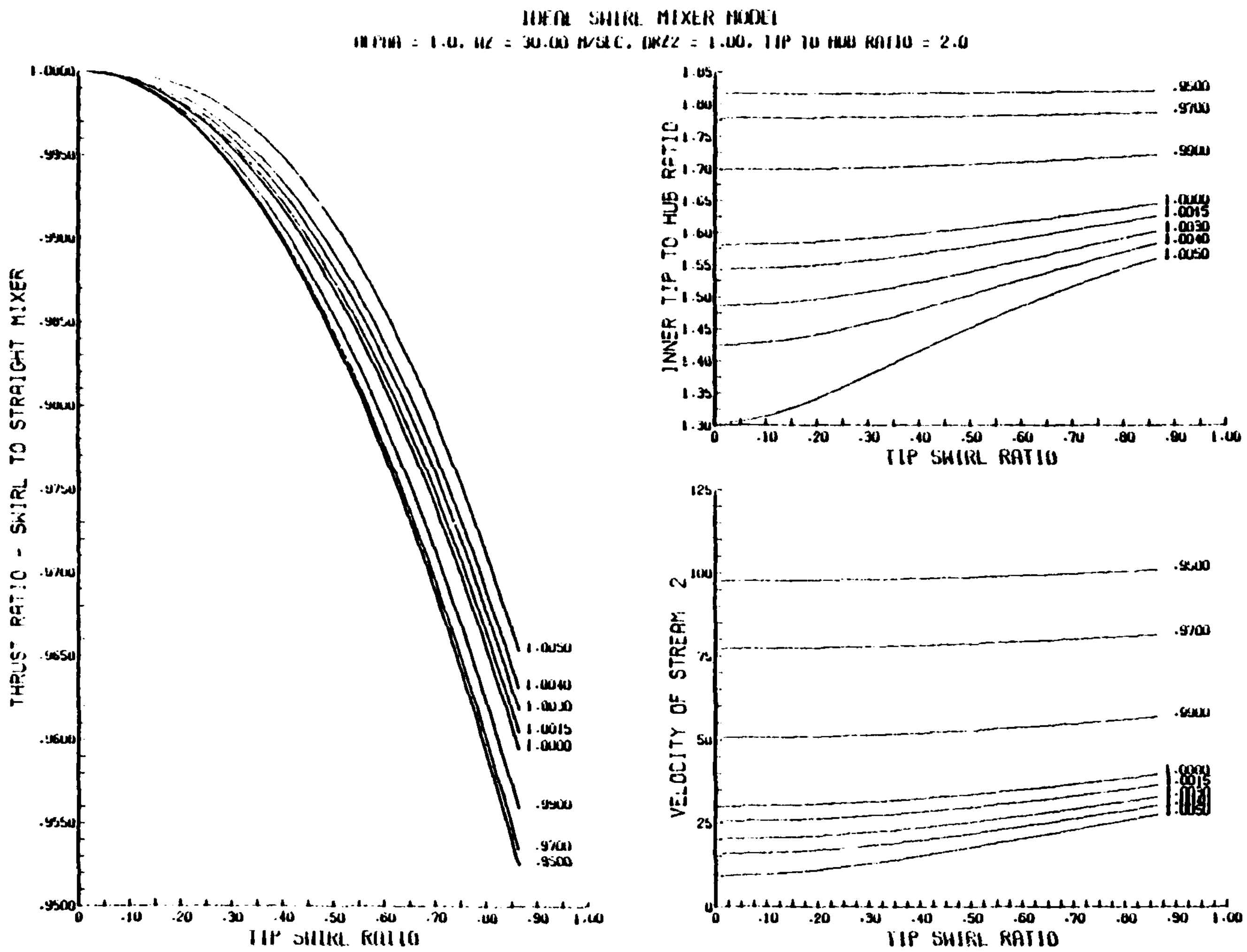

Figure 2-10 Performance Comparison of Ideal Swirl Mixer to Ideal Straight Mixer, $\alpha = 1$, $\rho_0/\rho_2 = 1$

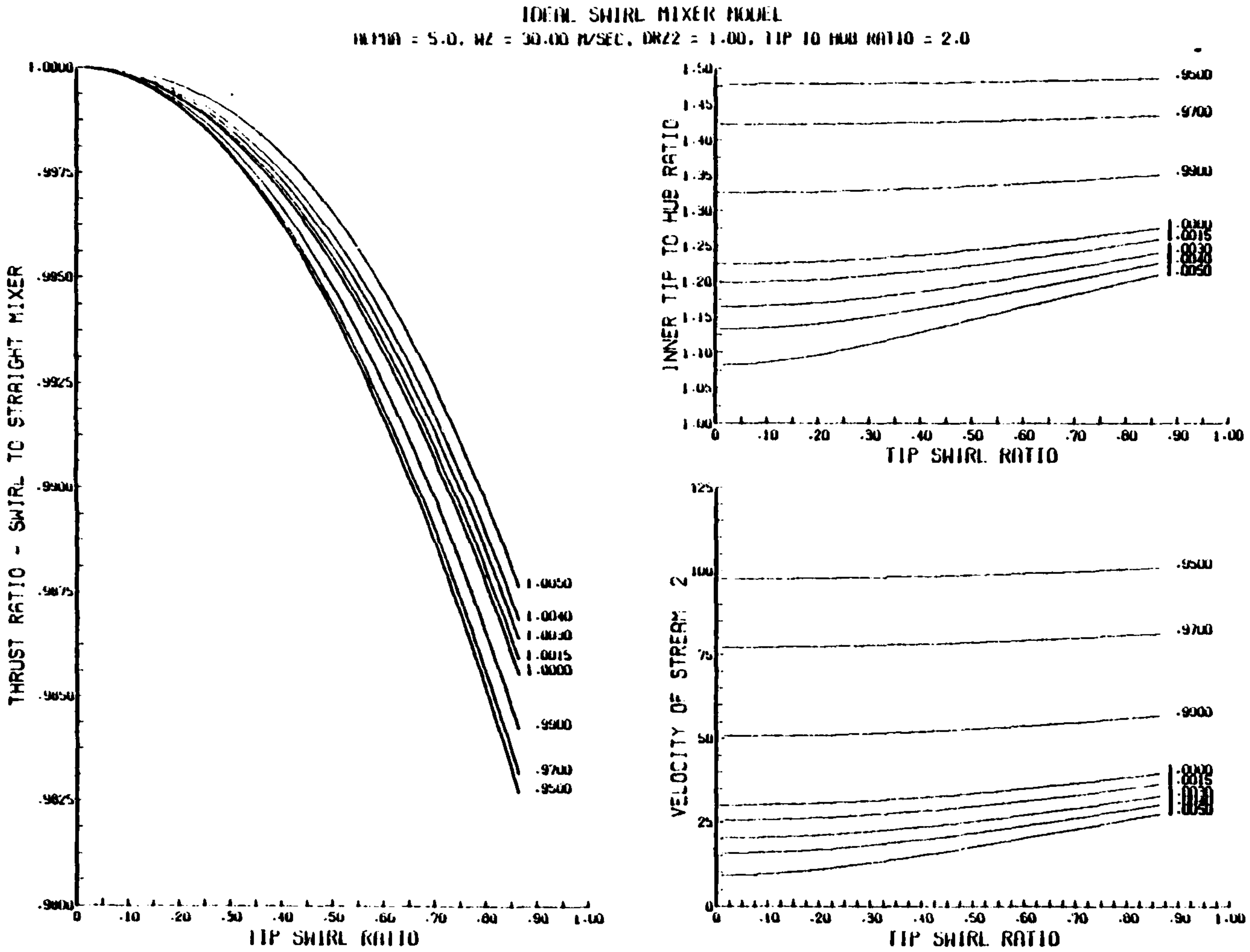

Figure 2-11 Performance Comparison of Ideal Swirl Mixer to Ideal Straight Mixer, $\alpha = 5$, $\rho_0/\rho_2 = 1$

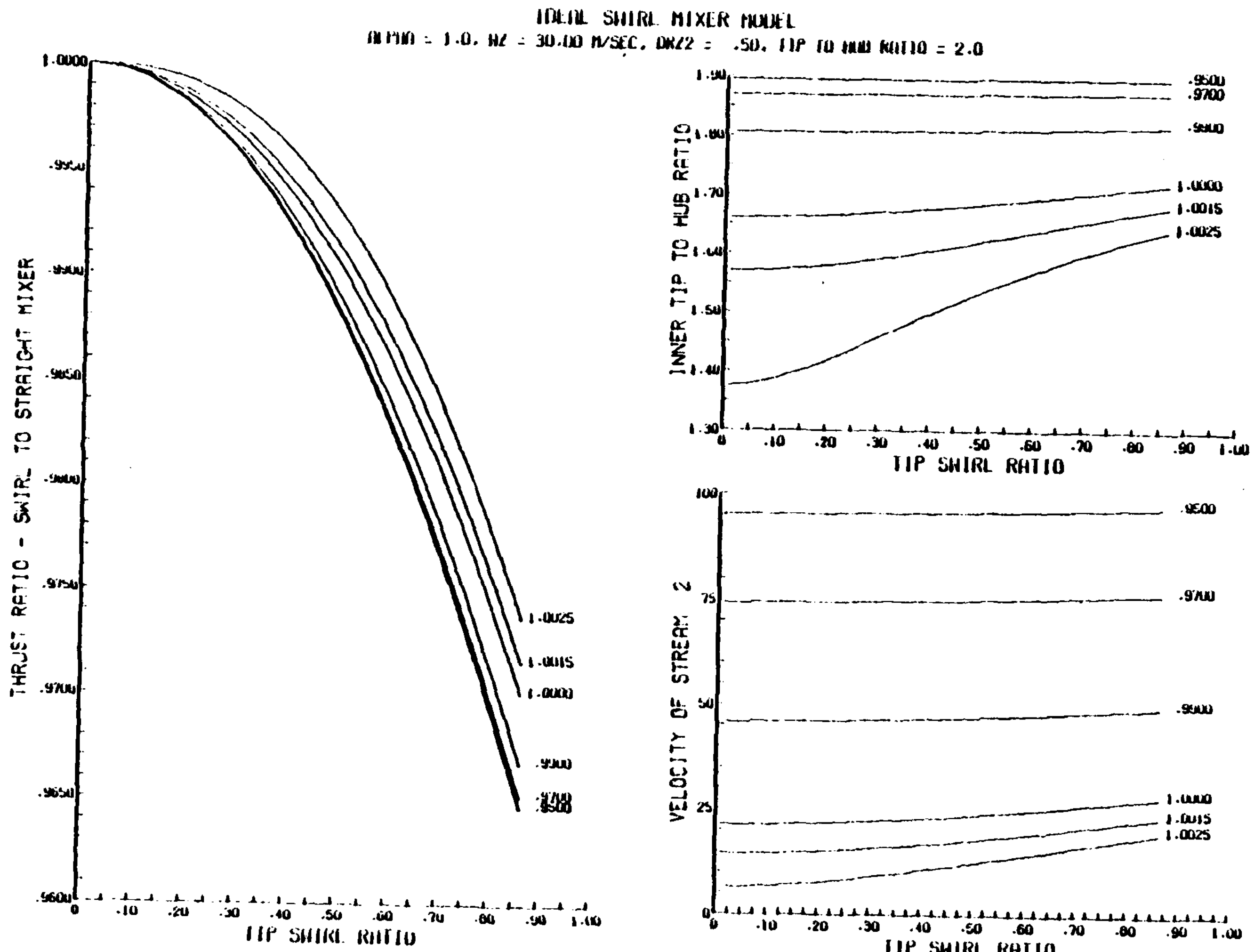

Figure 2-12 Performance Comparison of Ideal Swirl Mixer to Ideal Straight Mixer, $\alpha = 1$, $\rho_0/\rho_2 = 0.5$

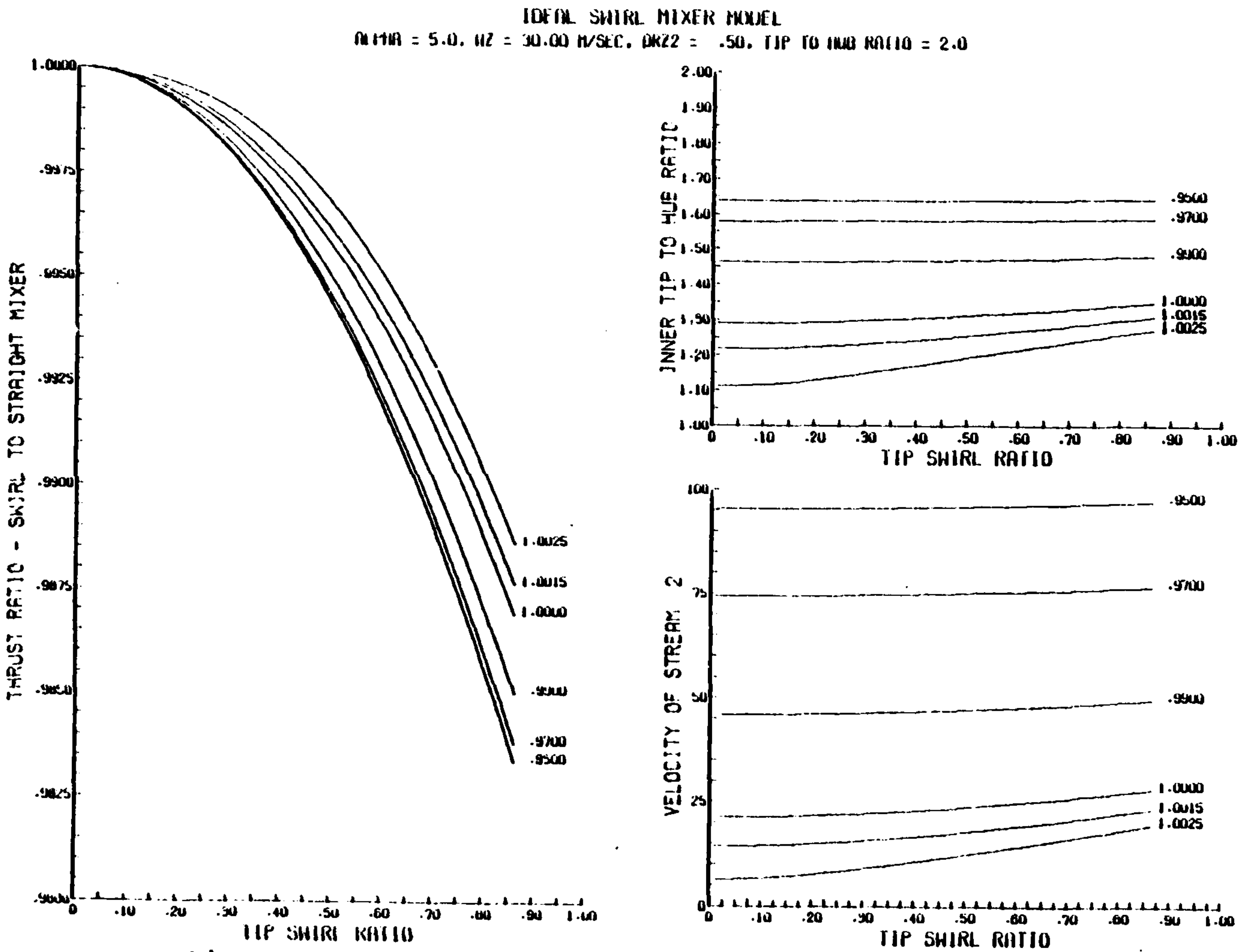

Figure 2-13 Performance Comparison of Ideal Swirl Mixer to Ideal Straight Mixer, $\alpha = 5$, $\rho_0/\rho_2 = 0.5$

CHAPTER 3

EXPERIMENTAL MEASUREMENTS

I. INTRODUCTION

The mixing of two coaxial air streams (inner stream with swirl) was measured in four set of experiments. These sets of experiments used the test apparatus and measurement systems, described in Chapter 4, and the two five-hole probes, described in Chapter 5. The first three sets of experiments were done in test sections that had no outside wall and used the initial measurement system and the first five-hole probe, Probe #1. The fourth set of experiments was performed with an outside wall on the test section and used the improved measurement system and the second five-hole probe, Probe #2.

The first three sets of experiments were run to get an understanding of the mixing of the two coaxial air streams when no outside wall is present. The initial sets of experiments also provided a learning environment for the final set of experiments, mixing of two coaxial air streams in a constant area mixer.

The following sections of this chapter describe the test

arrangement for each set of experiments and the data gathering procedures used in the experiments. Reduction of the experimental data for these experiments is described in Chapter 6 and the results are presented and discussed in Chapter 7.

II. FIRST THREE SETS OF EXPERIMENTS

The first set of experiments was performed with the test section in the configuration shown in Figure 3-1. In this configuration, a single swirling stream of air from a circular annulus in a flat wall flows into stagnant surroundings. Probe #1 was used at three axial locations to make experimental measurements for one mass flow rate. Table 3-1 lists the conditions for the three test runs in this set of experiments.

The configuration of the test section for the second set of experiments is shown in Figure 3-2. In this set of experiments, two streams of air (inner stream with swirl) from concentric annuli in a flat wall flow into stagnant surroundings. Experimental measurements were made at three axial locations for a mass flow ratio (α) of one using Probe #1. Table 3-1 lists the conditions for the three test runs in this set of experiments.

The test section for the third set of experiments is shown in Figure 3-3. In this arrangement, two streams of air (inner stream with swirl) from concentric annuli in a flat wall flow into an open region. This set of experiments differed from the second set of experiment by the addition of an extension of the inner wall of the inner annulus (centerbody) into the open region. Probe #1 was used to make experimental measurements at five axial locations for a mass flow ratio (α) of one. The conditions for the five test runs in this set of experiments are listed in Table 3-1.

The measurement system used for the first three sets of experiments is shown in Figure 4-19 and the set-up of the data gathering system is presented in Table 3-2. A Scanivalve with a single pressure transducer and 48 ports was used in all three sets of experiments to measure the pressure at the five ports of Probe #1, the total pressure of both plenums, and the static pressures on the outside wall of the inner annulus. In the third set of experiments, the static pressure along the centerbody were also measured. The Scanivalve, with one pressure transducer, was able to measure all the static pressure taps on the centerbody by changing the pressure taps

being measured from one test run to the next.

III. DATA GATHERING PROCEDURE FOR THE FIRST THREE SETS OF EXPERIMENTS

The initial measurement system, shown in Figure 4-19, was used for the first three sets of experiments. The procedure for taking data was also the same for the first three sets of experiments and consisted of the following steps:

1. Required choked orifice plates were installed in each supply line.

2. Supply voltage from each signal conditioner was checked.

3. Reference position of Probe #1 was set and the output voltage corresponding to r, z and α_p were recorded.

4. The Scanivalve was stepped from port #1 through port #48 while the output of signal conditioner "F" and the output of the voltage staircase from the Controller were monitored.

5. The output of signal conditioner "D" was adjusted to zero for a pressure difference across the differential pressure tranducer of zero.

6. Pressure regulating valve V-1, shown in Figure 4-1,

was adjusted to give the required supply line pressure.

7. Probe #1 was positioned in the radial and axial location of interest.

8. Probe #1 was rotated to give an output voltage of about zero from signal conditioner "D".

9. Time, supply line pressure, and tank pressure were manually recorded.

10. The Controller was given a "start" signal and the Controller stepped the Scanivalve through the 48 positions. The Datalogger received a "scan" command from the Controller about half a second after the Scanivalve completed each step and then all eight channels were scanned, measured, recorded on magnetic tape, and displayed on the CRT terminal (see Figure 4-19). A complete scan of all 48 positions took about 60 seconds.

11. Steps #7 through #10, above, were repeated for each desired measurement location of Probe #1 for the test run.

IV. FOURTH SET OF EXPERIMENTS

The final and most extensive set of experiments was performed with the test section in the configuration shown in Figure 3-4. In this configuration, two streams of air (inner stream with swirl) from concentric annuli

flow into a constant area annular duct. Probe #2 was used to make experimental measurements at seven axial locations for mass flow ratios of 0.47, 1.0, 2.13, and 3.91 and at eight axial locations for flow from only the inner annulus. Table 3-3 lists the conditions for the 36 test runs in this set of experiments. The improved measurement system used for this set of experiments is shown in Figure 4-18 and 4-20 and its set-up is presented in Table 3-4. All static pressures in the test section were measured by the Scanivalve with two pressure transducers. The pressure at each of the five ports of Probe #2 was measured by individual pressure transducers as described in Chapter 4.

V. DATA GATHERING PROCEDURE FOR THE FOURTH SET OF EXPERIMENTS

The improved measurement system, shown in Figures 4-18 and 4-20, was used for this set of experiments. The data taking procedure for this set of experiments consisted of the following steps:

1. Probe #2 and its section of outside wall (see Figure 4-17) were installed at the desired axial location.

2. Required choked orifice plates (see Table 3-3) were

installed in each supply line.

3. Probe #2 was moved to a known radial position. The output voltage from the linear variable differential transformet (LVDT) corresponding to this radial position was recorded.

4. The output of signal conditioners "J", "L", and "M" were recorded.

5. The length of tubing connecting Probe #2 to its block of five pressure transducers was disconnected so that atmospheric pressure was applied to both ports of each pressure transducer.

6. The Scanivalve was moved to its "home" position (location #48).

7. The Datalogger was set to continuously scan channel "Ø1" and then the pressure regulating valve V1 (see Figure 4-18) was manually positioned to give the desired line pressure (see Table 3-3).

8. The Datalogger was set to scan channels "ØØ" through "17" on receipt of a remote "scan" signal and send the measured values to the Data Tape Recorded and CRT monitor.

9. Probe #2 was positioned at the desired radial location.

1Ø. The "scan" button on the front panel of the Controller was pressed to initiate scan #1.

11. The length of tubing connecting Probe #2 to its block of five pressure transduccers was reconnected.

12. Probe #2 was rotated while monitoring the output of signal conditioner "F" (using a digital volt meter) until the output voltage reached a minimum.

13. The "start" button on the front panel of the Controller was pressed to initiate the automatic stepping of the Scanivalve through its 48 positions. The Datalogger received a "scan" command from the Controller about a half second after the Scanivalve completed each step and all seventeen channels were scanned, measured, recorded on magnetic tape, and displayed on the CRT terminal (see Figure 4-20). A complete scan of all 48 Scanivalve positions took about 75 seconds.

14. At the completion of the automatic stepping of the Scanivalve, the length of tubing connecting Probe #2 to its block of five pressure transducers was disconnected and the "scan" button on the front panel of the Controller was pressed to initiate scan #49.

15. Steps #9 through #14, above, were repeated for each radial location in the test run.

16. Steps #2 through #15, above, were repeated for each test run (mass flow ratio) at that axial position.

17. Steps #1 through #16, above, were repeated for each axial location of Probe #2 in this set of experiments.

TABLE 3-1

TEST RUNS FOR FIRST, SECOND, AND THIRD
SETS OF EXPERIMENTS

Set Run No.	Orifice Size*		Line Pressure (psig)	Probe Axial Location	Name of Data Files		
	Inside	Outside			Raw	Fine	Output
1/1	2	1	500	0.28"	RAW11	D1A	PLT1A
1/2	2	1	500	1.01"	RAW12	D1B	PLT1B
1/3	2	1	500	2.01"	RAW13	D1C	PLT1C
2/1	2	2	300	0.24"	RAW21	D2A	PLT2A
2/2	2	2	300	1.00"	RAW22	D2B	PLT2B
2/3	2	2	300	4.01"	RAW23	D2C	PLT2C
3/1	2	2	500	0.26"	RAW31	D3A	PLT3A
3/2	2	2	500	1.00"	RAW32	D3B	PLT3B
3/3	2	2	500	4.01"	RAW33	D3C	PLT3C
3/4	2	2	500	8.88"	RAW34	D3D	PLT3D
3/5	2	2	500	23.99"	RAW35	D3E	PLT3D

* Orifice Size	$\dot{m}$ at 600 psia
1	0.000 lb/sec
2	0.493 lb/sec

TABLE 3-2

DATALOGGER/TRANSDUCERS/SIGNAL CONDITIONERS

USED IN FIRST THREE SETS OF EXPERIMENTS

DATALOGGER			SIGNAL CONDITIONER		TRANSDUCER
CHANNEL	SCALE	VARIABLE	UNIT	VOLTAGE	
00	400 mV	r	LVDT Conditioner	-	LVDT
01	40 V	Scanivalve Port #	Controller Output	-	Scanivalve Encoder
02	40 mV	z	A	10 VDC	10k Ohm Potentiometer
03	4 V	T_i	B	10 VDC	Thermistor
04	4 V	T_o	C	10 VDC	Thermistor
05	400 mV	$P_1 - P_3$	D	5 VDC	Statham PM-283TC±0.15
06	4 V	α_p	E	10 VDC	10k Ohm
07	40 mV	P_x	F	5 VDC	Statham PM-131TC±2.5

Variables P_T and P_L were read from gauges on the control panel and manually recorded. The pressure drop across each flow orifice plate, ΔP_i and ΔP_o, were recorded on the strip chart recorder in the control panel.

TABLE 3-3

TEST RUNS FOR THE FOURTH SET OF EXPERIMENTS

Run No.	Orifice Size*		Line Pressure (psig)	Probe Axial Location	Name of Data Files		
	Inside	Outside			Raw	Fine	Output
1	3	1	500	0.25"	RAW001	DAT001	PLT001
2	3	2	333	0.25"	RAW002	DAT002	PLT002
3	2	2	500	0.25"	RAW003	DAT003	PLT003
4	2	3	333	0.25"	RAW004	DAT004	PLT004
5	2	4	200	0.25"	RAW005	DAT005	PLT005
6	3	1	500	2.25"	RAW021	DAT021	PLT021
7	3	2	333	2.25"	RAW022	DAT022	PLT022
8	2	2	500	2.25"	RAW023	DAT023	PLT023
9	2	3	333	2.25"	RAW024	DAT024	PLT024
10	2	4	200	2.25"	RAW025	DAT025	PLT025
11	3	1	500	4.25"	RAW041	DAT041	PLT041
12	3	2	333	4.25"	RAW042	DAT042	PLT042
13	2	2	500	4.25"	RAW043	DAT043	PLT043
14	2	3	333	4.25"	RAW044	DAT044	PLT044
15	2	4	200	4.25"	RAW045	DAT045	PLT045
16	3	1	500	6.25"	RAW061	DAT061	PLT061
17	3	2	333	6.25"	RAW062	DAT062	PLT062
18	2	2	500	6.25"	RAW063	DAT063	PLT063
19	2	3	333	6.25"	RAW064	DAT064	PLT064
20	2	4	200	6.25"	RAW065	DAT065	PLT065
21	3	1	500	8.25"	RAW081	DAT081	PLT081
22	3	1	500	12.25"	RAW121	DAT121	PLT121
23	3	2	333	12.25"	RAW122	DAT122	PLT122
24	2	2	500	12.25"	RAW123	DAT123	PLT123
25	2	3	333	12.25"	RAW124	DAT124	PLT124
26	2	4	200	12.25"	RAW125	DAT125	PLT125
27	3	1	500	18.25"	RAW181	DAT181	PLT181
28	3	2	333	18.25"	RAW182	DAT182	PLT182
29	2	2	500	18.25"	RAW183	DAT183	PLT183
30	2	3	333	18.25"	RAW184	DAT184	PLT184
31	2	4	200	18.25"	RAW185	DAT185	PLT185
32	3	1	500	24.25"	RAW241	DAT241	PLT241
33	3	2	333	24.25"	RAW242	DAT242	PLT242
34	2	2	500	24.25"	RAW243	DAT243	PLT243
35	2	3	333	24.25"	RAW244	DAT244	PLT244
36	2	4	200	24.25"	RAW245	DAT245	PLT245

* Orifice Size	$\dot{m}$ at 600 psia
1	0.000 lb/sec
2	0.493 lb/sec
3	1.052 lb/sec
4	1.928 lb/sec

TABLE 3-4

DATALOGGER/TRANSDUCERS/SIGNAL CONDITIONERS

USED IN THE FOURTH SET OF EXPERIMENTS

DATALOGGER			SIGNAL CONDITIONER		TRANSDUCER
CHANNEL	SCALE	VARIABLE	UNIT	VOLTAGE	
00	4 V	α_p	I	10 VDC	10k Ohm Potentiometer
01	40 mV	P_L	J	5 VDC	Statham PG-146TC-800
02	40 mV	P_T	K	5 VDC	Statham PG-146TC-5M
03	4 V	r	LVDT Conditioner	-	LVDT
04	40 V	Scanivalve Port #	Controller Output	-	Scanivalve Encoder
05	J	T_i	-	-	Thermocouple
06	J	T_o	-	-	Thermocouple
07	Skip	-	-	-	
08	40 mV	P_1	G	12 VDC	ScanCo PDCR-22+1 #47153
09	40 mV	P_2	H	12 VDC	ScanCo PDCR-22+1 #40166
10	40 mV	P_3	A	12 VDC	ScanCo PDCR-22+1 #45699
11	40 mV	P_4	B	12 VDC	ScanCo PDCR-22+1 #45811
12	40 mV	P_5	C	12 VDC	ScanCo PDCR-22+1 #47148
13	40 mV	P_x	D	12 VDC	ScanCo PDCR-22+1 #47149
14	40 mV	P_x	E	12 VDC	Scanco PDCR-22+1 #47152
15	40 mV	$P_1 - P_3$	F	5 VDC	Statham PM-283TC+0.15
16	40 mV	ΔP_i	L	5 VDC	Statham PM-80TC #532
17	40 mV	ΔP_o	M	5 VDC	Statham PM-80TC #531

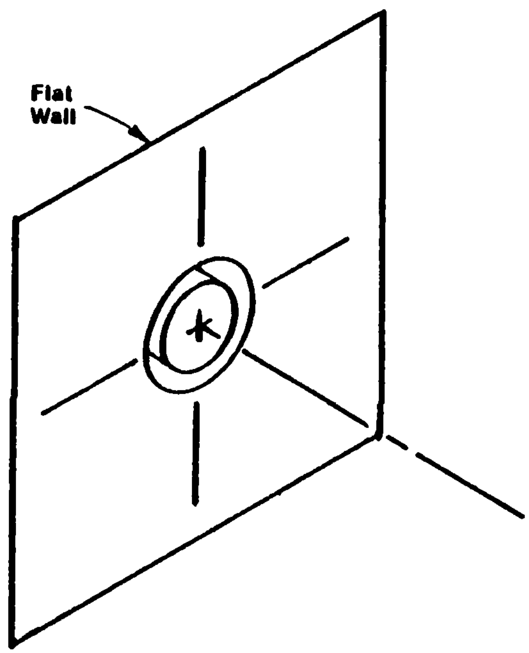

Figure 3-1

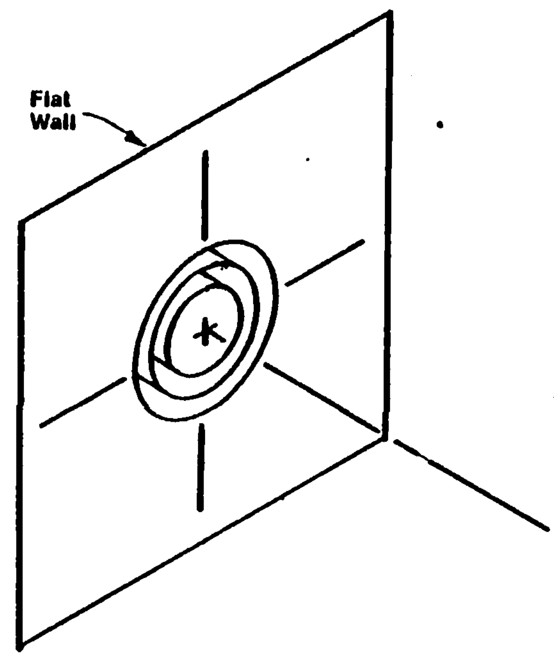

Figure 3-2

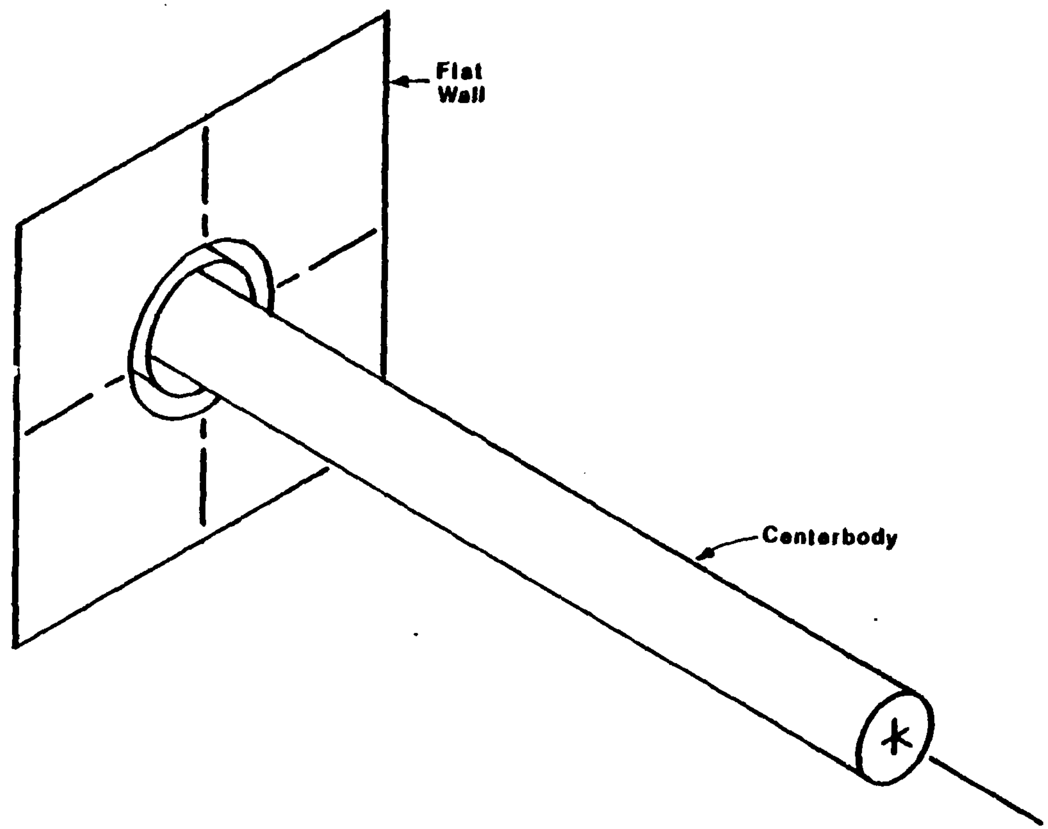

Figure 3-3 Test Section for Third Set of Experiments

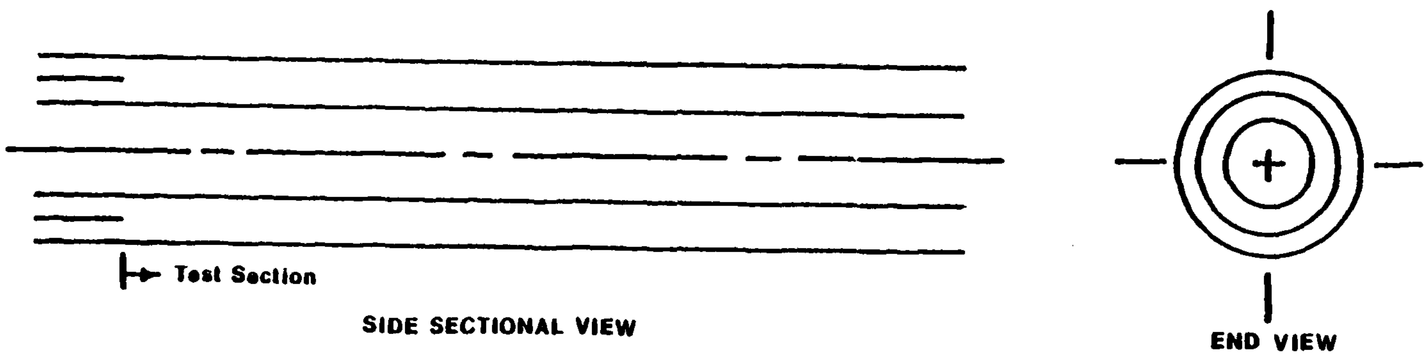

Figure 3-4 Test Section for Fourth Set of Experiments

CHAPTER 4

TEST APPARATUS

I. INTRODUCTION

The test apparatus consists of five major portions:

1. High pressure dual air supply system
2. Concentric dual plenum section
3. Swirl generator and nozzles section
4. Test section
5. Measurement equipment

A diagram of the high pressure air supply system is shown in Figure 4-1. Figure 4-2 shows the next three major portions of the test apparatus as listed above. The following sections of this chapter will discuss the five major portions of the test apparatus in the order listed.

II. HIGH PRESSURE DUAL AIR SUPPLY SYSTEM

The high pressure air supply system consisting of an air compressor, air receiver and single pressure supply piping was modified to supply two separate air streams at different stagnation pressures. This modification was accomplished by connecting a new supply line to the

existing air receiver and installing the piping and valving shown in Figure 4-1. Control valve V1 can be set to maintain a downstream pressure of up to 600 psig. The medium pressure air, downstream of control valve V1, is then piped into two separate and controllable streams. Initially, the stagnation pressure of supply air stream #1 was controlled by control valve V2 to maintain a supply pressure of up to 39 psig and its mass flow rate measured by orifice plate 01. Also, the stagnation pressure of supply air stream #2 was controlled by control valve V3 to maintain a supply pressure of up to 30 psig and its mass flow rate measured by orifice plate 02. This supply system had severe stability problems at the low mass flow rates required for these experiments and modification was required. The two control valves, V2 and V3, were replaced by orifice plates sized for specific mass flow rates and operating under choked conditions. Further discussion of the choked orifice plates is included in the "Measurement Equipment" section of this chapter.

III. CONCENTRIC DUAL PLENUM SECTION

The concentric dual plenum section, shown in Figure 4-3, consists of a 30-inch diameter cylinder supported inside

a 40-inch diameter cylinder and this section is 90 inches long. The air enters the inner plenum through a two-inch pipe that is aligned with the centerline of the plenum and this air stream is dispersed by a "core buster". The air enters the outside plenum through four pipes of two-inch diameter spaced evenly around the annulus and each entering air stream is dispersed by a "core buster". Both the air stream in the inner circular plenum and the air stream in the outer annular plenum then pass through two sets of screens, three sets of honeycomb and four sets of screens. The two concentric air streams leaving this dual plenum section are essentially uniform and have a low turbulence level.

The concentric dual plenum section is connected to the high pressure dual air supply system by two sections of two-inch diameter schedule 40 pipe. These sections of pipe are connected to the dual plenum section by rubber hose and connected to the high pressure dual air supply system by bolted flanges. Each section of pipe contains a rupture disc to prevent overpressurization of the dual plenum section.

The dual plenum section is designed to handle stagnation pressures of up to 10 psig, however, in these

experiments, the stagnation pressures were below 1 psig. The design and construction of the dual plenum section was influenced by the space limitations for the test apparatus and the size of the doorway leading into the space that houses the test apparatus.

The "core busters" consist of 1/2-inch thick aluminum plates mounted to the common plenum end cap by threaded rods (for adjustment). The "core buster" for the inner plenum measures 7"x11" with 75 holes of one-half inch diameter distributed evenly over its surface and was mounted about six inches away from the plenum end cap. The four "core busters" for the outer plenum each measure 4.5"x11" with 75 holes of one-half inch diameter distributed evenly over each surface and each was mounted about four inches away from the plenum end cap.

A set of screens was placed upstream of the honeycomb sections to break up the large eddies and provide a more even flow upstream of the honeycomb. Commercial 18x14 mesh brass screen fabric was used for the screens which gave a mesh size of 0.0625 inches. Using Figure 1.18 on Page 19 of Reference 1, this mesh size and a mean velocity of 5 ft/sec give a Reynolds Number of 163 and the value of $\overline{u}^2 / \overline{u'^2}$ reaches a value of about 5,000 within

four inches downstream of the screen. This dampening of the turbulence intensity is acceptable as a minimum and the minimum distance between screens was selected as four inches. This agrees with the suggestions of Schubauer, et al, (Reference 2).

Screens are capable of reducing the magnitude of the turbulence intensity in the direction of the mean flow. Honeycomb is capable of aligning the mean flow and reducing the lateral components of turbulence; however, the longitudinal component of turbulence is increased (Reference 3). An essentially uniform and low turbulence stream is obtained by having the air stream first pass through three sets of honeycomb to align the flow, reduce lateral components of turbulence and reduce longitudinal non-uniformity in the mean velocity. The air stream then passes through two sets of screens to reduce the longitudinal components of turbulence. The resulting air streams can then be accelerated through nozzles to the test section velocity and for a contraction ratio of 25 and 45, the ratio of the turbulence intensity to the mean velocity is reduced to 0.16 and 0.12, respectively (Reference 4).

The effect of multiple sections of honeycomb on reducing

longitudinal non-uniformity in the mean velocity was analyzed using the model shown in Figure 4-4. The model is composed of a frictionless duct (section 1-2) which allows both the high velocity and low velocity streams to adjust before entering the honeycomb (section 2-3). The honeycomb is assumed to be composed of small circular pipes. The two air streams are assumed to have equal static pressures at points 1 and 3. The sum of the area of the high velocity flow plus the area of the low velocity flow is constant and the area of the honeycomb is constant. For 1/8-inch diameter honeycomb, a Reynolds Number of 195 corresponds to a mean velocity of 3 ft/sec and a Reynolds Number of 1950 corresponds to a mean velocity of 30 ft/sec. Since the design overall mean velocity is 5 ft/sec, the flow through the honeycomb is assumed to be developing laminar flow. Application of the continuity and momentum equations to the model give the following relationships for incompressible flow:

$$\frac{V_{H_1}}{V_{H_3}} = 1 + \frac{A_{L_1}}{A_{H_1}}\left[1 - \frac{V_{L_1}}{V_{L_3}}\right] \qquad (4\text{-}1)$$

$$\frac{A_{L_3}}{A_{H_3}} = \frac{A_{L_1}}{A_{H_1}} \frac{V_{L_1}}{V_{L_3}} \frac{V_{H_3}}{V_{H_1}} \qquad (4\text{-}2)$$

$$P_1 - P_3 = 1/2\ \rho\ V_{H_3}^2\left[\frac{64L\nu}{d^2 V_{H_3}} + 2.41\right] - 1/2\ \rho\ V_{H_1}^2 \qquad (4\text{-}3)$$

$$P_1 - P_3 = 1/2\,\rho\, V_{L_3}^2 \left[\frac{64L\nu}{d^2 V_{L_3}} + 2.41 \right] - 1/2\,\rho\, V_{L_1}^2 \qquad (4\text{-}4)$$

The frictional loss term contained within the brackets in Equations 4-3 and 4-4 was obtained from Equation 44 on Page 308 of Reference 5. Since the pressure difference

$P_1 - P_3$ of the two streams are equal, Equations 4-2 and 4-3 can be equated to give the following relationship:

$$\left[\frac{V_{L_3}}{V_{L_1}}\right]^2 = \frac{1 + \left[\frac{V_{H_3}}{V_{H_1}}\right]^2 \left[\frac{V_{H_1}}{V_{L_1}}\right]^2 \left[\frac{64L\nu}{d^2 V_{H_1}} \frac{V_{H_1}}{V_{H_3}} + 2.41\right] - \frac{V_{H_1}}{V_{L_1}}}{\frac{64L\nu}{d^2 V_{H_1}} \frac{V_{H_1}}{V_{L_1}} \frac{V_{L_1}}{V_{L_3}} + 2.41} \qquad (4\text{-}5)$$

Thus Equations 4-1, 4-2 and 4-5 give a system of equations that can be solved to determine the downstream velocity discontinuity and distribution given the upstream velocity discontinuity and distribution.

A comparison between the performance of three two-inch thick sections of honeycomb and one six-inch thick section of honeycomb was made using the following input data:

V_{H_1} = 18 ft/sec	d = 1/8 inch
V_{L_1} = 3 ft/sec	ρ = 0.075 lb/ft
A_{L_1}/A_{H_1} = 9	ν = 0.00016 ft/sec

The model gives the following results for the two different configurations:

	Three - 2" Sections	One - 6" Section
V_{H_3} =	4.544 ft/sec	6.064 ft/sec
V_{L_3} =	4.435 ft/sec	3.840 ft/sec
A_{L_3}/A_{H_3} =	0.68311	2.3687
P =	0.0397 in H_2O	0.0129 in H_2O

From the above example, the superiority of multiple sections of honeycomb versus one section of the same total thickness is evident in its ability to even out mean velocity variations. In both cases, the mean velocity has an average value of 4.5 ft/sec with an incoming standard deviation of 4.5 ft/sec. The leaving standard deviation for the three two-inch sections of honeycomb is 0.0535 ft/sec whereas the standard deviation for the air stream leaving the one six-inch section of honeycomb is 1.016 ft/sec. The multiple sections of honeycomb produce a larger pressure loss than a single section of honeycomb with the same total thickness of six inches due to the multiple entrance losses.

Because only a limited amount of two-inch thick honeycomb with 1/8-inch cells was available, the honeycomb was used to align the flow and reduce the mean velocity variations

by using three sections of honeycomb in each plenum. The position of the three honeycomb sections is shown in Figure 4-3.

Downstream of the honeycomb, two sets of screens were placed to reduce the longitudinal component of turbulence as recommended by Scheiman and Brooks in Reference 3. The position of these sets of screens in the dual plenum is shown in Figure 4-3.

IV. SWIRL GENERATOR AND NOZZLES SECTION

The swirl generator and nozzles section is shown in Figure 4-5. This section is composed of the swirl generator, swirl generator housing, inner annulus between the four-inch OD center body and the six-inch ID cantilevered tube and outer annulus between the outside nozzle and inner nozzle.

The swirl generator was designed to give a swirling air stream with uniform axial velocity and free vortex angular velocity. This type of velocity profile was obtained by bringing the air stream radially into a one-inch slot, passing the air stream over adjustable stators which impart an angular velocity and then turn

the air stream into an annular passage which converts the radial velocity into axial velocity. An isometric cross-section of the swirl generator is shown in Figure 4-6. The outside diameter of the swirl generator is 18 inches and the air enters the radial slot around the perimeter through a bell mouth-type entrance whose length is 1/2 inch. The stator blades are positioned so that the leading edge of each blade falls on a circle whose diameter is 16 inches; the pivot shaft of each blade falls on a circle whose diameter is 14 inches and the trailing edge of each blade falls on a circle whose diameter is 12 inches. The stator blades were made using a symmetric NACA 0024 airfoil shape whose centerline was curved to give the desired exit angle. The geometry of the stator cascade is shown in Figure 4-7. Constant's rule, which is given below in empirical form, was used to determine the desired departing stagger angle for a turning angle of 45. Constant's rule, as given on Pages 179 and 180 of Reference 6, is:

$$\delta/\theta^{*} = 0.25/\sqrt{\sigma} \qquad (4\text{-}6)$$

where (refer to Figure 4-8)

$\Phi = \beta_1 - \beta_2$ = turning angle $\quad \gamma_1$ = stager angle

$\sigma = c/s$ = solidarity $\quad \theta^{*} = \gamma_1 - \gamma_2$

$\alpha = \beta_1 - \gamma_1$ = angle of attack $\quad \delta = \beta_2 - \gamma_2$

The following values apply for the design shown in Figure 4-7:

$\beta_1 = 0, \gamma_1 = 0, \gamma_2 = -60^\circ, c = 2.32", s = 2.20"$

Thus $\sigma = 1.055$ and, from Equation 6, $\beta_2 = -45.4^\circ$. This value of departure angle is very close to the desired value of -45° and was used for the swirl generator design. The stator cascade consists of twenty stator blades which can be adjusted in unison to give a value of β_1, from -30 to 30. Each blade has a symmetric NACA 0024 shape about its centerline whose radius is 2.75 inches (see Figure 4-7). For the geometry shown in Figure 4-7 and an entering radial velocity of 35 ft/sec at the blade leading edge, the radial and angular velocities at the blade trailing edge are 46.7 ft/sec and 47.3 ft/sec, respectively, for $\beta_2 = -45.4^\circ$. The air stream leaving the stator blades then enters a channel as shown in Figure 4-9.

Application of conservation of mass and angluar momentum to the flow in the channel shown in Figure 4-9 gives the following relationships for invisid incompressible axisymmetric flow in radial equilibrium:

$$v_3 = v_2 r_2 / r \qquad r_i \leq r \leq r_o \qquad (4\text{-}7)$$

$$w_3 = 2\, u_2 r_2 / (r_o^2 - r_i^2) \qquad (4\text{-}8)$$

The values of r_2 , r_o , and r_i for this design are 6 inches, 3 inches and 2 inches, respectively. Thus for u_2 = 46.7 ft/sec and v_2 = 47.3 ft/sec, Equations 4-7 and 4-8 give

w_3 = 112 ft/sec and

$$v_3 = 94.6 \times r_o/r \text{ ft/sec} \qquad 2 \leq r \leq 3 \qquad (4\text{-}9)$$

The angular velocity will vary in accordance with Equation 4-9 from 94.6 ft/sec at r = 3 inches to 141.9 ft/sec at r = 2 inches. The angle that the velocity vector makes with the centerline will vary from 40.2° at r = 3 inches to 51.7° at r = 2 inches for the above design data.

The shape of the channel which transforms the radial slot into an annulus was chosen to be circular in cross-section as shown in Figure 4-9. Although other transitions could have been used, the circular cross-section was easiest to manufacture and gave the required gradual transition.

For a design mass flow of 0.916 lb/sec, the velocities at each section of the swirl generator are as follows:

Entering the swirl generator housing		2.49 ft/sec
Swirl generator:		
at entrance to bell mouth		15.56 ft/sec
at leading edge of stator blade		35.00 ft/sec
at trailing edge of " "	u =	46.7 ft/sec
	v =	47.3 ft/sec
at exit for r=3 inches	w =	112.0 ft/sec
	v =	94.6 ft/sec
at exit for r=2 inches	w =	112.0 ft/sec
	v =	141.9 ft/sec

The annular channel has a mean length of 32.5 inches. Because of this length, an analysis of the development of the boundary layer was performed using the Waltz method for turbulent boundary layer for axisymmetric flow as described by Waltz in Reference 7. The mean velocity along a line half way between the channel walls, corrected for the displacement thickness, was used to determine the imposed pressure gradient and the properties of the turbulent boundary layer. The variation of this mean velocity with the axial distance for this annulus is plotted in Figure 4-10. The boundary layer properties at the exit from this channel for the above

design values are as follows for both walls of the annular channel:

$$\delta_1 = 0.098 \text{ inches} \qquad H_{12} = 1.350$$

$$\delta_2 = 0.072 \text{ inches} \qquad H_{32} = 1.763$$

The outer portion of the swirl generator housing, shown in Figure 4-5, is an extension of the outer plenum. This extension of the outer plenum is connected to the section containing the inside nozzle and outside nozzle. The two concentric nozzles were designed using the following empirical relationship due to Vitoshinski in Reference 8.

$$r = r_o \left[1 - \left(1 - \frac{r_o^2}{r_i^2} \right) \frac{\left(1 - z^2/L^2\right)^2}{\left(1 + z^2/L^2\right)^3} \right]^{1/2} \qquad (4\text{-}10)$$

where r_o = outlet radius ($z = L$)

r_i = inlet radius ($z = 0$)

L = nozzle length

For design, a nozzle length of 36 inches was used in Equation 4-10 and the actual nozzle length was limited to the first 29.75 inches. The following values for r and r. were used for the nozzles:

Inside nozzle: r_i = 15 inches & r_o = 3.003 inches

Outside nozzle: r_i = 20 inches & r_o = 3.95 inches

The nozzle profiles generated by Equation 4-10 agree very

well, over the majority of the nozzle length, with the profiles generated using the method of Tsien contained in Reference 9 and the profiles generated using the method of Szczeniowski contained in Reference 10. As shown in Figure 4-5, the inner nozzle wall and the outer wall of the inner annulus are machined from the same piece of material for over half the nozzle's length. This common wall ends at the entrance to the test section and its thickness at this point is 0.033 inches.

Static pressure taps were placed on the inside of the outer wall in the inner annulus to get a measure of the adjustment of the swirling flow as it approaches the exit. The placement of these static pressure taps and a detail of a typical pressure tap are shown in Figure 4-11. Stainless steel tubing with o.021-inch ID and 0.010-inch wall thickness was used and placed in grooves machined in the outer wall of the six-inch ID cantilever tube. The grooves in the outside wall were filled before final machining of the inner nozzle surface. Holes of 0.021-inch diameter were drilled through the inside wall of the six-inch ID cantilever tube at all positions listed below, except the end positions:

Pressure Tap Number	Z	Angular Position
29 - 35 - 41	end	90, -30, -150
30 - 36 - 42	-0.10"	70, -50, -170
31 - 37 - 43	-0.25"	50, -70, 170
32 - 38 - 44	-0.50"	30, -90, 150
33 - 39 - 45	-1.00"	10, -110, 110
34 - 40 - 46	-2.00"	-10, -130, 110

An analysis of the development of the turbulent boundary layers on each nozzle was performed using the Waltz method for axisymmetric flow as described by Waltz in Reference 7. For an entering velocity of 4.48 ft/sec, the calculated boundary layer properties on both nozzle walls at exit are as follows: $\delta_1 = 0.045$ inches $H_{12} = 1.39$

$\delta_2 = 0.032$ inches $H_{32} = 1.74$

The variation of the mean velocity with the axial distance is plotted in Figure 4-12.

V. TEST SECTION

The test section was designed so that it could be set up in one of three different test configurations. The three test configurations are shown in Figure 4-13 and listed below.

Configuration	Description
One	Flow with swirl from inner annulus with outside flat wall and with or without a centerbody
Two	Flow from two annull (axial flow from outer and swirl flow from inner) with outside flat wall and with or without a centerbody
Three	Flow from two annull (axial flow from outer and swirl flow from inner) with constant radius outer wall and centerbody

The test section has a length of 48 inches. Measurements of the total and static pressures and flow direction for test configurations one and two (without outside wall) are possible using Probe #1 and its traversing mechanism, as shown in Figure 4-14, which is mounted on rails parallel to the centerline of the test section. The probe's traversing mechanism allows for rotating the probe face to align the probe with the flow direction and radial positioning of the probe. The probe's radial position is measured by the linear variable differential transformer (LVDT). The probe's angle is measured by a

potentiometer on the traversing mechanism and the axial position is measured by a potentiometer on the axial traversing bed.

An outer flat wall is provided by a 36 inch outside diameter piece of pressboard that mounts to the end of the outer nozzle for test configurations one and two. The outer flat wall is extended inward to the 6- inch OD annulus for test configuration one by insertation of a large disc into the annulus between the nozzle walls.

The 4-inch OD centerbody of the swirl generator can be ended at the beginning of the test section by insertation of an end cap or extended through the test section by attaching the 4-inch centerbody sections shown in Figure 4-15. The centerbody, for use in the test section, was made in three pieces: one section of two-foot length with twenty wall pressure taps; one section of two-foot length with eight wall pressure taps, and an end support. All three pieces of this centerbody are interchangeable. As shown in Figure 4-15, the wall static pressure taps are located at the following axial positions:

Tap #	1	2	3	4	5	6	7	8
z (in)	0.125	0.250	0.375	0.50	0.75	1.00	1.25	2.25

Tap #	9	10	11	12	13	14	15	16
z (in)	3.25	4.25	5.25	6.25	8.25	10.25	12.25	14.25

Tap #	17	18	19	20	21	22	23
z (in)	16.25	18.25	20.25	22.25	24.25	26.25	28.25

Tap #	24	25	26	27	28
z (in)	30.25	34.25	38.25	42.25	46.25

The static pressure tap holes in the wall of the 4-inch OD centerbody have a diameter of 0.021 inches and are connected to stainless tubing of the same inside diameter.

The eight-inch ID outer wall for test configuration three is made from plexiglass tubing of 1/2-inch wall thickness that was cut into five interchangeable sections. Each section has wall static pressure taps of 0.021-inch diameter which are located every two inches along the length. The length of each section of outer wall and the pressure tap locations are shown in Figure 4-16 and listed below.

Section	A											
Length	24"											
Tap #	47	48	49	50	51	52	53	54	55	56	57	58
Location	1"	3"	5"	7"	9"	11"	13"	15"	17"	19"	21"	23"

Section	B						C			D		E
Length	12"						6"			4"		2"
Tap #	59	60	61	62	63	64	65	66	67	68	69	70
Location	1"	3"	5"	7"	9"	11"	1"	3"	5"	1"	3"	1"

Measurement of the total and static pressures and flow direction for test configuration three (with outside wall) were performed using Probe #2 and its traversing mechanism with section of outer wall, as shown in Figure 4-17. The section that contains Probe #2 and its traversing mechanism has a length of 2.375 inches and the head of the probe is located 0.250 inches from the entrance of the section. The probe head can be traversed radially between outside and inside walls on the side of the centerbody opposite the traversing mechanism. Measurement at different axial locations is accomplished by interchanging the sections of the outer wall and the probe section of the outer wall. The progressive section lengths allow location of the probe section at 1/4 inch into the test section and in increments of two inches

through the test section. The probe section of the outer wall has two static pressure taps 1/4" from the leading edge as shown in Figure 4-17.

The outside wall of the test section is supported at its entrance by connection with the end of the outside nozzle, along its length by supporting rails and at its exit by connection to the outlet section of the outside wall that is itself supported by a spider connected to the centerbody end support. The outlet section of the outside wall has a slight nozzle at its exit with an exit to entrance area ratio of Ø.84 to provide slight pressuration of the test section above the pressure in the surrounding room.

VI. MEASUREMENT EQUIPMENT

The measurement equipment is divided into two systems. One system consists of the measurement equipment associated with the high pressure dual air supply system. The other system consists of the measurement equipment associated with the concentric dual plenum section, the swirl generator and nozzles section and the test section.

A. High Pressure Dual Air Supply System

The measurement equipment associated with the high pressure dual air supply system is shown in Figure 4-18. Control valves V2 and V3, shown in Figure 4:1, have been replaced by orifice plates sized to supply specific mass flow rates for choked flow conditions. The empirical relationship for choked flow through an orifice plate is given on Page 21 of Reference 6. This relationship solved for the orifice area (A^*) in terms of the mass flow rate ($\dot{m}$) and upstream gas properties is given below for isentropic flow.

$$A^* = \dot{m}\sqrt{R\ T_T}\ /\left(\Gamma\ P_T\right) \tag{4-11}$$

where P_T and T_T are the upstream stagnation pressure and temperature, respectively, R is the gas constant and Γ is a symbol for the equation written below in terms of γ, the ratio of specific heats.

$$\Gamma = \sqrt{\gamma}\left(\frac{2}{\gamma+1}\right)^{\frac{\gamma+1}{2(\gamma-1)}}$$

Choked flow orifice plates were sized using Equation 4-11 for mass flow rates of 0.493 lb/sec, 1.052 lb/sec, 1.928

lb/sec and 3.15 lb/sec with an upstream stagnation pressure of 600 psia and stagnation temperature of 500 R. The actual mass flow rate was calculated using the relationship:

$$\dot{m} = \dot{m}_o (P_T / P_{T_o}) \ (T_{T_o} / T_T)^{1/2} \qquad (4\text{-}12)$$

where the zero subscripted quantities are design values, listed above, and the non-subscripted quantities are the actual values measured during a test.

Flow meter orifice plates were sized using the procedures listed in Reference 11 for a pressure drop of 100 inches of water and upstream stagnation conditions of 600 psia and 500 R. Identical orifice plates with 1.000-inch diameter bore were installed in both supply lines. These orifice plates have a pressure drop of 100 inches of water for a flow rate of 1.09 lb/sec of dry air at the design conditions. The actual flow rate in each supply line is calculated using the relationship:

$$\dot{m}\ (\text{lb/sec}) = 1.0907 \times \left[\frac{\Delta P\ (\text{in } H_2O)}{100\ \text{in } H_2O} \quad \frac{P(\text{psia})}{600\ \text{psia}} \quad \frac{500^\circ R}{T(^\circ R)} \right] \qquad (4\text{-}13)$$

where the pressure drop across each orifice plate (ΔP) is

measured and recorded, the pressure (P) in both supply lines is measured and recorded and the temperature (T) of the air is obtained from the measurement of the stagnation temperature and pressure in each plenum, thermodynamic properties of dry air and the assumption of adiabatic flow from each orifice plate to the plenum section. The pressure drop across each orifice plate is measured and recorded by two separate systems. Each orifice plate is connected to a pneumatic transmitter that transmits a pressure, proportional to the measured pressure drop, to the strip chart recorder. Each orifice plate is also connected to a strain gauge-type differential pressure transducer.

The two types of orifice plates, choked and flow meter, in each supply line allows for comparison. The choked orifice plate fixes the mass flow rate for a constant supply line pressure. However, due to the characteristics of the pressure regulating valve, the supply line pressure does vary slightly during a test run and the flow meter orifice plates measure the corresponding variation in mass flow rate.

B. Plenum, Swirl Generator/Nozzles and Test Section

The measurement system associated with the concentric dual plenum section, the swirl generator and nozzles section and the test section is shown in Figure 4-19 for tests without the 8-inch outside wall and in Figure 4-20 for tests with the 8-inch outside wall. This system will be discussed by considering each of the following subsystems:

a. Scanivalve

b. Sensors and Signal Conditioners

c. Data Measurement, Recording & Monitoring

d. Controller

1. Scanivalve

The scanivalve, shown in Figure 4-21, is a Model SGM having three valve assemblies with 48 pressure tabulations in each valve assembly, solenoid drive, an odd-even tube marker position transmitter and pressure transducers. The Scanivalve, with its pressure transducers, was used to measure all static pressures. The stepping of the Scanivalve and determination of its position were performed by the Controller, which will be discussed later in this section.

2. Sensors and Signal Conditioners

A Model PM131TC+2.5 Statham pressure transducer was used in the Scanivalve for all tests without the 8-inch outside wall. During these tests, this pressure transducer was used to measure wall static pressures and the five pressures of Probe #1. The pressure difference between ports #1 and #3 of Probe #1 was measured using a Model PM283TC+0.15 Statham pressure transducer which gave the capability of approximately nulling the flow angle (α_r) of the air stream relative to this probe.

Seven Model PDCR22+1 ScanCo differential pressure transducers were added to the measurement system for tests conducted with the 8-inch outside wall. In addition, two Model PM80TC+100 Statham pressure transducers were installed for measuring the pressure drop across the two flow orifice plates, one Model PG146TC-5M Statham pressure transducer was installed to measure the pressure of the air upstream of the pressure regulating valve and one Model PG146TC-800 Statham pressure transducer was installed to measure the pressure of the air downstream of this same valve. Two of the seven Model PDCR22+1 ScanCo differential pressure transducers were added to the Scanivalve so that all wall

static pressures were scanned on each scan. Five of the seven Model PDCR22+1 ScanCo differential pressure transducers were mounted in a special block for simultaneous measurement of all pressure ports on the five-hole probe as shown in Figure 4-22. The Model PM283TC+0.15 Statham pressure tranducer was used to measure the difference between the pressures at port #1 and port #3 of the five-hole probe which gave the capability of approximately nulling the flow angle (α_r) of the air stream relative to the probe.

The air temperatures inside both the inner and outer plenums were measured by Veco thermistors manufactured by Victory Engineering Corp. for tests without the 8-inch outside wall and were measured by iron/constantan thermocouples for tests with the 8-inch outside wall. The angle of the probe relative to the centerline of the experimental apparatus (α_p) was measured by a 10K Ohm precision potentiometer that was connected by gearing to the shaft of the probe. The axial position of the probe for tests without the 8-inch outside wall was measured by a Model WR8-1132/158 position transducer manufactured by Lockheed Electronics Company. The radial position of the probe was measured by a Model H-3000-S3R LVDT manufactured by Columbia Research.

All the sensors, except the LVDT, were connected using the wiring configuration shown in Figure 4-23 to separate Model 3511C Strain Gage Power Supply and Signal Conditioner units manufactured by Systems Research Corporation. These units are of the "plug-in" type construction with designer cards for bridge completion and can be mounted in a rack. Six of these units were used for tests without the 8-inch outside wall and 14 of these units were used for tests with the 8-inch outside wall. The sensors that were not a full bridge with a full active circuit were wired as shown in Figure 4-23 and their bridge circuit completed on the designer card. The type of bridge and active circuit for the four types of sensors are listed below:

Sensor	Bridge Type	Active Circuit
Pressure Transducer	Full	Full
Temperature Thermistor	Half	Half
Probe Angle	Half	Full
Axial Position Transducer	Full	Full

The LVDT was connected to a Model 300B Daytronic Differential Transformer Indicator which provided the necessary electronics to give an output signal that was proportional to the movement of the core in the LVDT. Calibration of the LVDT and the Probe Angle Potentiometer yielded nonlinear characteristics near the ends of each's range. Both calibrations fit the characteristic equation for the half bridge type with full active circuit given in Reference 12 and rewritten below in the form used.

$$V = V_o + A\ (x-x_o)/(1+B(x-x_o)^2) \qquad (4\text{-}14)$$

where V_o is the output voltage, x is the variable being measured, A and B are calibration coefficients and the subscript " o " represents the center of the range of operation.

Equation 4-14 was used to represent the calibration of all sensors that had linear characteristics over their operating range by setting B equal to zero. The results of sensor/signal conditioner calibration are listed below using Equation 4-14.

Measured Variable (x)	Calibration Coefficients A	B
P_x (psig) Statham	1.626mV/psi	0
P_x (psig) ScanCo	19.60mV/psi	0
P_3-P_1 (psi)	140.0mV/psi	0
Tank Pressure (psig)	0.00715mV/psi	0
Line Pressure (psig)	0.0473mV/psi	0
Flow Meter DP (in H_2O)	0.00476mV/psi	0
T_i (°C)	23.95 mV/°C	0
T_o (°C)	27.25 mV/°C	0
α_p (degrees) Probe #1	53.163mV/deg	-3.3227×10^{-5}
α_p (degrees) Probe #2	9.741mV/deg	0
z (inches)	-1.3245mV/inch	0
r (inches)	283.75mV/inch	0

3. Data Measurement, Recording and Monitoring

The output of all signal conditioners and the Scanivalve position voltage from the Controller were scanned and measured by a Model 2200B Datalogger manufactured by the John Fluke Co. This instrument contains an A-D converter that measures DC voltages on four ranges: 40mV, 400 mV, 4V and 40V. Resolution on the 40mV range is 1 μV. A measurement speed of 15 readings per second was selected

for all test runs. The Datalogger was equipped with the RS-232-C interface option and outputted the measured data at a baud rate of 4800 for recording on an external tape recorder. The Datalogger was set up tp scan and measure all inputs on receipt of a scan signal from the Controller.

A Columbia Data Corporation Model 300C Data Cartridge Tape Recorder was connected via its MODEM/CPU cable to the Datalogger for receipt and recording of data at a baud rate of 4800. The terminal port of this tape recorder was connected to a Tele-video Model 920C CRT terminal for monitoring and review of data during test runs.

A Preston Model 723 Digital Volt Meter (DVM) was connected to specific channels for monitoring via a selector switch. This DVM was used to monitor the following channels:

a. Differential pressure between ports #1 and #3 of the five-hole probe during nulling of these two pressures by manually rotating the probe.

b. Radial position of the five-hole probe as indicated by the output of the LVDT system during manual positioning of the probe.

c. Axial position of probe transversing mechanism used with Probe #1 during manual positioning of the probe's axial position.

d. Supply line pressure during the manual setting of the pilot pressure to the pressure regulating valve shown in Figure 4-18.

4. Controller

The Controller was designed using off-the-shelf integrated circuits (IC's) and References 13 through 16 to perform the following functions:

a. Step the Scanivalve from position #1 through #48 at a preset rate after receipt of a start command.

b. Initiate scan of Datalogger for each step of Scanivalve after a preset time delay.

c. Count steps and output both an analog voltage signal proportional to the Scanivalve position and a digital display of the step count.

The Controller was constructed in two physical parts. The first part houses all the integrated circuits and requires an external 5V DC power supply. The second part houses the switching circuit for the high current 20V DC power that is sent to the stepping solenoid of the

Scanivalve. The IC's used in the first part of the Controller are:

IC#	Device	Description
1,2,4,5,9&10	74LS00	Quad NAND Gate
3,6&7	555	Timer
8	74LS161	4-Bit Up Counter
11&12	74LS90	BCD (Decade) Counter
13&14	74LS75	4-Bit Latch
15&16	74LS47	BCD to 7-segment Decoder/Driver
17&18	-	7-segment LED Single-Digit Readout
19 thru 25	74LS90	BCD (Decade) Counter

IC's #11 through #18 were mounted on two Radio Shack Catalog Number 277-103 Single Digit Counter Project Boards to give the two digit counter. IC's #19 through #25 were mounted on a portion of a Radio Shack Catalog Number 277-115 Time Base Generator Project Boards as shown by the top circuit board in Figure 4-24. IC's #1 through #10 were mounted onto a plug-in experimentor card as shown by the bottom circuit board in Figure 4-24.

A circuit diagram of the first part of the Controller is shown in Figure 4-25. Quad NAND gates (74LS00) were used to provide the basic digital logic switching. The pin

connections for the Quad NAND gate, NAND gate symbol and truth table are shown in Figure 4-26. Figure 4-25 shows the 23 NAND gates used in the circuit. The particular NAND gate used on a 74LS00 is designated by the letter (A, B, C or D) following the IC number (1,2,4,5,9 or 10) contained within the NAND symbol in Figure 4-25.

Integrated circuits #3, #6 and #7 are 555 timers; IC #3 is set up to generate an adjustable clock pulse. The user can select either this internal clock pulse or one from an external source with a selector switch. The selected clock pulse is then inputted into a series of seven decade counters (IC #19 through #25) where the clock period can be multiplied by 10, where n is selectable from zero to seven. This multiplied clock output is then inputted into the logic circuit at connector "L" and also connected to a light-emitting diode (LED) for the operator to view. The waveform of this multiplied clock pulse is shown at the top of Figure 4-27.

The position transmitter of the Scanivalve is connected to pins D, E and F in Figure 4-25 and during operation gives the waveforms shown in the upper portion of Figure 4-27. The printed circuit pattern of the position transmitter module is shown in Figure 4-21 and was used

with a 5V DC common. Four NAND gates (1A, 1B, 1C & 1D) are used to generate an output pulse which goes low when the Scanivalve is between locations (see IC 1D out waveform in Figure 4-27). This output is used to trigger IC #6 which is connected as a single shot with an adjustable length of output pulse. The output waveform of IC #6 is shown in Figure 4-27. IC #6 is adjusted so that its output pulse goes low during the time that the multiplied clock pulse input (pin L) is also low. The rise in the output of IC #6 is used to turn off the power applied to the solenoid of the Scanivalve. Thus the signal (IC 9C out) to the solenoid is turned off just as soon as it is known that the Scanivalve is at the new location and thus reduces both the power consumption and the chance of skipping a location. The output of NAND gate 9B is used to initiate a scan by the Datalogger. The scan signal starts at the beginning of the second half of the multiplied clock pulse (low signal input to pin L) and ends when the output of the single shot IC #6 drops to low. Thus the length of the output pulse from IC #6 determines the length of the scan signal and care must be taken so that this signal is long enough to initiate the scan but not too long so as to initiate a second scan.

IC #7 is connected as a single shot that is triggered by

either the output of NAND gate 1D or a manual count switch depending on the position of the manual-auto selector switch. This single shot gives a clear count pulse to the two-digit counter (IC's #11 through #18) and the voltage staircase (IC #8). The output of the voltage staircase versus the Scanivalve position is shown in Figure 4-28.

The zero (reset or stop) signal from the Scanivalve position transmitter is connected to pin E in Figure 4-25. When pin E is high (zero signal), then the signal at pin K remains high and the signal at pin R remains low. A cycle of the stepping of the Scanivalve is initiated by bringing the reset signal at pin J to the low state and the waveforms as shown in Figure 4-27 will then occur.

The circuit of the second portion of the Controller is shown in Figure 4-29. The output signal from the first portion of the Controller is used to turn on the RS-2039 transistor which then energizes the relay. The Scanivalve can be stepped by either pressing the step button when the selector switch is in the manual position or by energizing the relay when the selector switch is in the auto position. The Scanivalve can be reset or homed to

the zero or 48 position by pressing the reset button and holding until the unit has stopped.

REFERENCES

1. Cebeci, T. and Smith, A. M. O., Analysis of Turbulent Boundary Layers, Academic Press, 1974.

2. Schubauer, G. B., Spangenberg, W. G., and Klebanoff, P. S., "Aerodynamic Characteristics of Damping Screens," NACA TN-20001, Jan. 1950.

3. Scheiman, J. and Brooks, J. D., "A Comparison of Experimental and Theoretical Turbulence Reduction from Screens, Honeycomb and Honeycomb-Screen Combinations," AIAA-80-0433.

4. Dryden, H. L. and Abbott, I. H., "The Design of Low-Turbulence Wind Tunnels," NACA TR-940, 1949.

5. Goldstein, S., Modern Developments in Fluid Dynamics, Volume 1, Dover, 1965.

6. Oates, G. C., Notes on Rockets and Airbreathing Engines, USAF Academy, 1975.

7. Waltz, A., Boundary Layers of Flow and Temperature, MIT Press, 1969, pp. 262-270.

8. Gorlin, Wind Tunnels and Their Instrumentation, (Translated from Russian), NASA TTF-346, US Dept of Commerce, Springfield, VA.

9. Tsien, Hsue-Shen, "On the Design of the Contraction Cone for a Wind Tunnel, JAS, Feb. 1943, pp 68-70.

10. Szczeniowski, B., "Contraction Cone for a Wind Tunnel," JAS, Feb. 1943, pp. 311 & 312.

11. Cusick, C. F., Flow Meter Engineering Handbook, Minneapolis-Honeywell Regulator Company, Third Edition, 1961.

12. Perino, P. r., "Wheatstone Bridge Transducer Equations," Statham Instrument Notes No. 38, Feb. 1966.

13. Mims, F. M., III, Engineer's Notebook, Integrated Circuit Applications, Radio Shack, First Edition, 1979.

14. Grinich, V. H. and Jackson, H. G., Introduction to Integrated Circuits, McGraw-Hill, New York, NY, 1975.

15. Lenk, J. D. Handbook of Integrated Circuits: for Engineers & Technicians, Reston Publishing Co, Reston, VA, 1978.

16. CMOS Databook, National Semiconductor Corp, Santa Clara, CA, 1977.

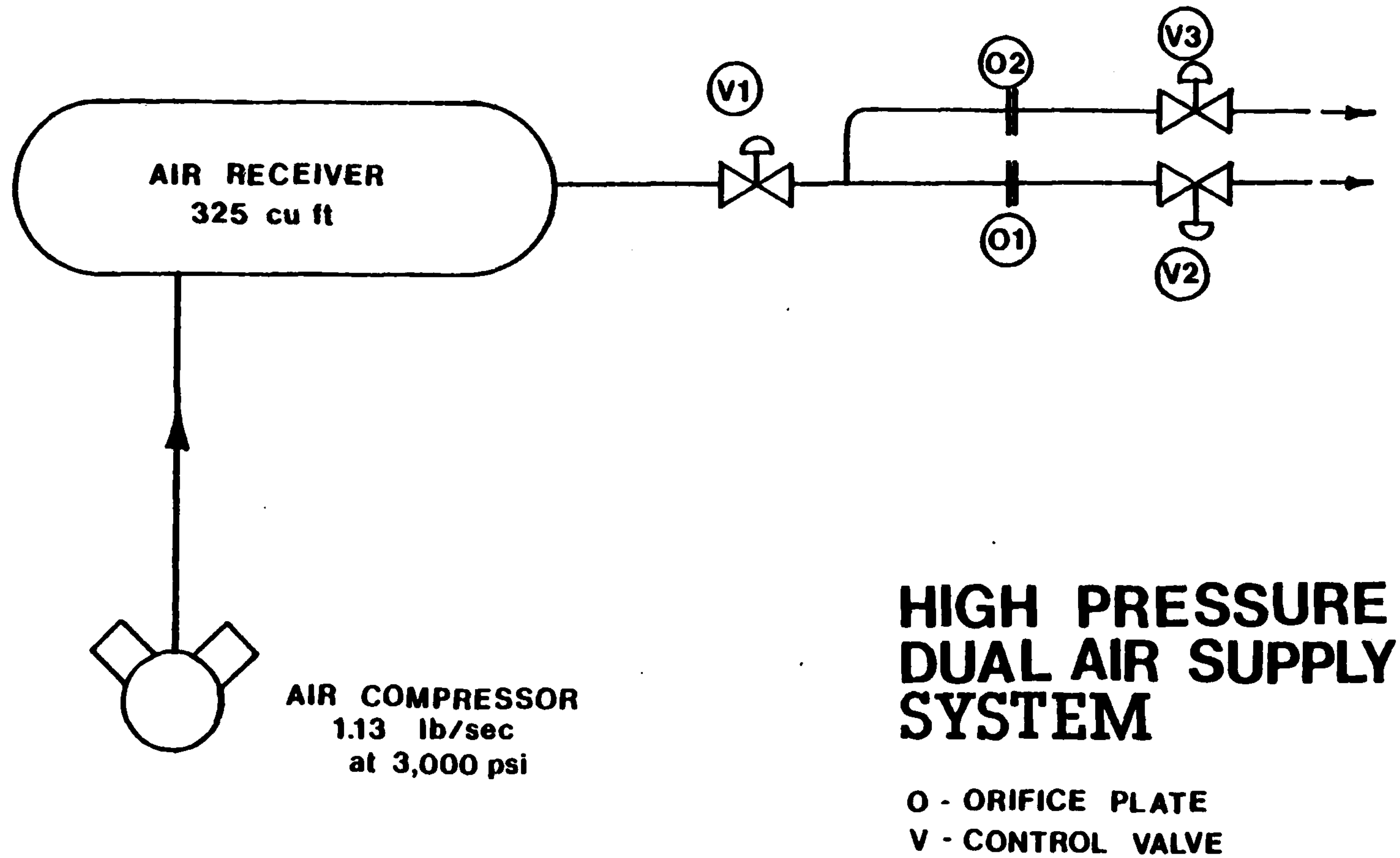

Figure 4-1 Original High Pressure Dual Air Supply System

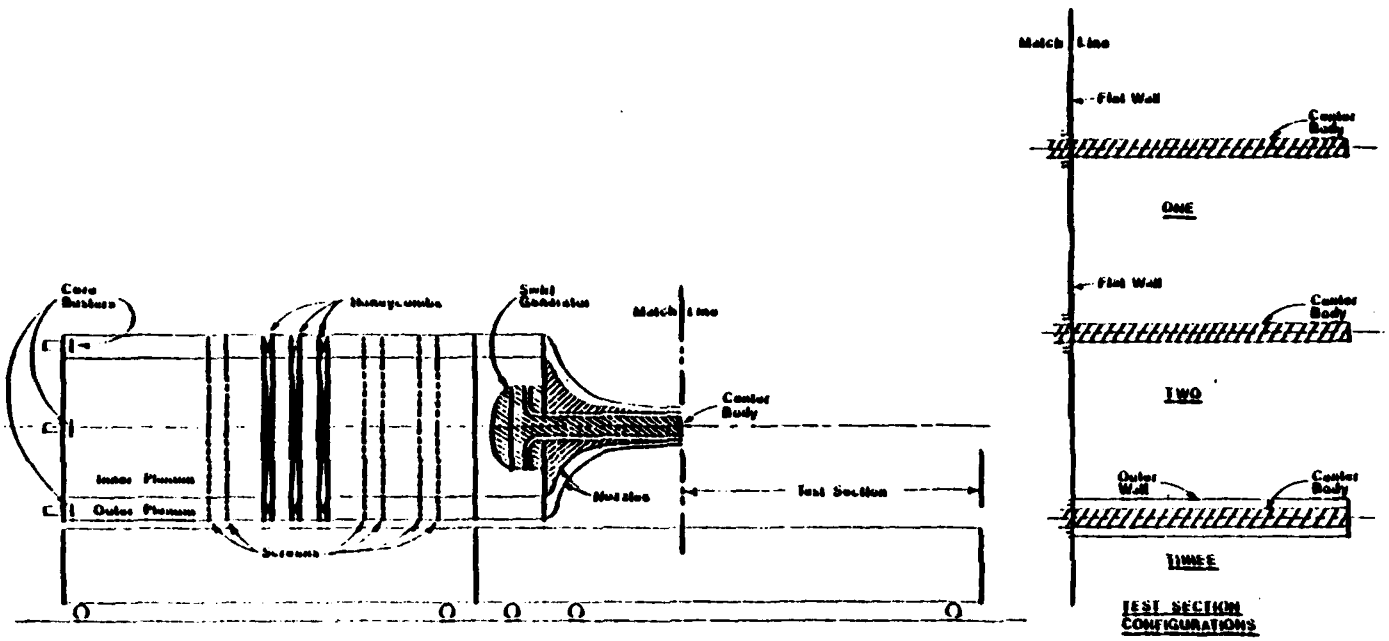

TEST APPARATUS

Figure 4-2 Test Apparatus

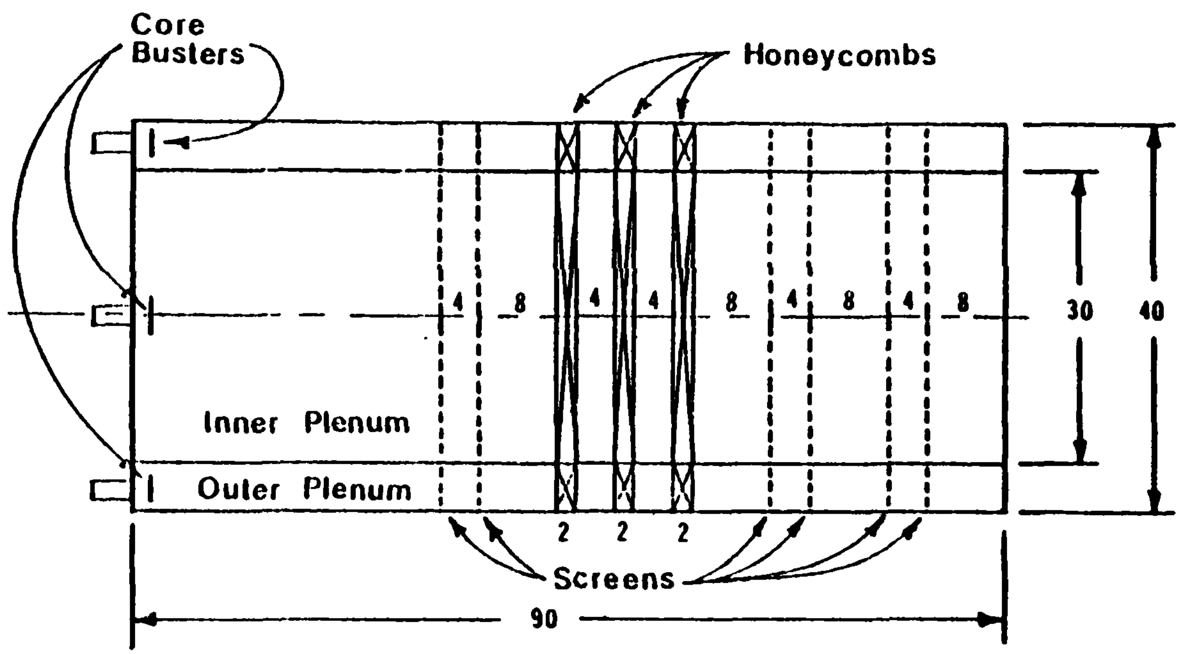

Figure 4-3 Dual Concentric Plenum System

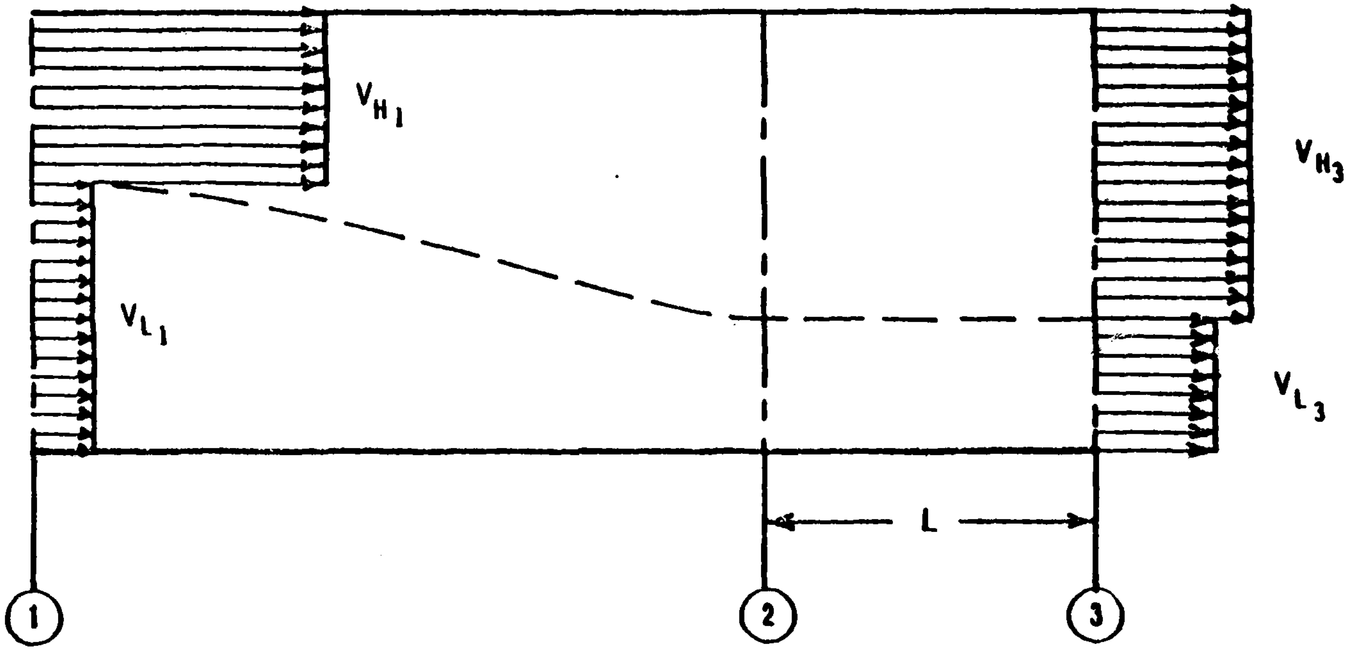

Figure 4-4 Model for Flow Through Honeycomb

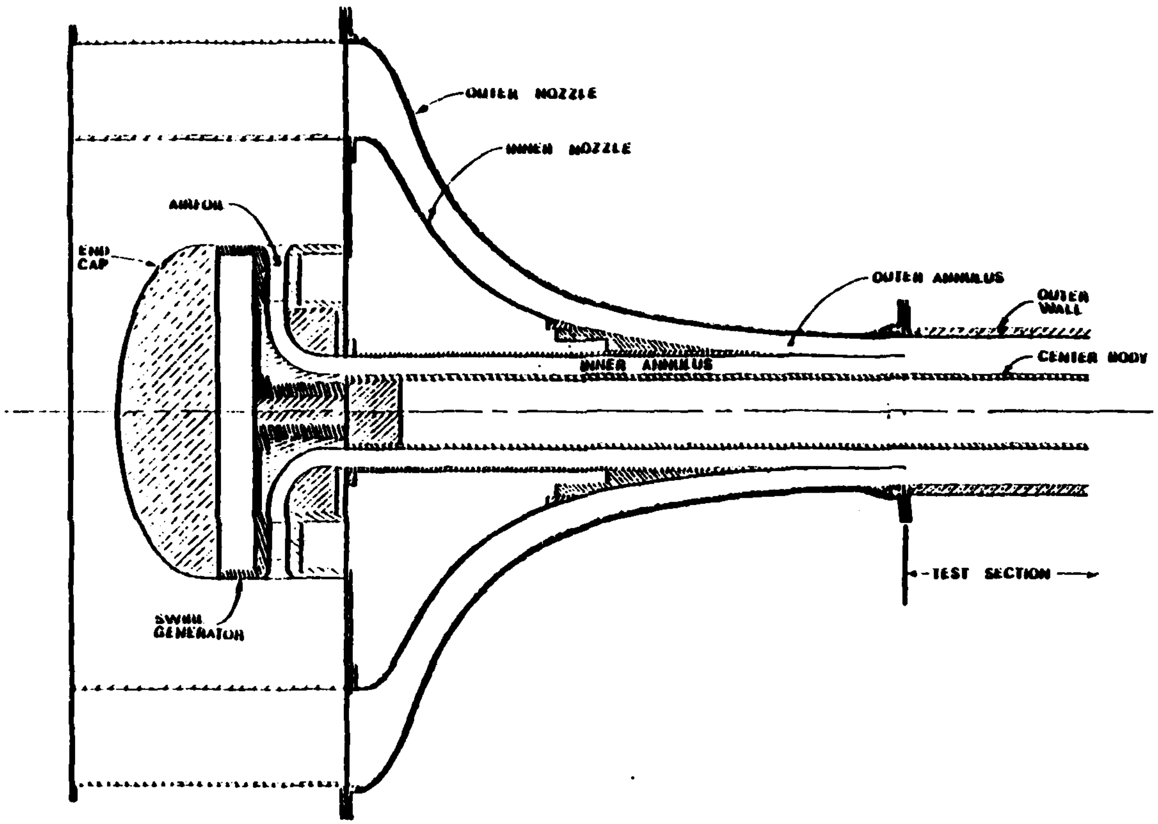

Figure 4-5 Swirl Generator and Nozzles

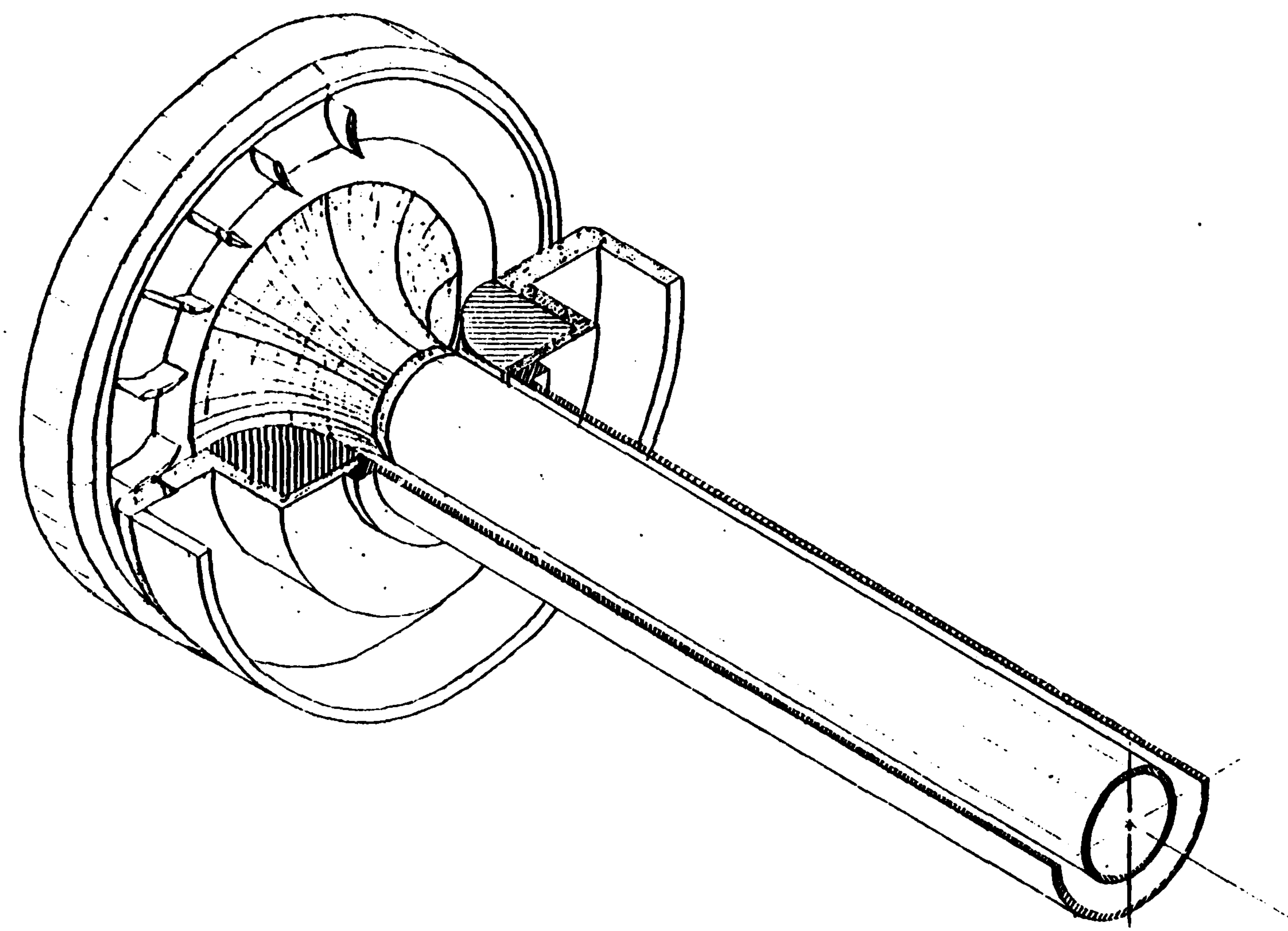

Figure 4-6   Isometric Section of Swirl Generator

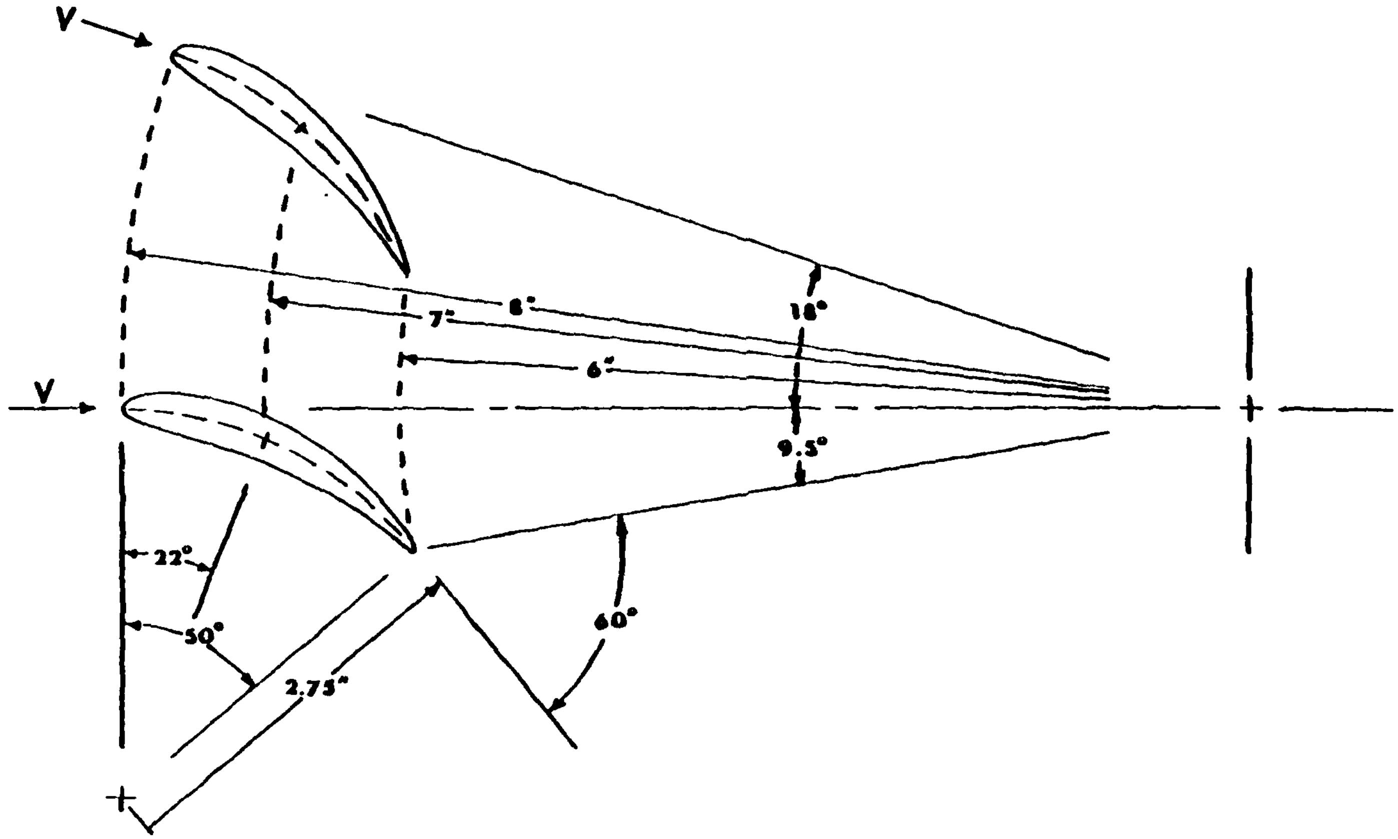

Figure 4-7 Swirl Generator Stator Cascade Geometry

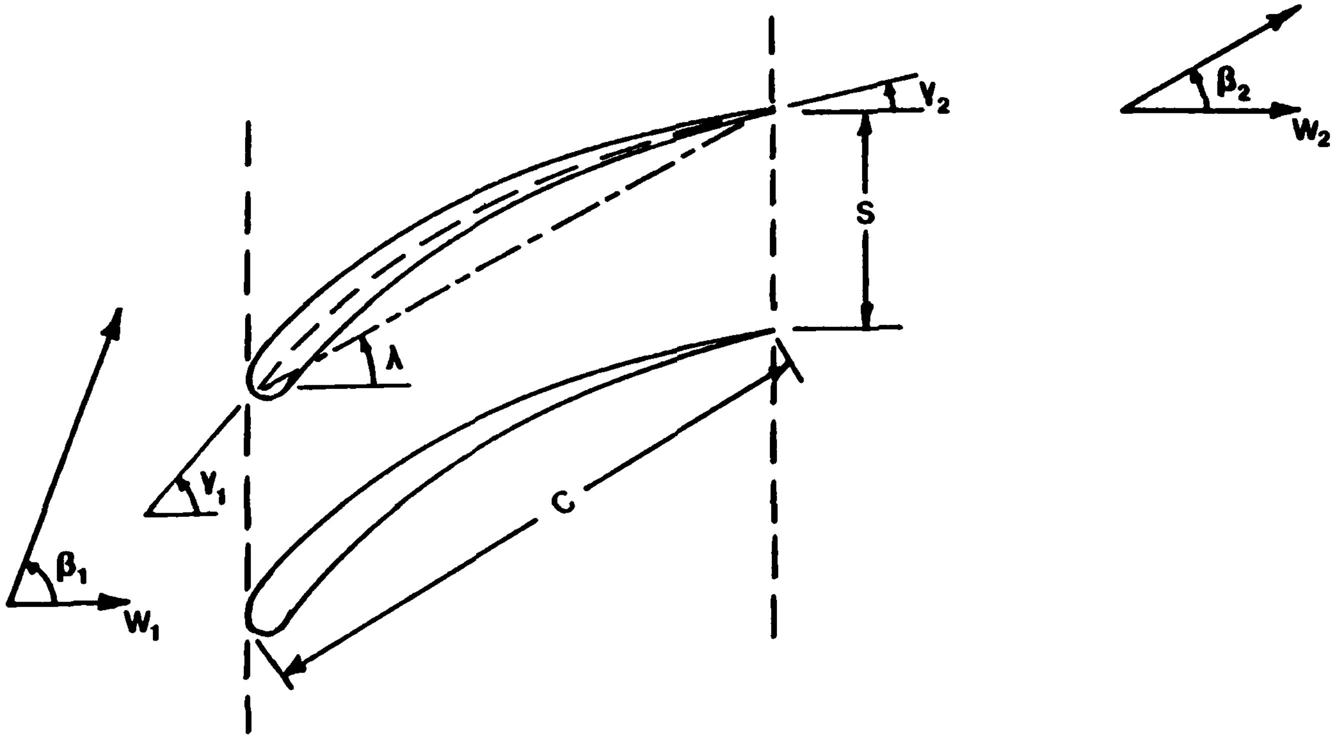

Figure 4-8 Stator Cascade Geometry

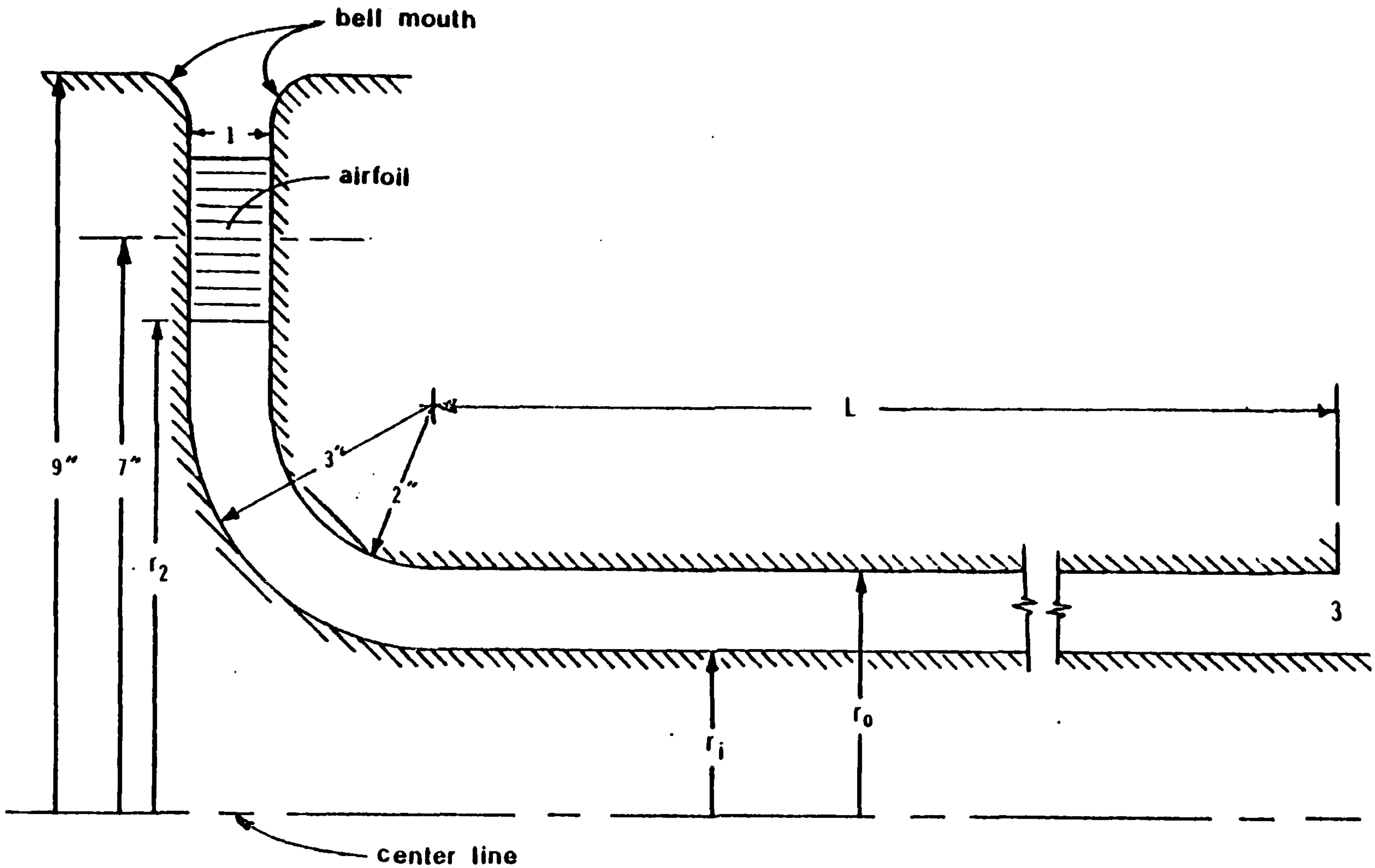

Figure 4-9 Flow Annulus for Swirling Stream

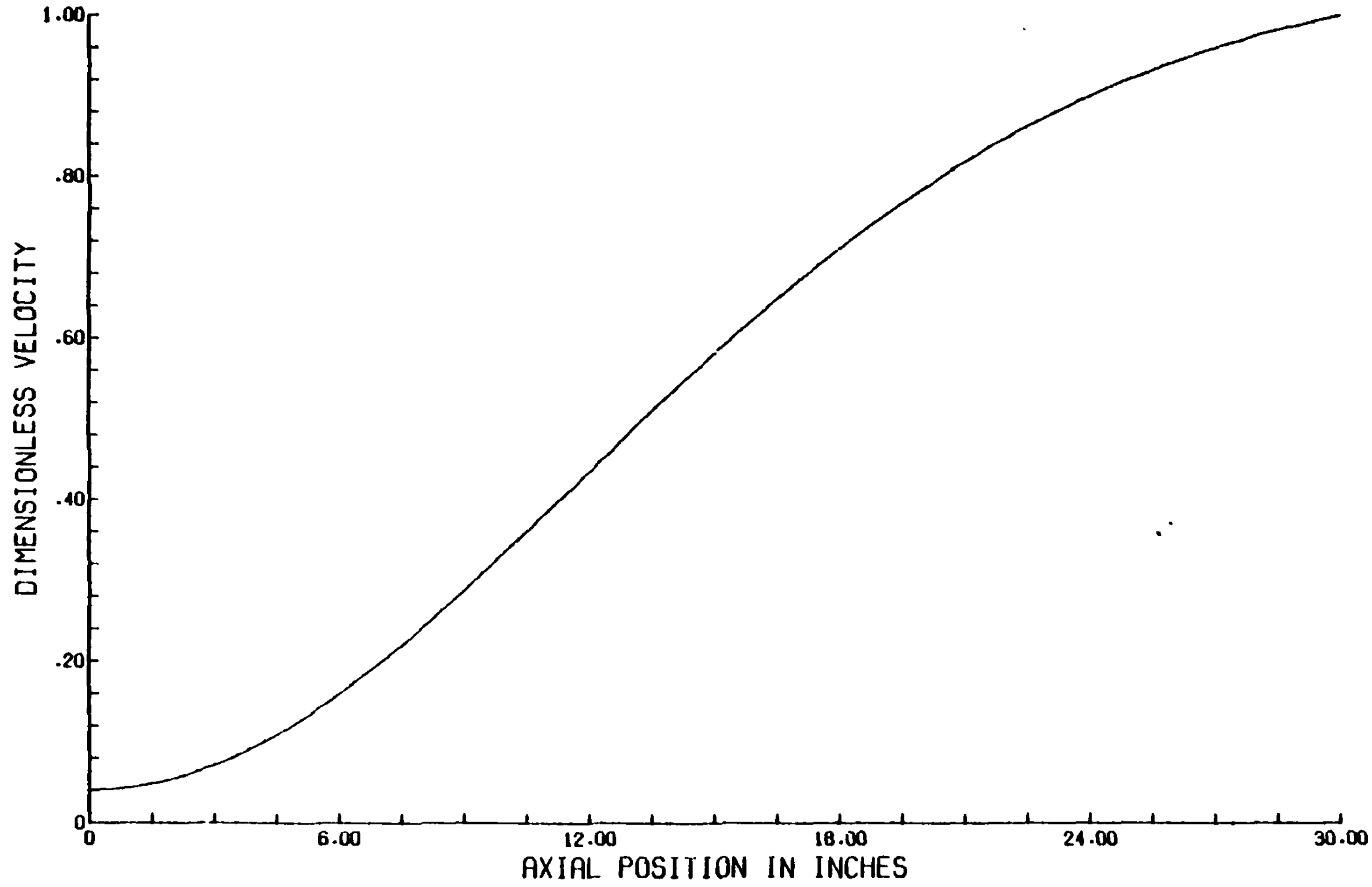

Figure 4-10 Axial Velocity Variation Through Nozzles
- Outer Annulus

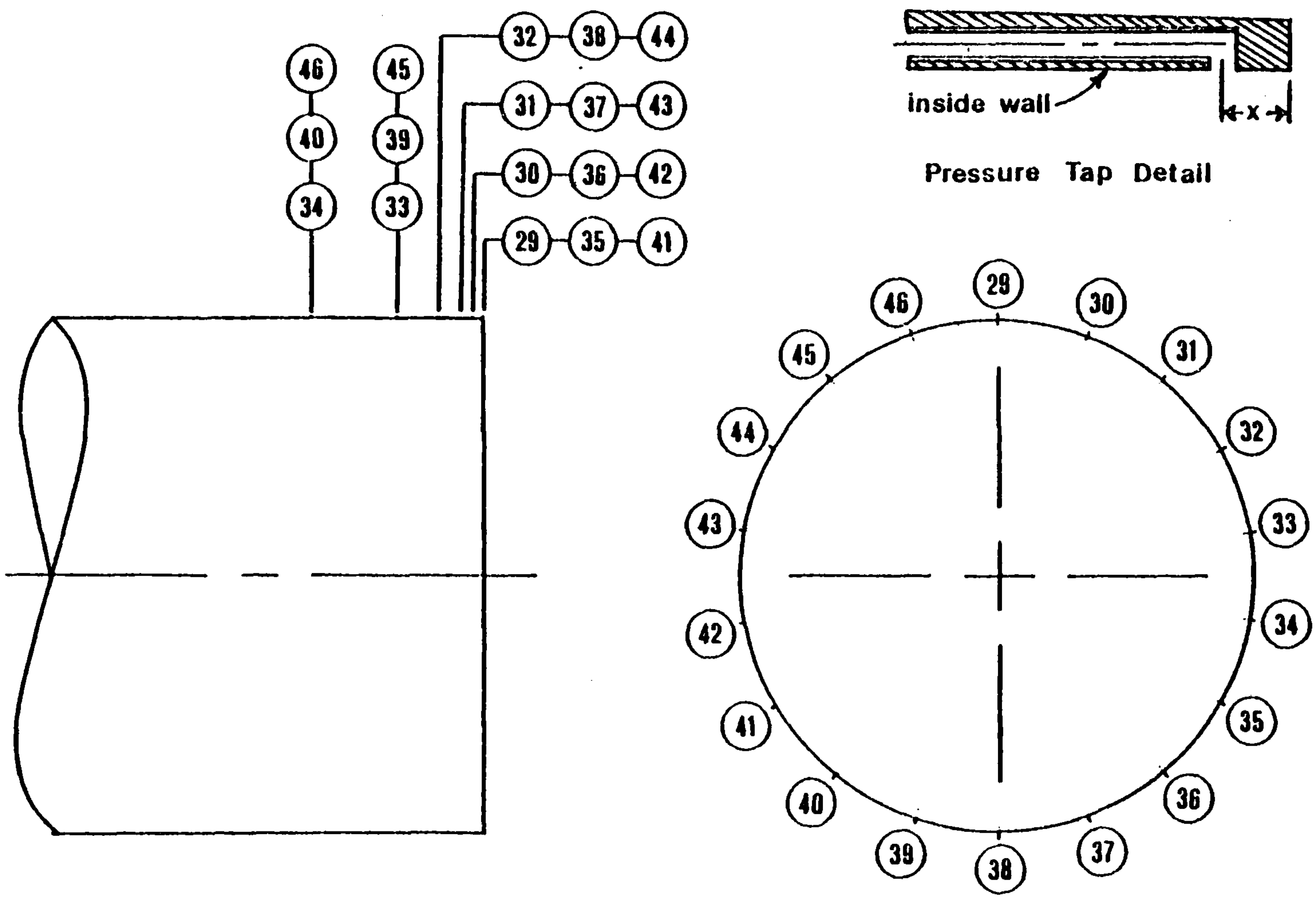

Figure 4-11 Static Pressure Tap Locations on Outside Wall of Inner Annulus

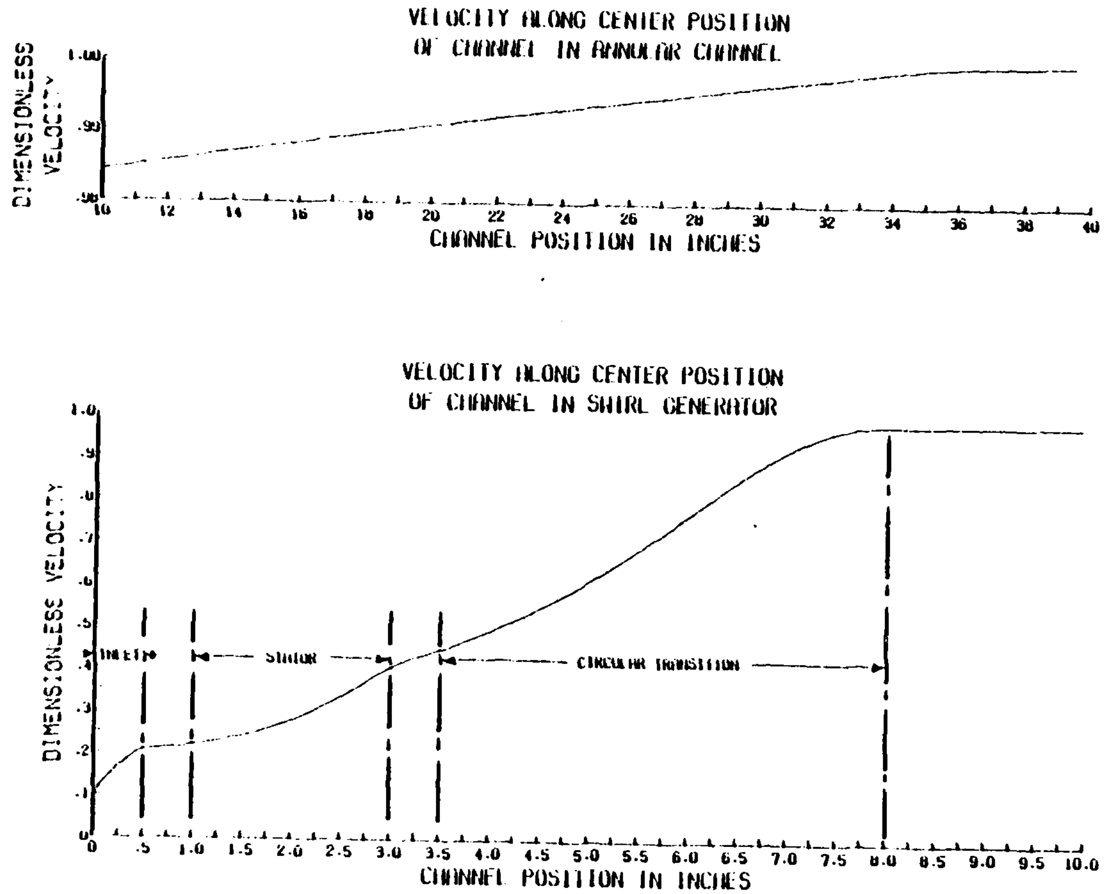

Figure 4-12 Velocity Variation of Swirling Stream Through Inner Annulus

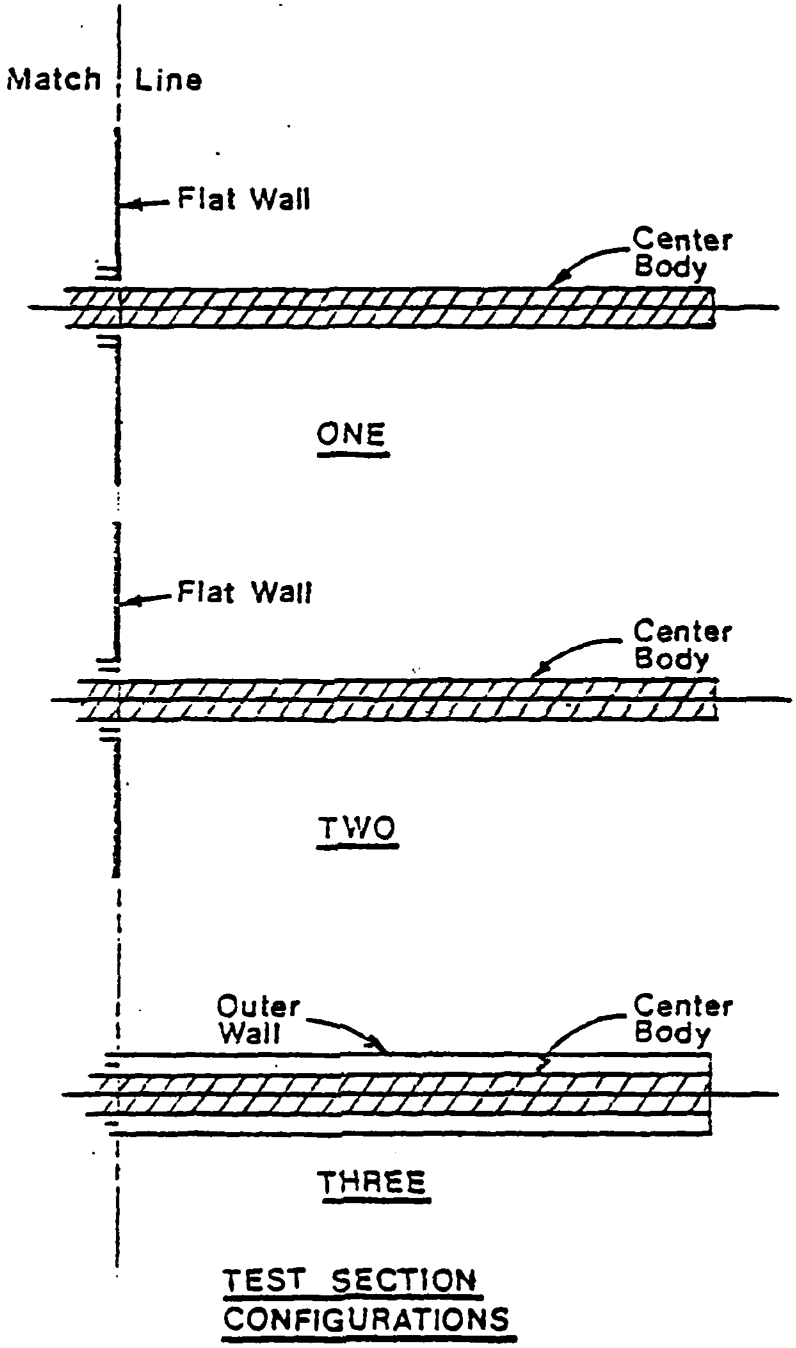

Figure 4-13 Test Section Configurations

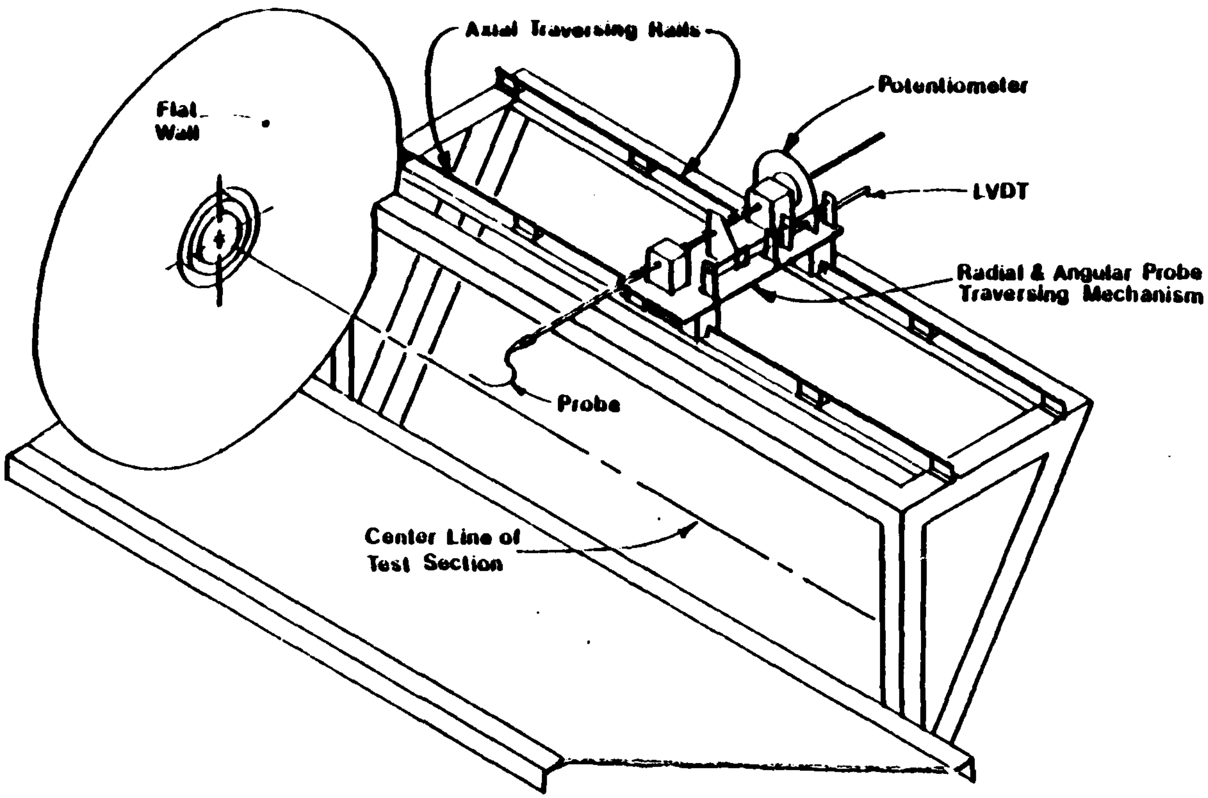

Figure 4-14 Probe #1 and Traversing Mechanism

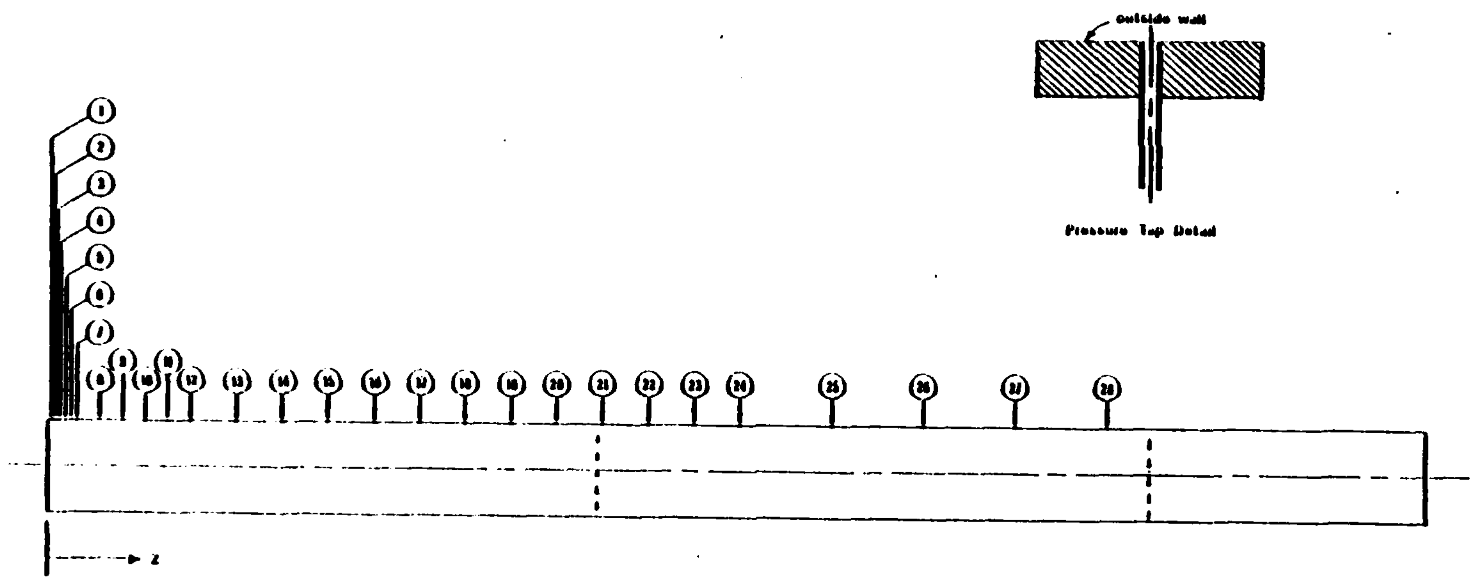

Figure 4-15 Static Pressure Tap Locations on Center Body

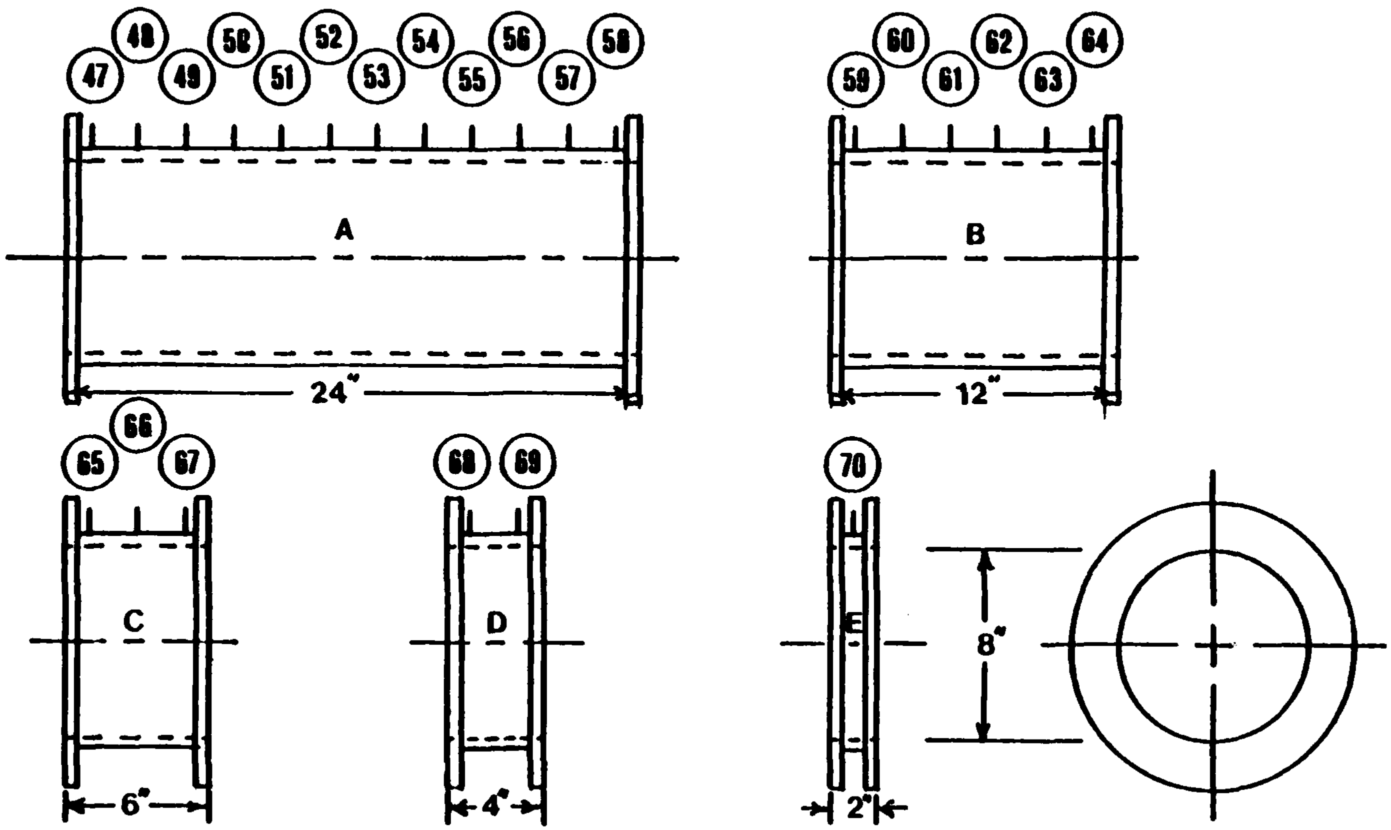

Figure 4-16 Multiple Sections of Outside Wall and Static Pressure Tap Locations

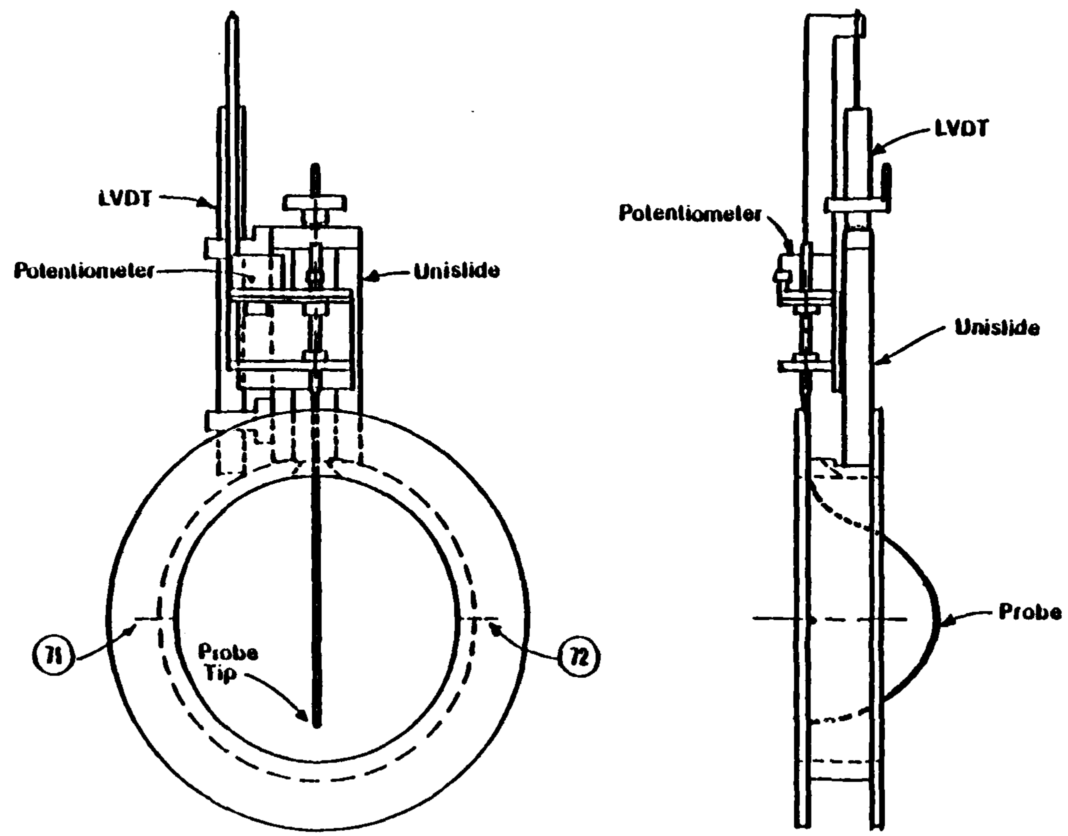

Figure 4-17 Probe #2, Traversing Mechanism and Section of Outside Wall

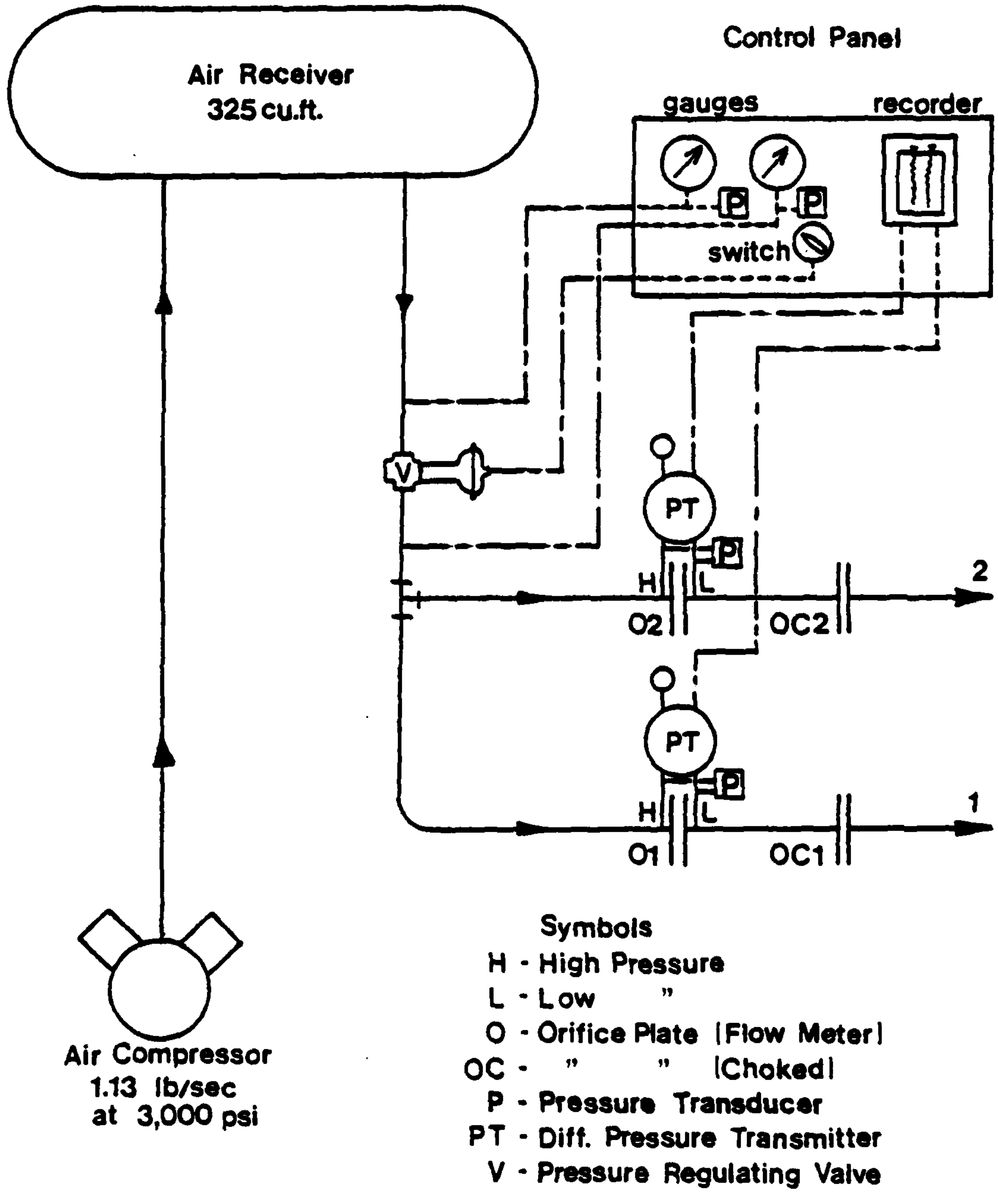

Figure 4-18 Modified High Pressure Dual Air Supply System

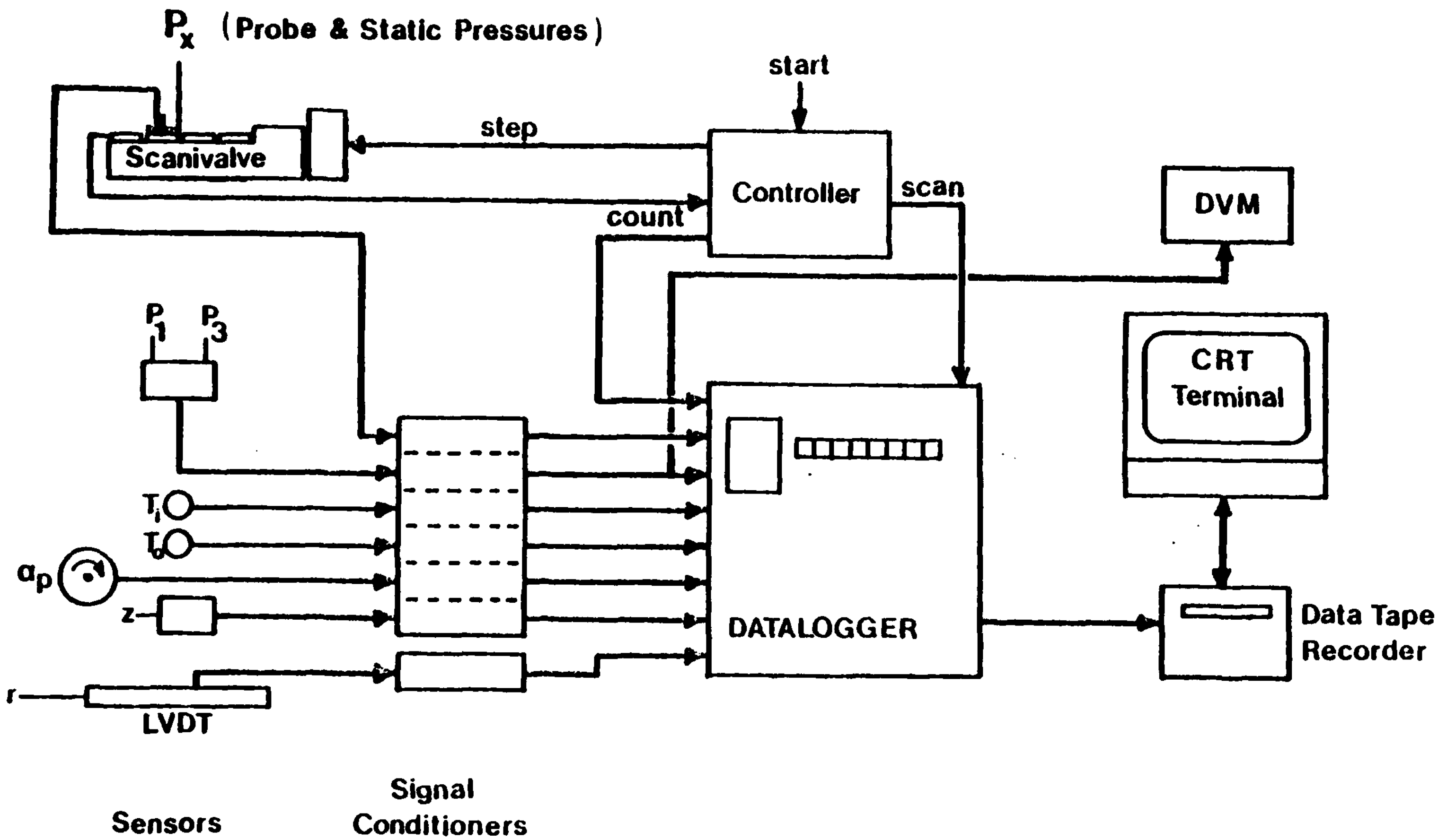

Figure 4-19 Measurement System for Tests without 8" Outside Wall

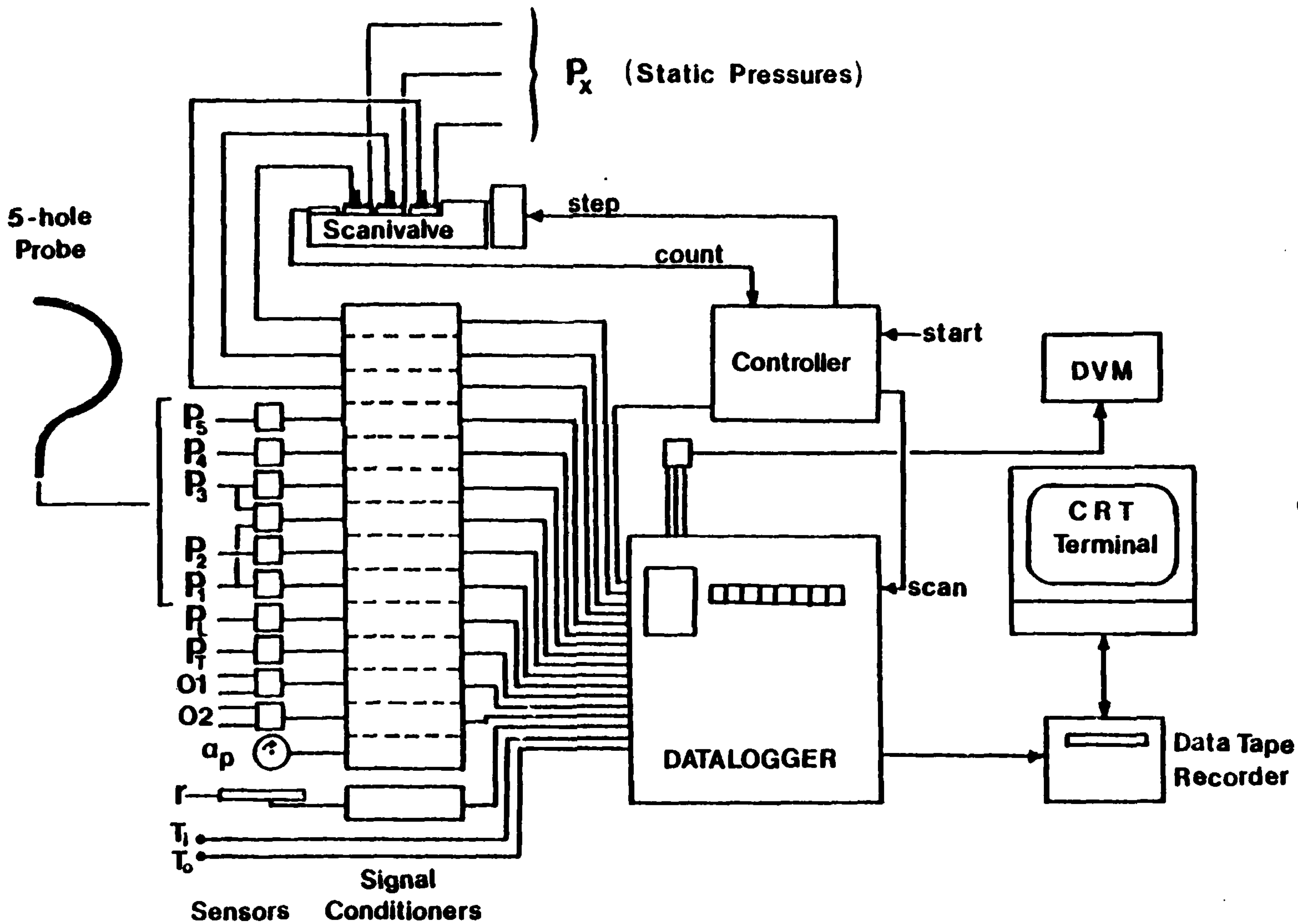

Figure 4-20 Measurement System for Tests with 8" Outside Wall

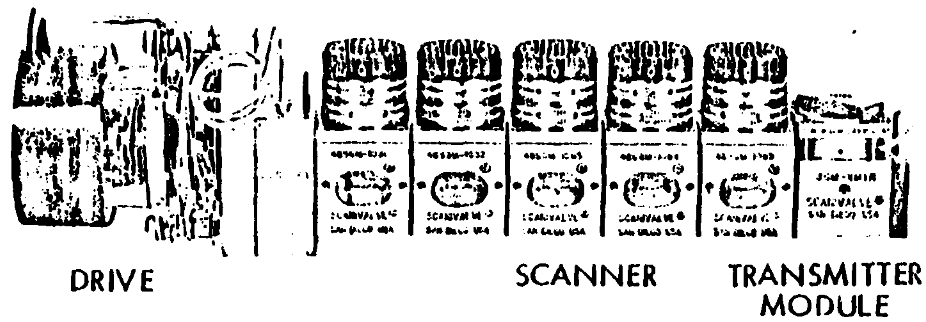

Figure 4-21a Scanivalve

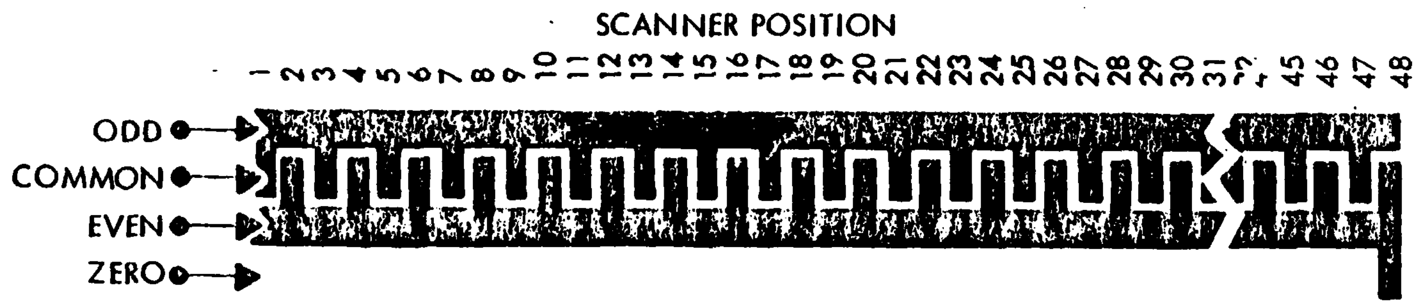

Figure 4-21b Scanivalve Position Encoder Pattern

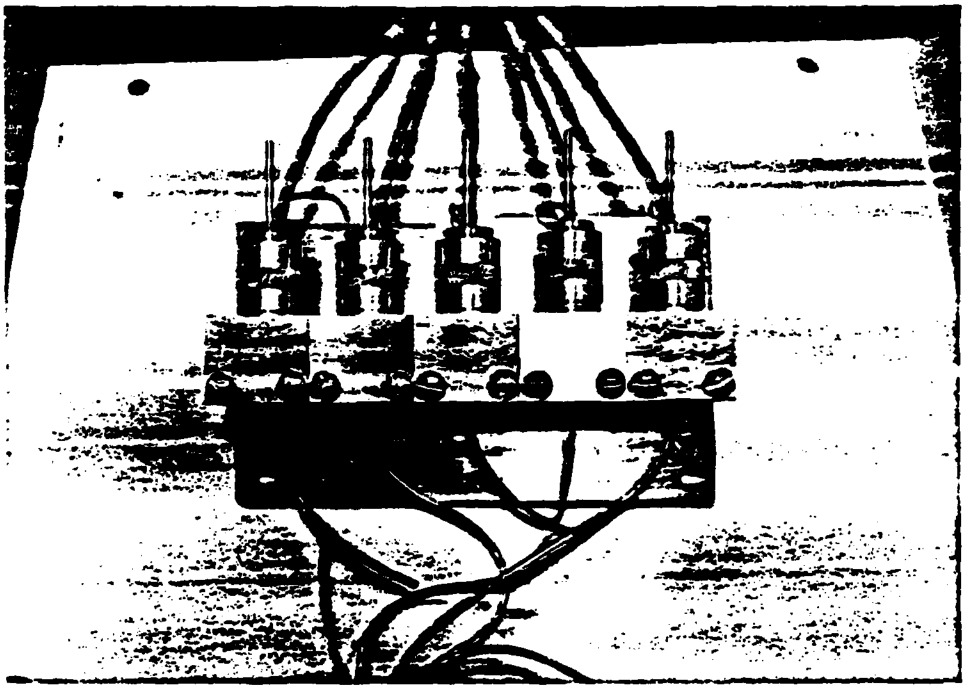

Figure 4-22 Block of Five Pressure Transducers for Probe #2

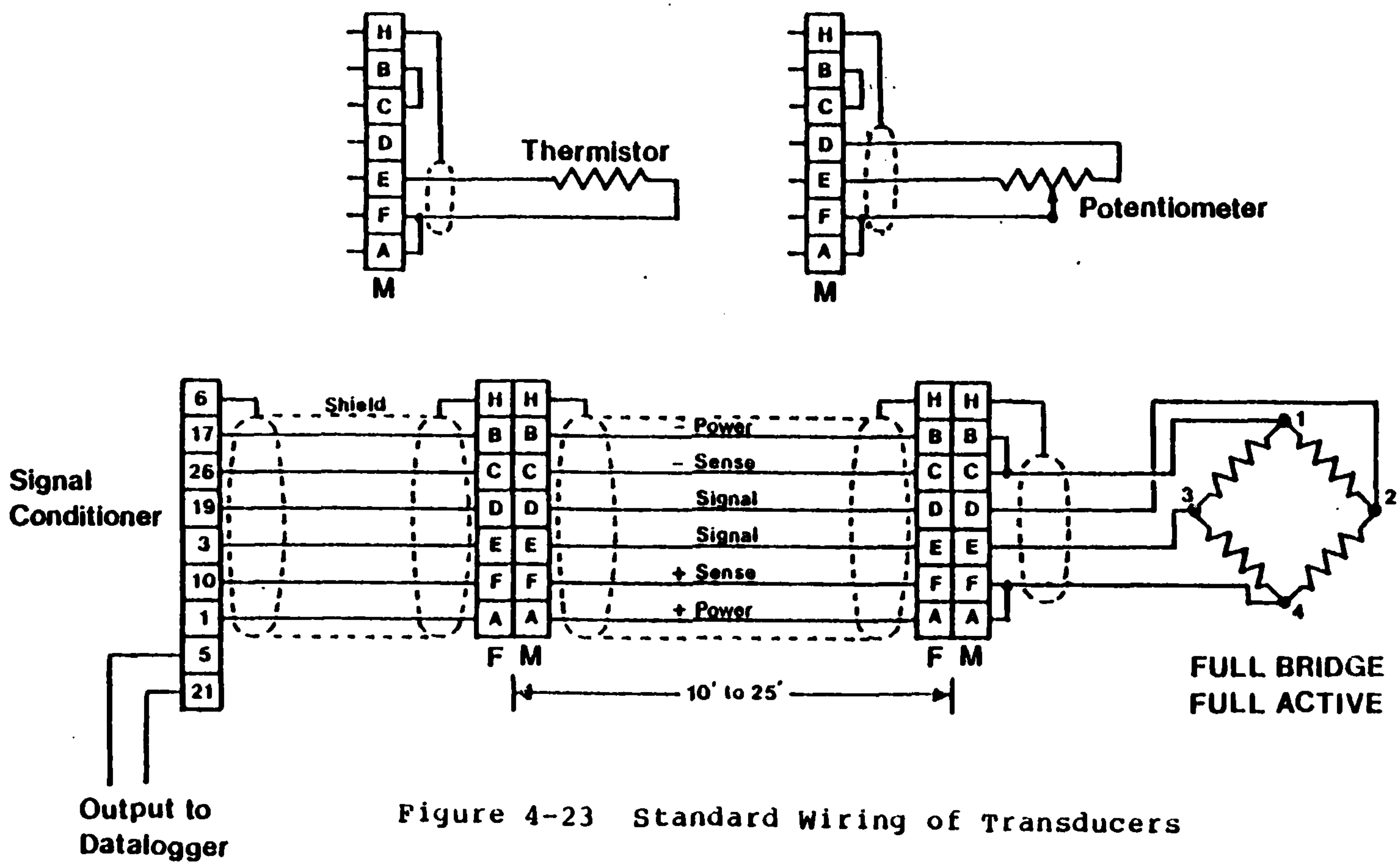

Figure 4-23 Standard Wiring of Transducers

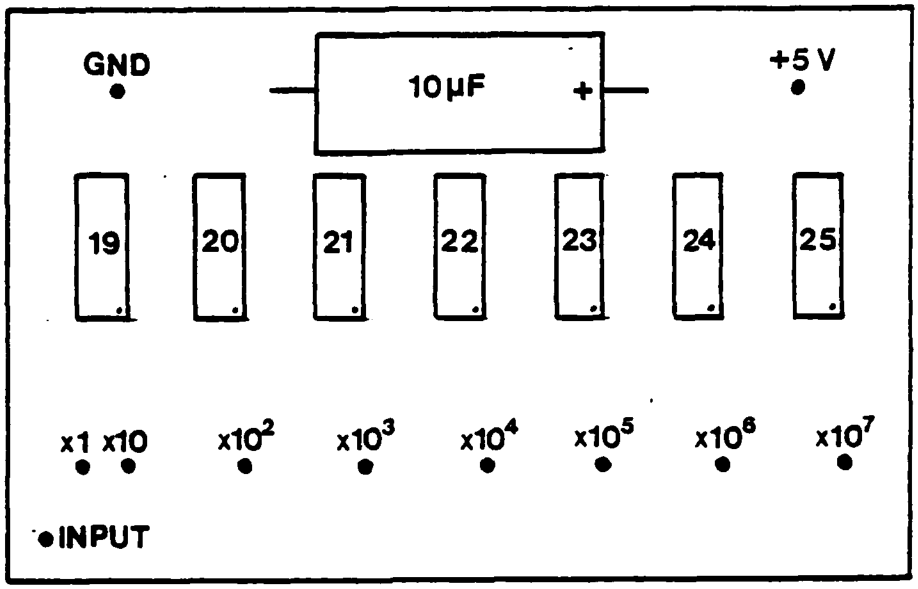

Figure 4-24a Circuit Board of Frequency Multiplier

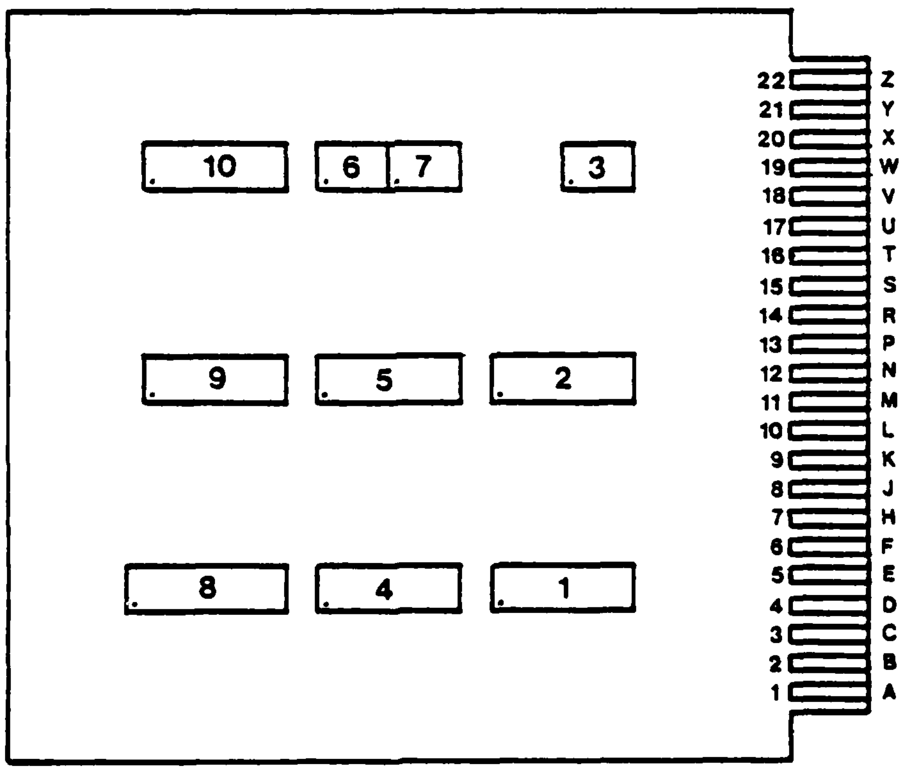

Figure 4-24b Main Controller Circuit Board

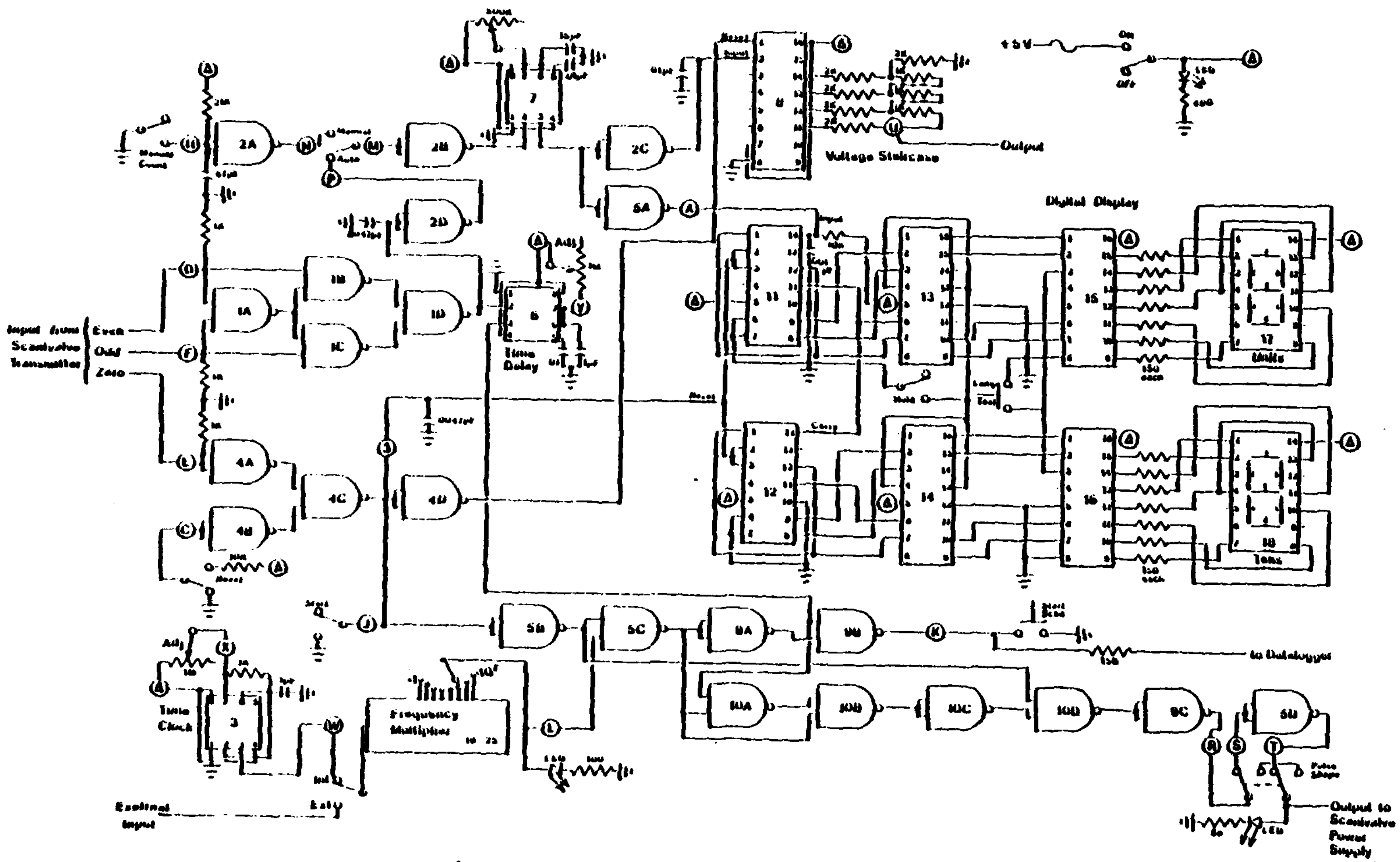

Figure 4-25 Controller Circuit Diagram

74LS00 QUAD NAND GATE

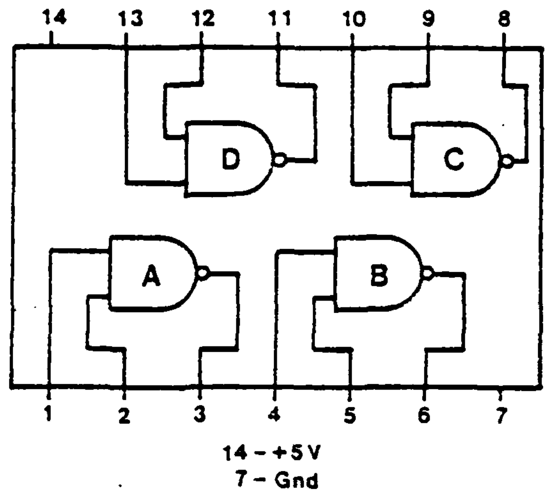

NAND GATE

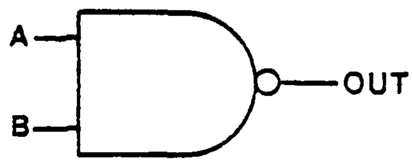

TRUTH TABLE

A	B	OUT
L	L	H
L	H	H
H	L	H
H	H	L

Figure 4-26 Quad NAND Gate Schematic

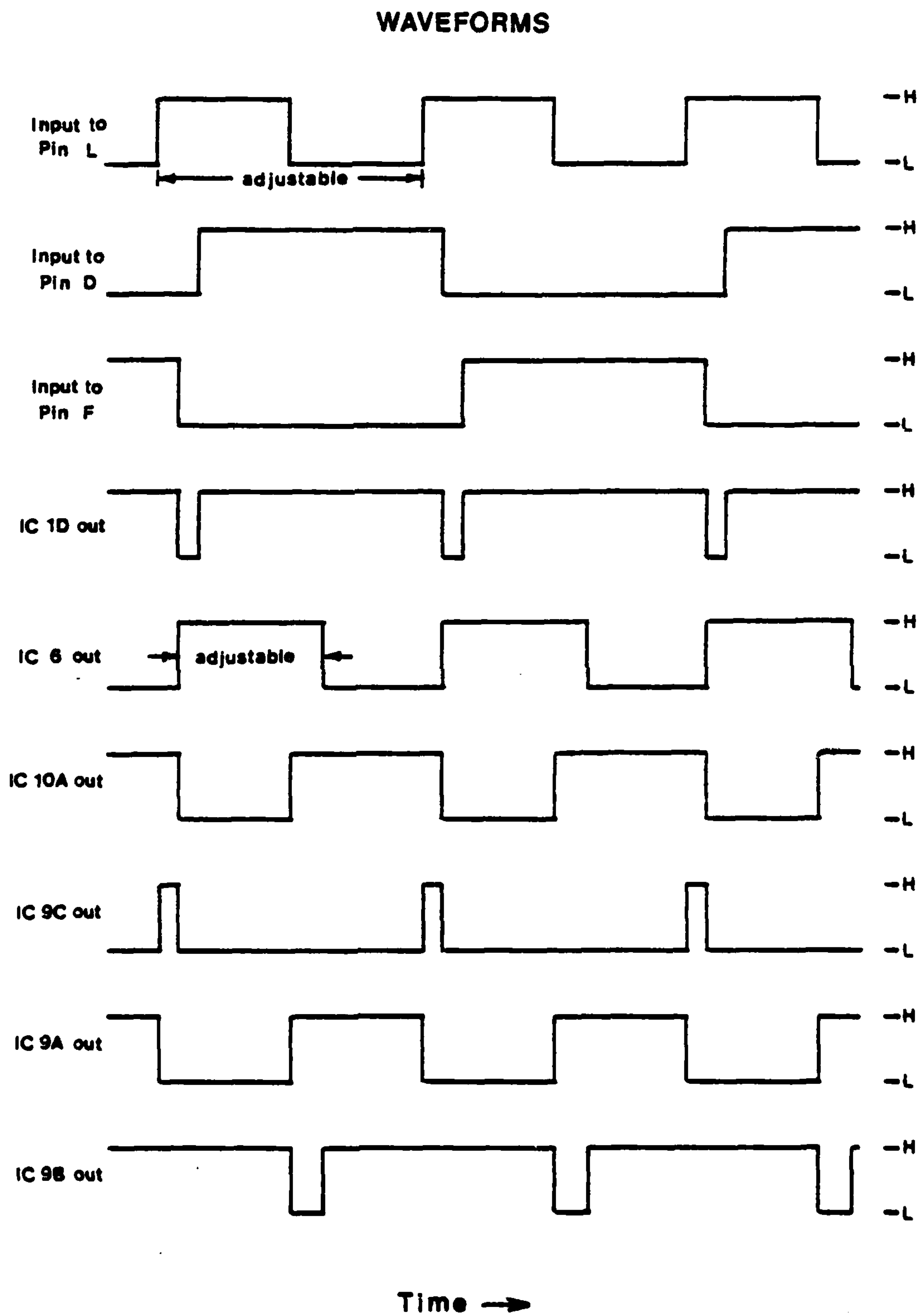

Figure 4-27 Controller Timing Waveforms

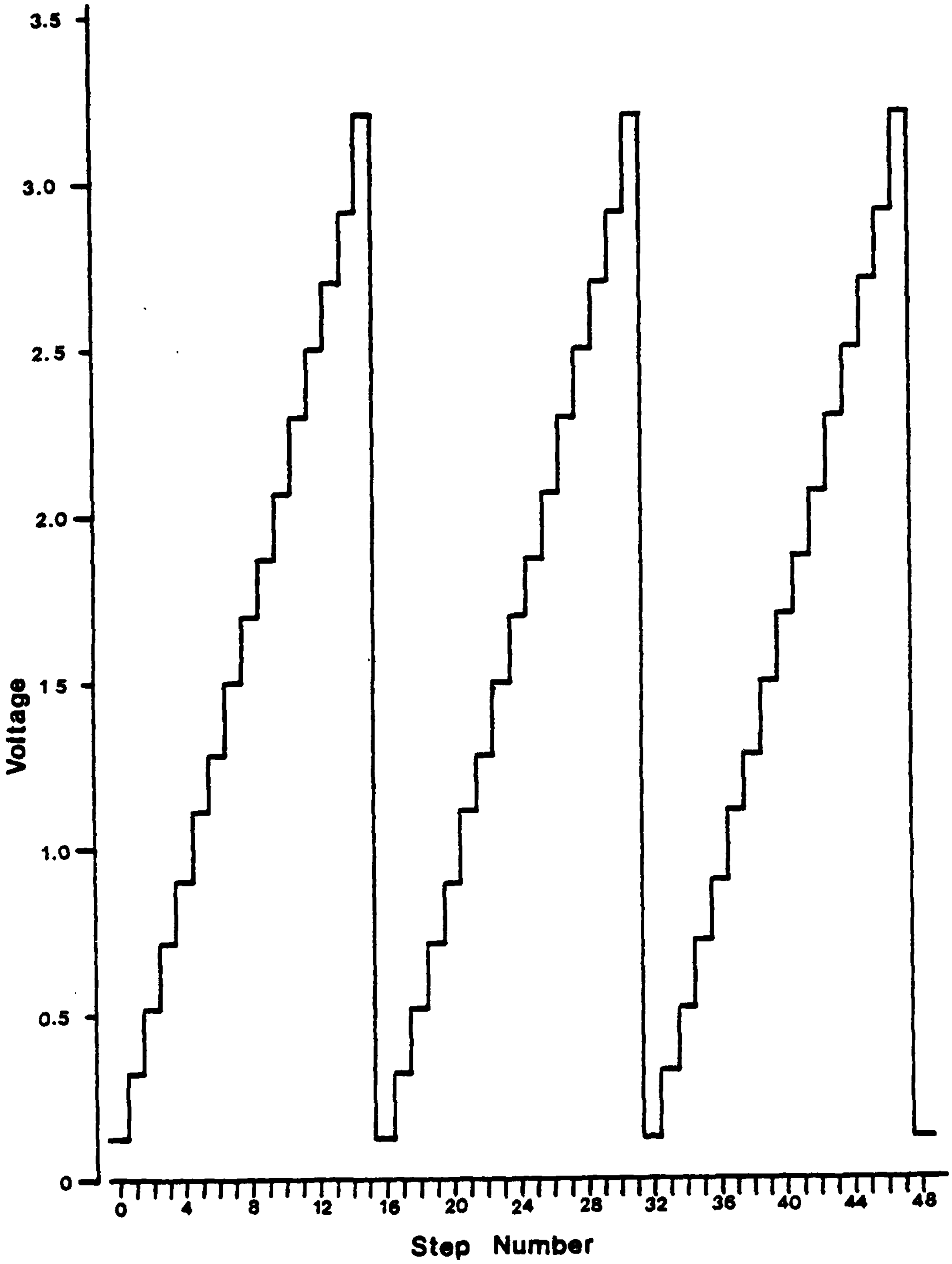

Figure 4-28 Scanivalve Position Voltage Staircase

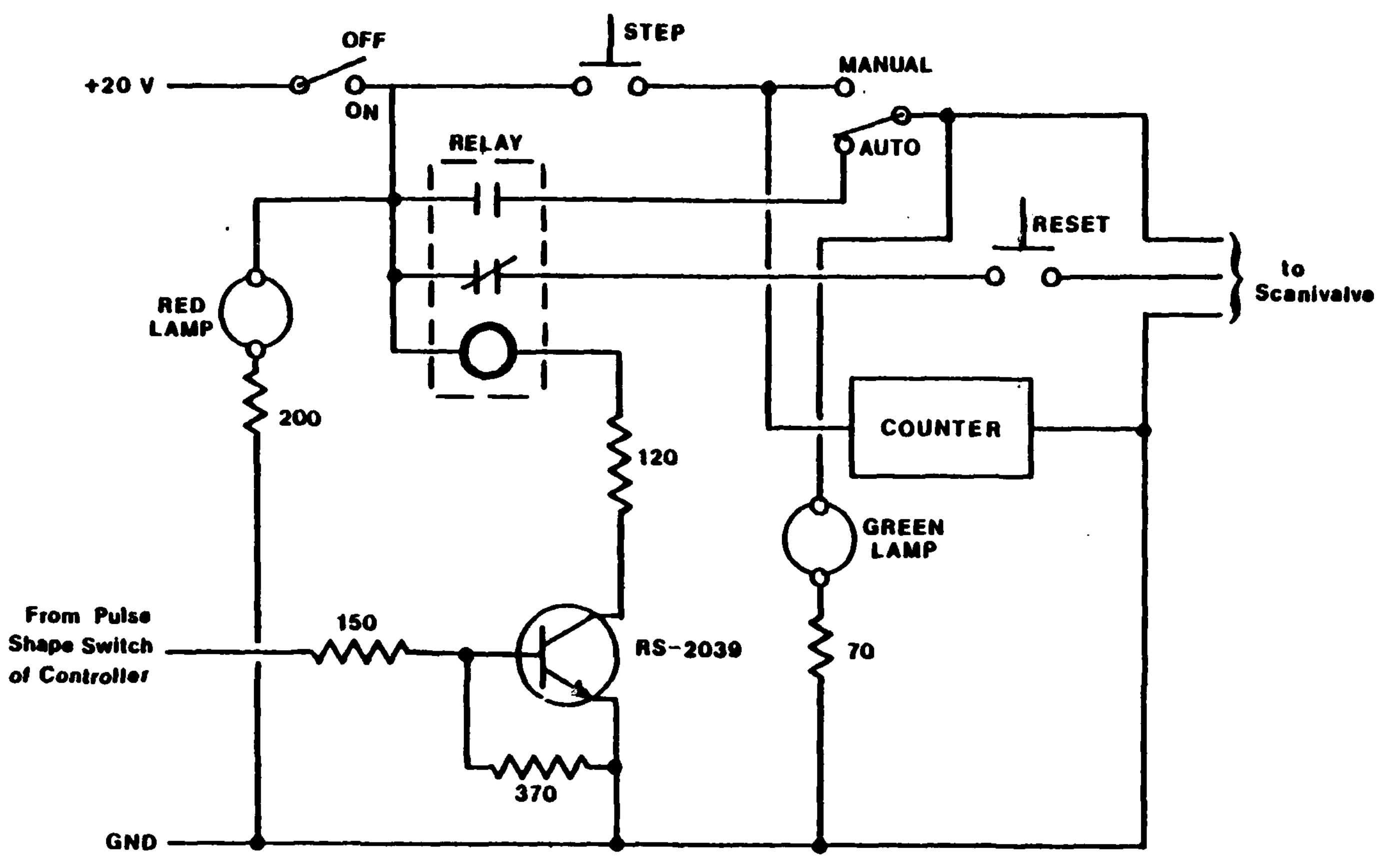

Figure 4-29 High Current Switching Relay Circuit for Scanivalve Solenoid

CHAPTER 5

FIVE-HOLE PROBES

I. INTRODUCTION

A five-hole probe is essential to the measurement of mean flow in the incompressible mixing of concentric jets with swirl in the inner stream. This type of probe is constructed with a single forward hole surrounded by four holes on a conical surface eminating from the forward hole. Erwin (Reference 1) describes the general characteristics of this type of probe and gives typical calibration data for a five-hole probe. The procedure described by Erwin to use this type of probe requires that the pressures from two holes on opposite sides of the conical surface be nulled, first for determination of one flow angle, and then the other flow angle is determined by the other three pressures and the calibration curve. Baker, Gallington and Minster (Reference 2) describe a calibration procedure for this type of probe which does not require that the probe be moved to a null position during measurement. The probe described by Erwin is not practical for use in a blow-down system and the location of the probe head changes when the probe is rotated. The calibration procedure described by Baker et al alleviates

these drawbacks, however, the accuracy of measurement is degraded due to the larger calibration regime. Dring, Joslyn and Hardin (Reference 3) describe the use of a modified five-hole probe that keeps the probe head essentially in a constant position when the probe is rotated. However, this modified probe, as calibrated by Dring et al, requires that two pressures be nulled during measurement. The required high accuracy and the limited time of measurement are satisfied by the use of a probe as described by Dring et al, but using a modification of the calibration and measurement procedures described by Baker et al.

Several small probes were constructed using the methods described by Gallington and Hollenbaugh (Reference 4). These probes were calibrated using the methods of Baker et al over a small range of angle of attack (α) and a large range of angle of sideslip (β). During measurement, the probe is rotated to minimize the pressure difference between the two pressure holes on the conical surface that are directly related to the angle of attack (α). Since nulling is not required for determining the exact angle of attack, the time for measurement of the flow by the five-hole probe is reduced considerably. The accuracy of measurement still remains high since the probe is

calibrated for a small difference in the flow's angle of attack relative to the probe's axis and for a large range of angle of sideslip.

II. THEORETICAL SECTION

A. Calibration Equations

The coordinate system for the five-hole conical probe is shown in Figure 5-1 and the port numbering system is shown in Figure 5-2. Figure 5-1 shows the end of the pressure probe and only the forward hole - port 5. The velocity components in the radial, tangential and axial directions (u, v and w) can be written in terms of the magnitude of the velocity, V, and the flow angles, α and β, as follows:

$$u = V \sin\beta \qquad (5\text{-}1)$$

$$v = V \sin\alpha \cos\beta \qquad (5\text{-}2)$$

$$w = V \cos\alpha \cos\beta \qquad (5\text{-}3)$$

As recommended by Baker, Gallington and Minster (reference 2), four pressure coefficients are defined in terms of the pressures measured from each of the five pressure ports on the probe and the measured total and

static pressures.

$$C_\alpha = \frac{P_3 - P_1}{3\,(P_5 - 1/4\,P_\Sigma)} \qquad (5\text{-}4)$$

$$C_\beta = \frac{P_2 - P_4}{3\,(P_5 - 1/4\,P_\Sigma)} \qquad (5\text{-}5)$$

$$C_o = \frac{P_T - P_5}{P_5 - 1/4\,P_\Sigma} \qquad (5\text{-}6)$$

$$C_q = \frac{P_5 - 1/4\,P_\Sigma}{P_T - P_S} \qquad (5\text{-}7)$$

where P_1 through P_5 are the pressures measured at pressure ports 1 through 5 shown in Figure 5-2; P_Σ is the sum of P_1, P_2, P_3 and P_4; P_T is the total pressure; and P_S is the static pressure.

For a fixed flow angle β and small changes in the flow angle α, the coefficient C_α is roughly proportional to v/W. Similarly, for small changes in the flow angle β, the coefficient C_β is roughly proportional to u/V. The coefficient C_o is the difference between the actual total pressure and the pressure measured by port 5 nondimensionalized by the difference between P_5 and 1/4 P_Σ. The coefficient C_q is a ratio of that portion of the dynamic pressure sensed by the probe, $P_5 - 1/4\,P_\Sigma$, to the actual dynamic pressure, $P_T - P_S$.

For calibration of a particular probe, the following fourth-order equation for C_o , C_q , u/V and v/V is used as recommended by Barker et al (Reference 2):

$$\begin{aligned} A = {} & K_{A_1} + K_{A_2} C_\alpha + K_{A_3} C_\beta + K_{A_4} C_\alpha^2 + K_{A_5} C_\alpha C_\beta + \\ & K_{A_6} C_\beta^2 + K_{A_7} C_\alpha^3 + K_{A_8} C_\alpha^2 C_\beta + K_{A_9} C_\alpha C_\beta^2 + \\ & K_{A_{10}} C_\beta^3 + K_{A_{11}} C_\alpha^4 + K_{A_{12}} C_\alpha^3 C_\beta + K_{A_{13}} C_\alpha^2 C_\beta^2 + \\ & K_{A_{14}} C_\alpha C_\beta^3 + K_{A_{15}} C_\beta^4 \end{aligned} \tag{5-8}$$

where A = C_o , C_q , u/V, v/V as applicable and the 15 subscripted K's are calibration coefficients to be determined for each of the four A's. From a large number of data points, the calibration coefficients can be determined by using matrix operations as discussed by Neter and Wasserman (Reference 5) and the resulting calibration automatically incorporates a least squares fit. Nine matrices are required in this calibration process:

$$[D] = \begin{bmatrix} 1 & C_{\alpha_1} & C_{\beta_1} & C_{\alpha_1}^2 & C_{\alpha_1} C_{\beta_1} & C_{\beta_1}^2 & \cdots & C_{\beta_1}^4 \\ 1 & C_{\alpha_2} & C_{\beta_2} & C_{\alpha_2}^2 & C_{\alpha_2} C_{\beta_2} & C_{\beta_2}^2 & \cdots & C_{\beta_2}^4 \\ 1 & C_{\alpha_3} & C_{\beta_3} & C_{\alpha_3}^2 & C_{\alpha_3} C_{\beta_3} & C_{\beta_3}^2 & \cdots & C_{\beta_3}^4 \\ \vdots & \vdots & \vdots & \vdots & \vdots & \vdots & & \vdots \\ 1 & C_{\alpha_n} & C_{\beta_n} & C_{\alpha_n}^2 & C_{\alpha_n} C_{\beta_n} & C_{\beta_n}^2 & \cdots & C_{\beta_n}^4 \end{bmatrix} \tag{5-9}$$

where the subscripts on C_α and C_β denote the particular

data point.

$$\left[{}^{u}/V\right] = \begin{bmatrix} {}^{u}/V_1 \\ {}^{u}/V_2 \\ {}^{u}/V_3 \\ \vdots \\ {}^{u}/V_n \end{bmatrix} \qquad \left[K_{u/V}\right] = \begin{bmatrix} K_{u/V_1} \\ K_{u/V_2} \\ K_{u/V_3} \\ \vdots \\ K_{u/V_{15}} \end{bmatrix}$$

$$\left[{}^{v}/V\right] = \begin{bmatrix} {}^{v}/V_1 \\ {}^{v}/V_2 \\ {}^{v}/V_3 \\ \vdots \\ {}^{v}/V_n \end{bmatrix} \qquad \left[K_{v/V}\right] = \begin{bmatrix} K_{v/V_1} \\ K_{v/V_2} \\ K_{v/V_3} \\ \vdots \\ K_{v/V_{15}} \end{bmatrix} \tag{5-10}$$

$$\left[C_o\right] = \begin{bmatrix} C_{o_1} \\ C_{o_2} \\ C_{o_3} \\ \vdots \\ C_{o_n} \end{bmatrix} \qquad \left[K_{C_o}\right] = \begin{bmatrix} K_{C_{o_1}} \\ K_{C_{o_2}} \\ K_{C_{o_3}} \\ \vdots \\ K_{C_{o_{15}}} \end{bmatrix}$$

$$\left[C_q\right] = \begin{bmatrix} C_{q_1} \\ C_{q_2} \\ C_{q_3} \\ \vdots \\ C_{q_n} \end{bmatrix} \qquad \left[K_{C_q}\right] = \begin{bmatrix} K_{C_{q_1}} \\ K_{C_{q_2}} \\ K_{C_{q_3}} \\ \vdots \\ K_{C_{q_{15}}} \end{bmatrix} \tag{5-11}$$

By use of the matrix notation, Equation 5-8 can be written for all data points as follows:

$$\left[A\right] = \left[D\right]\left[K_A\right] \tag{5-12}$$

where $A = u/V$, v/V, C_o, C_q and

$K_A = K_{u/V}$, $K_{v/V}$, K_{C_o}, K_{C_q} as applicable

Solving Equation 5-12 for the calibration coefficients that give the least square error between the actual data and the value predicted by the calibration can be done as follows for the u/V matrix:

1. Write Equation 5-12 in terms of u/V

$$[u/V] = [D]\left[K_{u/V}\right] \tag{5-13}$$

2. Multiply each side of Equation 5-13 by the transpose of the $[D]$ matrix, Equation 5-9

$$[u/V][D]^T = [D]^T[D]\left[K_{u/V}\right] \tag{5-14}$$

3. Multiply each side of Equation 5-14 by the inverse of the newly formed $[D^T D]$ matrix

$$[D^T D]^{-1}[u/V][D^T] = [D^T D]^{-1}[D^T D]\left[K_{u/V}\right] \tag{5-15}$$

4. Noting that the product of a matrix and its inverse is the identity matrix, Equation 5-15 becomes

$$\left[K_{u\,V}\right] = [D^T D]^{-1}[u/V][D^T] \tag{5-16}$$

The same derivation is followed to derive the following equations for the calibration coefficients $K_{v/V}$, K_{C_o} and K_{C_q}:

$$\left[K_{v/V}\right] = [D^T D]^{-1} [v/V] [D^T] \tag{5-17}$$

$$\left[K_{C_o}\right] = [D^T D]^{-1} [C_o] [D^T] \tag{5-18}$$

$$\left[K_{C_q}\right] = [D^T D]^{-1} [C_q] [D^T] \tag{5-19}$$

Thus, from a given set of data, the D, u/V, v/V, C_o, and C_q matricies are calculated and, by matrix operations, the calibration coefficients $K_{u/V}$, $K_{v/V}$, K_{C_o}, and K_{C_q} are calculated, using Equations 5-16, 5-17, 5-18 and 5-19, respectively.

B. Prediction of Static and Dynamic Pressures

Once the calibration coefficients have been determined, then the static pressure, P_S, and the dynamic pressure, $P_T - P_S$, can be predicted from the five pressures measured by the probe, P_1 through P_5, and Equations 5-4 through 5-8 as follows:

1. From the pressures P_1 through P_5, use Equations 5-4 and 5-5 to calculate C_α and C_β.

2. Using the calculated C_α and C_β and the calibration coefficients K_{C_o} and K_{C_q}, calculate the predicted value of C_o and C_q, using Equation 5-8.

3. From the predicted value of C_q and the five measured pressures, P_1 through P_5, calculate the dymanic pressure, $P_T - P_S$, from Equation 5-7, written as follows:

$$P_T - P_S = (P_5 - 1/4\ P_\Sigma)/C_q \qquad (5\text{-}20)$$

4. From the predicted values of C_q, C_o and $P_T - P_S$ and the five measured pressures, P_1 through P_5, calculate the static pressure, P_S, from the combination of Equations 5-6 and 5-7, written in the following form:

$$P_S = P_5 - (1/C_q - C_o)\ (P_5 - 1/4 P_\Sigma) \qquad (5\text{-}21)$$

The predicted value of the total pressure, P_T, can also be calculated from Equation 5-6, written as follows:

$$P_T = P_5 + C_o\ (P_5 - 1/4 P_\Sigma) \qquad (5\text{-}22)$$

C. Prediction of Momentum

In axisymmetric flow, the tangential and axial momentum fluxes are quantities of interest. By aligning the x-axis of the five-hole probe with the radial direction of flow and the z-axis of the probe with the axial direction of flow, this probe can be used to determine the radial,

tangential and axial velocities and the static pressure at a point. Figure 5-3a shows this type of alignment.

These probes will be used in measurement where air streams are provided by a blow-down system. For accurate determination of the flow direction, the probe will be rotated about its x-axis to essentially null the flow angle α as shown in Figure 5-3b. When the probe is rotated, as shown in Figure 5-3b, the u, v and w velocity components can be determined with respect to the probe's body fixed coordinate system (x,y',z') and then the rotation of the probe can be taken into account in determining the values of the v and w velocity components with respect to the x,y,z coordinate system. The resulting u, v and w velocity components are then the radial, tangential and axial velocity components, respectively, in the cylindrical coordinate system (r,θ ,z), shown in both Figures 5-3a and 5-3b.

The axial and tangential momentum fluxes can be written as follows for incompressible axisymmetric flow:

$$M_z = P_S - P + \rho w^2 \tag{5-23}$$

$$M_z' = \rho (w^2 - v^2/2) \tag{5-24}$$

$$M_\theta = \rho vw \tag{5-25}$$

where M_z and M_z' are the axial momentum fluxes, M_θ is the

tangential momentum flux, P_o is a reference pressure, and is the density of the incompressible fluid.

Since the dynamic pressure, $P_T - P_S$, equals $\rho V/2$ for the case of incompressible flow, then the equations for the axial and tangential momentum fluxes can be written in terms of the values predicted, using the five-hole probe as follows:

$$M_z = P_S - P_o + 2(P_T - P_S)(w/V)^2 \qquad (5\text{-}26)$$

$$M_z' = 2(P_T - P_S)((w/V) - (v/V)/2) \qquad (5\text{-}27)$$

$$M_\theta = 2(P_T - P_S)(v/V)(w/V) \qquad (5\text{-}28)$$

$$\text{where} \quad w/V = (1-(u/V)^2 - (v/V)^2)^{1/2}$$

Thus Equations 5-26, 5-27, and 5-28 can be used to determine M_z, M_z', and M_θ from the redicted values of P_S, $P_T - P_S$, u/V and v/V.

D. Measure of Accuracy

The calibration procedure consists of measuring the seven pressures (P_1, P_2, P_3, P_4, P_5, P_T & P_S) and the two angles (α and β) at each point of interset. From this given set of data, the D, u/V, v/V, C_o and C_q. matrices are calculated using Equations 5-16, 5-17, 5-18 and 5-19. Once the four sets of calibration coefficients

are determined, the values of u/V, v/V, C_o and C_q can be calculated using Equation 5-8 and compared to the experimental values of these quantities at each data point. This comparison of calculated and experimental values of u/V, v/V, C_o and C_q constitute a validity test of the calibration.

As discussed by Barker, Gallington and Minster, the accuracy, as defined by the validity test of the calibration, is dependent on the way the calibration data samples are taken, the manufacturing anomalies of the probe, and the associated measuring equipment used with the probe. Since the calibration procedure utilizes a curve fitting routine, the greater accuracy is afforded in the region where the calibration data samples have the higher density. Thus, the density of the data points effects the accuracy and the distribution of the data points should be selected in such a way as to insure that the accuracy is constant over the probe's range of use.

When calibrating a five-hole probe, the range of flow angles, α and β, to be measured should be known beforehand. The range and density of the calibration points can then be selected to insure a high accuracy where desired.

The standard deviation, S, of the calculated values of the four desired outputs (u/V, v/V, C_o and C_q) obtained from the experimental values of these quantities gives an overall measure of the accuracy of the calibration. This standard deviation can be estimated using the following equation:

$$S_A = \left[\frac{\sum_n (A_e - A_c)^2}{n} \right]^{1/2} \qquad (5\text{-}29)$$

where A = u/V, v/V, C_o and C_q in turn, n is the number of data points being compared, and e and c are subscripts that refer to experimental and calculated values, respectively.

Assuming a normal distribution of errors, one then finds a 95% probability that the actual value will be within 1.96 standard deviations of that calculated from the curve fit.

An important point to note is that the calibration process for the five-hole probe is limited to incompressible flow because the calibration depends on C_α and C_β , which are pressure coefficients that are dependent on Mach number.

III. EXPERIMENTAL SECTION

A. Apparatus - Probe #1

The calibration experiment was conducted in the 30-inch hexagonal subsonic venturi wind tunnel at the University of Washington. The five-hole probe to be tested (Probe #1) was mounted to its traversing mechanism which allowed variations in the flow angle α and radial position. This probe/transversing mechanism assembly was attached to a calibration fixture which allowed variations in the flow angle β . Both flow angles, α and β , were changed manually. Pressures P_1 , P_2, P_3, P_4, P_5, P_T and P_S were measured using a Scanivalve with a Statham pressure transducer and a digital volt meter (DVM), as shown in Figure 5-4a. The positioning of Probe #1, in the tunnel for calibration, is shown in Figure 5-4b.

Figure 5-5 shows the shape and dimensions of Probe #1. This probe has a hook shape so that rotation of the probe's mounting shaft (a part of the probe/transversing mechanism) only rotates the probe's face and does not change the location of the probe's face. The probe has an outside diameter of 0.158 inches with each of the five tubes having an inside diameter of 0.021 inches. The

probe tip has a conical half-angle of 45 degrees.

B. Initial Calibration - Probe #1

The probe was mounted to its traversing mechanism, leveled on a surface plate and the resistance of the potentiometer that measures the angle of the probe, with respect to the traversing mechanism, was measured to establish a zero for the flow angle α. The calibration fixture was mounted to the wind tunnel and aligned with the flow. The probe/traversing mechanism, with the probe attached, was mounted to the calibration fixture for a flow angle β of zero and the probe position adjusted for a flow angle of zero. The flow angle α of the probe versus the output voltage of a bridge circuit that included the potentiometer connected to the shaft of the traversing mechanism was used to set the flow angle α. For each flow angle β, the flow angle α was varied manually and the seven pressures and temperatures recorded. The position of the traversing mechanism on the calibration fixture was changed manually to a new flow angle β and the measurements repeated over the range of flow angle α. The wind tunnel was operated at a velocity of approximately 82 ft/sec during this phase of the calibration. Data was taken for the following flow

angles:

$$\alpha = 0, \pm 1.9, \pm 3.8, \pm 5.7, \pm 7.5, \pm 11.3, \pm 15.1, \pm 18.9, \pm 23.6, \pm 28.3, \pm 32, \pm 36.2, \pm 40.2, \pm 48 \ \& \ \pm 51.5$$

$$\beta = 0, \pm 2, \pm 4, \pm 6, \pm 8, \pm 10, +15, +20, +25, +30 \ \& \ +35$$

This phase of the calibration was performed over a larger range of flow angle α than the actual probe will encounter, so that the complete characteristics of this probe could be determined and compared with other probes whose characteristics are documented. The pressure coefficients C_o, C_q, C_α and C_β are plotted versus the flow angle α for values of the flow angle β of -10°, 0°, $+10^\circ$, $+25^\circ$ and $+35^\circ$ in Figures 5-6, 5-7, 5-8, 5-9 and 5-10, respectively. Note the near linear characteristic of the four pressure coefficients versus α in the range of α from -7.5° to $+7.5^\circ$. The pressure coefficients C_o, C_q, C_α and C_β are plotted versus the flow angle β for $\alpha=0$ in Figure 5-11 and the need for two distinct calibration regions is shown as the characteristics of the pressure coefficients C_o, C_q and C_β change from nearly constant for values of β between -10° and $+10^\circ$ to significant changes for values of β greater than $+10^\circ$.

The calibration data was separated into two regions for calibration. The first calibration region being for values of β between -10 and +10 and the second calibration region being for values of β greater than +10 . Since Probe #1 would be subjected to only small values of the flow angle α, the probe was calibrated using data which extended from α equal to -7.5 to +7.5 . The first calibration region has 99 data points ($\pm\alpha$ = 0, 1.9 , 3.8 , 5.7 & 7.5 and $\pm\beta$ = 0, 2 , 4 , 6 , 8 & 10) and the second calibration region has 54 data points ($\pm\alpha$ = 0 , 1.9 , 3.8 , 5.7 & 7.5 and β = 10 , 15 , 20 , 25 , 30 & 35). Both calibration regions have the 9 data points at the flow angle of β=+10 in common.

C. Calibration Coefficients - Probe #1

For the calibration regions, the appropriate set of data was read into the University of Washington's CDC computer for reduction into the five matrices $[D]$, $[u/V]$, $[v/V]$, $[C_o]$ and $[C_q]$ using Equations 5-1 through 5-10. Then the calibration coefficients $K_{u/V}$, $K_{v/V}$, K_{C_o} and K_{C_q} of Probe #1 were calculated for each region using Equations 5-16 through 5-19. The computer program for calibration is written in Fortran and includes call to the linear algebra library package LINPACK for solution of Equations

5-16 through 5-19. Equation 9 was used to calculate the predicted values of u/V, v/V, C_o and C_q, using the measured values of C_α & C_β and the specific calibration coefficients for that region for comparison with the calibration values of these variables.

The results of the calibration are presented in Figures 5-12 through 5-18. Lines of constant C_α and C_β are plotted on a u/V versus v/V plot in Figures 5-12 and 5-13 for the first and second calibration regions, respectively. For the first calibration region, constant contours of C_o plotted against C_α and C_β are shown in Figure 5-14 and constant contours of C_q plotted against C_α and C_β are shown in Figure 5-16. Contours of C_o and C_q for the second calibration region are plotted in Figures 5-15 and 5-17, respectively. The value of the pressure coefficient C_β is used to determine which set of calibration coefficients are to be used to calculate the flow properties. The first region's calibration coefficients are used for values of C_β less than 0.35 and the second region's calibration coefficients are used for values of C_β greater than or equal to 0.35. Figure 5-18 provides a comparison between the actual and predicted values of u/V and v/V. The difference between the two values represents the error in determining the

flow direction.

D. Apparatus - Probe #2

The five-hole probe for measuring the mixing with swirl between and eight-inch outer tube and a four-inch inner tube is shown in Figure 5-19. This probe also has a hook shape so that rotation of the probe's shaft only rotates the face of the probe and doesn't change the location of the probe's face. The probe has an outside diameter of 0.158 inches with each of the five tubes having an inside diameter of 0.021 inches. The probe tip has a conical half-angle of 45 .

Probe #2 and its tranversing mechanism was removed from its section of eight-inch tubing and mounted to a calibration fixture which allowed variations in the flow angle β . The transversing mechanism for this probe allowed for radial transversing and variation of the flow angle α . This transversing mechanism is shown in Figure 5-20 and its potentiometer was used to determine the flow angle . Both flow angles, α and β , were changed manually. Pressures P_1 , P_2 , P_3 , P_4 , P_5 , P_T and P_S were measured using seven separate ScanCo pressure transducers. The measurement system for the calibration of Probe #2 is

shown in Figure 5-21a. The positioning of Probe #2 for calibration in the 30-inch hexagonal subsonic venturi wind tunnel at the University of Washington is shown in Figure 5-21b.

E. Initial Calibration - Probe #2

Probe #2 was manually positioned at different values of the flow angles α and β in the same manner as described for Probe #1 in Section B. The wind tunnel was operated at a velocity of approximately 75 ft/sec during this phase of calibration. Data was taken for the following flow angles:

$$\alpha = 0, \pm 5, \pm 10, \pm 15, \pm 20, \pm 25, \pm 30, \pm 35, \pm 40, \pm 45 \;\&\; \pm 50$$

$$\beta = 0, \pm 2, \pm 4, \pm 6, \pm 8, \pm 10, +15 \;\&\; +20$$

This phase of calibration was performed over a larger range of flow angles α and β than the actual probe will encounter, so that the complete characteristics of this probe could be determined and compared with Probe #1 and other probes whose characteristics are documented. The pressure coefficients C_α , C_β , C_o and C_q are plotted versus the flow angle α for values of the flow angle β = -10, 0, +10 and +20 in Figures 5-22, 5-23, 5-24 and 5-25, respectively. Pressure coefficients C_α , C_β and C_q are

nearly linear versus the flow angle α in the range of α from -20 to +20. The pressure coefficient C_o has a minimum near the flow angle α value of +5, indicating a degree of asymmetry in the construction of Probe #2.

Probe #2 was to be used in a diverse environment which would extend over a large range in the value of the flow angle α . Ideally, the probe would be adjusted to null pressures P_1 and P_3 , thus giving a C_α value of zero. However, the probe was also to be subjected to large values of the flow angle α that could be aslarge as -50. The four pressure coefficients are plotted versus the flow angle α for values of α from -50 to +50 for a value of the flow angle β equal to +4 in Figure 5-26. The pressure coefficients C_α and C_β are nearly linear versus α in the range of from -50 to +20. However, the pressure coefficients C_o and C_q vary nonlinearly with the flow angle α . Two calibration regions were selected to meet the operating range of Probe #2.

Calibration data were separated into the following two regions:

Region	Range of Flow Angles
1	$-20 \leq \alpha \leq +20, -10 \leq \beta \leq +10$
2	$-50 \leq \alpha \leq -20, -6 \leq \beta \leq +8$

The range of the flow angle β for calibration of the second region is smaller than that for the first region because the probe would be operating in the second region when measuring confined flows that had small swirl angle and a resultant small radial angle (β). The first calibration region has 99 data points (α=0,±5,±10,±15 & ±20 and β=0,±2,±4,±6,±8 &±10) and the second calibration region has 56 data points (α=-20,-25,-30,-35,-40,-45 & -50 and β=0,±2,±4,±6 & +8). Both calibration regions have 7 data points at the flow angle of $\alpha = -20^\circ$ in common.

F. Calibration Coefficients - Probe #2

The calibration coefficients $K_{u/V}$, $K_{v/V}$, K_{C_o} and K_{C_q} of Probe #2 were calculated for each region using the same method as described previously for Probe #1. The predicted values of u/V, v/V, C_o and C_q were calculated using Equation 5-8, the measured values of C_α & C_β and the specific calibration coefficients for that region so that these values could be compared with the calibration values of these variables.

The results of the calibration are presented in Figures 5-27 through 5-33. Lines of constant C_α and C_β are

plotted on a u/V versus v/V plot in Figures 5-27 and 5-28 for the first and second calibration regions, respectively. For the first calibration region, constant contours of C_o plotted against C_α and C_β are presented in Figure 5-29 and constant contours of C_q plotted against C_α and C_β presented in Figure 5-31. Contours of C_o and C_q for the second calibration region are plotted in Figures 5-30 and 5-32, respectively. The value of the pressure coefficient C_α is used to determine which set of calibration coefficients are to be used to calculate the flow properties. The first region's calibration coefficients are used for values of C_α greater than or equal to -0.65 and the second region's calibration coefficients are used for values of C_α less than -0.65. Figure 5-33 gives a comparison between the actual and predicted values of u/V and v/V.

IV. DISCUSSION

It is convenient to separate the discussion of each probe's behavior into sub-sections regarding flow angles, total and dynamic pressures and accuracy.

A. Flow Angles - Probe #1

A comparison between the actual values of u/V and v/V and the values predicted using the polynominals of Equation 5-8 are given in Figure 5-18. The error in determining the flow angle is indicated by the difference between each set of predicted and actual values of u/V and v/V. This figure shows that the fit is most accurate near the origin of the tangential velocity ratio, v/V (flow angle $\alpha=0$). This is not surprising since the density of data points was greatest in this region, thus forcing a higher accuracy in this region. This figure also shows that the error varies in an unpredictable way. Both of the above observations concerning the comparison between actual and predicted values of u/V and v/V were also noted by Baker, et al, in Reference 2. Figure 5-18 also shows that the error is greater in the second calibration region (values of the radial velocity ratio, u/V, greater than 0.15) than in the first calibration region. This difference is due mainly to the lower density of data points in the second calibration region and to the severe flow angle β.

Figures 5-12 and 5-13 are plots of u/V versus v/V showing lines of constant C_α and C_β for the first and second

calibration regions, respectively. The lines of constant C_α generally tend to be vertical and the lines of constant C_β generally tend to be horizontal. It is apparent from the almost vertical C_α lines and almost horizontal C_β lines that C_α is almost independent of u/V and C_β almost independent of v/V. The location of the C_α equal zero line in both Figures 5-12 and 5-13 gives the value of the flow angle α at which the pressure coefficient C_α is nulled. The location of the C_β equal to zero line in only Figure 5-12 gives the value of the flow angle β at which the pressure coefficient C_β is nulled. The location of the C_β equal zero line in Figure 5-13 does not give the value of the flow angle at which the pressure coefficient C_β is nulled because the null value of this pressure coefficient is outside the calibration region and plotted from extrapolation to show an overlap with the region shown in Figure 5-12.

B. Total and Dynamic Pressures - Probe #1

Constant contours of C is plotted against C_α and C_β are shown in Figures 5-14 and 5-15 for the first and second calibration regions, respectively. As indicated in Equation 5-6, C_o is proportional to the difference between the actual total pressure, P_T , and the total

pressure measured by pressure port 5 of the probe, P_5. Figure 5-14 shows that, for small angles, P_5 gives an accurate reading of the actual total pressure. The larger the angle, the larger the difference between P_T and P_5. The constant contours of C_o are not perfectly circular in Figure 5-14 which indicates a degree of probe asymmetry. The relatively flat section of the constant contours of C_o in Figure 5-15, for values of v/V near zero, show relative independence of P_5 on the flow angle α for large values of the flow angle β. The accuracy of the curve fit procedure for C_o is shown by the relative position of the labeled data points with respect to the lines of constant C_o.

Constant contours of C_q plotted against C_α and C_β are shown in Figures 5-16 and 5-17 for the first and second calibration regions, respectively. Equation 5-7 defines C_q as the ratio of the dynamic pressure measured by the probe, $P_5 - 1/4P_\Sigma$, to the actual dynamic pressure, $P_T - P_S$ Figure 5-16 shows that C_q has a maximum value for $C_\alpha \simeq 0.25$ & $C_\beta \simeq -0.35$ and that C_q has values greater that 0.475 for values of C_β less than -0.1. This indicates a degree of physical asymmetry of the probe. Figure 5-17 shows some degree of physical asymmetry of the probe and the decreasing trend of C_q with increasing

C_β The accuracy of the curve fit for C is shown by the relative position of the labeled data points with respect to the lines of constant C_q.

C. Accuracy - Probe #1

Table 5-1 shows the average accuracy achieved over all the data points used in calibration.

TABLE 5-1

PARAMETER ACCURACY

PROBE # 1

Variable	1.96σ
C_o	0.036
C_q	0.017
u/V	0.49°
v/V	0.56°

Since the probe was used by approximately nulling C_α before making measurements, a more realistic measure of the accuracy is obtained by comparison of the actual values and the predicted values of all parameters for the five central values of the flow angle α (i.e. $\alpha = \pm 3.8$, $\alpha = \pm 1.9$ and $\alpha = 0$). Table 5-2 shows the average accuracy achieved over this set of data points for the four parameters and five variables of interest.

TABLE 5-2 CENTRAL ACCURACY PROBE # 1	
Variable	1.96σ
C_o	0.035
C_q	0.016
u/V	0.55°
v/V	0.51°
P_T	.00083 psig
P_S	.00194 psig
V	1.53 ft/sec
M_z	6.2%
M_θ	.00092 psig

With 95% certainty, the above table gives the accuracy in determining the listed variable from the five pressures measured by the probe. As indicated above, the angles are predicted to about the nearest half a degree. The total pressure is indicated to 3.5% of P_5 - 1/4 P_Σ or 1.5% of the dynamic pressure and the static pressure is indicated to 3.5% of the dynamic pressure. The velocity is indicated to 1.9% of the actual velocity. The axial momentum flux, M_z , is indicated to 6.2% of the actual axial momentum flux and the tangential or angular

momentum flux, M_θ, is indicated to 1.7% of the dynamic pressure.

D. Flow Angles - Probe #2

A comparison between the actual values of u/V and v/V and the values predicted using the polynominals of Equation 5-8 are given in Figure 5-33. The error in determining the flow angle is indicated by the difference between each set of predicted and actual values of u/V and v/V. The fit is most accurate near the origin of the tangential velocity ratio, v/V (flow angle $\alpha = 0$). The error is greatest in the second calibration region (values of the tangential velocity ratio, v/V, less than -0.3) than in the first calibration region.

Figures 5-27 and 5-28 are plots of u/V versus v/V showing lines of constant C_α and C_β for the first and second calibration regions, respectively. It is apparent from the almost vertical C_α lines and almost horizontal C_β lines that C_α is almost independent of u/V and C_β almost independent of v/V in the first calibration region. The location of the C_β equal zero line in both Figures 5-27 and 5-28 gives the value of the flow angle β at which the

pressure coefficient C_β is nulled. The location of the C_α equal zero line in Figure 5-27 gives the value of the flow angle α at which the pressure coefficient C_α is nulled.

E. Total and Dynamic Pressures - Probe #2

Constant contours of C_o plotted against C_α and C_β are shown in Figures 5-29 and 5-30 for the first and second calibration regions, respectively. Figure 5-29 shows that, for small angles, P_5 gives an accurate reading of the actual total pressure. The larger the angle, the larger the difference between P_T and P_5. The constant contours of C_o are not perfectly circular in Figure 5-29 which indicates a degree of probe asymmetry. The relative flat section of the constant contours of C_o in Figure 5-30 for values of v/V near -0.25 show relative independence of P_5 on the flow angle β for large values of the flow angle α. The accuracy of the curve fit procedure for C_o is shown by the relative position of the labeled data points with respect to the lines of constant C_o.

Constant contours of C_q plotted against C_α and C_β are

shown in Figures 5-31 and 5-32 for the first and second calibration regions, respectively. Figure 5-31 shows that C_q has a maximum value for $C_\alpha = -0.07$ & $C_\beta = -0.08$ and that C_q has a saddle at about $C_\alpha = -0.3$ & $C_\beta = 0.24$. The elliptical shape of the contours and the saddle indicate a degree of physical asymmetry of the probe. Figure 5-32 shows contours that are extensions of ellipses for values of C_q greater than 0.5 and asymmetric contours for values of C_q less than 0.5. The accuracy of the curve fit for C_q is shown by the relative position of the labeled data points with respect to the lines of constant C_q .

F. Accuracy - Probe #2

Table 5-3 shows the average accuracy achieved over the 148 data points used in calibration for the four parameters and five variables of interest. With 95% certainty, Table 5-3 gives the accuracy in determining the listed variable from the five pressures measured by the probe. The total pressure is indicated to 3.0% of the dynamic pressure and the static pressure is indicated to 11.8% of the dynamic pressure. The velocity is indicated to 5.2% of the actual velocity. The axial momentum flux, M_z, is indicated to 9.0% of the actual momentum flux and

the tangential or angular momentum flux, M_θ, is indicated to 4.5% of the dynamic pressure. The flow angles are predicted to about the nearest 1.5 degrees.

TABLE 5-3

CENTRAL ACCURACY

PROBE # 2

Variable	1.96σ
C_o	0.054
C_q	0.062
u/V	1.5
v/V	1.3
P_T	.00136 psig
P_S	.00539 psig
V	3.90 ft/sec
M	9.0%
M_θ	.00206 psig

The accuracy of Probe #2, shown above, is significantly different than that of Probe #1, shown in Table 5-2, due to the very large range of flow angles that Probe #2 will measure. Probe #1's accuracy is for the approximate nulling of the flow angle α and Probe #2's accuracy includes values of the flow angle α as large as -50 degrees.

REFERENCES

1. Erwin, J.R., "Experimental Techniques", Aerodynamics of Turbines and Compressors, High Speed Aerodynamics and Jet Propulsion, Vol. X, Section D, Princeton, 1964.

2. Barker, K., Gallington, R., and Minster, S., "Calibration of Five-Hole Probes for On-Line Data Reduction", Aeronautics Digest, Spring 1979, USAFA-TR-79-7, USAF Academy, CO, July 1979.

3. Dring, R.P., Joslyn, H.D., and Hardin, l.w., "Experimental Investigation of Compressor Rotor Wakes", United Technologies Research Center Technical Report AFAPL-TR-79-2107, Jan 1980.

4. Gallington, R.W. and Hollenbaugh, C.F., "A Fast Method for Accurate Manufacture of Small Five-Hole Probes", Aeronautics Digest, Spring 1979, USAFA-TR-79-7, USAF Academy, CO, July 1979.

5. Neter, J. and Wasserman, W., Applied Linear Statistical Models, Homewood, IL, Richard D. Irvin Inc., 1974.

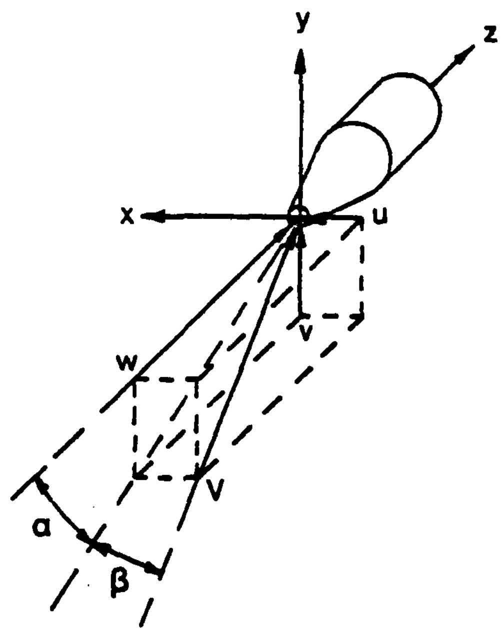

$u = V \sin\beta$
$v = V \sin\alpha \cos\beta$
$w = V \cos\alpha \cos\beta$

Figure 5-1 Body-Fixed Co-ordinate System

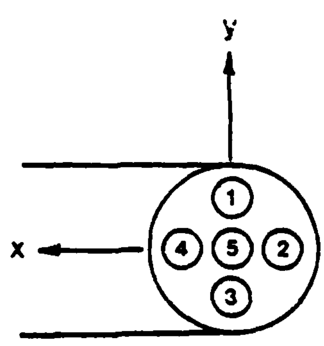

Figure 5-2 Port Numbering System

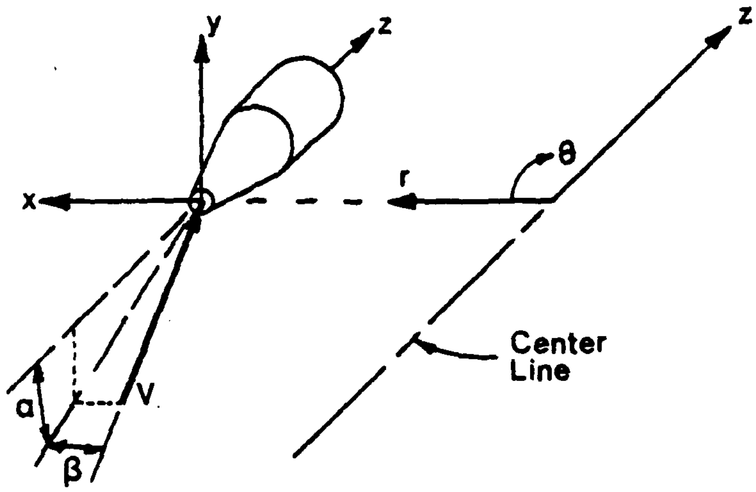

Figure 5-3a Alignment of Body-Fixed and Axisymmetric Coordinate Systems

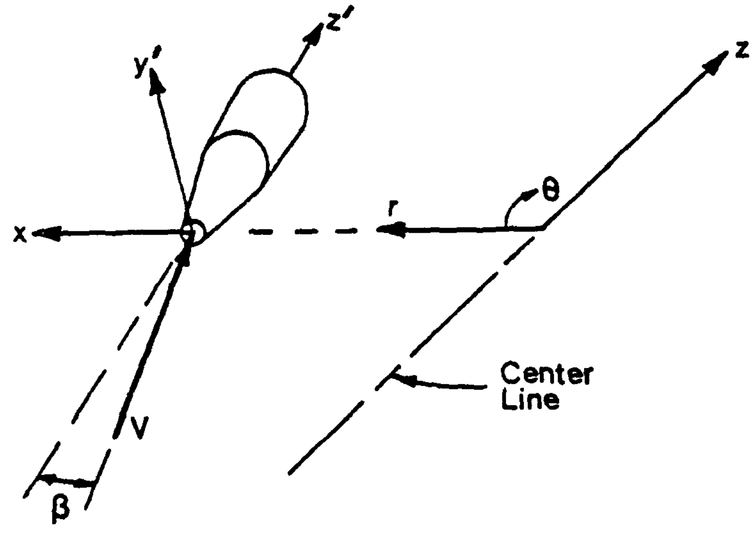

Figure 5-3b Probe Rotated to Null Flow Angle

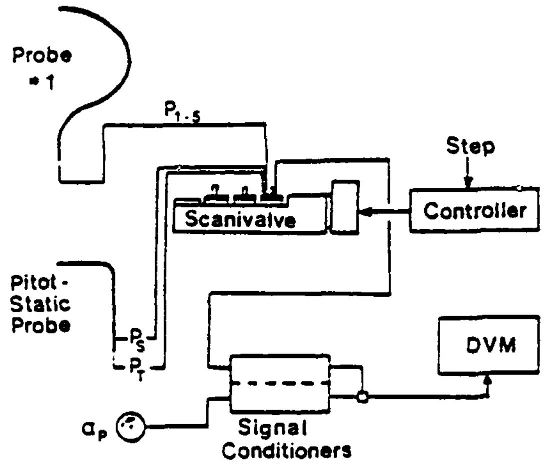

Figure 5-4a Calibration Instrumentation for Probe #1

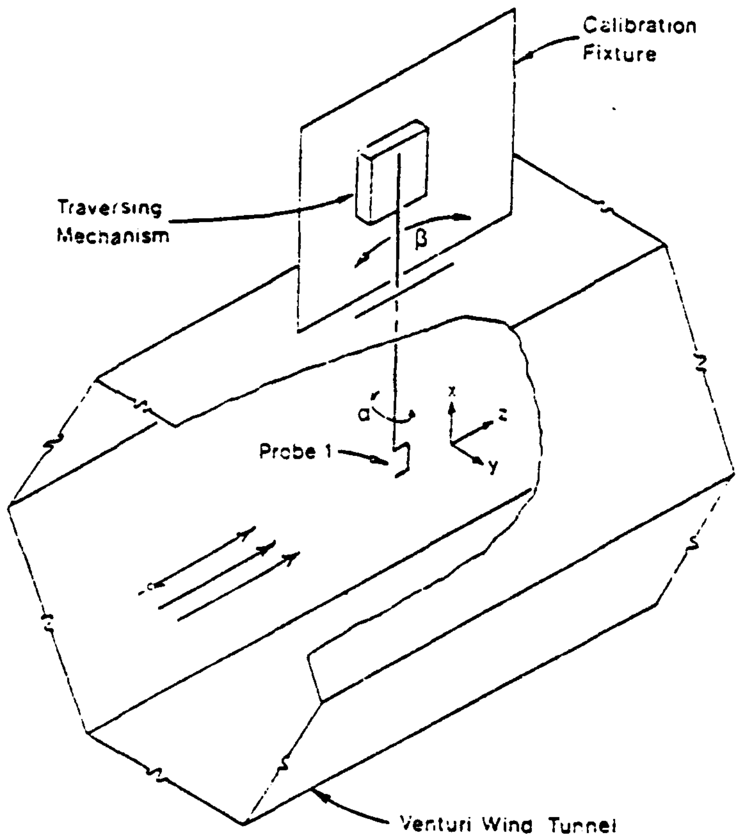

Figure 5-4b Calibration System for Probe #1

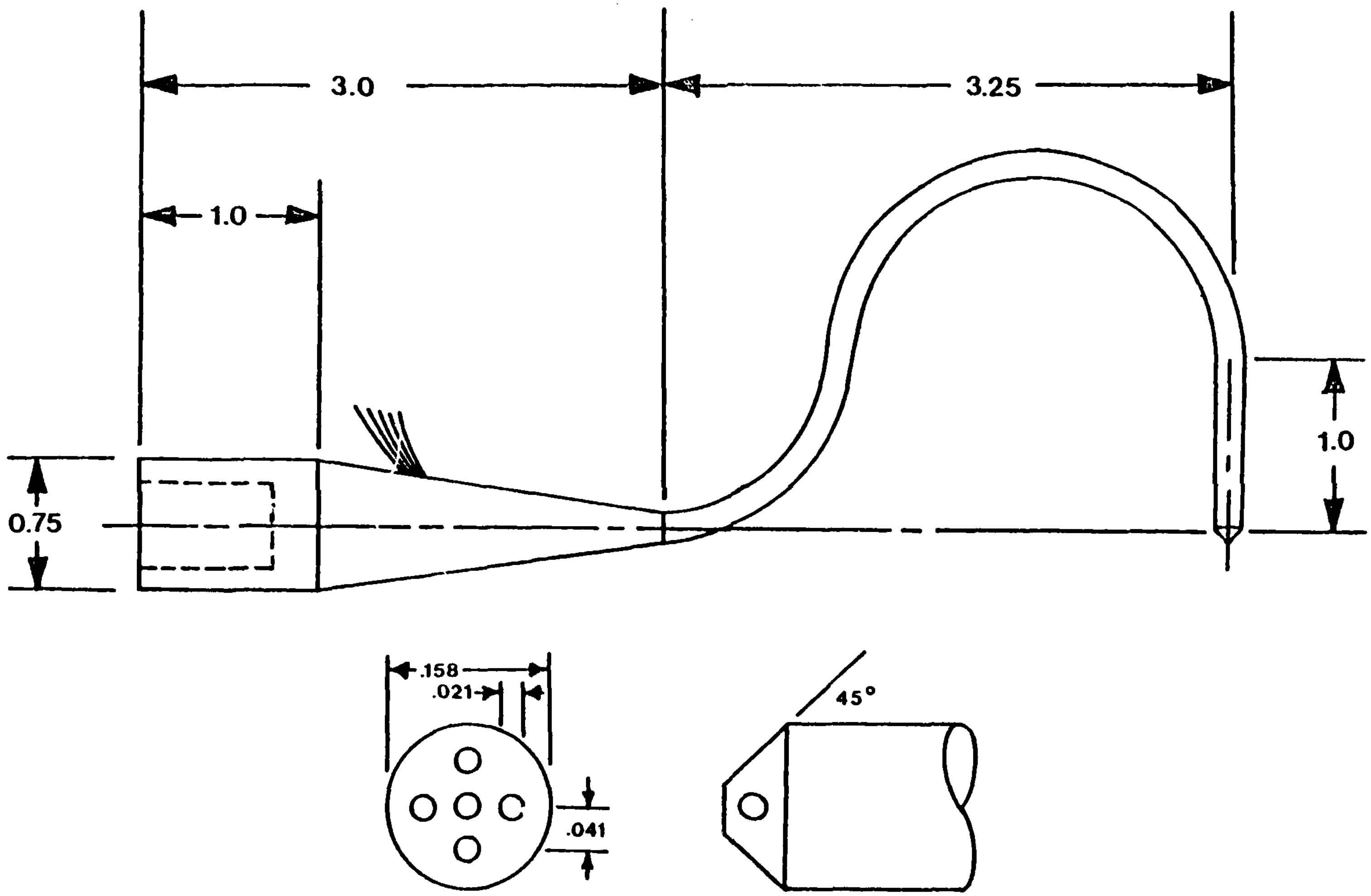

Figure 5-5 Dimensions of Probe #1

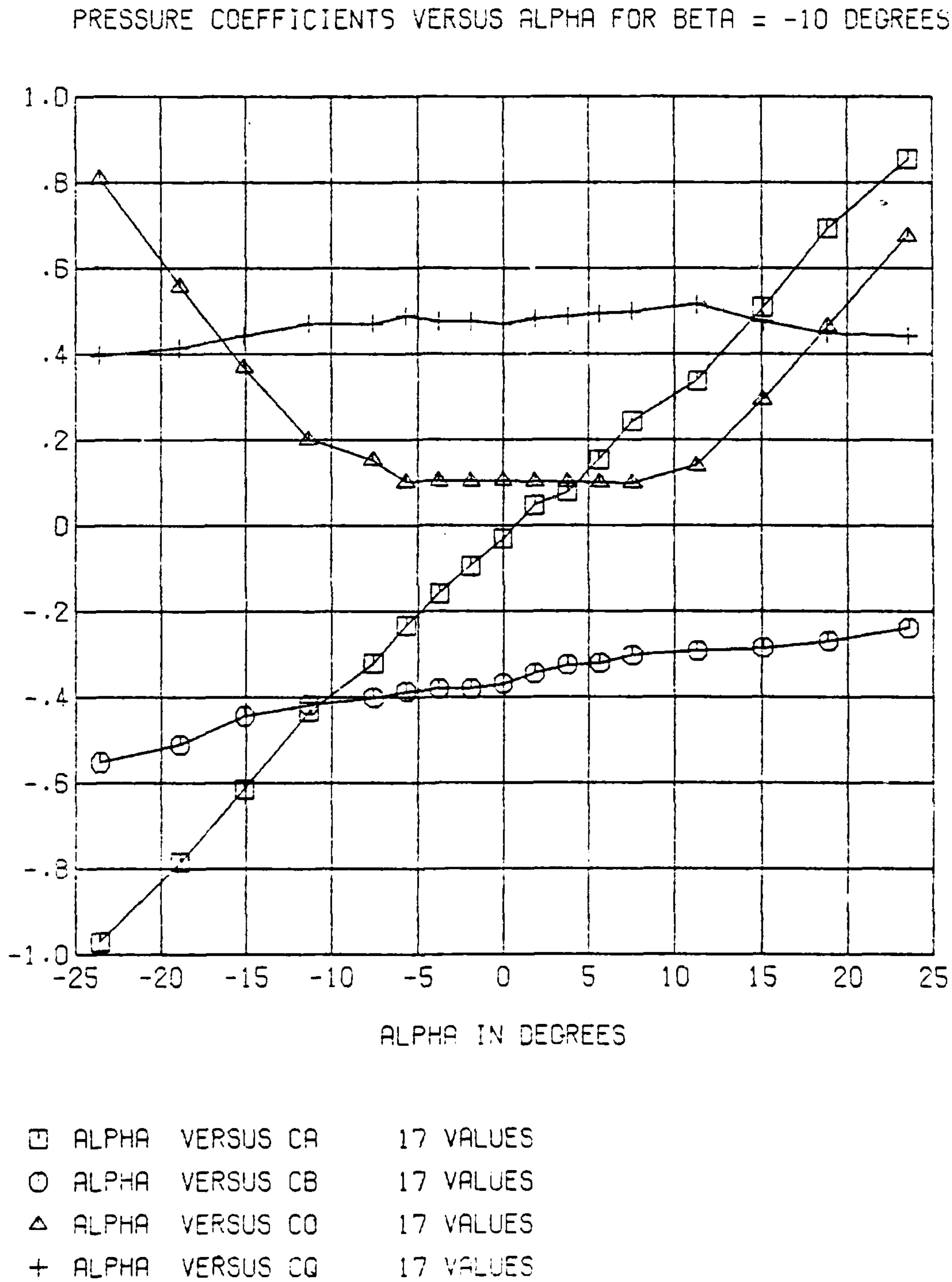

Figure 5-6 Pressure Coefficients for Probe #1, β=-10

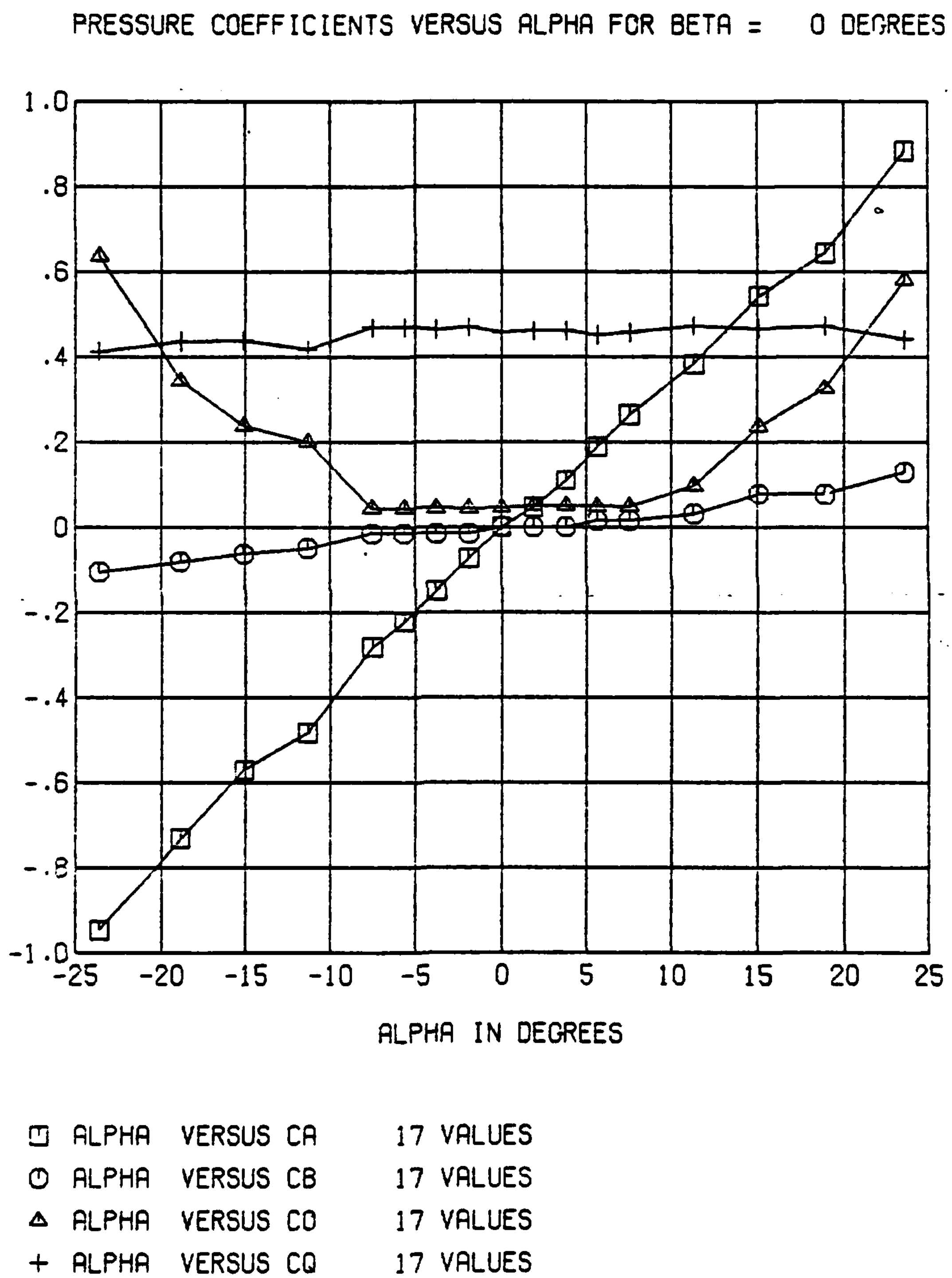

Figure 5-7 Pressure Coefficients for Probe #1, β= 0

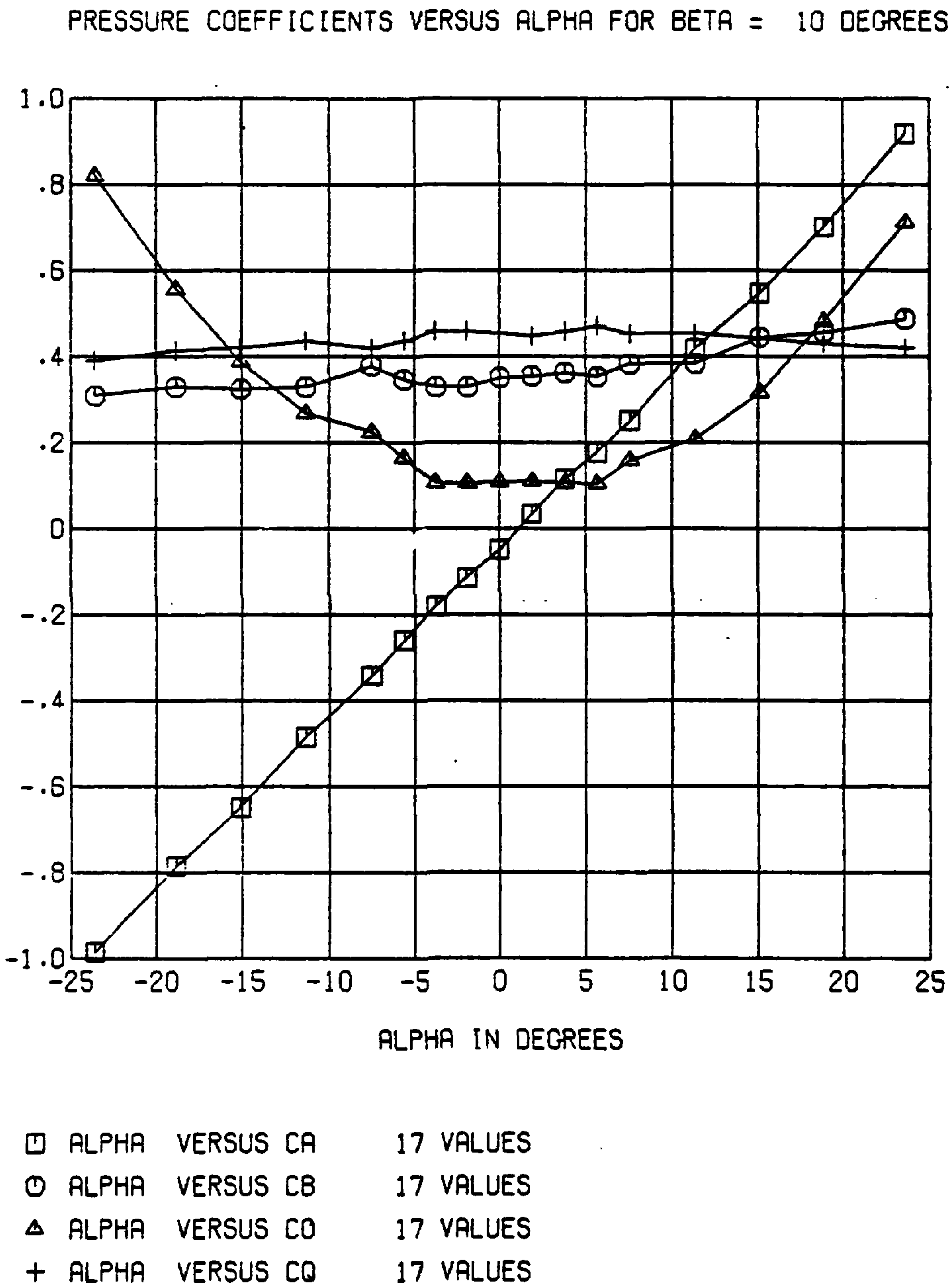

Figure 5-8 Pressure Coefficients for Probe #1, ß = 10

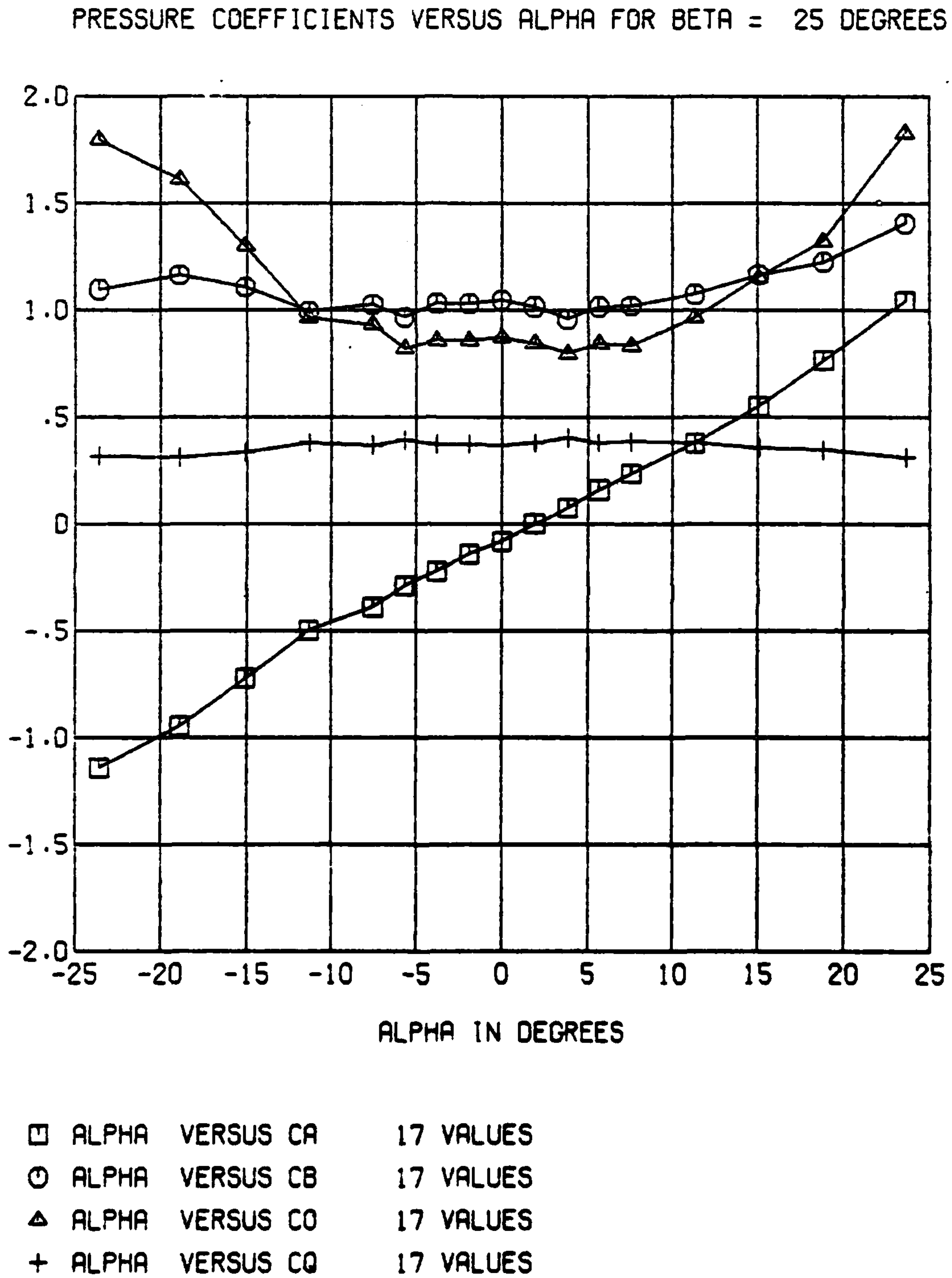

Figure 5-9 Pressure Coefficients for Probe #1, β = 25

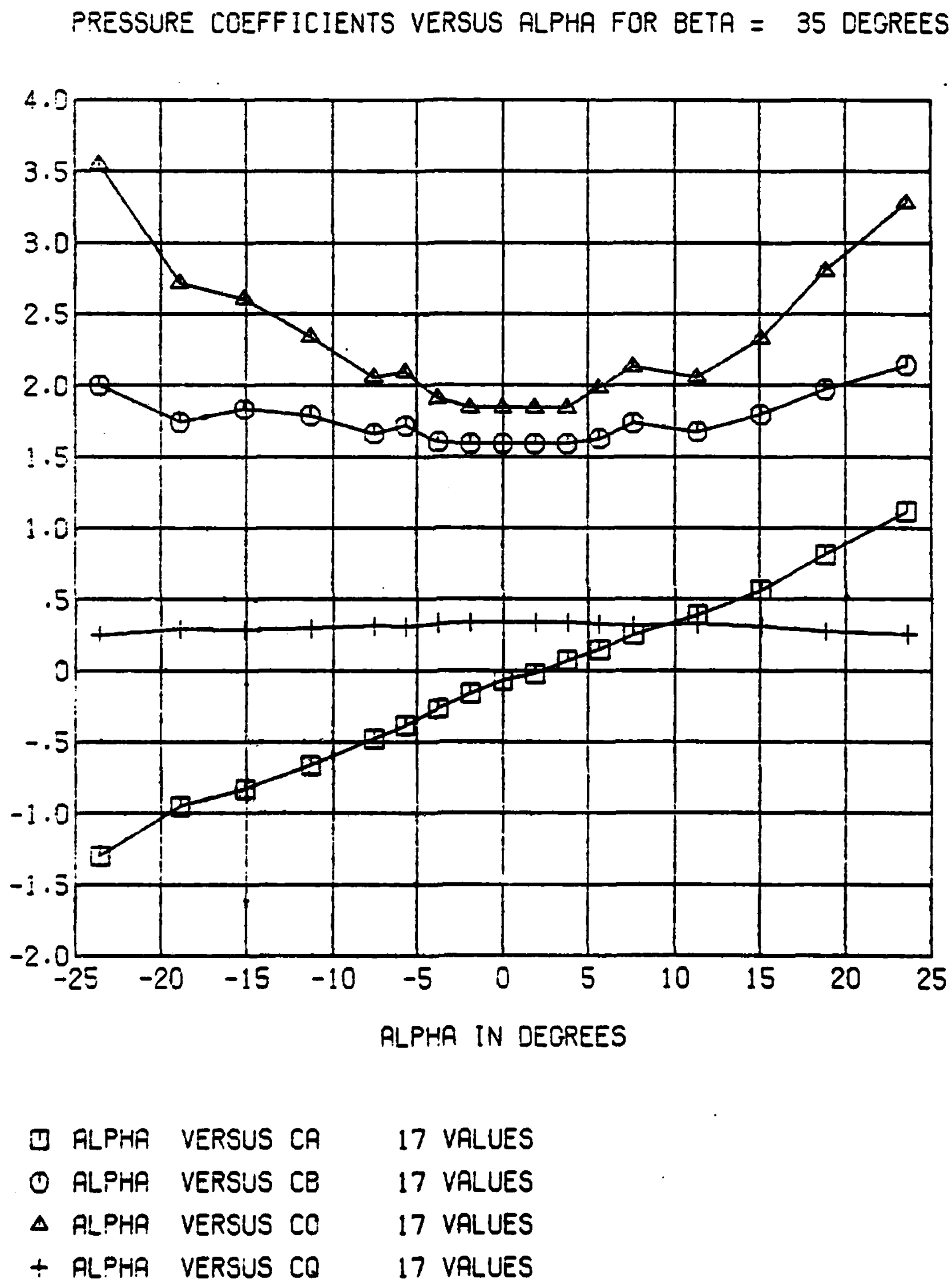

Figure 5-10 Pressure Coefficients for Probe #1, β = 35

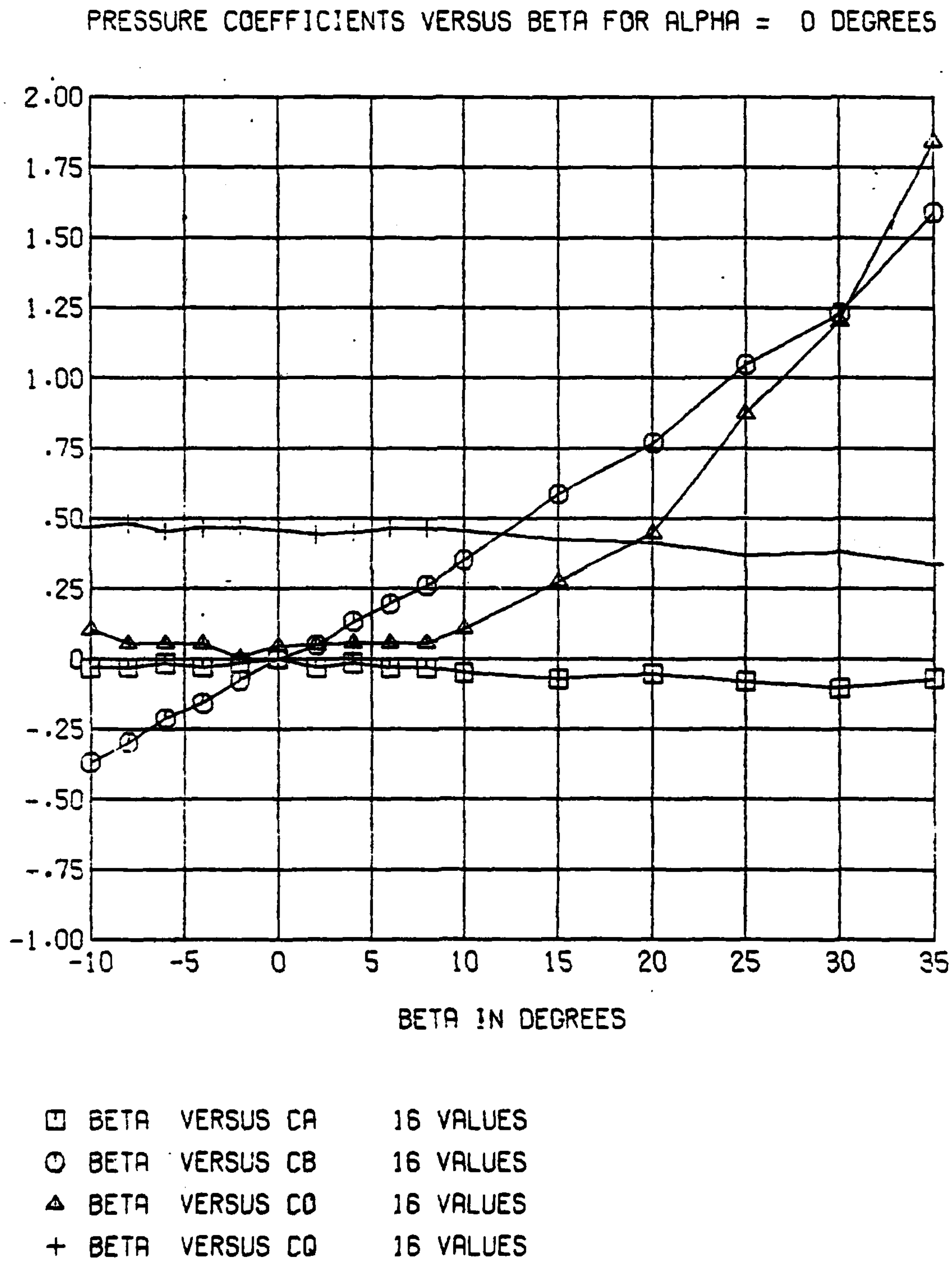

Figure 5-11 Pressure Coefficients for Probe #1, $\alpha = 0$

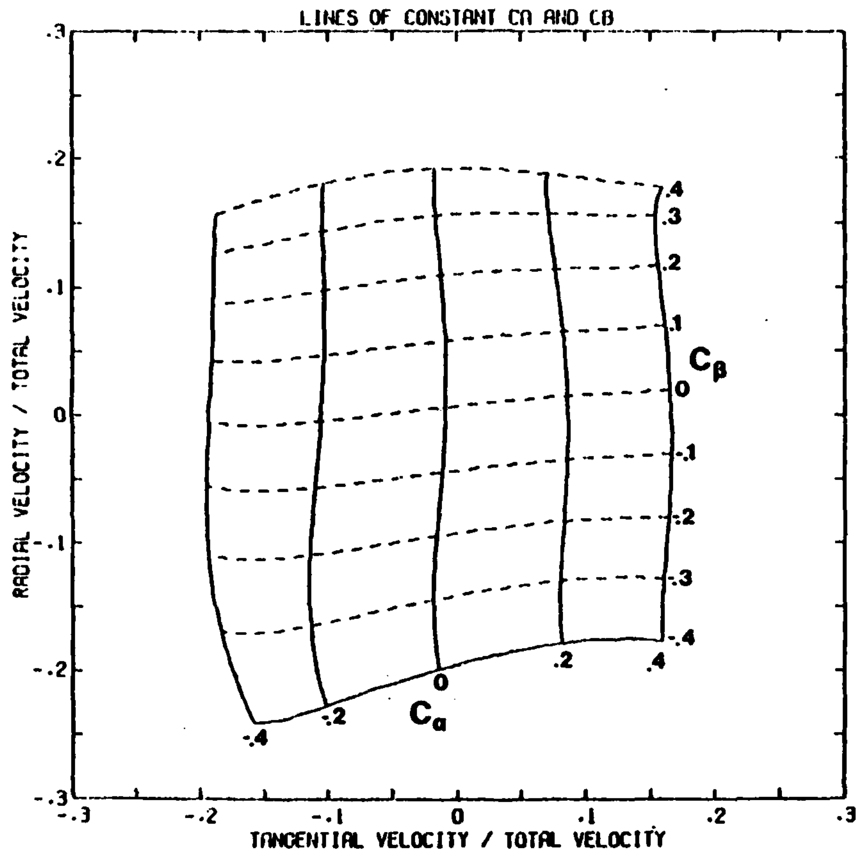

Figure 5-12 Constant C_α and C_β Contour Lines, Probe #1, Calibration Region #1

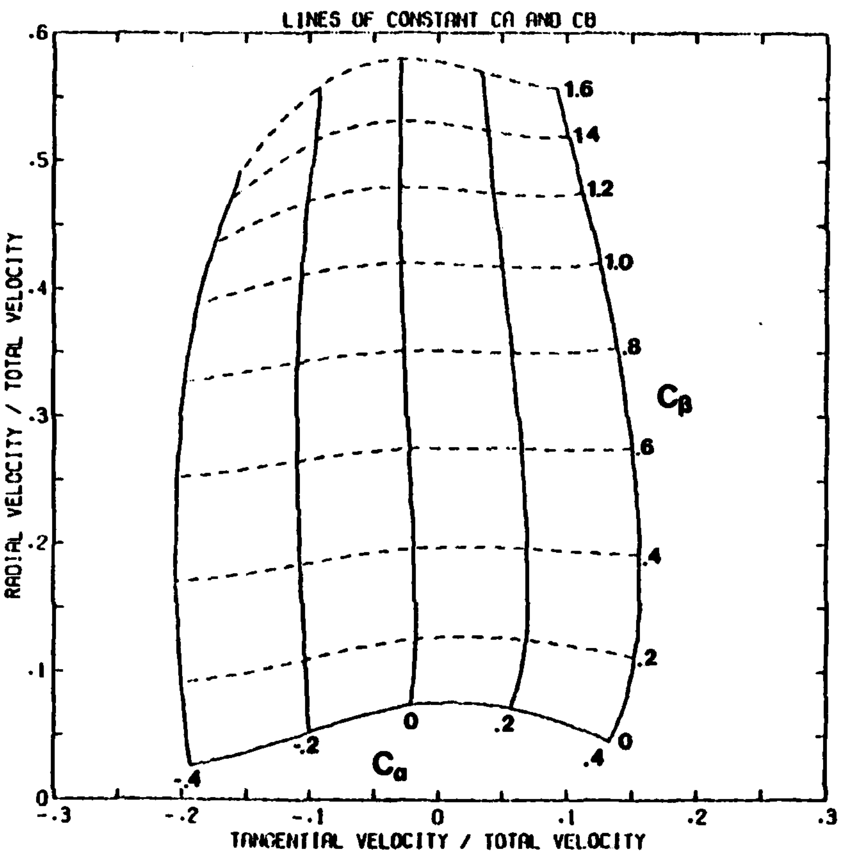

Figure 5-13 Constant C_α and C_β Contour Lines, Probe #1, Calibration Region #2

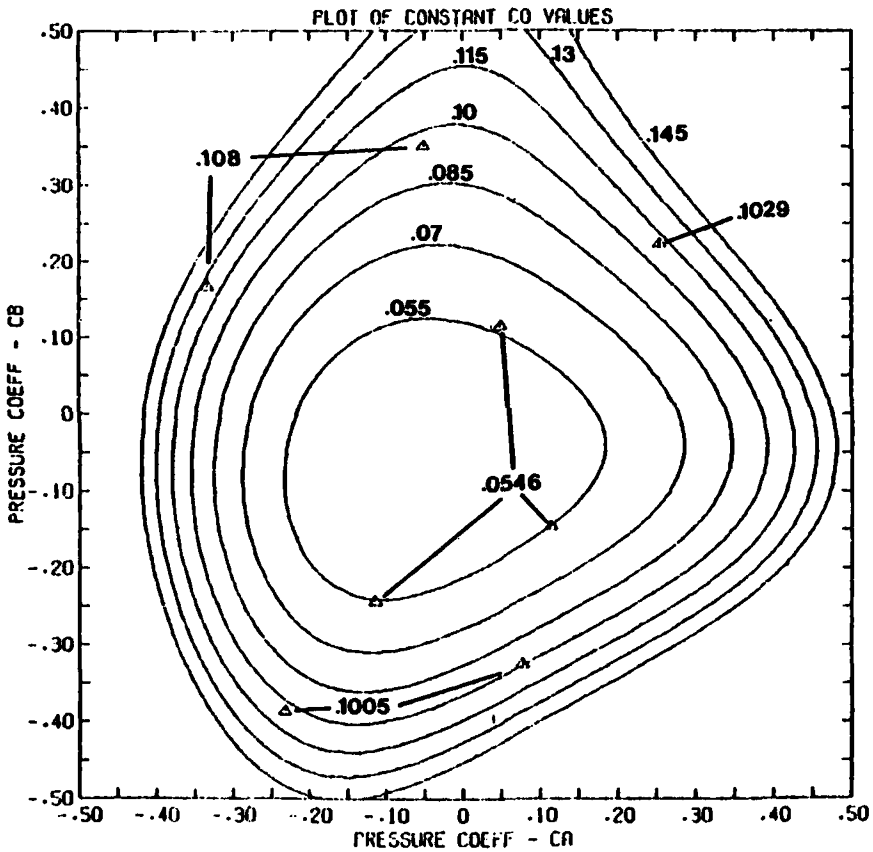

Figure 5-14 Constant C_o Contour Lines, Probe #1, Calibration Region #1

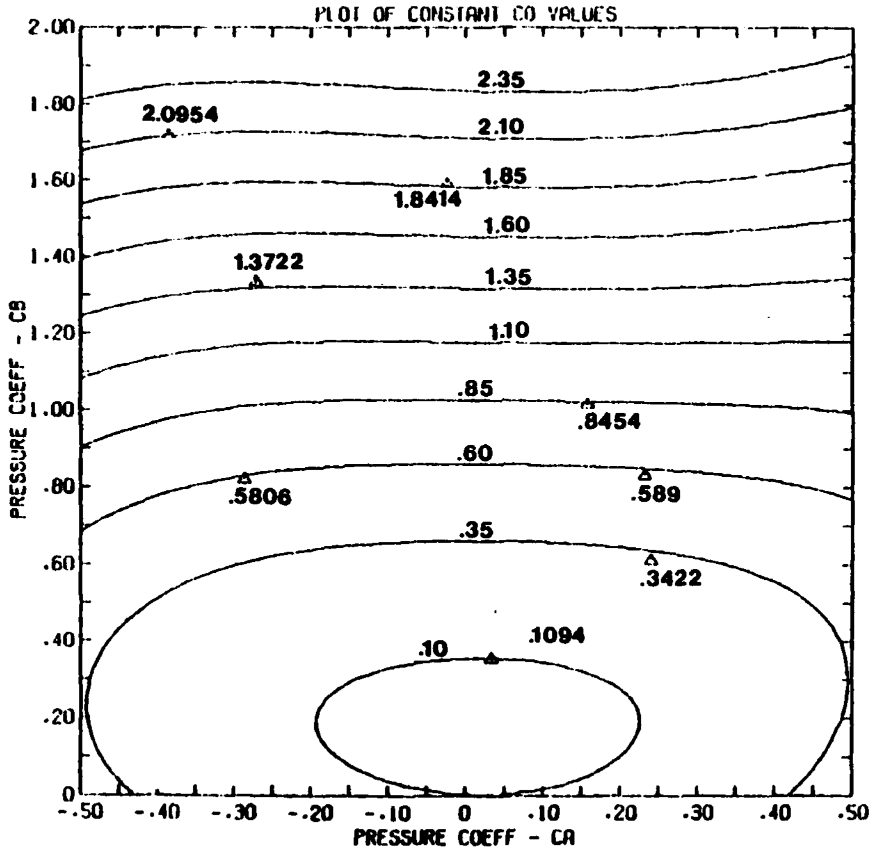

Figure 5-15 Constant C_o Contour Lines, Probe #1, Calibration Region #2

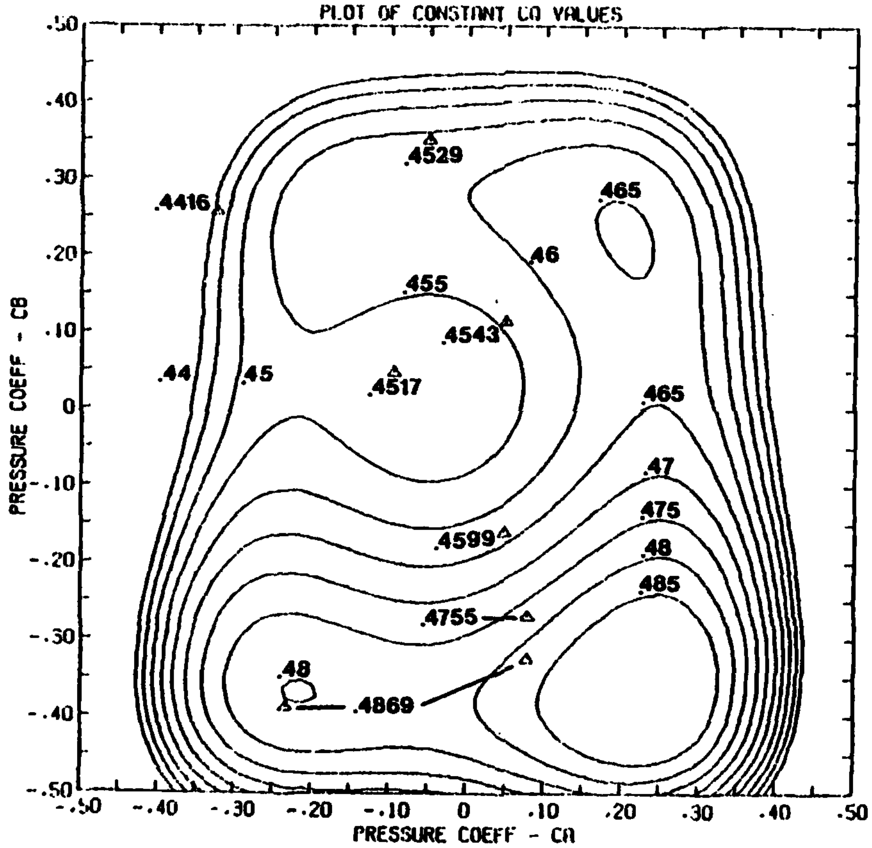

Figure 5-16 Constant C_q Contour Lines, Probe #1, Calibration Region #1

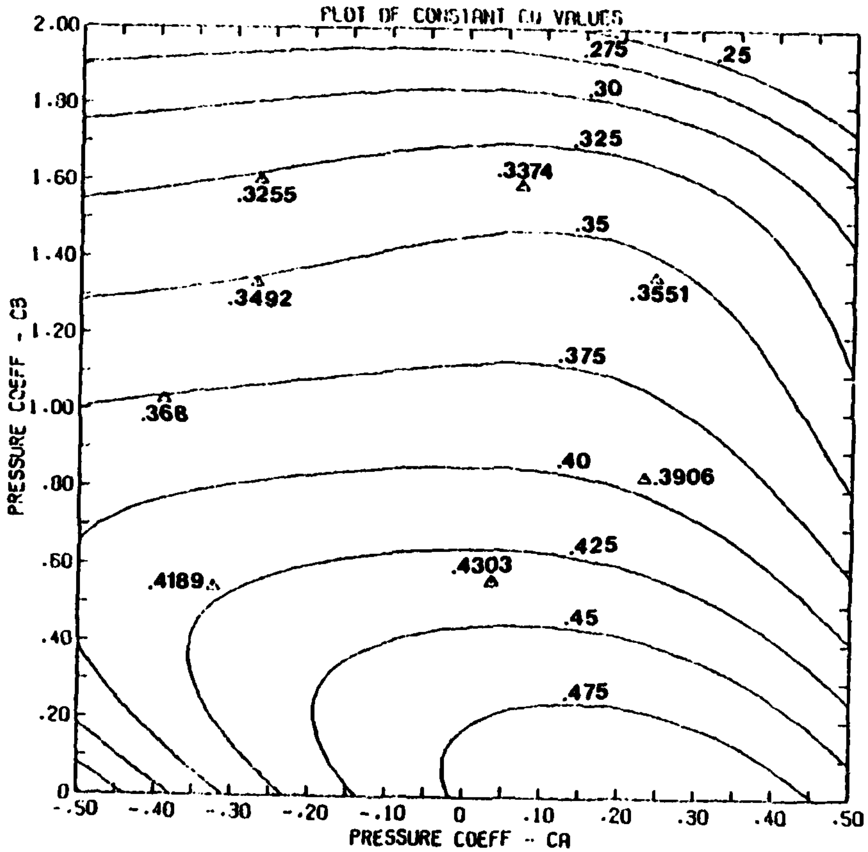

Figure 5-17 Constant C_q Contour Lines, Probe #1, Calibration Region #2

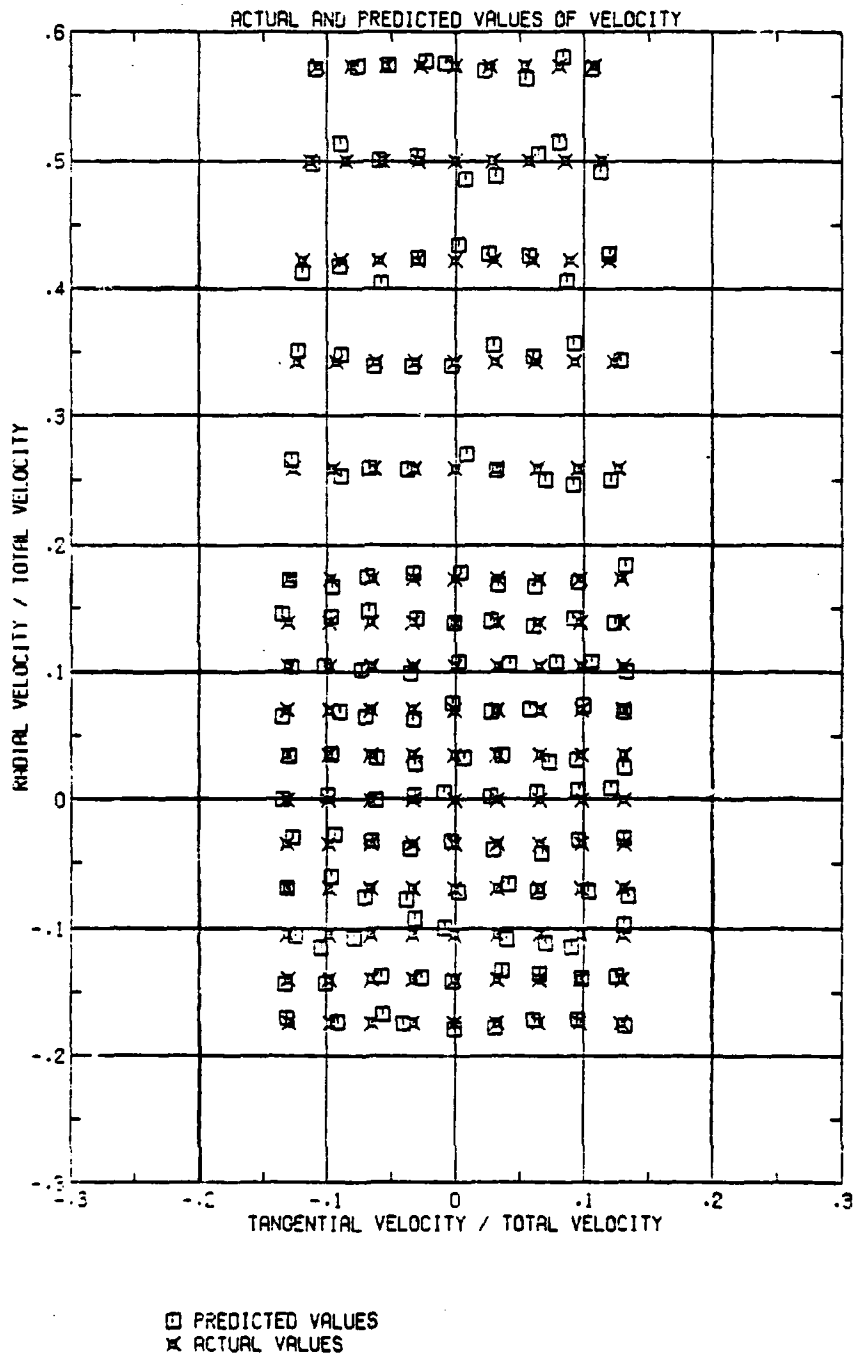

Figure 5-18 Actual and Predicted Values of u/V and v/V for Probe #1

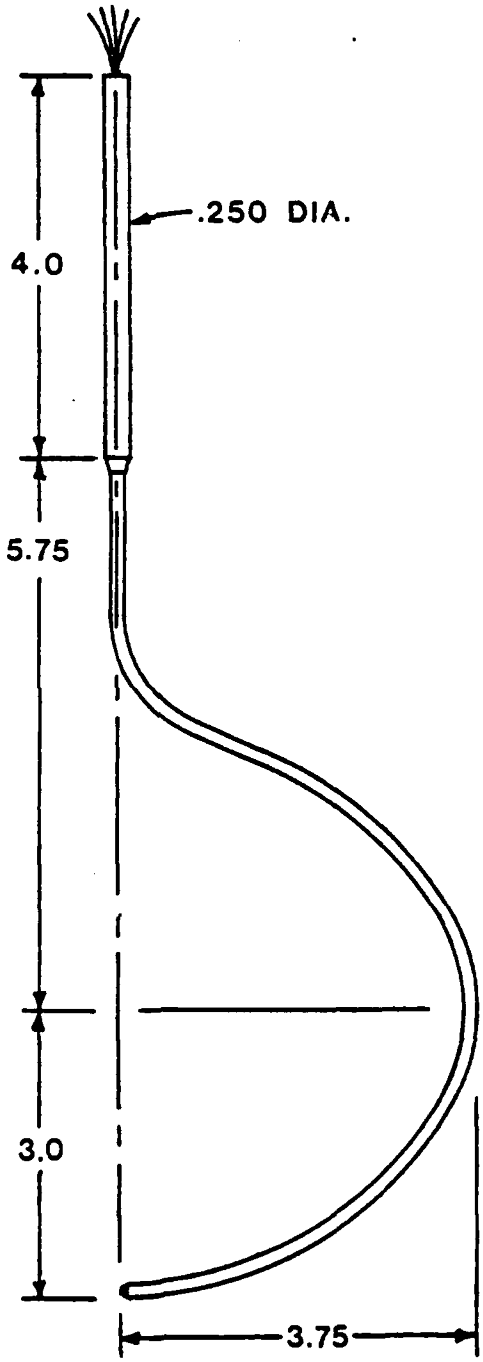

Figure 5-19 Dimensions of Probe #2

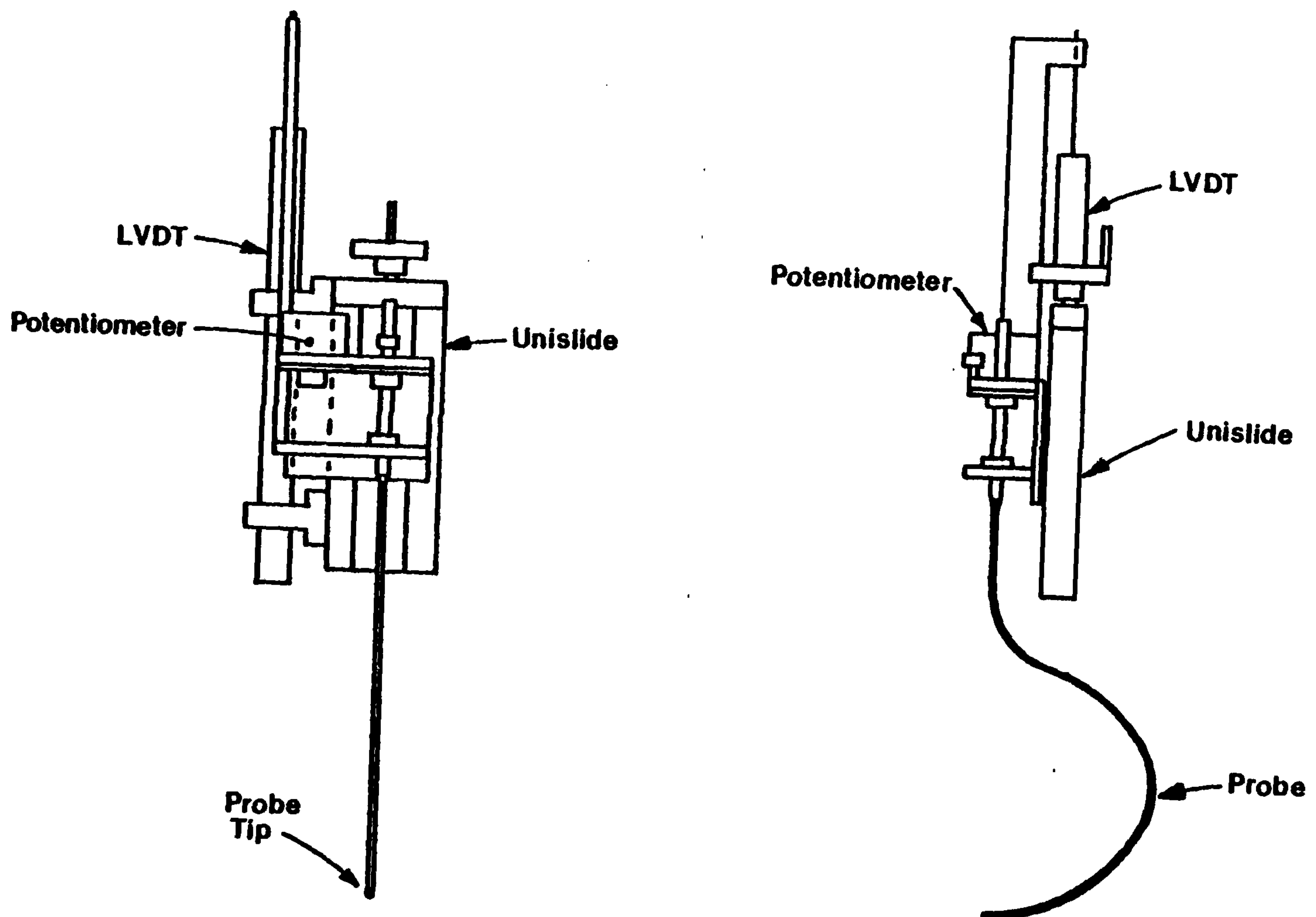

Figure 5-20 Probe #2 and Traversing Mechanism for Calibration

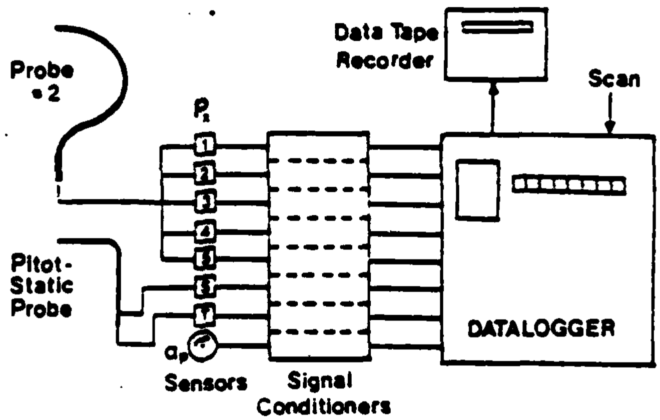

Figure 5-21a Calibration Instrumentation for Probe #2

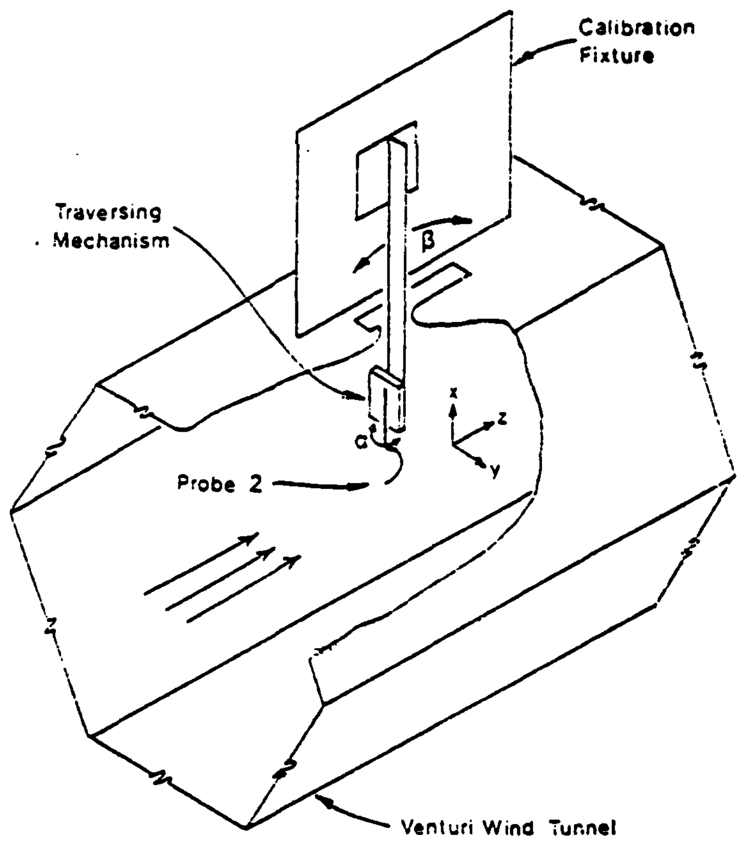

Figure 5-21b Calibration System for Probe #2

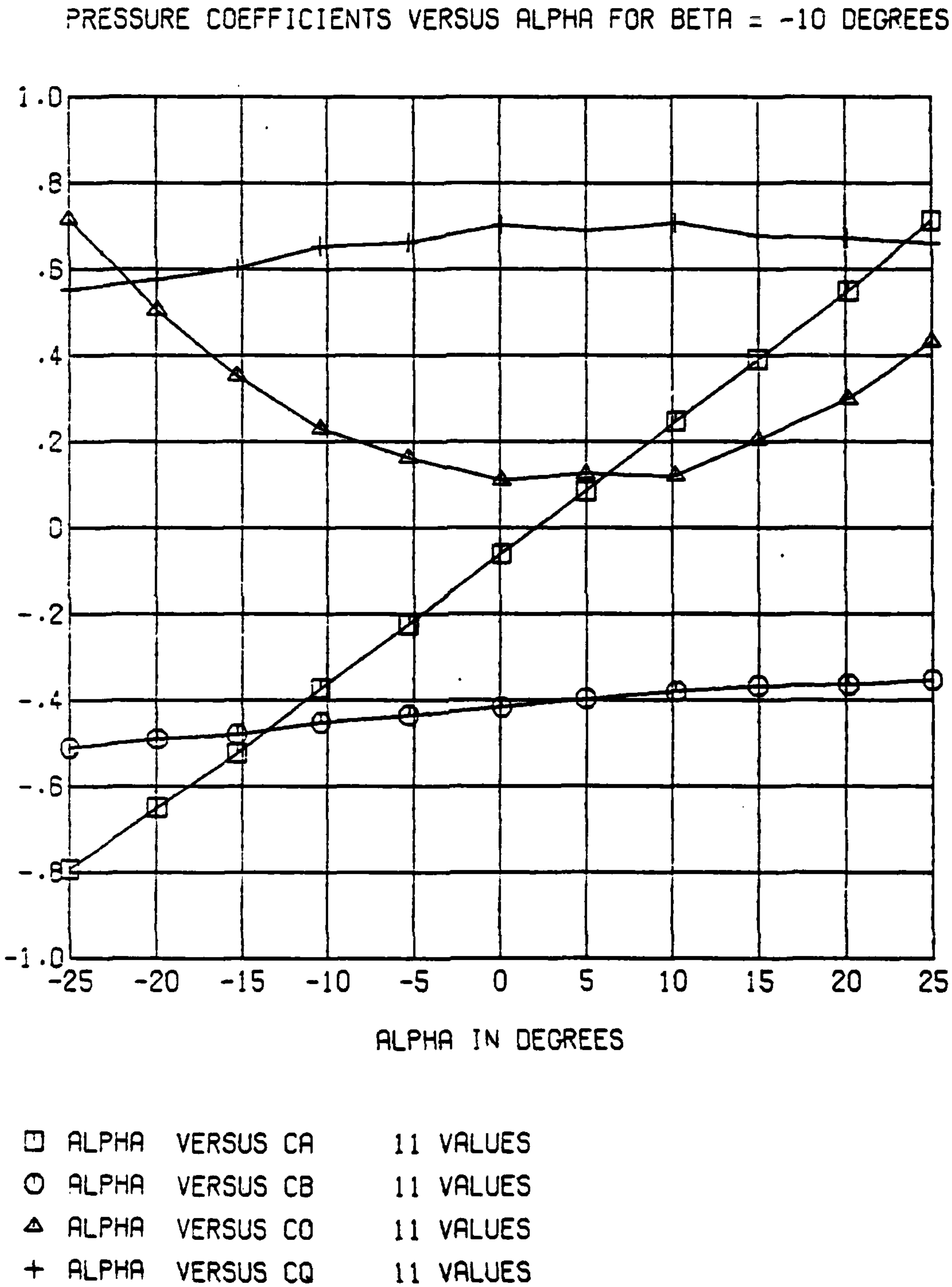

Figure 5-22 Pressure Coefficients for Probe #2, β=-10

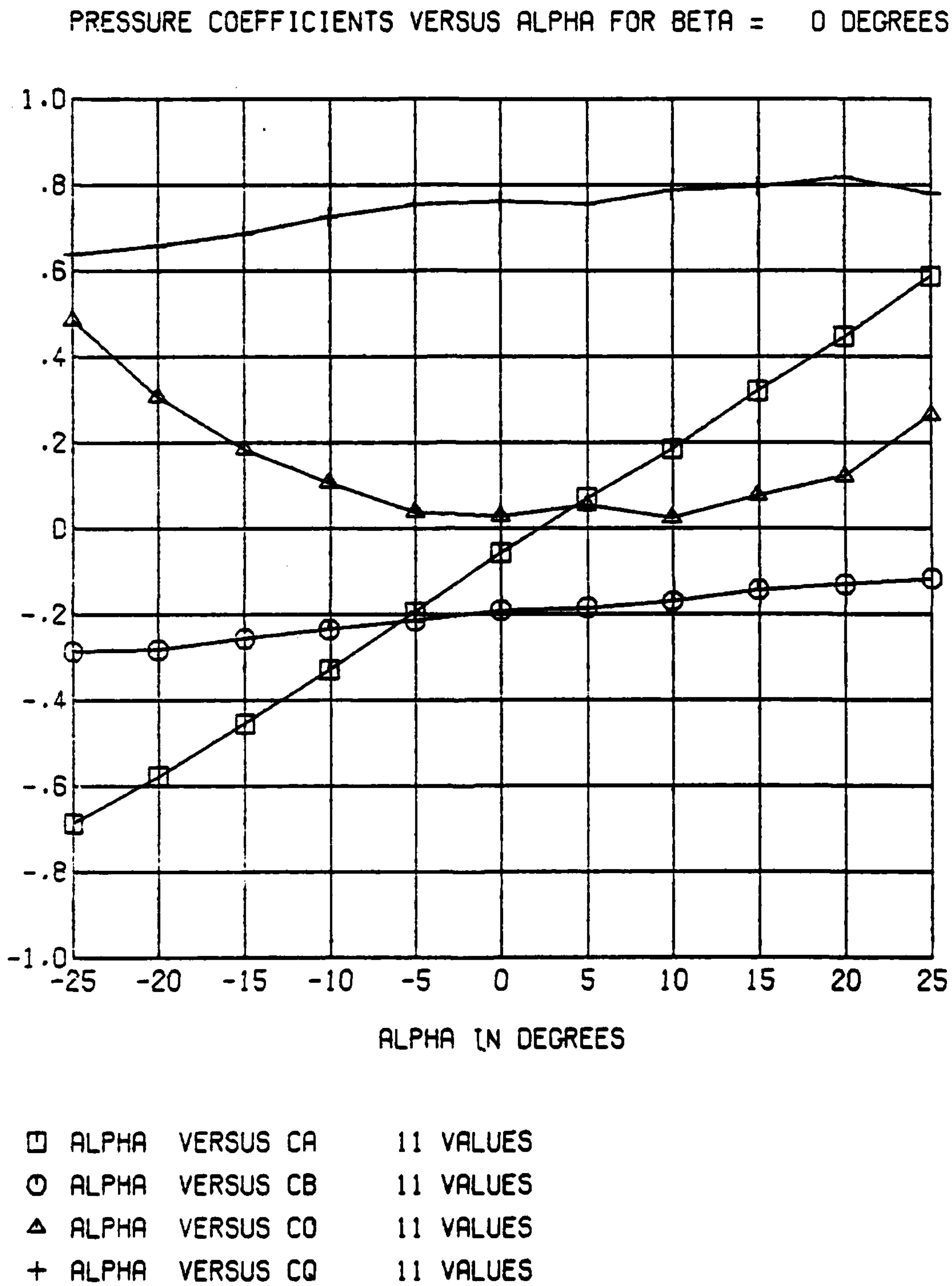

Figure 5-23 Pressure Coefficients for Probe #2, β = 0

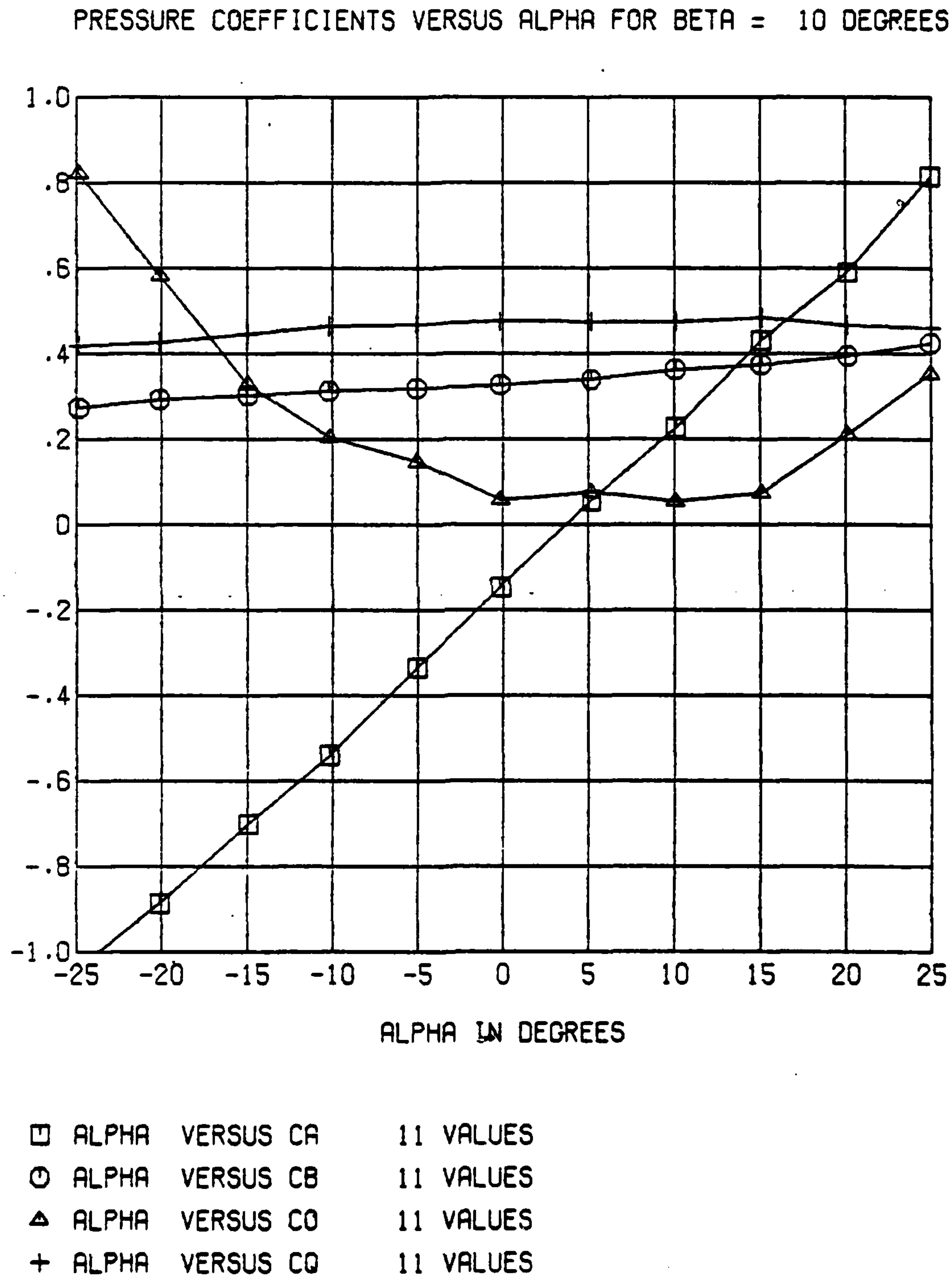

Figure 5-24 Pressure Coefficients for Probe #2, β = 10

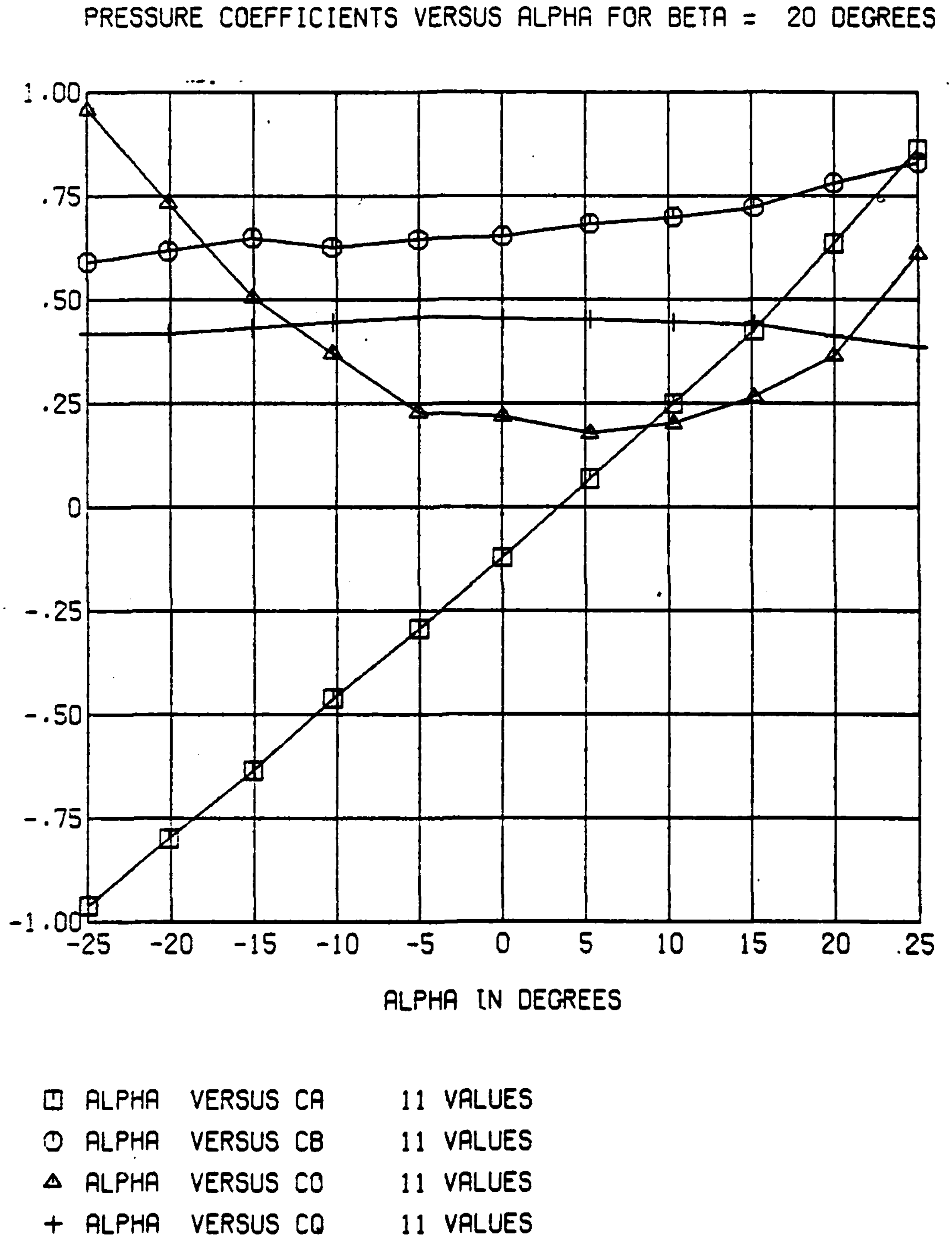

Figure 5-25 Pressure Coefficients for Probe #2, β = 20

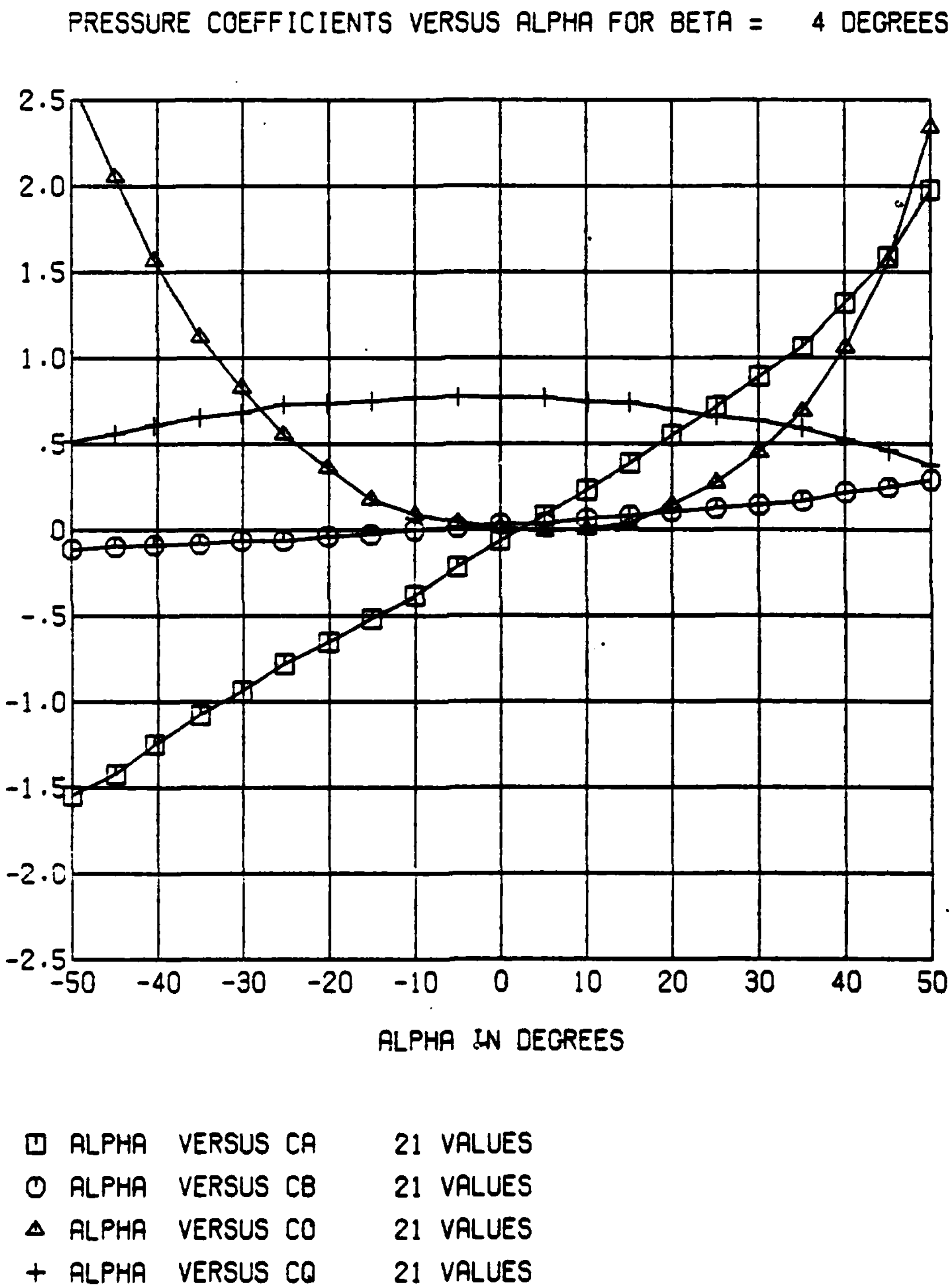

Figure 5-26 Pressure Coefficients for Probe #2, β = 4, Large Variation in α's

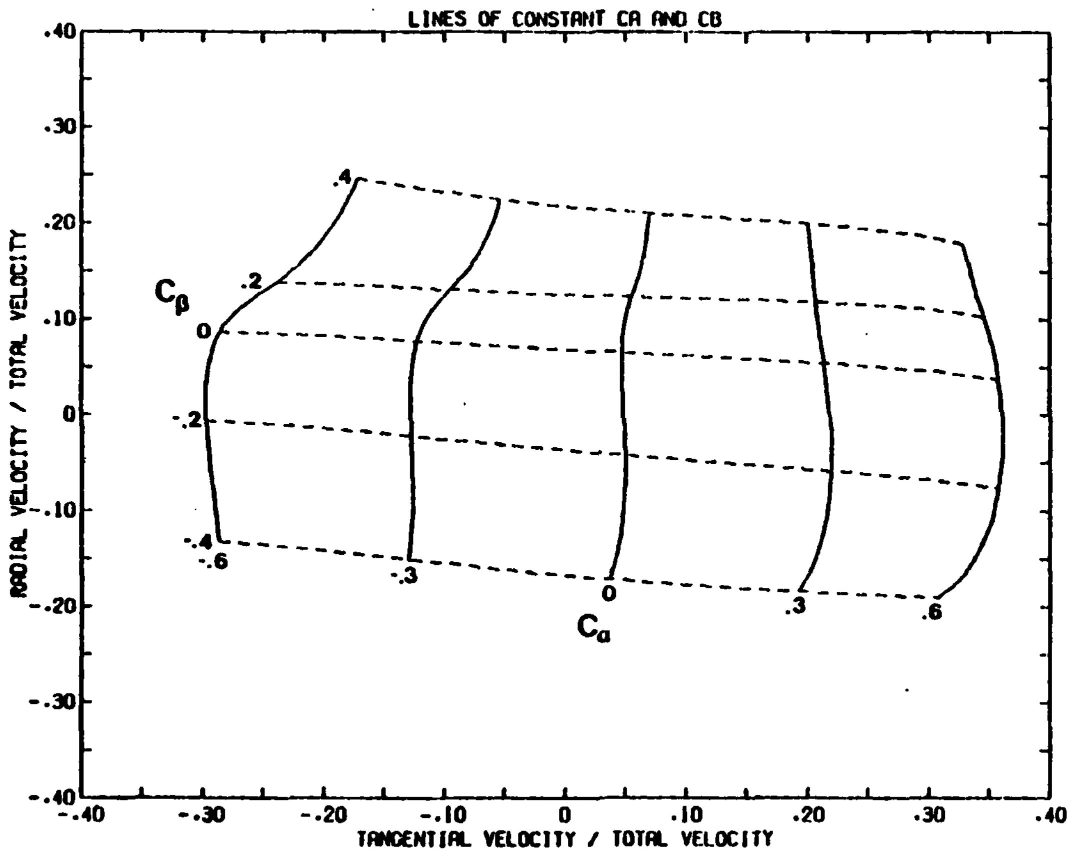

Figure 5-27 Constant C_α and C_β Contour Lines, Probe #2, Calibration Region #1

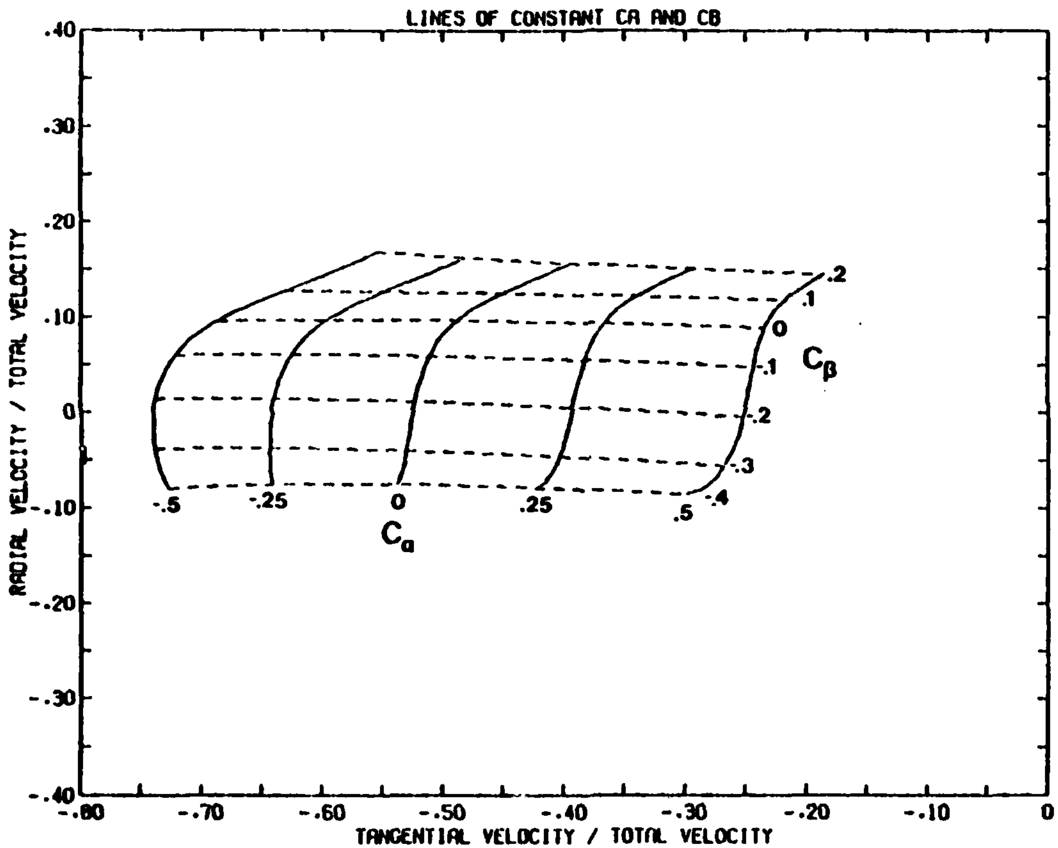

Figure 5-28 Constant C_α and C_β Contour Lines, Probe #2, Calibration Region #2

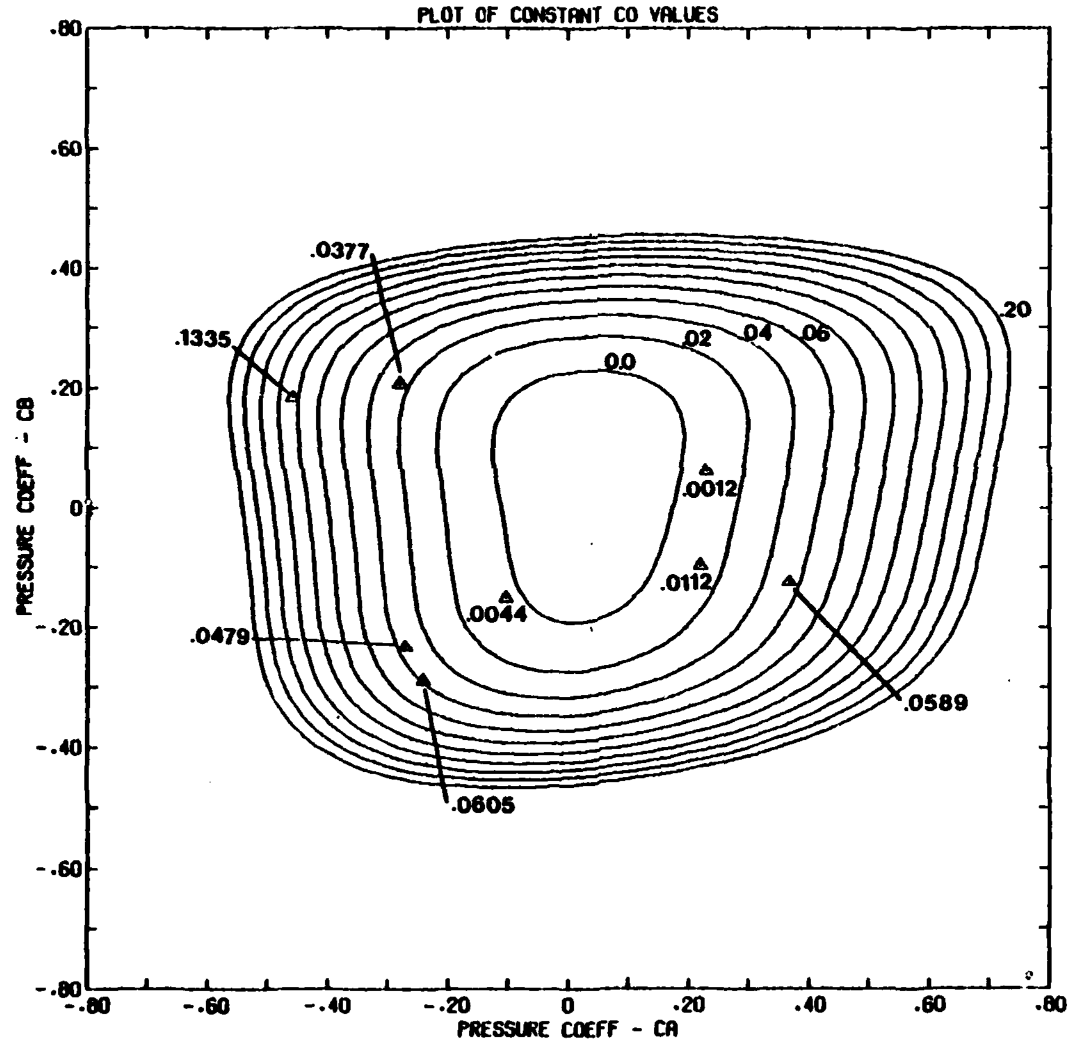

Figure 5-29 Constant C_o Contour Lines, Probe #2, Calibration Region #1

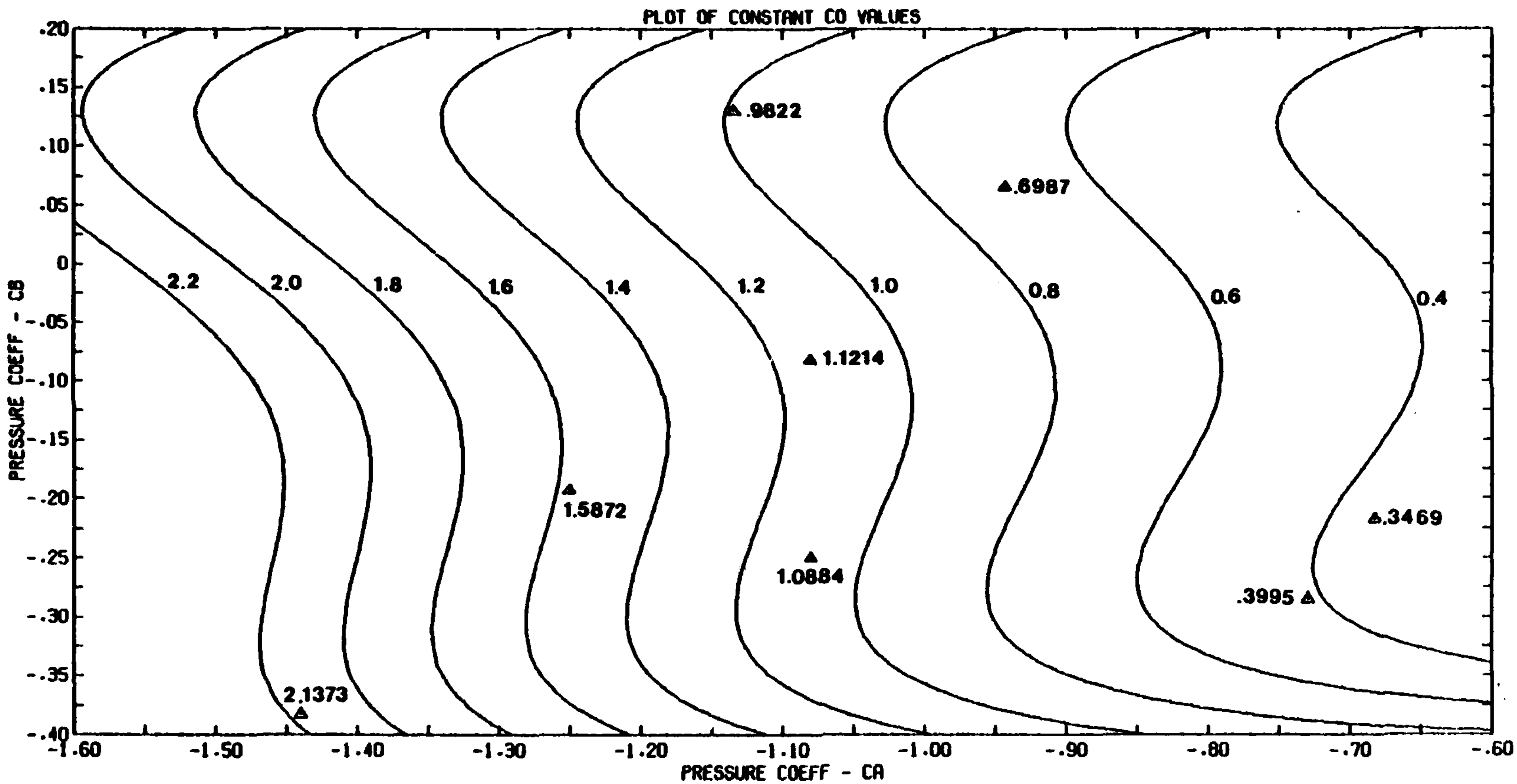

Figure 5-3Ø Constant C_o Contour Lines, Probe #2, Calibration Region #2

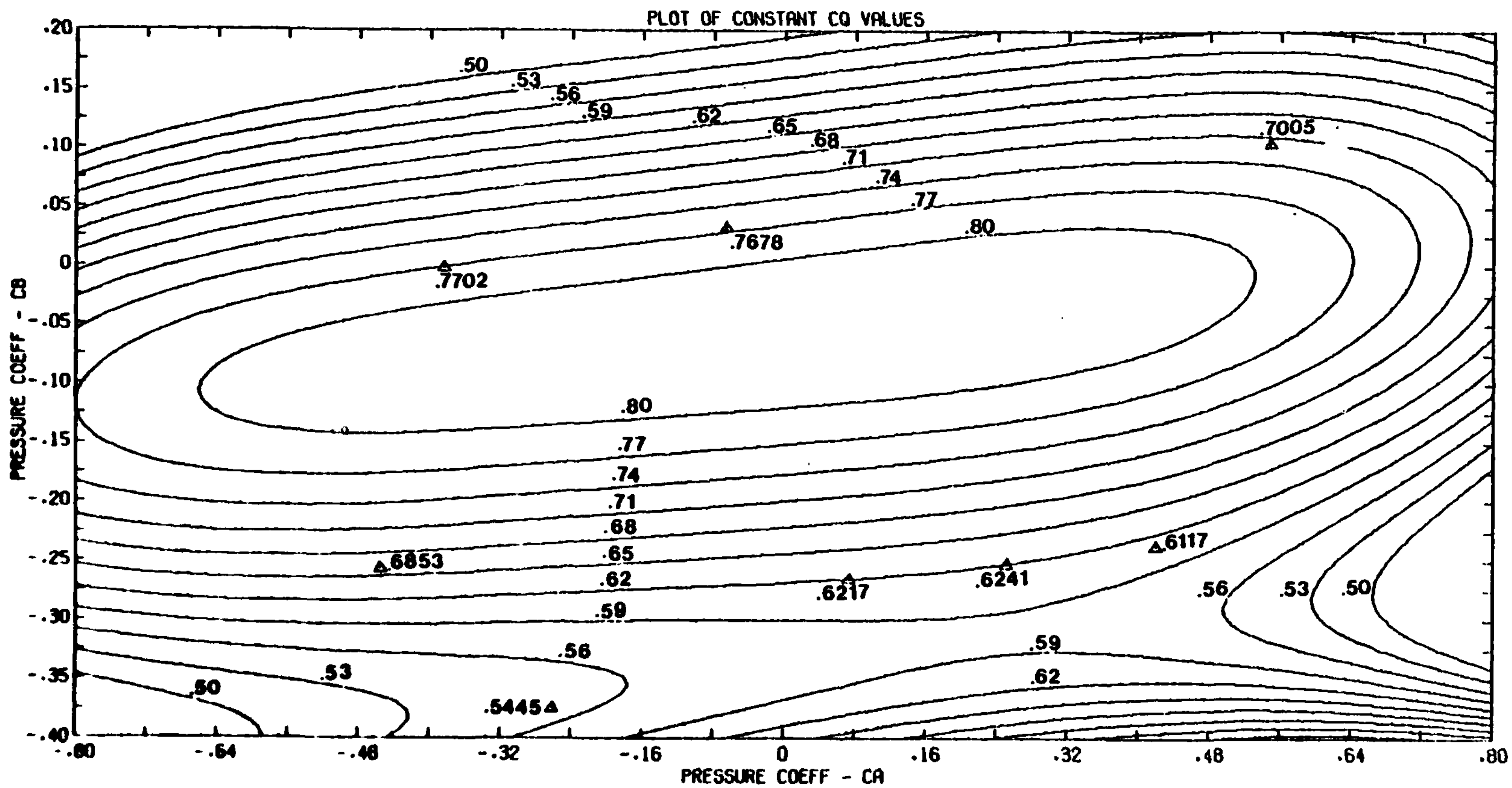

Figure 5-31 Constant C_q Contour Lines, Probe #2, Calibration Region #1

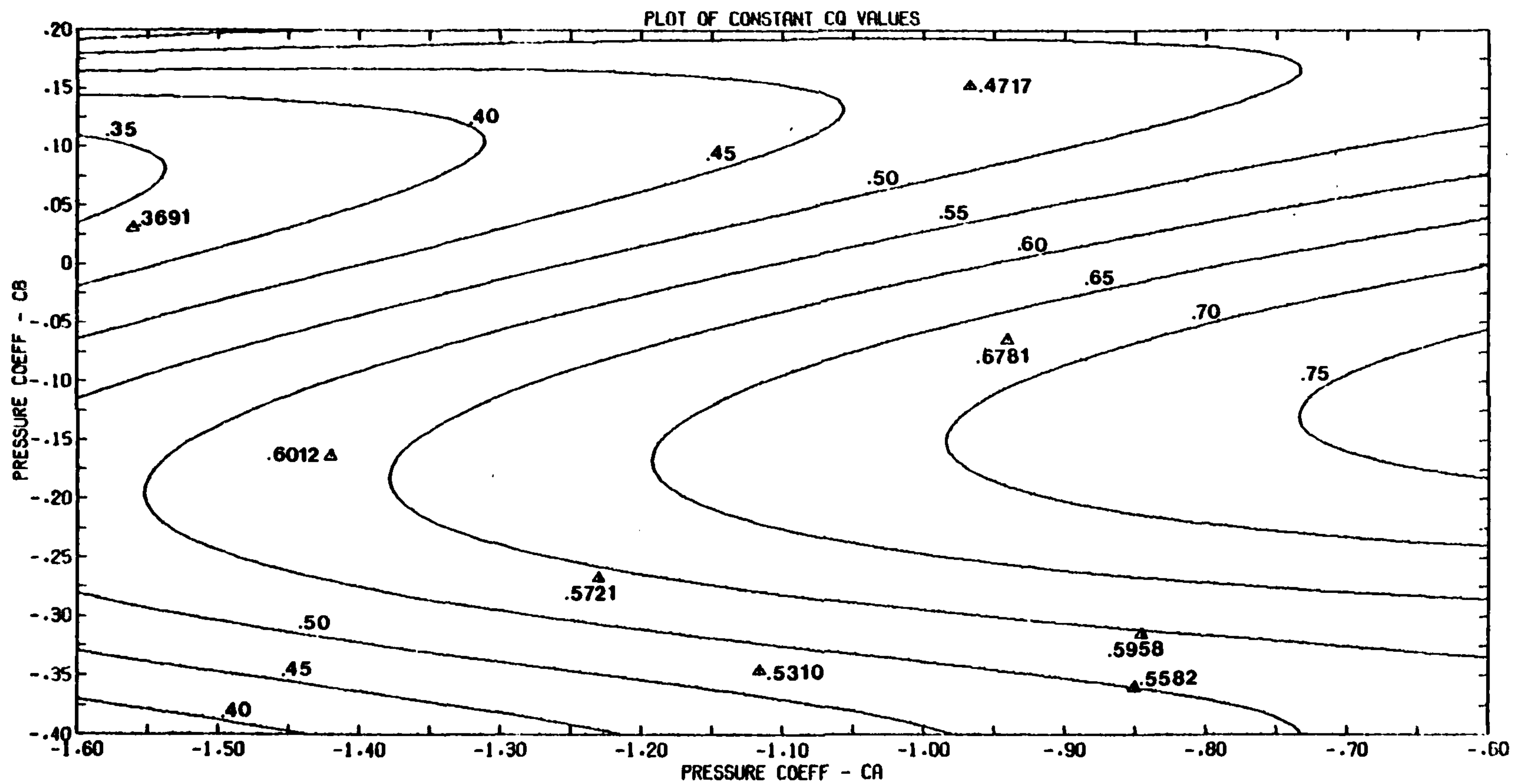

Figure 5-32 Constant C_q Contour Lines, Probe #2, Calibration Region #2

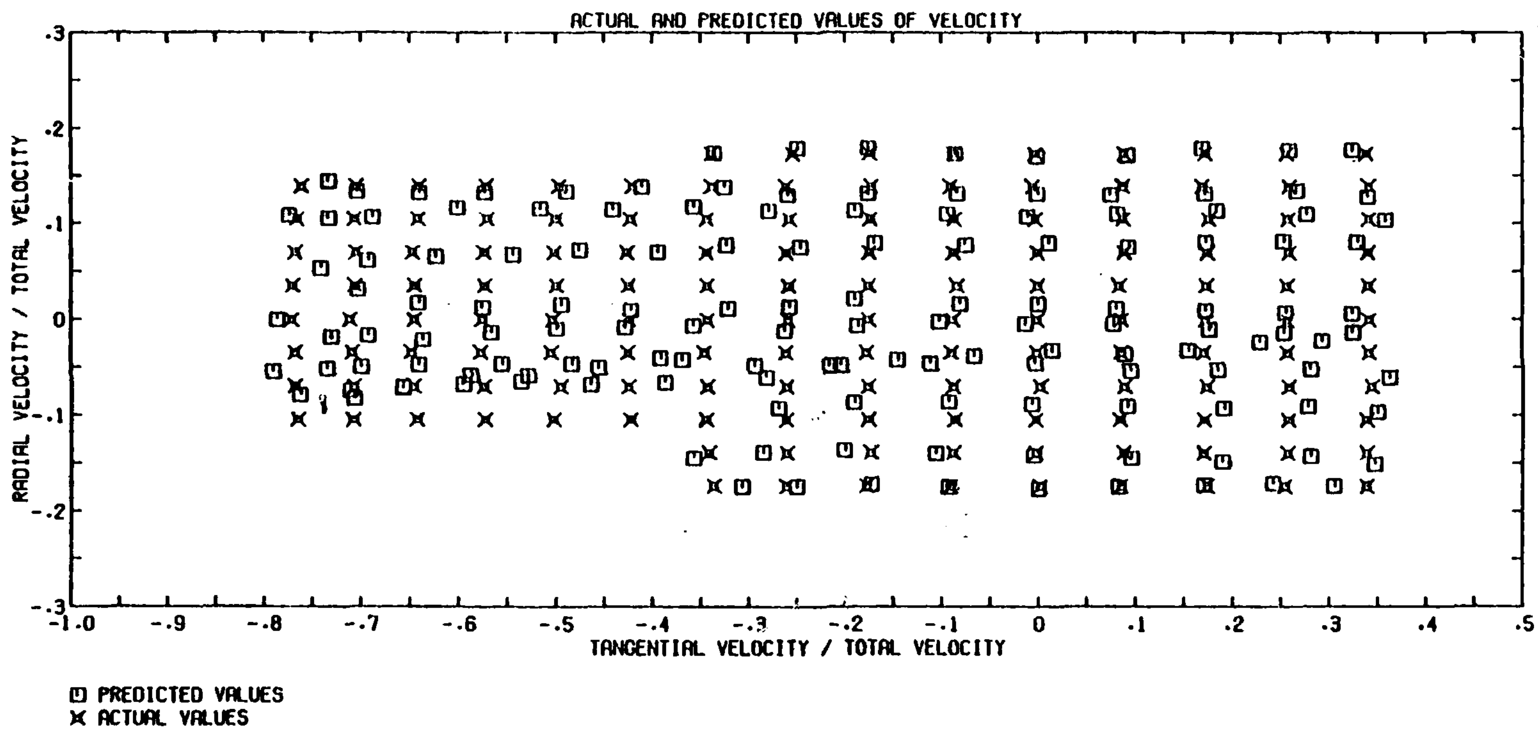

Figure 5-33 Actual and Predicted Values of u/V and v/V for Probe #2

CHAPTER 6

DATA REDUCTION

I. INTRODUCTION

The data set for each test run was reduced on the University of Washington's CDC computer using the following four step procedure:

1. The recorded raw data set was loaded from magnetic tape onto a disc file from a remote CRT terminal via campus phone lines.

2. The raw data set was initially reduced by time averaging certain data points and removing the time dependent zero drift of each low pressure transducer measurement.

3. The flow properties for the test run were calculated and recorded on disc file for later plotting.

4. The reduced data sets with the same mass flow ratio were plotted for analysis.

The following sections describe each step of data reduction as shown in Figures 6-1a and 6-1b.

II. LOADING RECORDED RAW DATA

A set of raw data for each test run was recorded on magnetic tape using the Fluke Datalogger and the Columbia 300 Data Tape Recorder as shown at the top of Figure 6-1a. The Columbia 300 Data Tape Recorder was then connected in series between a TeleVideo 920C CRT Terminal and a 1200 baud MODEM for entry of each set of raw data into the computer. Communications was then established between the remote terminal and the CDC computer using the campus phone system. The raw data set recorded on the magnetic tape and manual entries from the CCT terminal were read by the computer's ICE Text Editor and then saved on disc as a RAW DATA FILE (shown in Figure 6-1a). The ICE Text Editor was selected to read the data because this text editor used a carriage return to indicate the end of a line of data (the same format as the data recorded on magnetic tape using the Fluke Datalogger). Also this text editor sent a sequential line number prompt for each line of data read that was monitored for the progress and status of loading. The format of the initial part of a RAW DATA FILE is shown in Table D-2 where the first two lines are manual entries from the CRT terminal. The number of subruns, the subrun number and

the number of scans for a subrun were manually entered from the CRT terminal. The number of each test run was incorporated into that data file's filename for later identification. After loading of the raw data file for a test run, this file was available for the first step of data reduction.

III. INITIAL DATA REDUCTION - PROGRAM "REDUCE"

Each raw data file for a test run consisted of twenty or more subruns. Each subrun corresponded to a location of the five-hole probe and consists of 49 datalogger scans of the 18 measured quantities (the time and 17 voltages). Scans #2 through #49 corresponded to positions 1 through 48 of the Scanivalve and scan #1 corresponded to the initial scan of position 48 of the Scanivalve.

The five lengths of tygon tubing between the five-hole probe and its six pressure transducers were disconnected during scans #1 and #49, allowing zero pressure measurements of these six pressure transducers and the two Scanivalve pressure transducers during scans #1 and #49. Considerable drift in the output from each low pressure transducer was experienced and this drift is shown in Figure 6-2. The magnitude of the time variation

in the output voltage from each low pressure transducer was found to be independent of the input pressure's magnitude. The period of the time variation was found to be much larger than the length of time required for a subrun, $t_f - t_i$. Program REDUCE calculated the output voltage for a zero input pressure, $V_o(t)$, for each low pressure transducer from the data gathered on scan #1 (initial) and scan #49 (final) and assuming that $V_o(t)$ varied linearly between t_i and t_f using the following relationship:

$$V_o(t) = V_o(t_i) + \frac{V_o(t_f) - V_o(t_i)}{t_f - t_i} \times (t - t_i)$$

The time variation of the output voltage from the low pressure transducers was removed by calculating the corrected transducer voltage, V_c , using the measured output voltage, V(t), and subtracting the output voltage for zero input pressure, V_o (t), at the same time, t, calculated from the above equation.

Program REDUCE averaged the following inputs over fourty measurements (scan #6 through scan #45) for each subrun of a test run:

1. The corrected transducer voltage for the six low pressure transducers connected to the five-hole probe.

2. The voltages from the tank and line pressure

transducers.

3. The voltages from the two flow orifice plate differential pressure transducers.

4. The voltage from the potentiometer corresponding to the probe angle α_p.

5. The temperatures of the inside and outside plenums and the LVDT output voltage corresponding to the probe's radial position.

The output from REDUCE for each subrun consisted of the subrun number, the hour and minute at the start of the subrun, the corrected transducer voltage for scan #1 through scan #49 of both Scanivalve tranducers and the averaged measurements listed above. Typical output from REDUCE is shown in Table D-3 (FINE DATA FILE) for Run #4. The first four lines of the FINE DATA FILE in Table D-3 are test conditions which were manually loaded onto the data file from the CRT terminal and the remainder of the FINE DATA FILE is output from program REDUCE for two of the twenty-nine subruns in this test run.

This initial data reduction is shown in the bottom portion of the flow chart in Figure 6-1a. Program REDUCE and a description of input and output variables for this program are contained in Appendix D.

IV. CALCULATION OF FLOW PROPERTIES - PROGRAM "DATAR4"

Program DATAR4 used the FINE DATA FILE for each test run as the input data file as is shown in Figure 6-1b. Program DATAR4 also required the following data files:

1. Probe Calibration Coefficients of Regions 1 and 2
2. Layout of Pressures on Scanivalve

Program DATAR4 and a description of input and output variables for DATAR4 are contained in Appendix E. Program DATAR4 has seven subroutines to calculate specific properties and one subroutine to plot out the results on the printer. The main program portion of DATAR4 performs all input of data from disc files and output of results to the printer (except the printer plots) and to the output disc file, REDUCED DATA FILE. The main program portion of DATAR4 also averaged the wall static pressures over all subruns within the test run and calculated the axial momentum, the angular momentum, the swirl number, the average axial velocity and the mass average total pressure from the five-hole probe measurements at the axial location of the test run. The seven subroutines called by the main program portion of DATAR4 are explained in the following paragraphs in the order they are contained in Appendix E.

Subroutine PVPLOT plots out the results on the printer, using the Numerical Plotting System (NPS) software of the University of Washington's CDC computer. This subroutine produced the following eleven plots for the axial location of the test run:

1. Wall static pressure versus axial location on the four-inch diameter centerbody.

2. Wall static pressure versus axial location on the eight-inch diameter outer wall.

3. Wall static pressure versus axial location on the inside of the six-inch diameter tube separating the two air streams.

4. The following probe measured quantities versus the radial position of the probe (r):

   a. Axial velocity (w)

   b. Radial velocity (u)

   c. Tangential velocity (v)

   d. Total velocity (V)

   e. Static pressure (P_S)

   f. Total pressure (P_T)

   g. Axial momentum flux (M_z or M_z')

   h. Tangential momentum flux (M_θ)

Subroutine LOCATN determined the location and the pressure of each static pressure tap, using the coded Scanivalve location for each of the 74 static pressure taps (contained in FILE 1, LAYOUT) and the starting location of each section of the eight-inch diameter outer wall (contained in FILE 2, FINE DATA FILE for the test run). The file LAYOUT, containing the coded Scanivalve location for each of the 74 static pressure taps, is shown in Table E-2. The starting location of each section of the eight-inch diameter outer wall for test run #4 is shown in the fourth line of the FINE DATA FILE in Table D-3.

Subroutine PRESS calculated the pressure measured by the twelve pressure transducers, using the calibration coefficient of the respective transducer, the measured output voltage of the pressure transducer and the output voltage of the pressure transducer for zero input pressure. The output voltage of the eight low-pressure transducers had already been corrected in the initial data reduction program REDUCE. The output voltages of the other four pressure transducers for zero input pressure are contained in the third line of the FINE DATA FILE as shown in Table D-3 for test run #4.

Subroutine DENSTY calculated the density of the air in both plenums from the plenum's total pressure and temperature. This subroutine also calculated the mass average density, the axial velocity and the dynamic pressure based on this axial velocity for the test section. This subroutine used the mass flow rates of the two air streams determined by the subroutine FLOW.

Subroutine POSITN calculated the five-hole probe's radial position for each subrun based on the voltage from the Linear Variable Differential Transformer (LVDT), the calibration coefficients of the LVDT and the reference voltage and position of the probe. The reference radial position and its corresponding voltage are the last two entries contained in the first line of the FINE DATA FILE as shown in Table D-3 for test run #4.

Subroutine FLOW calculated the mass flow rates through both plenums, using two different methods. The first method of calculating the mass flow rate is based on choked flow and knowing the area of the choked orifice, the total pressure upstream of the choked orifice and an estimate of the total temperature upstream of the choked orifice. The second method of calculating the mass flow rate is based on a calibrated flow orifice plate and

knowing the differential pressure across the flow orifice plate, the total pressure upstream of the flow orifice plate and an estimate of the total temperature upstream of the flow orifice plate.

Subroutine PROBE calculated the flow properties at the five-hole probe's radial position, using the probe's calibration coefficients for regions #1 and #2, the pressures at each of the probe's five ports, the voltage from the probe's angular position measuring system and the method described in the Chapter 5. The following flow quantities were determined for the point in the flow measured by the probe:

1. Axial velocity to total velocity ratio (w/V)
2. Radial velocity to total velocity ratio (u/V)
3. Tangential velocity to total velocity ratio (v/V)
4. Total velocity (V)
5. Flow angle alpha (α)
6. Flow angle beta (β)
7. Static pressure (P_S)
8. Total pressure (P_T)
9. Axial momentum flux (M_z or M_z')
10. Tangential momentum flux (M_θ)

Subroutine INTERGR used the trapezoid rule and data at each radial position to integrate flow properties between the inner radius and the outer radius of the flow channel. This subroutine was used by the main portion of DATAR4 to calculate the axial momentum, the angular momentum, the swirl number, the average axial velocity and the mass average total pressure.

V. OUTPUT FROM PROGRAM "DATAR4"

Typical printer output from program DATAR4 is shown in Table E-3 in Appendix E for test run #061. The printer output includes listings of the following quantities:

1. Input data for the test run
2. Wall static pressure versus axial position
3. Output data from probe measurements
4. Printer plots

Program DATAR4 also wrote the results of each test run onto a separate disc file (Reduced Data File XXX) as shown in Figure 6-1b. The Reduced Data Files were used as input data for the plotting program PLDATA that is discussed in the next section.

VI. PLOTTING PROGRAM "PLDATA"

Program PDATA plots the reduced data files as shown in Figure 6-1b. This program was developed for plotting results using the TEKTRONIX PLOT-10/Terminal Control System contained on the PDP-11/23 computer system in the Aeronautics Laboratory at the United States Air Force Academy. Program PLDATA and a description of input and output variables for this program are contained in Appendix F.

The main portion of this program performed all input of data from disc files and the interactions with the user. The subroutine PVPLOT accomplished all the plotting of the results by directly calling on PLOT-10 subroutines and by indirectly calling on PLOT-10 subroutines in the subroutines SYMBLS and GRID. Subroutine SCALE performed the necessary scaling of the data before plotting. Subroutine SYMBLS plots one of eleven possible symbols at each data point. Subroutine GRID draws a two dimensional grid and numbers both axes.

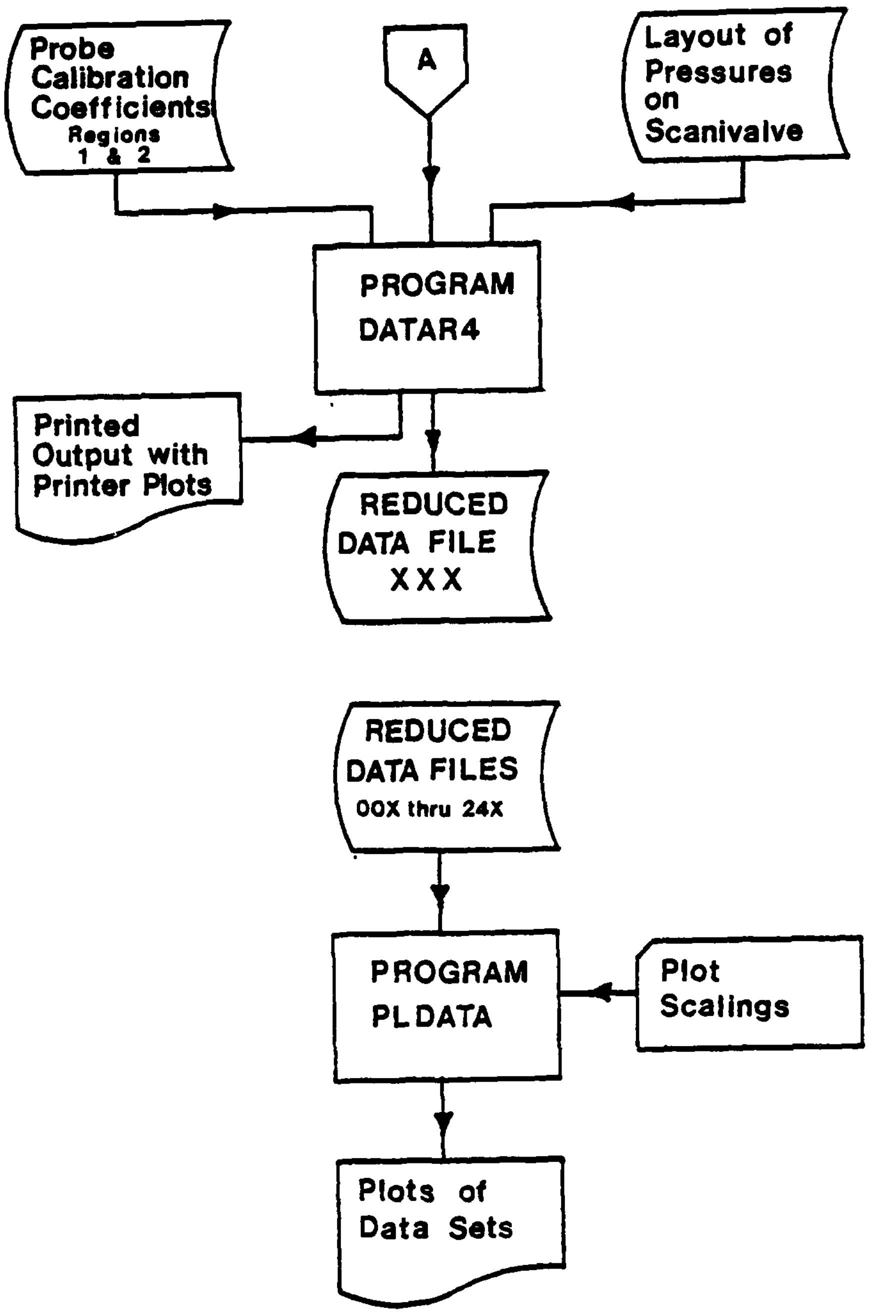

Figure 6-1a Data Reduction Flow Chart, Part I

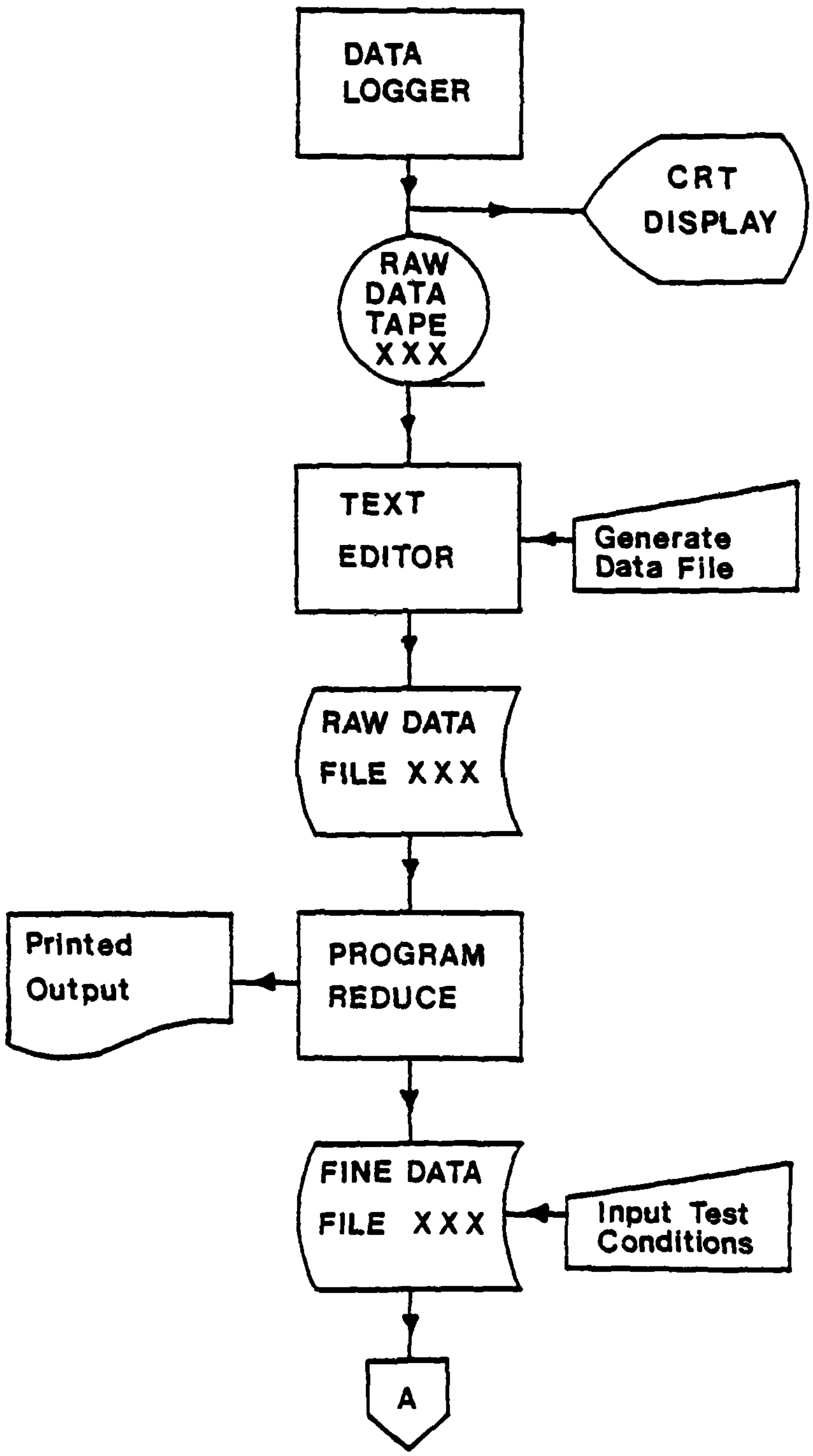

Figure 6-1b Data Reduction Flow Chart, Part II

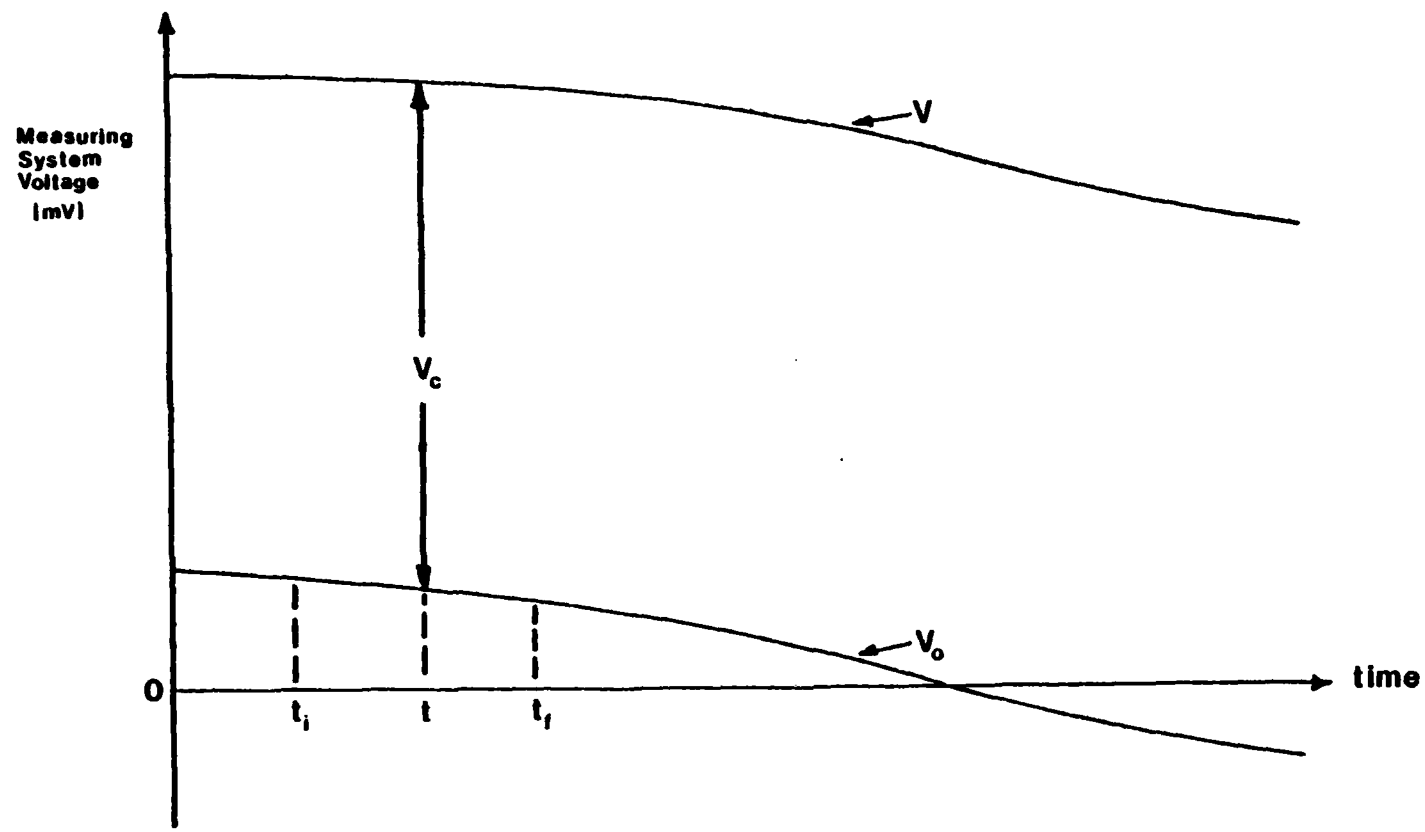

Figure 6-2 Time Variation of Measuring System Voltage

CHAPTER 7

RESULTS & CONCLUSIONS

I. INTRODUCTION

This chapter discusses the experimental results of the four tests conducted to measure the turbulent mixing of coaxial air streams with swirl present. The data for the tests is presented in Appendix A and the experimental measurements, test apparatus, five-hole probes, and data reduction are discussed in Chapters 3, 4, 5, and 6, respectively.

II. TEST #1

A limited amount of data was taken for the mixing of a swirling stream from an annulus in a flat wall into a stagnant environment (the test configuration is shown in Figure 3-1). The reduced data for this test is contained in Figures A-1 through A-8 in Appendix A. The inside boundary of the swirling stream grows toward the centerline and the outside boundary of this stream grows away from the centerline into the stationary surrounding air. The growth of the outside boundary of the swirling stream is expected because this boundary is unstable due

to the decrease in fluid angular momentum in the radial direction. The inward growth of the swirling stream's inside boundary can be attributed to the zone of recirculation (sketched below) that is present about the centerline near the entrance.

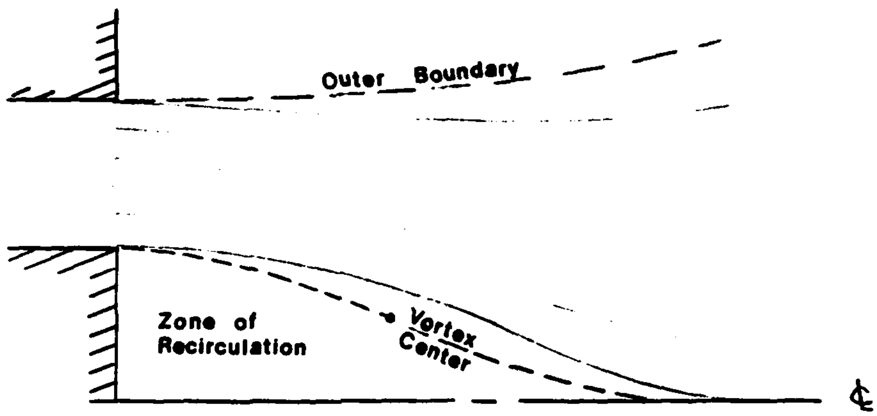

III. TEST #2

Data was taken of the mixing of two coaxial air streams (inner stream with swirl) from concentric annuli in a flat wall into stagnant surroundings (see Figure 3-2 for test configuration). The reduced data for this test is contained in Figures A-9 through A-17 in Appendix A. The outside boundary of the inner swirling stream does not grow as quickly when surrounded by a coaxial air stream as was the case for this boundary in stagnant surroundings (Test #1). The reduced growth of the outside

boundary of the swirling stream can be attributred to the presence of the outer stream and the reduction in the intensity of the instability of this boundary. The outer stream has a much higher velocity, axial momentum, and static pressure than was the case for Test Set #1. The inside boundary of the swirling stream grows toward the centerline due to the zone of recirculation that is present about the centerline near the entrance.

IV. TEST #3

The test section for the third set of experiments is shown in Figure 3-3. Two streams of air (inner stream with swirl) from concentric annuli in a flat wall flow into an open region. This set of experiments differed from the second set of experiments by the addition of an extension of the inner wall of the inner annulus (centerbody) into the open region. The reduced data for this test is contained in Figures A-18 through A-35 in Appendix A. The presence of the centerbody prevents the inward growth of the swirling stream's inside boundary and the growth rate of the swirling stream's outside boundary is increased over its growth rate in Test #2.

The scatter of data for measurements at the two far

downstream axial locations is attributed to the intermittency of the turbulent flow at these locations.

V. COMPARISON OF TEST #1, #2, AND #3

The growth of the outside boundary of the swirling stream is presented for the first three tests in Figure 7-1 as a plot of the tangential velocity's half-radius versus axial location. Both the absence of a centerbody and the presence of an outer coflowing stream retard the growth of the swirl velocity.

VI. TEST #4

The final and most extensive set of experiments was performed with the test section in the configuration shown in Figure 3-4. In this configuration, two streams of air (inner stream with swirl) from concentric annuli flow into a constant area annular duct. The reduced data for this set of experiments is contained in Figures A-36 through A-90 in Appendix A. Measurements were taken for five different mass flow ratios, α's, or runs. Table 7-1 lists these five mass flow ratios, the three character abbreviations used to differentiate the data runs of each mass flow rate, the Figures in Appendix A containing the

reduced data for the data runs, and the swirl number, S_o (defined by Equation G-16 in Appendix G), at the first axial location, z = 0.25 inches.

TABLE 7-1

MASS FLOW RATIOS FOR TEST #4

Mass Flow Ratio ($\alpha = \dot{m}_o/\dot{m}_i$)	Abbreviation of Data Runs	Figures	Swirl S_o
0.00	XX1	A-36 - A-46	.1762
0.47	XX2	A-47 - A-57	.1579
1.00	XX3	A-58 - A-68	.1096
2.13	XX4	A-69 - A-79	.0379
3.91	XX5	A-80 - A-90	.0125

In runs XX1 (α = 0.00), a region of recirculation is established at the entrance of the test section between the inner swirling stream and the outside wall. At about four inches downstream of the test section entrance, the inner swirling stream separates from the centerbody due to the large adverse pressure gradient (see Figure 7-2) and a region of flow reversal is produced. Further downstream (at about eight inches from entrance), the flow re-attaches to the centerbody. The streamline pattern for runs XX1 is sketched in Figure 7-3.

In runs XX2 (α = 0.47), the flow from the outer annulus prevents the establishment of an outer region of

recirculation and reduces the magnitude of the adverse pressure gradient on the centerbody (see Figure 7-4) preventing separation. The flow from the outer annulus also reduces the rate of outward growth of the tangential velocity.

In runs XX3 (α = 1.00), the adverse pressure gradient on the centerbody is further reduced by the flow from the outer annulus (see Figure 7-5). The initial difference in axial momentum flux between the inner and outer streams is lower than for runs XX2 and the rate of outward growth of the tangential velocity is further reduced.

In runs XX4 (α = 2.13), the outside wall of the test section and the higher velocity of the outside stream cause the boundary between the two streams to move inward before any significant outward growth of tangential velocity. The inward growth of axial momentum flux reduces the outward transfer of tangential momentum flux and its associated tangential velocity. The magnitude of the adverse pressure gradient present on the initial section of centerbody (see Figure 7-6) is reduced by the inward growth of the outer stream.

In runs XX5 (α = 3.91), both walls of the test section

have adverse pressure gradients (see Figure 7-7). The adverse pressure gradient on the outside wall is due to the inward spread of the outer stream. The inward transfer of axial momentum flux further reduces the outward transfer of tangential momentum flux as compared to runs XX4.

The half-radius growth of the swirl (tangential) velocity versus axial location is plotted in Figure 7-8 for runs XX1, XX2, XX3, XX4, and XX5 of test #4. The increase in outward growth with increased swirl agrees with the results for a swirling jet (Reference 1). The rate of outward growth of the swirl velocity is reduced by a flowing outer stream and the higher the mass flow ratio (with its outer stream axial velocity and axial momentum flux), the slower the rate of this growth. When the initial axial momentum flux of the outer stream is greater that that of the inner stream (runs XX4 and XX5), the rate of inward transfer of axial momentum more than offsets the outward transfer of tangential momentum in the initial portion of the test section and the half-radius of the swirl velocity is reduced.

The variation of the swirl number (S), with axial distance for runs XX1, XX2, XX3, XX4, and XX5 of test

#4,is plotted in Figure 7-9. The swirl number has been normalized by its value at the first axial location (S_{o}). This initial value of the swirl number is listed in Table 7-1. The results indicate that the decay of the swirl number with axial distance for runs XX1, XX2, and XX3 is dominated by the decay of the tangential momentum with axial distance. This agrees with the results of swirl dominated flows (Reference 2). The results for runs XX4 seem to indicate that this region of flow is dominated by the decay of the axial momentum with axial distance. The author is unable to explain the variation of the swirl number for runs XX5 except to note that the five-hole probe was being used in the outer edge of its calibration and small errors in predicted flow direction had a much larger effect on the tangential momentum flux than on the axial momentum flux.

The variation of the static pressure along the outside wall of the inner annulus upstream of the test section is presented in Figures 7-10 and 7-11 for runs XX1, XX2, XX3, XX4, and XX5 of test #4. The static pressures in Figure 7-10 have been nondimensionalized by the dynamic pressure associated with the mean axial velocity in the test section and those in Figure 7-11 have been nondimensionalized by the dynamic pressure associated

with the mean axial velocity in the inner annulus. The influence of the outer stream on the pressure along the outside wall of the inner annulus can be seen for runs XX3, XX4, and XX5 by comparing Figures 7-10 and 7-11. For runs XX1 and XX2, the static pressure on the outside wall and at the end of this wall are only a function of the dynamic pressure of the inner stream and the axial location (see Figure 7-11). The upstream influence for runs XX3, XX4, and XX5 can be seen in Figure 7-11 (i.e. the higher the mass flow ratio, α, the further upstream the influence).

The variation of the static pressure along the outside wall of the inner annulus upstream of the test section is presented in Figure 7-12 for test sets #1, #2, #3, and #4 (runs XX1 and XX2 only). The decrease in static pressure for test sets #1, #3, and #4 indicates an increase in the fluid velocity near the outside wall at the exit. However, the increase in static pressure for test set #2 indicates a decrease in fluid velocity near the outer wall at the exit for this test set.

Static pressure measurements in test #4 along the centerbody and the outside wall were used to calculate the coefficient of friction (c_f) for this flow. The

coefficient of friction for both the inside wall and the outside wall are presented in Table 7-2 for each test. Calculation of the coefficient of friction was based on the dynamic pressure associated with the mean axial velocity in the test section.

TABLE 7-2

COEFFICIENT OF FRICTION, TEST #4

RUNS	Centerbody	Outside Wall
XX1	0.0016	0.0140
XX2	0.0031	0.0108
XX3	0.0059	0.0093
XX4	0.0048	0.0048
XX5	0.0043	0.0043

The higher values of the coefficient of friction at the outer wall reflect the existence of larger tangential velocities near this wall and the higher turbulence present due to this extremely unstable boundary layer. Scott and Rask (Reference 3) explain that this increase in the coefficient of friction at the outer wall is due to unstable flow which increases the turbulent production and promotes turbulent transfer.

VII. CONCLUSIONS

On the basis of the experimental results, the following remarks can be made regarding the initial mixing region

(for the swirl rates tested):

1. For annular swirling jet, the addition of a concentric outside annular jet decreases the growth of the outer boundary of tangential (angular) momentum in the initial region.

2. For concentric annular streams without an outside wall, the addition of a centerbody increases the radial transfer of tangential (angular) momentum.

3. For concentric annular streams with a centerbody, the addition of an outside wall decreases the radial transfer of tangential (angular) momentum.

4. For concentric annular streams with a centerbody and an outside wall,

a. an increase in the axial momentum of the outer stream reduces the radial transfer of tangential (angular) momentum.

b. an increase in the mass flow ratio (outside to inside flow rates) increases the influence of the outside stream on upstream pressures on the outer wall of the inner annulus.

REFERENCES

1. Pratte, B.D. and Keffer, J.F., "The Swirling Turbulent Jet", Journal of Basic Engineering, Vol. 95, 1973.

2. Lilley, D.G., "Swirl Flows in Combustion: A Review", AIAA Journal, Vol. 15, No. 8, August 1977, pp. 1063-1078.

3. Scott, C.J. and Rask, D.R., "Turbulent Viscosities for Swirling Flow in a Stationary Annulus", Journal of Fluids Engineering, Trans. ASME, Dec. 1973, pp. 557-566.

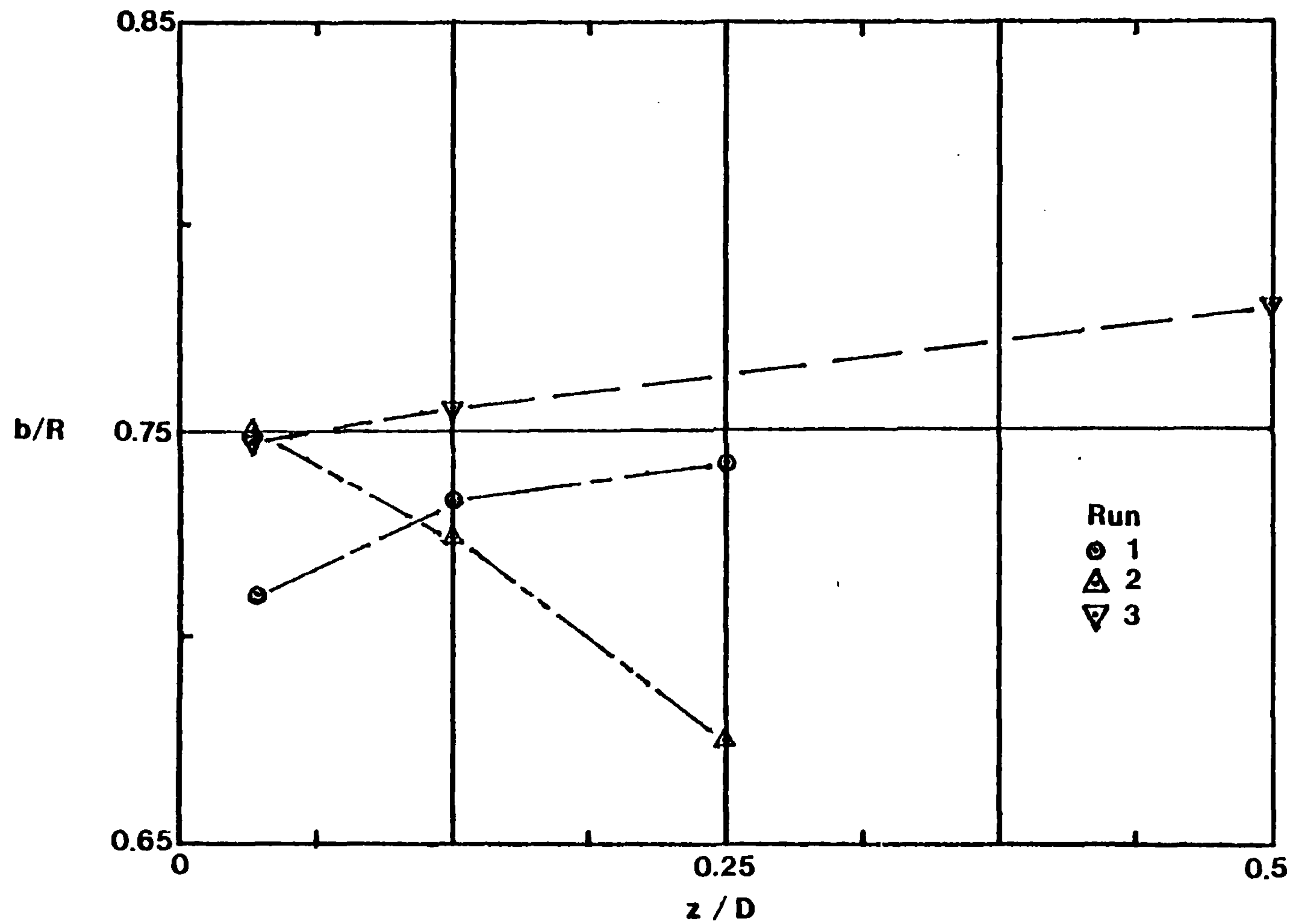

Figure 7-1 Half-Radius Growth of Swirl Velocity for Tests #1. #2, and #3

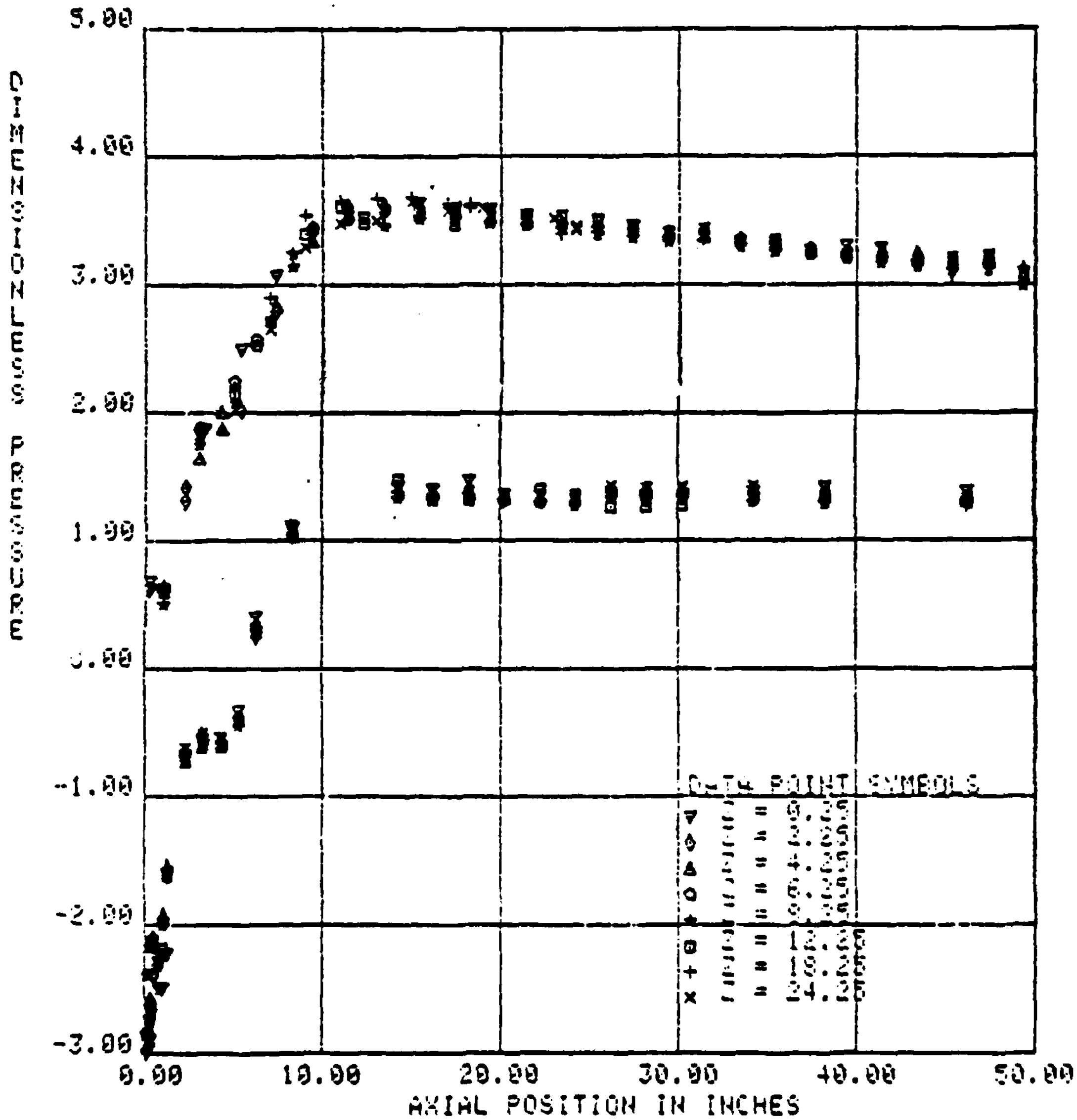

Figure 7-2   Static Pressure on 4 Inch and 8 Inch Tubes, Test #4, Runs XX1

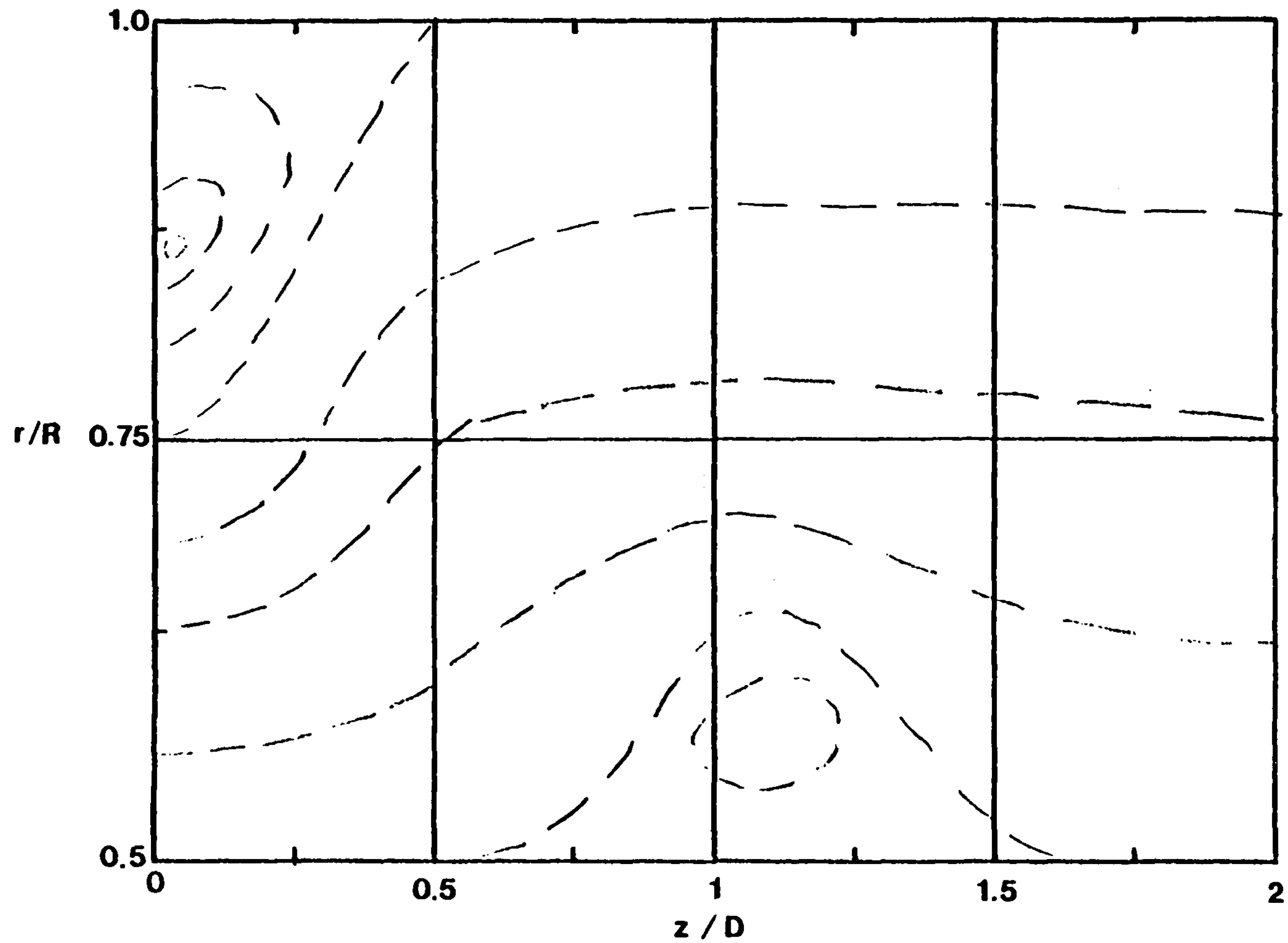

Figure 7-3 Streamline Pattern for Runs XX1 of Test #4

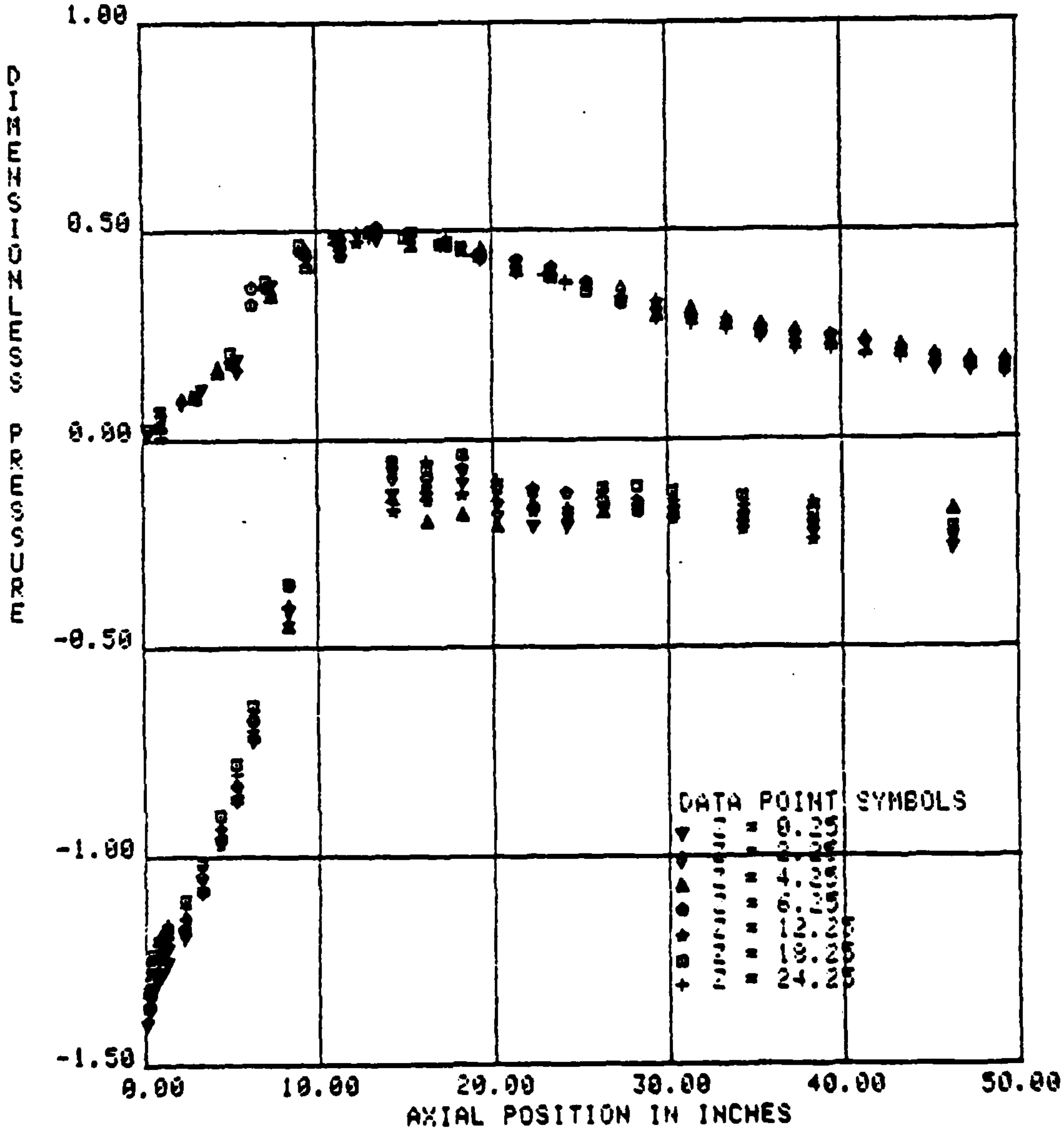

Figure 7-4 Static Pressure on 4 Inch and 8 Inch Tubes, Test #4, Runs XX2

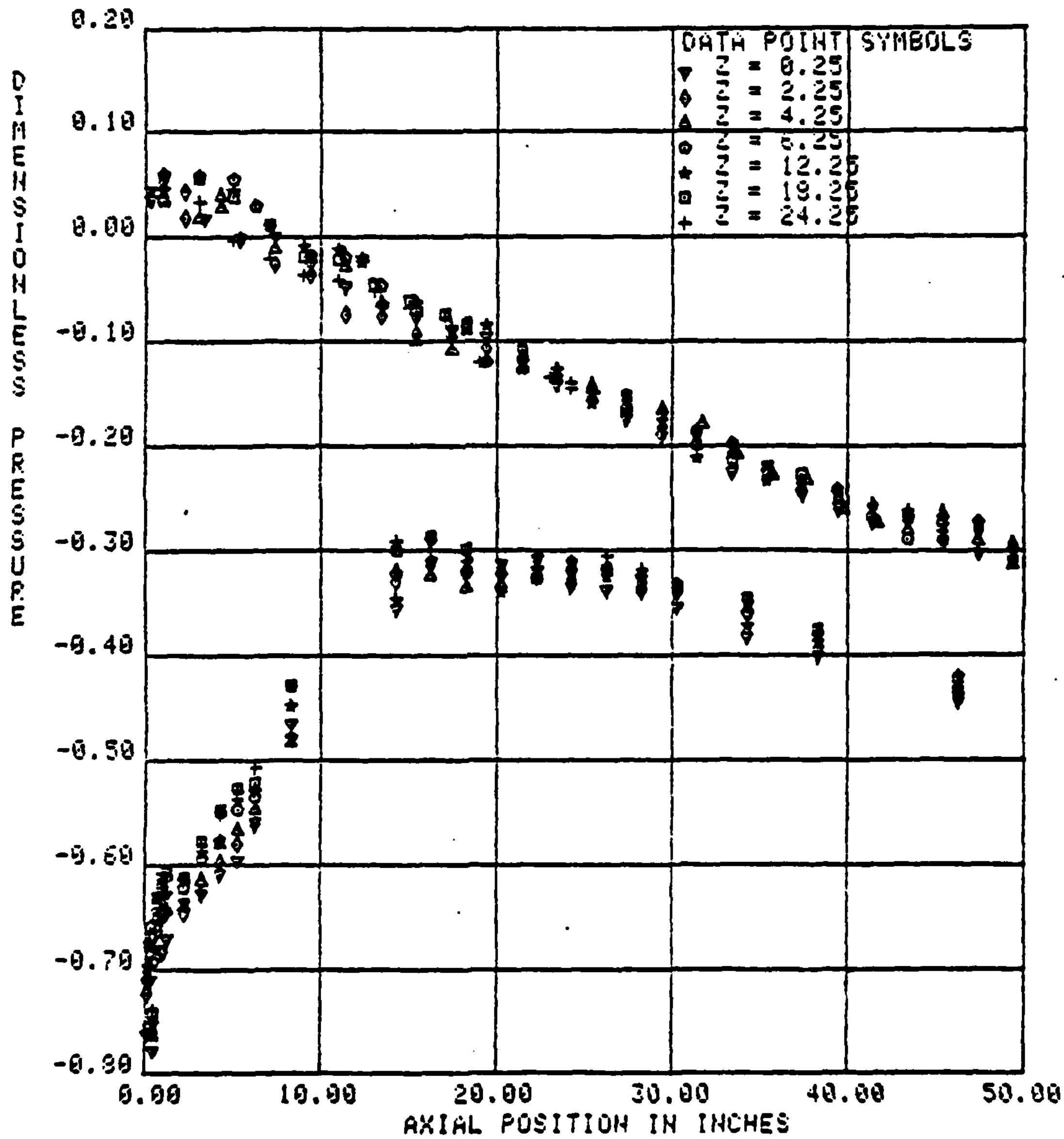

Figure 7-5 Static Pressure on 4 Inch and 8 Inch Tubes, Test #4, Runs XX3

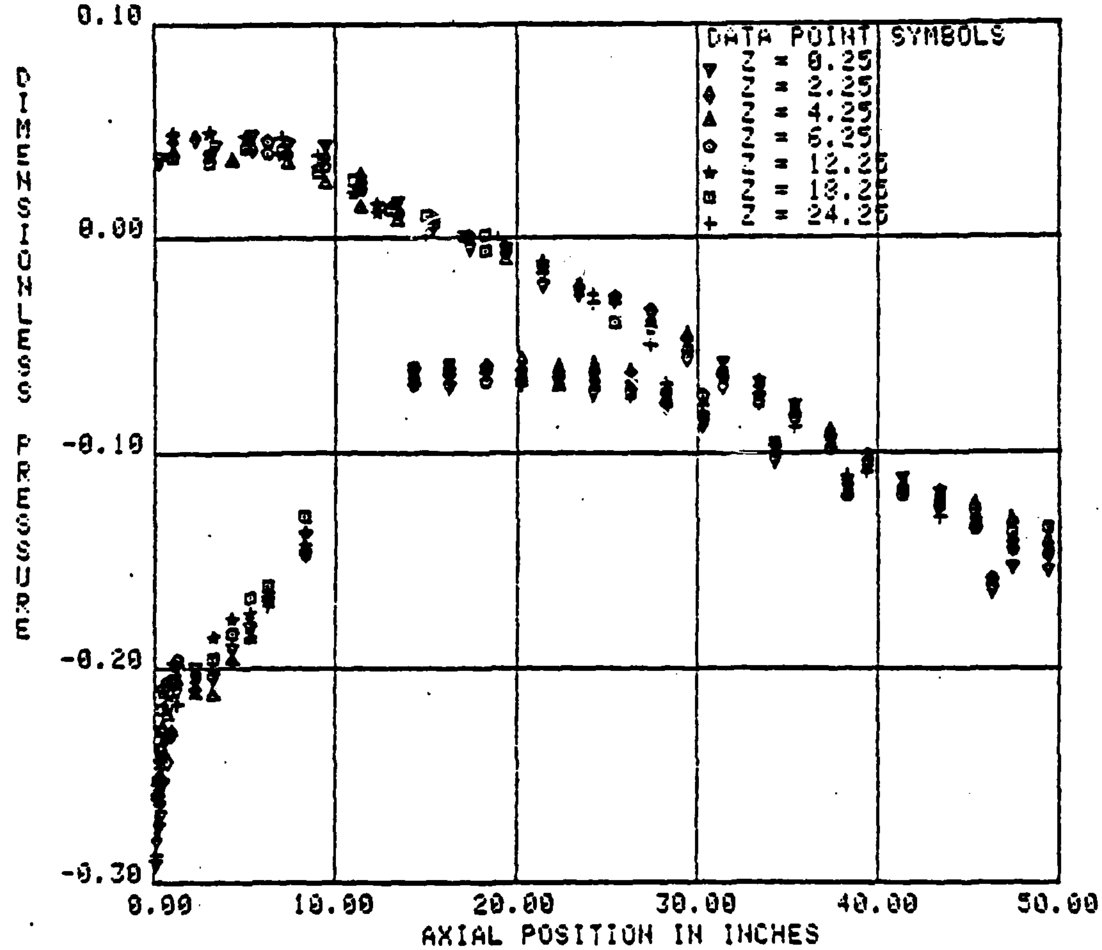

Figure 7-6 Static Pressure on 4 Inch and 8 Inch Tubes, Test #4, Runs XX4

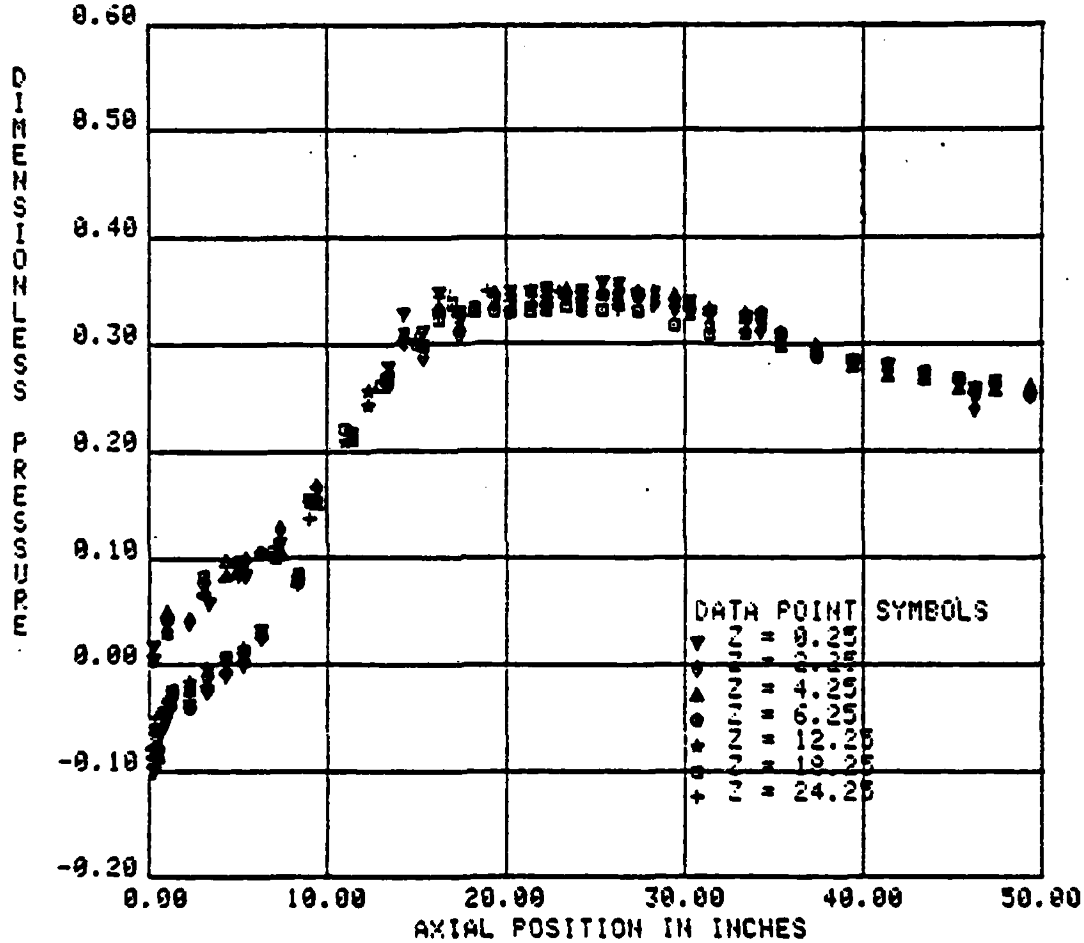

Figure 7-7 Static Pressure on 4 Inch and 8 Inch Tubes, Test #4, Runs XX5

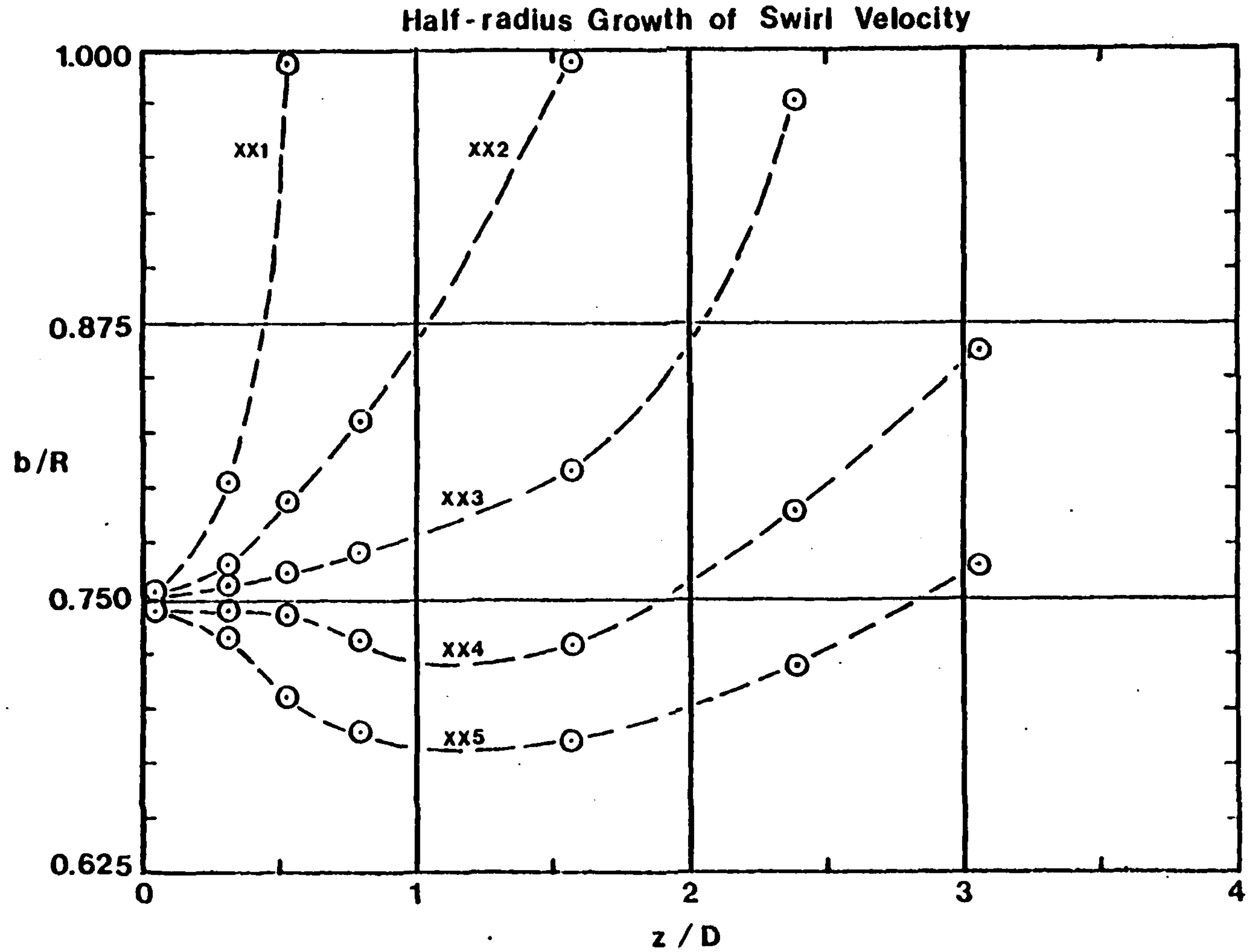

Figure 7-8 Half-Radius Growth of Swirl Velocity for Test #4

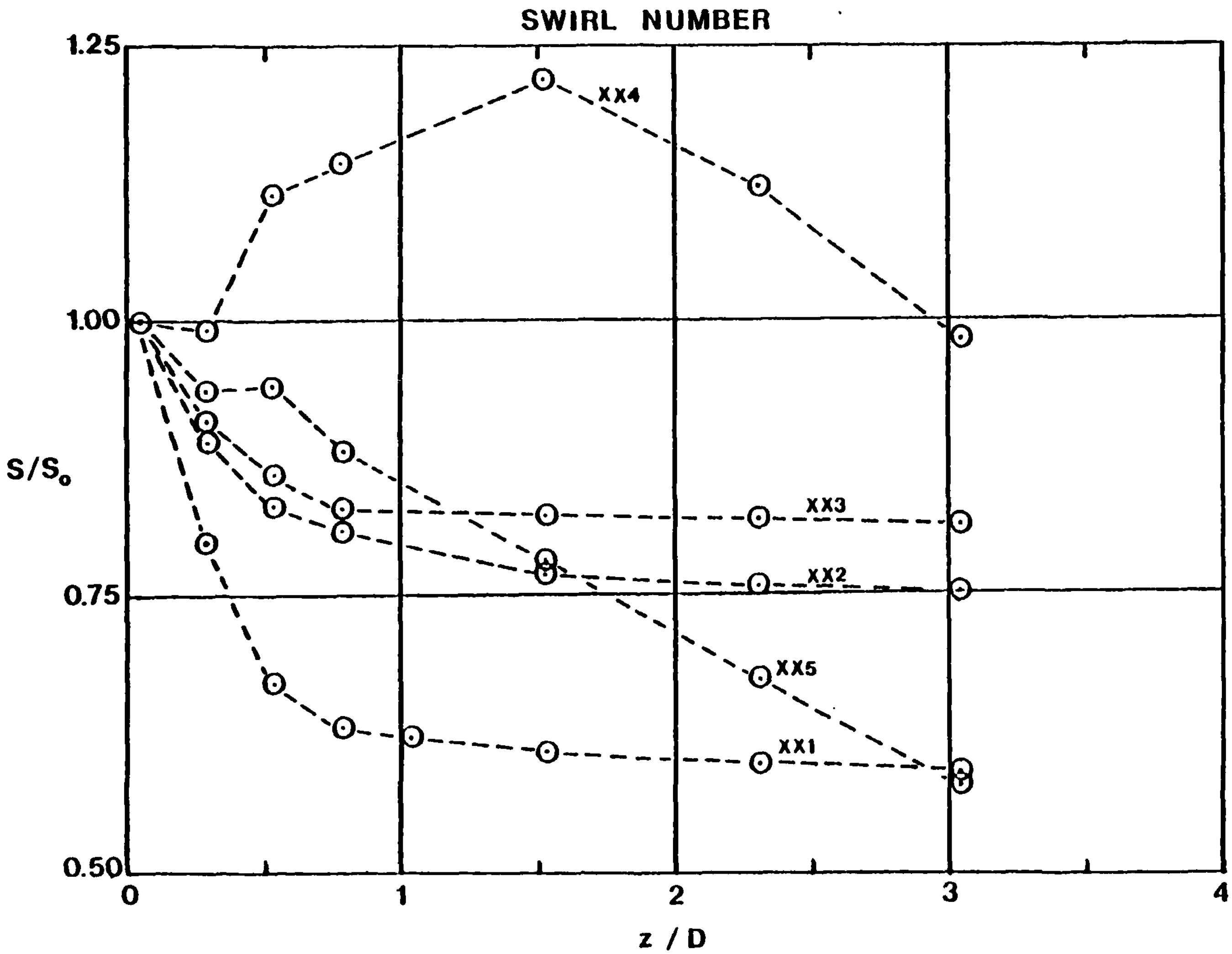

Figure 7-9   Swirl Number Decay, Test #4

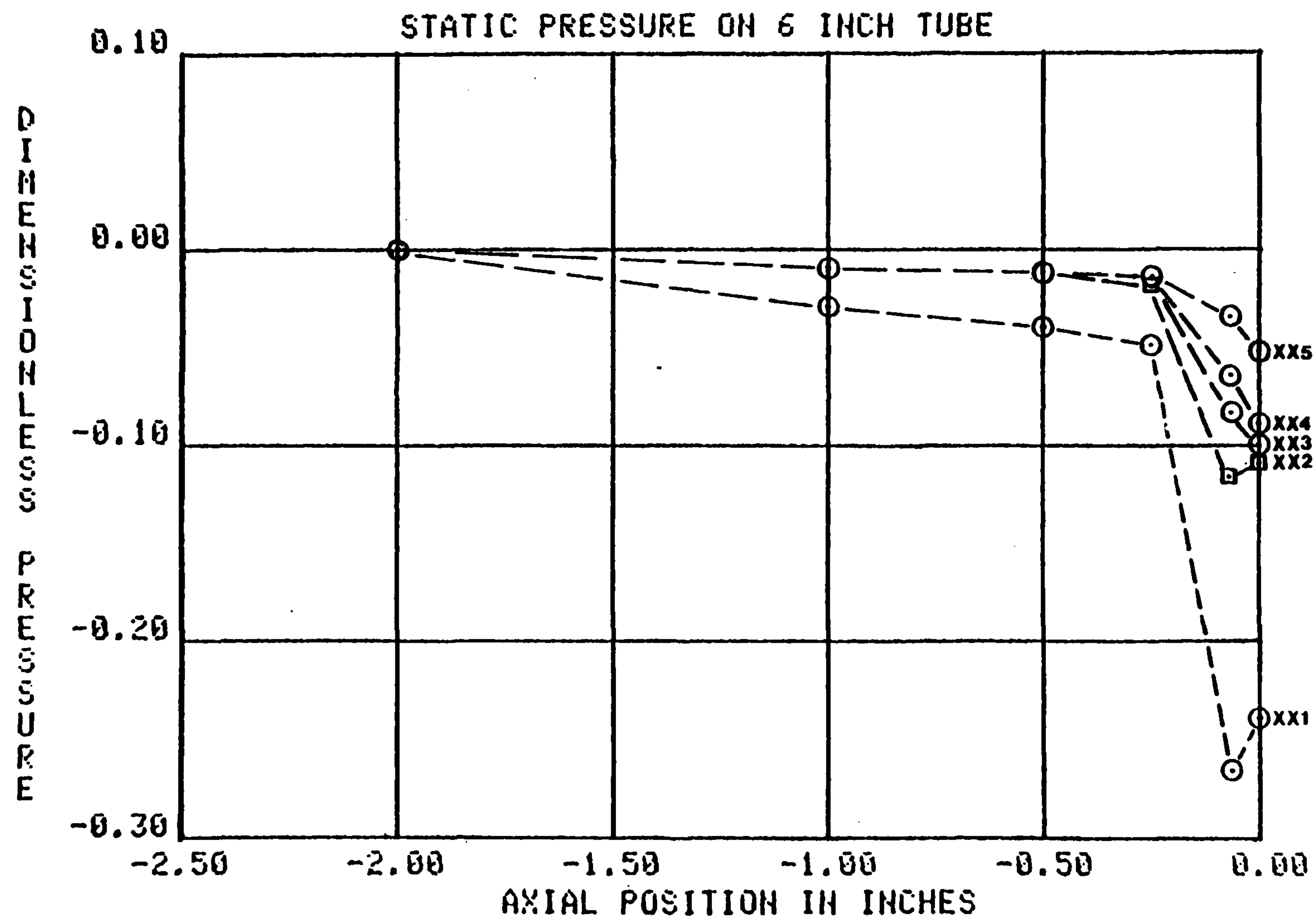

Figure 7-10 Static Pressure on 6 Inch Tube, Test #4

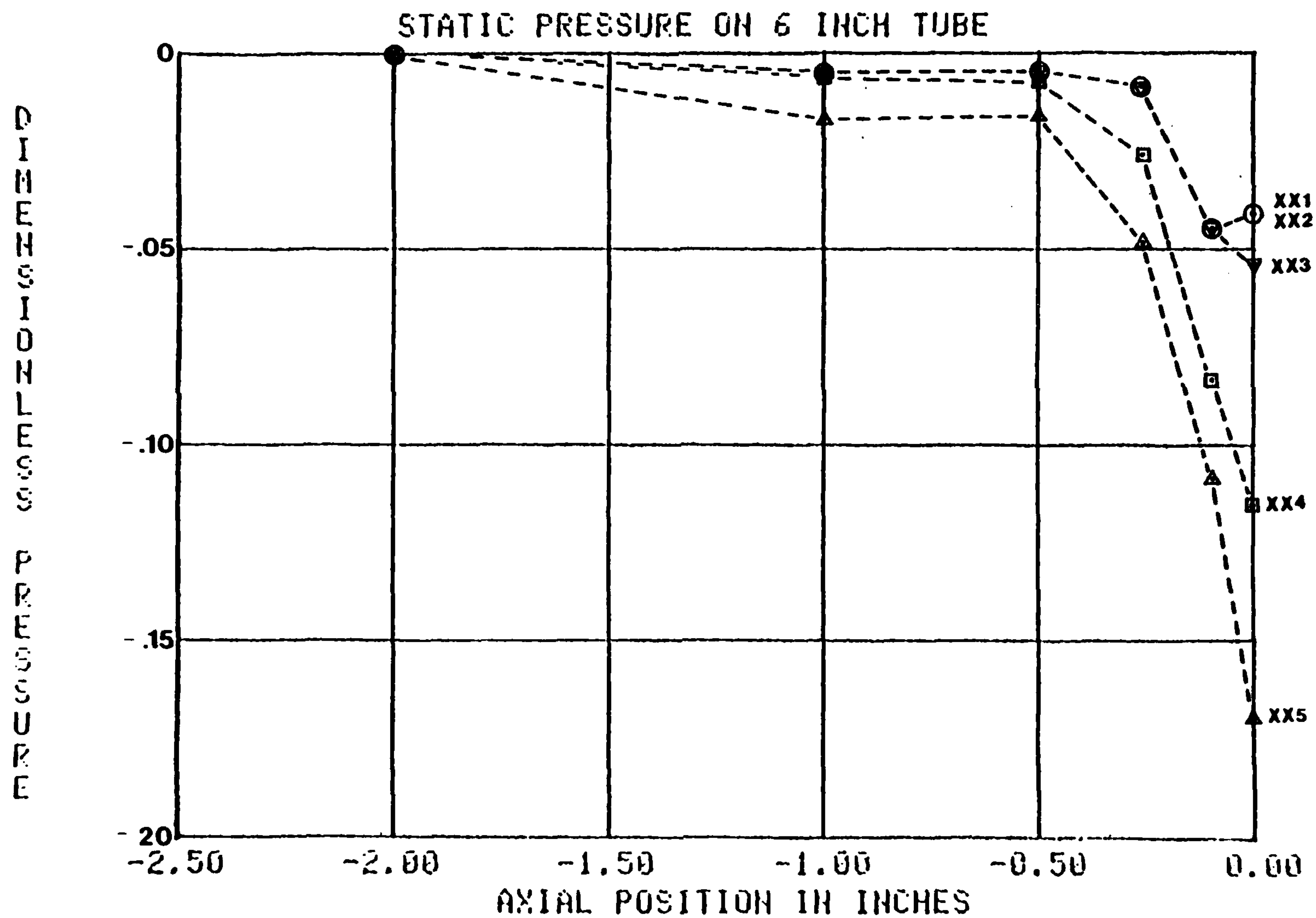

Figure 7-11 Static Pressure on 6 Inch Tube, Test #4

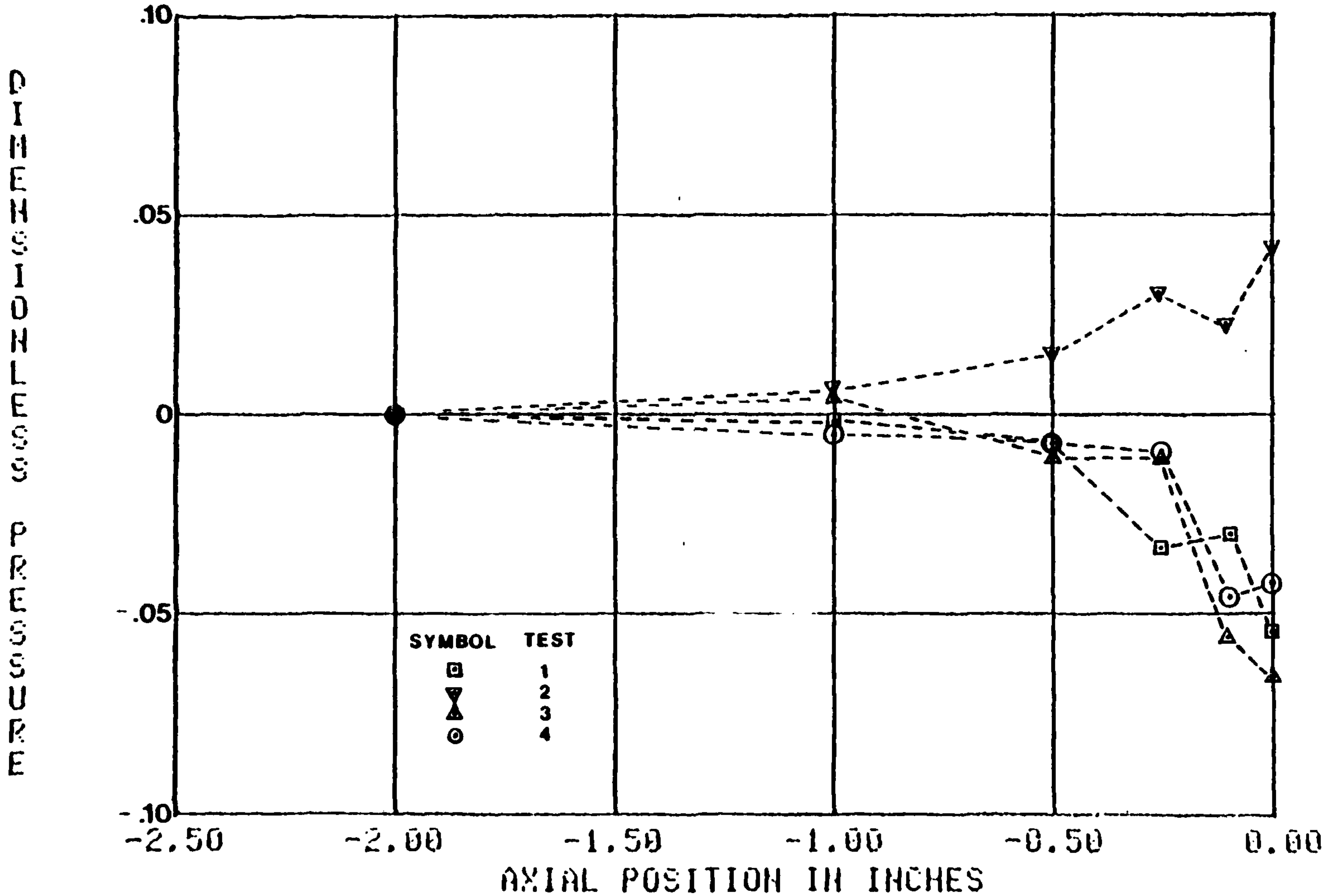

Figure 7-12 Static Pressure on 6 Inch Tube, Tests #1, #2, #3, and #4

BIBLIOGRAPHY

Abramovich, G.N., The Theory of Turbulent Jets, MIT Press, Cambridge, Mass., 1960 (English edition)

Alpinieri, L.J., "Turbulent Mixing of Coaxial Jets", AIAA Journal, Vol. 2, No. 9, Sept. 1964, pp. 1560-1567.

Barker, K., Gallington, R., and Minster, S., "Calibration of Five-Hole Probes for On-Line Data Reduction", Aeronautics Digest, Spring 1979, USAFA-TR-79-7, USAF Academy, CO, July 1979.

Bird, R.B., Stewart, W.E., and Lightfoot, E.N., Transport Phenomena, Wiley, 1960.

Bradshaw, P., "The Analogy Between Streamline Curvature and Buoyancy in Turbulent Shear Flow", Journal of Fluid Mechanics, Vol. 36, Part 1, 1969, pp. 177-191.

Betchow, R. and Criminale, W.O., Jr., Stability of Parallel Flows, Applied Mathematics and Mechanics, Volume 10, Academic Press, 1967.

Bradshaw, P., "The Understanding and Prediction of Turbulent Flow", Aeronautical Journal, July 1972, pp. 403-418.

Cebeci, T. and Smith, A.M.O., Analysis of Turbulent Boundary Layers, Academic Press, 1974.

Chervinsky, A. and Lorenz, D., "Decay of Turbulent Axisymmetrical Free Flows with Rotation", Journal of Applied Mechanics, Trans. ASME, Dec. 1967, pp. 806-812.

Chigier, N.A. and Beer, J.M., "Velocity and Static-Pressure Distributions in Swirling Air Jets Issuing From Annular and Divergent Nozzles", Journal of Applied Mechanics, Trans. ASME, June 1967, pp. 788-796.

Chigier, N.A. and Beer, J.M., "The Flow Region Near the Nozzle in Double Concentric Jets", Journal of Basic Engineering, Trans. ASME, Dec. 1964, pp. 797-804.

Chigier, N.A. and Chervinsky, A., "Experimental Investigation of Swirling Vortex Motion in Jets", Journal of Applied Mechanics, Trans. ASME, June 1967, pp. 443-451.

CMOS Databook, National Semiconductor Corporation, Santa Clara, CA, 1977.

Coles, D., "A Note on Taylor Instability in Circular Couette Flow", Journal of Applied Mechanics, Trans. ASME, Sept. 1967, pp. 529-534.

Cusick, C.F., Flow Meter Engineering Handbook, Minneapolis-Honeywell Regulator Company, Third Edition, 1961.

Dring, R.P., Joslyn, H.D., and Hardin, L.W., "Experimental Investigation of Compressor Rotor Wakes", United Technologies Research Center Technical Report AFAPL-TR-79-2107, Jan 1980.

Dryden, H.L. and Abbott, I.H., "The Design of Low-Turbulence Wind Tunnels", NACA TR-940, 1949.

Erwin, J.R., "Experimental Techniques", Aerodynamics of Turbines and Compressors, High Speed Aerodynamics and Jet Propulsion, Vol. X, Section D, Princeton, 1964.

Fujii, S., Eguchi, K., and Gomi, M., "Swirling Jets With and Without Combustion", AIAA Journal, Vol. 19, No. 11, Nov. 1981, pp. 1438-1442.

Gallington, R.W. and Hollenbaugh, C.F., "A Fast Method for Accurate Manufacture of Small Five-Hole Probes", Aeronautics Digest, Spring 1979, USAFA-TR-79-7, USAF Academy, CO, July 1979.

Goldstein, S., Modern Developments in Fluid Dynamics, Volumes 1 and 2, Dover, 1965.

Gorlin, Wind Tunnels and Their Instrumentation, (Translated from Russian), NASA TTF-346, US Dept. of Commerce, Springfield, VA.

Grinich, V.H. and Jackson, H.G., Introduction to Integrated Circuits, McGraw-Hill, New York, NY, 1975.

Habib, M.A. and Whitelaw, J.H., "Velocity Characteristics of Confined Coaxial Jets With and Without Swirl", Journal of Fluids Engineering, Vol. 102, March 1980, pp. 47-53.

Harlow, F.H., Editor, Turbulence Transport Modeling, AIAA Selected Reprint Series, Volume XIV, Feb. 1973.

Higuchi, H. and Rubesin, M.W., "An Experimental and Computational Investigation of the Transport of Reynolds Stress in an Axisymmetric Swirling Boundary Layer", AIAA-81-0416, Jan. 1981.

Hinze, J.L., Turbulence, McGraw-Hill, New York, 1959.

Holman, J.P., Experimental Methods for Engineers, McGraw-Hill, New York, Second Edition, 1971.

King, M.K., Rothfus, R.R., and Kermode, R.I., "Static Pressure and Velocity Profiles in Swirling Incompressible Tube flow", A.I.Ch.E. Journal, Vol. 15, No. 6, Nov. 1969, pp. 837-842.

Kreith, F. and Sonju, O.K., "The Decay of a Turbulent Swirl in a Pipe", Journal of Fluid Mechanics, Vol. 22, Part 2, 1965, pp. 257-271.

Launder, B.E. and Morse, A., "Some Experiments on the Turbulent Swirling Jet With and Without an External Stream", Unpuplished Paper.

Launder, B.E. and Morse, A., "Numerical Prediction of Axisymmetric Free Shear Flows with a Reynolds Stress Closure", Turbulent Shear Flows I, edited by F. Durst, B.E. Launder, F.W. Schmidt, and J.H. Whitelaw, Springer-Verlag,Berlin,1979, pp. 279-294.

Lenk, J.D., Handbook of Integrated Circuits: for Engineers & Technicians, Reston Publishing co, Reston, VA, 1978.

Lilley, D.G., "Prediction of Inert Turbulent Swirl Flows", AIAA Journal, Vol. 11, No. 7, July 1973, pp. 955-960.

Lilley, D.G., "Swirl Flows in Combustion: A Review", AIAA Journal, Vol. 15, No. 8, August 1977, pp 1063-1078.

Long, M.B. and Chu, B.T., "On the Mixing and Structure of an Axisymmetric Turbulent Mixing Layer", AIAA-80-1354, July 1980.

Mellor, G.L. and Herring, H.J., "A Survey of the Mean Turbulent Field Closure Models", AIAA Journal, Vol. 11, No. 5, May 1973, pp. 590-599.

Milne-Thomson, L.M., Theoretical Aerodynamics, Dover, 1973.

Mims, F.M., III, Engineer's Notebook, Integrated Circuit Applications, Radio Shack, First Edition, 1979.

Neter, J. and Wasserman, W., Applied Linear Statistical Models, Homewood, IL, Richard D. Irvin Inc., 1974.

Oates, G.C., and Knight, C.J., "Throughflow Theory for Turbomachines", USAF Aero Propulsion Laboratory Technical Report, AFAPL-TR-73-61.

Oates, G.C., Notes on Rockets and Airbreathing Engines, USAF Academy, 1975.

Oates, G.C., Editor, "The Aerothermodynamics of Aircraft Gas Turbine Engines", USAF Aero Propulsion Laboratory Technical Report, AFAPL-TR-78-52.

Pai, S.I., Fluid Dynamics of Jets, D. Van Nostrand, New York, 1954.

Perino, P.R., "Wheatstone Bridge Transducer Equations", Statham Instrument Notes No. 38, Feb. 1966.

Pratte, B.D. and Keffer, J.F., "The Swirling Turbulent Jet", Journal of Basic Engineering, Vol. 95, 1973.

Rao, V.K. and Dey, J., "A Note on Turbulent Swirling Flows", AIAA Journal, Vol. 16, No. 4, April 1978, pp. 409-411.

Reynolds, A.J., "Similarity in Swirling Wakes and Jets", Journal of Fluid Mechanics, Vol. 14, 1962, pp. 241-243.

Ribeiro, M.M. and Whitelaw, J.H., "Coaxial Jets With and Without Swirl", Journal of Fluid Mechanics, Vol. 96, Part 4, 1980, pp. 769-795.

Rochino, A. and Lavan, Z., "Analytical Investigation of Incompressible Turbulent Swirling Flow in Stationary Ducts", Journal of Applied Mechanics, Trans. ASME, June 1969, pp. 151-158.

Rodi, W., "Progress in Turbulence Modeling for Incompressible Flows", AIAA-81-0045, Jan. 1981.

Rose, W.G., "A Swirling Round Turbulent Jet, 1 - Mean-Flow Measurements", Journal of Applied Mechanics, Trans. ASME, Dec. 1962, pp. 615-625.

Scheiman, J. and Brooks, J.D., "A Comparison of Experimental and Theoretical Turbulence Reduction from Screens, Honeycomb and Honeycomb-Screen Combinations", AIAA-80-0433.

Schetz, J.A., Injection and Mixing in Turbulent Flow, Progress in Astronautics and Aeronautics, Volume 68, American Institute of Aeronautics and Astronautics, New York, 1980.

Schlichting, H., Boundary Layer Theory, 5th Ed., McGraw-Hill, New York, 1978.

Schubauer, G.B., Spangenberg, W.G., and Klebanoff, P.S., "Aerodynamic Characteristics of Damping Screens", NACA TN-2001, Jan. 1950.

Scott, C.J. and Rask, D.R., "Turbulent Viscisities for Swirling Flow in a Stationary Annulus", Journal of Fluids Engineering, Trans. ASME, Dec. 1973, pp. 557-566.

Sharma, B.I., Launder, B.E., and Scott, C.J., "Computation of Annular, Turbulent Flow With Rotating Core Tube", Journal of Fluids Engineering, Trans. ASME, Dec. 1976, pp. 753-758.

Shavit, G. and Lavan, Z., "Analytical and Experimental Investigations of Laminar Mixing of Confined Heterogeneous Jets", AIAA Journal, Vol. 11, No. 3, March 1973, pp. 352-358.

So, R.M.C. and Mellor, G.L., "Experiment on Convex Curvature Effects in Turbulent Boundary Layers", Journal of Fluid Mechanics, Vol. 60, Part 4, 1973, pp. 45-62.

Szczeniowski, B., "Contraction Cone for a Wind Tunnel", JAS, Feb. 1943, pp. 311 & 312.

Tabakoff, W. and Blasenak, J., "Non-Isoenergetic Turbulent Jet Mixing in a Constant Area Duct", AIAA-81-0347, Jan. 1981.

Tennekes, H. and Lumley, J.L., A First Course in Turbulence, MIT Press, Cambridge, Mass., 1972.

Townsend, A.A., "Entrainment and Structure of Turbulent Flow", Journal of Fluid Mechanics, Vol. 41, Part 1, 1970, pp. 13-46.

Tsien, H.S., "On the Design of the Contraction Cone for a Wind Tunnel", JAS, Feb. 1943, pp. 68-70.

Waltz, A., Boundary Layers of Flow and Temperature, MIT Press, 1969, pp. 262-270.

White, F.M., Viscous Fluid Flow, McGraw-Hill, New York, 1974.

Wolf, L., Jr, Lavan, Z., and Fejer, A.A., "Measurement of the Decay of Swirl in Turbulent Flow", AIAA Journal, Vol. 7, No. 5, May 1969, pp. 971-972.

Yajnik, K.S. and Subbaiah, M.V., "Experiments on Swirling Turbulent Flows. Part 1. Similarity in Swirling Flows", Journal of Fluid Mechanics, Vol. 60, Part 4, 1973, pp. 665-687.

Zakkay, V., Krause, E., and Woo, S.D.L., "Turbulent Transport Properties for Axisymmetric Heterogeneous Mixing", AIAA Journal, Vol. 2, No. 11, Nov. 1964, pp. 1939-1947.

Zelazny, S.W., Morgenthaler, J.H., and Herendeen, D.L., "Shear Stress and Turbulence Intensity Models for Coflowing Axisymmetric Streams", AIAA Journal, Vol. 11, No. 8, Aug. 1973, pp. 1165-1173.

APPENDIX A

EXPERIMENTAL RESULTS

This appendix presents the experimental data gathered in four sets of experiments using the test apparatus described in Chapter 4 and the five-hole probes described in Chapter 5. The experimental data was reduced and plotted in Figures A-1 through A-90 using the programs described in Chapter 6. The experimental data has been nondimensionalized for presentation and ease of analysis. The quantities used to nondimensionalize are shown in Table A-1. Table A-2 lists the test section configuration and data plot Figures for each test number. Table A-3 presents the values used to nondimensionalize the data and the average reference values for each test.

Plots of the static pressure on the 4 inch tube, the 6 inch tube, and the 8 inch tube for tests #3 and #4 have individual data points for each run contained in the test. However the plots of the static pressure on the 6 inch tube for tests #1 and #2 (Figures A-1 & A-9) have data points that are the average of the runs in the test. The variations of velocity, pressure, momentum, etc. with radial and axial position for tests #1 and #4 are plotted in a format having individual subplots for each axial

position measured. The variations of these properties for tests #2 and #3 are plotted on a combined radial/axial position scale with error bounds (dots) plotted for each data point. The horizontal location of the variable's zero is repositioned to correspond to the axial location of the test run as shown on the axial position scale at the top of these plots (see Figure A-21).

TABLE A-1
Dimensionless Quantities for Data Plots

Dimensional Symbol	Dimensional Quantity	Dimensionless Quantity
w	Axial Velocity	w/U
v	Tangential Velocity	v/U
u	Radial Velocity	u/U
V	Total Velocity	V/U
P_T	Total Pressure	$(P_T-P_o)/(1/2\,\rho U^2)$
P_S	Static Pressure	$(P_S-P_o)/(1/2\,\rho U^2)$
P	Wall Static Pressure	$(P-P_o)/(1/2\,\rho U^2)$
M_z	Axial Momentum Flux	$M_z/(1/2\,\rho U^2)$
M_z'	Axial Momentum Flux	$M_z'/(1/2\,\rho U^2)$
M_θ	Tangential Momentum Flux	$M_\theta/(1/2\,\rho U^2)$

where

Symbol	Description	Test Sets
U	Mean Axial Velocity of Inner Stream	1 - 3
U	Mean Axial Velocity in Test Section	4
P_o	Atmospheric Pressure	1 - 3
P_o	Static Pressure on Outer Wall of Inner Stream at z = -2 inches	4

TABLE A-2
Test Sets/Configuration/Figures

Test Set Number	Test Section Figure	Configuration			Data Figures
		Outer Stream	Center Body	Outside Wall	
1	3-1	No	No	No	A-1 - A-8
2	3-2	Yes	No	No	A-9 - A-17
3	3-3	Yes	Yes	No	A-18 - A-35
4	3-4	Yes	Yes	Yes	A-36 - A-90

TABLE A-3
Average Reference Values

Test Set	Runs	$\dot{m}$ (lb /sec)	α	U (ft/sec)	P_o (psig)
1	1 - 3	.577	0	70	0
2	1 - 3	.494	1.0	30	0
3	1 - 5	.807	1.0	49	0
4	XX1	.652	0	33	-0.010
4	XX2	.652	0.47	33	0.015
4	XX3	.652	1.0	33	0.016
4	XX4	.652	2.13	33	0.014
4	XX5	.652	3.91	33	0.008

Reference Density = 0.079 lbm/ft^3

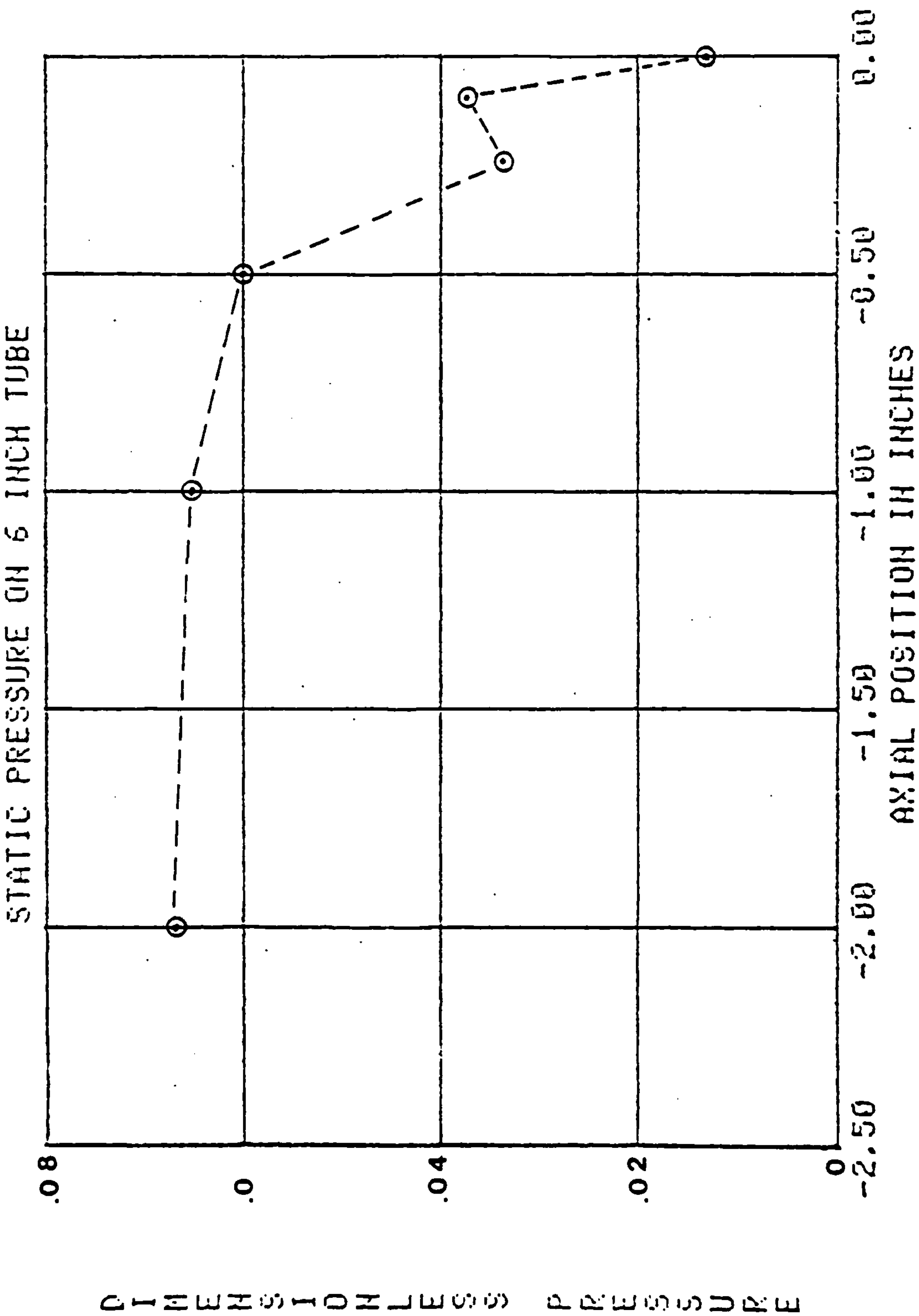
STATIC PRESSURE ON 6 INCH TUBE
AXIAL POSITION IN INCHES
DIMENSIONLESS PRESSURE
-2.50
-2.00
-1.50
-1.00
-0.50
0.00
0
.02
.04
.0
.08

Figure A-1

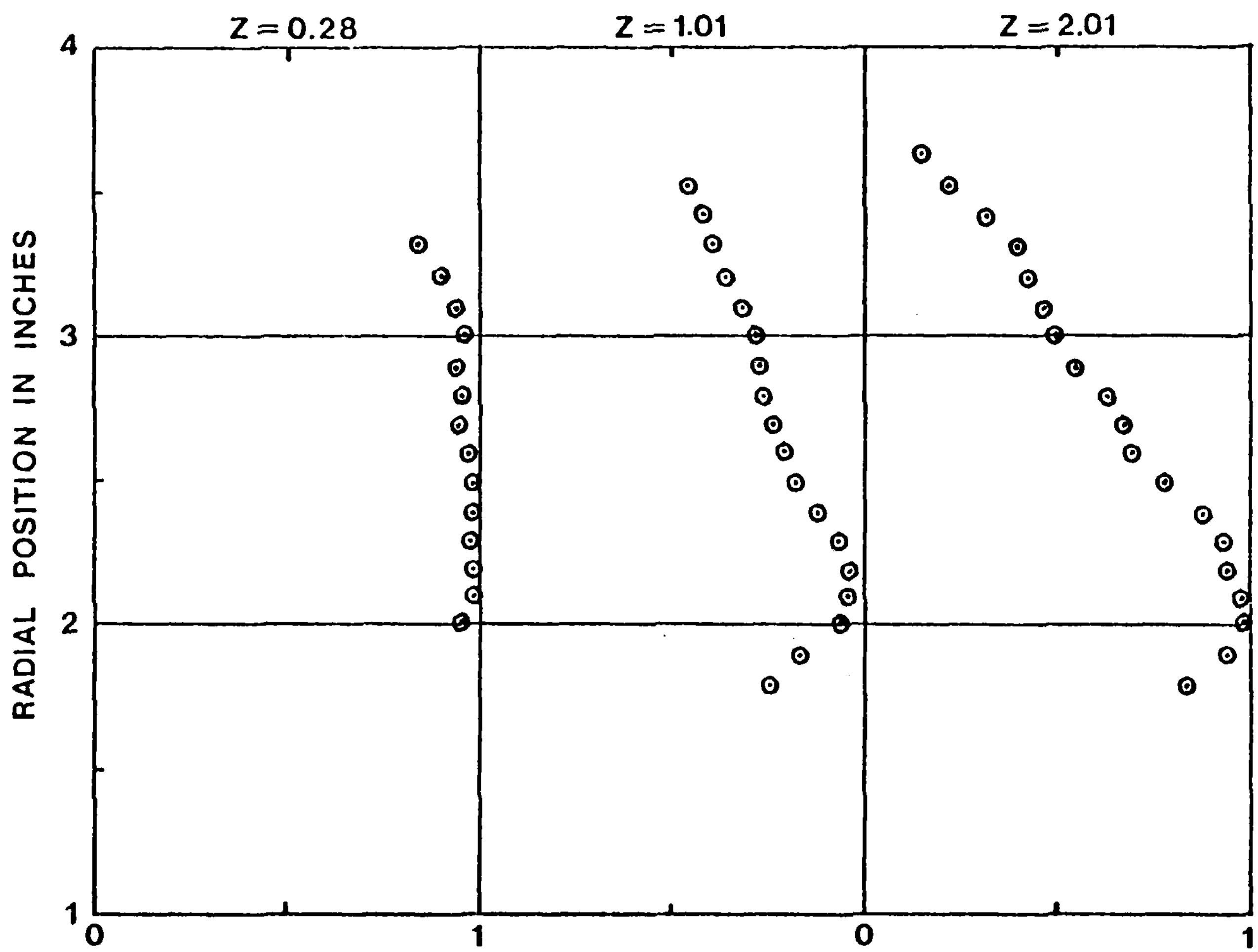

Figure A-2 Dimensionless Axial Velocity, Test #1

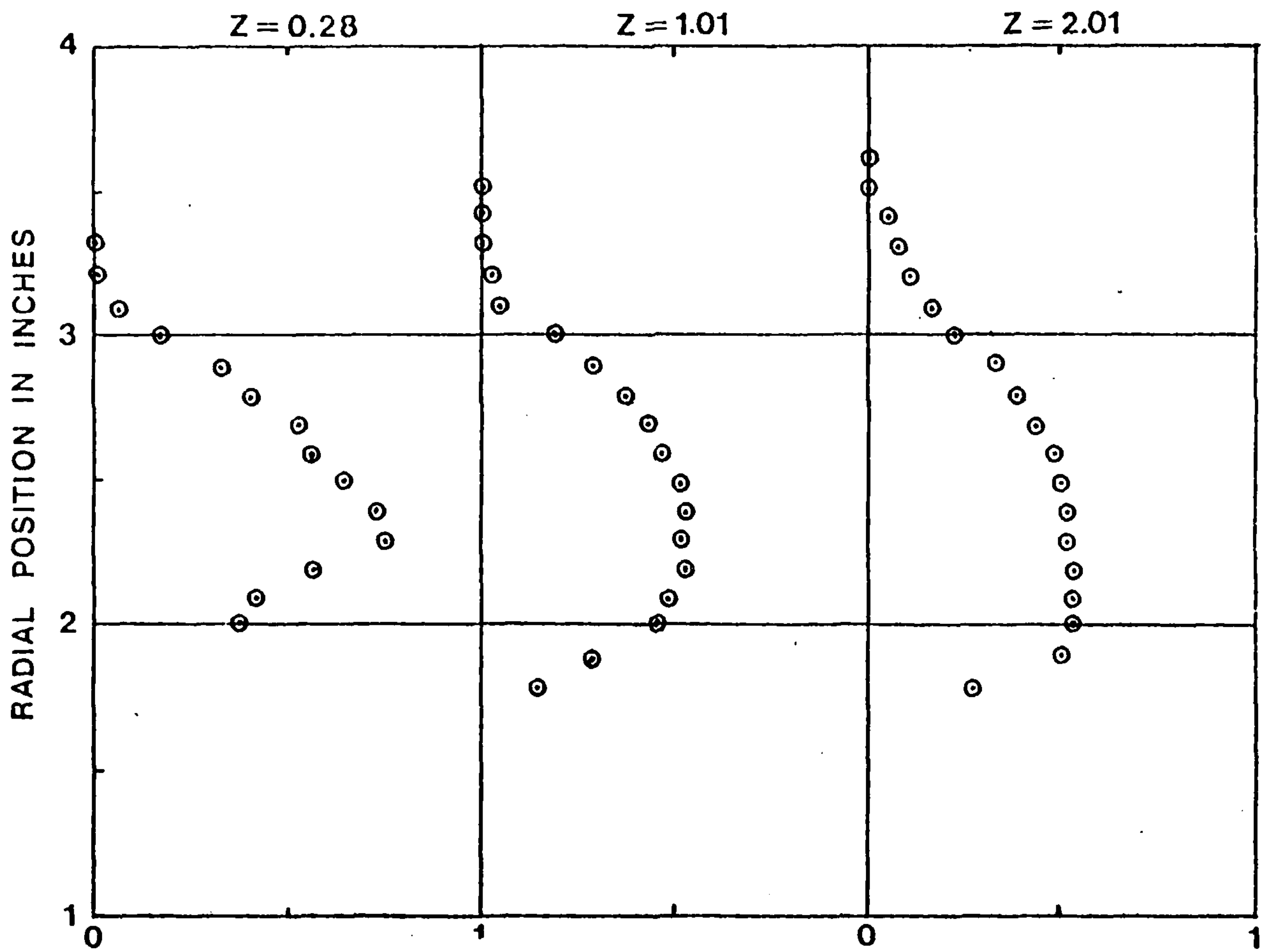

Figure A-3 Dimensionless Tangential Velocity, Test #1

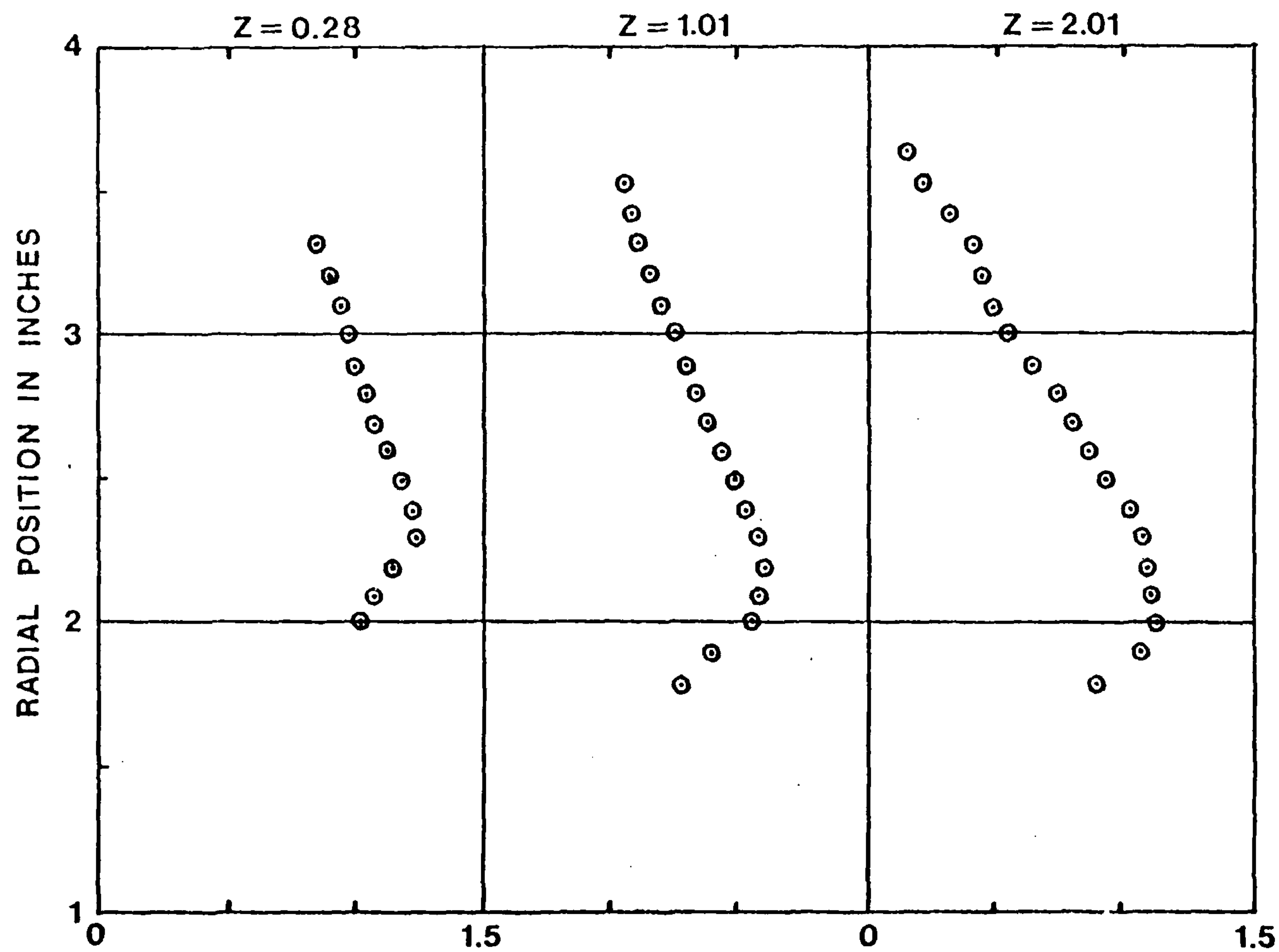

Figure A-4 Dimensionless Velocity, Test #1

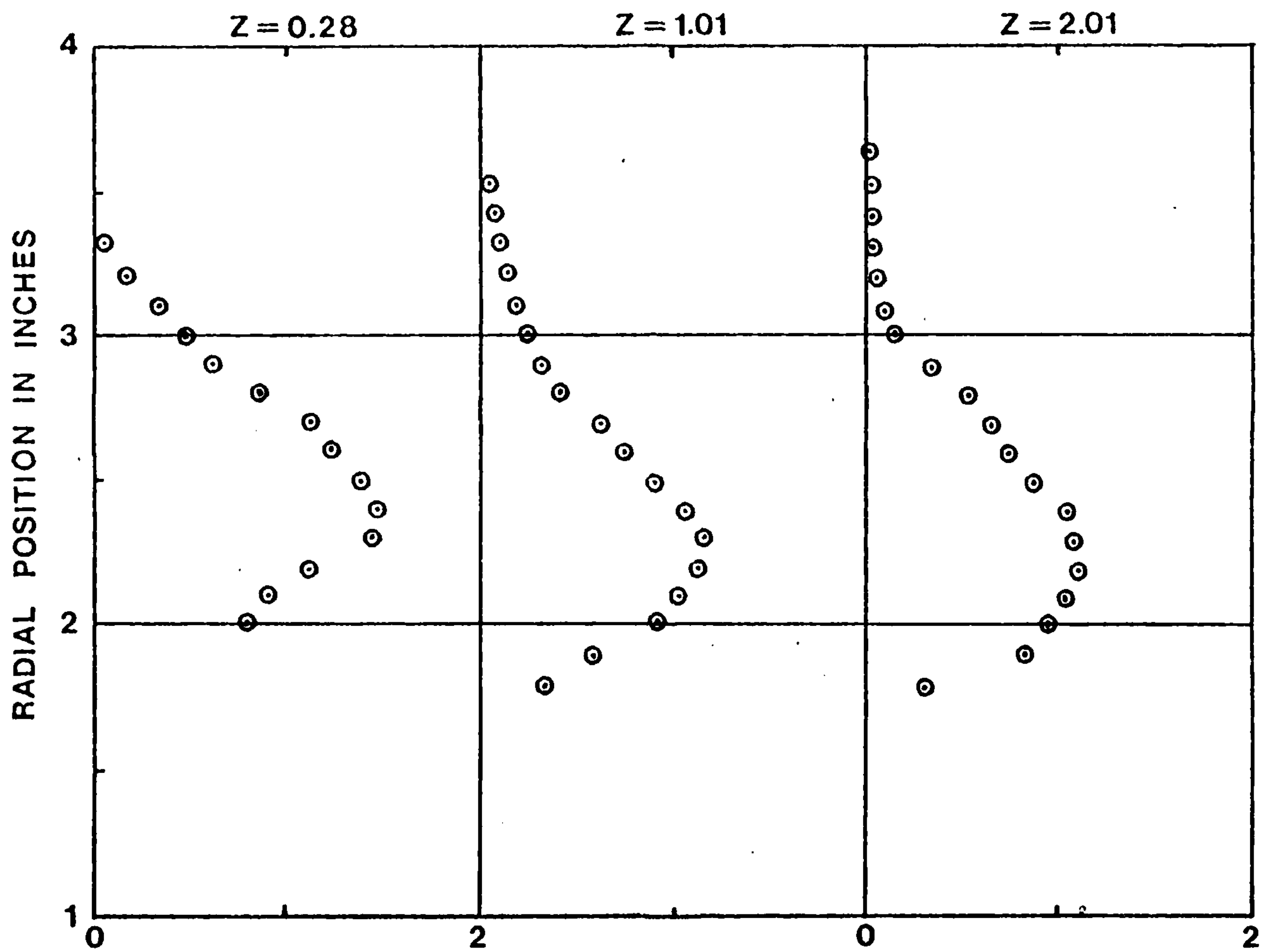

Figure A-5 Dimensionless Total Pressure, Test #1

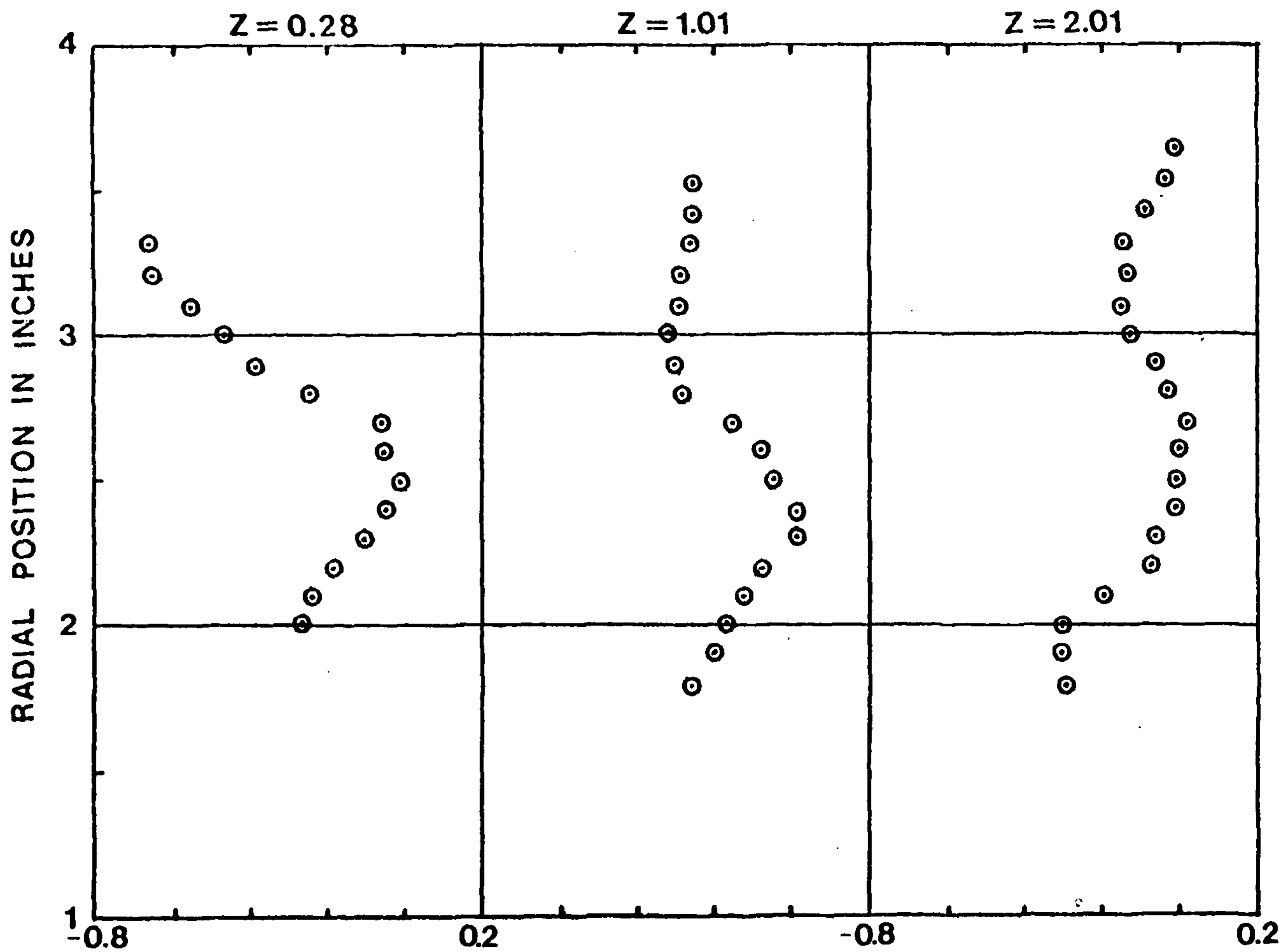

Figure A-6 Dimensionless Static Pressure, Test #1

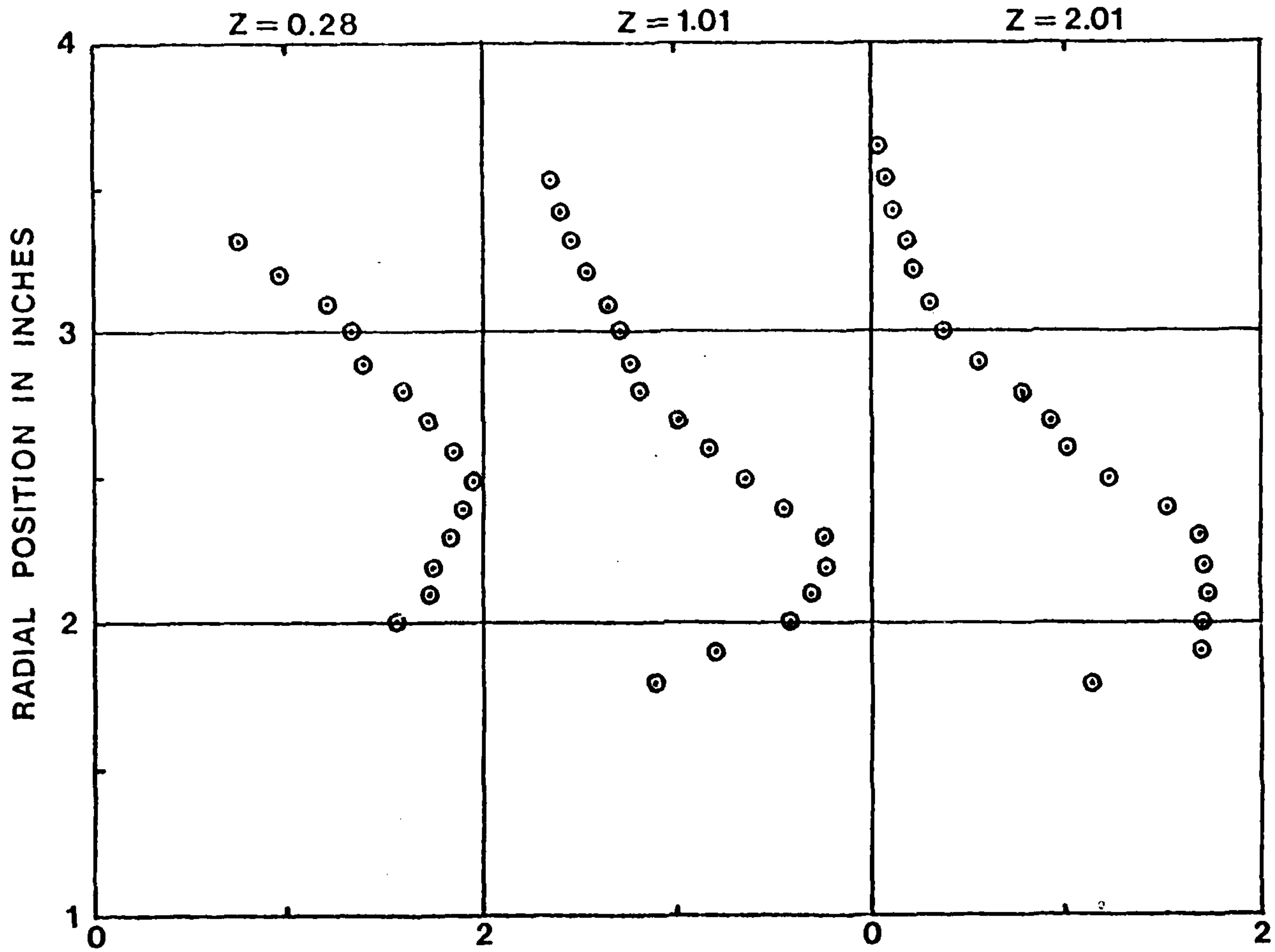

Figure A-7 Dimensionless Axial Momentum Flux, Test #1

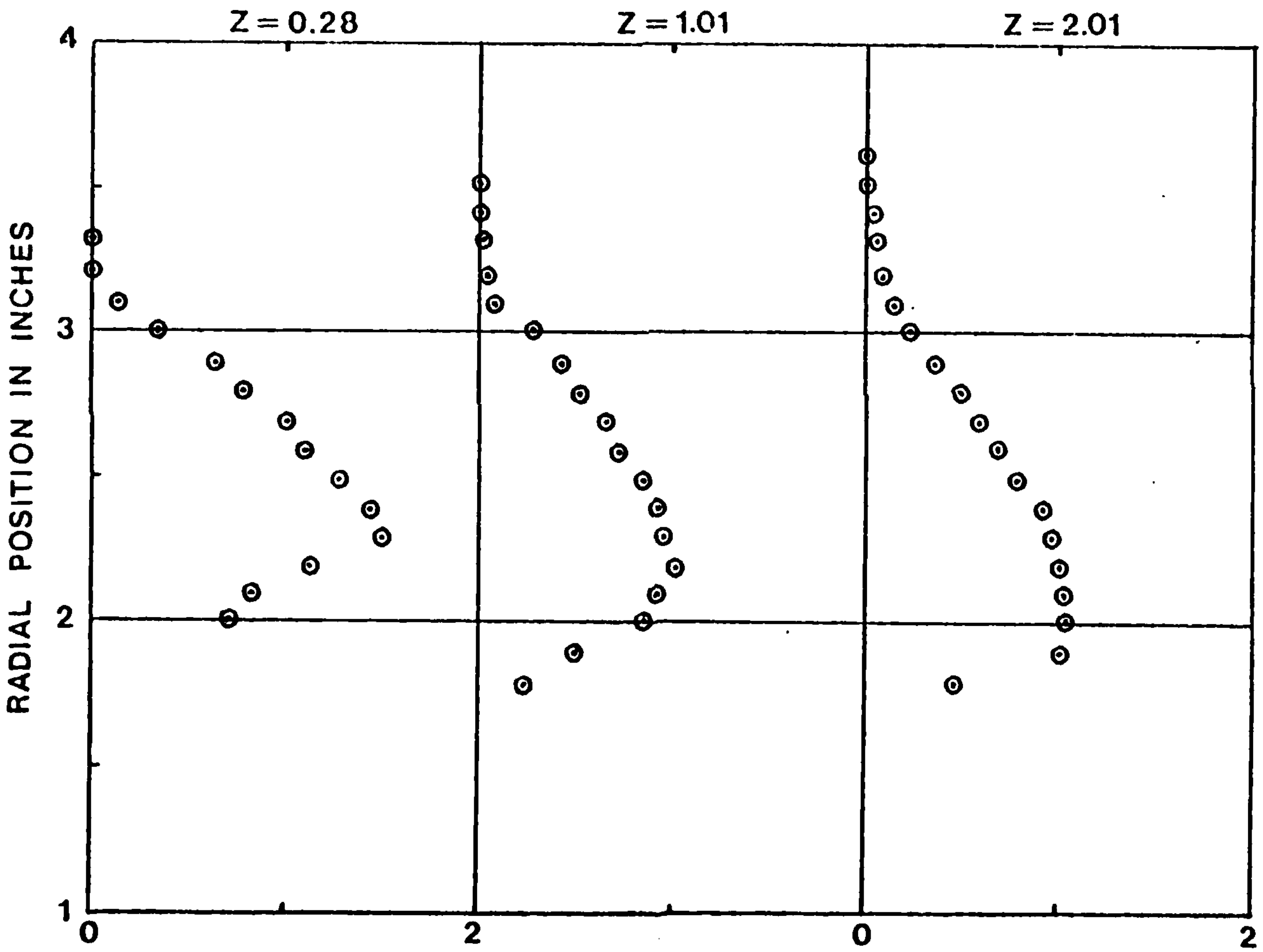

Figure A-8 Dimensionless Tangential Momentum Flux, Test #1

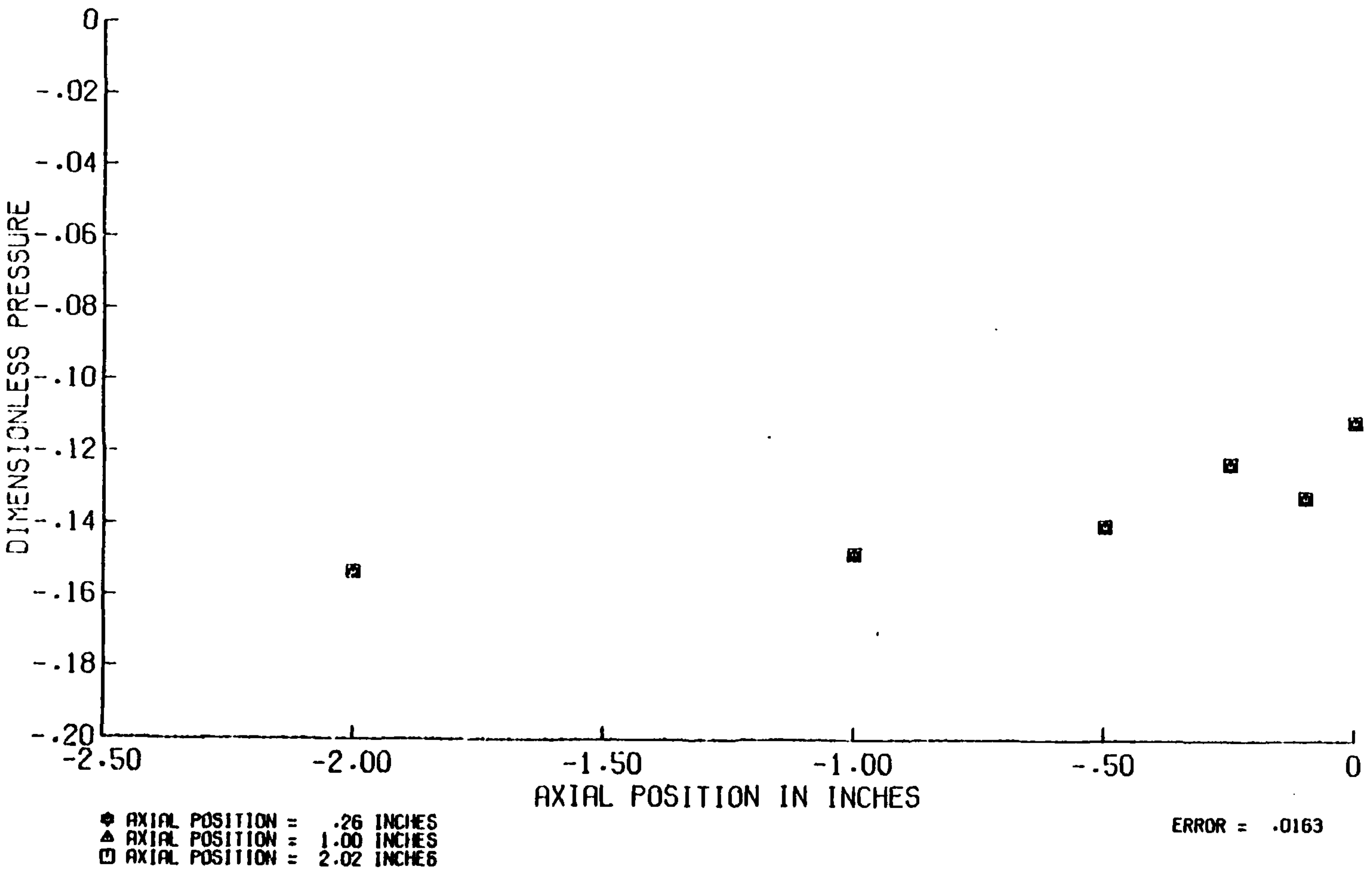

Figure A-9 Dimensionless Static Pressure on 6 Inch Tube, Test #2

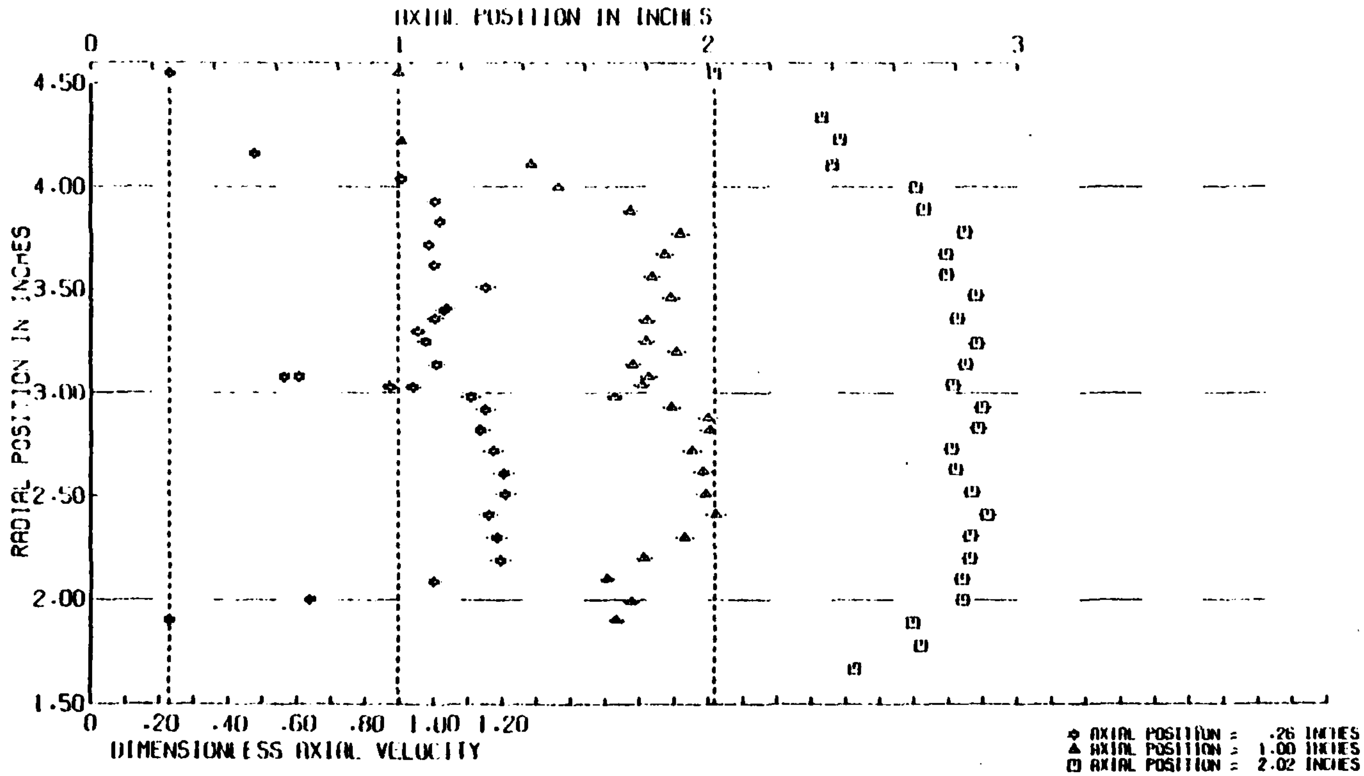

Figure A-10 Dimensionless Axial Velocity, Test #2

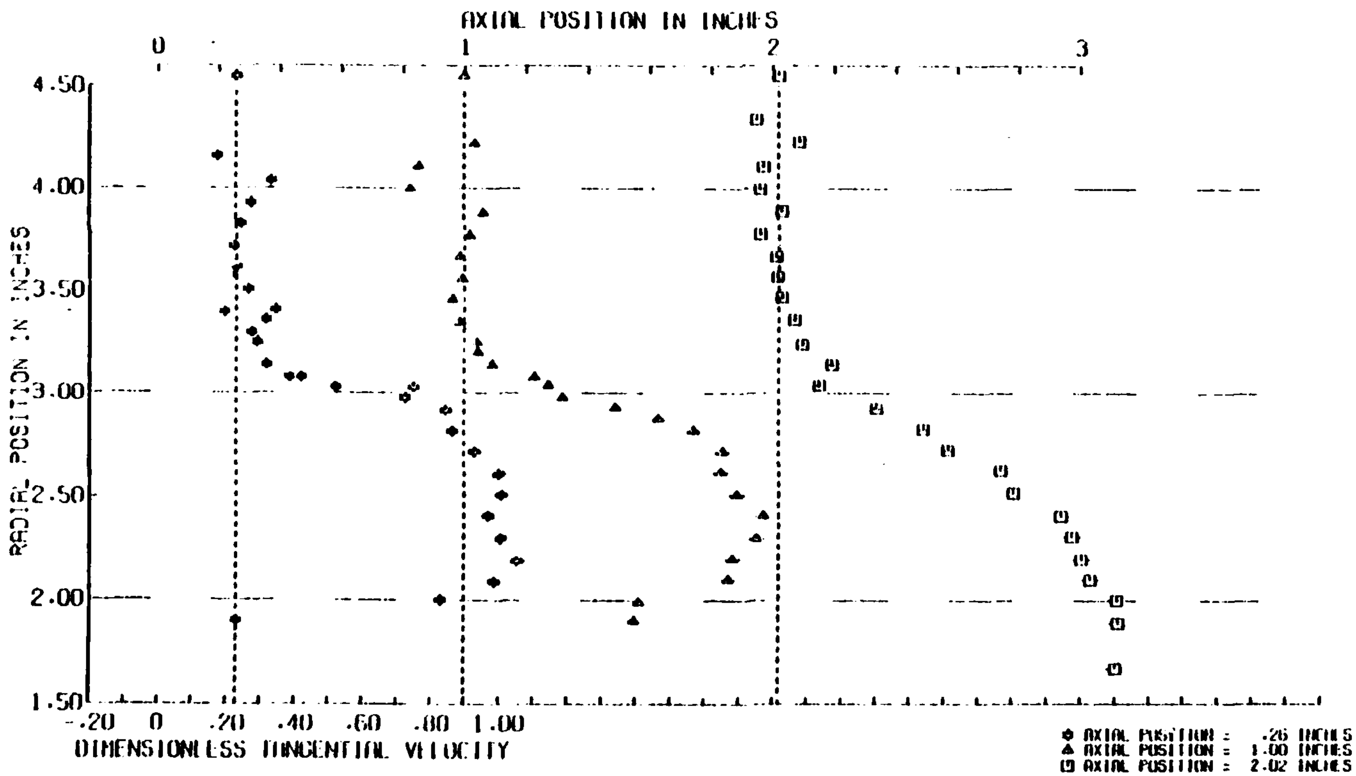

Figure A-11 Dimensionless Tangential Velocity, Test #2

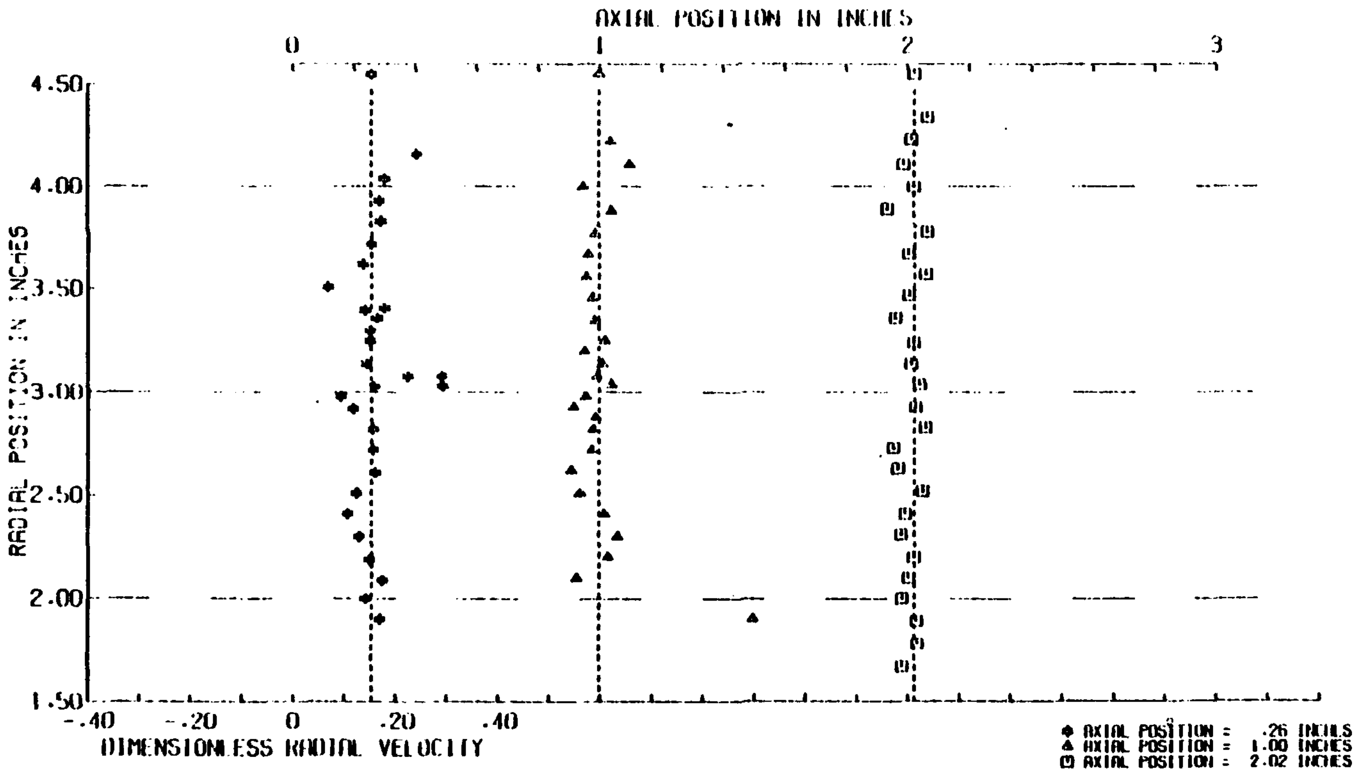

Figure A-12 Dimensionless Radial Velocity, Test #2

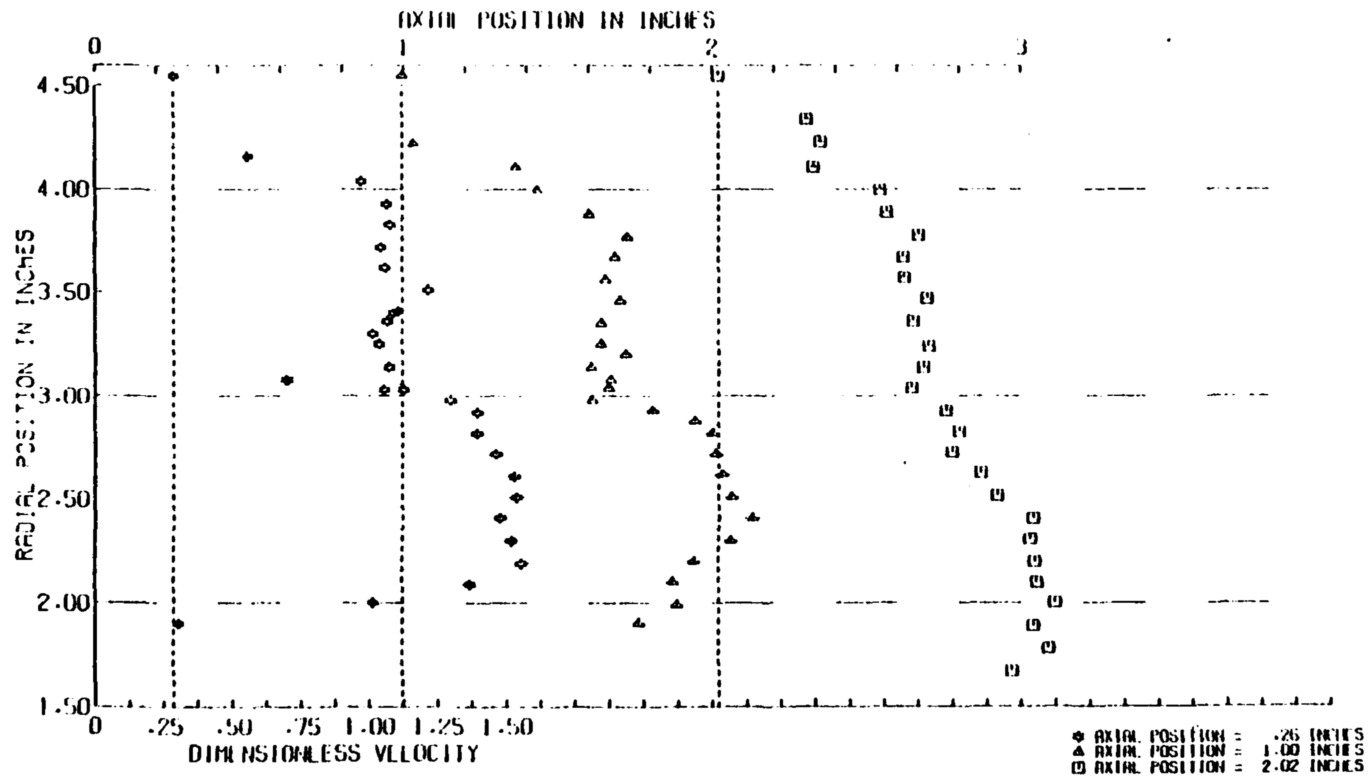

Figure A-13 Dimensionless Velocity, Test #2

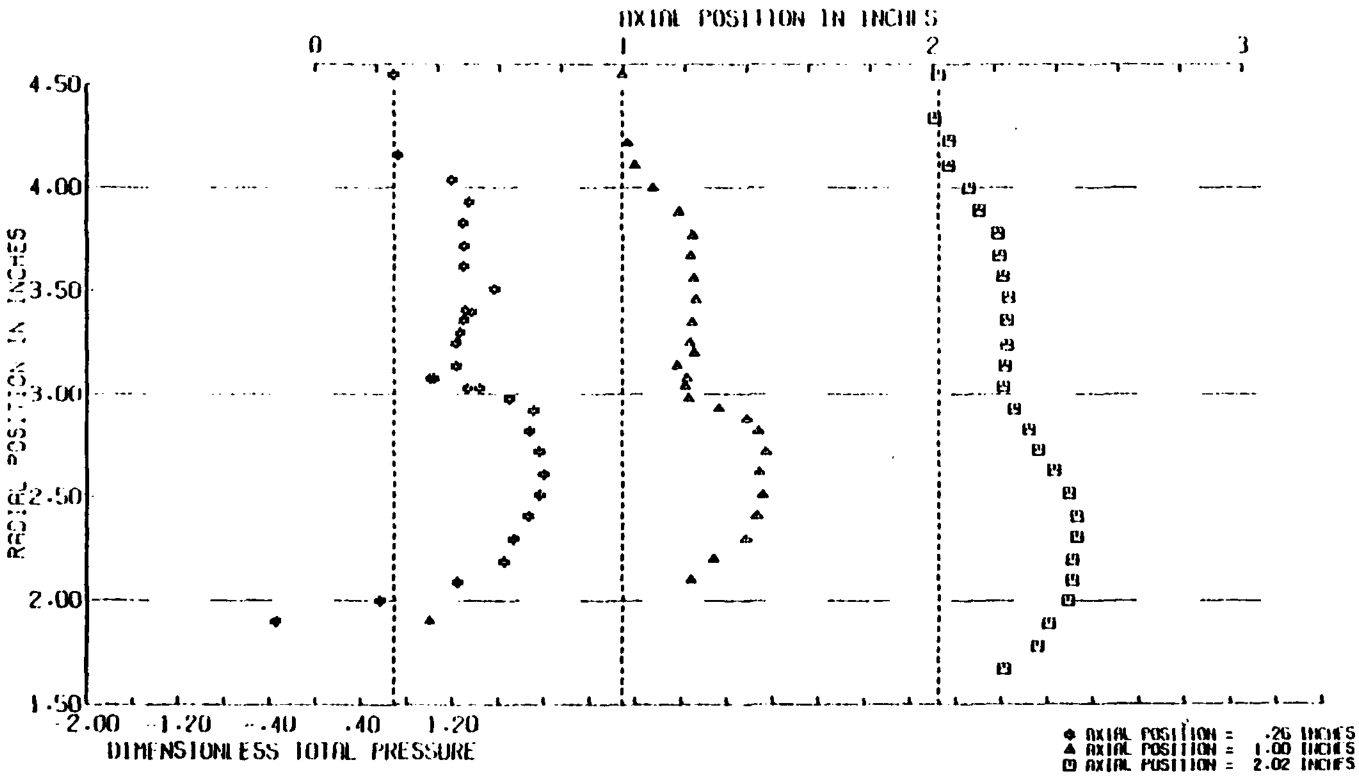

Figure A-14 Dimensionless Total Pressure, Test #2

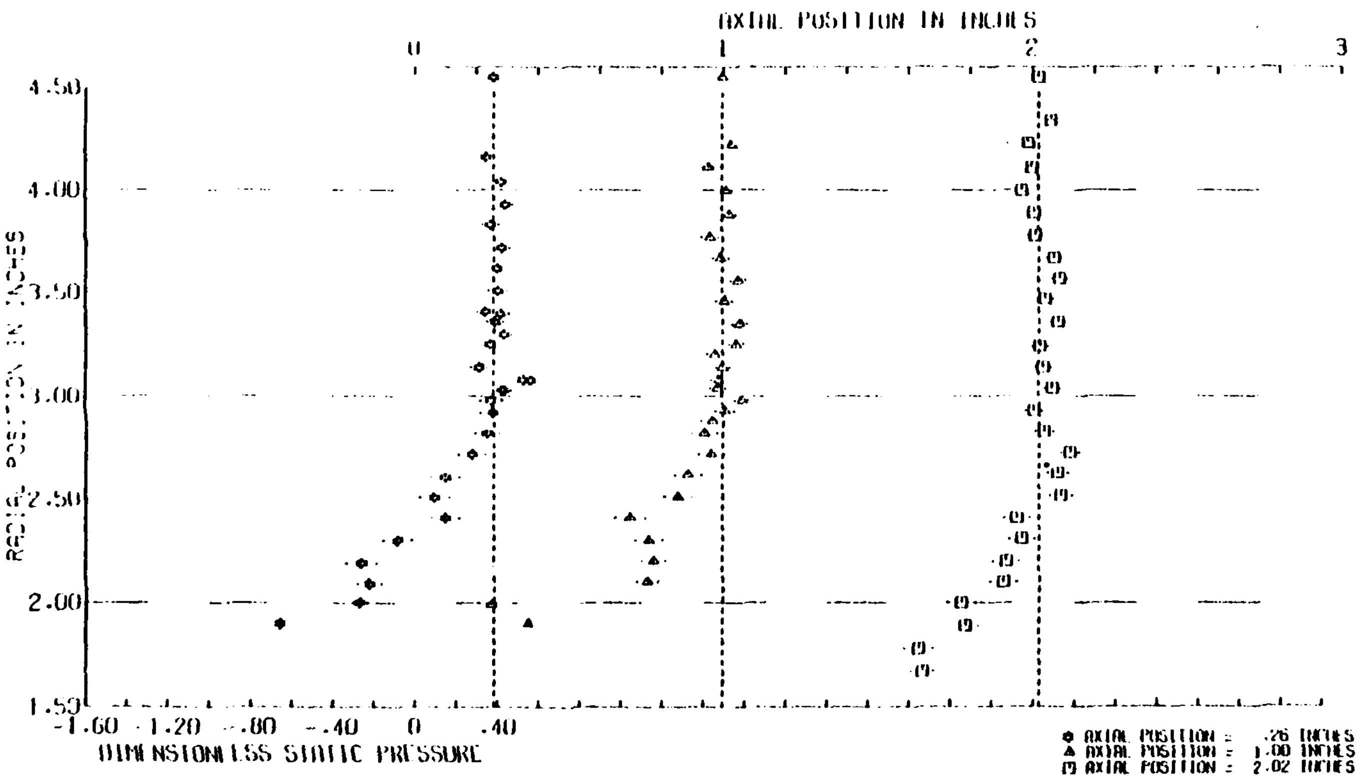

Figure A-15 Dimensionless Static Pressure, Test #2

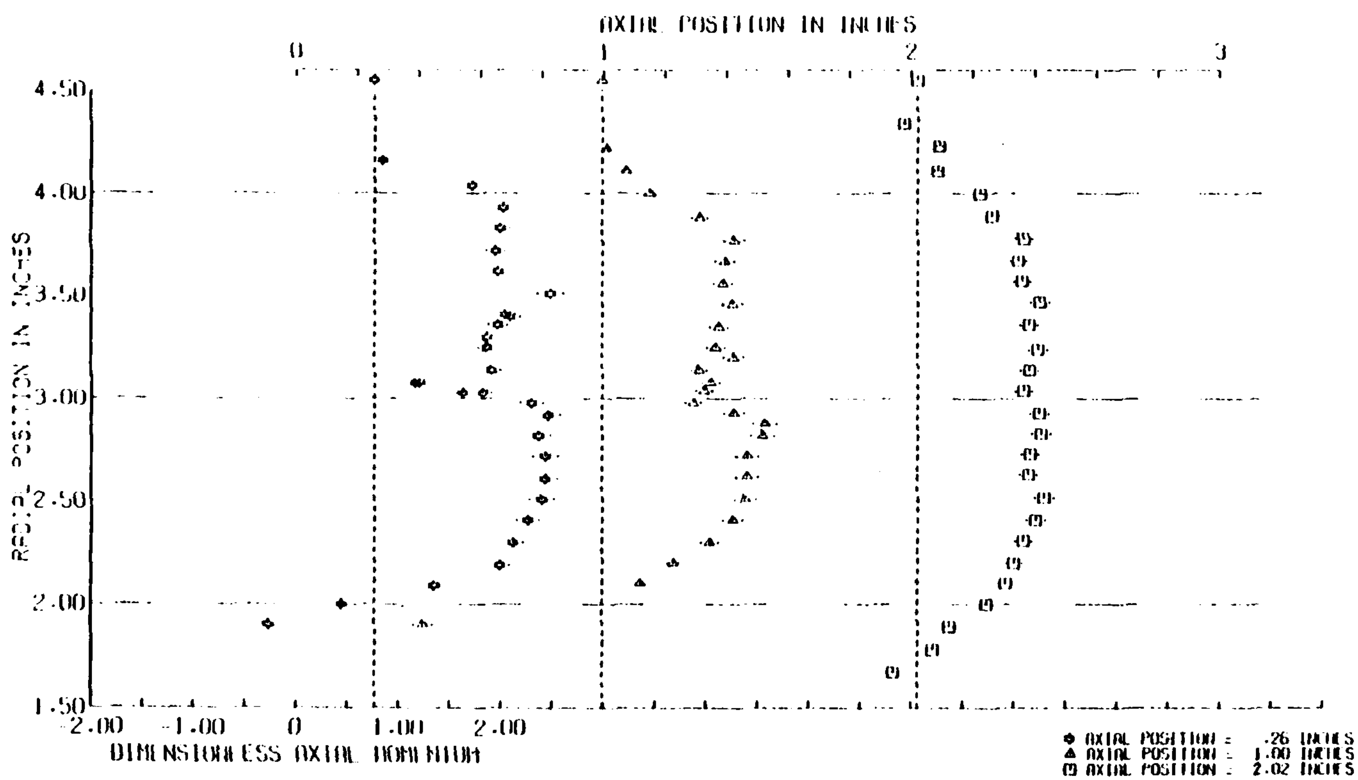

Figure A-16 Dimensionless Axial Momentum Flux, Test #2

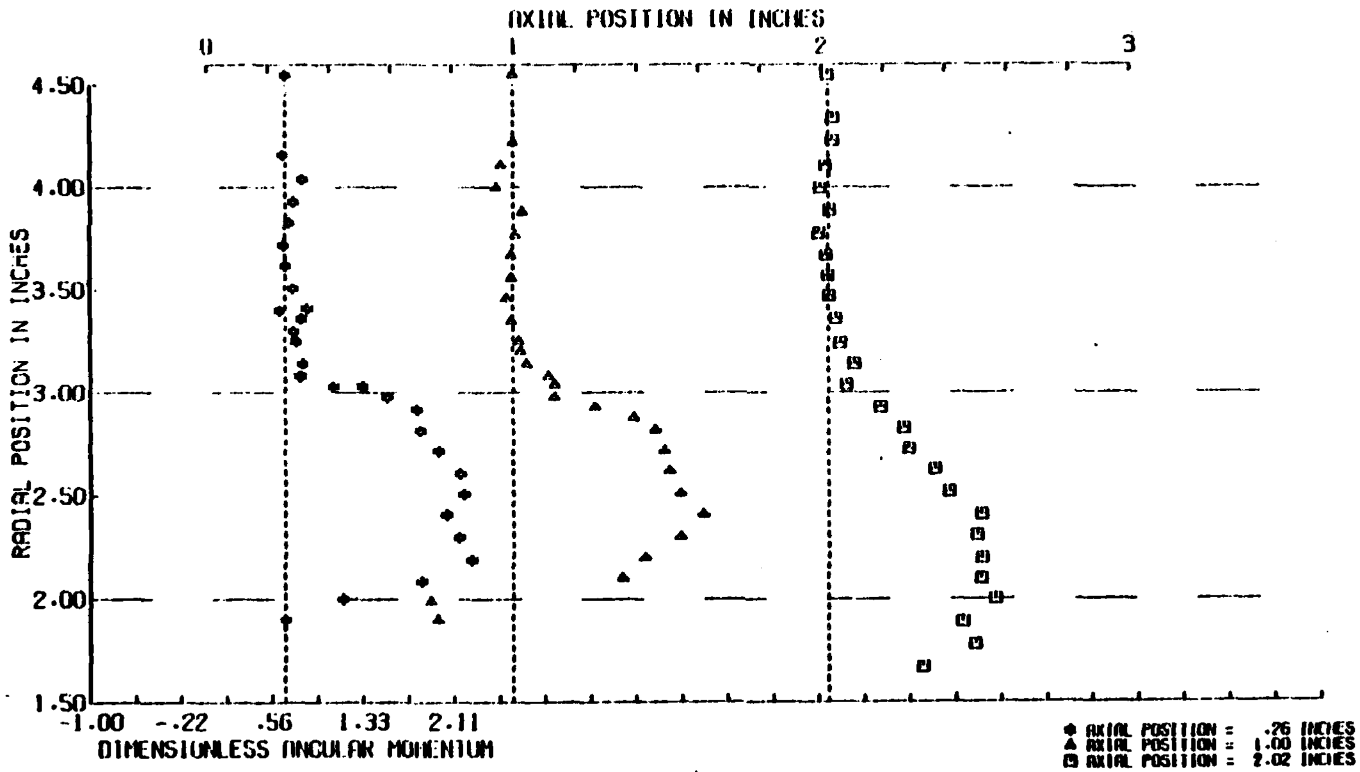

Figure A-17 Dimensionless Angular Momentum Flux, Test #2

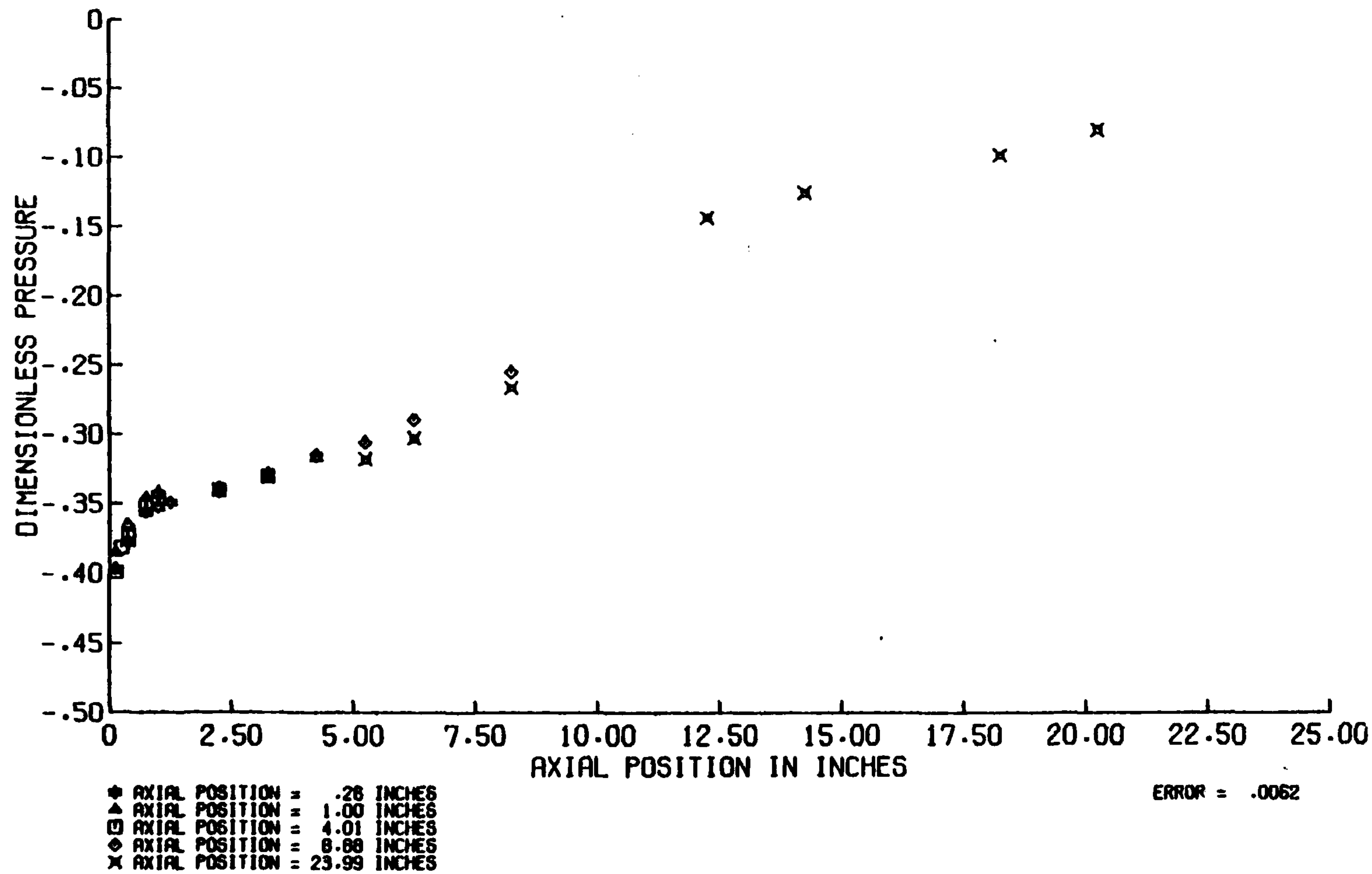

Figure A-18 Dimensionless Static Pressure on 4 Inch Tube, Test #3

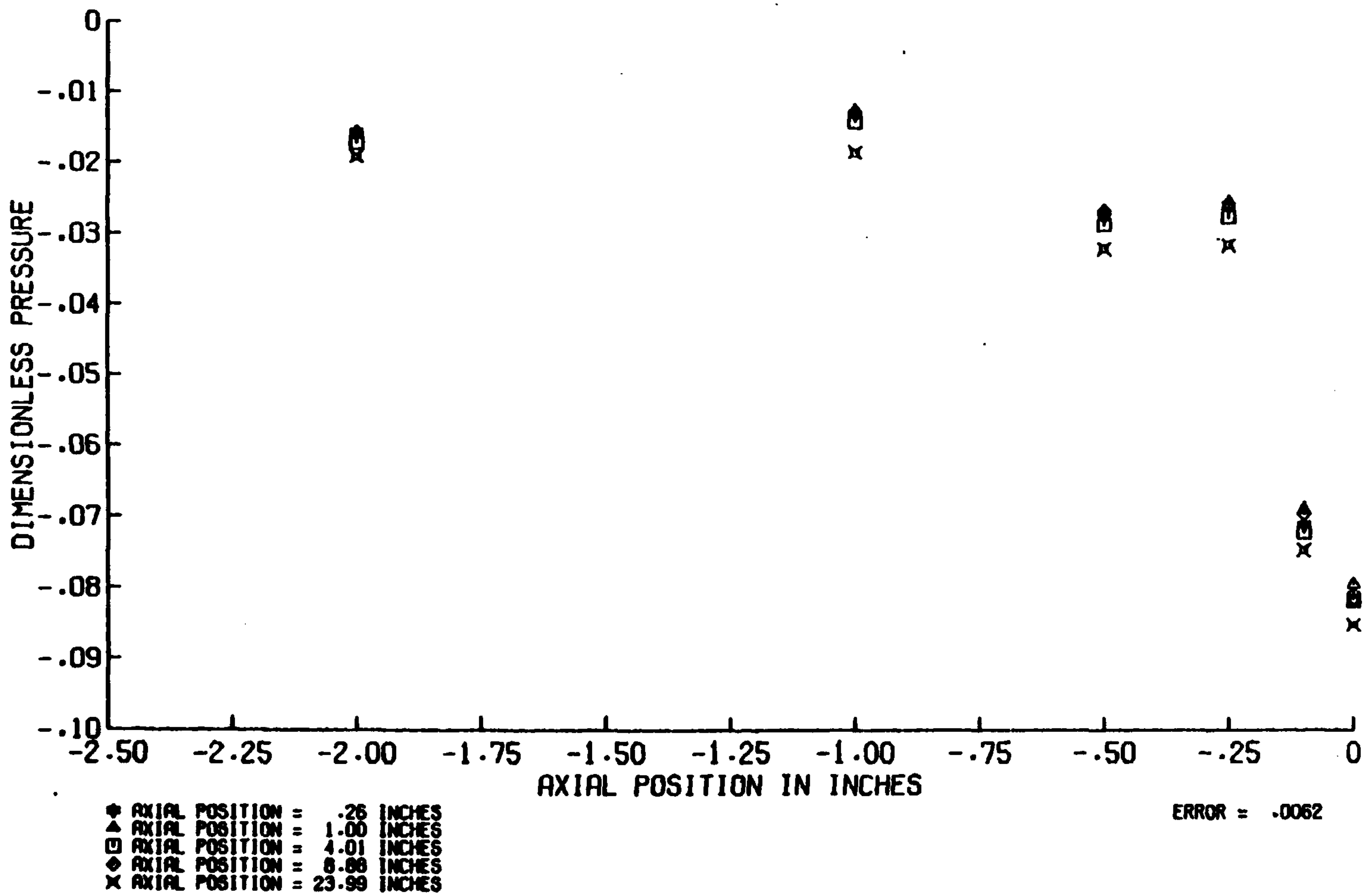

Figure A-19 Dimensionless Static Pressure on 6 Inch Tube, Test #3

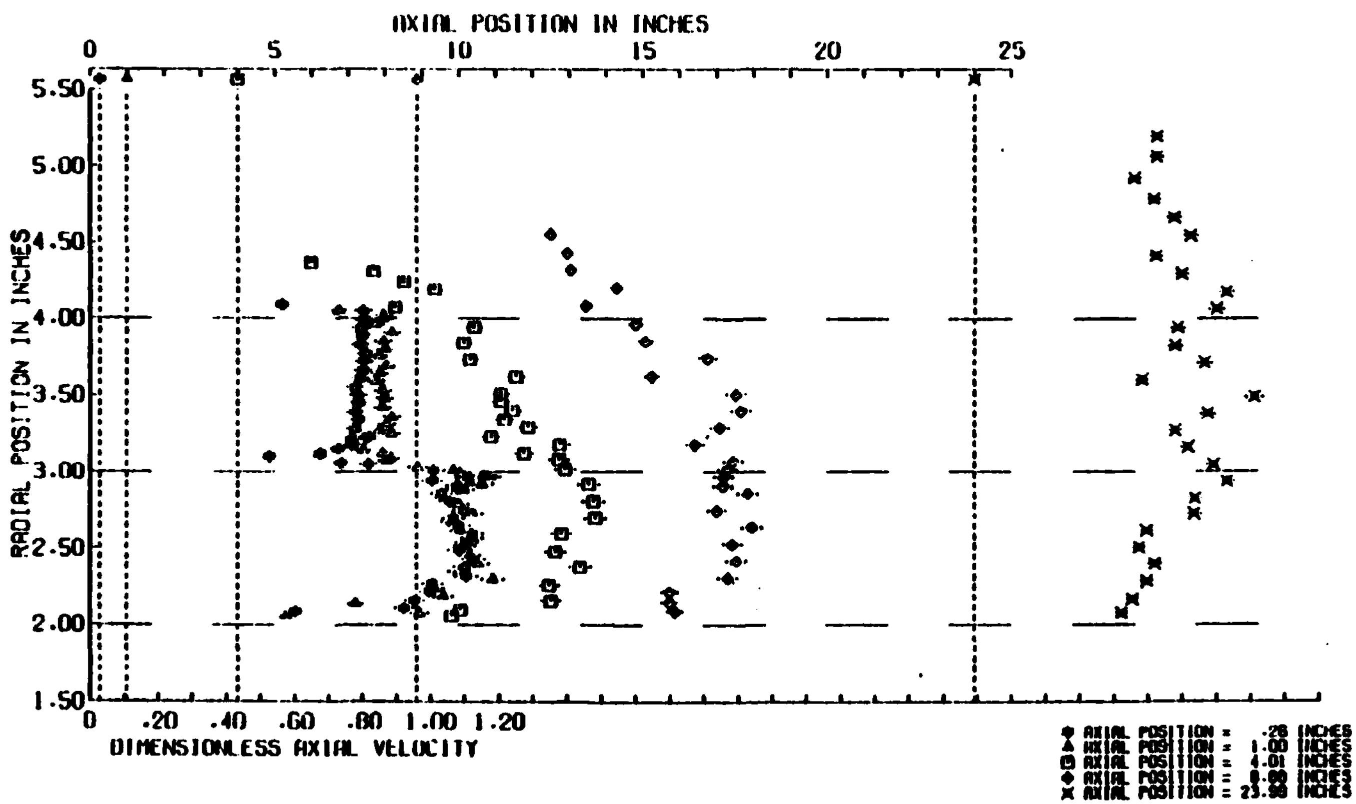

Figure A-20 Dimensionless Axial Velocity, Test #3, Five Axial Locations

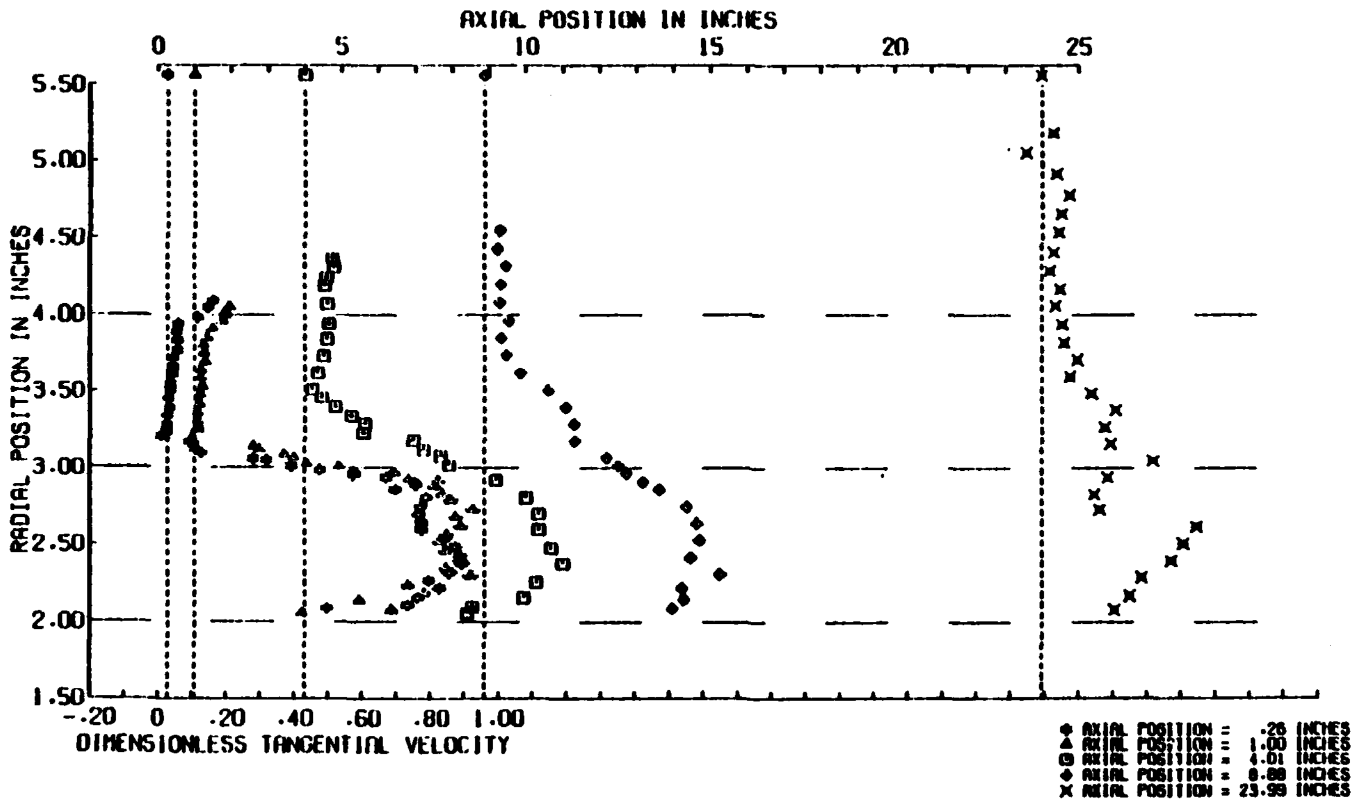

Figure A-22 Dimensionless Tangential Velocity,
Test #3, Five Axial Locations

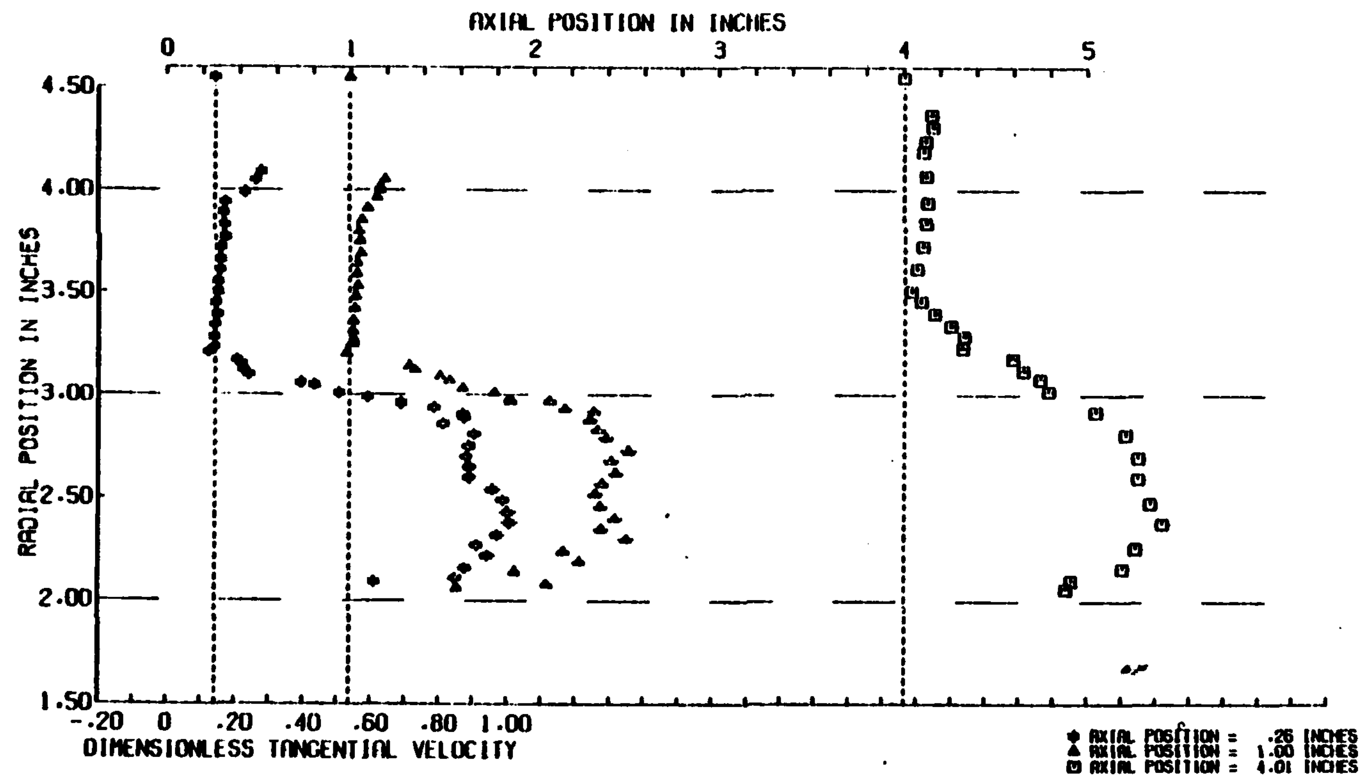

Figure A-23 Dimensionless Tangential Velocity, Test #3, Three Axial Locations

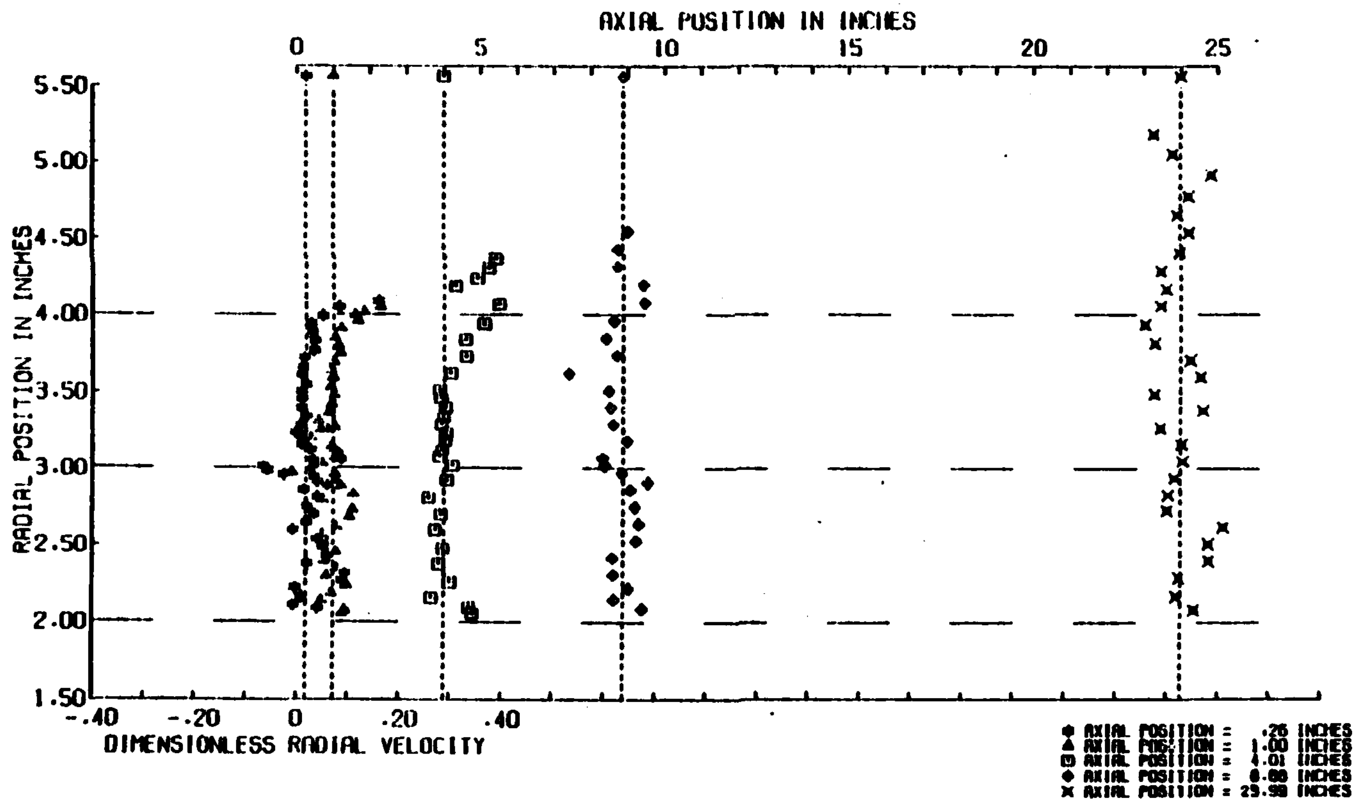

Figure A-24 Dimensionless Radial Velocity, Test #3, Five Axial Locations

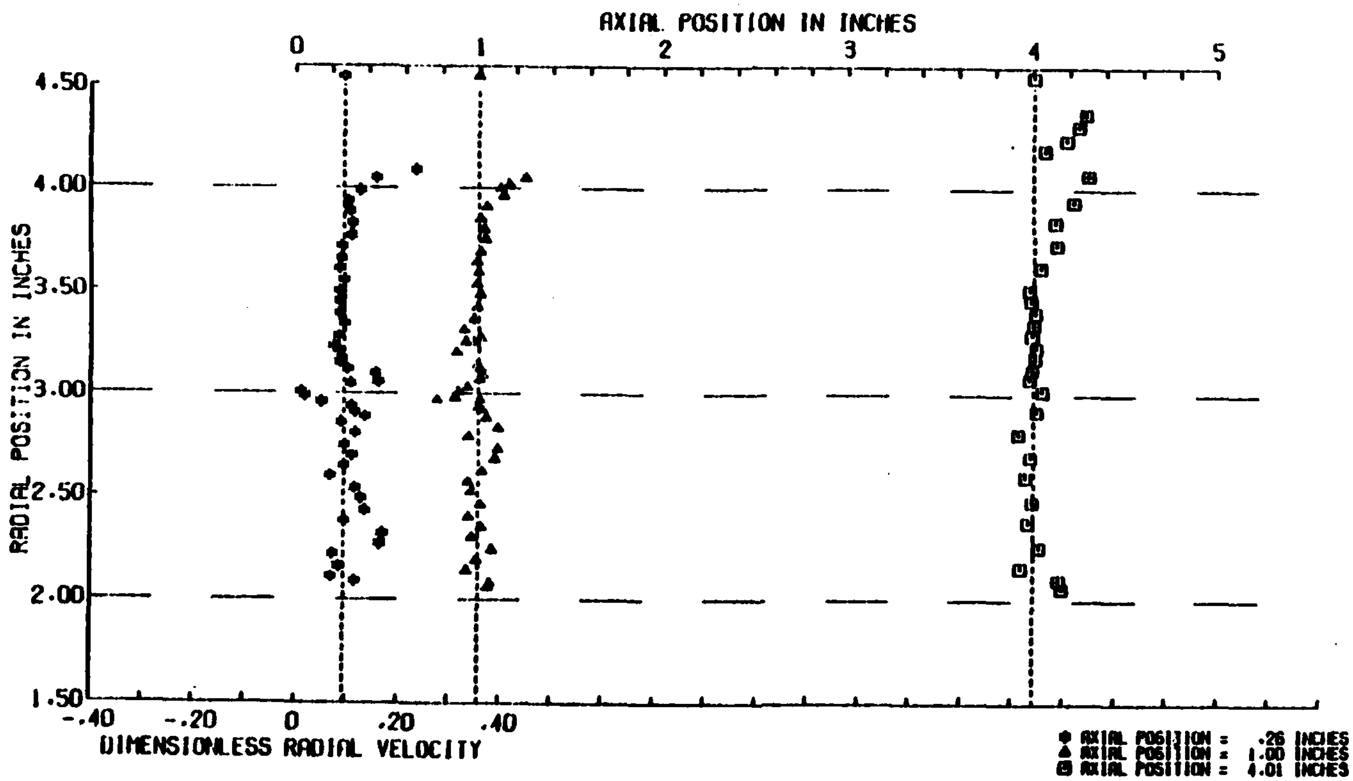

Figure A-25 Dimensionless Radial Velocity, Test #3, Three Axial Locations

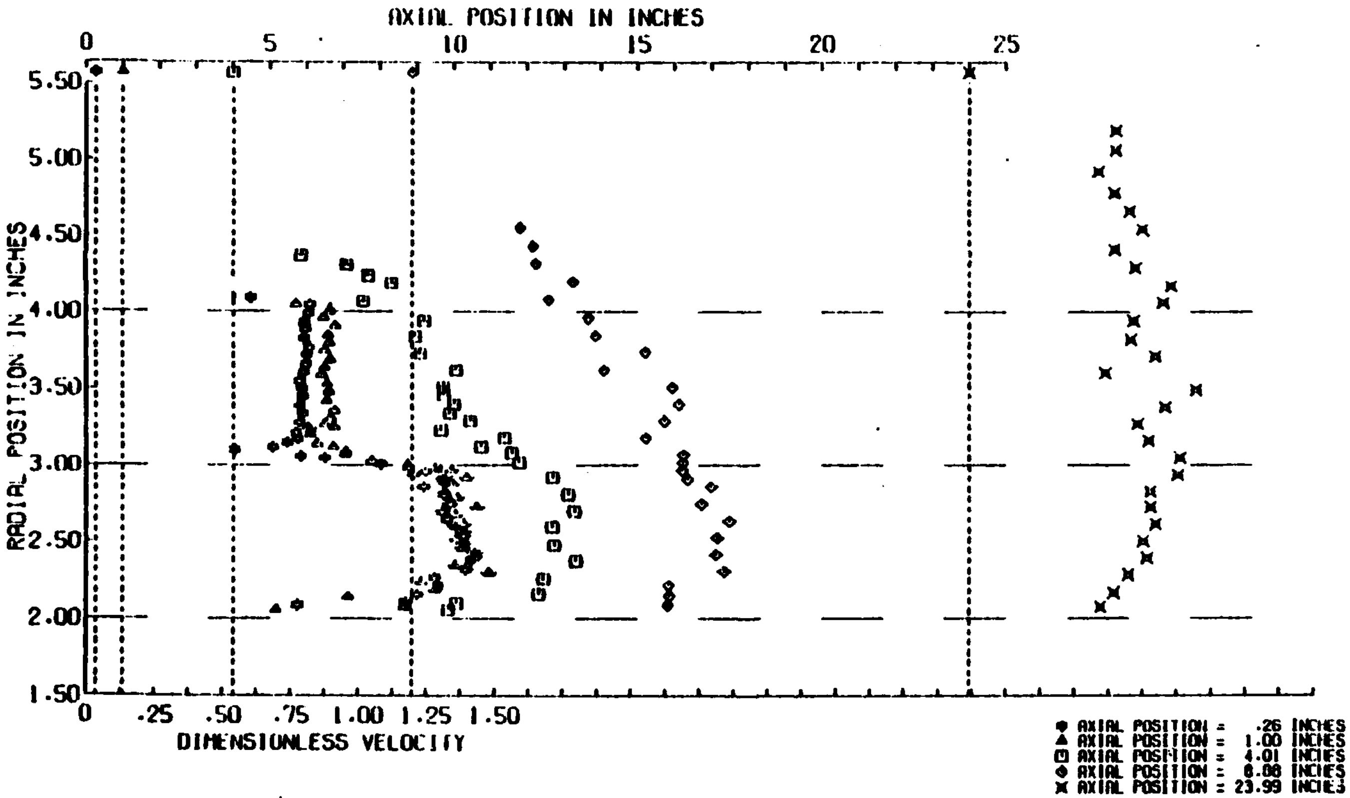

Figure A-26 Dimensionless Velocity, Test #3, Five Axial Locations

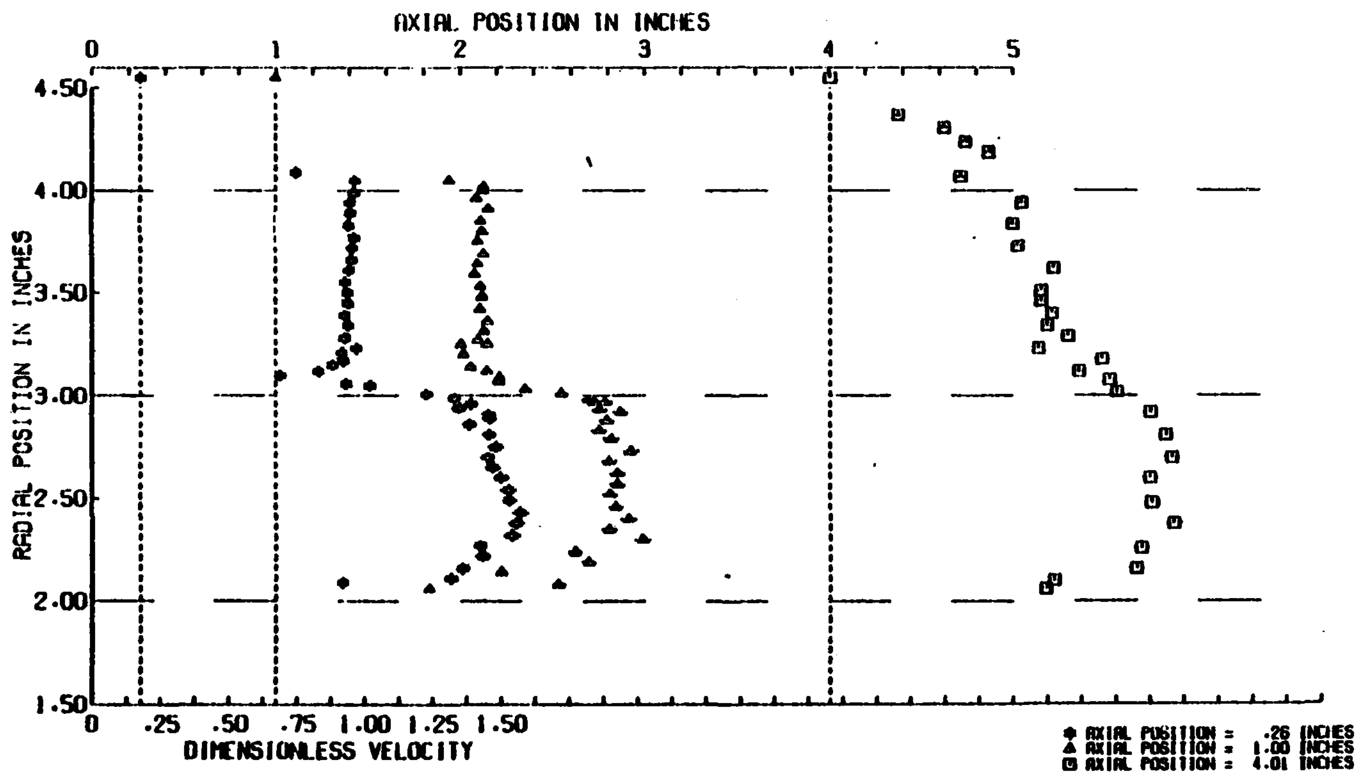

Figure A-27 Dimensionless Velocity, Test #3, Three Axial Locations

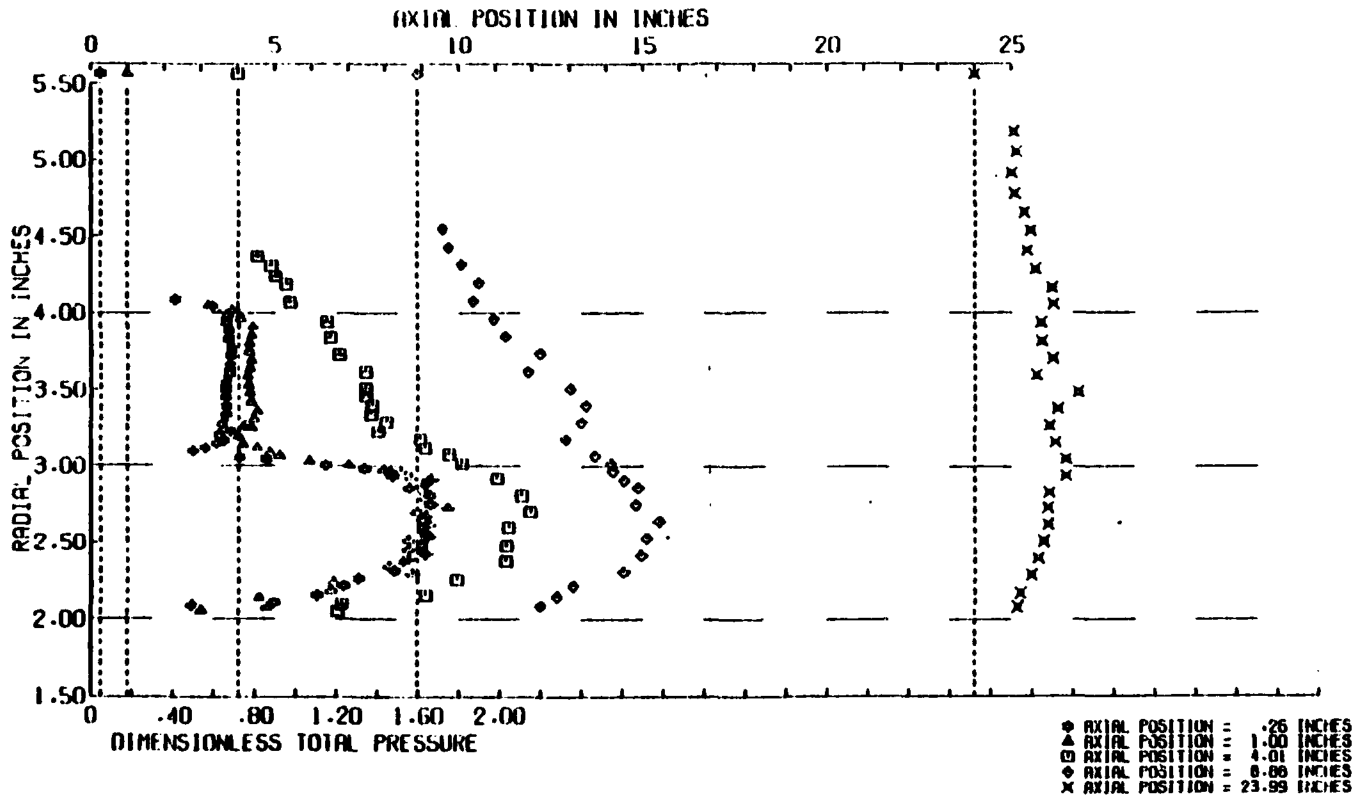

Figure A-28 Dimensionless Total Pressure, Test #3, Five Axial Locations

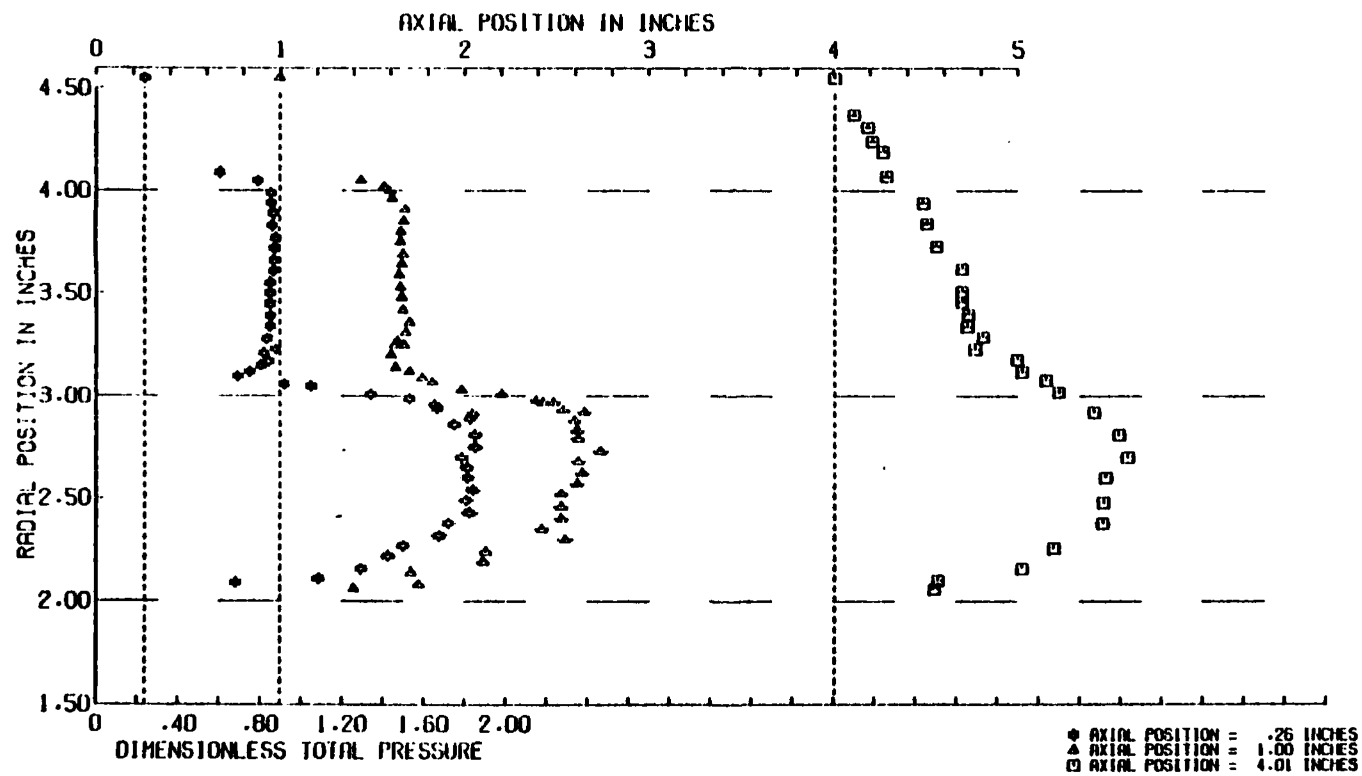

Figure A-29 Dimensionless Total Pressure, Test #3, Three Axial Locations

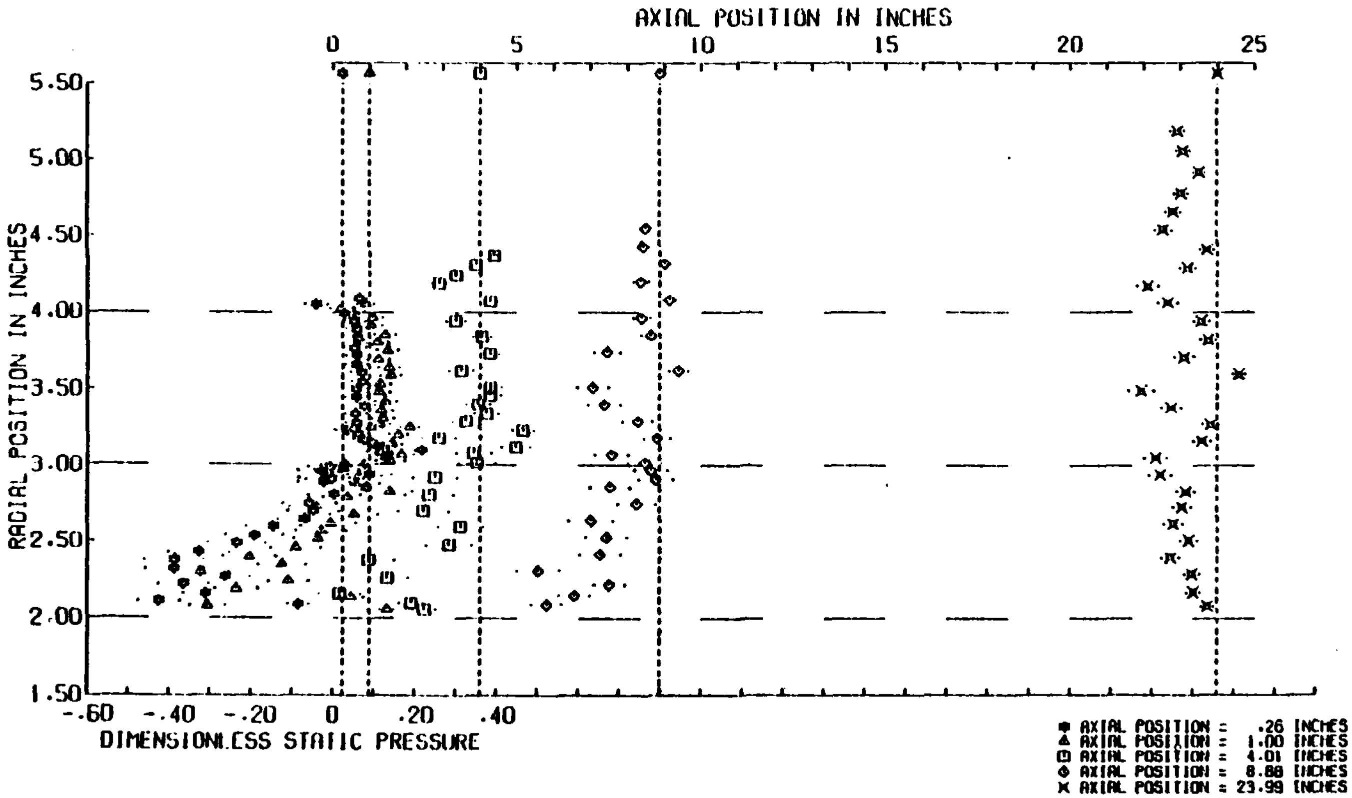

Figure A-30 Dimensionless Static Pressure, Test #3, Five Axial Locations

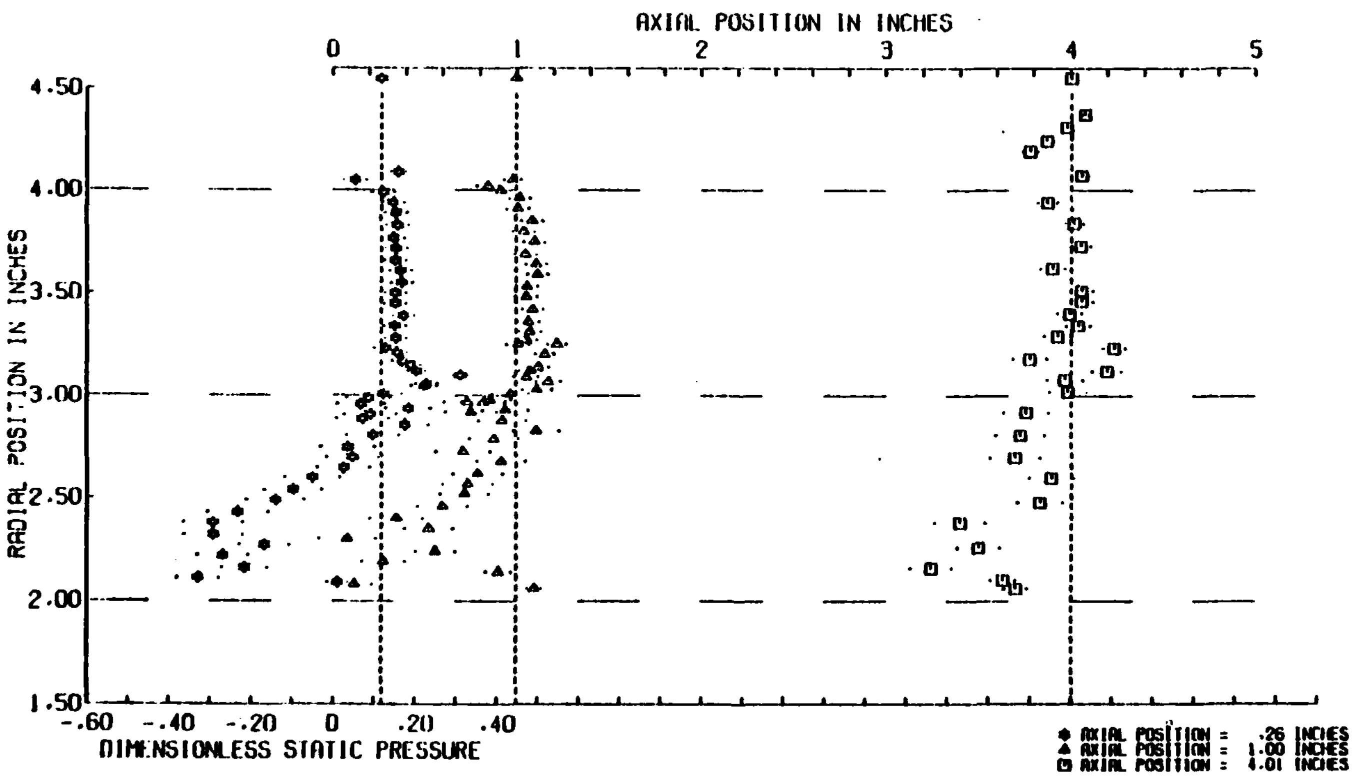

Figure A-31 Dimensionless Static Pressure, Test #3, Three Axial Locations

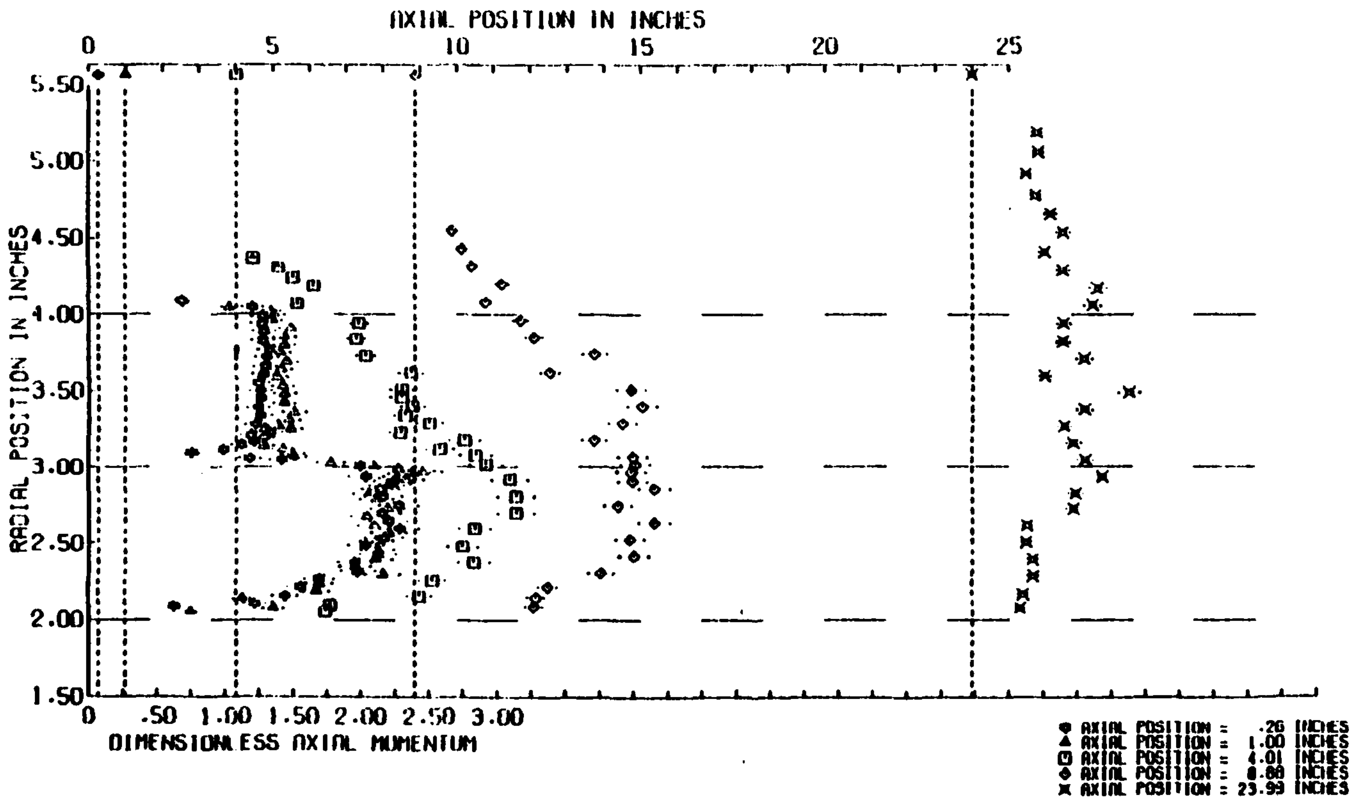

Figure A-32 Dimensionless Axial Momentum Flux,
Test #3, Five Axial Locations

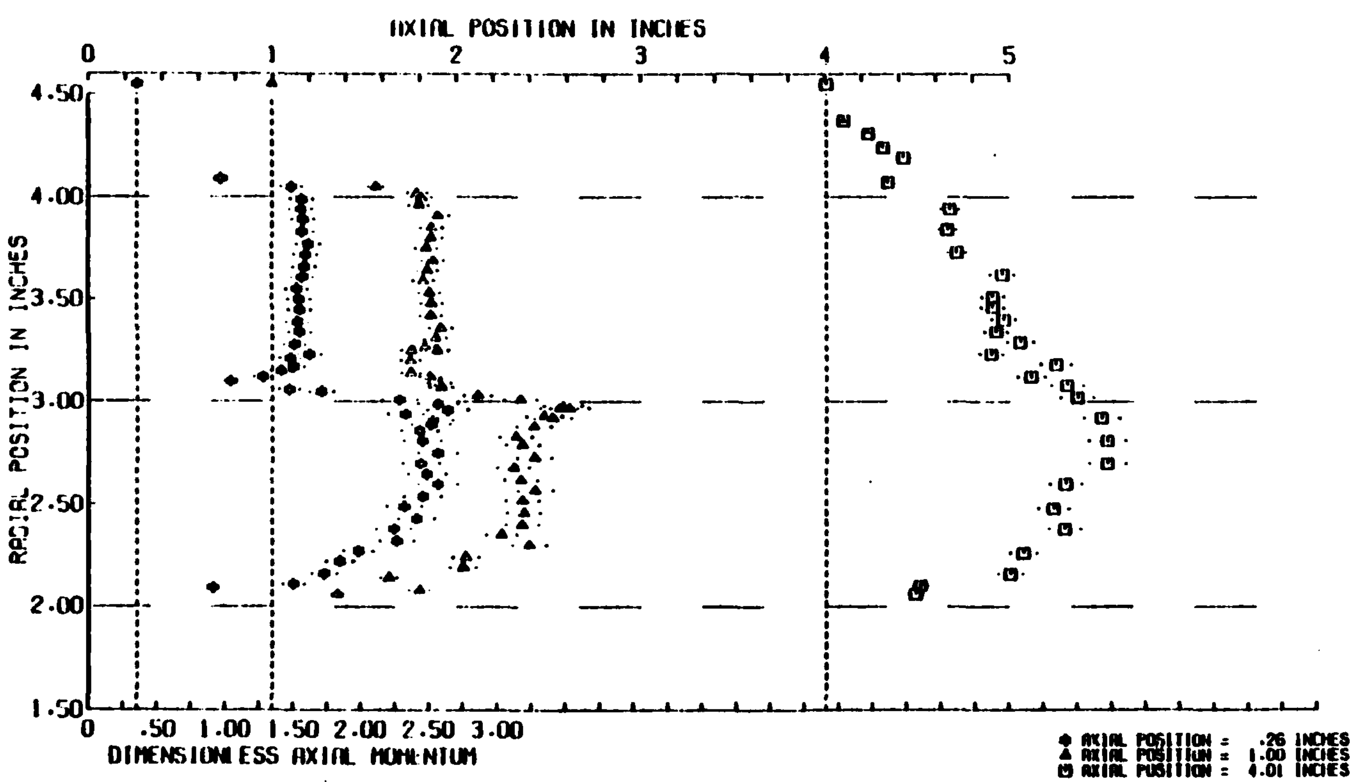

Figure A-33 Dimensionless Axial Momentum Flux, Test #3, Three Axial Locations

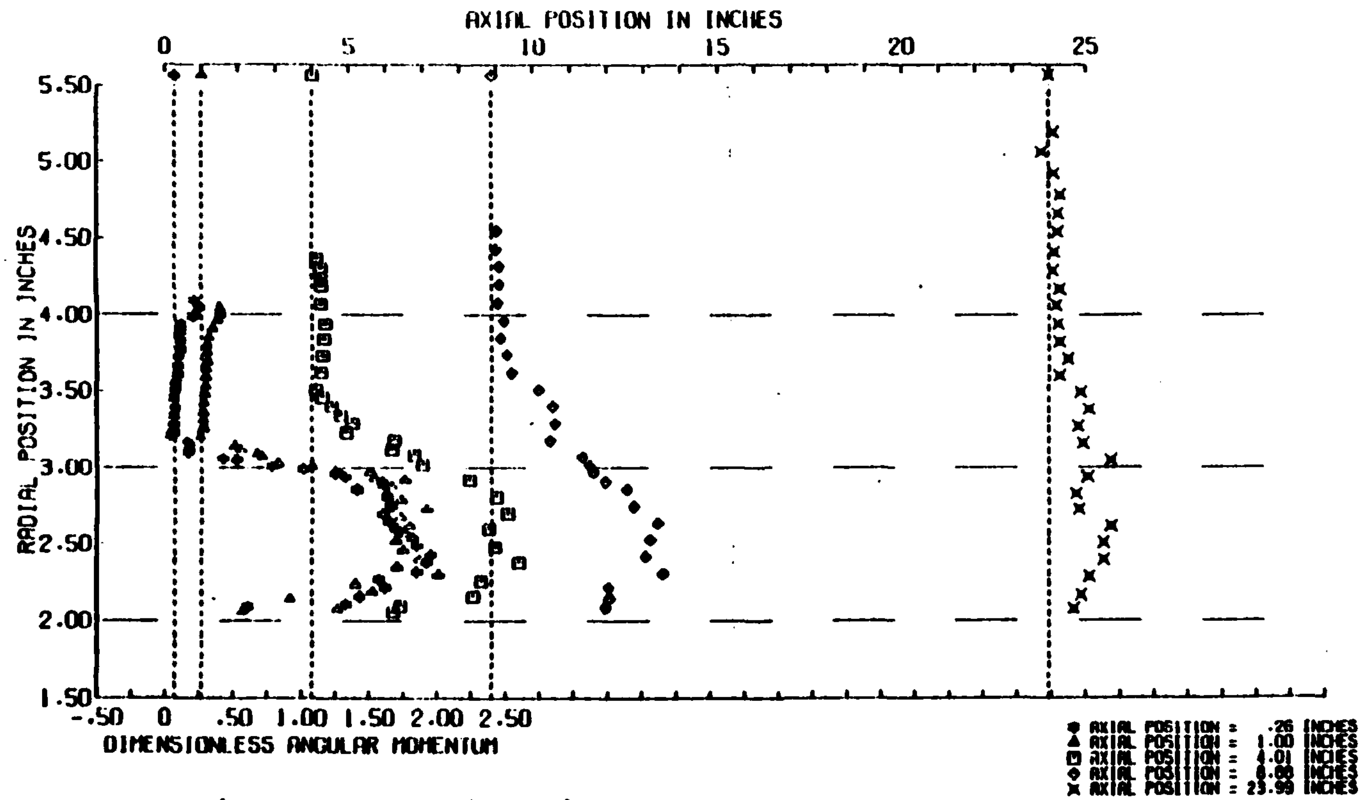

Figure A-34 Dimensionless Angular Momentum Flux, Test #3, Five Axial Locations

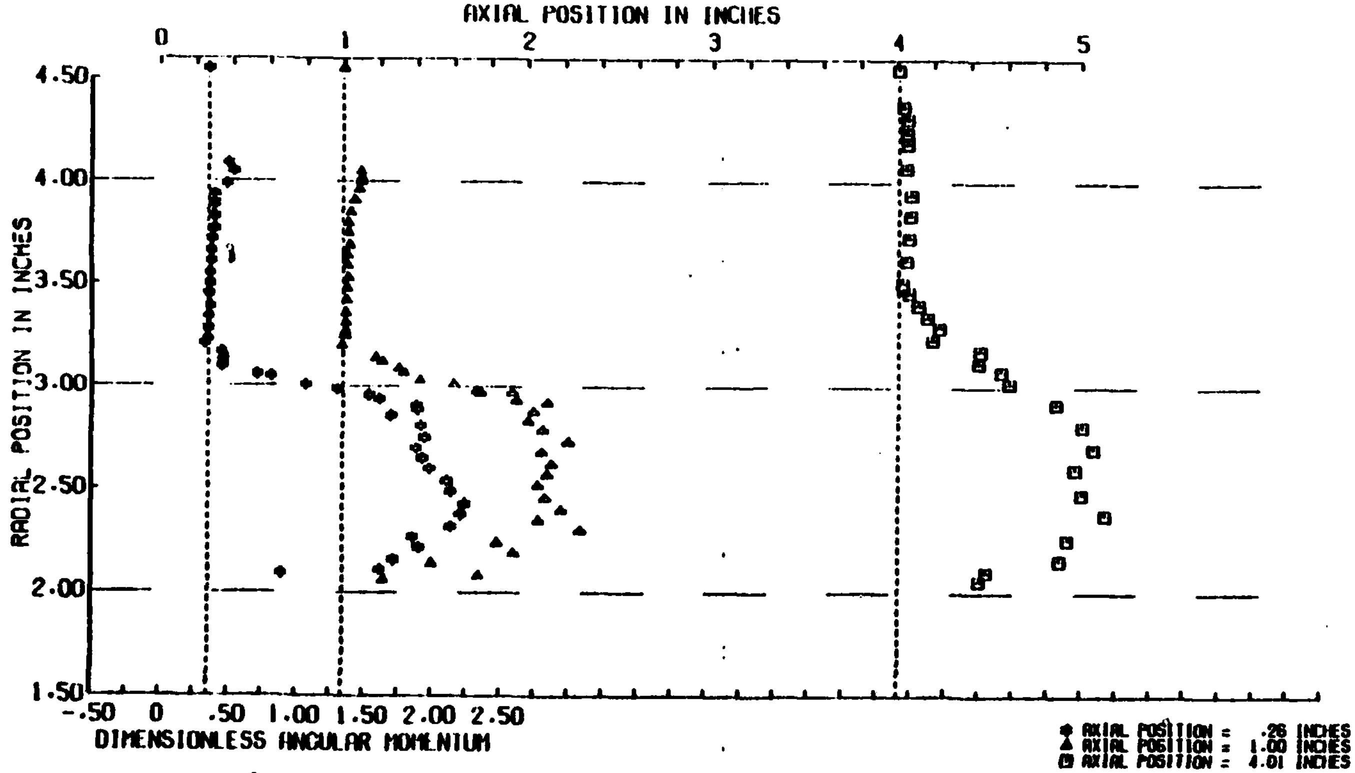

Figure A-35 Dimensionless Angular Momentum Flux, Test #3, Three Axial Locations

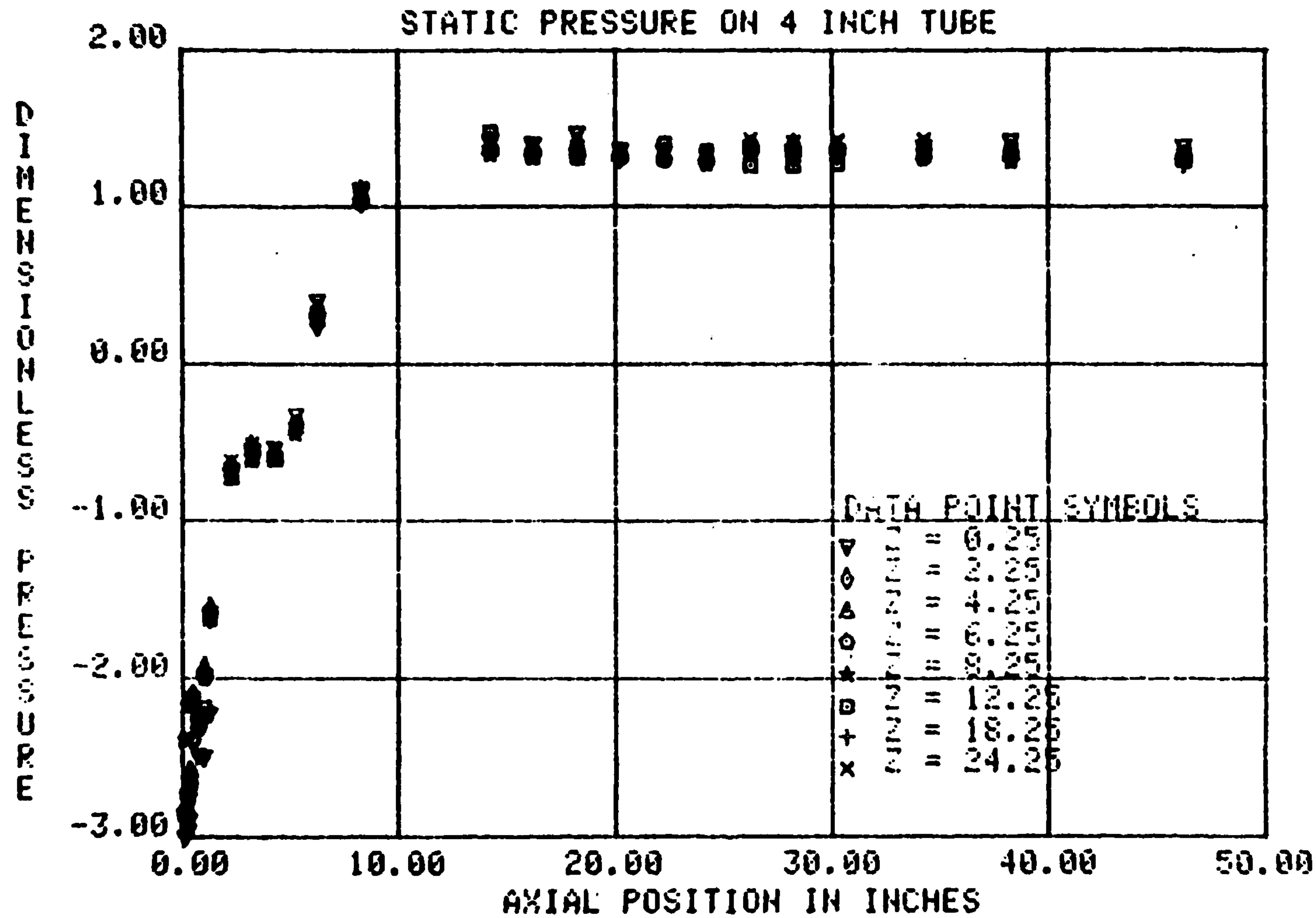

Figure A-36 Dimensionless Static Pressure on 4 Inch Tube, Test #4, Runs XX1

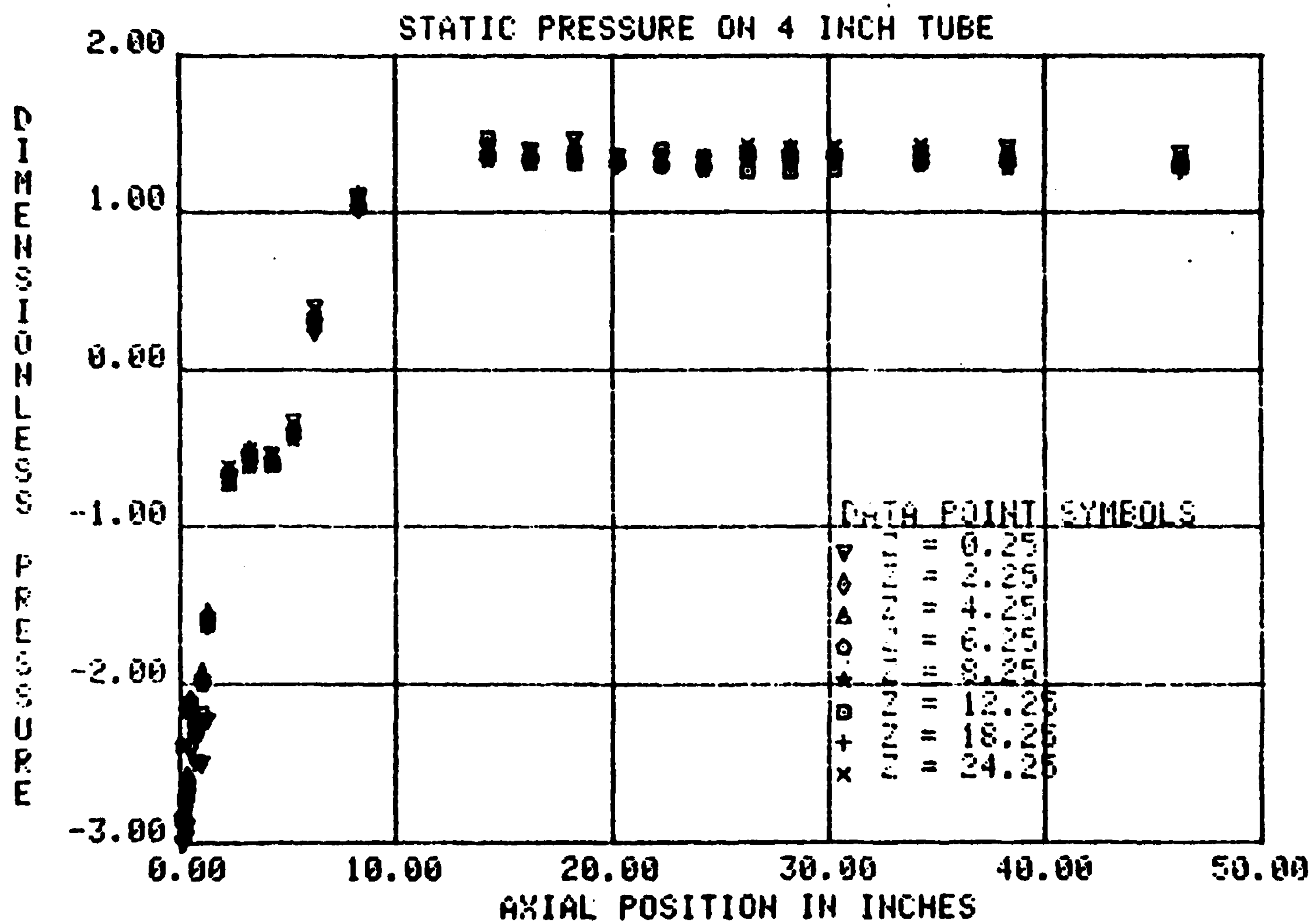

Figure A-36 Dimensionless Static Pressure on 4 Inch Tube, Test #4, Runs XX1

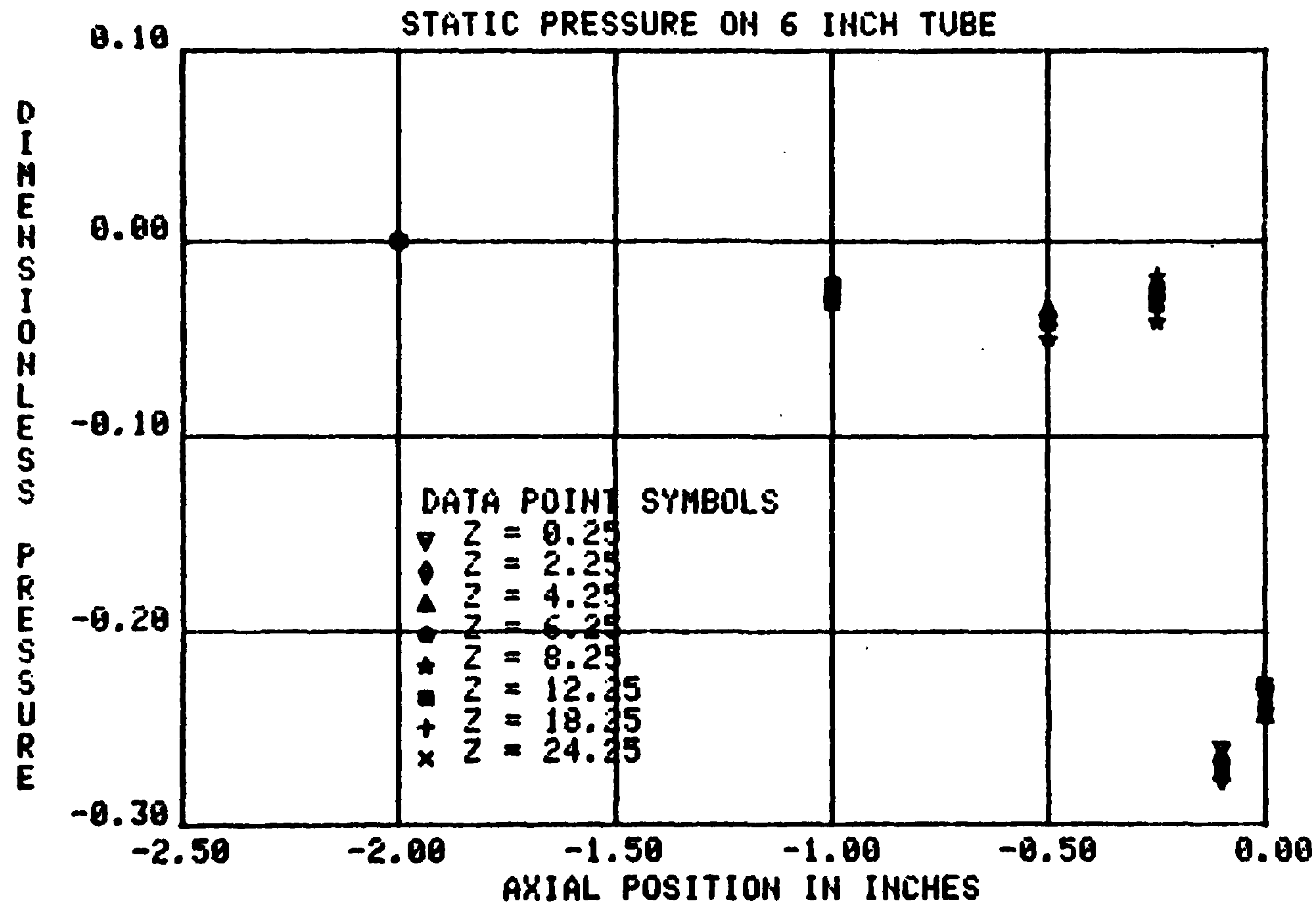

Figure A-37 Dimensionless Static Pressure on 6 Inch Tube, Test #4, Runs XX1

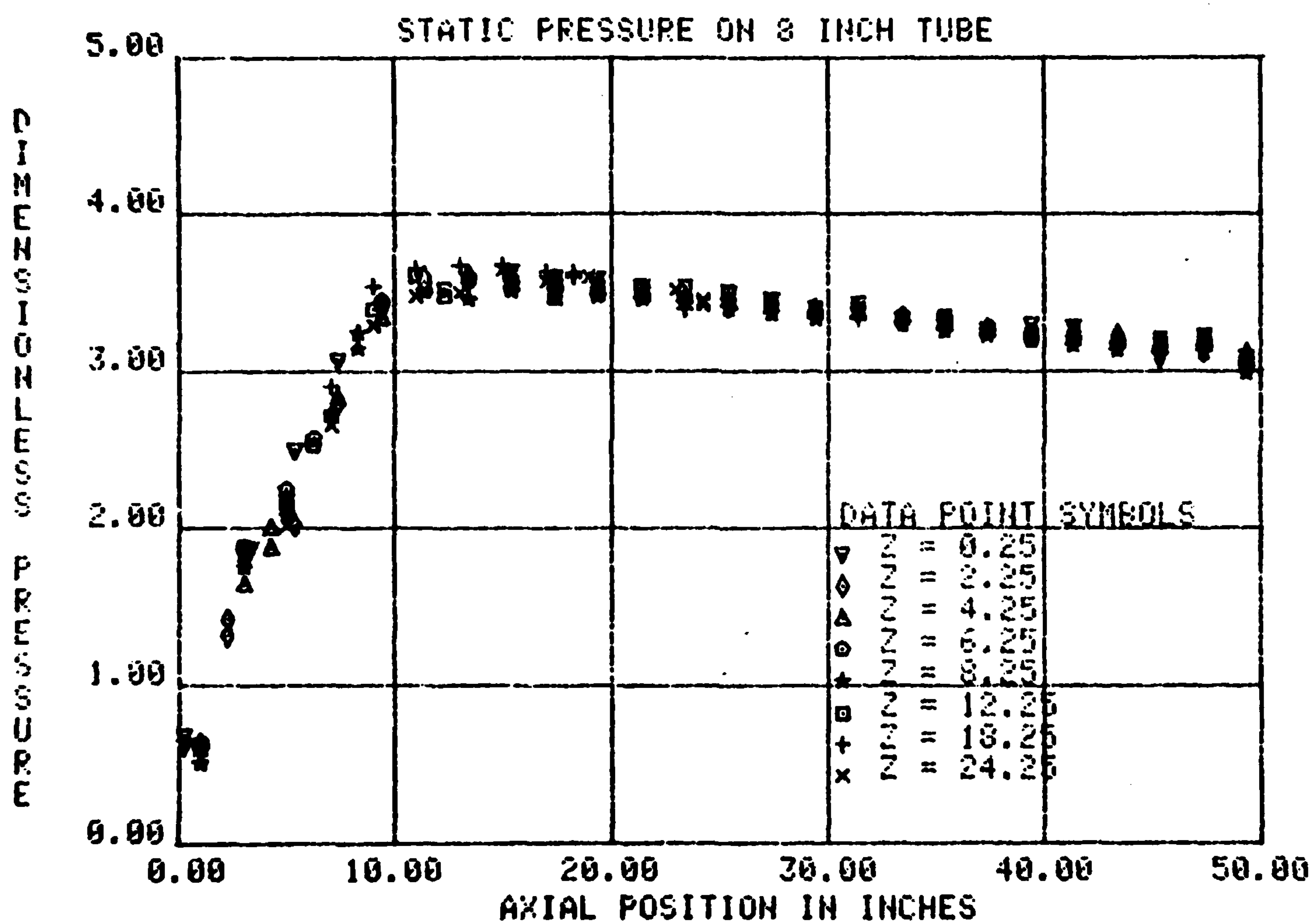

Figure A-38 Dimensionless Static Pressure on 8 Inch Tube, Test #4, Runs XX1

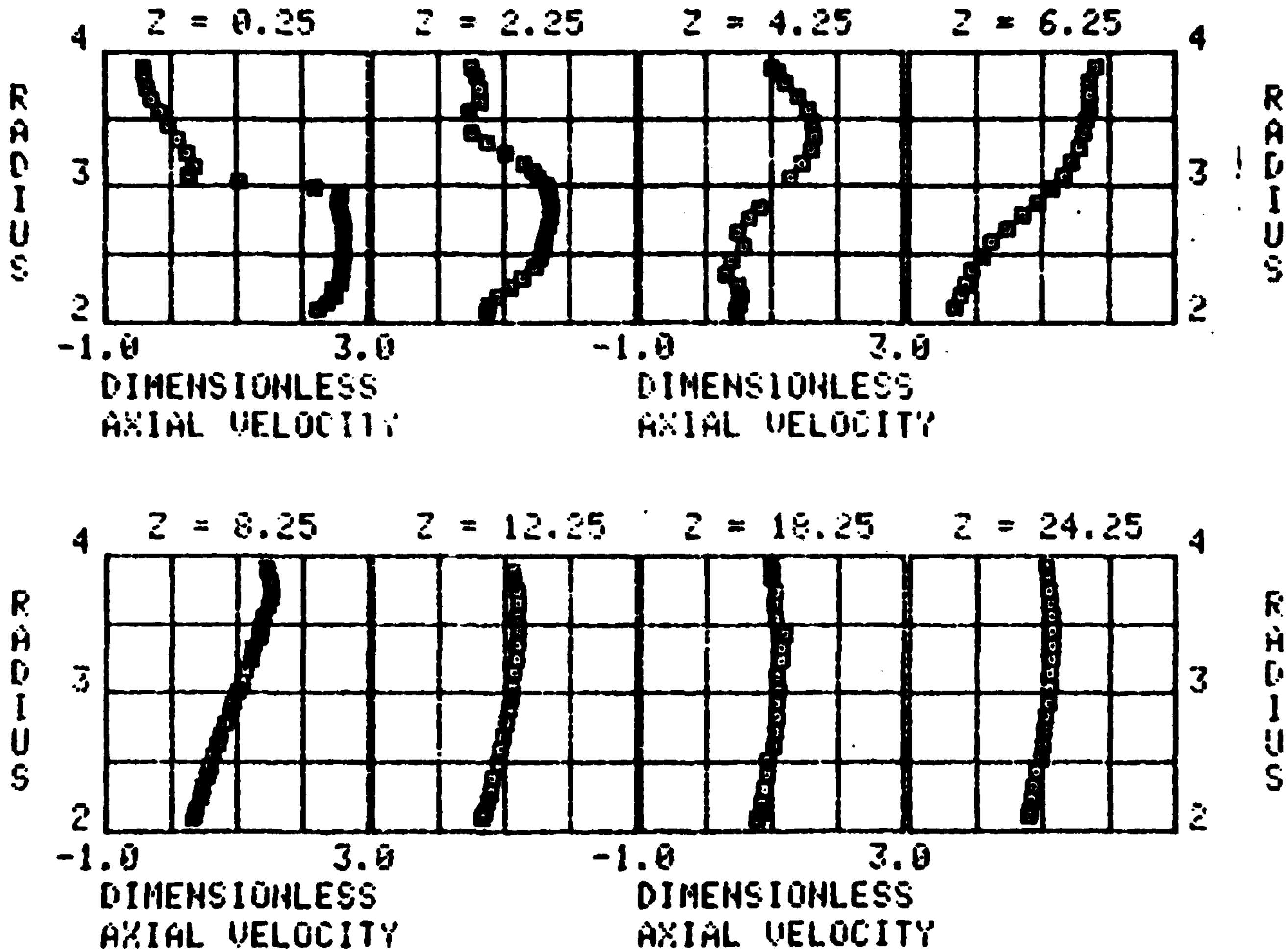

Figure A-39 Dimensionless Axial Velocity, Test #4, Runs XX1

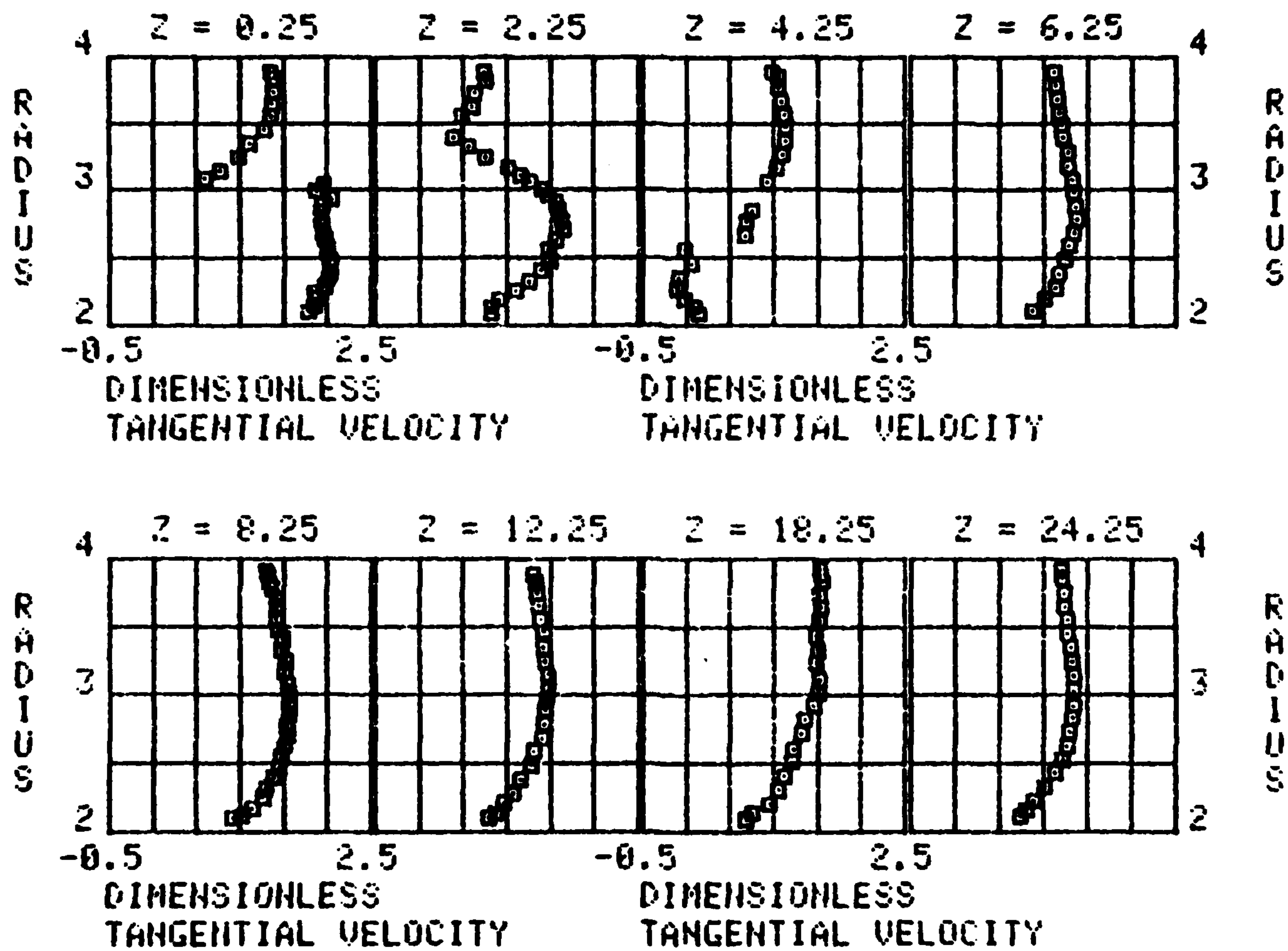

Figure A-40 Dimensionless Tangential Velocity, Test #4, Runs XX1

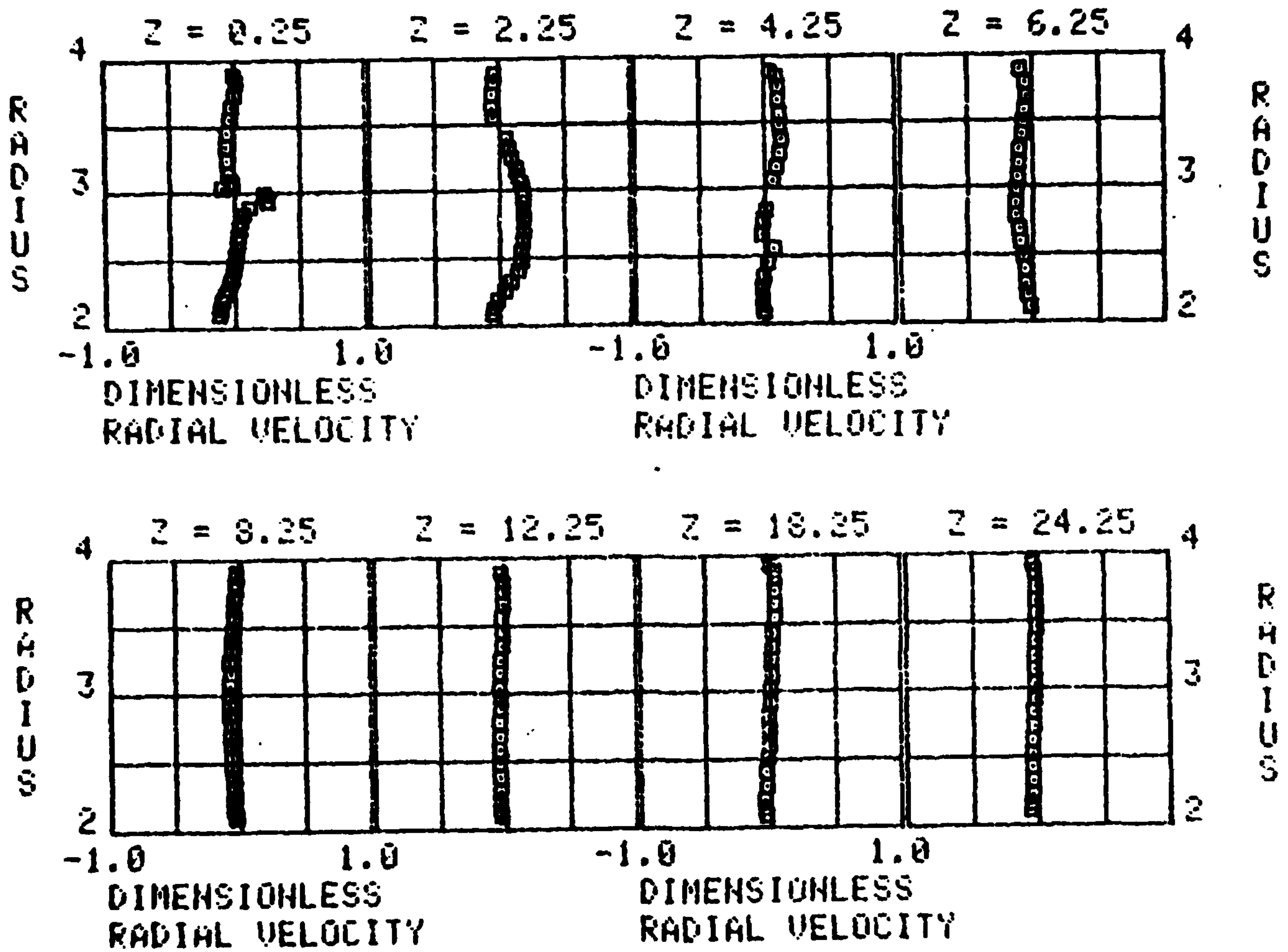

Figure A-41 Dimensionless Radial Velocity, Test #4, Runs XX1

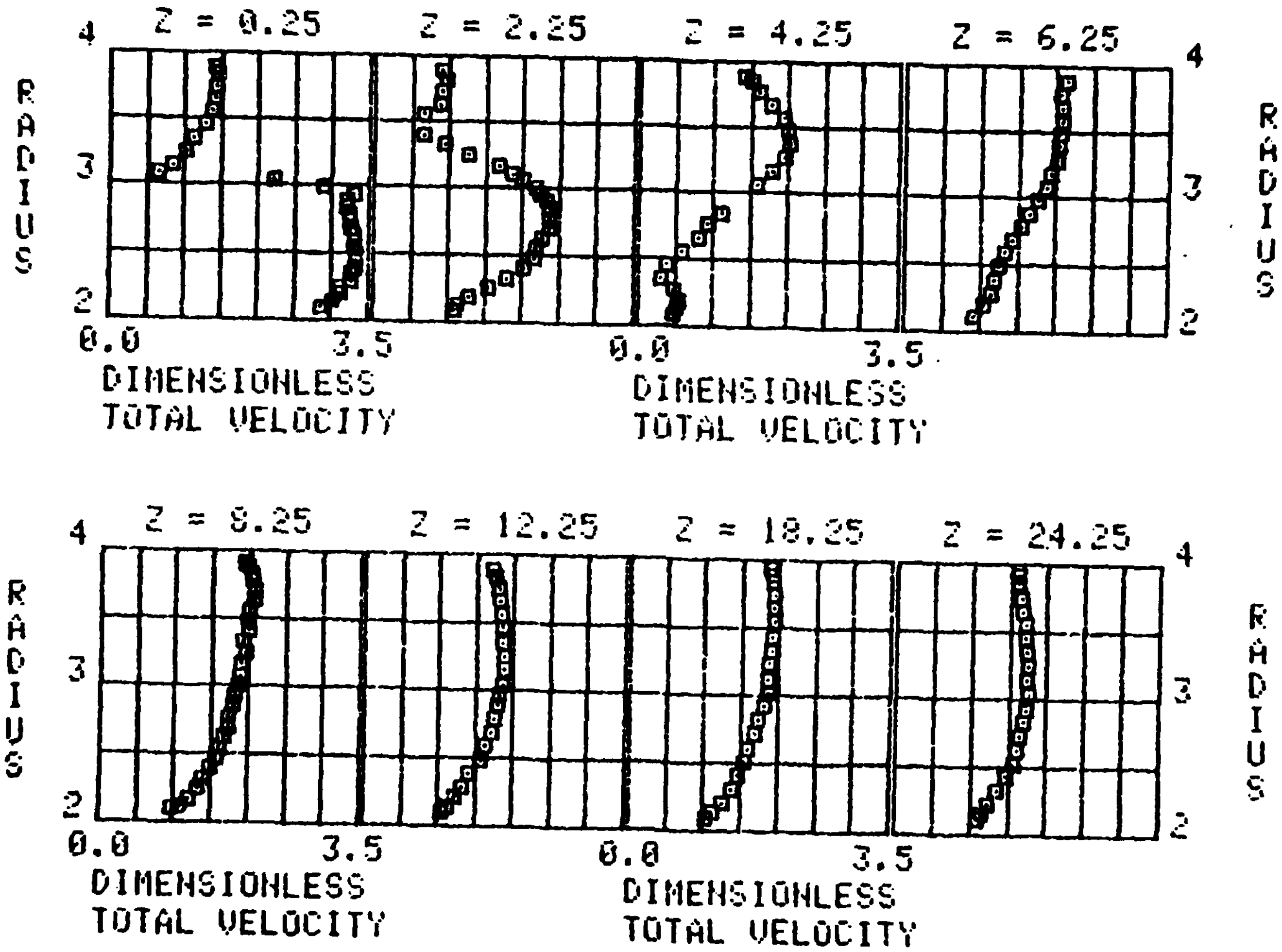

Figure A-42 Dimensionless Velocity, Test #4, Runs XX1

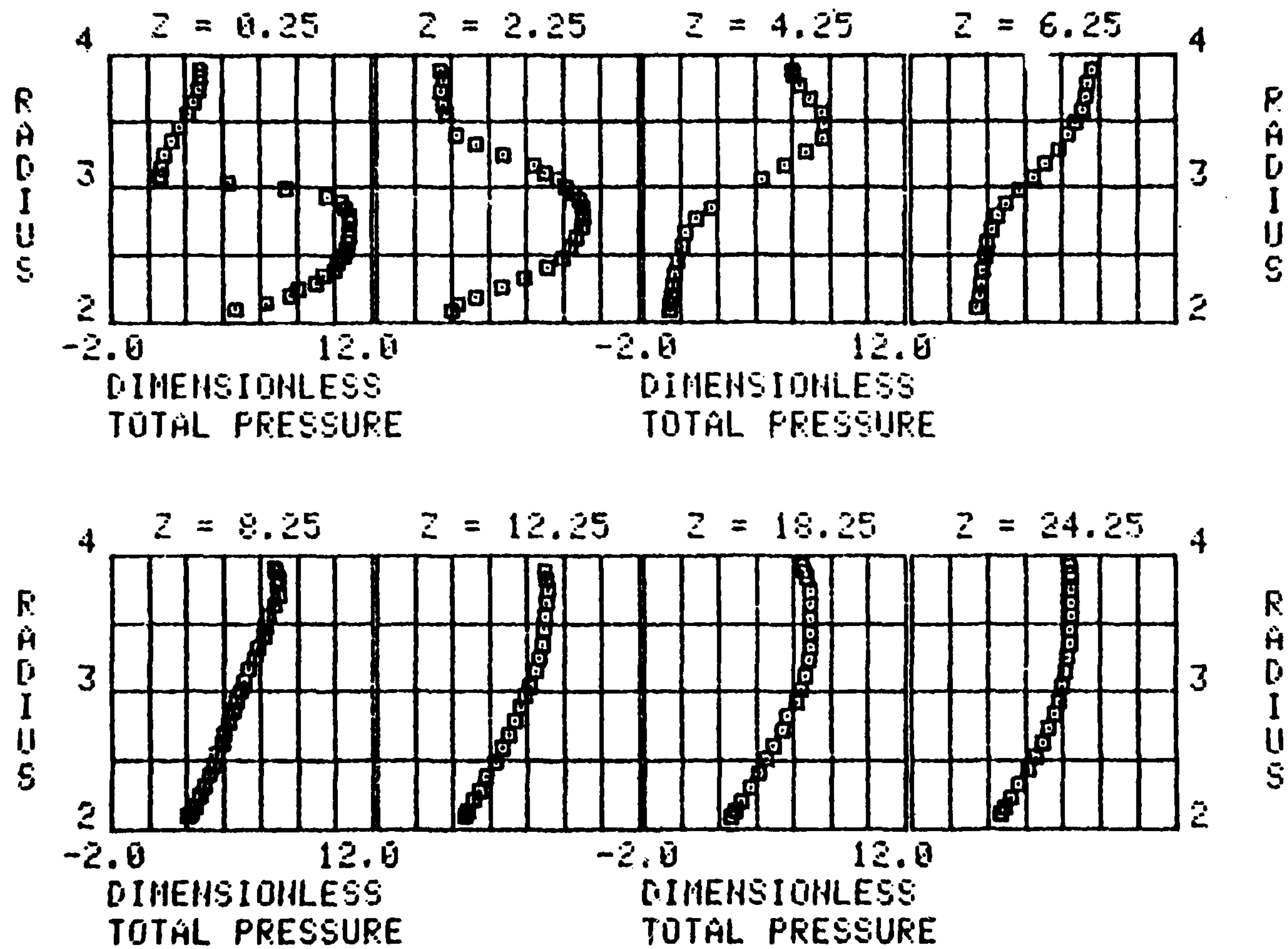

Figure A-43 Dimensionless Total Pressure, Test #4, Runs XX1

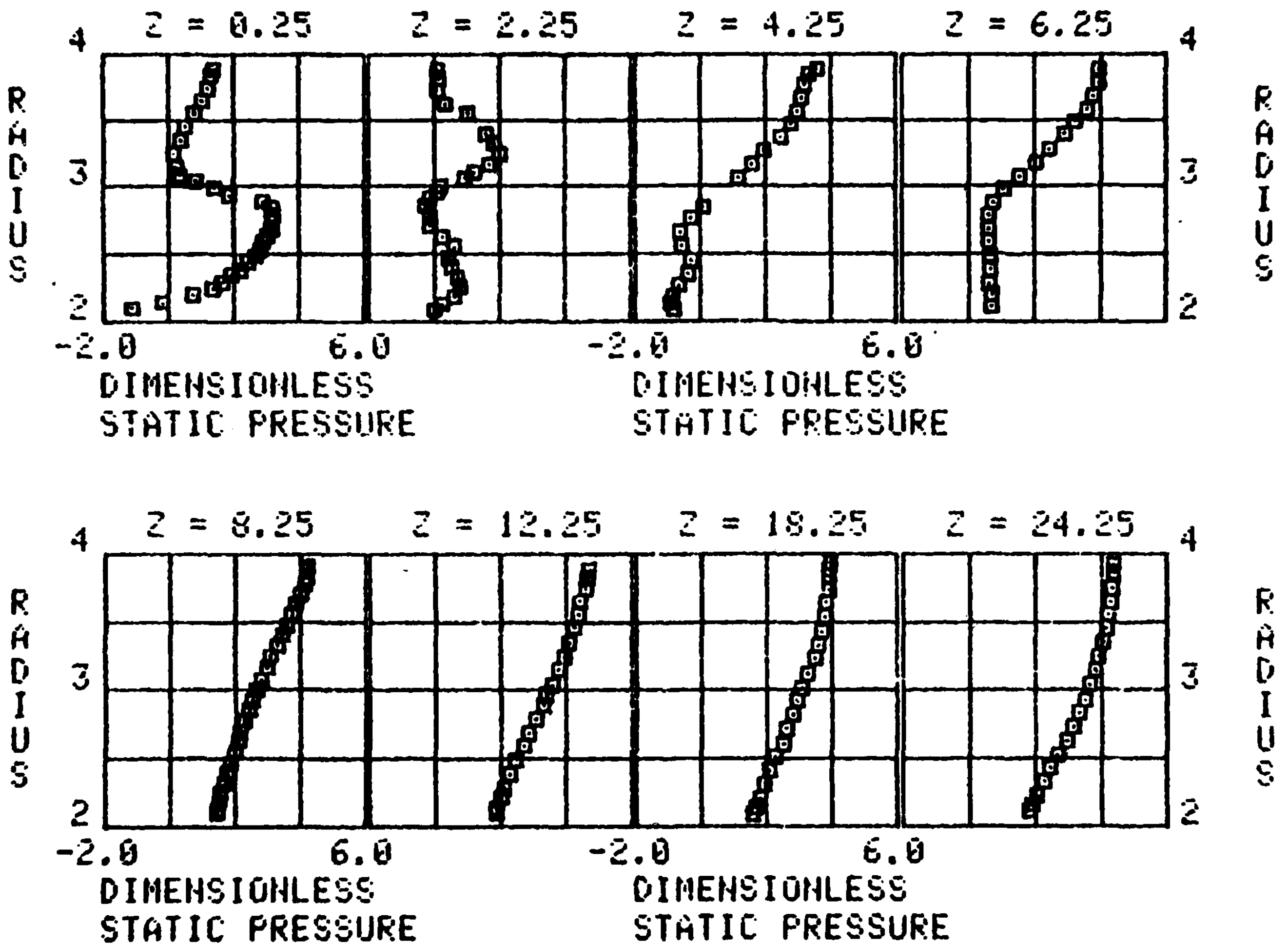

Figure A-44 Dimensionless Static Pressure, Test #4, Runs XX1

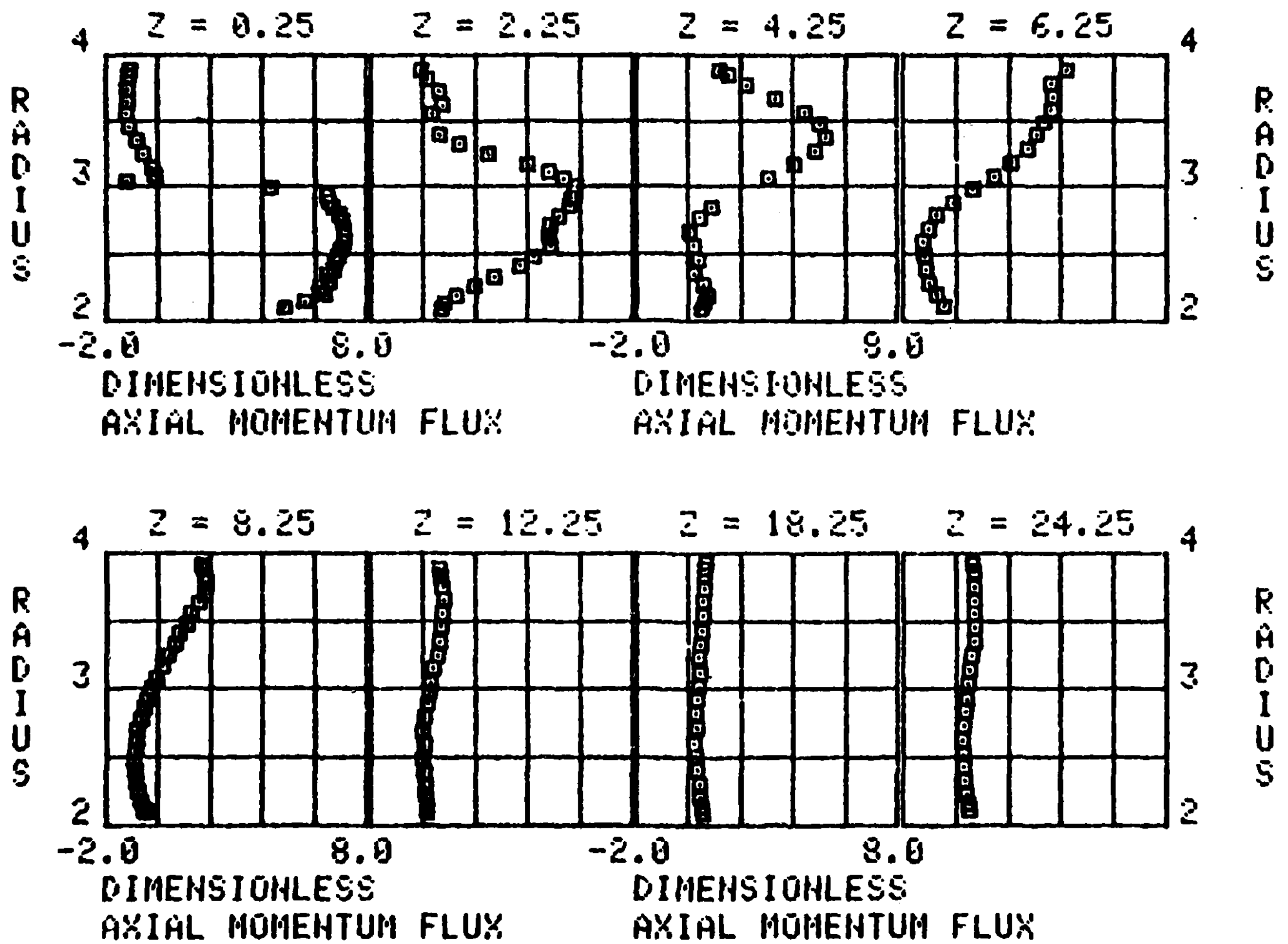

Figure A-45 Dimensionless Axial Momentum Flux, Test #4, Runs XX1

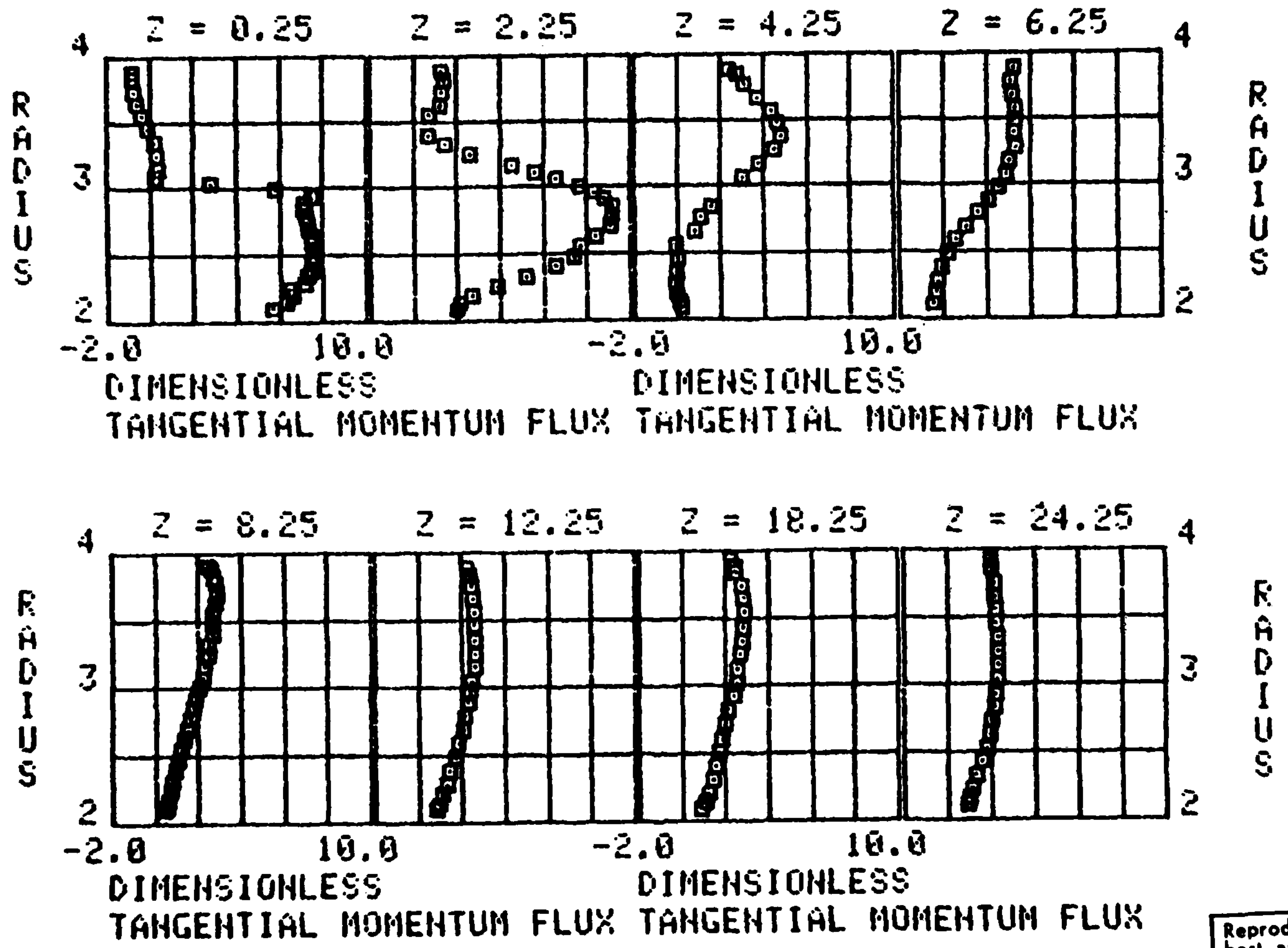

Figure A-46 Dimensionless Tangential Momentum Flux, Test #4, Runs XX1

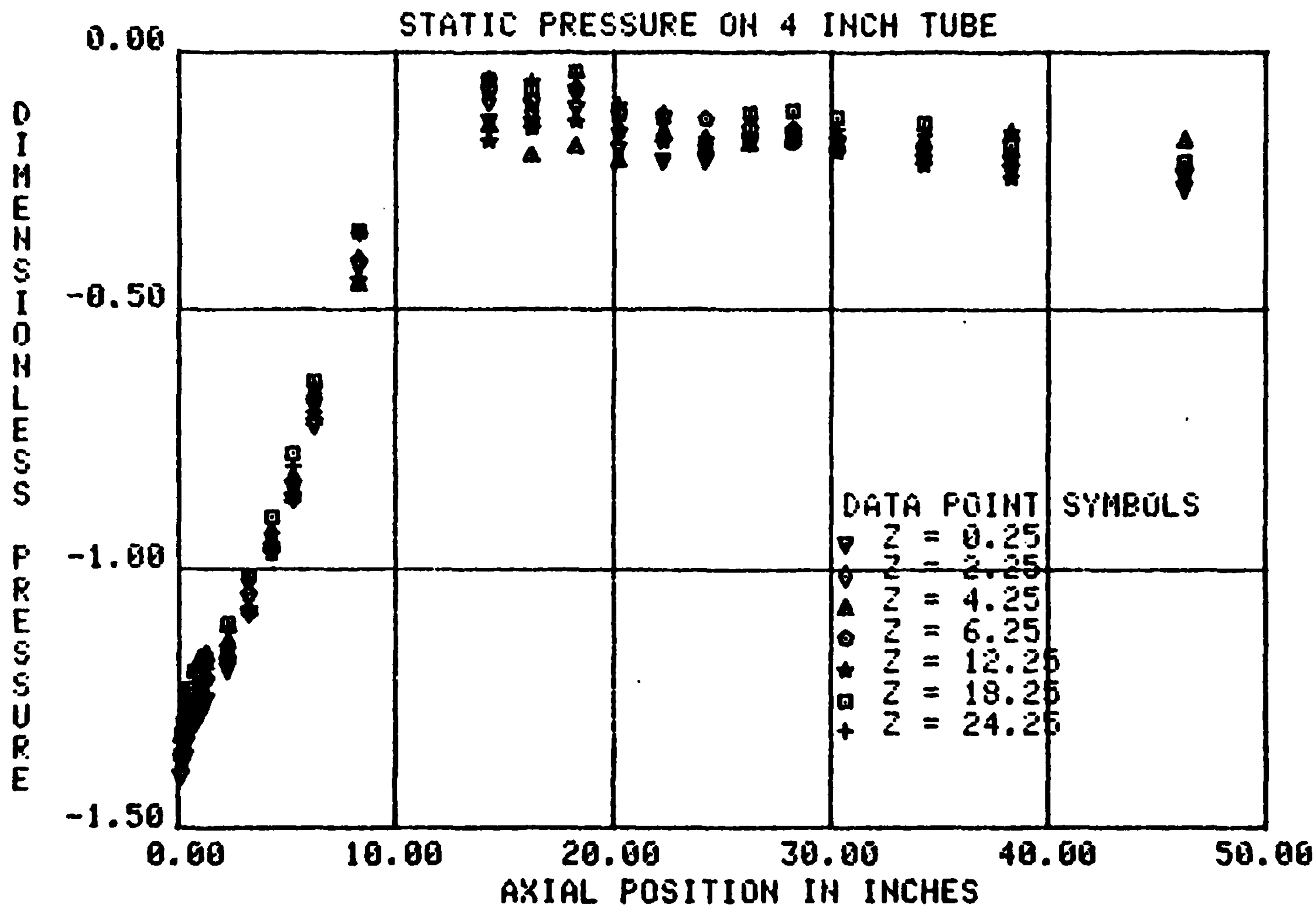

Figure A-47 Dimensionless Static Pressure on 4 Inch Tube, Test #4, Runs XX2

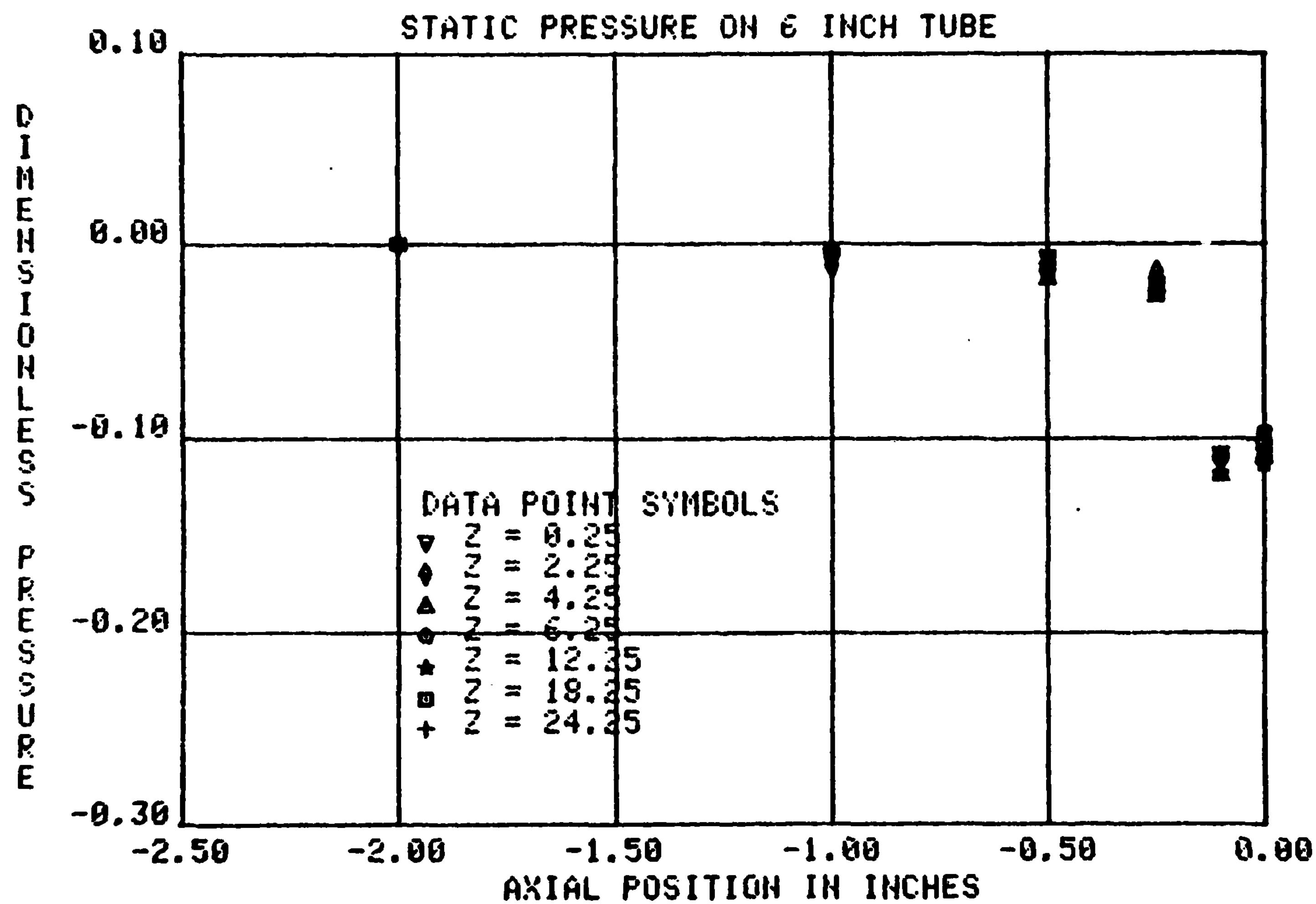

Figure A-48 Dimensionless Static Pressure on 6 Inch Tube, Test #4, Runs XX2

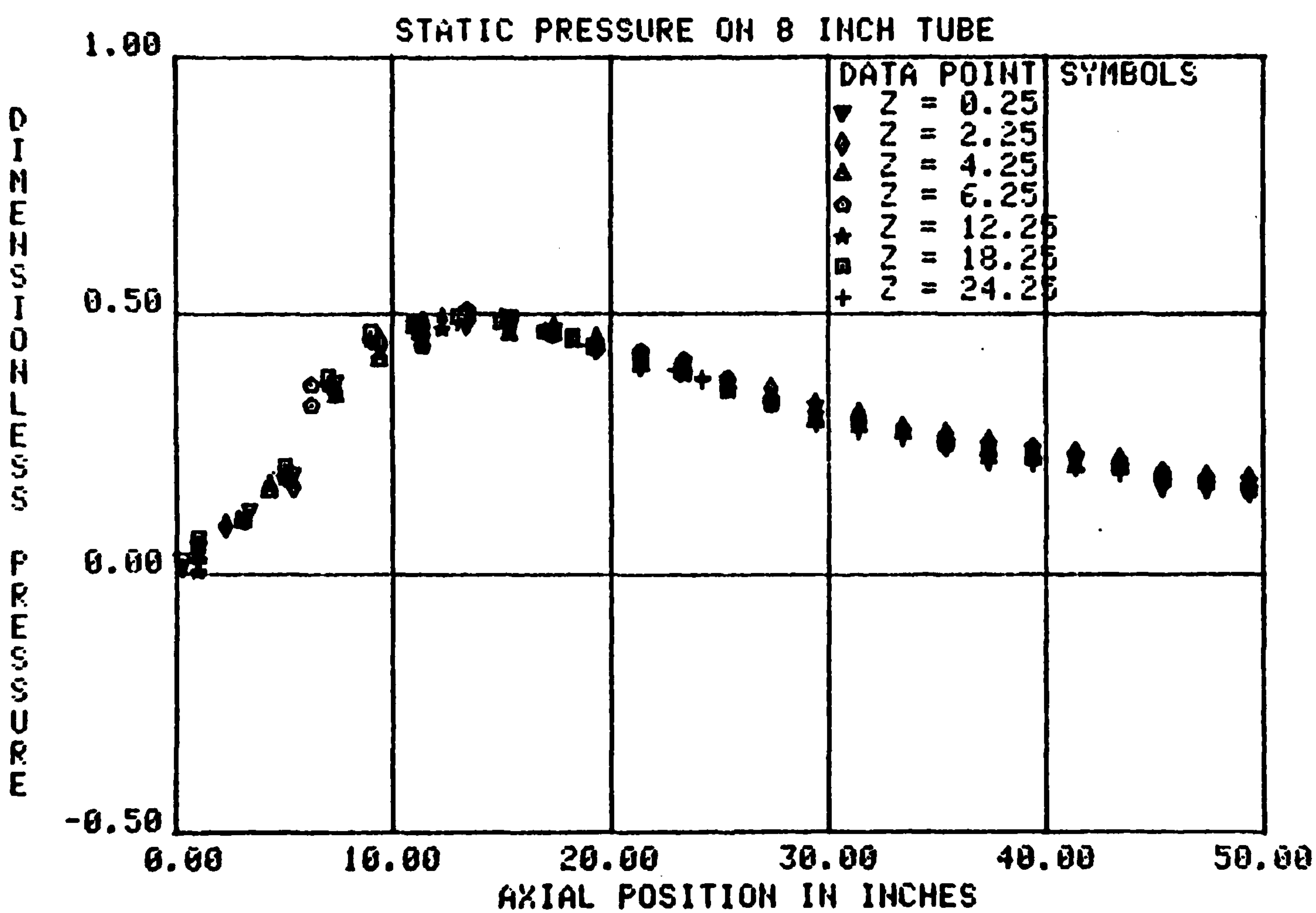

Figure A-49 Dimensionless Static Pressure on 8 Inch Tube, Test #4, Runs XX2

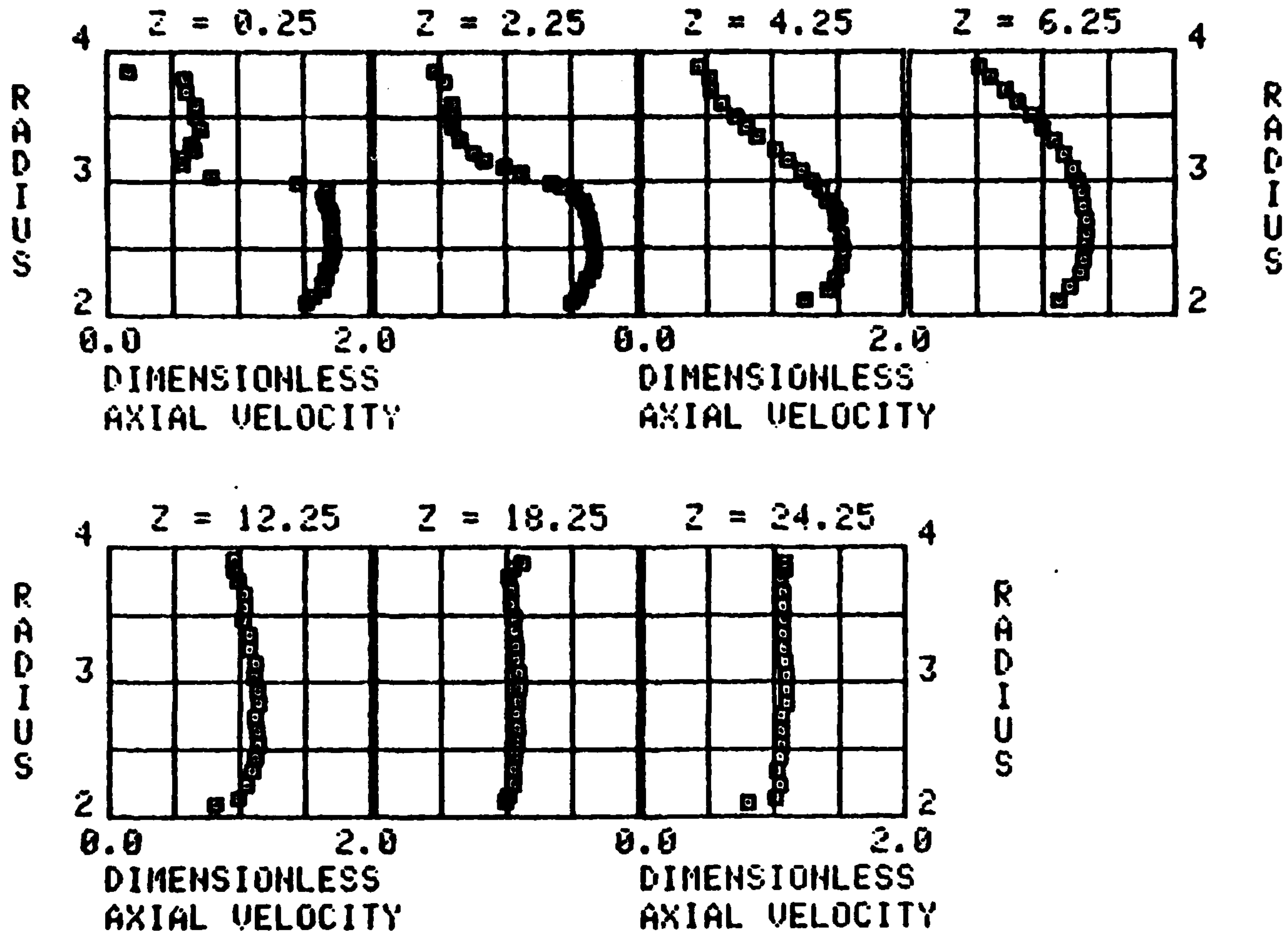

Figure A-50 Dimensionless Axial Velocity, Test #4, Runs XX2

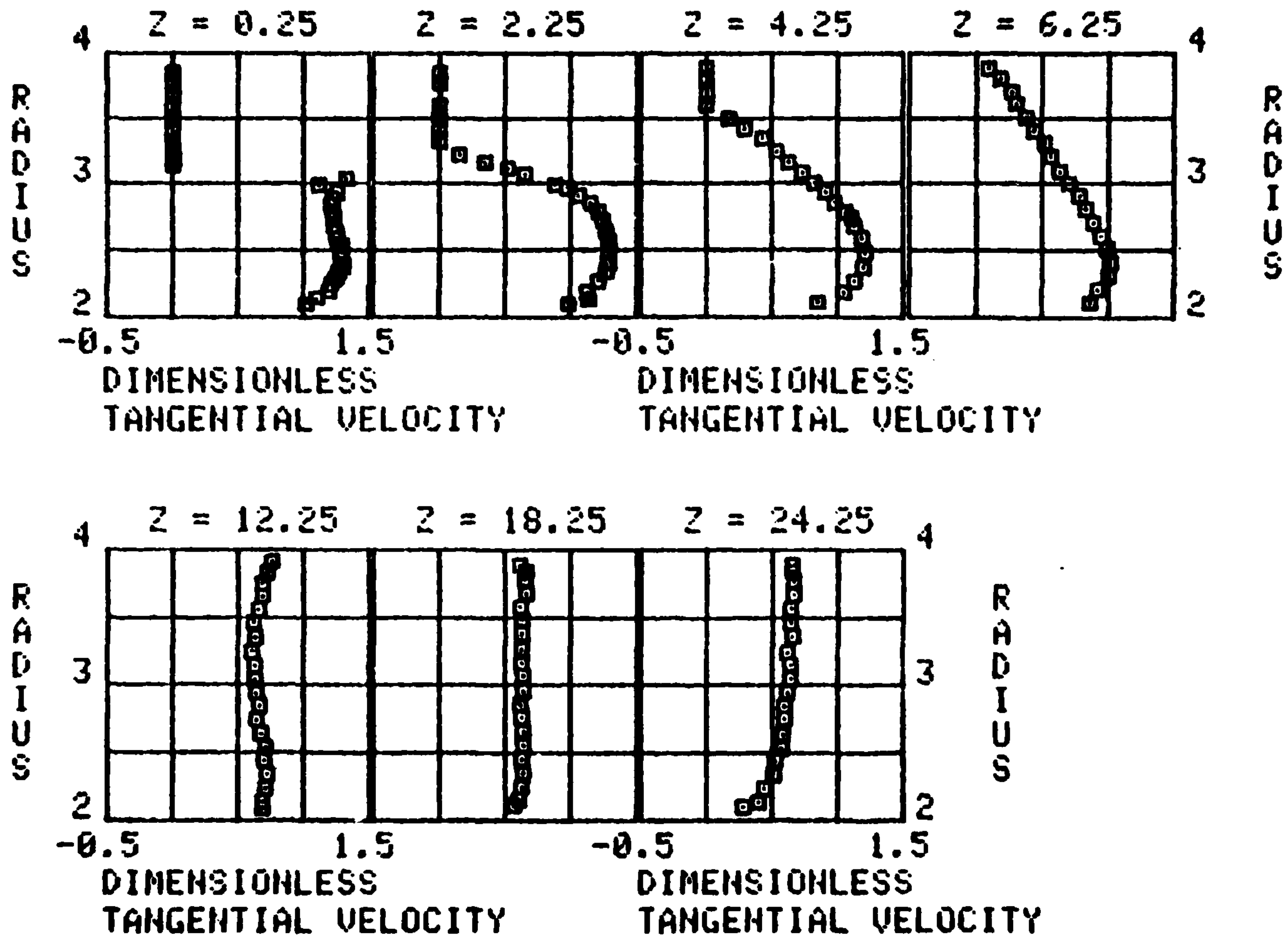

Figure A-51 Dimensionless Tangential Velocity, Test #4, Runs XX2

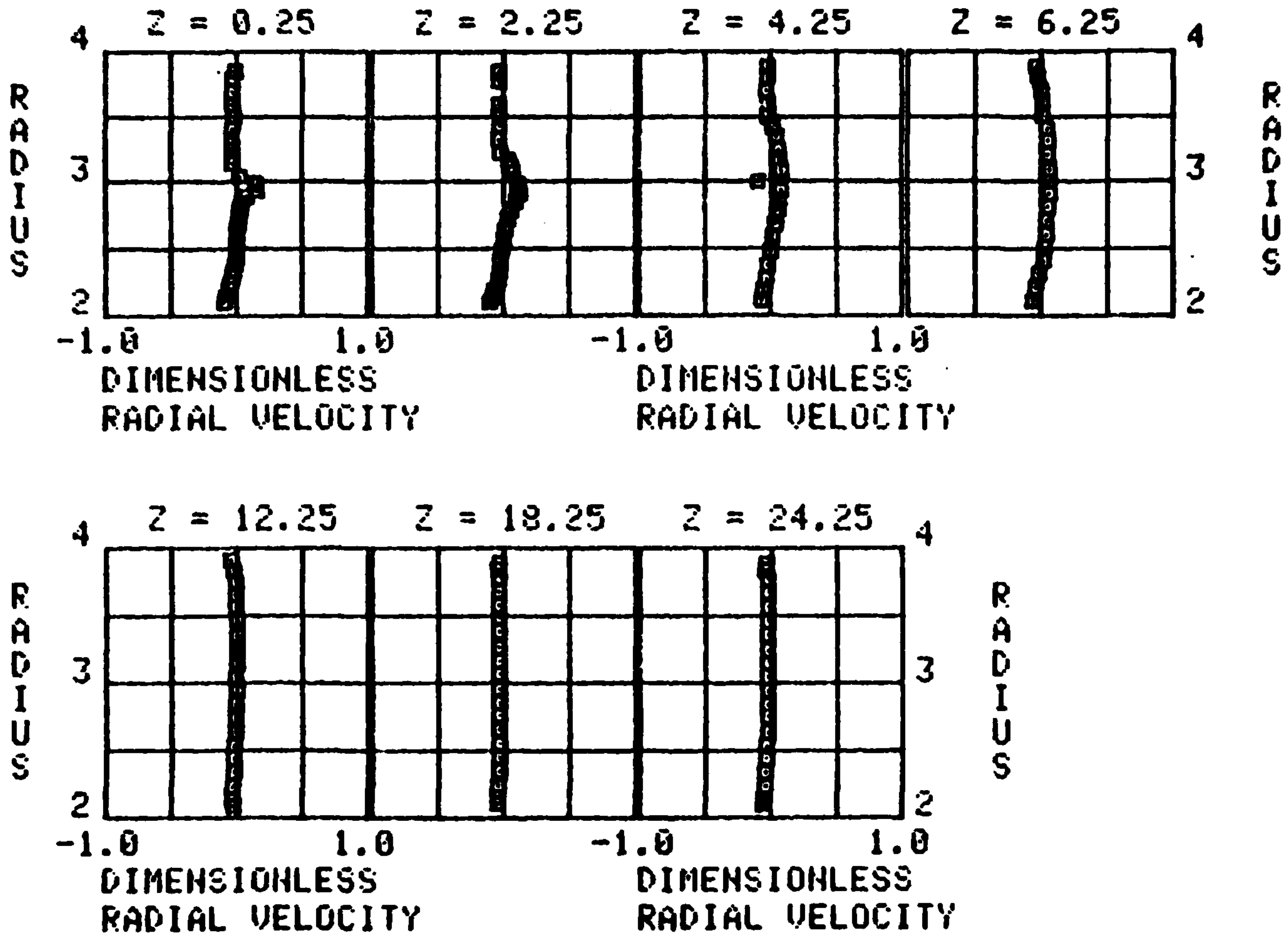

Figure A-52 Dimensionless Radial Velocity, Test #4, Runs XX2

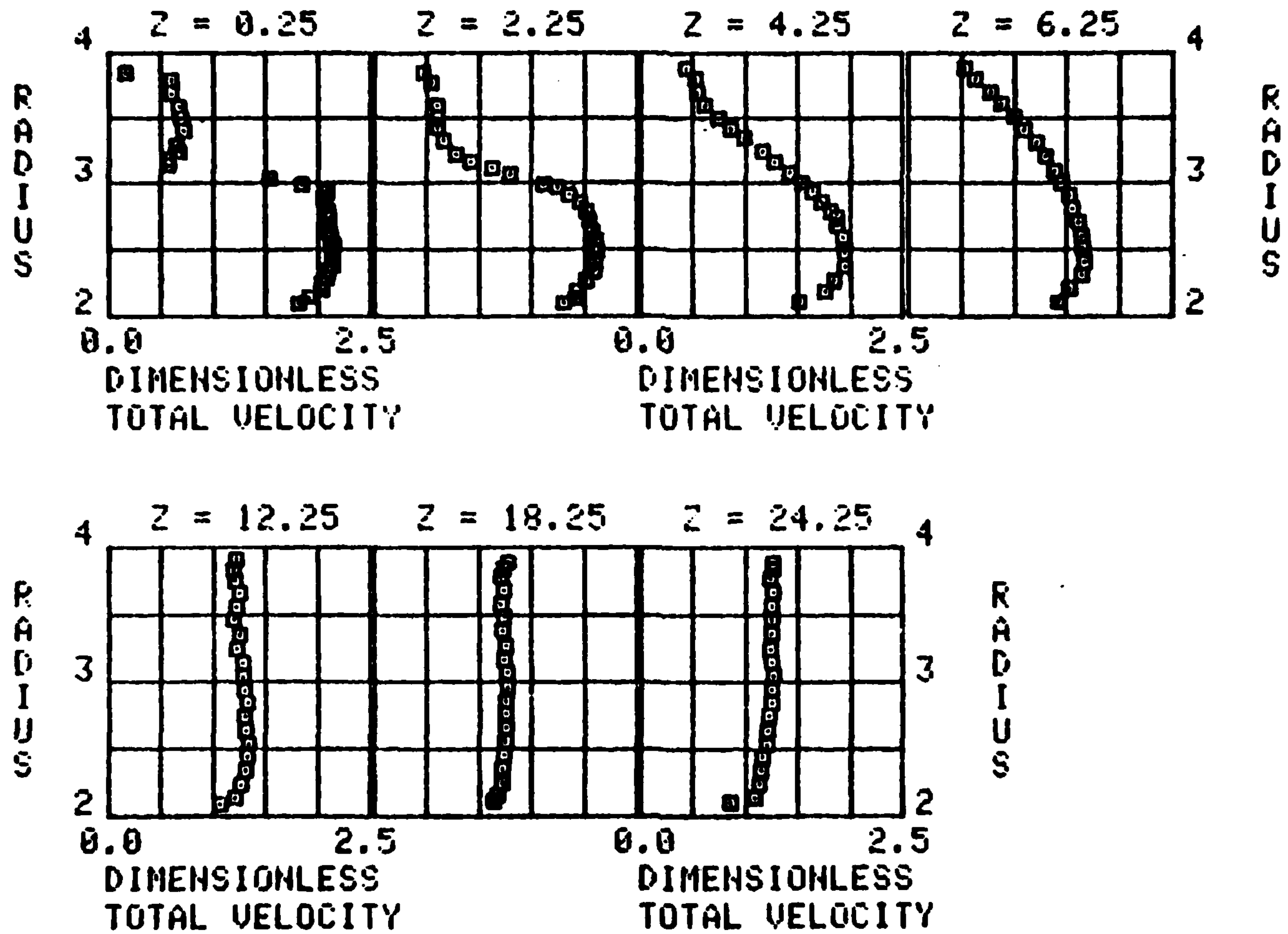

Figure A-53 Dimensionless Velocity, Test #4, Runs XX2

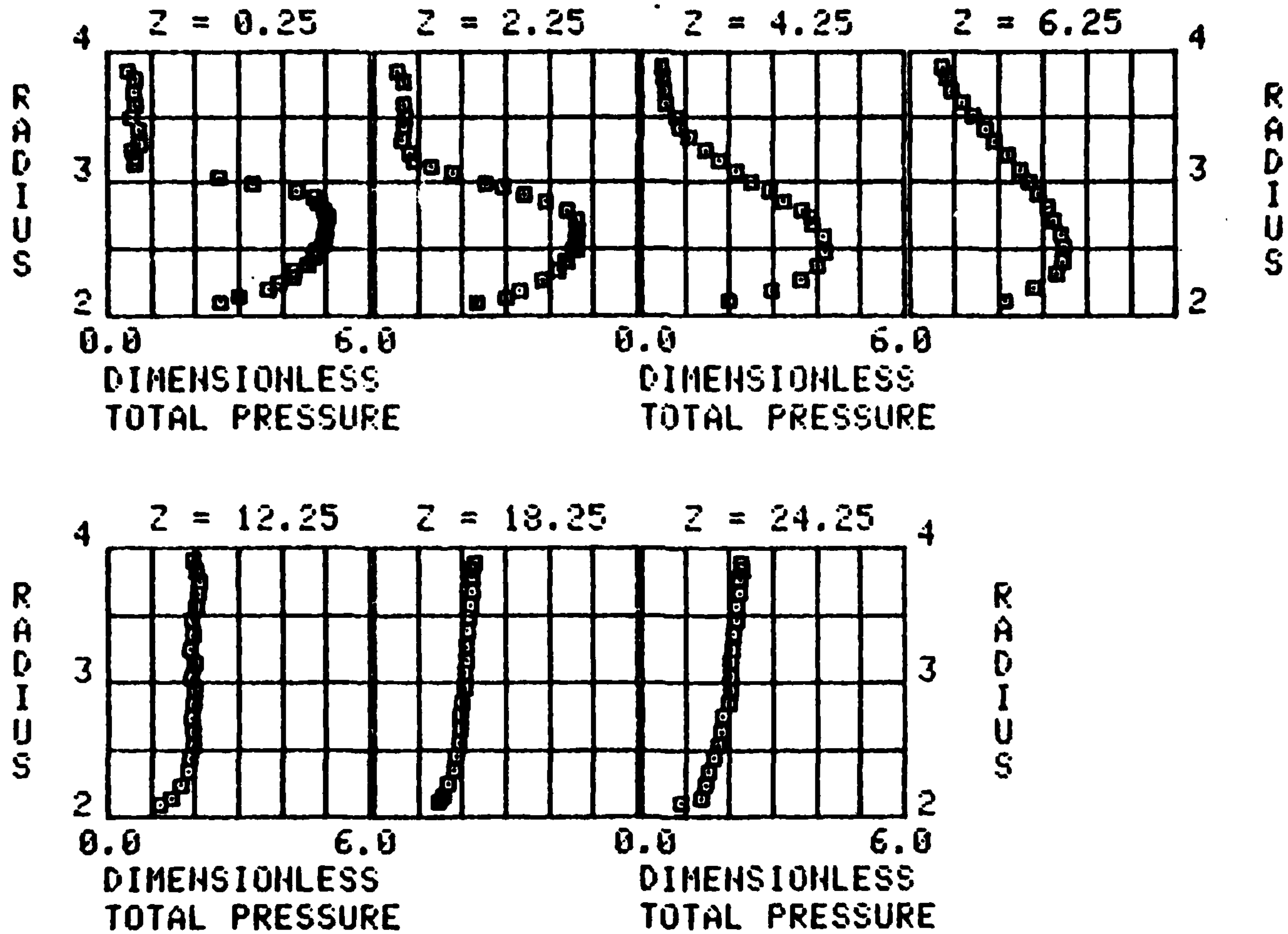

Figure A-54 Dimensionless Total Pressure, Test #4, Runs XX2

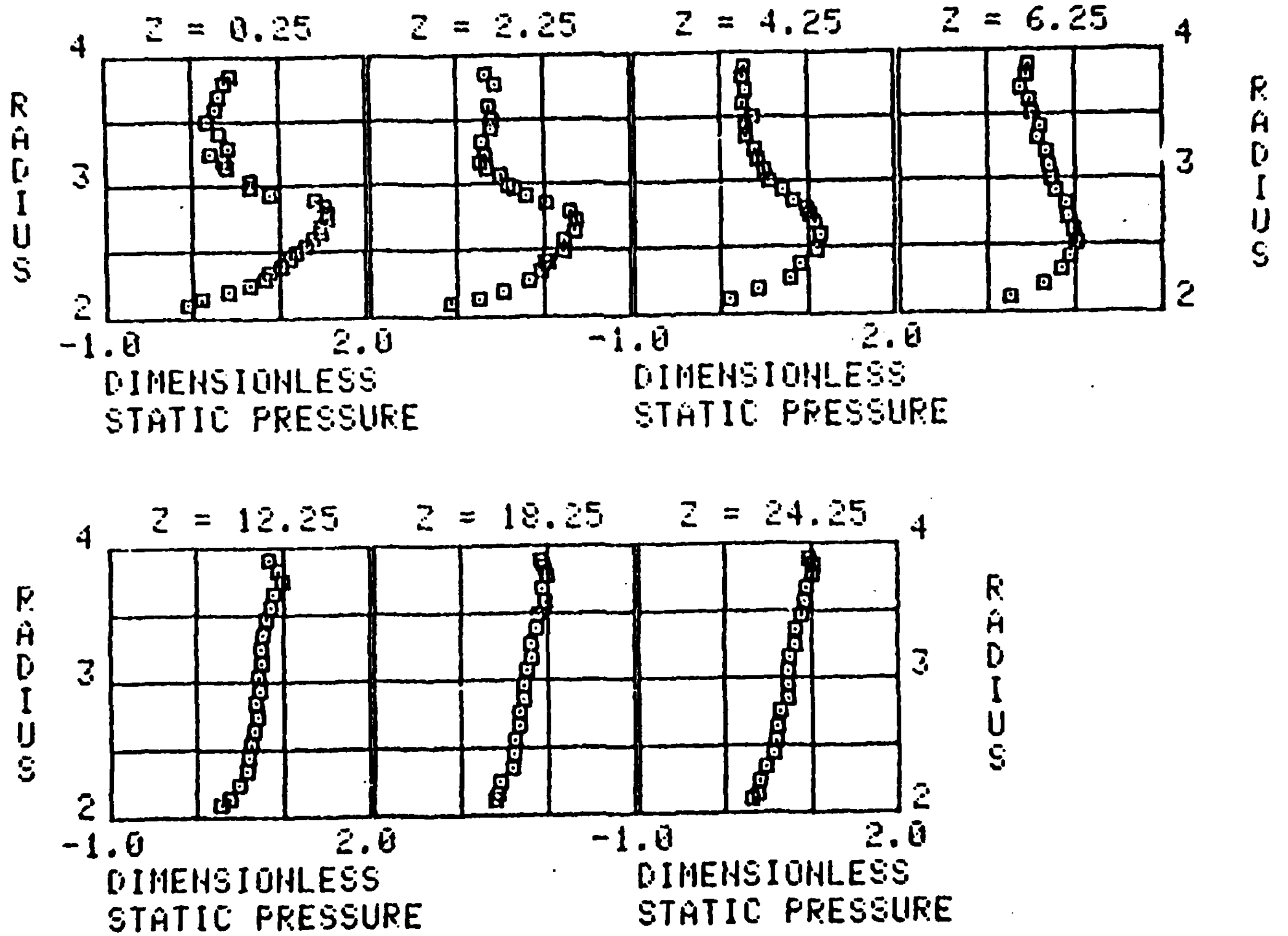

Figure A-55 Dimensionless Static Pressure, Test #4, Runs XX2

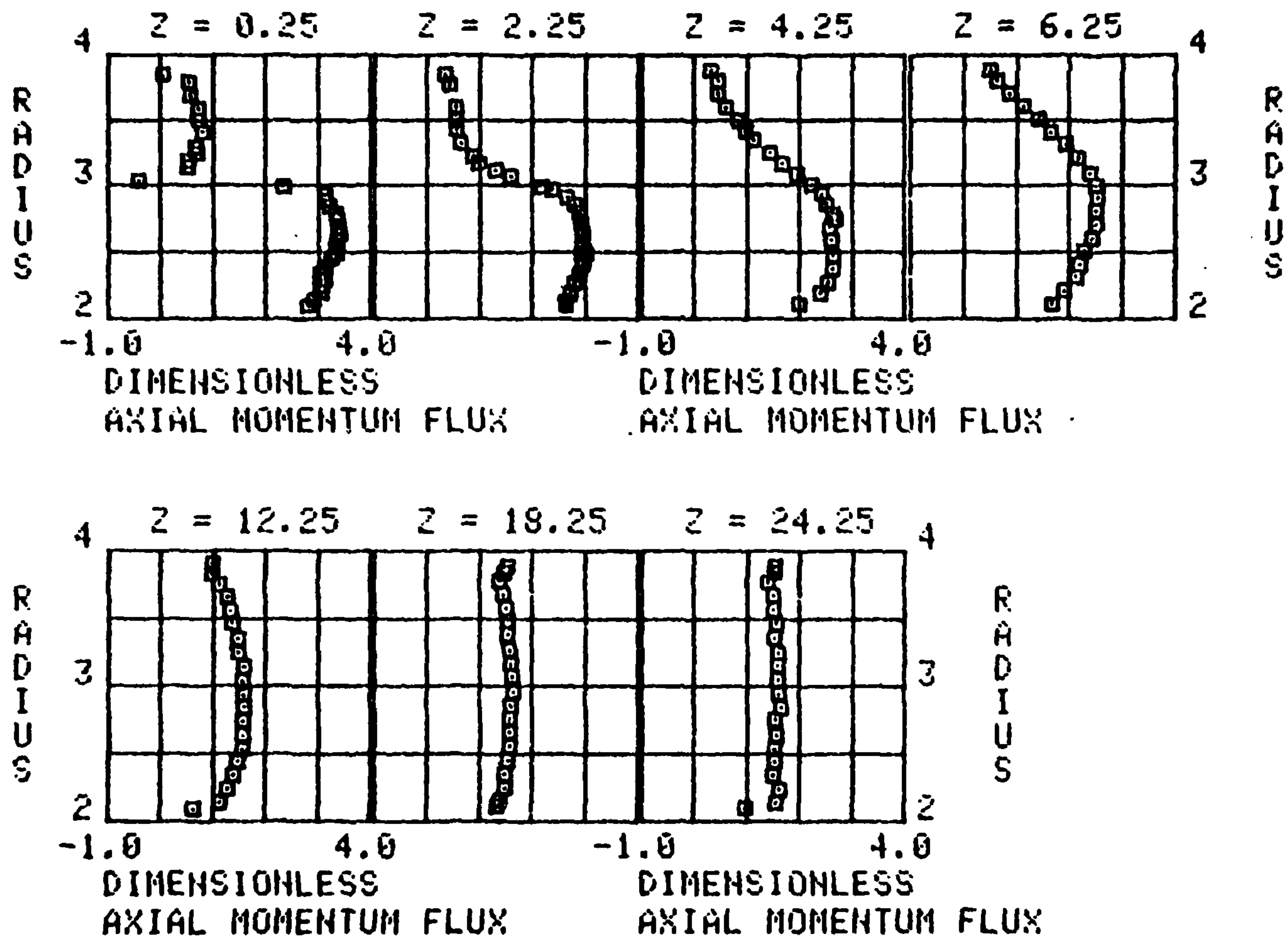

Figure A-56 Dimensionless Axial Momentum Flux, Test #4, Runs XX2

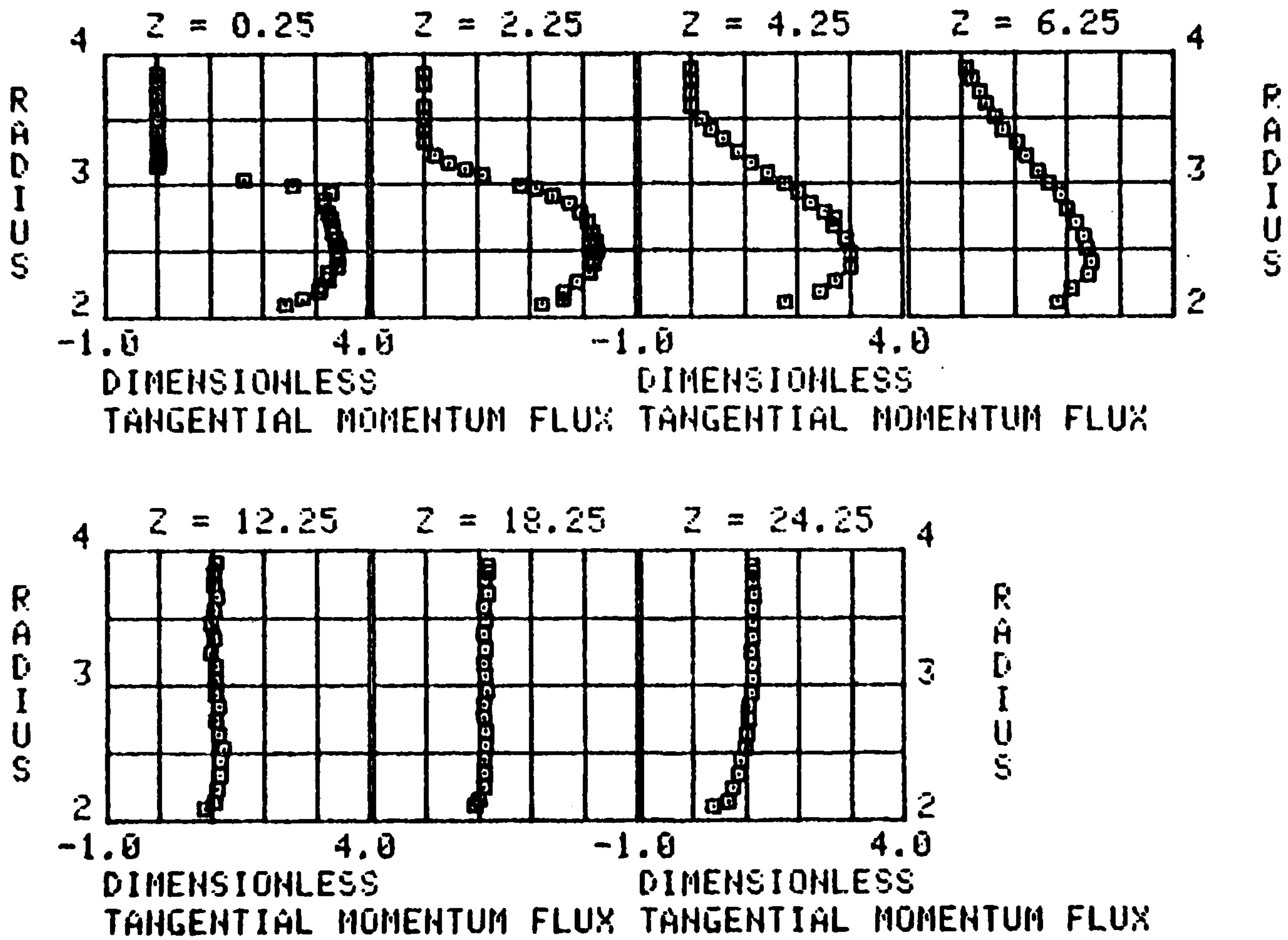

Figure A-57 Dimensionless Tangential Momentum Flux, Test #4, Runs XX2

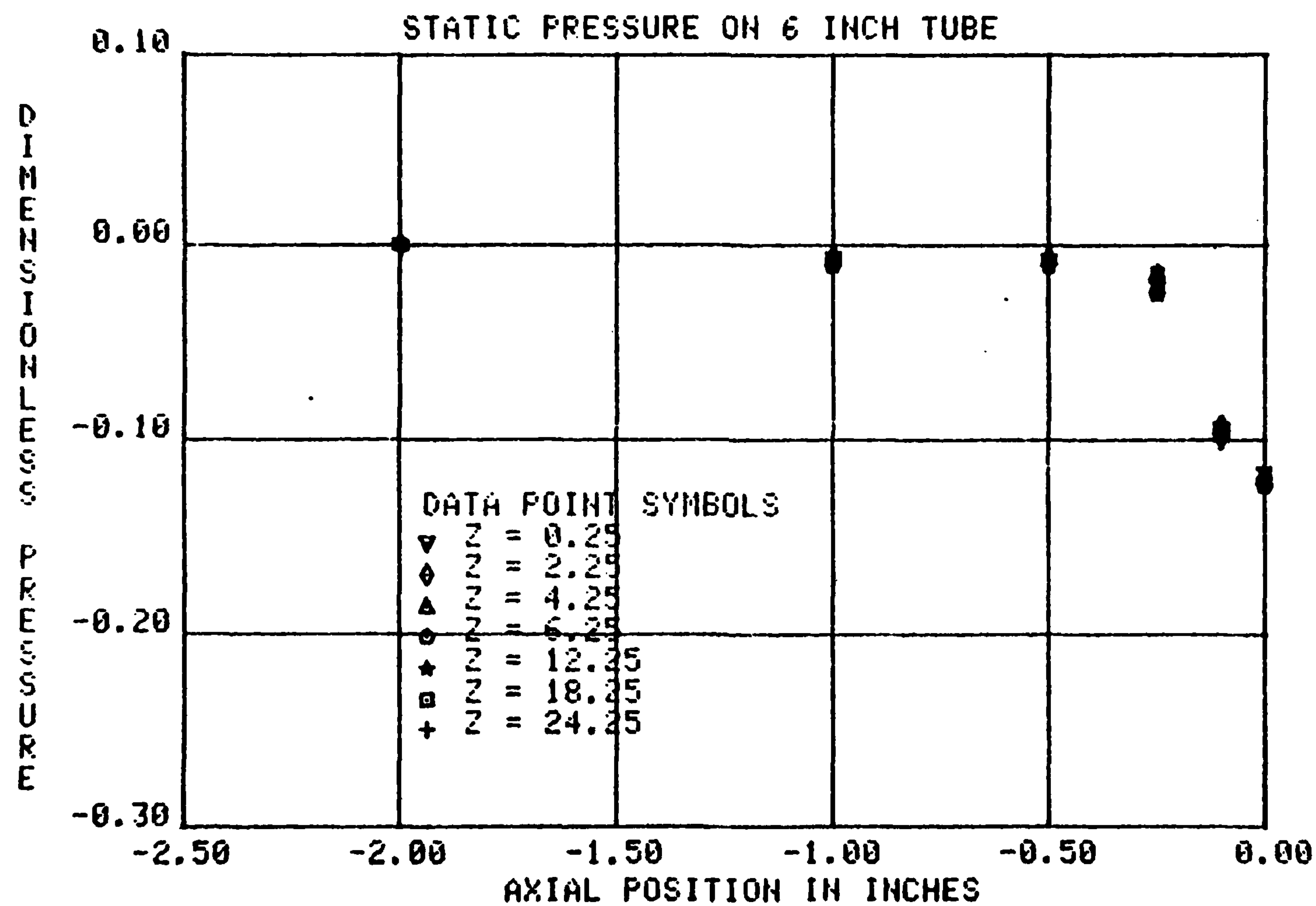

Figure A-59 Dimensionless Static Pressure on 6 Inch Tube, Test #4, Runs XX3

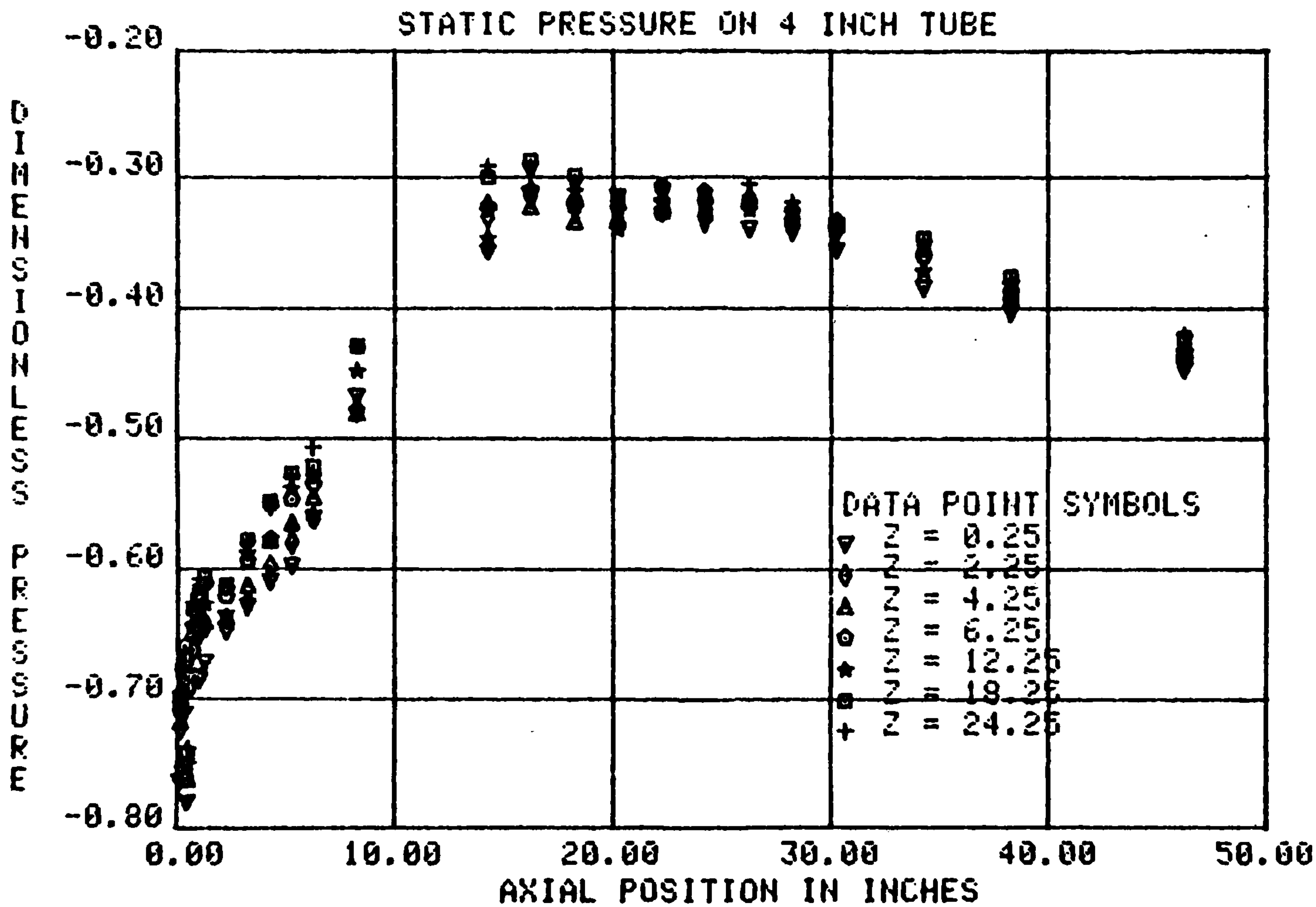

Figure A-58 Dimensionless Static Pressure on 4 Inch Tube, Test #4, Runs XX3

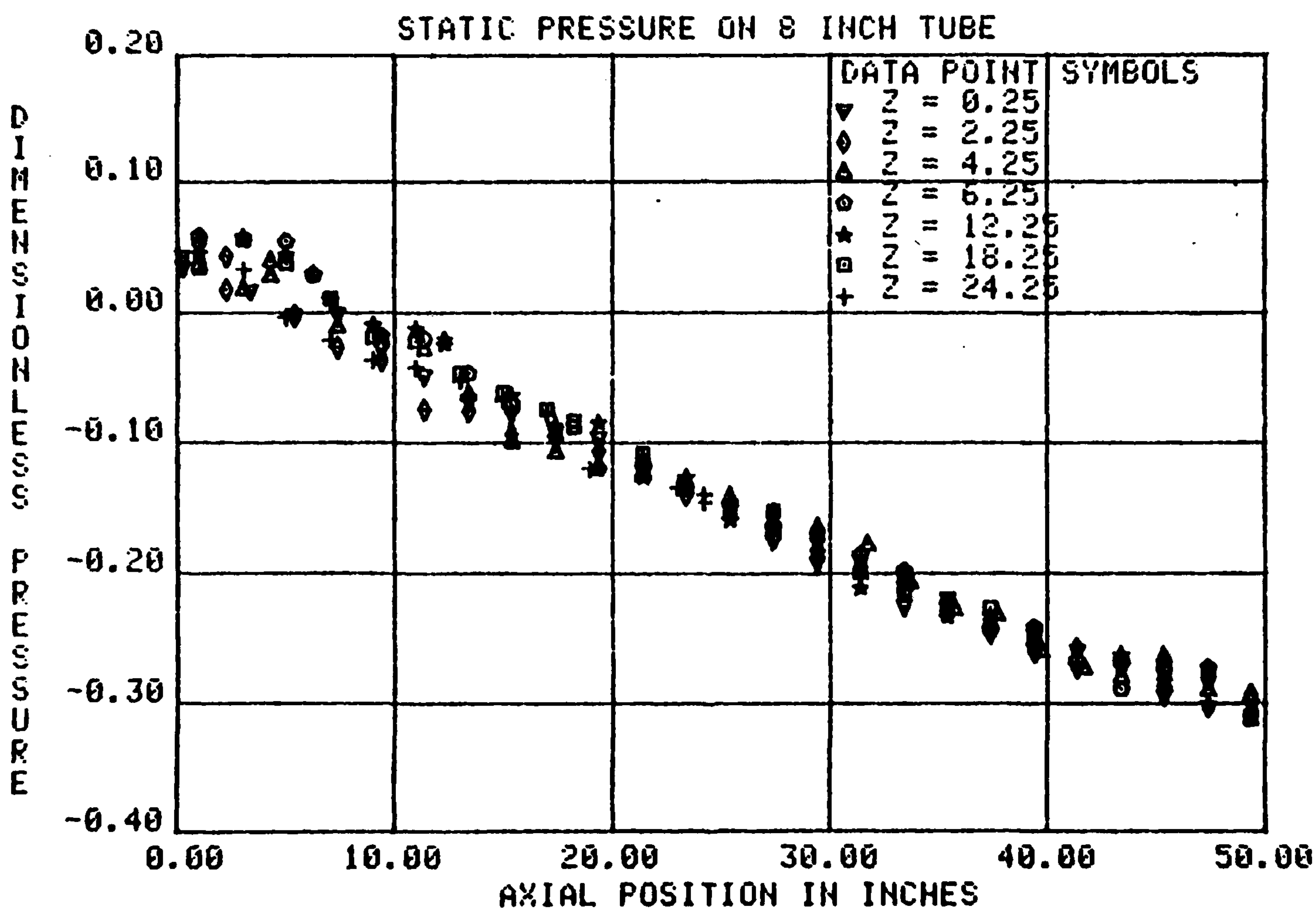

Figure A-60 Dimensionless Static Pressure on 8 Inch Tube, Test #4, Runs XX3

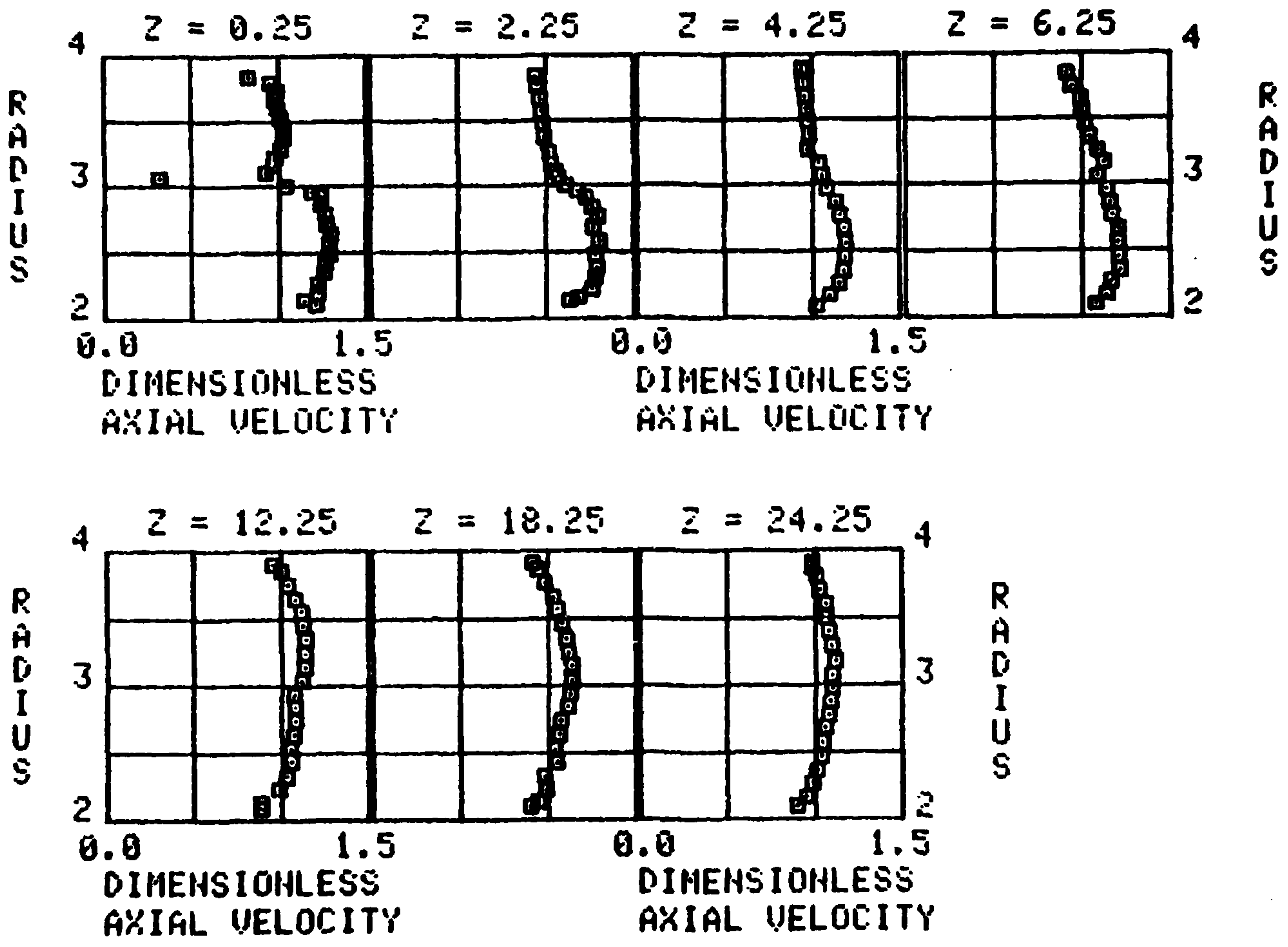

Figure A-61 Dimensionless Axial Velocity, Test #4, Runs XX3

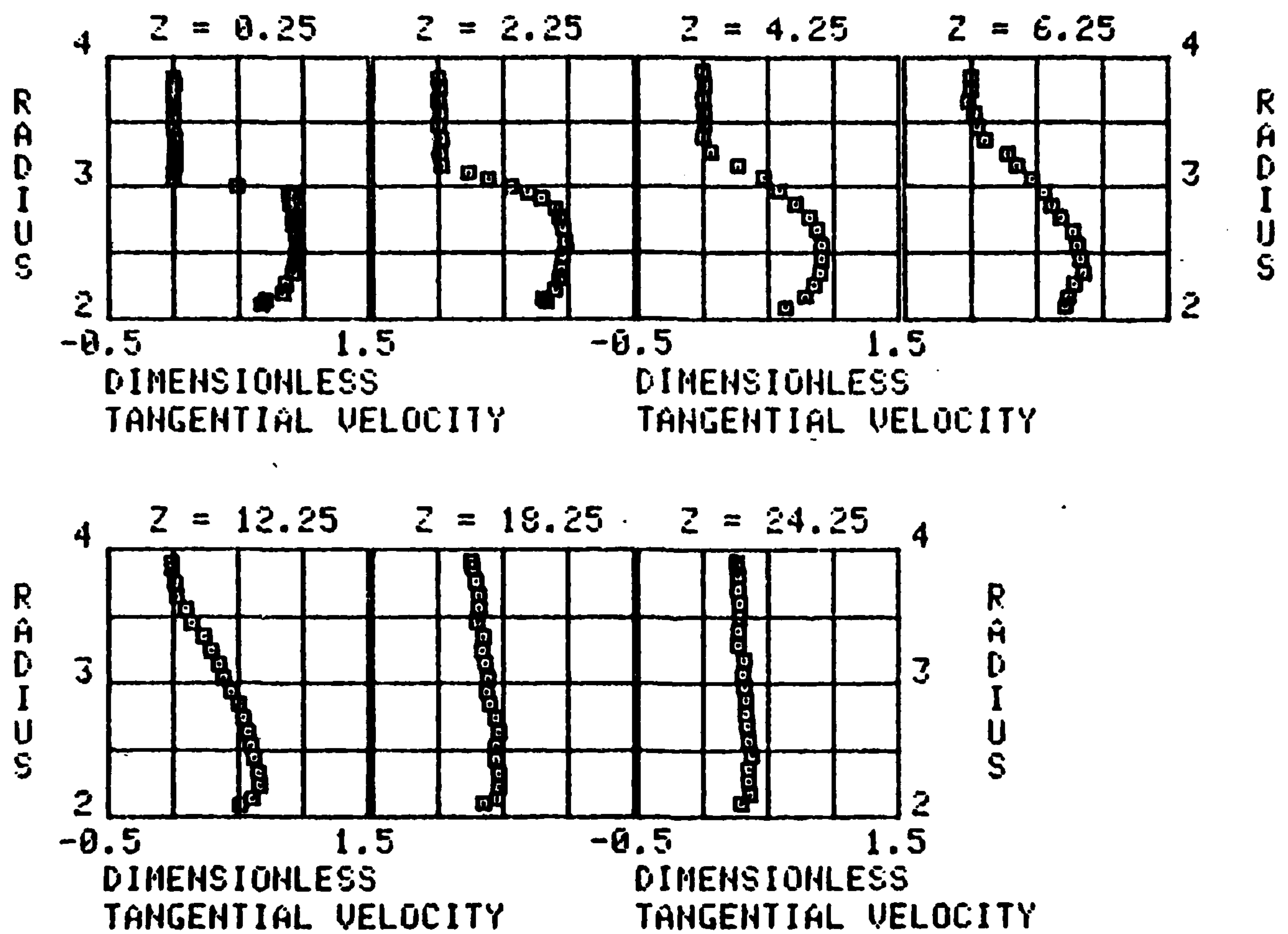

Figure A-62 Dimensionless Tangential Velocity, Test #4, Runs XX3

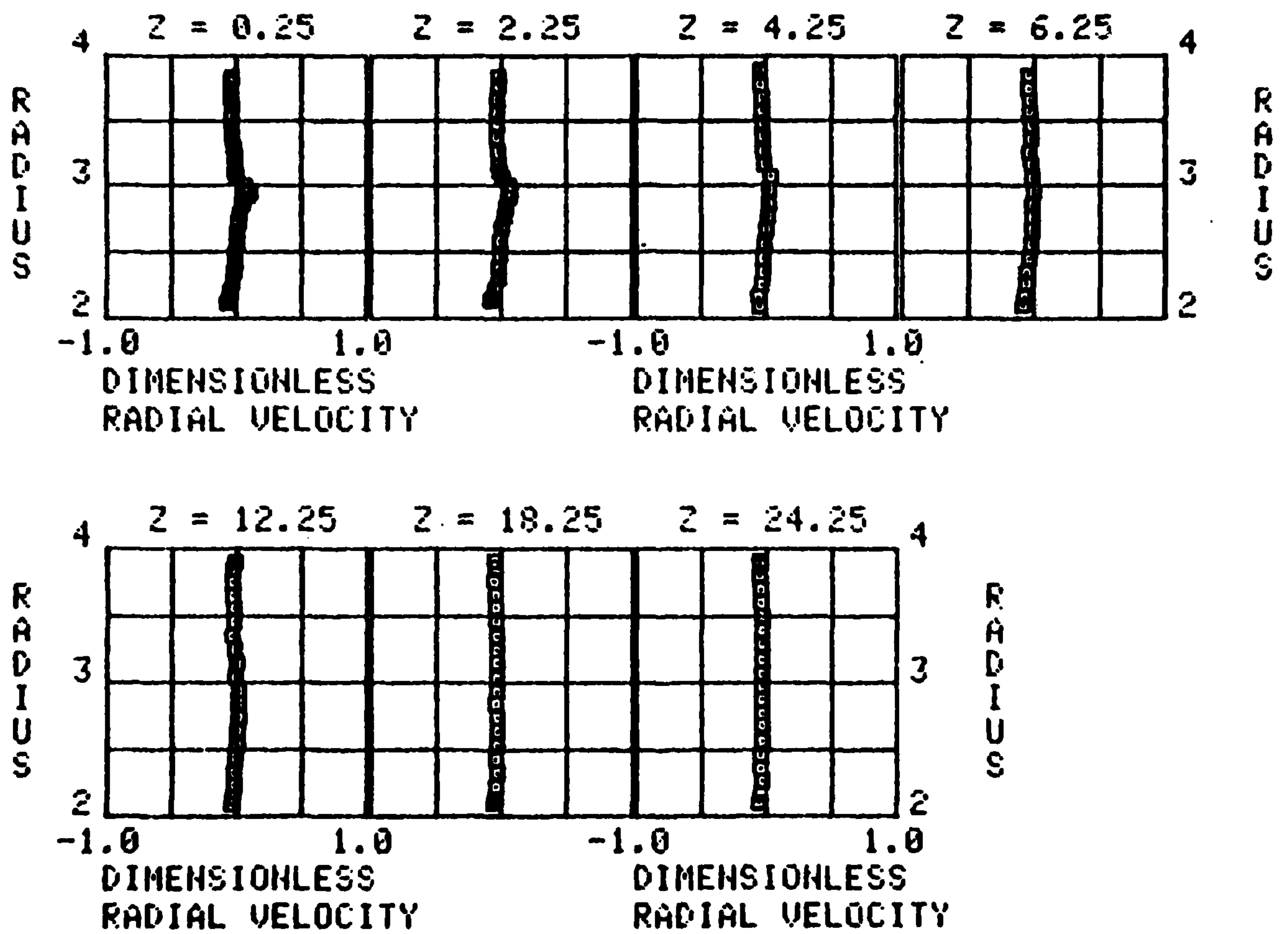

Figure A-63 Dimensionless Radial Velocity, Test #4, Runs XX3

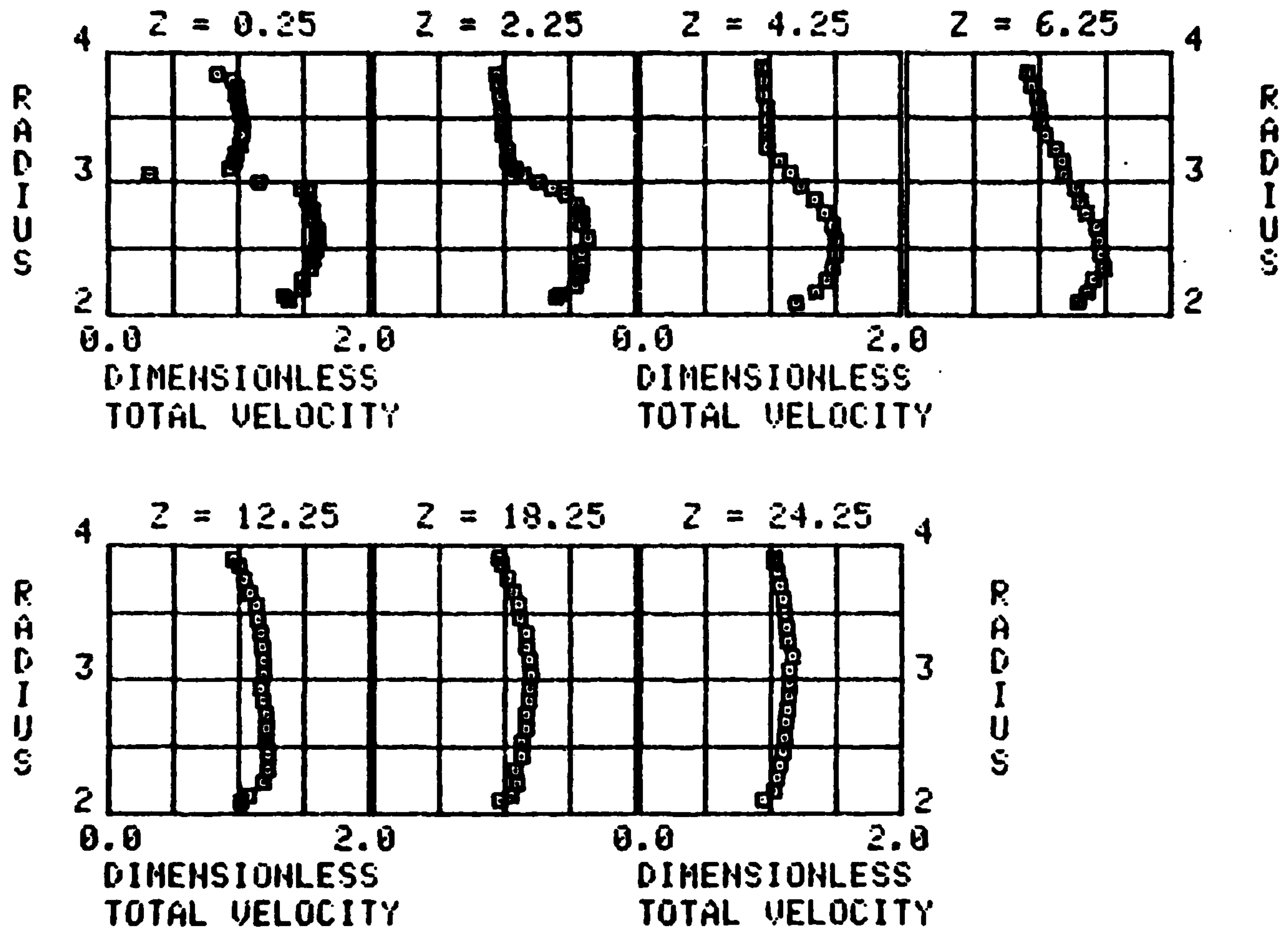

Figure A-64 Dimensionless Velocity, Test #4, Runs XX3

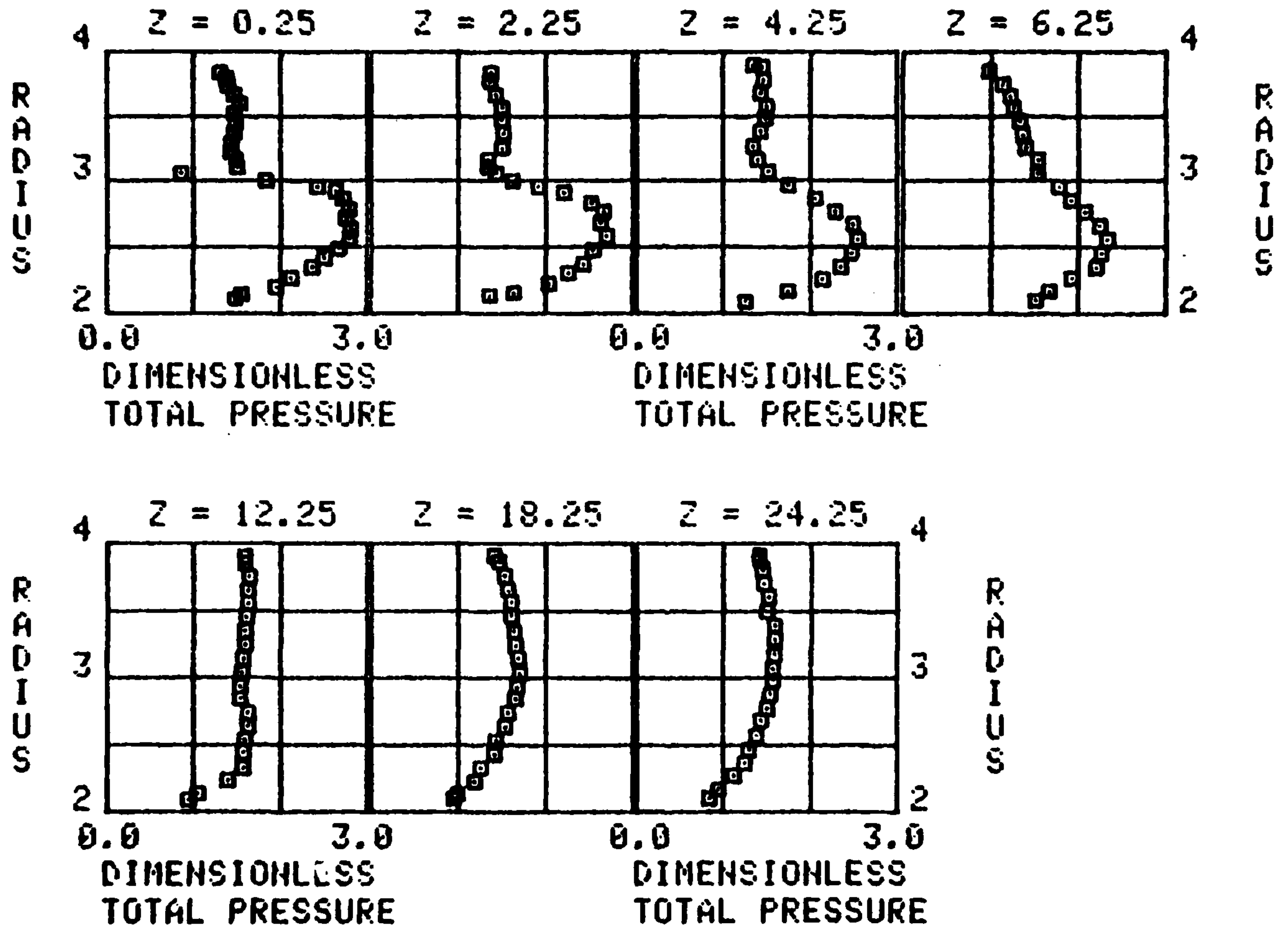

Figure A-65 Dimensionless Total Pressure, Test #4, Runs XX3

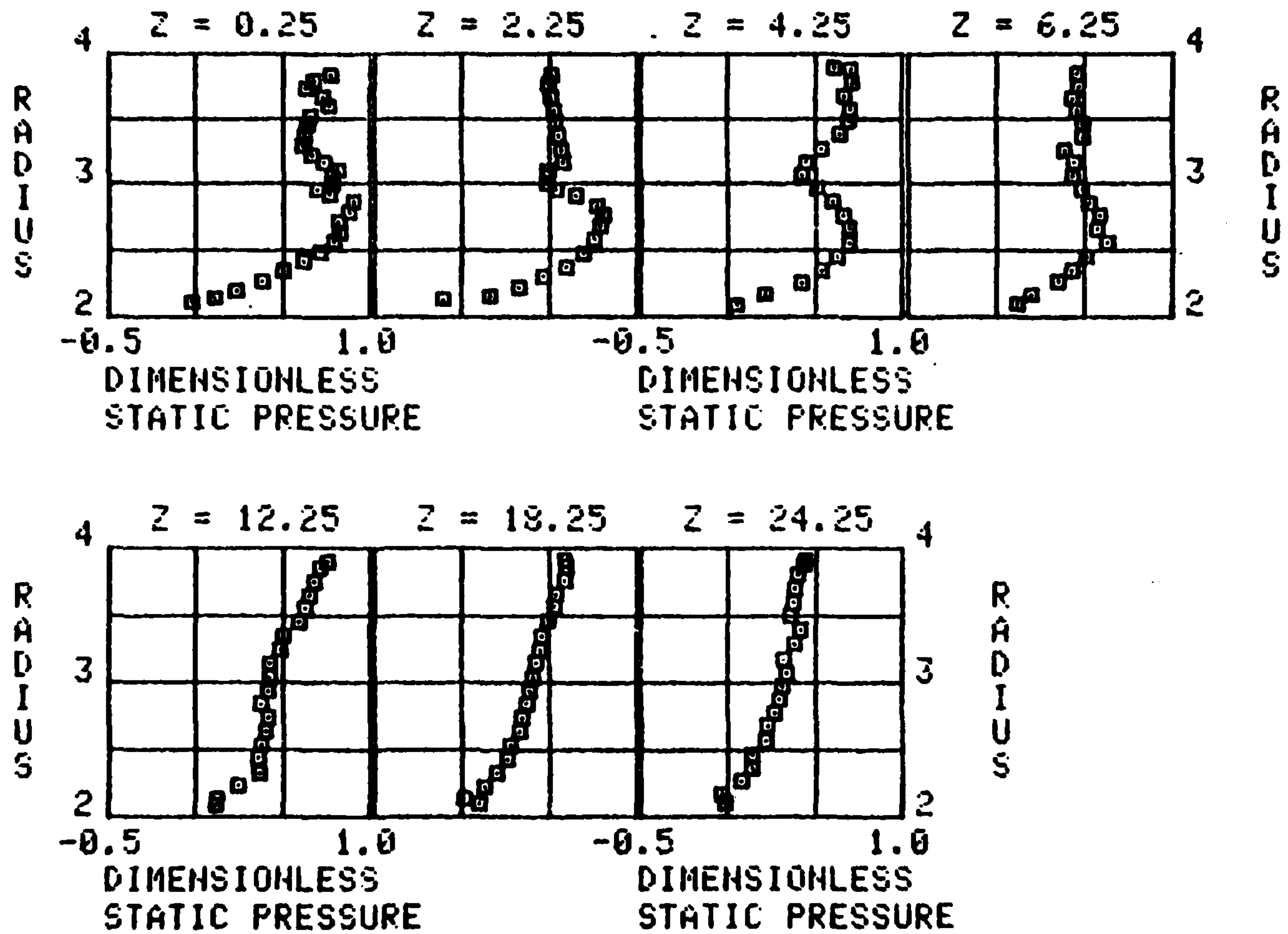

Figure A-66 Dimensionless Static Pressure, Test #4, Runs XX3

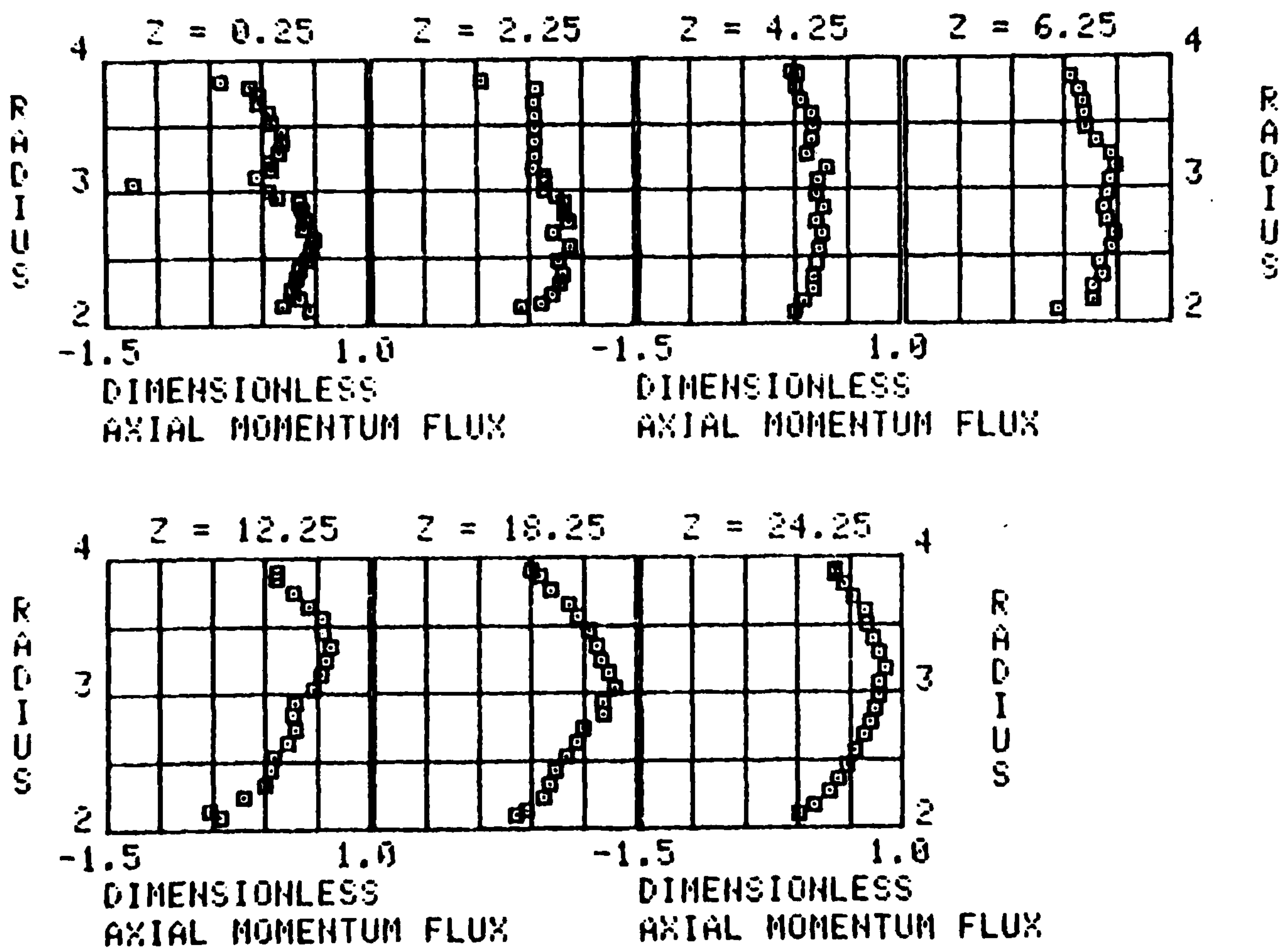

Figure A-67 Dimensionless Axial Momentum Flux,
Test #4, Runs XX3

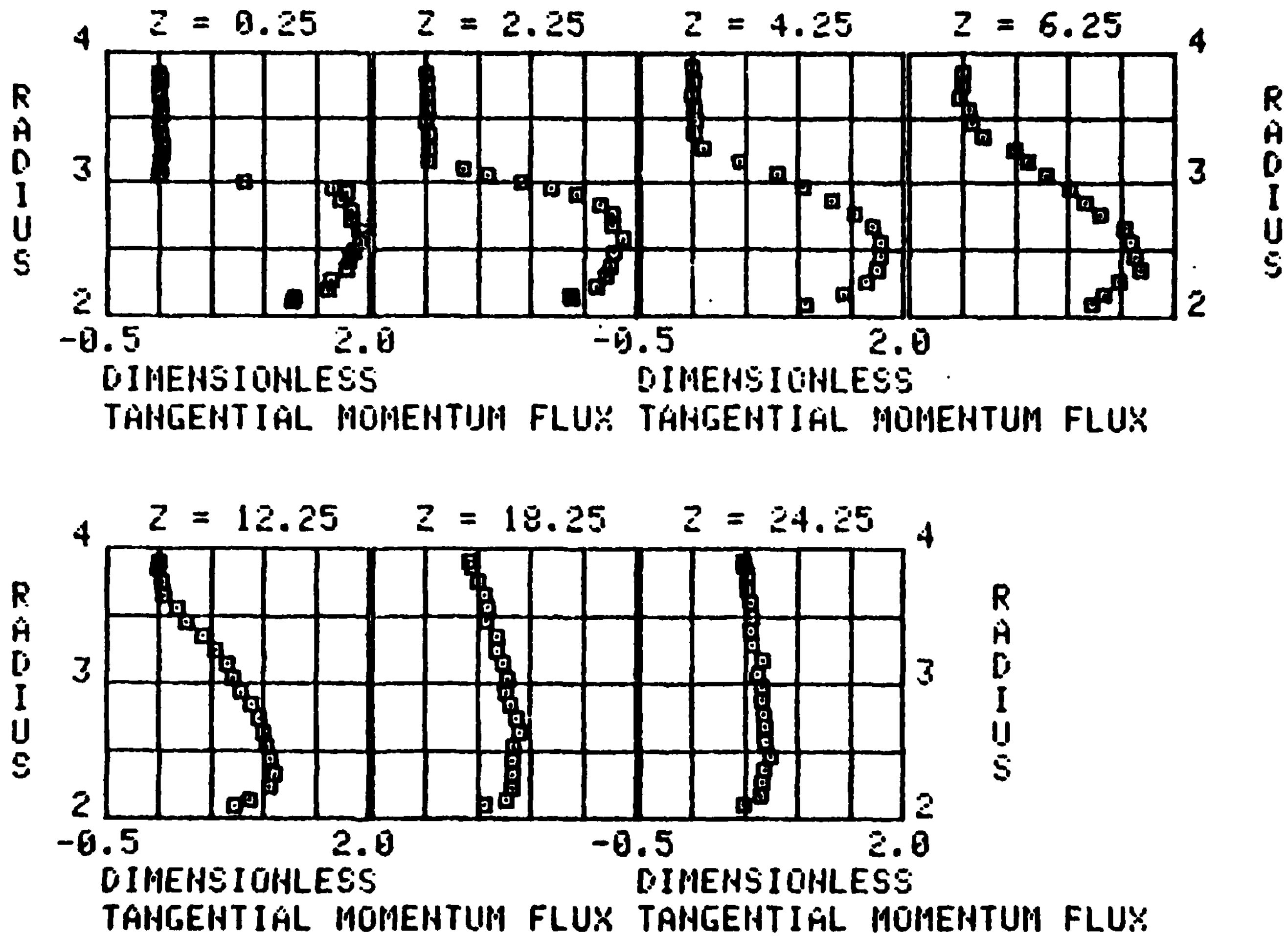

Figure A-68 Dimensionless Tangential Momentum Flux, Test #4, Runs XX3

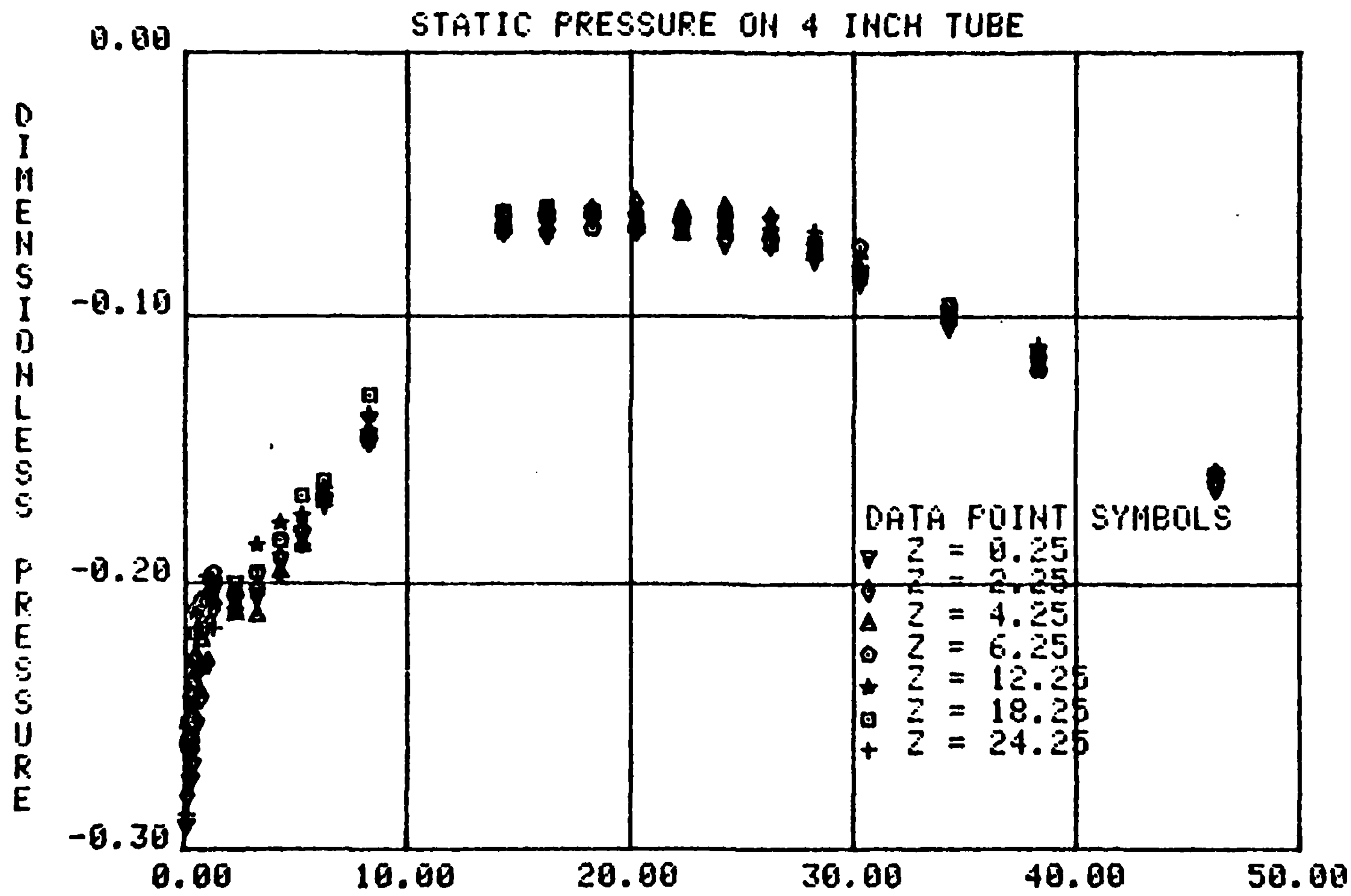

Figure A-69 Dimensionless Static Pressure on 4 Inch Tube, Test #4, Runs XX4

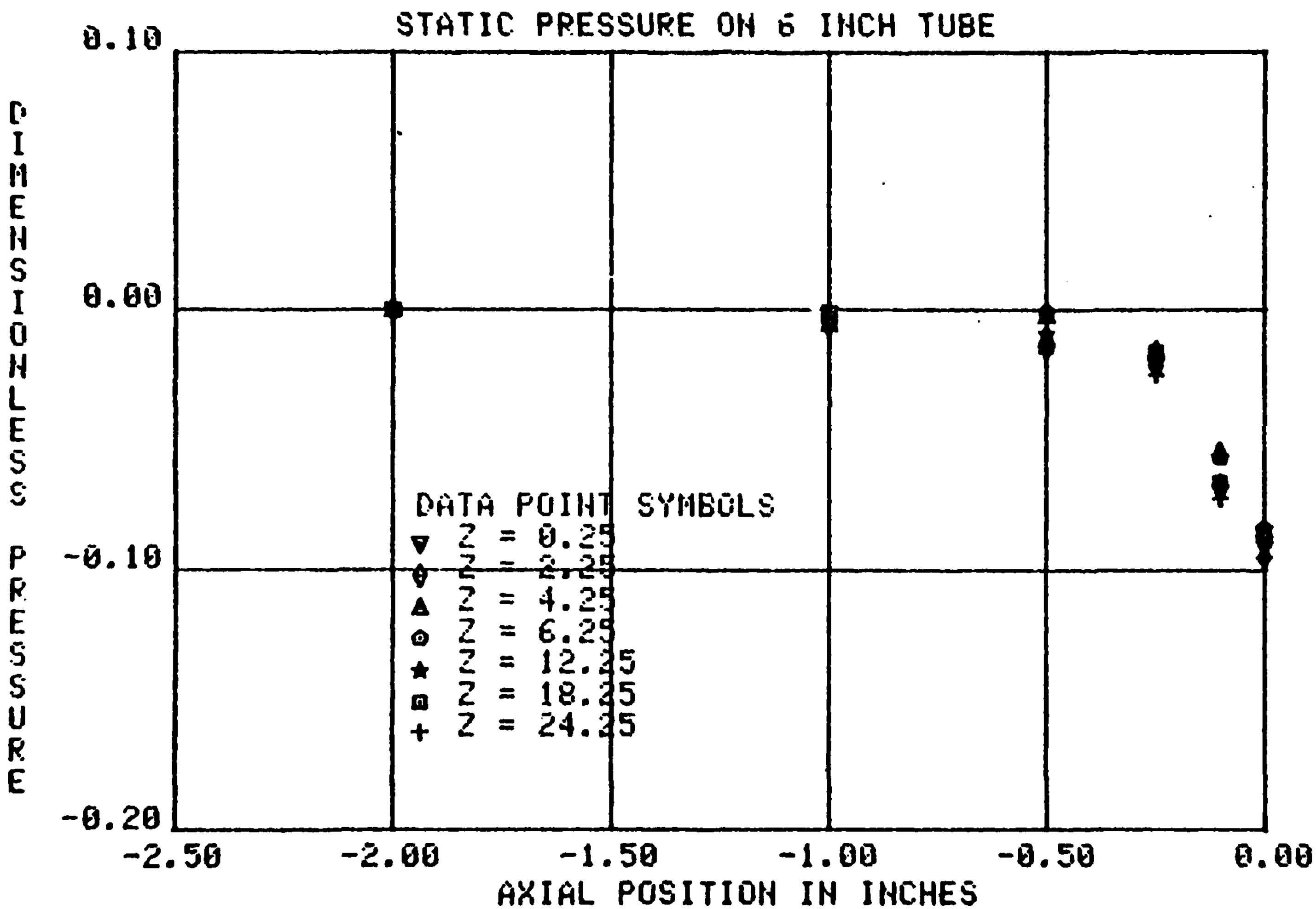

Figure A-70 Dimensionless Static Pressure on 6 Inch Tube, Test #4, Runs XX4

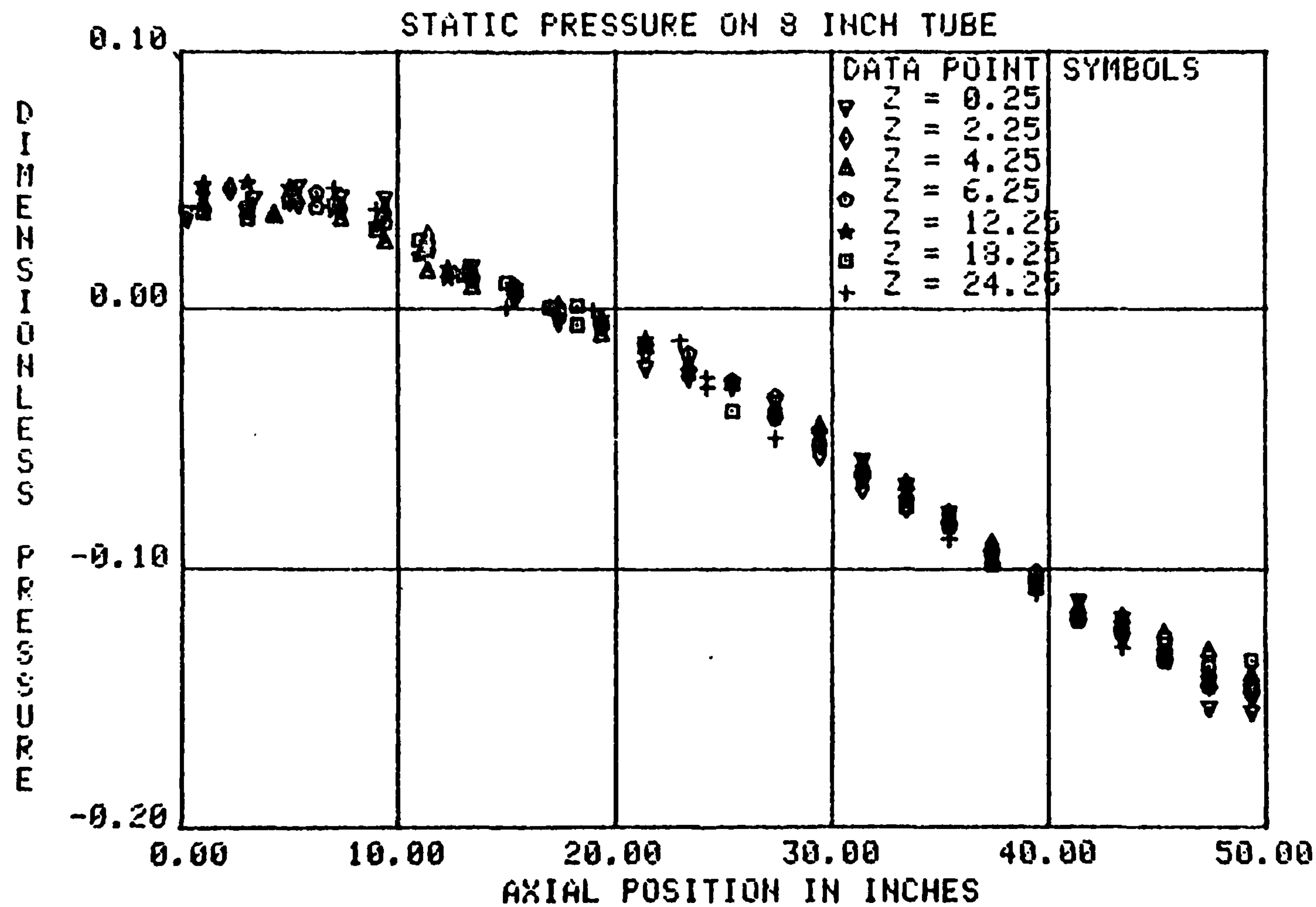

Figure A-71 Dimensionless Static Pressure on 8 Inch Tube, Test #4, Runs XX4

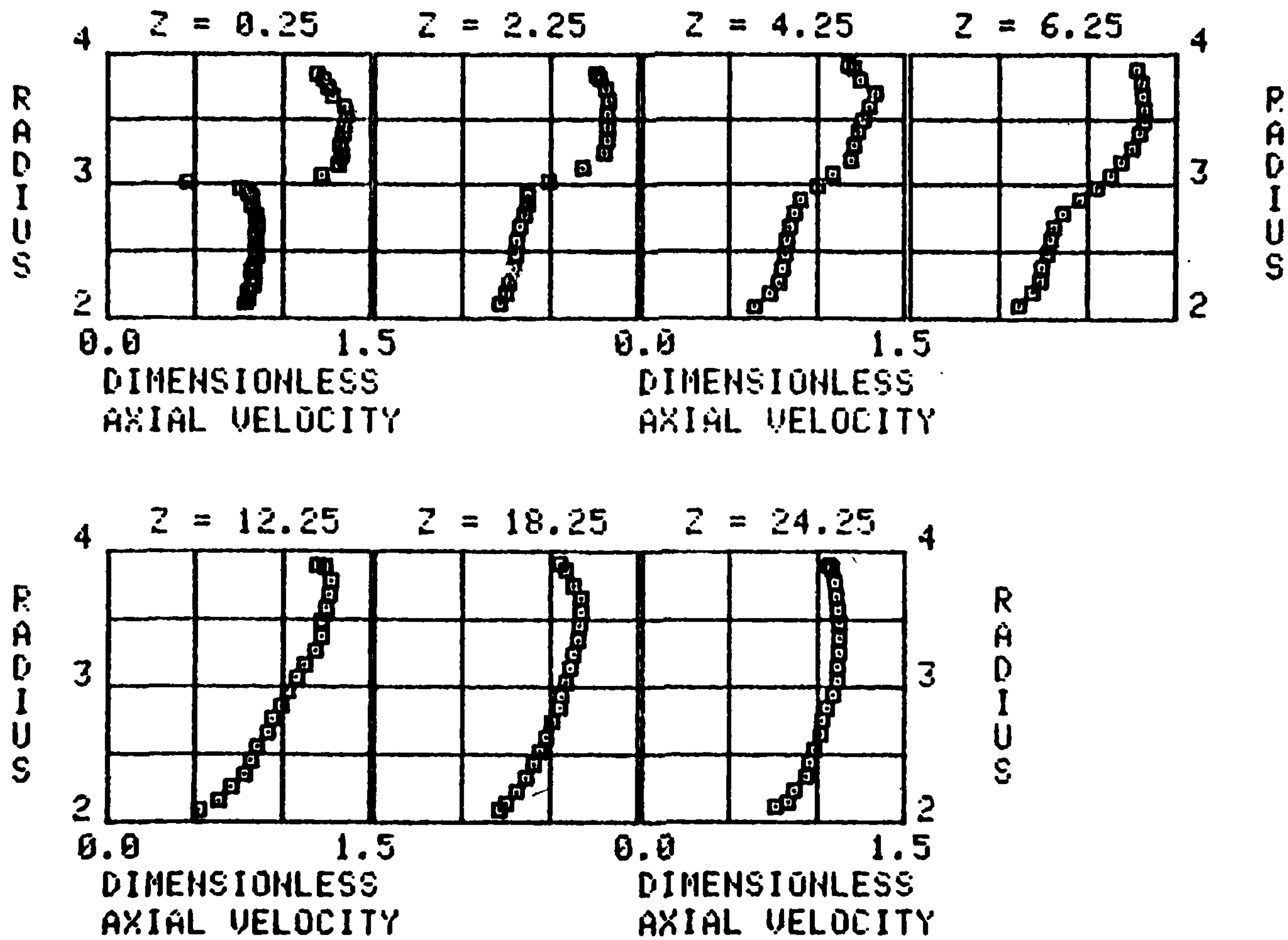

Figure A-72 Dimensionless Axial Velocity, Test #4, Runs XX4

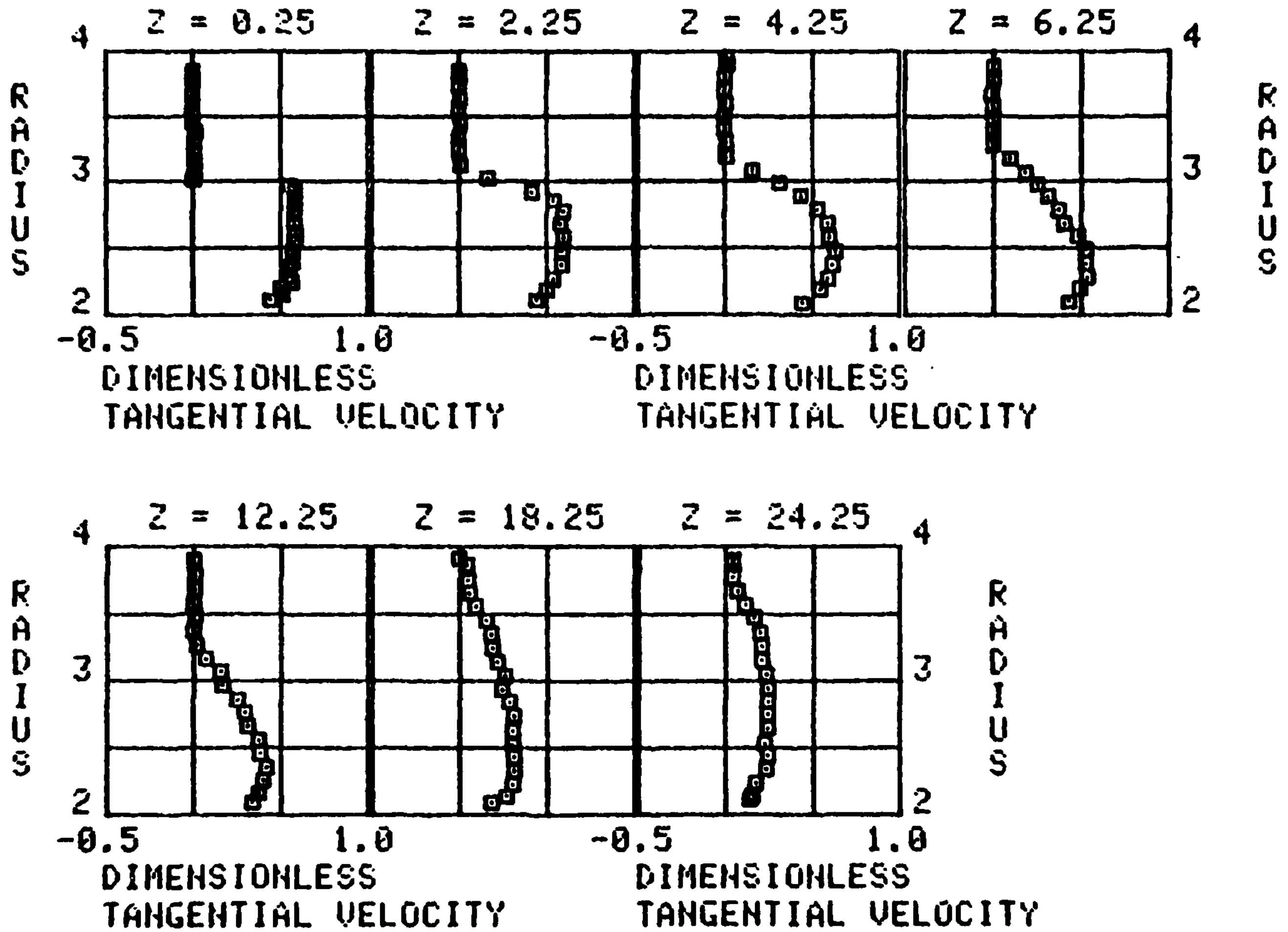

Figure A-73 Dimensionless Tangential Velocity, Test #4, Runs XX4

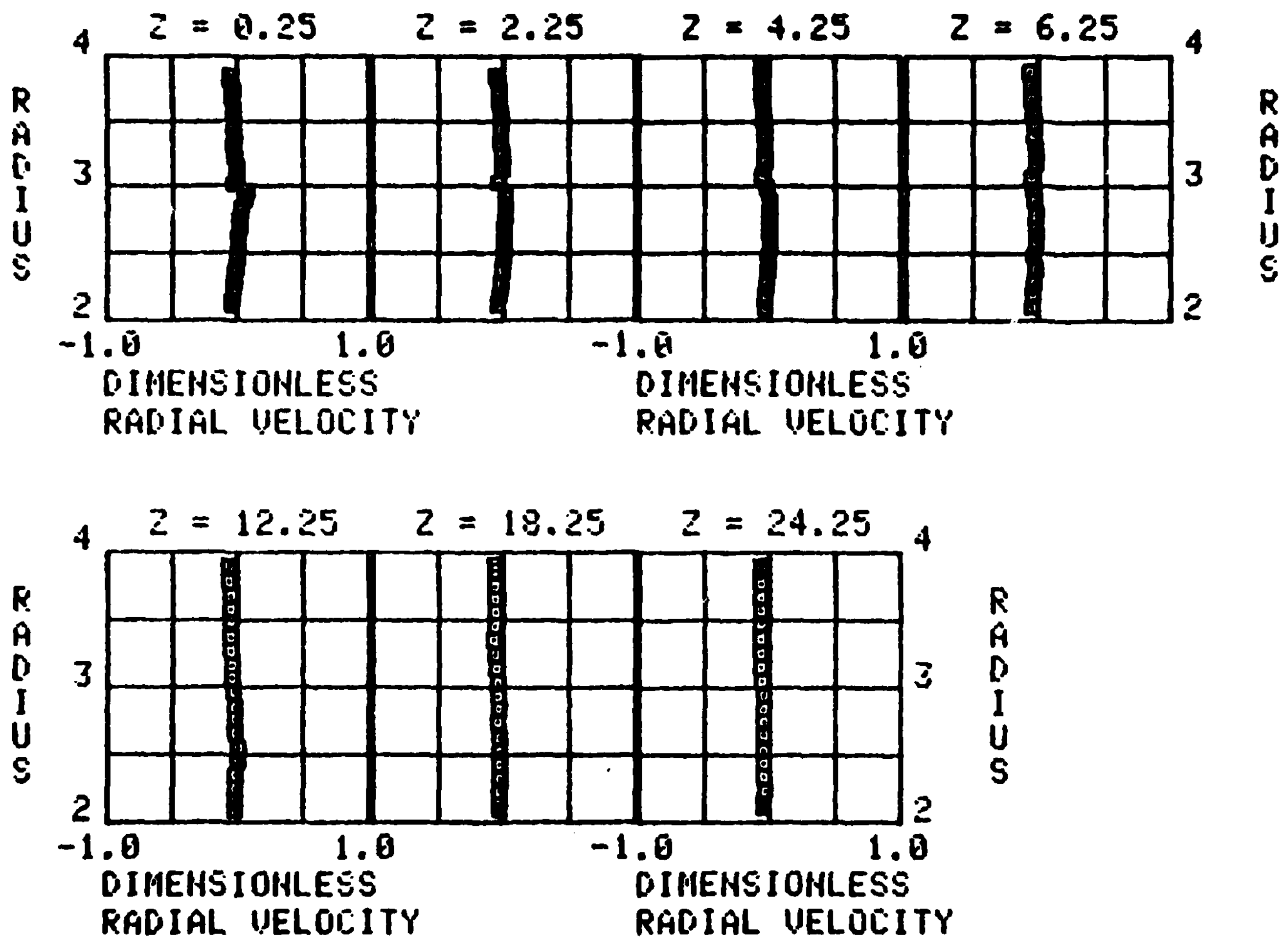

Figure A-74 Dimensionless Radial Velocity, Test #4, Runs XX4

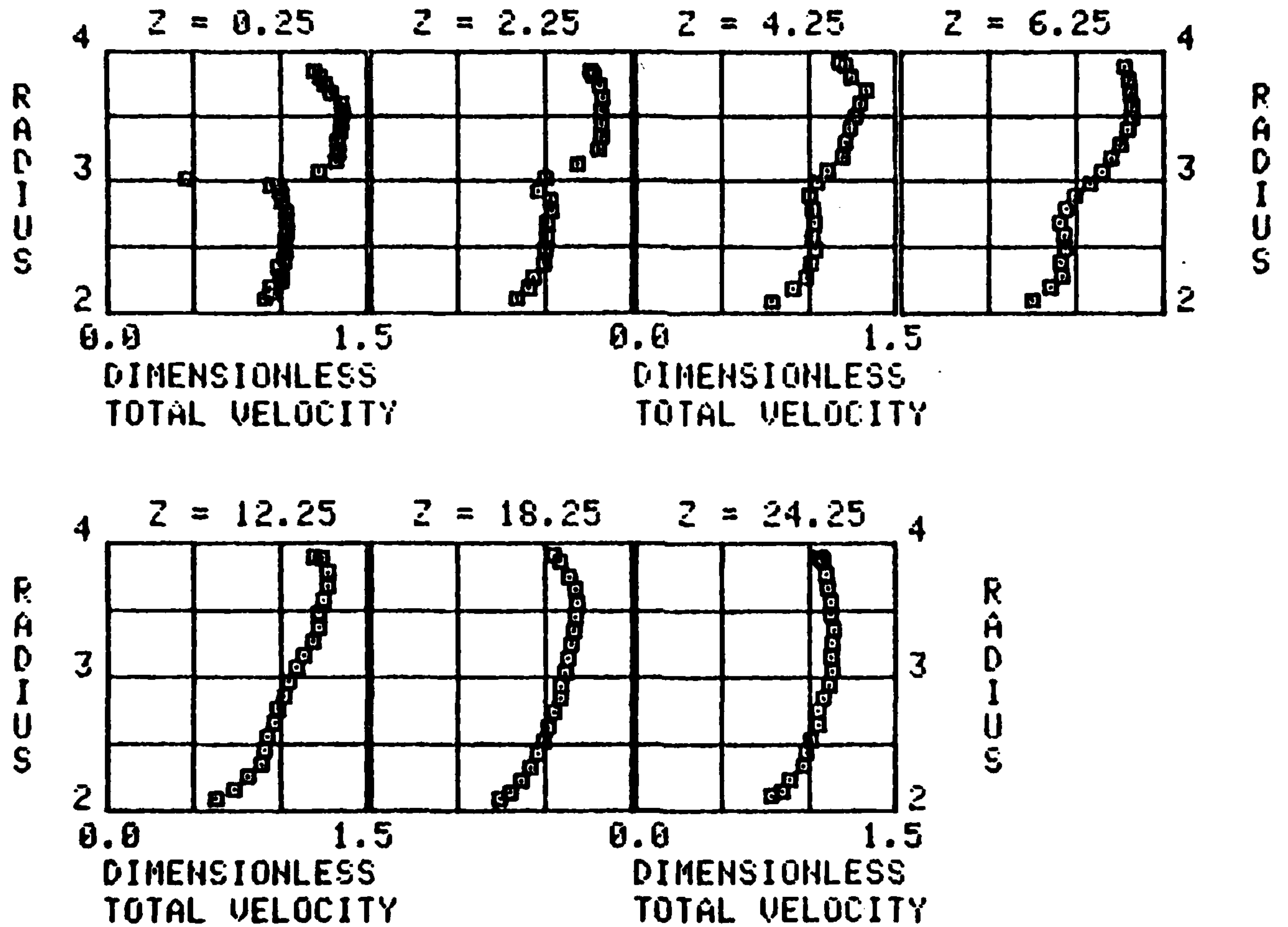

Figure A-75 Dimensionless Velocity, Test #4, Runs XX4

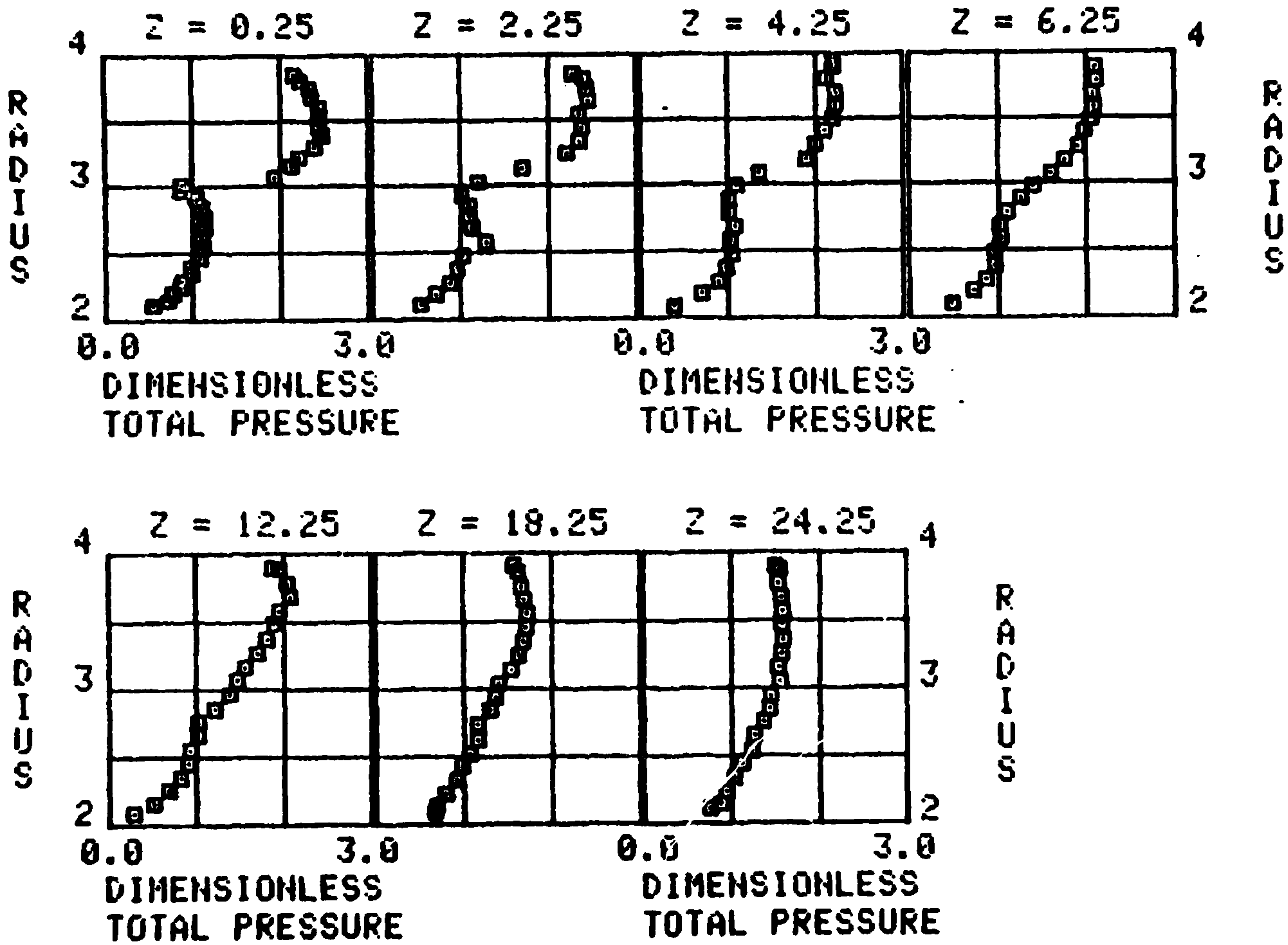

Figure A-76 Dimensionless Total Pressure, Test #4, Runs XX4

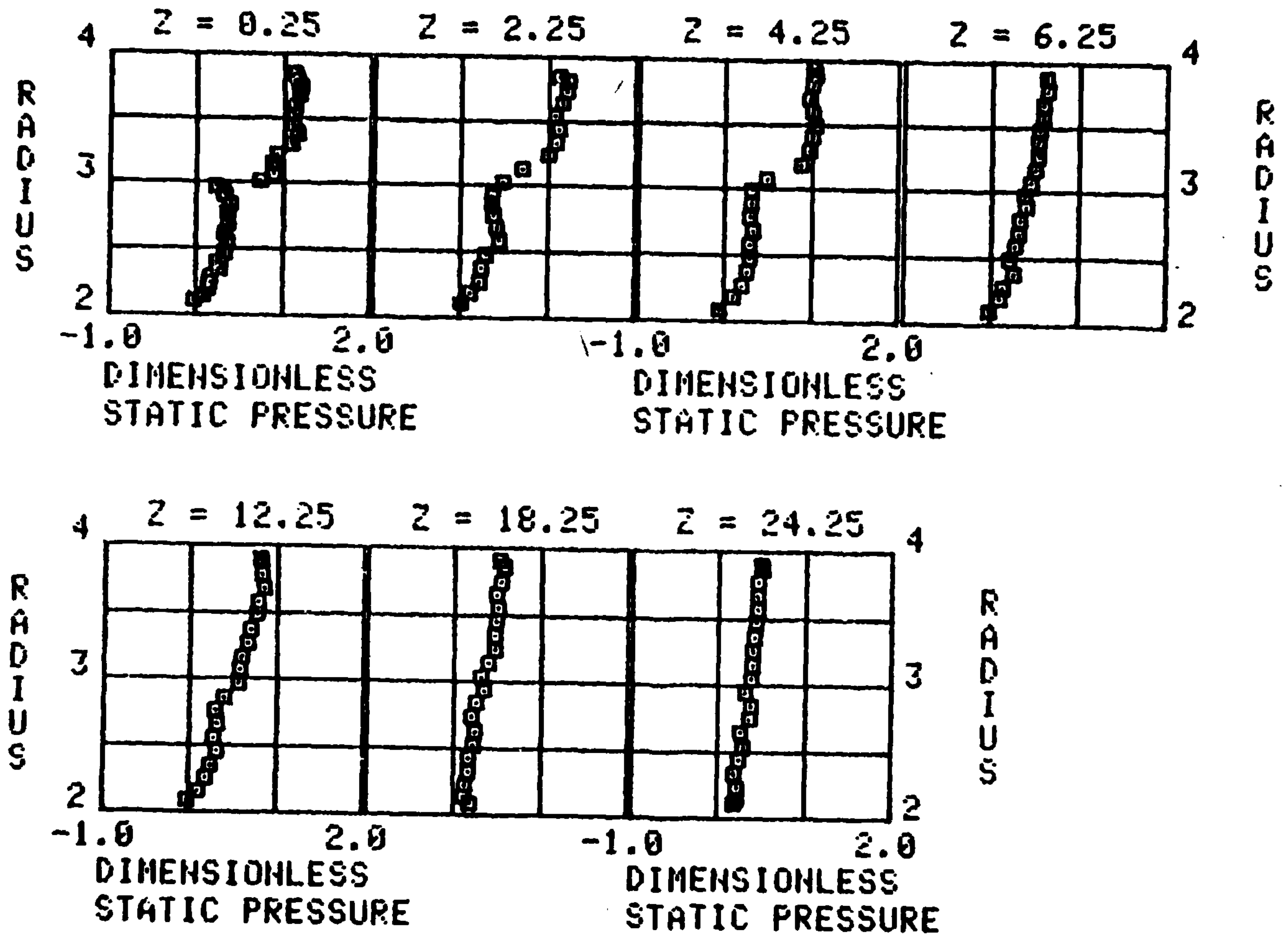

Figure A-77 Dimensionless Static Pressure, Test #4, Runs XX4

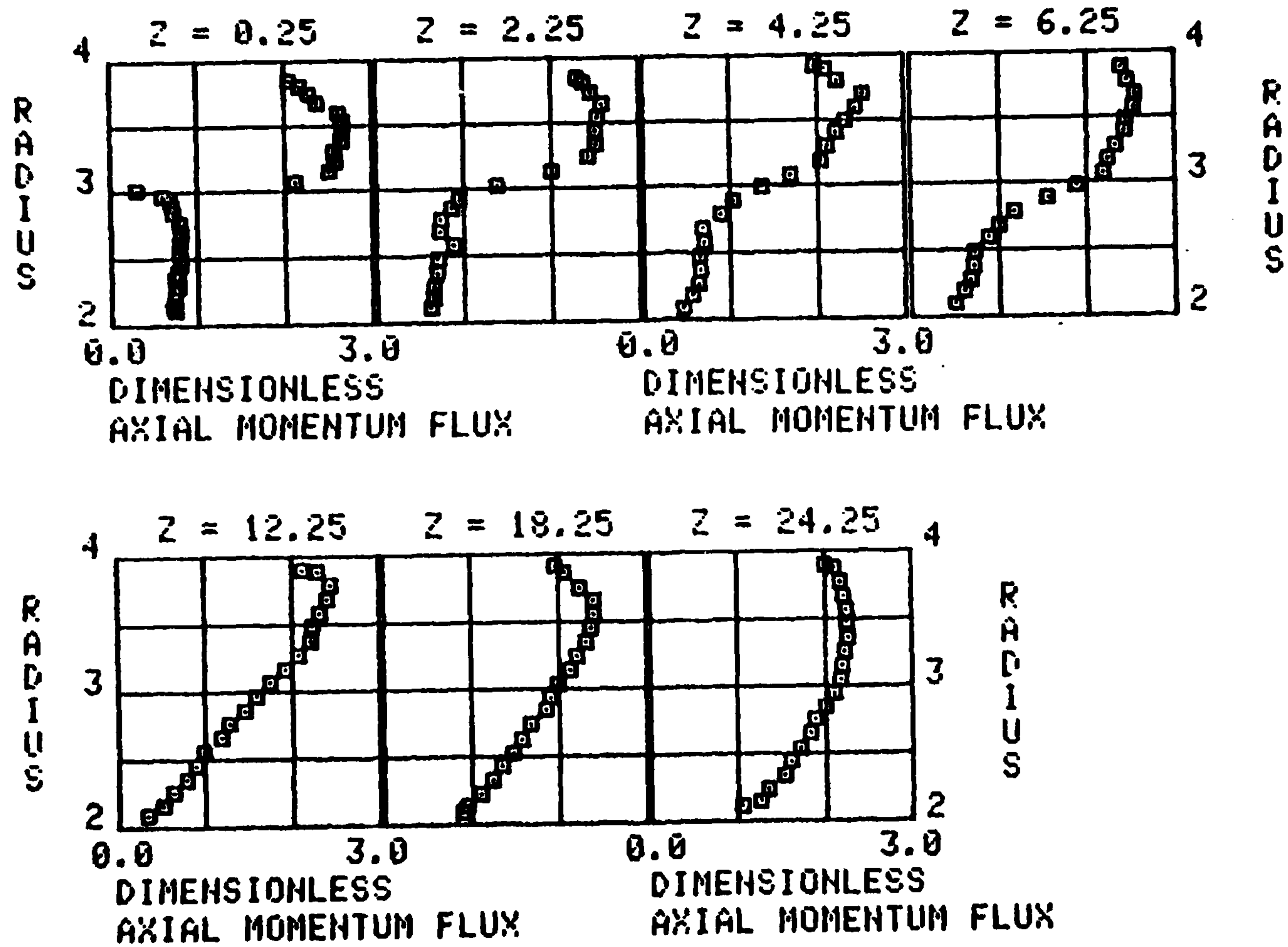

Figure A-78 Dimensionless Axial Momentum Flux, Test #4, Runs XX4

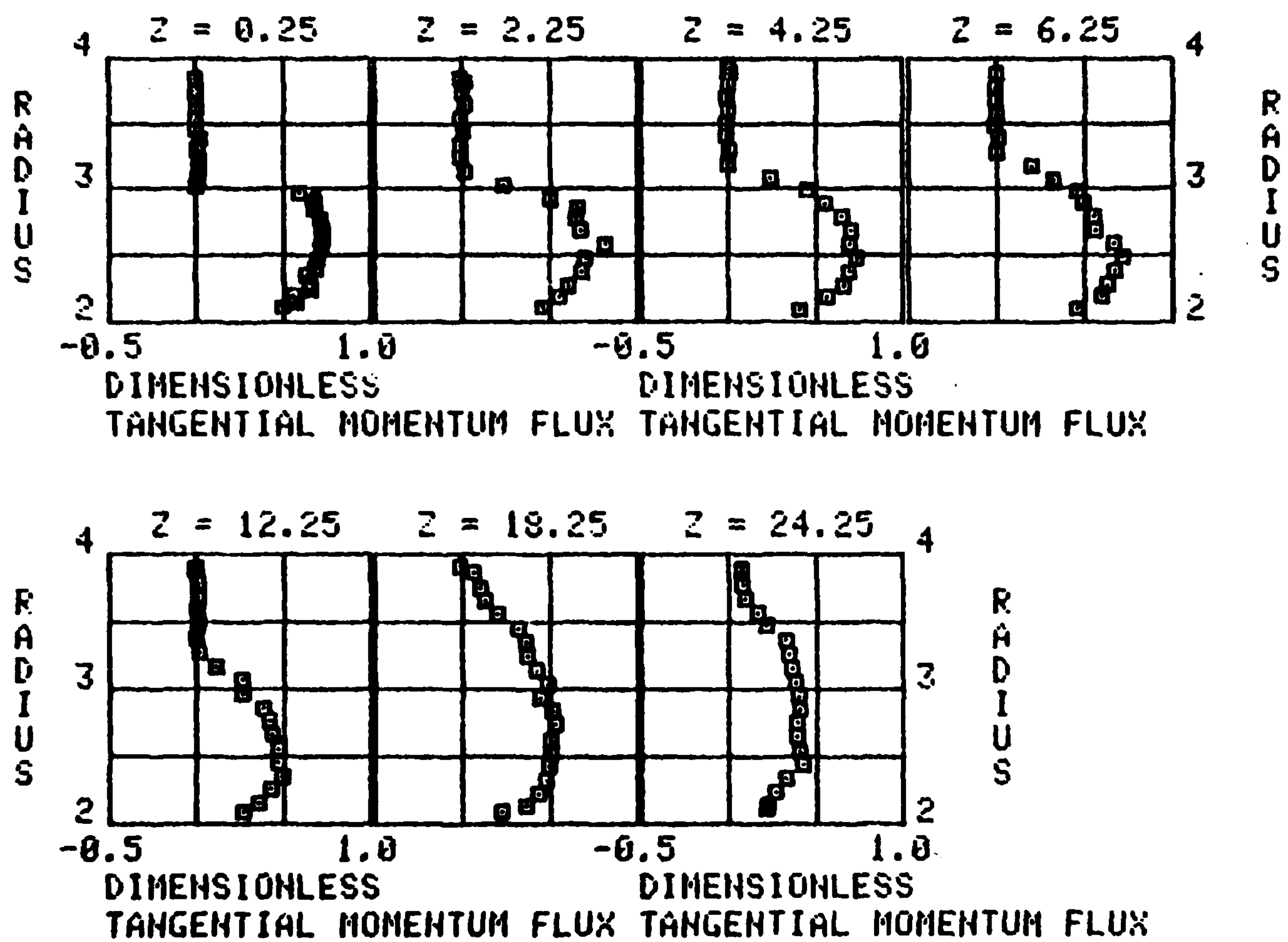

Figure A-79 Dimensionless Tangential Momentum Flux, Test #4, Runs XX4

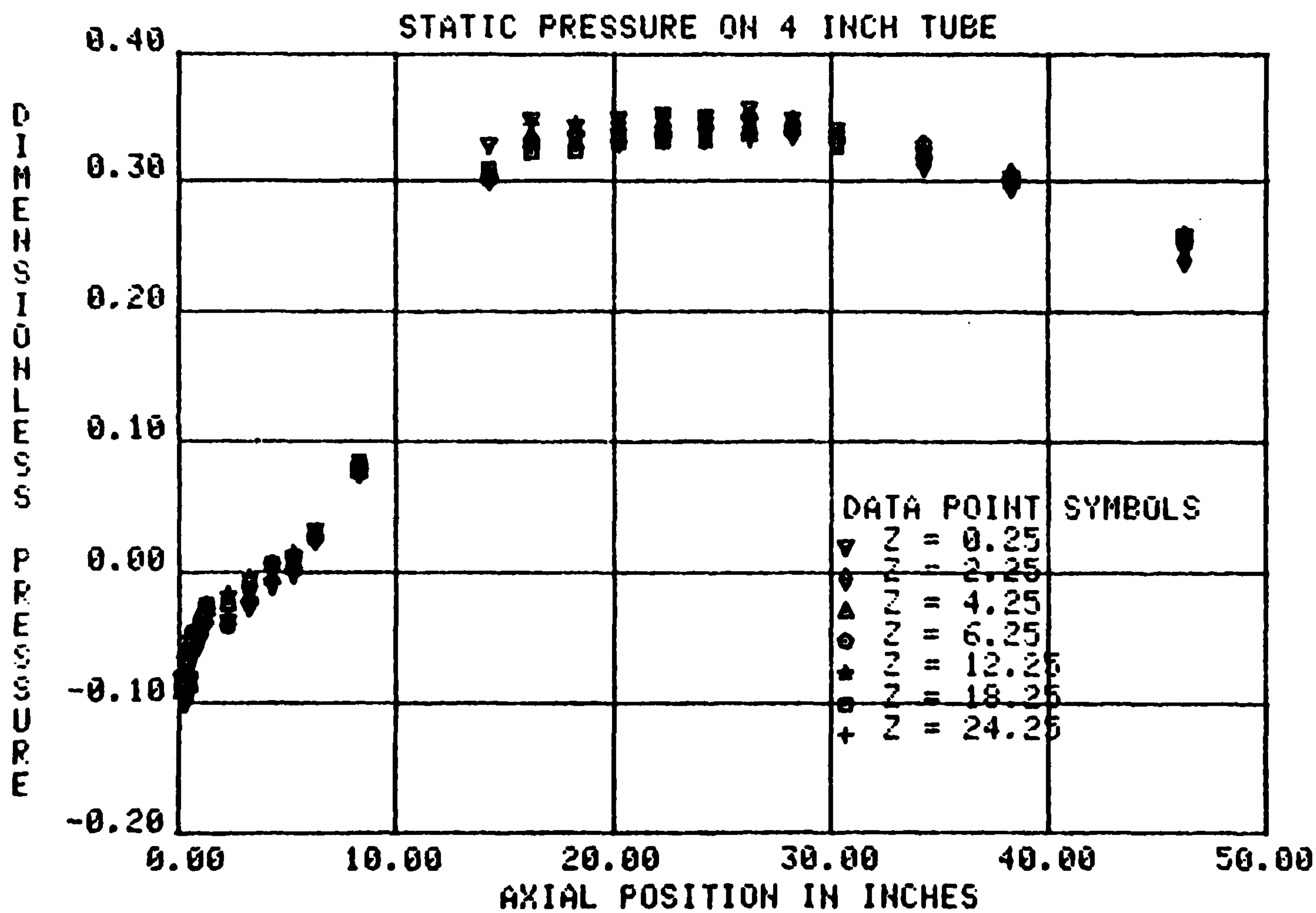

Figure A-8Ø Dimensionless Static Pressure on 4 Inch Tube, Test #4, Runs XX5

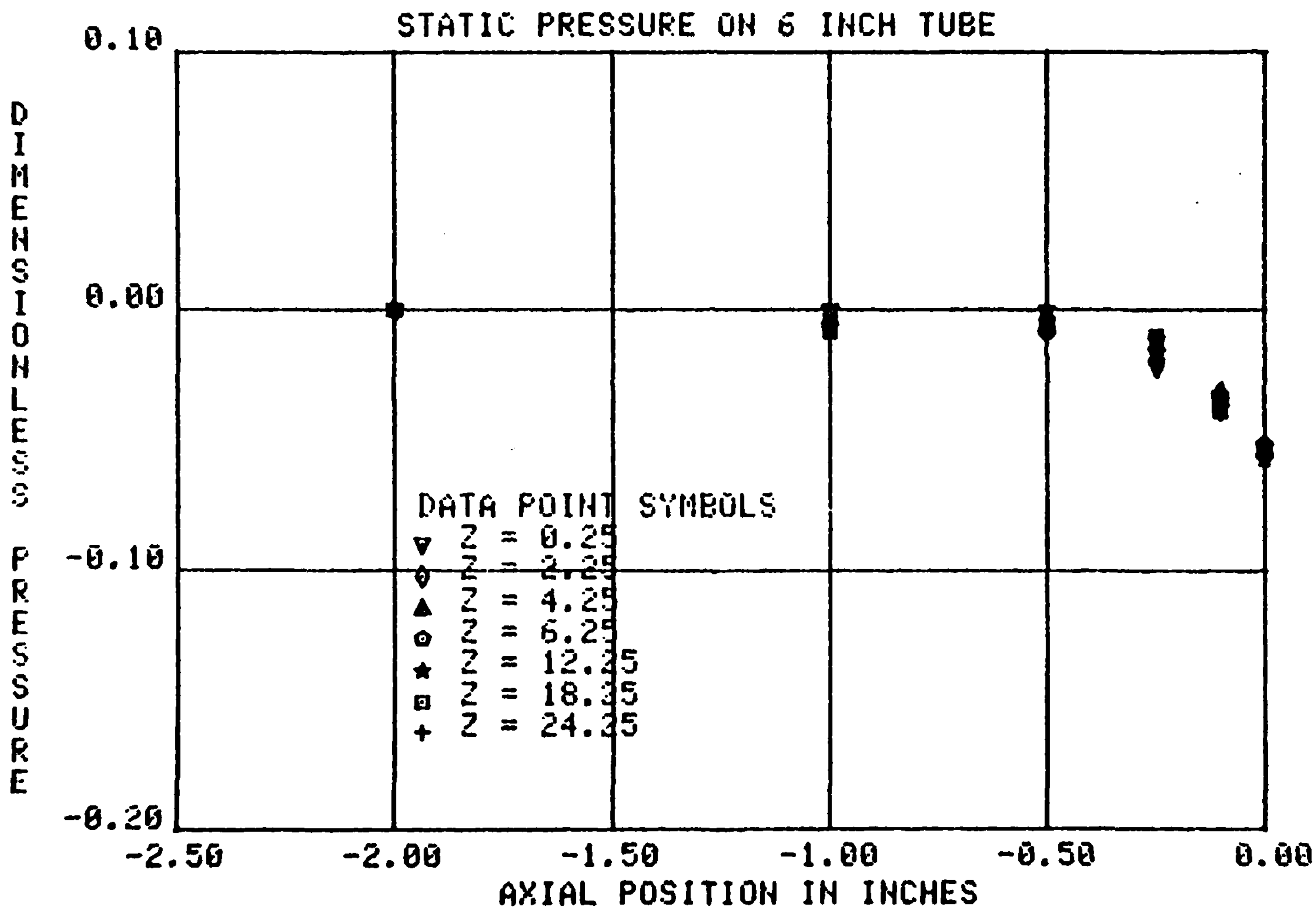

Figure A-81 Dimensionless Static Pressure on 6 Inch Tube, Test #4, Runs XX5

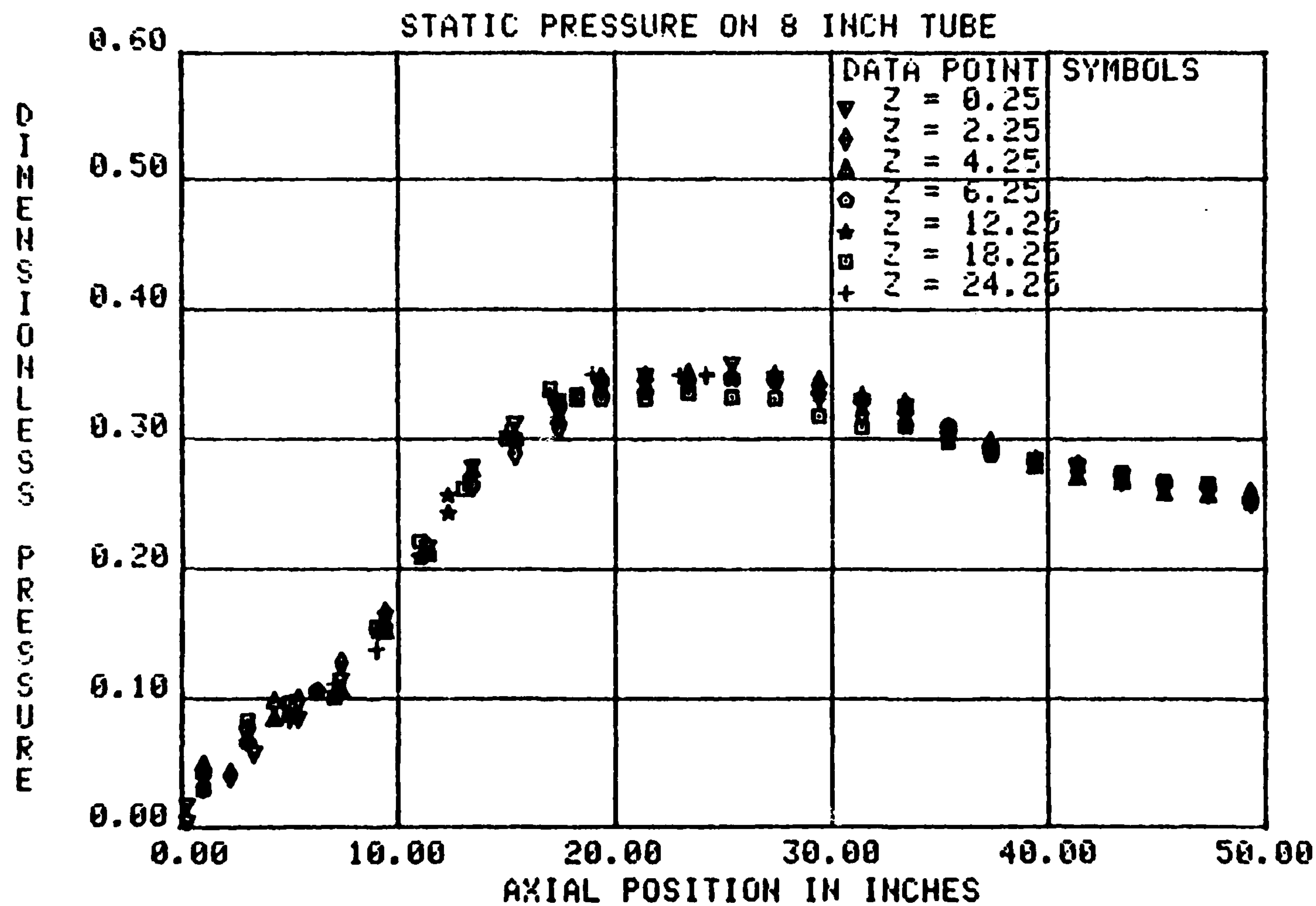

Figure A-82 Dimensionless Static Pressure on 8 Inch Tube, Test #4, Runs XX5

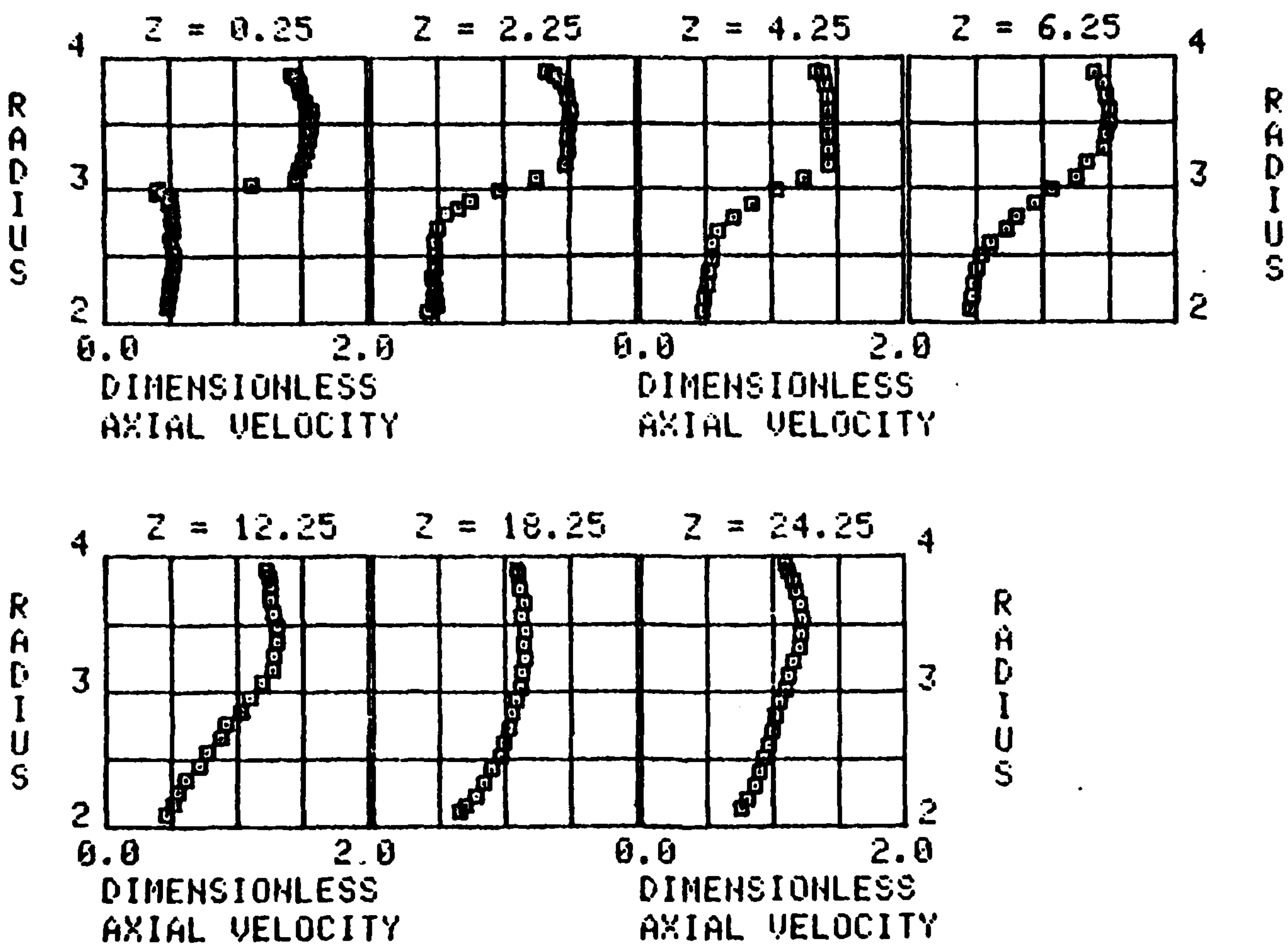

Figure A-83 Dimensionless Axial Velocity, Test #4, Runs XX5

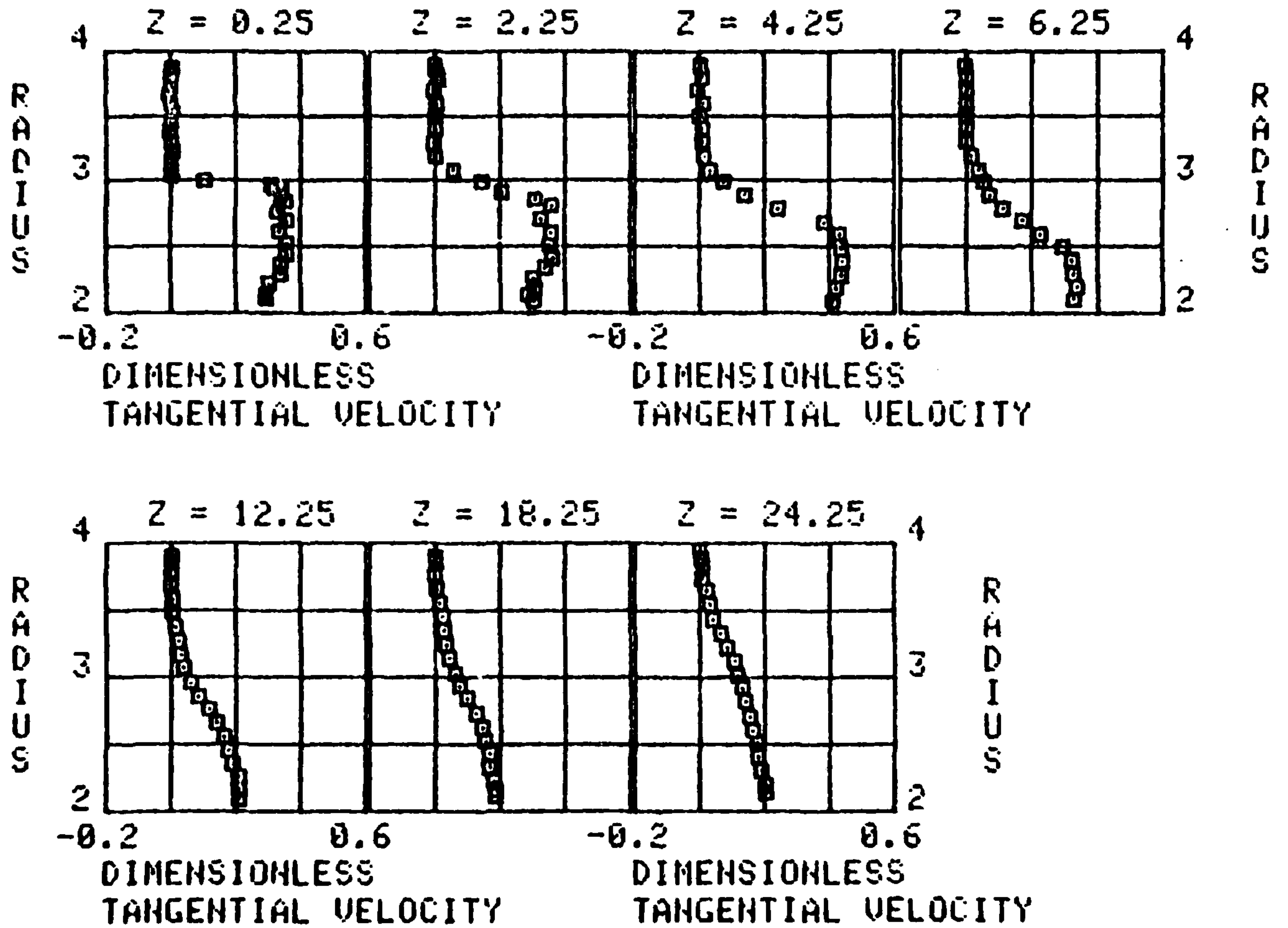

Figure A-84 Dimensionless Tangential Velocity, Test #4, Runs XX5

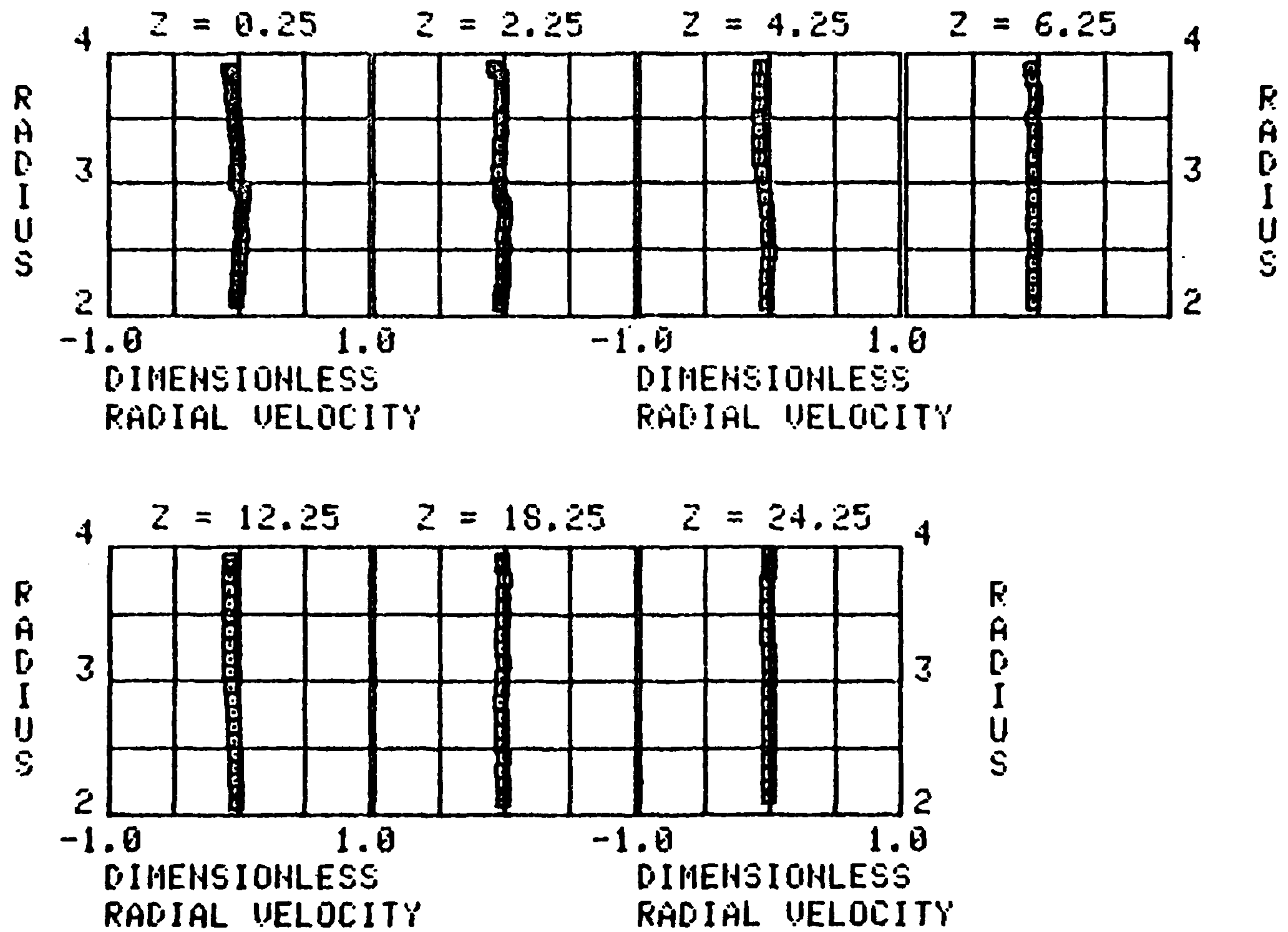

Figure A-85 Dimensionless Radial Velocity, Test #4, Runs XX5

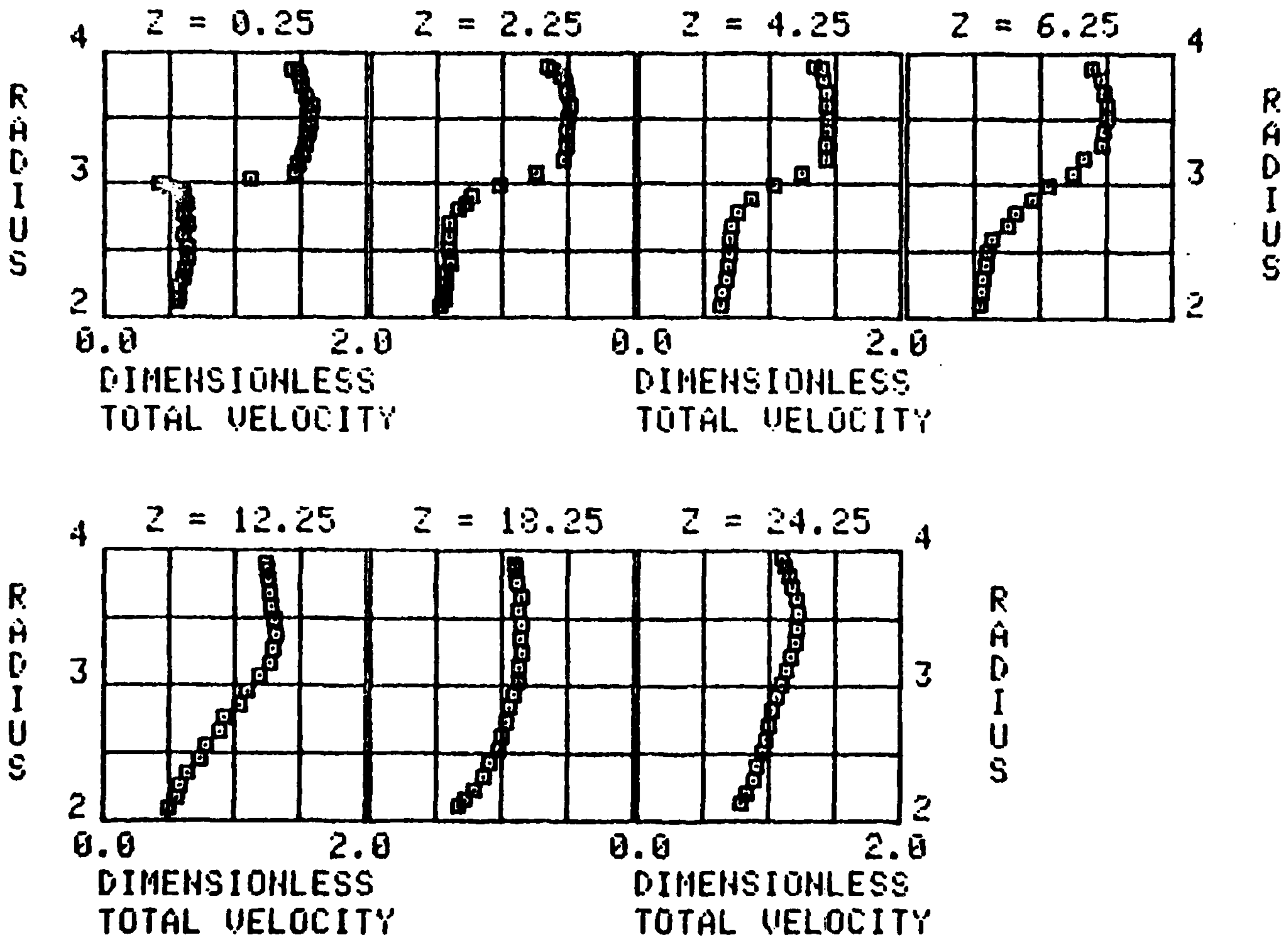

Figure A-86 Dimensionless Velocity, Test #4, Runs XX5

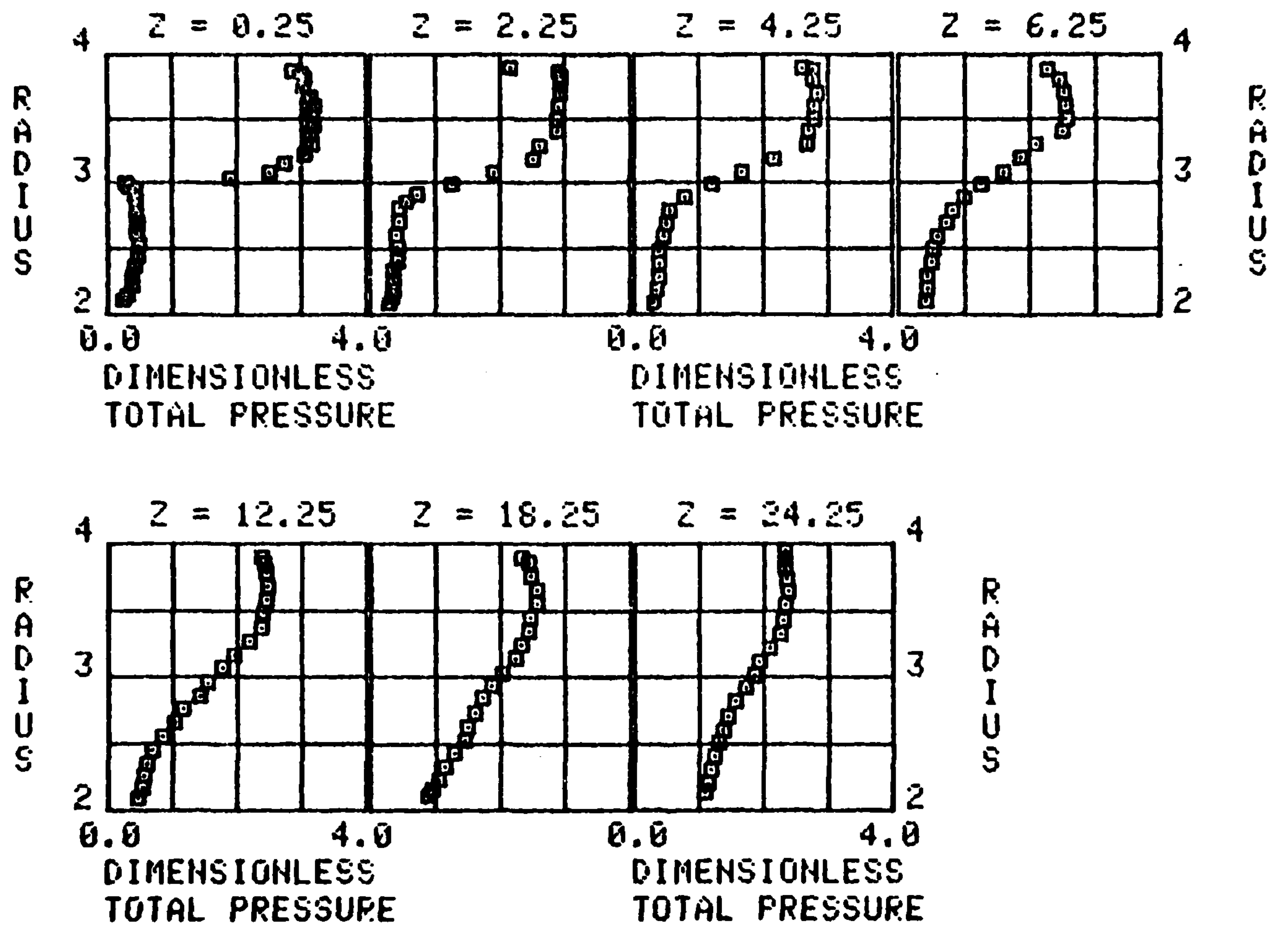

Figure A-87 Dimensionless Total Pressure, Test #4, Runs XX5

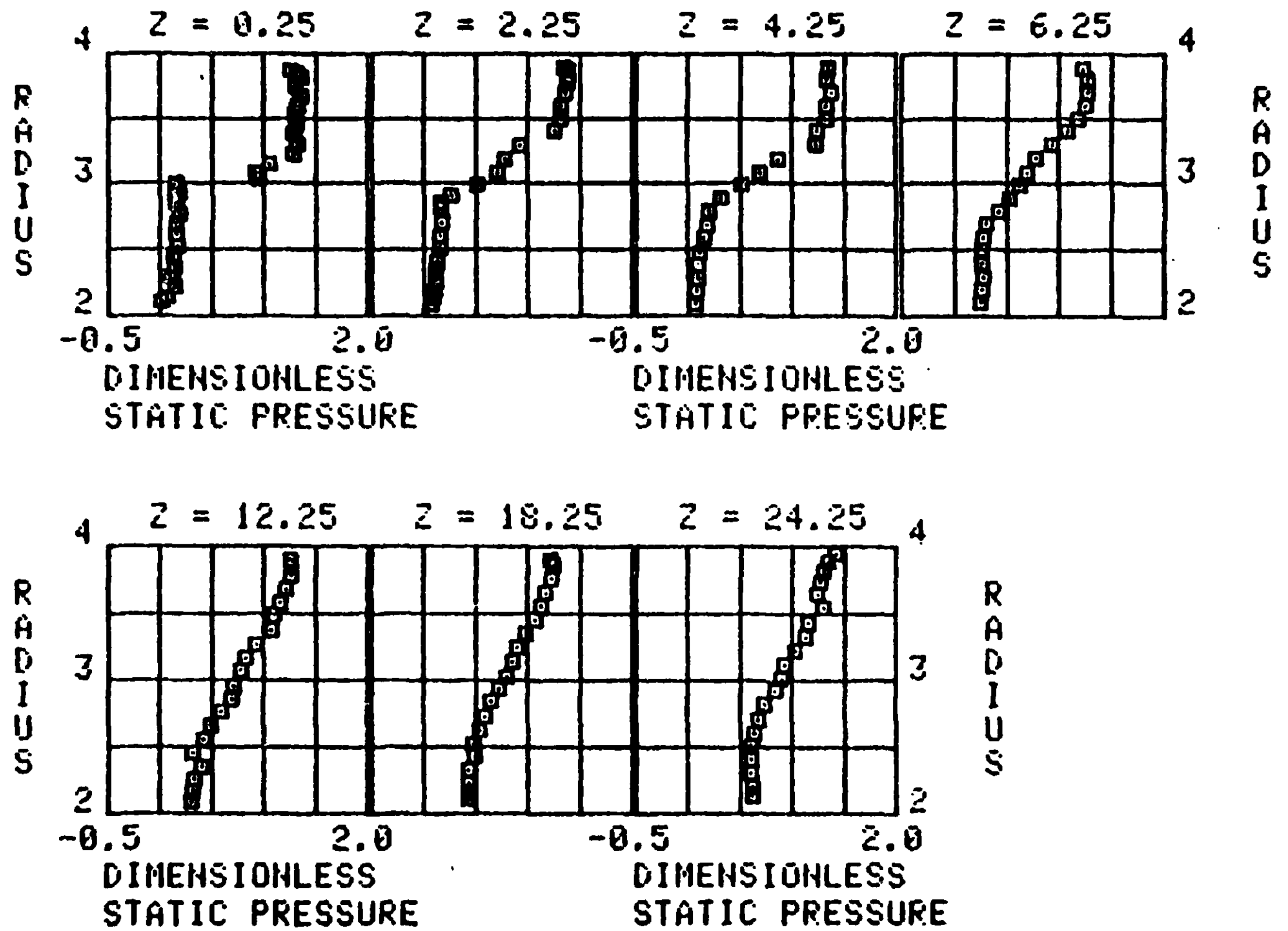

Figure A-88 Dimensionless Static Pressure, Test #4, Runs XX5

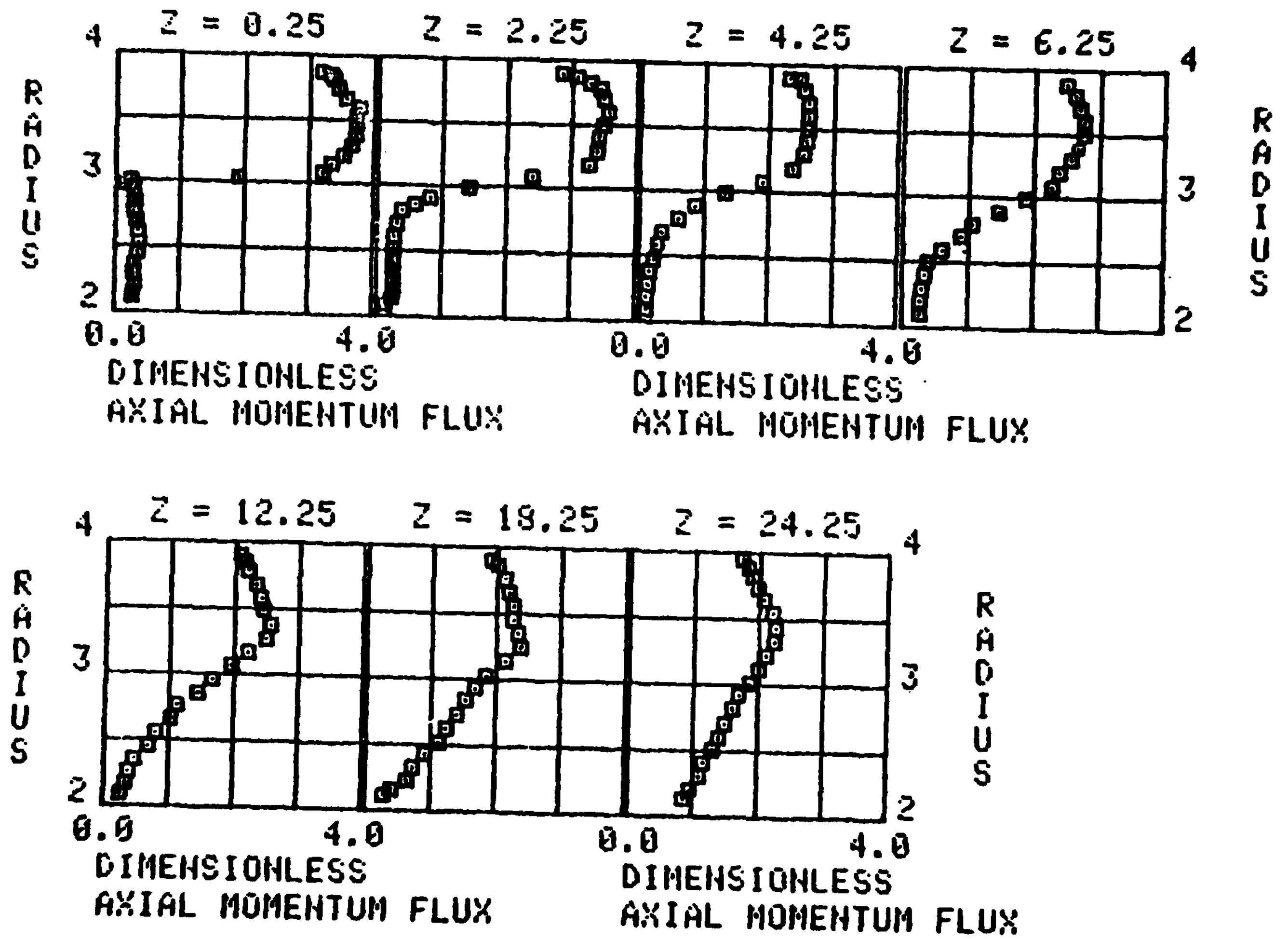

Figure A-89 Dimensionless Axial Momentum Flux,
Test #4, Runs XX5

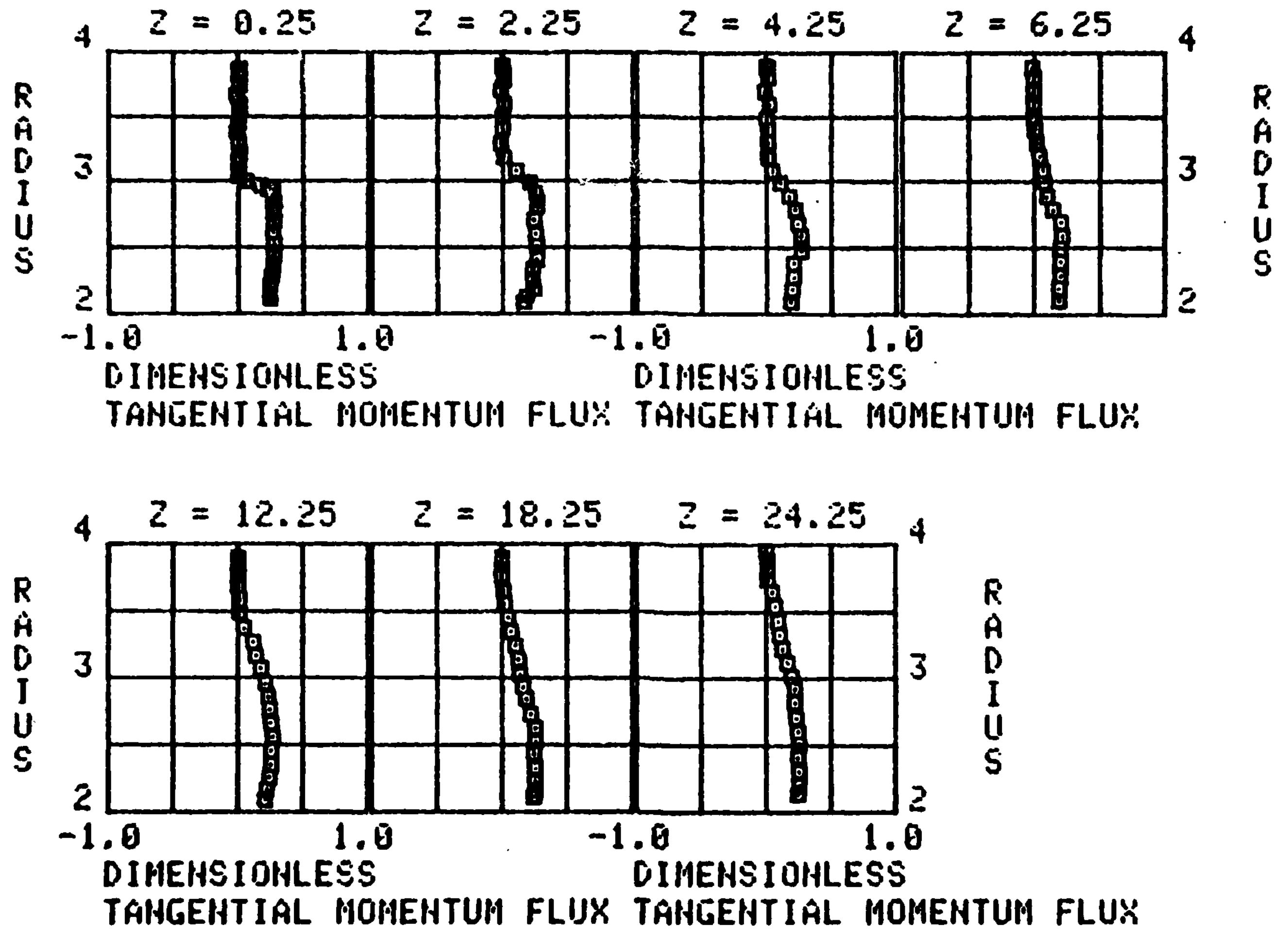

Figure A-90 Dimensionless Tangential Momentum Flux, Test #4, Runs XX5

APPENDIX B

DEVELOPMENT OF A MODEL OF IDEAL INCOMPRESSIBLE MIXER WITH SWIRL

I. INTRODUCTION

As a model of an ideal mixer with swirl, consider inviscid incompressibleone-dimensional flow in the constant area mixer shown in Figure 2-1. The outer stream (2) enters the mixer at a uniform axial velocity, w_2, and uniform total pressure, P_{T_2}. The inner stream (Ø) enters the mixer at a uniform axial velocity, w_0, and uniform total pressure, P_{T_0}. The inner stream then passes through a free vortex stator before entering the mixing region. The mixed stream (3) is assumed to have uniform axial velocity, w_3 , and an angular velocity profile corresponding to solid body rotation. The mixed stream then passes through a stator that removes this solid body rotation and the departing mixed stream (4) has uniform static pressure, P_4 , and no angular velocity. This departing stream (4) is then accelerated through a nozzle to an exit static pressure of P_e .

Each section of the model will be considered separately in order to develop the equations needed for analysis. After all sections of the ideal swirl mixer are analyzed, the equations for thrust, using an ideal constant area mixer and the thrust for unmixed flow, will be developed. Then the equations for comparing the performance of the ideal swirl mixer to the ideal constant area mixer, or to the unmixed flow thrust, will be listed in the order used for analysis.

II. UNIFORM ENTERING STREAMS

Both the inner stream (Ø) and the outer stream (2) enter the ideal mixer with uniform axial velocity and total pressure. The following equations apply to these two streams:

A) Total Pressure

$$P_{T_0} = P_0 + 1/2\ \rho_0 w_0^2 \qquad \text{(B-1)}$$

$$P_{T_2} = P_2 + 1/2\ \rho_2 w_2^2 \qquad \text{(B-2)}$$

B) Mass Flow Ratio (α)

$$\alpha = \frac{\dot{m}_2}{\dot{m}_0} = \frac{\rho_2 w_2 A_2}{\rho_0 w_0 A_0} \qquad \text{(B-3)}$$

C) Area Ratio

$$\frac{A_2}{A_0} = \frac{R_t^2 - r_t^2}{r_t^2 - r_h^2} = \frac{g^2 - f^2}{f^2 - 1} \qquad \text{(B-4)}$$

where $f = r_t / r_h$ and $g = R_t / r_h$

III. FREE VORTEX STATOR AND DEPARTING SWIRLING STREAM

For an ideal free vortex stator, the total pressure is constant on streamlines. Because the entering stream has uniform axial velocity (w_0) and uniform total pressure (P_{T_0}), the departing stream will have uniform axial velocity and uniform total pressure. Thus, the entering and departing total pressures are equal ($P_{T_1} = P_{T_0}$). Also, the entering and departing axial velocities are equal ($w_1 = w_0$) because the flow is incompressible and the area is constant. The following equations apply to the stream departing the free vortex stator:

A) Total Pressure

$$P_{T_1} = P_t + 1/2\,\rho_0 (w_0^2 + v_1^2) \qquad \text{(B-5)}$$

B) Angular Velocity and Static Pressure

$$v_1 = v_{t_1}\, r_t / r \qquad \text{(B-6)}$$

$$P_1 = P_d - 1/2\,\rho_0\, v_{t_1}^2 \,(r_t^2/r^2 - 1) \qquad \text{(B-7)}$$

where v_{t_1} is the value of v_1 at $r=r_t$

and P_d is the value of P_1 at $r=r_t$

The axial force (F_1) on the free vortex stator in the constant area annulus is determined by considering the actuator disc limit axial force on a blade row given by

Equation 45 in Reference 1 and listed below.

$$F_1 = 2\pi \left[M'\right] \tag{B-8}$$

$$\text{where } M' = \int_{r_h}^{r_t} (H - P_o/\rho + 1/2(w^2 - v^2 - u^2))\, r\, dr$$

P_o = Reference pressure

H = Stagnation enthalpy

and $[\;]$ = Change across

The axial force (F_1) on the free vortex stator using Equation B-8 and assuming radial equilibrium is given by

$$F = -\pi \rho_0 \int_{r_h}^{r_t} v_1^2\, r\, dr$$

$$\text{or } F = -\pi \rho_0\, v_{t_1}^2\, r_t^2\, \ln(f) \tag{B-9}$$

IV. MIXED STREAM

The mixed stream is assumed to have uniform axial velocity, solid body angular velocity and no radial velocity. The angular velocity and static pressure are given by

$$v_3 = v_{t_3} \ r / R_t \tag{B-10}$$

$$P_3 = P_{R_{t_3}} + 1/2 \ \rho_3 \ v_{t_3}^2 \ (r^2/R_t^2 - 1) \tag{B-11}$$

where v_{t_3} is the value of v_3 at $r=R_t$

and $P_{R_{t_3}}$ is the value of P_3 at $r=R_t$

The density of the mixed stream can be written in terms of the density of the two entering streams and the mass flow ratio (α) since the volume flow rate is constant.

$$\rho = \frac{\dot{m}_0 + \dot{m}_2}{\dot{m}_0/\rho_0 + \dot{m}_2/\rho_2} = \frac{1 + \alpha}{1 + \alpha\rho/\rho_2} \tag{B-12}$$

The axial velocity can be written in terms of the properties of the entering streams by application of the conservation of mass to the one-dimensional constant area flow.

$$\dot{m}_0 + \dot{m}_2 = (A_0 + A_2)\rho_3 w_3$$

$$\text{or} \quad w_3 = w_0 \frac{1 + \alpha\, \rho_0/\rho_2}{1 + \alpha \dfrac{\rho_0 w_0}{\rho_2 w_2}} \tag{B-13}$$

A) Axial Momentum Equation

Application of the axial momentum to the mixing region gives the following relationship which can be solved to give $P_{R_{t_3}}$ in terms of other properties

$$\int_1 P_1\, dA + \rho_0 w_0^2 A_0 + (P_2 + \rho_2 w_2^2)A_2 = \int_3 P_3\, dA + \rho_3 w_3^2 (A_0 + A_2) \tag{B-14}$$

The first integral is given by

$$\int_1 P_1\, dA = (P_d + \rho_0 v_{t_1}^2/2)\, A - \pi \rho_0 v_{t_1}^2 r_t^2 \ln(f) \tag{B-15}$$

and the second integral is given by

$$\int_3 P_3\, dA = (P_{R_{t_3}} - \rho_3 v_{t_3}^2/2)(A_0 + A_2) + \pi \rho_3 \frac{v_t^2}{R_t^2} \frac{R_t^4 - r_h^4}{4} \tag{B-16}$$

Substitution of Equations B-15 and B-16 into Equation B-14 give the following relationship for $P_{R_{t_3}}$

$$P_{R_{t_3}} = \frac{A_0}{A_0 + A_2}\left[P_{T_0} + \frac{\rho_0 w_0^2}{2} - \frac{\rho_0 v_{t_1}^2 f^2}{f^2 - 1} \ln(f)\right] + \frac{A_2}{A_0 + A_2}\left[P_{T_2} + \frac{\rho_2 w_2^2}{2}\right] - \rho_3 w_3^2$$
$$+ \rho_3 v_{t_3}^2 (1 - h^2)/4 \tag{B-17}$$

where $h = r_h / R_t = 1/g$

B) Conservation of Angular Momentum

Application of the conservation of angular momentum to the mixing region gives the following relationship which can be solved to give v_{t_3} in terms of upstream properties

$$\int_{A_0} \rho_0 w_0 v_1 \, r \, dA = \int_{A_0+A_2} \rho_3 w_3 v_3 \, r \, dA \qquad \text{(B-18)}$$

Substitution of Equations B-6 and B-1Ø into Equation B-18 and integration gives the following relationship for v_{t_3}.

$$v_{t_3} = 2 \, v_{t_1} \frac{\rho_0 \, w_0}{\rho_2 \, w_2} \; \frac{r_t \, R_t \, (r_t^2 - r_h^2)}{R_t^4 - r_h^4}$$

$$\text{or} \quad v_{t_3} = \frac{2 \, v_{t_1}}{1+\alpha} \; \frac{gf}{g^2 + 1} \qquad \text{(B-19)}$$

V. SOLID BODY ROTATION STATOR AND DEPARTING STREAM (4)

The ideal stator between stations 3 and 4 is assumed to remove all angular velocity from the mixed stream. Since the flow is assumed to be inviscid, the torque on this stator is equal to the torque on the free vortex stator but opposite in direction. Thus, the net torque on the mixer is zero. To determine the axial force on this

stator, the axial velocity profile of the departing stream (4) is required. Since the departing stream (4) has no swirl and is in radial equilibrium, the static pressure (P_4) will be uniform.

A) Properties of Departing Stream

The stream function (ψ) is defined as follows in terms of the axial velocity of the mixed stream (w_3).

$$d\Psi = - r\, w_3\, dr$$

Since w_3 is constant, the above equation integrates to give the radius in terms of the stream function.

$$r^2 = R_t^2 + 2\ (\psi_t - \psi)\ /\ w_3$$

where Ψ_t is the value of the stream function, Ψ, at $r = R_t$

Thus the angula velocity of the mixed stream, given by Equation B-10, can be written in terms of the stream function, Ψ , to give

$$v_3^2 = v_{t_3}^2 \left[1 - \frac{2}{w_3 R_t^2} (\Psi - \Psi_t) \right]$$

Now the stagnation enthalpy, H , can be written in terms of the stream function to give

$$H_3(\Psi) = K - \frac{2\ v_{t_3}^2}{w_3 R_t^2}(\Psi - \Psi_t) \qquad \text{(B-20)}$$

where K is a constant $(= \frac{P_{R_{t_3}}}{\rho_3} + \frac{w_3^2}{2} + \frac{v_{t_3}^2}{2})$

The stagnation enthalpy is constant on a streamline across the ideal stator

$$H_3(\Psi) = H_4(\Psi) \qquad \text{(B-21)}$$

and we have from Reference 2 for radial equilibrium

$$\frac{dH_3}{d\Psi} = \frac{dH_4}{d\Psi} \qquad \text{(B-22)}$$

where Equation B-22 can be evaluated for the mixed stream by using Equation B-20 to get

$$\frac{dH_3}{d\Psi} = -\frac{2\ v_{t_3}^2}{w_3 R_t^2} \qquad \text{(B-23)}$$

The axial velocity of the departing stream, w_4, is related to the stagnation enthalpy and the stream function for radial equilibrium flow with no swirl by

$$\frac{1}{r}\frac{dw_4}{dr} = -\frac{dH_4}{d\Psi} \qquad \text{(B-24)}$$

Substitution of Equation B-23 into Equation B-24 and integration gives

$$w_4 = \frac{v_{t_3}^2}{w_3} \frac{r^2}{R_t^2} + C \qquad \text{(B-25)}$$

The constant, C, in the above equation is evaluated by application of the conservation of mass between stations 3 and 4 to give the following resulting relationship for the axial velocity w_4.

$$w_4 = w_3 + 1/2 \frac{v_{t_3}^2}{w_3}\left[2 \frac{r^2}{R_t^2} - (1+h^2)\right] \qquad \text{(B-26)}$$

The value of the static pressure at the departing stream, P_4, can be determined by evaluating H_3 at $r=R_t$, H_4 at $r=R_t$ and then equating H_3 and H_4 to get

$$P_4 = P_{R_{t_3}} + 1/2\ \rho_3 (w_3^2 + v_{t_3}^2 - w_{t_4}^2) \qquad \text{(B-27)}$$

$$\text{where } w_{t_4} = w_3 + 1/2 \frac{v_{t_3}^2}{w_3} (1-h^2) \qquad \text{(B-28)}$$

B) Axial Thrust on Solid Body Rotation Stator

The axial thrust on the stator is given by Equation B-8, rewritten below with the upper limit of integration changed to R_t

$$F_2 = 2\pi\rho_3\left[M_3'\right] \qquad \text{(B-29)}$$

where

$$M_3' = \int_{r_h}^{R_t} \left\{ \left(H_4 + w_4^2/2\right) - \left(H_3 + (w_3^2 - v_3^2)/2\right) \right\} r\, dr$$

Using Equations B-1Ø, B-11, B-26, B-27 and B-28, the two terms within the integral can be written as

$$H_3 + (w_3^2 - {}_1v_3^2)/2 = P_{R_{t_3}}/\rho_3 + w_3^2 + v_{t_3}^2\ (r^2/R_t^2 - 1)$$

$$H_4 + w_4^2/2 = P_{R_{t_3}}/\rho_3 + w_3^2 + v_{t_3}^2\ (r^2/R_t^2 - 1)/2 + G$$

$$\text{where } G = \frac{v_{t_3}^2}{2}\left[\frac{3r^2}{R_t^2} - (1+h^2)\right] + \frac{v_{t_3}^4}{8w_3^2}\left[2(2\frac{r^2}{R_t^2} - 1 - h^2)^2 - (1-h^2)^2\right]$$

(B-3Ø)

Substitution of the above relationships into Equation B-29 gives

$$F_2 = 2\pi\rho_3 \int_{r_h}^{R_t} G\ r\ dr$$

Integration of the above equation for F_2 gives the following relationship

$$F_2 = \frac{\rho_3 \pi v_{t_3}^2 R_t^2\ (1-h^2)}{24}\left[6(1+h^2) - \left(\frac{v_{t_3}^2}{w_3^2}\right)(1-h^2)^2\right] \qquad \text{(B-31)}$$

IV. NOZZLE THRUST, INCOMPRESSIBLE FLOW

For ideal incompressible flow through a nozzle exhausting to a static pressure of P_e , the velocity of the exiting stream is given by

$$w_e = \left\{2\left(H_4 - P_e/\rho_3\right)\right\}^{1/2} \tag{B-32}$$

Since H_4 varies, the above equation will be applied to each streamline and the result used in calculating the nozzle thrust, F_N . The stagnation enthalpy, H_4 , can be expressed in terms of a stream function, Ψ, by defining

$$w_4 = -\frac{1}{r}\frac{d\Psi}{dr}$$

S''bstitution of Equation B-26 into the above equation and integration gives

$$\Psi - \Psi = \left[w_3 - \frac{V_{t_3}^2}{2w_3}(1+h\ )\right]\left(R_t^2/2\right)(1-r^2/R_t^2) + \frac{V_{t_3}^2 R_t^2}{4\ w_3}(1-r^4/R_t^4)$$

where Ψ_t is the value of the stream function at $r=R_t$

Solving the above equation for (r/R_t) and substituting into Equation B-26 yields

$$w_4(\psi) = w_3\left\{\left[1+\frac{v_{t_3}^2}{2w_3}(1-h^2)\right]^2 - \frac{4v_{t_3}^2}{w_3^2}\,\frac{\Psi-\Psi_t}{w_3 R_t^2}\right\}$$

Using the above equation for w_4, the stagnation enthalpy, H_4, can now be expressed in terms of the stream function as

$$H_4(\psi) = \frac{P_4}{\rho_3} + \frac{w_3^2}{2}\left\{\left[1+\frac{v_{t_3}^2}{2w_3^2}(1-h^2)\right]^2 - \frac{4v_{t_3}^2}{w_3^2}\,\frac{\Psi-\Psi_t}{w_3 R_t^2}\right\} \tag{B-33}$$

Now substituting Equation B-33 into Equation B-22 gives the nozzle exit velocity, w_e, in terms of the stream function,

$$w_e(\psi) = \left[2\,\frac{P_4-P_e}{\rho_3} + w_3^2\left\{\left[1+\frac{v_{t_3}^2}{2w_3^2}(1-h^2)\right]^2 - \frac{4v_{t_3}^2}{w_3^2}\,\frac{\Psi-\Psi_t}{w_3 R_t^2}\right\}\right]^{1/2} \tag{B-34}$$

The mass flow rate for incompressible flow can be written in terms of the stream function as

$$d\dot{m} = -\,2\pi\,\rho_3\,d\Psi \tag{B-35}$$

The nozzle thrust is equal to the momentum flux of the exiting stream

$$F_N = \int_{A_e} w_e \, d\dot{m}$$

Using Equation B-35, F_N can be written as

$$F_N = -2\pi \int_{\Psi_h}^{\Psi_t} \rho_3 \, w_e \, d\Psi \qquad \text{(B-36)}$$

Defining $\Psi_t = 0$, then $\Psi_h = w_3 R_t^2 (1-h^2)/2$

Defining a new variable $\Phi = 2\Psi v_{t_3}^2/(w_3 R_t^2)$ (B-37)

Then $\Phi = 0$, $\Phi = (1-h^2) v_{t_3}^2$ and $d\Phi = 2 v_{t_3}^2/(w_3 R_t^2) \, d\Psi$

Rewriting Equation B-34 in terms of the new variable gives

$$w_e(\Phi) = \left\{ 2\frac{P_4 - P_e}{\rho_3} + w_3^2 \left[1 + \frac{v_{t_3}^2}{2 w_3}(1-h^2) \right]^2 - 2\Phi \right\}^{1/2} \qquad \text{(B-38)}$$

Substituting Equations B-37 and B-38 into Equation B-36 yields the following equation for F_N

$$F = \sqrt{2}\, \rho_3 \pi R_t^2 (w_3/v_{t_3}^2) \int_0^{(1-h^2) v_{t_3}^2} (D - \Phi) \, d\Phi \qquad \text{(B-39)}$$

where $D = [w_e(\Phi_t)]^2/2$ (B-40)

Integration of Equation B-39 gives the following result for the nozzle thrust

$$F_N = \frac{\dot{m}_0 + \dot{m}_2}{3v_{t_3}^2(1-h^2)} \left\{ \left[w_e(\Phi_t)\right]^3 - \left[w_e(\Phi_h)\right]^3 \right\} \tag{B-41}$$

where $$w_e(\Phi_t) = \left\{ 2\frac{P_4 - P_e}{\rho_3} + w_3^2\left[1 + \frac{v_{t_3}^2}{2w_3^2}(1-h^2)\right] \right\}^{1/2} \tag{B-42}$$

and $$w_e(\Phi_h) = \left\{ 2\frac{P_4 - P_e}{\rho_3} + w_3^2\left[1 - \frac{v_{t_3}^2}{2w_3^2}(1-h^2)\right] \right\}^{1/2} \tag{B-43}$$

VII. NOZZLE THRUST, COMPRESSIBLE FLOW

For isentropic flow of a perfect gas through a nozzle exhausting to a static pressure of P_e, the velocity of the exiting stream is given by

$$w_e = 2\gamma(H_4 - P_e/\rho_e)/(\gamma-1) \tag{B-44}$$

Substituting Equation B-33 into the above equation and defining Φ by Equation B-37 we get

$$w_e(\Phi) = \sqrt{\frac{2\gamma}{\gamma-1}} \left\{ \frac{P_4}{\rho_3} - \frac{P_e}{\rho_e} + \frac{w_3^2}{2}\left[1 + \frac{v_{t_3}^2}{2w_3^2}(1-h^2)\right] - \Phi \right\}^{1/2}$$

Substituting the above equation into the thrust equation, Equation B-36, and integrating gives the following result for the thrust for compressible flow through a nozzle:

$$F = \frac{\gamma-1}{3\gamma} \frac{\dot{m}_0 + \dot{m}_2}{v_{t_3}^2(1-h^2)} \left\{ \left[w_e(\Phi_t)\right]^3 - \left[w_e(\Phi_h)\right]^3 \right\} \tag{B-45}$$

$$\text{where} \quad w_{e}(\Phi_t) = \sqrt{\frac{2\gamma}{\gamma-1}} \left\{ \frac{P_4}{\rho_3} - \frac{P_e}{\rho_e} + \frac{w_3^2}{2} \left[1 + \frac{v_{t_3}^2}{2w_3^2} (1-h^2) \right]^2 \right\}^{1/2} \quad \text{(B-46)}$$

$$\text{and} \quad w_{e}(\Phi_h) = \sqrt{\frac{2\gamma}{\gamma-1}} \left\{ \frac{P_4}{\rho_3} - \frac{P_e}{\rho_e} + \frac{w_3^2}{2} \left[1 + \frac{v_{t_3}^2}{2w_3^2} (1-h^2) \right]^2 \right\}^{1/2} \quad \text{(B-47)}$$

VIII. TOTAL THRUST FOR SWIRL MIXER WITH NOZZLE

The total thrust for the swirl mixer with nozzle, F_{SM}, is the sum of the thrust of each of the two stators and of the thrust of the nozzle.

$$F_{SM} = F_1 + F_2 + F_N \quad \text{(B-48)}$$

where F_1 is given by Equation B-9

F_2 is given by Equation B-31

F_N is given by either Equation B-41 or Equation B-45

IX. CONSTANT AREA MIXER WITH NOZZLE

The performance of constant area mixer with nozzle will be developed in this section for comparison with the performance of the swirl mixer with nozzle. The physical configuration of the constant area mixer with nozzle is the same as shown in Figure 1 without the two stators. Thus, the flow properties are unchanged from station "Ø" to station "1" and from station "3" to station "4". The Kutta condition at the splitter plate requires that the

two entering static pressures be equal ($P_0 = P_2$). Equations B-1 through B-4, B-12 and B-13 apply for this case. Using Equations B-1 and B-2 and the condition that $P_0 = P_2$ gives the following equation for the axial velocity, w_2.

$$w_2 = \left\{\left[\rho_0 w_0^2 + 2\ (P_{T_2} - P_{T_0})\right]/\rho_2\right\}^{1/2} \qquad \text{(B-49)}$$

Application of the axial momentum equation across the mixing region gives the following equation for P_{T_3}.

$$P_{T_3} = P_{T_0} - \frac{\rho_0 w_0^2}{2}\left\{\frac{(1+\alpha)\,(1+\alpha\rho_0/\rho_2)}{\left[1+\alpha\,\rho_0 w_0/(\rho_2 w_2)\right]^2} - 1\right\} - \frac{2\,\alpha\,\rho_0 w_0/(\rho_2 w_2)}{1+\alpha\,\rho_0 w_0/(\rho_2 w_2)}\,(P_{T_0} - P_{T_2}) \qquad \text{(B-50)}$$

The thrust for ideal incompressible flow through a nozzle with uniform entering conditions is given by

$$F_{ST} = (\dot{m}_0 + \dot{m}_2)\, w_0 \sqrt{\beta_3} \qquad \text{(B-51)}$$

$$\text{where } \beta_3 = w_e^2/w_0^2 = 2P_{T_3}(1 - P_e/P_{T_3})/(\rho_3 w_0^2) \qquad \text{(B-52)}$$

The thrust for ideal compressible flow through a nozzle with uniform entering conditions is given by Equation B-51 but with β_3 given by

$$\beta_3 = \frac{\gamma}{\gamma-1}\;\frac{2\,P_{T_3}}{\rho_3 w_0^2}\left[1 - \frac{P_3}{P_T}\left(\frac{P_e}{P_3}\right)^{\frac{\gamma-1}{\gamma}}\right] \qquad \text{(B-53)}$$

X. UNMIXED FLOW THRUST

The thrust for two unmixed streams flowing ideally and incompressibly through separate nozzle to the same exhaust pressure, P_e, is given by

$$F_{UM} = (\dot{m}_0 + \dot{m}_2)\, w_0 (\sqrt{\beta_1} + \alpha\sqrt{\beta_2})/(1+\alpha) \tag{B-54}$$

where $\beta_1 = 2(P_{T_0} - P_e)/(\rho_0 w_0^2)$ (B-55)

and $\beta_2 = 2(P_{T_2} - P_e)/(\rho_2 w_2^2)$ (B-56)

The thrust for two unmixed streams flowing ideally and compressibly through separate nozzles to the same exhaust pressure, P_e, is given by Eqn B-54 and

$$\beta_1 = \frac{\gamma}{\gamma-1} \; \frac{P_{T0} - (P_e)^{\frac{\gamma-1}{\gamma}} (P_{T0} - \rho_0 w_0^2/2)^{1/\gamma}}{\rho_0 w_0^2/2} \tag{B-57}$$

$$\beta_2 = \frac{\gamma}{\gamma-1} \; \frac{P_{T2} - (P_e)^{\frac{\gamma-1}{\gamma}} (P_{T2} - \rho_2 w_2^2/2)^{1/\gamma}}{\rho_2 w_0^2/2} \tag{B-58}$$

XI. WORKING EQUATIONS FOR SWIRL MIXER PERFORMANCE COMPARISON

The equations developed in the previous sections are presented in this section in a form which facilitates computer calculations. The ratio of the swirl velocity leaving the free vortex stator to the axial velocity at $r=r_t$, v_{t_1}/w_0, is an input variable that is used to vary the degre of swirl during a series of calculations to determine the swirl mixer performance over a range of swirl. This velocity ratio is defined by

$$S_{t_1} = v_t / w_0 \qquad \text{(B-59)}$$

The ratio S_t has a minimum value when P_{T_0}, P_{T_2}, ρ_0 and w_0 are defined because the modified Kutta condition, value of P_2/P_d, at the splitter plate and the velocity of stream 2, w_2, must be real. For $w_2=0$, we get from Equations B-2, B-5 and B-7 the following relationship for the minimum value of S_t

$$(S_t^2)_{min} = \frac{P_{T_0} - P_{T_2}(P_d/P_2)}{\rho_0 w_0^2/2} - 1 \qquad \text{(B-60)}$$

S_t has a minimum value of zero for values of $(S_t^2)_{min}$ less than or equal to zero.

The input variables were selected to permit comparison of mixers and are listed below. Also listed are the output variables and the equations in the order of calculation

INPUT VARIABLES: P_{T_0}, ρ_0, w_0, P_{T_2}, ρ_2, α, g, S_t, P_e/P_{T_0}, P_d/P_2, & γ

OUTPUT VARIABLES: w/w, A/A, f, w/w, v_t/w, $F_1/(\dot{m}+\dot{m})w$, $F_2/(\dot{m}+\dot{m})w$, and the thrust ratios F_{SM}/F_{ST}, F_{SMC}/F_{STC}, F_{ST}/F_{UM}, & F_{STC}/F_{UMC}

WORKING EQUATIONS

$$(S_t^2)_{min} = \frac{P_{T_0} - P_{T_2}(P_d/P_2)}{\rho_0 w_0^2/2} - 1$$

if $(S_t^2)_{min}$ is less than zero, then $S_{t_{min}} = \emptyset$

A. Swirl Mixer $\quad S_t \geq S_{t_{min}} > \emptyset$

$$P_d = P_{T_0} - \rho_0 w_0^2 (1+S_t^2)/2$$

$$P_2 = P_d/(P_d/P_2)$$

$$w_2 = \left[2(P_{T_2} - P_2)/\rho_2 \right]^{1/2}$$

$$A_2/A_0 = \alpha\rho_0 w_0/(\rho_2 w_2)$$

$$f = (g^2 + A_2/A_0)/(1 + A_2/A_0)$$

$$\rho_3/\rho = (1+\alpha)/(1+\alpha\rho_0/\rho_2)$$

$$w_3/w = (1+\alpha\rho_0/\rho_2)/(1 + A_2/A_0)$$

$$h = 1/g$$

$$v_{t_3}/v_{t_1} = 2fg/(1+\alpha)(1+h^2)$$

$$v_{t_3}/w_3 = S_t\,(v_{t_3}/v_{t_1})(w_3/w_0)$$

$$w_{t_4}/w_3 = 1 + (v_{t_3}/w_3)^2\,(1-h^2)/2$$

$$\frac{F_1}{(\dot m_0+\dot m_2)w_0} = -\,S_t^2\,\frac{f^2\,\ln(f)}{(1+\alpha)(f^2-1)}$$

$$\frac{F_2}{(\dot m_0+\dot m_2)w_0} = \frac{w_3}{w_0}\left(\frac{v_{t_3}}{w_3}\right)^2\frac{1}{24}\left[6(1+h^2) - \left(\frac{v_{t_3}}{w_3}\right)^2(1-h^2)^2\right]$$

$$P_4 = \frac{\rho_3\,w_3^2/2}{(1+\alpha)(w_3/w_0)}\left\{\left(\frac{2P_{T_0}}{\rho_0 w_0^2} + 1 + \frac{2(1+\alpha)\,F_1}{(\dot m_0+\dot m_2)w_0}\right) + \alpha\frac{w_2}{w_0}\left(\frac{P_{T_2}}{\rho_2 w_2^2/2} + 1\right)\right\}$$
$$+\,(\rho_3\,w_3^2/2)\left\{(v_{t_3}/w_3)^2(3-h^2)/2 - 1 - (w_{t_4}/w_3)^2\right\}$$

1. Nozzle with Incompressible Flow

$$w_{e_t} = \left\{\frac{2(P_4 - P_e)}{\rho_3} + w_3^2\left(1 + \frac{v_{t_3}^2}{2w_3^2}(1-h^2)\right)^2\right\}^{1/2}$$

$$w_{e_h} = \left\{\frac{2(P_4 - P_e)}{\rho_3} + w_3^2\left(1 - \frac{v_{t_3}^2}{2w_3^2}(1-h^2)\right)^2\right\}^{1/2}$$

$$\frac{F_N}{(\dot m_0+\dot m_2)w_0} = \frac{w_{e_t}^3 - w_{e_h}^3}{3w_0\,v_{t_3}^2\,(1-h^2)}$$

$$\frac{F_{SM}}{(\dot m_0+\dot m_2)w_0} = \frac{F_1 + F_2 + F_N}{(\dot m_0+\dot m_2)w_0}$$

2. Nozzle with Compressible Flow

$$w_{e_t} = \left[\frac{\gamma}{\gamma-1} \left\{ \frac{2P_4}{\rho_3} \left[1 - \left(\frac{P_e}{P_4} \right)^{\frac{\gamma-1}{\gamma}} \right] + w_3^2 \left[1 + \frac{V_{t_3}^2}{2w_3^2} (1-h^2) \right]^2 \right\} \right]^{1/2}$$

$$w_{e_h} = \left[\frac{\gamma}{\gamma-1} \left\{ \frac{2P_4}{\rho_3} \left[1 - \left(\frac{P_e}{P_4} \right)^{\frac{\gamma-1}{\gamma}} \right] + w_3^2 \left[1 - \frac{V_{t_3}^2}{2w_3^2} (1-h^2) \right]^2 \right\} \right]^{1/2}$$

$$\frac{F_N}{(\dot{m}_0 + \dot{m}_2) w_0} = \frac{\gamma - 1}{3} \frac{w_{e_t}^3 - w_{e_h}^3}{w_0 V_{t_3}^2 (1-h^2)}$$

$$\frac{F_{SMC}}{(\dot{m}_0 + \dot{m}_2) w_0} = \frac{F_1 + F_2 + F_N}{(\dot{m}_0 + \dot{m}_2) w_0}$$

B. Constant Area Mixer ($S_t = \emptyset$)

$$P_2 = P_d$$

$$w_2 = \left[2 (P_{T_2} - P_{T_0} + \rho_0 w_0^2/2)/\rho_2 \right]^{1/2}$$

$$P_{T_3} = P_{T_0} - \frac{\rho_0 w_0^2}{2} \left[\frac{(1+\alpha)(1+\alpha\rho_0/\rho_2)}{(1+\alpha\rho_0 w_0/(\rho_2 w_2))^2} - 1 \right]$$

$$- \frac{2\alpha\rho_0 w_0/(\rho_2 w_2)}{1 + \alpha\rho_0 w_0/(\rho_2 w_2)} (P_{T_0} - P_{T_2})$$

1. Nozzle with Incompressible Flow

$$\frac{F_{ST}}{(\dot{m}_0 + \dot{m}_2) w_0} = \left(\frac{P_{T_3} - P_e}{\rho_3 w_0^2/2} \right)^{1/2}$$

2. Nozzle with Compressible Flow

$$\beta_3 = \frac{\gamma}{\gamma-1}\left(P_{T_3} - (P_e)^{\frac{\gamma-1}{\gamma}}(P_{T_3} - \rho_3 w_3^2/2)^{1/\gamma}\right)/(\rho_3 w_0^2/2)$$

$$\frac{F_{STC}}{(\dot{m}_0 + \dot{m}_2)\,w_0} = \sqrt{\beta_3}$$

C. Unmixed Flow Thrust ($S_t = \emptyset$)

1. Nozzle with Incompressible Flow

$$\frac{F_{UM}}{(\dot{m}_0 + \dot{m}_2)\,w_0} = \frac{1}{1+\alpha}\left\{\sqrt{\frac{P_{T_0} - P_e}{\rho_0 w_0^2/2}} + \alpha\sqrt{\frac{P_{T_2} - P_e}{\rho_2 w_2^2/2}}\right\}$$

2. Nozzle with Compressible Flow

$$\beta_1 = \frac{\gamma}{\gamma-1}\left[P_{T_0} - (P_e)^{\frac{\gamma-1}{\gamma}}(P_{T_0} - \rho_0 w_0^2/2)^{1/\gamma}\right]/(\rho_0 w_0^2/2)$$

$$\beta_2 = \frac{\gamma}{\gamma-1}\left[P_{T_2} - (P_e)^{\frac{\gamma-1}{\gamma}}(P_{T_2} - \rho_2 w_2^2/2)^{1/\gamma}\right]/(\rho_2 w_0^2/2)$$

$$\frac{F_{UMC}}{(\dot{m}_0 + \dot{m}_2)\,w_0} = \frac{\sqrt{\beta_1} + \alpha\sqrt{\beta_2}}{1 + \alpha}$$

REFERENCES

1. Oates, G.C., and Knight, C.J., "Throughflow Theory for Turbomachines", USAF Aero Propulsion Laboratory Technical Report, AFAPL-TR-75-61.

2. Oates, G.C., Editor, "The Aerothermodynamics of Aircraft Gas Turbine Engines", USAF Aero Propulsion Laboratory Technical Report, AFAPL-TR-78-52.

APPENDIX C

CONSTANT AREA MIXER WITH SWIRL COMPUTER PROGRAM - "SWIRL"

This appendix contains a listing of the computer program SWIRL. This program uses the equations developed in Appendix B and listed at the end of that appendix. Table C-1 contains a list of the variables used in program SWIRL.

TABLE C-1

Variables Used in Program SWIRL

A) INPUT VARIABLES (listed in the order used)

NDR	- Number of density ratios for this run
RHOZ	- Density of stream "Ø"
PTZ	- Total pressure of stream "Ø"
DRZ2	- Ratio of the density of stream "Ø" to the density of stream "2"
RTHR	- Over ll tip to hub ratio of mixer
SM	- Maximum tip swirl ratio
PREZ	- Ratio of static pressure of exhaust stream to the total pressure of steam "Ø"
SPRD2	- Ratio of the static pressure at point "d" to the static pressure in stream "2"
GAM	- Ratio of specific heats
NW	- Number of axial velocities, W, of stream "Ø"
NAL	- Number of mass flow ratios, AL
NP	- Number of total pressure ratios, P
W	- Axial velocity of stream "Ø"
AL	- Ratio of the mass flow rate of steam "2" to the mass flow rate of stream "Ø".
P	- Ratio of the total pressure of stream "Ø" to the total pressure of stream "2"

B) OUTPUT VARIABLES (listed in the output order)

PT2	- Total pressure of stream "2"
RHO2	- Density of stream "2"

1) CONSTANT AREA MIXER WITHOUT SWIRL

PDP	- Static pressure at point "d"
P2P	- Static pressure of stream "2"
W2P	- Axial velocity of stream "2"
A2Az	- Ratio of cross-sectional area of stream "2" to that of stream "Ø"
W3	- Axial velocity of mixed stream
F	- Tip to hub ratio of inner annulus
FUM	- Thrust of unmixed flow with incompressible flow through the nozzles
FUMC	- Thrust of unmixed flow with isentropic flow through the nozzles
PT3P	- Total pressure of the mixed stream
PTAM	- Mass average total pressure of the two incoming streams
RD2	- Location of dividing streamline at the entrance to the mixer

RD3 - Location of dividing streamline at the exit of the mixer

FSTUM - Ratio of the thrust of mixed flow with incompressible flow through the nozzle to the thrust of unmixed flow, FUM

FSTUMC- Ratio of the thrust of mixed flow with isentropic flow through the nozzle to the thrust of unmixed flow, FUMC

2) CONSTANT AREA MIXER WITH SWIRL (values of the following for each iteration of S)

S - Tip swirl ratio leaving stator "1"

VT3W3 - Tip swirl ratio of mixed stream at "3"

W2WZ - Ratio of the axial velocity of stream "2" to that of stream "Ø"

W3WZ - Ratio of the axial velocity of stream "3" to that of stream "Ø"

A2AZ - Ratio of the cross-sectional area of stream "2" to that of stream "Ø"

F - Tip to hub ratio of inner annulus

F1 - Thrust on stator-1

F2 - Thrust on stator-2

FN - Incombressible nozzle thrust

FNC - Isentropic nozzle thrust

FSWFST - Ratio of the thrust of swirl mixed flow with incompressible flow through the nozzle to that of mixed flow without swirl

FSWSTC - Ratio of the thrust of swirl mixed flow with isentropic flow through the nozzle to that of mixed flow without swirl

FSW - Thrust of swirl mixer with incompressible flow through the nozzle

FUM - Thrust of unmixed flow with incompressible flow through the nozzles

FSWUM - Ratio of the thrust of swirl mixed flow with incompressible flow through the nozzle to that of unmixed flow

FSWUMC - Ratio of the thrust of swirl mixed flow with isentropic flow through the nozzle to that of unmixed flow

SW - Swirl number

```
      PROGRAM SWIRL(INPUT,OUTPUT,TAPE5=INPUT,TAPE6=OUTPUT)
      DIMENSION IMAGE(2501),POINT(10)
      DIMENSION AL(10),W(10),P(10),M(10)
      DATA POINT/ 1H0,1H1,1H2,1H3,1H4,1H5,1H6,1H7,1H8,1H9/
C     READ INPUT DATA
      READ(5,20)NDR
      DO 12 ND=1,NDR
      READ(5,10) RHOZ,PTZ,DRZ2,KTHR,SM,PREZ,SPRD2,GAM
      READ(5,20) NW,NAL,NP
      READ(5,30)(W(I),I=1,NW)
      READ(5,40)(AL(I),I=1,NAL)
      READ(5,40)(P(I),I=1,NP)
      H=1.0/KTHR
      DO 1 I=1,NW
      WZ=W(I)
      DO 2 J=1,NAL
      ALPHA=AL(J)
      CALL PLOT1(0,20,5,10,10)
      CALL PLOT2(IMAGE,1.0,0.0,1.0,0.98)
      DO 3 K=1,NP
      TPRZ2=P(K)
      L=0
      M(K)=0
C     CALCULATE BASIC PROPERTIES
      PT2=PTZ/TPRZ2
      PE=PT2*PREZ
      RHO2=RHOZ/DRZ2
      RHO3=RHOZ*(1.0+ALPHA)/(1.0+ALPHA*DRZ2)
      DUMB=0.5*RHOZ*WZ*WZ
      SMINS=((PTZ-PT2*SPRD2)/DUMB-1.0)
      IF(SMINS.GT.0.0) GO TO 5
      PDP=PT2-0.5*RHOZ*WZ*WZ
      P2P=PDP/SPRD2
      IF((P2P.GT.PT2).OR.(PE.GT.PT2)) GO TO 5
```

```
      W2P=(2.0*(PT2-P2P)/RHO2)**0.5
C     CALCULATE UNMIXED INCOMPRESSIBLE THRUST
      FUM=(((PTZ-PE)/(0.5*RHOZ*WZ*WZ))**0.5+ALPHA*((PT2-PE)/(0.5*RHO2*
     *WZ*WZ))**0.5)/(1.0+ALPHA)
      DUMA=RHOZ*WZ*ALPHA/(RHO2*W2P)
      PT3P=PTZ-0.5*RHOZ*WZ*WZ*((1.0+ALPHA)*(1.0+ALPHA*RHOZ/RHO2)/(1.0+
     *DUMA)**2.0-1.0)-2.0*DUMA*(PTZ-PT2)/(1.0+DUMA)
      A2AZ=DUMA
      PTAM=PT2*(TPRZ2+ALPHA)/(1.0+ALPHA)
      IF(PE.GT.PT3P) GO TO 5
C     CALCULATE STRAIGHT MIXER INCOMPRESSIBLE THRUST
      FSM=(2.0*(PT3P-PE)/(RHO3*WZ*WZ))**0.5
      F=((RTHR*RTHR+A2AZ)/(1.0+A2AZ))**0.5
      RD2=H*F
      W3=WZ*(1.0+ALPHA*DRZ2)/(1.0+A2AZ)
      W2WZ=W2P/WZ
      RD3=1.0-(ALPHA+W2WZ/RHOZ)*(1.0-H*H*F*F)/(1.0+ALPHA)
      RD3=SQRT(RD3)
      P3P=PT3P-0.5*RHO3*W3*W3
      GAMR=(GAM-1.0)/GAM
      PZ=PTZ-DUMB
      BETA1=(PTZ -(PE**GAMR)*(PZ **(1.0/GAM)))/(GAMR*DUMB)
      BETA2=(PT2 -(PE**GAMR)*(P2P**(1.0/GAM)))/(GAMR*DUMB)
      BETA3=(PT3P-(PE**GAMR)*(P3P**(1.0/GAM)))/(GAMR*DUMB)
      IF((BETA1.LT.0.0).OR.(BETA2.LT.0.0).OR.(BETA3.LT.0.0)) GO TO 5
C     CALCULATE UNMIXED AND STRAIGHT MIXER COMPRESSIBLE THRUSTS
      FUMC=(SQRT(BETA1)+ALPHA*SQRT(BETA2))/(1.0+ALPHA)
      FSMC=SQRT(BETA3)
      FSTUM=FSM/FUM
      FSTUMC=FSMC/FUMC
      GO TO 7
C     CALCULATE MAX SWIRL AND MIN SWIRL NUMBERS
    5 CONTINUE
      M(K)=1
```

```
      FSM=1.0
      FSMC=1.0
    7 SMAX=(PTZ/DUMB-1.0)**0.5
      WRITE(6,50)
      WRITE(6,100) PTZ,RHOZ,WZ,ALPHA,PT2,RHO2,SPRD2,PREZ,RTHR,GAM
      IF(M(K).EQ.1) GO TO 11
      WRITE(6,105) PDP,P2P,W2P,A2AZ,W3,F,FUM,FUMC,PT3P,PTAM,RD2,RD3
      WRITE(6,110) FSTUM,FSTUMC
   11 WRITE(6,115)
      SD=0.025
      IF(SMINS.LE.6.25E-4) SMIN=SD
      IF(SMINS.GT.6.25E-4) SMIN=SQRT(SMINS)
      IF(SMAX.GT.SM) SMAX=SM
      IMAX=100.0*SMAX
      IMIN=100.0*SMIN+0.99
      SMAX=0.01*IMAX
      SMIN=0.01*IMIN
      S=SMIN
C     CALCULATE PROPERTIES OF INCOMPRESSIBLE MIXED FLOW WITH SWIRL
      AC=1.0-2.0*F*F*ALOG(F)/(F*F-1.0)
      SW=S/(1.0+0.5*S*S*AC)
    4 L=L+1
      PD=PTZ-DUMB*(1.0+S*S)
      P2=PD/SPRD2
      W2=(2.0*(PT2-P2)/RHO2)**0.5
      W2WZ=W2/WZ
      A2AZ=RHOZ*WZ*ALPHA/(RHO2*W2)
      F=((RTHR*RTHR+A2AZ)/(1.0+A2AZ))**0.5
      W3WZ=(1.0+ALPHA*DRZ2)/(1.0+A2AZ)
      W3=WZ*W3WZ
      VT31=2.0*F/((1.0+ALPHA)*(RTHR+H))
      VT3W3=VT31*S/W3WZ
      WT4W3=1.0+0.5*VT3W3*VT3W3*(1.0-H*H)
C     CALCULATE THRUST ON STATORS
```

```
      F1=-(S*S*F*F/((1.0+ALPHA)*(F*F-1.0)))*ALOG(F)
      F2=W3WZ*VT3W3*(6.0*(1.0+H*H)-VT3W3*VT3W3*(1.0-H*H)**2.0)/24.0
      F2=F2*VT3W3
C     CALCULATE NOZZLE THRUST FOR BOTH INCOMPRESSIBLE FLOW AND
C     COMPRESSIBLE FLOW
      A=PTZ/DUMB+1.0+2.0*(1.0+ALPHA)*F1+ALPHA*W2WZ*(2.0*PT2/(RHO2*W2*
     *W2)+1.0)
      PRT3=0.5*RHO3*W3*W3*(A/((1.0+ALPHA)*W3WZ)-(2.0-0.5*VT3W3*VT3W3*(
     *1-H*H)))
      P4=PRT3+0.5*RHO3*W3*W3*(1.0+VT3W3*VT3W3-WT4W3*WT4W3)
      WETS=2.0*(P4-PE)/RHO3+W3*W3*(1.0+0.5*VT3W3*VT3W3*(1.0-H*H))**2.0
      WEHS=2.0*(P4-PE)/RHO3+W3*W3*(1.0-0.5*VT3W3*VT3W3*(1.0-H*H))**2.0
      FN=(WETS**1.5-WEHS**1.5)/(3.0*WZ*W3*W3*VT3W3*VT3W3*(1.0-H*H))
      WETCS=((2.0*P4/RHO3)*(1.0-(PE/P4)**GAMR)+W3*W3*(1.0+0.5*VT3W3*
     *VT3W3*(1.0-H*H))**2.0)/GAMR
      WEHCS=((2.0*P4/RHO3)*(1.0-(PE/P4)**GAMR)+W3*W3*(1.0-0.5*VT3W3*
     *VT3W3*(1.0-H*H))**2.0)/GAMR
      FNC=(WETCS**1.5-WEHCS**1.5)*GAMR/(3.0*WZ*W3*W3*VT3W3*VT3W3*(1.0-
     *H*H))
C     CALCULATE THRUST OF SWIRL MIXER WITH NOZZLE AND THE
C     THRUST RATIOS
      FSW=F1+F2+FN
      FSWFST=FSW/FSM
      FSWC=F1+F2+FNC
      FSWSTC=FSWC/FSMC
      FSWUM=FSW/FUM
      FSWUMC=FSWC/FUMC
      IF(M(K).EQ.1) GO TO 6
C     WRITE OUT RESULTS FOR THIS SWIRL NUMBER
      WRITE(6,120)L,S,VT3W3,W2WZ,W3WZ,A2AZ,F,F1,F2,FN,FNC,FSWFST,FSWSTC,
     *FSW,FUM,FSWUM,FSWUMC,SW
      CALL PLOT3(POINT(K),SW,FSWFST,1)
C     INCREMENT SWIRL RATIO
    6 S=S+SD
```

```
      AC=1.0-2.0*F*F*ALOG(F)/(F*F-1.0)
      SW=S/(1.0+0.5*S*S*AC)
      IF(L.GT.60) GO TO 25
      IF(S.LE.SMAX) GO TO 4
    3 CONTINUE
      DO 8 K=1,NP
      IF(M(K).EQ.0.0) GO TO 9
    8 CONTINUE
      GO TO 2
C     PLOT OUT RESULTS ON PRINTER
    9 WRITE(6,50)
      CALL PLOT4(39,39H THRUST RATIO - SWIRL TO STRAIGHT MIXER)
      WRITE(6,126)
      WRITE(6,127)((POINT(K),P(K)),K=1,NP)
    2 CONTINUE
    1 CONTINUE
   12 CONTINUE
      WRITE(6,50)
   10 FORMAT(F6.4,F8.1,6F6.4)
   20 FORMAT(3I4)
   30 FORMAT(10F6.2)
   40 FORMAT(10F6.4)
   50 FORMAT(1H1)
  100 FORMAT(1X,'INPUT DATA', /,1X,'PTZ = ',F8.1,' PA',3X,'RHOZ = ',F5.2
     *,' KG/M3',3X,'WZ = ',F5.2,' M/S',3X,'ALPHA = ',F6.4,/,1X,'PT2 = ',
     *F8.1,' PA',3X,'RHO2 = ',F5.2,' KG/M3',3X,'SPRD2 = ',F6.4,4X,
     *'PREZ = ',F6.4,/,1X,'TIP TO HUB RATIO = ',F6.4,5X,'GAMMA = ',
     *F6.4,//,1X,'ZERO SWIRL')
  105 FORMAT( 1X,'PDP = ',F8.1,' PA',3X,'P2P = ',F8.1,' PA',3X,'W2P =',
     *F6.2,' M/S',4X,'A2AZ =' ,F7.4,/,2X,'W3 = ',F6.2,' M/S',6X,'F = ',
     *F6.4,8X,'FUM = ',F6.4,7X,'FUMC =',F7.4,/,1X,'PT3P= ',F8.1,' PA',
     *3X,'PTAM= ',F8.1,' PA',3X,'RD2 = ',F6.4,7X,'RD3  = ',F6.4,/)
  110 FORMAT(1X,'THRUST RATIO - MIXED TO UNMIXED',/,1X,'INCOMPRESSIBLE '
     *,'NOZZLE FLOW = ',F6.4,/,3X,'COMPRESSIBLE NOZZLE FLOW = ',F6.4,//
```

```
     *,1X,17(3H***),' SWIRL - MIXER ', 18(3H***) )
 115 FORMAT(78X,'THRUST RATIOS',/,5X,2('SWIRL '),'VELOCITY RATIO',14X,
     *'STATOR THRUST',4X,'NOZZLE THRUST',1X,'SWIRL TO STRAIGHT',/,3X,
     *'N',3X,'U',5X,'3',5X,'2/2',5X,'3/2',2X,'A2A2',5X,'F',5X,'1',7X,'3'
     *,5X,2('INCOMPR  COMPR',1X),1X,'FSW',4X,'FUM',1X,'FSWUM',1X,
     *'FSWUMC',2X,'SW',/)
 120 FORMAT(1X,I3,2F6.3,2F7.4,F6.4,F7.4,F7.4,F8.4,1X,2F8.4,1X,2F7.4,
     *2F7.3,2F6.4,F7.4)
 126 FORMAT(1H0,40X,'SWIRL NUMBER - S',//)
 127 FORMAT(10X,'KEY TO DATA POINTS: ',10(2X,A1,' = TPRZ2 OF ',F10.8,
     */,30X))
  25 CONTINUE
     STOP
     END
```

APPENDIX D

INITIAL DATA REDUCTION PROGRAM - "REDUCE"

This appendix contains a listing of the computer program REDUCE as described in Chapter 6. Table D-1 is a list of the variables used in the program REDUCE, Table D-2 is a partial listing of a RAW data file, and Table D-3 is a partial listing of a FINE data file.

TABLE D-1

Variables Used in Program REDUCE

A) INPUT VARIABLES (listed in the order used)

NSRUNS - Number of subruns within this run
(the following is input for each subrun)
NSUB - Subrun number
NSCANS - Number of data scans for this subrun
(the following is input for each scan "K")
NHR - Hour of scan
NMIN - Minute of scan
NSEC - Second of scan
DATA(1) - Scanivalve position from controller voltage staircase
DATA(2) - Alpha, voltage corresponding to the angle of the probe
DATA(3) - Voltage from supply line pressure transducer
DATA(4) - Voltage from supply tank pressure transducer
DATA(5) - Voltage from LVDT, radial position of probe head
DATA(6) - Temperature of inside plenum (C)
DATA(7) - Temperature of outside plenum (C)
DATA(8) - Voltage from P(1) pressure transducer
DATA(9) - Voltage from P(2) pressure transducer
DATA(10) - Voltage from P(3) pressure transducer
DATA(11) - Voltage from P(4) pressure transducer
DATA(12) - Voltage from P(5) pressure transducer
DATA(13) - Voltage from P(1)-P(3) pressure transducer
DATA(14) - Voltage from outside flow orifice plate differential pressure transducer
DATA(15) - Voltage from inside flow orifice plate differential pressure transducer
VPRESA(K) - Voltage of Scanivalve pressure transducer A
VPRESB(K) - Voltage of Scanivalve pressure transducer B

B) OUTPUT VARIABLES (listed in the order used)

L - Subrun number
MHR - Hour of subrun
MMIN - Minute of subrun
VPRESA(1) through VPRESA(49) - Input value less the transducer zero value
VPRESB(1) through VPRESB(49) - Input value less the transducer zero value
DATA(2) through DATA(15) - Average of scan #6 through scan #45 (transducer zero has been subtracted for DATA(8) through DATA(15))

```
      PROGRAM REDUCF(DATAIN,DOUT1,OUTPUT,TAPE1=DATAIN,
     *TAPE2=DOUT1,TAPE6=OUTPUT)
C
C*****************************************************************
C
C     DATA(1) = SCANIVALVE POSITION FROM CONTROLLER
C     DATA(2) = ALPHA, ANGLE OF THE PROBE
C     DATA(3) = PRESSURE OF THE SUPPLY LINE
C     DATA(4) =    "      "   "     "   TANK
C     DATA(5) = RADIAL POSITION OF PROBE HEAD
C     DATA(6) = TEMPERATURE OF INSIDE PLENUM
C     DATA(7) =       "      "  OUTSIDE   "
C     DATA(8) = P(1)
C     DATA(9) = P(2)
C     DATA(10)= P(3)
C     DATA(11)= P(4)
C     DATA(12)= P(5)
C     DATA(13)= P(1)-P(3)
C     DATA(14)= FLOW METER PRESSURE DROP - OUTSIDE FLOW
C     DATA(15)=  "     "       "      "     INSIDE   "
C     VPRESA  = VOLTAGE FROM SCANIVALVE TRANSDUCER A
C     VPRESB  = VOLTAGE FROM SCANIVALVE TRANSDUCER B
C
C*****************************************************************
C
      DIMENSION DATA(15),VPRESA(52),VPRESB(52)
      DIMENSION X(10),VPO(4),ZP(6),N(4)
      DIMENSION D(52,17),Z(52,17),TIME(52)
C     IF NWRITE = 0, THERE IS NO PRINTED OUTPUT
      NWRITE=0
C     READ FIRST FOUR LINES ON OUTPUT FILE SO THAT OUTPUT DATA
C     WILL BE ADDED AT THE END OF THESE FOUR LINES
      READ(2,100) N(1),N(2),(X(I),I=1,6)
      READ(2,101) N(3),(X(I),I=7,10),N(4)
```

```
      READ(2,102) (VP)(I),I=1,4)
      READ(2,103) (ZP(I),I=1,6)
C
C*************************************************************
C
C     READ INPUT DATA FILE
C
      READ(1,10,ERR=11,END=90) NSRUNS
      GO TO 13
   11 WRITE(6,12)
   12 FORMAT(//,1X,27HERROR ON FIRST LINE OF DATA,//)
      GO TO 90
   13 CONTINUE
      DO 1 L=1,NSRUNS
      READ(1,5,ERR=14,END=90) NSUB,NSCANS
      IF(NSUB.LT.1) NSUB=1
      IF(NSCANS.LT.34) NSCANS=49
      GO TO 17
   14 WRITE(6,16)L
   16 FORMAT(//,1X,30HERROR ON FIRST LINE OF SUBRUN ,I3,//)
      NSUB=0
      NSCANS=49
   17 IF(NWRITE.NE.0) WRITE(6,15)L,NSUB
      DO 2 K=1,NSCANS
      READ(1,20,ERR=18,END=90) NHR,NMIN,NSEC
      GO TO 19
   18 NHR=0
      NMIN=0
      NSEC=0
   19 READ(1,30,ERR=21,END=90)(DATA(I),I=2,5),DATA(1)
      GO TO 23
   21 WRITE(6,22)K,L
   22 FORMAT(//,1X,29HERROR ON SECOND LINE OF SCAN ,I3,11H IN SUBRUN ,I3
     *,//)
```

```
      DATA(1)=0.0
      DATA(2)=0.0
      DATA(3)=0.0
      DATA(4)=0.0
      DATA(5)=0.0
   23 READ(1,40,ERR=24,END=90)DATA(6),DATA(7),VPRESA(K),VPRESB(K),
     *DATA(8)
      GO TO 26
   24 WRITE(6,25)K,L
   25 FORMAT(//,1X,28HERROR ON THIRD LINE OF SCAN ,I3,11H IN SUBRUN ,I3,
     *//)
      VPRESA(K)=0.0
      VPRESB(K)=0.0
      DATA(6)=0.0
      DATA(7)=0.0
      DATA(8)=0.0
   26 READ(1,41,ERR=27,END=90)(DATA(I),I=9,13)
      GO TO 29
   27 WRITE(6,28)K,L
   28 FORMAT(//,1X,28HERROR ON FURTH LINE OF SCAN ,I3,11H IN SUBRUN ,I3,
     *//)
      DO 8 I=9,13
      DATA(I)=0.0
    8 CONTINUE
   29 READ(1,42,ERR=31,END=90) DATA(14),DATA(15)
      GO TO 33
   31 WRITE(6,32)K,L
   32 FORMAT(//,1X,28HERROR ON FIFTH LINE OF SCAN ,I3,11H IN SUBRUN,I3,
     *//)
      DATA(14)=0.0
      DATA(15)=0.0
   33 DO 34 I=1,15
      D(K,I)=DATA(I)
   34 CONTINUE
```

```
C     CALCULATE THE TIME OF MEASUREMENT
      T=NSEC+NMIN*60+NHR*3600
      TIME(K)=T/3600.0
      D(K,16)=VPRESA(K)
      D(K,17)=VPRESB(K)
      IF(NWRITE.EQ.0) GO TO 83
      WRITE(6,50) K,NHR,NMIN,NSEC,DATA(1),VPRESA(K),VPRESB(K),(DATA(I),
     *I=2,15)
   83 IF(K.EQ.2) GO TO 3
      GO TO 4
    3 MHR=NHR
      MMIN=NMIN
    4 CONTINUE
    2 CONTINUE
C
C     END OF READING THE INPUT RAW DATA FILE FOR FIRST SET OF DATA
C     POINTS
C
C**********************************************************************
C
C     CALCULATE THE LINEAR TIME VARIATION OF EACH ZERO OF THE
C     MEASUREMENT SYSTEM USING THE INITIAL AND FINAL ZERO READINGS.
C     THEN SUBTRACT THE CALCULATED ZERO OFFSET FROM DATA POINTS 8
C     THROUGH 17.
C
      DO 36 I=8,17
      SLOPE=(D(NSCANS,I)-D(1,I))/(TIME(NSCANS)-TIME(1))
      Z0=D(1,I)
      DO 9 K=1,NSCANS
      DT=TIME(K)-TIME(1)
      Z(K,I)=Z0+DT*SLOPE
      IF((I.LT.16).AND.(I.GT.12)) Z(K,I)=0.0
      D(K,I)=D(K,I)-Z(K,I)
      IF(I.GT.15) GO TO 37
```

```
      DATA(I)=D(K,I)
   37 IF(I.EQ.16) VPRESA(K)=D(K,16)
      IF(I.EQ.17) VPRESB(K)=D(K,17)
    9 CONTINUE
   36 CONTINUE
C
C     AVERAGE DATA POINTS 2 THROUGH 15 OVER SCANS 6 THROUGH MSCANS
C
      KSCANS=NSCANS-9
      MSCANS=NSCANS-4
      DO 38 I=2,15
      SUM=0.0
      DO 39 K=6,MSCANS
      SUM=SUM+D(K,I)
   39 CONTINUE
      DATA(I)=SUM/KSCANS
   38 CONTINUE
C
C     WRITE FINE DATA ONTO OUTPUT DATA FILE
C
      WRITE(2,55)L,MHR,MMIN
      WRITE(2,60) (VPRESA(J),J=1,12)
      WRITE(2,60) (VPRESA(J),J=13,24)
      WRITE(2,60) (VPRESA(J),J=25,36)
      WRITE(2,65) (VPRESA(J),J=37,NSCANS)
      WRITE(2,60) (VPRESB(J),J=1,12)
      WRITE(2,60) (VPRESB(J),J=13,24)
      WRITE(2,60) (VPRESB(J),J=25,36)
      WRITE(2,65) (VPRESB(J),J=37,NSCANS)
      WRITE(2,70) (DATA(I),I=2,8)
      WRITE(2,70) (DATA(I),I=9,15)
    1 CONTINUE
    5 FORMAT(2I3)
   10 FORMAT(I3)
```

```
 15 FORMAT(1H1,4X,I3,4X,I3,/)
 20 FORMAT(4X,I2,1X,I2,1X,I2)
 30 FORMAT(4X,F7.3,8X,F7.3,8X,F7.3,8X,F7.4,8X,F7.3,2X)
 40 FORMAT(4X,F7.1,8X,F7.1,8X,F7.3,8X,F7.3,8X,F7.3,2X)
 41 FORMAT(4X,F7.3,4(8X,F7.3))
 42 FORMAT(4X,F7.3,8X,F7.3)
 50 FORMAT(5X,I3,2X,I2,':',I2,':',I2,/,4X,9F10.4,/,4X,8F10.4)
 55 FORMAT(I3,2I2)
 60 FORMAT(12F6.3)
 65 FORMAT(12F6.3,/,4F6.3)
 70 FORMAT(7F10.6)
    GO TO 95
 90 WRITE(6,91)
 91 FORMAT(//,1X,23HEND OF DATA ENCOUNTERED ,//)
100 FORMAT(I14,I3,F5.2,F5.1,2F5.2,2F5.3)
101 FORMAT(I8,2F5.2,2F5.0,I3)
102 FORMAT(4F10.6)
103 FORMAT(6F5.2)
 95 STOP
    END
```

```
29
 1 49
  :09:43:19
 0 - 0.713 V     1 -15.687MV     2 - 3.755MV     3 -0.2537 V     4 + 0.189 V
 5 +  19.7 C     6 +  19.6 C     8 + 0.000MV     9 - 0.013MV    10 - 0.016MV
11 - 0.060MV    12 - 0.056MV    13 - 0.058MV    14 - 0.020MV    15 + 0.006MV
16 - 0.208MV    17 - 0.105MV
  :09:43:44
 0 - 1.101 V     1 -15.677MV     2 - 3.674MV     3 -0.2544 V     4 + 0.385 V
 5 +  19.1 C     6 +  19.3 C     8 - 0.226MV     9 - 0.288MV    10 - 0.416MV
11 - 0.299MV    12 - 0.236MV    13 - 0.296MV    14 - 0.362MV    15 - 1.566MV
16 - 0.174MV    17 - 0.099MV
  :09:43:46
 0 - 1.101 V     1 -15.673MV     2 - 3.667MV     3 -0.2543 V     4 + 0.583 V
 5 +  19.1 C     6 +  19.3 C     8 - 0.202MV     9 - 0.261MV    10 - 0.392MV
11 - 0.304MV    12 - 0.229MV    13 - 0.292MV    14 - 0.374MV    15 - 1.560MV
16 - 0.189MV    17 - 0.100MV
  :09:43:48
 0 - 1.101 V     1 -15.674MV     2 - 3.661MV     3 -0.2544 V     4 + 0.785 V
 5 +  19.1 C     6 +  19.3 C     8 - 0.226MV     9 - 0.297MV    10 - 0.380MV
11 - 0.287MV    12 - 0.226MV    13 - 0.283MV    14 - 0.367MV    15 - 1.481MV
16 - 0.193MV    17 - 0.100MV
  :09:43:51
 0 - 1.101 V     1 -15.671MV     2 - 3.654MV     3 -0.2543 V     4 + 0.991 V
 5 +  19.0 C     6 +  19.2 C     8 - 0.205MV     9 - 0.281MV    10 - 0.403MV
11 - 0.262MV    12 - 0.238MV    13 - 0.297MV    14 - 0.390MV    15 - 1.612MV
16 - 0.204MV    17 - 0.100MV
  :09:43:53
 0 - 1.101 V     1 -15.673MV     2 - 3.648MV     3 -0.2548 V     4 + 1.191 V
 5 +  16.9 C     6 +  19.2 C     8 - 0.234MV     9 - 0.021MV    10 - 0.393MV
11 - 0.312MV    12 - 0.245MV    13 - 0.303MV    14 - 0.351MV    15 - 1.386MV
16 - 0.205MV    17 - 0.099MV
```

Table D-2 RAW Data File

```
 0040060981323 4530.0 333.390.  -0.7 2.079-.262
0943104721.8 22.1  580. 420. 29
 0.0       0.001     0.0      -0.003
0.0  2.3826.3844.3838.3842.38
 1 943
    0 -.221 -.197 -.220 -.199 -.227 -.198 -.164 -.187 -.139 -.210 -.252
-.209 -.251 -.216 -.252 -.213  .001 -.211 -.245 -.221 -.001 -.232 -.241
-.252 -.002 -.252 -.004 -.240 -.003 -.238 -.239 -.256  .002 -.254 -.223
-.250 -.156 -.259 -.002 -.240 -.243 -.235 -.003 -.265 -.224 -.244 -.005
    0
    0 -.270 -.242 -.278 -.261 -.001 -.269 -.257 -.269 -.265 -.273 -.001
-.267 -.263 -.243 -.268 -.248 -.002 -.257 -.260 -.255 -.264 -.260 -.209
-.257 -.265 -.243 -.264 -.248 -.002 -.256 -.200 -.266 -.257 -.267 -.219
-.267 -.236 -.268 -.003 -.274 -.237 -.139  .002 -.738  .003 -.250 -.000
-.000
-1.101625-15.675100 -3.521625  -.254256 18.170000 18.812500  -.367534
 -.235401  -.182566  -.236501  -.354021 -1.452200  -.194300  -.098775
 2 945
    0 -.215 -.198 -.224 -.205 -.226 -.207 -.214 -.165 -.194 -.209 -.252
-.211 -.258 -.214 -.252 -.204  .002 -.206 -.253 -.212  .002 -.236 -.250
-.249 -.002 -.253 -.003 -.245 -.003 -.247 -.242 -.279  .000 -.253 -.232
-.254 -.214 -.257 -.002 -.255 -.242 -.237 -.006 -.268 -.243 -.238 -.006
    0
    0 -.270 -.241 -.260 -.257  .003 -.269 -.263 -.266 -.259 -.271  .003
-.262 -.265 -.243 -.267 -.245  .004 -.259 -.264 -.257 -.258 -.263 -.247
-.255 -.265 -.239 -.264 -.245  .007 -.250 -.248 -.265 -.256 -.263 -.287
-.266 -.234 -.265  .003 -.276 -.239 -.143 -.003 -.738  .001 -.249 -.001
-.000
-1.150350-15.729700 -3.130350  -.240800 16.190000 17.787500  -.385534
 -.266679  -.236353  -.279205  -.422946 -1.251900  -.206325  -.098900
```

Table D-3 FINE Data File

APPENDIX E

EXPERIMENTAL DATA REDUCTION PROGRAM -"DATAR4"

This appendix contains a listing of the computer program DATAR4 as described in Chapter 6. Table E-1 contains a list of the variables used in this computer program. Table E-2 is a list of the file LAYOUT that is the coded connection of the wall static pressure taps. Table E-3 is a sample output of the program DATAR4 for run #Ø61.

TABLE E-1

Variables Used in Program DATAR4

A) INPUT VARIABLES (From Files #1, #2, #3 & #4)

1) From File #1 (Layout of pressures on Scanivalve)

NTAPS - Number of static pressure taps used
N(1) - Number of static pressure taps on 4" OD tube
N(2) - Number of static pressure taps on 6" OD tube
N(3) - Number of static pressure taps on 8" ID tube
IP(1) through IP(74) - scanivalve port connections for the 74 possible static pressures(Can have a value of -1, 1 through 47 and 49 through 95. If =-1, then this static pressure is not connected)

2) From File #3 and #4 (Probe calibration coefficients)

KCX(K,J,I) - Probe calibration coefficients

I = 1,2 - Corresponds to calibration regions #1 & #2, respectively
J = 1,2,3,4,5 - Corresponds to C , C , v/V, u/V & w/V, respectively
K = 1 to 15 - Corresponds to the 15 calibration coefficients

3) From File #2 (FINE DATA FILE XXX)

NRUN - Run number
MONTH - Month of run
NDAY - Day of run
NYR - Year of run
NTCONF - Test configuration of run
NORF(1) - Inside choked orifice size
NORF(2) - Outside choked orifice size
NSVANE - Swirl vane setting
PATM - Atmospheric pressure (" Hg)
PLINEI - Supply line pressure setting (psig)
ALPHO - Calibration probe angle
VALPHO - Voltage from potentiometer for probe angle ALPHO
RDO - Calibration radial position of probe head
VRDO - Voltage from LVDT for probe position RDO
NTIMEH(1) - Hour at start of run
NTIMEM(1) - Minute at start of run
NTIMEH(2) - Hour at end of run
NTIMEM(2) - Minute at end of run
TRMS - Room temperature at start of run (C)

TRME - Room temperature at end of run (C)
PTANKS - Tank pressure at start of run (psig)
PTANKE - Tank pressure at end of run (psig)
NSRUNS - Number of subruns
VPO(7) - Zero of tank pressure transducer
VPO(8) - Zero of line pressure transducer
VPO(9) - Zero of outside flow orifice plate differential pressure transducer
VPO(10) - Zero of inside flow orifice plate differential pressure transducer
Z(1) to Z(6) - Axial position of probe section and 8" ID test section A, B, C, D & E, respectively

For each subrun "I"
NSRUN(I) - Subrun number
LTIMEH(I) - Hour at start of subrun
LTIMEM(I) - Minute at start of subrun
VPSV(1) to VPSV(96) - Scanivalve pressure transducer output voltages
VA - Voltage from potentiometer corresponding to probe angle
T(1) - Temperature of inside plenum (C)
T(2) - Temperature of outside plenum (C)
VP(1) - Voltage from P(1) pressure transducer
VP(2) - Voltage from P(2) pressure transducer
VP(3) - Voltage from P(3) pressure transducer
VP(4) - Voltage from P(4) pressure transducer
VP(5) - Voltage from P(5) pressure transducer
VP(6) - Voltage from P(1) - P(3) differential pressure transducer
VP(7) - Voltage from tank pressure transducer
VP(8) - Voltage from line pressure transducer
VP(9) - Voltage from outside flow orifice plate differential pressure transducer
VP(10) - Voltage from inside flow orifice plate differential pressure transducer

B) OUTPUT VARIABLES (To Files #6 and #7, the printer and REDUCED DATA FILE XXX, respectively)

1) The following input variables are used in the output unchanged (see INPUT VARIABLES for a description of each)

NRUN, MONTH, NDAY, NYR, NTCONF, NORF(1), NORF(2), NSVANE, PATM, PLINEI, NTAPS, N(1), N(2), N(3), NTIMEH(1),NTIMEM(1), NTIMEH(2), NTIMEM(2), TRMS, TRME, PTANKS, PTANKE & NSRUNS

2) Wall Static Pressures (averaged over all subruns) and their locations

PS4(J) - Static pressure on 4" OD centerbody at location "J" (J = 1 to N(1))
ZS4(J) - Axial location of static pressure PS4(J)
PS6(J) - Static pressure on inside wall of 6" tube at location "J" (J = 1 to N(2))
TH6(J) - Angular location of static pressure PS6(J)
ZS6(J) - Axial location of static pressure PS6(J)
NPA - Number of averaged static pressure locations on 6" tube
PS6A(J) - Average static pressure on inside wall of 6" tube at location "J" (J = 1 to NPA)
ZS6A(J) - Axial location of static pressure PS6A(J)
PS8(J) - Static pressure on 8" ID outer wall at location "J" (J = 1 to N(3))
ZS8(J) - Axial location of static pressure PS8(J)

3) For each subrun "I"

LTIMEH(I) - Hour at start of subrun
LTIMEM(I) - Minute at start of subrun
PNULL(I) - Pressure difference P(1) - P(3) (psi)
PTANK(I) - Tank pressure (psig)
PLINE(I) - Line pressure (psig)
FR1(I) - Inside flow orifice plate pressure drop (inches of water)
FR2(I) - Outside flow orifice plate pressure drop (inches of water)
TAI(I) - Inside plenum air temperature (C)
TAO(I) - Outside plenum air temperature (C)
PTI(I) - Inside plenum total pressure (psig)
PTO(I) - Outside plenum total pressure (psig)
RADIAL(I) - Radial position of probe head (inches)
AXIAL(I) - Axial location of probe head (inches)
ALPHA(I) - Flow angle alpha ( )
BETA(I) - Flow angle beta ( )
VEL(I) - Total velocity (ft/sec)
UV(I) - Ratio of radial to total velocity (u/V)
VV(I) - Ratio of tangential to total velocity (v/V)
WV(I) - Ratio of axial to total velocity (w/V)
PT(I) - Total pressure (psi)
PS(I) - Static pressure (psi)
MZ(I) - Axial momentum flux (psi)
MR(I) - Tangential momentum flux (psi)
FLOW1D(I) - Mass flow rate of inside flow choked orifice plate (lbm/sec)
FLOW2D(I) - Mass flow rate of outside flow choked orifice plate (lbm/sec)
FLOW1M(I) - Mass flow rate of inside flow meter

orifice plate (lbm/sec)

FLOW2M(I) - Mass flow rate of outside flow meter orifice plate (lbm/sec)

VELAVG(I) - Average axial velocity in test section (ft/sec)

PQAVG(I) - Dynamic pressure corresponding to VELAVG(I)

WI(I) = WZ(I) * RADIAL(I)

RAD(I) = RADIAL(I)

TI(I) = MR(I) * RADIAL(I)

XI(I) = WV(I) * VEL(I) * RADIAL(I)

PAI(I) = PT(I) * XI(I)

4) Output data for the run obtained by integration of data from the subruns

W - Axial momentum at axial location of run (lbf)

TO - Angular momentum at axial location of run (in-lbf)

S - Swirl number at axial location of run

WAVG - Average axial velocity of run from probe measurements (ft/sec)

PTM - Mass average total pressure at axial location of run (psi)

68251825
9092 2 4 6 8101214161820 1 3 5-1-11113151923222426283031-1356264666870727474767880
8284505254565860495155576163676973 75-18132343638404142454485894 68688

Table E-2 File LAYOUT

```
      PROGRAM DATAR4(DATAX1,DATAX2,KC1CAL,KC2CAL,OUTPUT,DATOUT,TAPE1=
     *DATAX1,TAPE2=DATAX2,TAPE3=KC1CAL,TAPE4=KC2CAL,TAPE6=OUTPUT,
     *TAPE7=DATOUT)
      REAL MZ(50),MR(50),KCX(15,4,2)
      DIMENSION PT(50),PS(50),UV(50),VV(50),WV(50),RAD(50)
      DIMENSION FLOW1D(50),FLOW2D(50),FLOW1M(50),FLOW2M(50)
      DIMENSION AXIAL(50),RADIAL(50),ALPHA(50),BETA(50),VEL(50)
      DIMENSION NORF(2),NTIMEH(2),NTIMEM(2),N(3),IP(79)
      DIMENSION Z(6),NSRUN(50),LTIMEH(50),LTIMEM(50),IPOINT(50)
      DIMENSION PTANK(50),PLINE(50),FR1(50),FR2(50),VPSV(96)
      DIMENSION PSV(96),PPB(6),ZS(80),PS1(80),TH6(18),ZS4(28),PS4(28)
      DIMENSION ZS6(18),PS6(18),ZS6A(6),PS6A(6),ZS8(26),PS8(26),T(2)
      DIMENSION OUT(10),FMDP(2),FLR1(2),FLR2(2),P(10),VP(10),VPO(10)
      DIMENSION X(60),Y(60),ERR(60,2),VELAVG(50),PQAVG(50),PNULL(50)
      DIMENSION TAI(50),TAO(50),PTI(50),PTO(50)
      DIMENSION WI(50),TI(50),XI(50),PAI(50),SVEL(2),SW(2),SU(2)
      DIMENSION SV(2),SPS(2),SPT(2),SMR(2),SMZ(2)
C
C
C*******************************************************************
C
C
C     INDEX FOR THE VARIABLES P(I), VP(I) AND VPO(I)
C
C            I = 1    PRESSURE ON PORT 1 OF FIVE HOLE PROBE
C            I = 2       "     "    "   2 "   "     "     "
C            I = 3       "     "    "   3 "   "     "     "
C            I = 4       "     "    "   4 "   "     "     "
C            I = 5       "     "    "   5 "   "     "     "
C            I = 6    DIFFERENTIAL PRESSURE BETWEEN PORTS 1 AND 3
C            I = 7    TANK PRESSURE
C            I = 8    LINE PRESSURE
C            I = 9    FLOW METER PRESSURE DROP - OUTSIDE FLOW
C            I = 10    "     "      "       "  - INSIDE   "
```

```
C
C
C     INDEX FOR THE VARIABLES T(I),FMDP(I),FLR1(I),FLR2(I) AND NORF(I)
C
C            I = 1   INSIDE FLOW STREAM
C            I = 2   OUTSIDE  "     "
C
C*****************************************************************
C
      DATA PS4/28*0.0/
      DATA PS6/16*0.0/
      DATA PS6A/6*0.0/
      DATA PS8/26*0.0/
      DATA SVEL/0.05471,0.0459/
      DATA SW/0.05548,0.04377/
      DATA SU/0.016843,0.038878/
      DATA SV/0.018912,0.028884/
      DATA SPS/0.1194,0.11615/
      DATA SPT/0.016633,0.05958/
      DATA SMR/0.04115,0.0525/
      DATA SMZ/0.09918,0.06729/
      NPLT=1
      PRD=0.0
      PRI=0.0
      ERROR=0.51
C
C     READ THE FIVE HOLE PROBE CALIBRATION COEFFICIENTS
C
      DO 17 I=1,2
      DO 18 J=1,4
      L=I+2
      READ(L,110)(KCX(K,J,I),K=1,8)
      READ(L,111)(KCX(K,J,I),K=9,15)
   18 CONTINUE
```

```
   17 CONTINUE
C
C     READ TEST NUMBER, DATE, CONFIGURATION,ETC.
C     READ ZERO'S OF TRANSDUCERS
C
      READ (2,100) NRUN,MONTH,NDAY,NYR,NTCONF,NORF(1),NORF(2),NSVANE,
     *PATM,PLINE1,ALPHO,VALPHO,RDO,VRDO
      READ (2,101)NTIMEH(1),NTIMEM(1),NTIMEH(2),NTIMEM(2),TRMS,TRME,
     *PTANKS,PTANKE,NSRUNS
      READ(2,114)(VPO(I),I=7,10)
C
C     READ PORT CONNECTION ON SCANIVALVE OF THE SEVENTY FOUR
C     PRESSURE TAPS
C
      READ(1,113) NTAPS,N(1),N(2),N(3)
      READ (1,102)(IP(I),I=1,40)
      READ (1,103)(IP(I),I=41,74)
      IF(N(3).EQ.0) GO TO 1
C
C     READ THE STARTING LOCATION OF EACH SECTION OF EIGHT
C     INCH TUBE
C
      READ (2,104)(Z(I),I=1,6)
    1 CONTINUE
      NRAUPT=NSPUNS
      DO 2 I=1,NSRUNS
      RI=I
      DO 16 J=1,6
      VPO(J)=0.0
   16 CONTINUE
C
C     READ INPUT DATA FOR EACH DATA POINT 'I'
C
      READ(2,115) NSRUN(I),LTIMEH(I),LTIMEM(I)
```

```
      READ(2,106) VPSV(48),(VPSV(J),J= 1,11)
      READ(2,106)(VPSV(J),J=12,23)
      READ(2,106)(VPSV(J),J=24,35)
      READ(2,106)(VPSV(J),J=36,47)
      READ(2,106) VPSV(48)
      READ(2,106) VPSV(96),(VPSV(J),J=49,59)
      READ(2,106)(VPSV(J),J=60,71)
      READ(2,106)(VPSV(J),J=72,83)
      READ(2,106)(VPSV(J),J=84,95)
      READ(2,106) VPSV(96)
      READ(2,107) VA,VP(8),VP(7),VRD,T(1),T(2),VP(1)
      READ(2,107) (VP(J),J=2,6),VP(9),VP(10)
      CALL PRESS(VPSV,PSV,0,VPO)
      CALL LOCATN(PSV,IP,Z,N,PTPI,PTPO,ZS,PS1,TH6,NPA)
      CALL PRESS(VP,P,I,VPO)
      DO 29 J=1,6
      PPB(J)=P(J)
   29 CONTINUE
      K=N(1)
      IF(N(1).EQ.0) GO TO 53
      DO 3 J=1,K
      ZS4(J)=ZS(J)
      PS4(J)=(PS4(J)*(RI-1.)+PS1(J))/RI
    3 CONTINUE
   53 K=K+1
      L=N(1)+N(2)
      IF(N(2).EQ.0) GO TO 54
      DO 4 J=K,L
      M=J-K+1
      ZS6(M)=ZS(J)
      PS6(M)=(PS6(M)*(RI-1.)+PS1(J))/RI
    4 CONTINUE
   54 K=L+1
      L=L+NPA
```

```
      IF(NPA.EQ.0) GO TO 55
      DO 5 J=K,L
      M=J-K+1
      ZS6A(M)=ZS(J)
      PS6A(M)=(PS6A(M)*(RI-1.)+PS1(J))/RI
    5 CONTINUE
   55 K=L+1
      L=L+N(3)
      IF(N(3).EQ.0) GO TO 56
      DO 6 J=K,L
      M=J-K+1
      ZS8(M)=ZS(J)
      PS8(M)=(PS8(M)*(RI-1.)+PS1(J))/RI
    6 CONTINUE
   56 FMDP(1)=P(10)
      FMDP(2)=P(9)
      PL=P(8)
      CALL FLOW(NURF,FMDP,PL,T,FLR1,FLR2)
      FLOW1D(I)=FLR1(1)
      FLOW2D(I)=FLR1(2)
      FLOW1M(I)=FLR2(1)
      FLOW2M(I)=FLR2(2)
      CALL DENSTY(PATM,PTP1,PIPO,FLR1,T,RHO,VAVG,PAVG)
      CALL PROBE(KCX,PPB,VA,VALPHO,ALPHO,RHO,I,OUT,J)
      IPOINT(I)=J
      ALPHA(I)=OUT(1)
      BETA(I)=OUT(2)
      VEL(I)=OUT(3)
      PT(I)=OUT(4)
      PS(I)=OUT(5)
      MZ(I)=OUT(6)
      MR(I)=OUT(7)
      UV(I)=OUT(8)
      VV(I)=OUT(9)
```

```
      WV(I)=OUT(10)
      PNULL(I)=P(6)
      PTANK(I)=P(7)
      PLINE(I)=P(8)
      FR1(I)=P(10)
      FR2(I)=P(9)
      PTI(I)=PTPI
      PTO(I)=PTPO
      TAI(I)=T(1)
      TAO(I)=T(2)
      VELAVG(I)=VAVG
      PWAVG(I)=PAVG
      CALL POSITN(RDO,VRDO,VRD,RD)
      AXIAL(I)=Z(1)+0.25
      RADIAL(I)=RD
    2 CONTINUE
C
C     WRITE OUT RESULTS ON PRINTER AND ON OUTPUT DATA FILE
C
      WRITE(6,209)
      WRITE(6,210)NRUN,MONTH,NDAY,NYR,NTCONF,NORF(1),NORF(2),NSVANE,
     *PATH,PLINEI
      WRITE(6,211)NTAPS,N(1),NTIMEH(1),NTIMEM(1),NTIMEH(2),NTIMEM(2),
     *N(2),TRMS,TRME,N(3),PTANKS,PTANKE
      WRITE(7,240)NSRUNS,N(1),NPA,N(3),NRADPT
      WRITE(6,220)
      DO 12 I=1,NSRUNS
      WRITE(6,221)NSRUN(I),LTIMEH(I),LTIMEM(I),PNULL(I),PTANK(I),
     *PLINE(I),FR1(I),FR2(I),TAI(I),TAO(I),PTI(I),PTO(I)
   12 CONTINUE
      WRITE(6,212)
      IF(N(1).EQ.0) GO TO 57
      K=N(1)
      MO=K-1
```

```
      DO 7 J=1,K
      WRITE(6,213) ZS4(J),PS4(J)
      WRITE(7,213) ZS4(J),PS4(J)
      IF(ZS4(J).LT.AXIAL(1)) MO=J
    7 CONTINUE
      PRI=0.5*(PS4(MO)+PS4(MO+1))
   57 IF(N(2).EQ.0) GO TO 59
      K=N(2)
      DO 8 J=1,K
      WRITE(6,214) ZS6(J),TH6(J),PS6(J)
    8 CONTINUE
      DO 9 J=1,NPA
      WRITE(6,215) ZS6A(J),PS6A(J)
      WRITE(7,215) ZS6A(J),PS6A(J)
    9 CONTINUE
   59 IF(N(3).EQ.0) GO TO 60
      K=N(3)
      DO 10 J=1,K
      WRITE(6,216) ZS8(J),PS8(J)
      WRITE(7,216) ZS8(J),PS8(J)
      ERRO=ZS8(J)-AXIAL(1)
      ERRO=ABS(ERRO)
      IF(ERRO.LT.ERROR) PRO=PS8(J)
   10 CONTINUE
   60 CONTINUE
      WRITE(6,217) NRUN
      DO 11 I=1,NSRUNS
      WRITE(6,218) I,RADIAL(I),AXIAL(I),ALPHA(I),BETA(I),VEL(I),UV(I),
     *VV(I),WV(I),IPOINT(I)
      WRITE(7,218) I,RADIAL(I),AXIAL(I),ALPHA(I),BETA(I),VEL(I),UV(I),
     *VV(I),WV(I),IPOINT(I)
   11 CONTINUE
      WRITE(6,230) NRUN
      NPT=NSRUNS+2
```

```
      NT=NSRUNS+1
      RAD(1)=2.0
      RAD(NPT)=4.0
      WI(1)=PRI*2.0
      WI(NPT)=PRO*4.0
      DO 15 I=1,NSRUNS
      WRITE(6,231) I,PT(I),PS(I),MZ(I),MR(I),FLOW1D(I),FLOW2D(I),
     *FLOW1M(I),FLOW2M(I),VELAVG(I),PQAVG(I)
      WRITE(7,231) I,PT(I),PS(I),MZ(I),MR(I),FLOW1D(I),FLOW2D(I),
     *FLOW1M(I),FLOW2M(I),VELAVG(I),PQAVG(I)
   15 CONTINUE
      WRITE(6,235)
      DO 70 I=1,NPT
      J=I-1
      IF(RADIAL(1).GT.3.0) J=NT+1-I
      IF((I.EQ.1).OR.(I.EQ.NPT)) GO TO 71
      RAD(I)=RADIAL(J)
      WI(I)=MZ(J)*RADIAL(J)
      TI(I)=MR(J)*RADIAL(J)
      XI(I)=WV(J)*VEL(J)*RADIAL(J)
      PAI(I)=PT(J)*XI(I)
      GO TO 73
   71 TI(I)=0.0
      XI(I)=0.0
      PAI(I)=0.0
      PB=PRO
      IF(I.EQ.1) PB=PRI
      WRITE(6,236) WI(I),PB,RAD(I),TI(I),XI(I),PAI(I),I,J
      GO TO 72
   73 WRITE(6,234) WI(I),MZ(J),RAD(I),TI(I),MR(J),WV(J),VEL(J),
     *XI(I),PT(J),PAI(I),I,J
   72 CONTINUE
   70 CONTINUE
C
```

```
C     CALCULATE THE AXIAL MOMENTUM, ANGULAR MOMENTUM, SWIRL
C     NUMBER, AVERAGE AXIAL VELOCITY AND MASS AVERAGE TOTAL
C     PRESSURE
C
      CALL INTERGR(WI,RAD,NPT,W)
      CALL INTERGR(TI,RAD,NPT,TO)
      CALL INTERGR(XI,RAD,NPT,XO)
      CALL INTERGR(PAI,RAD,NPT,PTM)
      PTM=PTM/XO
      S=TO/(W*4.0)
      WAVG=XO/6.0
      WRITE(6,232) W,TO,S,WAVG,PTM
      WRITE(7,233) W,TO,S,WAVG,PTM
      IF(NPLT.EQ.0) GO TO 241
      UNCP=0.00005
      DO 30 I=1,40
      ERR(I,1)=-UNCP
      ERR(I,2)=UNCP
   30 CONTINUE
      AX=0.0
      IF(N(1).EQ.0.0) GO TO 61
      NA=N(1)
      CALL PVPLOT(ZS4,PS4,NA,1,AX,ERR)
   61 IF(NPA.EQ.0.0) GO TO 62
      CALL PVPLOT(ZS6A,PS6A,NPA,3,AX,ERR)
   62 IF(N(3).EQ.0.0) GO TO 63
      NA=N(3)
      CALL PVPLOT(ZS8,PS8,NA,2,AX,ERR)
   63 CONTINUE
      DO 19 IA=4,11
      DO 14 I=1,NRADPT
      K=I
      IAT=IA-3
      J=IPOINT(I)
```

```
      PQ=PT(I)-PS(I)
      GO TO (20,21,22,23,24,25,26,27)IAT
   20 X(K)=WV(I)*VEL(I)
      ERR(K,1)=X(K)*(1.-SVEL(J))*(1.-SW(J))
      ERR(K,2)=X(K)*(1.+SVEL(J))*(1.+SW(J))
      GO TO 28
   21 X(K)=UV(I)*VEL(I)
      ERR(K,1)=X(K)*(1.-SVEL(J))*(1.-SU(J))
      ERR(K,2)=X(K)*(1.+SVEL(J))*(1.+SU(J))
      GO TO 28
   22 X(K)=VV(I)*VEL(I)
      ERR(K,1)=X(K)*(1.-SVEL(J))*(1.-SV(J))
      ERR(K,2)=X(K)*(1.+SVEL(J))*(1.+SV(J))
      GO TO 28
   23 X(K)=VEL(I)
      ERR(K,1)=X(K)*(1.-SVEL(J))
      ERR(K,2)=X(K)*(1.+SVEL(J))
      GO TO 28
   24 X(K)=PS(I)
      ERR(K,1)=X(K)-SPS(J)*PQ-UNCP
      ERR(K,2)=X(K)+SPS(J)*PQ+UNCP
      GO TO 28
   25 X(K)=PT(I)
      ERR(K,1)=X(K)-SPT(J)*PQ-UNCP
      ERR(K,2)=X(K)+SPT(J)*PQ+UNCP
      GO TO 28
   26 X(K)=MR(I)
      ERR(K,1)=X(K)-SMR(J)*PQ-UNCP
      ERR(K,2)=X(K)+SMR(J)*PQ+UNCP
      GO TO 28
   27 X(K)=MZ(I)
      ERR(K,1)=X(K)*(1.-SMZ(J))-UNCP
      ERR(K,2)=X(K)*(1.+SMZ(J))+UNCP
   28 Y(K)=RADIAL(I)
```

```
 14 CONTINUE
    NA=NRADPT
    AX=Z(1)+0.25
    CALL PVPLOT(X,Y,NA,IA,AX,ERR)
 19 CONTINUE
    WRITE(6,219)
100 FORMAT(I5,3I2,3I1,I3,F5.2,F5.1,2F5.2,2F5.3)
101 FORMAT(4I2,2F5.2,2F5.0,I3)
102 FORMAT(40I2)
103 FORMAT(34I2)
104 FORMAT(6F5.2)
106 FORMAT(12F6.3)
107 FORMAT(7F10.6)
110 FORMAT(6E12.6)
111 FORMAT(7E12.6)
113 FORMAT(4I2)
114 FORMAT(4F10.6)
115 FORMAT(I3,2I2)
209 FORMAT(1H1,24('*'),' INPUT DATA FOR RUN ',27('*'),/)
210 FORMAT(1X,'RUN NUMBER = ',I3,3X,'DATE: ',I2,'/',I2,'/',I2,//,1X,
   *'TEST CONFR = ',I3,3X,'ORIFICE SIZE: ',I1,'/',I1,3X,'SWIRL VANE ',
   *'SETTING = ',I3,/,1X,'PATM = ',F5.2,' IN HG',3X,'PLINE = ',F4.0,
   *' PSIG',//)
211 FORMAT(1X,'NO OF PRESS TAPS:',3X,'TOTAL = ',I2,10X,'READINGS AT:',
   * 1X,'START',2X,'END',/,19X,'4  TUBE = ',I2,10X,'TIME',9X,I2,':',
   *I2,I3,':',I2,/,19X,'6  TUBE = ',I2,10X,'ROOM TEMP',5X,F4.1,2X,
   *F4.1,1X,'C',/,19X,'8  TUBE = ',I2,10X,'TANK PRESS',3X,F5.0,1X,
   *F5.0,1X,'PSIG',//)
212 FORMAT(1H1,19('*'),' STATIC PRESSURE VS POSITION ',22('*'),//,
   *2X,'4 INCH TUBE',7X,'6 INCH TUBE',7X,'8 INCH TUBE',3X,
   *'AVG 6 IN TUBE',/,3X,'Z',4X,'PRESS',5X,'Z',3X,'THETA',2X,
   *'PRESS',5X,'Z',4X,'PRESS', 5X,'Z',4X,'PRESS',/)
213 FORMAT( 1X,F5.2,1X,F7.5)
214 FORMAT(16X,F5.2,1X,F5.1,1X,F7.5)
```

```
215 FORMAT(52X,F5.2,1X,F7.5)
216 FORMAT(37X,F5.2,1X,F7.5)
217 FORMAT(1H1,19('*'),' OUTPUT DATA FOR RUN NO. ',I3,2X,22('*'),//,
   *2X,'SUB',5X,'PROBE POSITION',5X,'VELOCITY MAGNITUDE AND DIRECTION'
   *,/,2X,'RUN',5X,'RADIAL',3X,'AXIAL',2X,'ALPHA',3X,'BETA',1X,
   *'VELOCITY',3X,'U/V',3X,'V/V',3X,'W/V',/,3X,'NO',5X,'(INCH)',2X,
   *'(INCH)',2X,'(DEG)',2X,'(DEG)',1X,'(FT/SEC)',23X,'J',/)
218 FORMAT(2X,I3,5X,F5.2,4X,F5.2,1X,F6.2,1X,F6.2,1X,F8.4,3F6.3,I6)
219 FORMAT(1H1)
220 FORMAT(//,1X,3HSUB,2X,4HTIME,4X,5HPNULL,4X,5HPTANK,2X,5HPLINE,3X,
   *3HFR1,3X,3HFR2,3X,2HTI,4X,2HTO,4X,3HPTI,5X,3HPTO,/)
221 FORMAT(1X,I3,2X,2I2,2X,F9.7,2F7.0,2F6.1,2F6.2,2F8.5)
230 FORMAT(1H1,19('*'),' OUTPUT DATA FOR RUN NO. ',I3,2X,22('*'),//,
   *2X,'SUB',6X,'PRESSURES',8X,'MOMENTUM',5X,'FLOW RATES (LBM/SEC)',
   */,2X,'RUN',5X,'TOTAL',2X,'STATIC',3X,'AXIAL',2X,'TANGTL',2X,
   *'DISC DISC  ORFP ORFP',/,3X,'NO',5X,'(PSI)',3X,'(PSI)',3X,'(PSI)',
   *3X,'(PSI)',3X,'1',4X,'2',5X,'1',4X,'2',4X,'VELAVG',2X,'PQAVG',/)
231 FORMAT(2X,I3,2X,2(1X,F7.5),2(2X,F6.4),2(1X,F5.3,F5.3),F8.2,F8.5)
232 FORMAT(///,5X,3HW =,F12.8,5X,3HT =,F12.8,5X,3HS =,F12.8,5X,
   *6HWAVG =,F8.4,5X,5HPTM =,F12.8,//)
233 FORMAT(5F12.8)
234 FORMAT(1X,10E12.6,2I5)
235 FORMAT(1H1,5X,2HWI,10X,2HMZ,10X,2HRD,10X,2HTI,10X,2HMR,10X,
   *2HWV,10X,2HVL,10X,2HXI,10X,2HPT,10X,3HPAI,9X,1HI,4X,1HJ,/)
236 FORMAT(1X,4E12.6,36X,E12.6,12X,E12.6,2I5)
240 FORMAT(10I5)
241 STOP
    END
```

```
      SUBROUTINE PVPLOT(X,Y,NPT,NUMP,AX,ERR)
C
C     PLOT OUT RESULTS ON PRINTER USING THE NPS SOFTWARE
C
      DIMENSION X(60),Y(60),A(3),ERR(60,2),XP(60),XM(60)
      DIMENSION XL(41),YL(41),YP(60),YM(60)
      CALL PRNTON
      CALL SIPRTT(1,8.0)
      CALL STS2OB(2.,9.,2.,9.)
      IF(NUMP.GT.3) GO TO 2
      NXMAX=X(NPT)/10.0+1
      XMAX=NXMAX
      XMAX=XMAX*10.0
      XMIN=0.0
      YMAX=0.0
      YMIN=0.0
      DO 1 I=1,NPT
      IF(Y(I).GE.YMAX) YMAX=Y(I)
      IF(Y(I).LE.YMIN) YMIN=Y(I)
    1 CONTINUE
      IF(NUMP.EQ.3) XMAX=0.0
      IF(NUMP.EQ.3) XMIN=-2.5
      NYMAX=YMAX*1000.0+1
      NYMIN=YMIN*1000.0-1.0
      YMAX=NYMAX
      YMAX=YMAX/1000.0
      YMIN=NYMIN
      YMIN=YMIN/1000.0
      GO TO 4
    2 YMAX=4.0
      YMIN=2.0
      NDY=4
      NU=NUMP-3
      GOTO(13,14,15,16,17,8,20,21)NU
```

```
C        SCALE FOR AXIAL VELOCITY
   13 XMAX=120.0
      XMIN=-20.0
      NDX=7
      GO TO 9
C       SCALE FOR RADIAL VELOCITY
   14 XMAX=20.0
      XMIN=-20.0
      NDX=4
      GO TO 9
C        SCALE FOR TANGENTIAL VELOCITY
   15 XMAX=60.0
      XMIN=-20.0
      NDX=5
      GO TO 9
C        SCALE FOR OTAL VELOCITY
   16 XMAX=120.0
      XMIN=0.0
      NDX=6
      GO TO 9
C        SCALE FOR STATIC PRESSURE
   17 XMAX=0.05
      XMIN=-0.05
      NDX=4
      GO TO 9
C        SCALE FOR TOTAL PRESSURE
    8 XMAX=0.16
      XMIN=-0.02
      NDX=9
      GO TO 9
C        SCALE FOR ANGLAR VELOCITY
   20 XMAX=0.1
      XMIN=-0.02
      NDX=6
```

```
      GO TO 9
C     SCALE FOR AXIAL MOMENTUM
   21 XMAX=0.2
      XMIN=-0.05
      NDX=5
    9 CONTINUE
    4 CALL STSUBJ(XMIN,XMAX,YMIN,YMAX)
      CALL AXLIL1
      IF(NUMP.GT.3) GO TO 5
      CALL STNDIV(5,5)
      CALL STNDEC(4)
      CALL NODLIL
      CALL STNCHR(16)
      CALL TITLEL(16HPRESSURE IN PSIG)
      CALL STNDEC(2)
      CALL NODLIB
      CALL STNCHR(24)
      CALL TITLEB(24HAXIAL POSITION IN INCHES)
      CALL STNCHR(30)
      IF(NUMP.EQ.1) CALL TITLET(30HSTATIC PRESSURE ON 4 INCH TUBE)
      IF(NUMP.EQ.2) CALL TITLET(30HSTATIC PRESSURE ON 8 INCH TUBE)
      IF(NUMP.EQ.3) CALL TITLET(30HSTATIC PRESSURE ON 6 INCH TUBE)
      GO TO 6
    5 CONTINUE
      CALL STNDIV(NDX,NDY)
      CALL STNDEC(2)
      CALL NODLIL
      CALL STNCHR(25)
      CALL TITLEL(25HRADIAL POSITION IN INCHES)
      CALL STNDEC(2)
      IF(NUMP.GT.7) CALL STNDEC(4)
      CALL NODLIB
      IF(NUMP.NE.6) CALL STNCHR(25)
      IF(NUMP.EQ.6) CALL STNCHR(29)
```

```
      IF(NUMP.EQ.7) CALL STNCHR(18)
      IF(NUMP.GT.7) CALL STNCHR(24)
      IF(NUMP.EQ.4) CALL TITLEB(25H AXIAL VELOCITY IN FT/SEC)
      IF(NUMP.EQ.5) CALL TITLEB(25HRADIAL VELOCITY IN FT/SEC)
      IF(NUMP.EQ.6) CALL TITLEB(29HTANGENTIAL VELOCITY IN FT/SEC)
      IF(NUMP.EQ.7) CALL TITLEB(18HVELOCITY IN FT/SEC)
      IF(NUMP.EQ.8) CALL TITLEB(24HSTATIC PRESSURE IN PSIG )
      IF(NUMP.EQ.9) CALL TITLEB(24H TOTAL PRESSURE IN PSIG )
      IF(NUMP.EQ.10)CALL TITLEB(24HANGULAR MOMENTUM IN PSI )
      IF(NUMP.EQ.11)CALL TITLEB(24H AXIAL MOMENTUM IN PSIG )
      ENCODE(30,7,A)AX
    7 FORMAT(17HAXIAL POSITION = ,F5.2,8H INCHES )
      CALL STNCHR(30)
      CALL STLNOR(0.)
      CALL OBLNST(3.0,9.5)
      CALL TITLEG(A)
      DO 10 J=1,NPT
      XP(J)=EKR(J,1)
      XM(J)=EKR(J,2)
   10 CONTINUE
      DO 11 LL=1,3
      DX=(XMAX-XMIN)/40.0
      DO 12 J=1,41
      XL(J)=XMIN+DX*(J-1)
      YL(J)=1.0+LL
   12 CONTINUE
      CALL STNPTS(41)
      CALL SITXTR(3)
      CALL SLLILI(XL,YL)
   11 CONTINUE
      CALL STNPTS(NPT)
      CALL STSYMB(13)
      CALL PSLILI(XP,Y)
      CALL STNPTS(NPT)
```

```
      CALL STSYMB(16)
      CALL PSLILI(XM,Y)
      GO TO 19
    6 CONTINUE
      DO 18 I=1,NPT
      YM(I)=Y(I)+ERR(I,1)
      YP(I)=Y(I)+ERR(I,2)
   18 CONTINUE
      CALL STNPTS(NPT)
      CALL STSYMB(13)
      CALL PSLILI(X,YP)
      CALL STNPTS(NPT)
      CALL STSYMB(16)
      CALL PSLILI(X,YM)
   19 CONTINUE
      CALL STNPTS(NPT)
      CALL PLILI(X,Y)
      CALL EXITPL
      RETURN
      END
```

```
      SUBROUTINE LOCATN(PSV,IP,Z,N,PTPI,PTPO,ZO,PS,TH6,NPA)
C
C     DETERMINE THE LOCATION AND STATIC PRESSURE OF EACH
C     STATIC PRESSURE TAP USING THE CODED SCANIVALVE
C     LOCATION FOR EACH OF THE 74 TAPS CONTAINED IN
C     'FILE1' AND THE STARTING LOCATION OF EACH SECTION
C     OF THE EIGHT INCH TUBE, Z(1), CONTAINED IN 'FILE2'.
C
      DIMENSION PSV(96),ZS(72),THS(18),IP(79),Z(6),N(3),ZS4(28)
      DIMENSION PS4(28),ZO(80),PS(80),ZS6(18),PS6(18),ZS6A(6),PS6A(6)
      DIMENSION ZS8(26),PS8(26),TH6(18)
      DATA THS/90.,70.,50.,30.,10.,350.,330.,310.,290.,270.,250.,230.,
     *210.,190.,170.,150.,130.,110./
      DATA ZS/0.125,0.25,0.375,0.5,0.75,1.0,1.25,2.25,3.25,4.25,5.25,
     *6.25,8.25,10.25,12.25,14.25,16.25,18.25,20.25,22.25,24.25,26.25,
     *28.25,30.25,34.25,38.25,42.25,46.25,0.0,-0.1,-0.25,-0.5,-1.0,-2.0,
     *0.0,-0.1,-0.25,-0.5,-1.0,-2.0,0.0,-0.1,-0.25,-0.5,-1.0,-2.0,1.0,
     *3.0,5.0,7.0,9.0,11.0,13.0,15.0,17.0,19.0,21.0,23.0,1.0,3.0,5.0,
     *7.0,9.0,11.0,1.0,3.0,5.0,1.0,3.0,1.0,0.25,0.25/
C     DETERMINE INSIDE AND OUTSIDE PLENUM TOTAL PRESSURES
      I=IP(1)
      PTPI=PSV(I)
      I=IP(2)
      PTPO=PSV(I)
      IF(N(1).EQ.0) GO TO 22
C     DETERMINE STATIC PRESSURES AND LOCATIONS ON 4 INCH INNER TUBE
      J=0
      DO 2 I=1,28
      K=IP(I+2)
      IF(K.EQ.-1) GO TO 2
      J=J+1
      ZS4(J)=ZS(I)
      PS4(J)=PSV(K)
    2 CONTINUE
```

```
   22 IF(N(2).EQ.0) GO TO 24
C     DETERMINE STATIC PRESSURES AND LOCATIONS ON 6 INCH TUBE
      J=0
      DO 3 I=29,46
      K=IP(I+2)
      IF(K.EQ.-1) GO TO 3
      J=J+1
      ZS6(J)=ZS(I)
      TH6(J)=THS(I-28)
      PS6(J)=PSV(K)
    3 CONTINUE
C     DETERMINE AVERAGE STATIC PRESSURES AT LOCATIONS ON 6 INCH TUBE
      J=I1=I2=I3=0
      DO 4 I=29,34
      K1=IP(I+2)
      K2=IP(I+8)
      K3=IP(I+14)
      IF(K1.NE.-1) I1=1
      IF(K2.NE.-1) I2=1
      IF(K3.NE.-1) I3=1
      IT=I1+I2+I3
      IF(IT.EQ.0) GO TO 4
      J=J+1
      IF(IT.EQ.1) GO TO 6
      IF(IT.EQ.2) GO TO 5
      PS6A(J)=(PSV(K1)+PSV(K2)+PSV(K3))/3.0
      GO TO 7
    5 IF(K1.EQ.-1) PS6A(J)=(PSV(K2)+PSV(K3))/2.0
      IF(K2.EQ.-1) PS6A(J)=(PSV(K1)+PSV(K3))/2.0
      IF(K3.EQ.-1) PS6A(J)=(PSV(K1)+PSV(K2))/2.0
      GO TO 7
    6 IF(K1.NE.-1) PS6A(J)=PSV(K1)
      IF(K2.NE.-1) PS6A(J)=PSV(K2)
      IF(K3.NE.-1) PS6A(J)=PSV(K3)
```

```
    7 ZS6A(J)=ZS(I)
      I1=I2=I3=0
    4 CONTINUE
   24 NPA=J
      IF(N(3).EQ.0) GO TO 29
C     DETERMINE AXIAL STATION LOCATIONS FOR THE SECTIONS OF EIGHT
C     INCH TUBES AND THE ASSOCIATED STATIC PRESSURES
      L=0
      DO 9 I=47,72
      K=IP(I+2)
      IF(K.EQ.-1) GO TO 9
      L=L+1
      J=1
      IF(I.LE.70) J=6
      IF(I.LE.69) J=5
      IF(I.LE.67) J=4
      IF(I.LE.64) J=3
      IF(I.LE.58) J=2
      ZS8(L)=ZS(I)+Z(J)
      PS8(L)=PSV(K)
    9 CONTINUE
C     ARRANGE PRESSURES AND LOCATIONS FOR OUTPUT FROM SUBROUTINE
   29 K=0
      IF(N(1).EQ.0) GO TO 16
      K=N(1)
      DO 10 I=1,K
      ZO(I)=ZS4(I)
      PS(I)=PS4(I)
   10 CONTINUE
   16 CONTINUE
      K=K+1
      J=N(1)+N(2)
      IF(N(2).EQ.0) GO TO 17
      DO 11 I=K,J
```

```
      L=I-K+1
      ZO(I)=ZS6(L)
      PS(I)=PS6(L)
   11 CONTINUE
      K=J+1
      J=J+NPA
      DO 12 I=K,J
      L=I-K+1
      ZO(I)=ZS6A(L)
      PS(I)=PS6A(L)
   12 CONTINUE
   17 CONTINUE
      K=J+1
      J=J+N(3)
      IF(N(3).EQ.0) GO TO 18
      DO 13 I=K,J
      L=I-K+1
      ZO(I)=ZS8(L)
      PS(I)=PS8(L)
   13 CONTINUE
      DO 14 I=K,J
      A=ZO(I)
      P=PS(I)
      DO 15 L=I,J
      IF(ZO(L).GT.A) GO TO 15
      LM=L
      A=ZO(L)
      P=PS(L)
   15 CONTINUE
      PS(LM)=PS(I)
      ZO(LM)=ZO(I)
      PS(I)=P
      ZO(I)=A
   14 CONTINUE
```

```
18 CONTINUE
   RETURN
   END
```

```
      SUBROUTINE PRESS(VPSV,PSV,N,VPO)
C
C     DETERMINE PRESSURES MEASURED BY SCANIVALVE PRESSURE TRANSDUCERS
C     AND ALL OTHER PRESSURE TRANSDUCERS
C
      DIMENSION VPSV(96),PSV(96),CAL(10),VPO(10)
      DATA CAL/-.054945,-.05102,-.05102,-.050378,-.050454,-.007143,
     *-139.933,-21.158,-211.0476,-210.6464/
      IF(N.NE.0) GO TO 3
      A=-.05102
      PSV(48)=0.0
      DO 1 I=1,47
      PSV(I)=(VPSV(I)-VPSV(48))*A
    1 CONTINUE
      A=-.051282
      PSV(96)=0.0
      DO 2 I=49,95
      PSV(I)=(VPSV(I)-VPSV(96))*A
    2 CONTINUE
      RETURN
    3 DO 4 I=1,10
      PSV(I)=(VPSV(I)-VPO(I))*CAL(I)
    4 CONTINUE
      RETURN
      END
```

```
      SUBROUTINE DENSTY(PATM,PTPI,PTPO,FLR1,T,RHO,VAVG,PAVG)
C
C     CALCULATE THE DENSITY OF BOTH AIRSTREAMS, THE MIXED STREAM'S
C     AVERAGE DENSITY AND BOTH THE AVERAGE VELOCITY AND DYNAMIC
C     PRESSURE OF THE INSIDE AIRSTREAM BASED ON THE MIXED DENSITY
C
      DIMENSION FLR1(2),T(2)
      PI=3.141593
      RHO1=(PATM*0.4912+PTPI)/((T(1)+273.15)*0.66675)
      RHO2=(PATM*0.4912+PTPO)/((T(2)+273.15)*0.66675)
      RHO=(FLR1(1)*RHO1+FLR1(2)*RHO2)/(FLR1(1)+FLR1(2))
      VAVG=(144.0*FLR1(1))/(RHO*PI*5.0)
      PAVG=0.5*RHO*VAVG*VAVG/(144.0*32.17)
      RETURN
      END
```

```
      SUBROUTINE POSITN(RDO,VRDO,VRD,RD)
C
C     DETERMINE THE RADIAL POSITION BASED ON THE CALIBRATION OF THE
C     LINEAR VARIABLE DIFFERENTIAL TRANSFORMER (LVDT)
C
      CRD=142.0
      DRD=20.164
      IF(VRDO.EQ.0) GO TO 3
      B=1.0-VRDO*VRDO/DRD
      B=SQRT(B)
      RDOO=RDO-CRD*(1.0-B)/VRDO
      GO TO 4
    3 RDOO=RDO
    4 IF(VRD.EQ.0) GO TO 1
      B=1.0-VRD*VRD/DRD
      B=ABS(B)
      B=SQRT(B)
      RD=RDOO+CRD*(1.0-B)/VRD
      GO TO 2
    1 RD=RDOO
    2 RETURN
      END
```

```
      SUBROUTINE FLOW(NFLOW,FMDP,PLINE,T,FLR1,FLR2)
C
C     DETERMINE THE MASS FLOW RATES IN BOTH AIR STREAMS
C
      DIMENSION NFLOW(2),FMDP(2),FLR1(2),FLR2(2),A(7),T(2),TLINE(2)
      DATA A/0.0,0.493,1.052,1.928,3.15,3.94,5.13/
      D=4.026
      FA=1.006
      FM=1.0
      PC=547.0
      PL=PLINE+14.696
      Z=1.000-0.02*PL/PC
C     CALCULATE FLOW RATES BASED ON CHOKED FLOW AT DISCS
      DO 1 I=1,2
      J=NFLOW(I)
      TLINE(I)=273.15+T(I)+(PLINE/14.696)*0.25
      FLR1(I)=A(J)*(PL/600.0)*(277.8/TLINE(I))**0.5
    1 CONTINUE
C     CALCULATE FLOW RATES BASED ON ORIFICE PLATES HAVING 1.00 INCH
C     ORIFICES AND MASS FLOW RATES BETWEEN 0.1 AND 3.0 LB/SEC
      DO 2 I=1,2
      FW2=2.702*PL/(TLINE(I)*Z)
      FW=SQRT(FW2)
      FHM2=FMDP(I)
      FHM=SQRT(FHM2)
      SO=0.0369
      FLR2(I)=0.099736*FA*D*D*FHM*FM*FW*SO
    2 CONTINUE
      RETURN
      END
```

```
      SUBROUTINE PROBE(KCX,P,VA,VAU,AO,RHO,L,OUT,J)
C
C     DETERMINE THE PROPERTIES OF THE FLOW AT THE POINT OF INTEREST
C     USING THE CALIBRATION COEFFICIENTS OF THE FIVE HOPE PROBE, THE
C     MEASURED PRESSURE AT EACH OF THE FIVE HOLES, THE DIFFERENTIAL
C     PRESSURE BETWEEN PORTS 1 AND 3 AND THE PROBE'S ANGULAR POSI-
C     TION VOLTAGE FROM THE POTENTIOMETER.
C
C     OUTPUT DATA FROM SUBROUTINE:
C          OUT(1) - FLOW ANGLE ALPHA
C          OUT(2) - FLOW ANGLE BETA
C          OUT(3) - TOTAL VELOCITY
C          OUT(4) - TOTAL PRESSURE
C          OUT(5) - STATIC PRESSURE
C          OUT(6) - AXIAL MOMENTUM FLUX
C          OUT(7) - ANGULAR MOMENTUM FLUX
C          OUT(8) - RADIAL/TOTAL VELOCITY RATIO
C          OUT(9) - TANGENTIAL/TOTAL VELOCITY RATIO
C          OUT(10)- AXIAL/TOTAL VELOCITY RATIO
C
      REAL KCX(15,4,2),MZ,MP
      DIMENSION P(6),OUT(10),R(15)
      RAD=57.296
      C=.00974074
      IF(L.EQ.1) WRITE(6,53)
      PS=0.25*(P(1)+P(2)+P(3)+P(4))
      CA=(P(3)-P(1))/(3.0*(P(5)-PS))
      ABSCA=ABS(CA)
C
C     IF THE MAGNITUDE OF PRESSURE COEFF CA IS LESS THAN 0.5,
C     THEN USE THE DIFFERENTIAL PRESSURE READING, P(6), AND
C     INCREASE THE ACCURACY OF THE CALCULATION.
C
      IF(ABSCA.LT.0.5) CA=-P(6)/(3.0*(P(5)-PS))
```

```
      CB=(P(2)-P(4))/(3.0*(P(5)-PS))
      ABSCB=ABS(CB)
C
C     IF THE MAGNITUDE OF PRESSURE COEFF CB IS GREATER THAN 1.0,
C     THE FLOW MEASUREMENT IS IN A SEVERE SHEAR FLOW ENVIRONMENT
C     AND TO STAY WITHIN THE CALIBRATION RANGE RESET THE MAGNITUDE
C     TO 0.5
C
      IF(ABSCB.GT.1.0) CB=(0.5*CB)/ABSCB
C
C     DETERMINE THE SET OF CALIBRATION COEFFICIENTS TO USE IN THE
C     CALCULATIONS BELOW
C
      J=1
      IF(CA.LT.-0.65) J=2
      IF(ABSCB.GT.0.4) J=1
C
C     CALCULATE CO, CQ, VV AND UV
C
      R( 1)=1.0
      R( 2)=CA
      R( 3)=CB
      R( 4)=CA*CA
      R( 5)=CA*CB
      R( 6)=CB*CB
      R( 7)=CA*CA*CA
      R( 8)=CA*CA*CB
      R( 9)=CA*CB*CB
      R(10)=CB*CB*CB
      R(11)=CA*CA*CA*CA
      R(12)=CA*CA*CA*CB
      R(13)=CA*CA*CB*CB
      R(14)=CA*CB*CB*CB
      R(15)=CB*CB*CB*CB
```

```
      CD=0.0
      CQ=0.0
      VV=0.0
      UV=0.0
      K=0
      DO 10 I=1,15
      CD=CD+KCX(I,1,J)*R(I)
      CQ=CQ+KCX(I,2,J)*R(I)
      VV=VV+KCX(I,3,J)*R(I)
      UV=UV+KCX(I,4,J)*R(I)
   10 CONTINUE
C
C     CALCULATE THE OTHER FLOW PROPERTIES
C
      VS=9273.6*(P(5)-PS)/(CQ*RHO)
      IF(VS.LT.0.0) K=1
      VS=ABS(VS)
      V=SQRT(VS)
      PT=P(5)+CD*(P(5)-PS)
      PS=P(5)-(1.0/CQ-CD)*(P(5)-PS)
      WRITE(6,52)(P(I),I=1,5),CD,CQ,VV,UV,CA,CB,L,J
      AUV=ABS(UV)
      IF(AUV.GT.1.0) WRITE(6,50) P(1),P(2),P(3),P(4),P(5),CD,CQ,VV,UV,L
      IF(AUV.GT.1.0) UV=UV/AUV
      BETA=ASIN(UV)-2./RAD
      UV=SIN(BETA)
      DUMB=VV/COS(BETA)
      ADU=ABS(DUMB)
      IF(ADU.GT.1.0) WRITE(6,51) P(1),P(2),P(3),P(4),P(5),CD,CQ,VV,UV,L
      IF(ADU.GT.1.0) DUMB=DUMB/ADU
      ALPHP=ASIN(DUMB)
      IF(VA.EQ.VAO) GO TO 11
      DALPHA=(VA-VAO)/C
      GO TO 12
```

```
11 DALPHA=0.0
12 CONTINUE
   ALPHA=(AU+DALPHA)/RAD+ALPHP
   VV=(SIN(ALPHA))*(COS(BETA))
   DUMA=1.0-UV*UV-VV*VV
   IF(DUMA.LT.0.0) K=2
   DUMA=ABS(DUMA)
   WV=SQRT(DUMA)
   OUT(1)=ALPHA*RAD
   ABSALP=ABS(OUT(1))
   IF(ABSALP.GT.90.0)WV=-WV
   MZ=PS+2.0*(PT-PS)*WV*WV
   MR=2.0*(PT-PS)*VV*WV
   OUT(2)=BETA*RAD
   OUT(3)=V
   OUT(4)=PT
   OUT(5)=PS
   OUT(6)=MZ
   OUT(7)=MR
   OUT(8)=UV
   OUT(9)=VV
   OUT(10)=WV
   ALPHP=ALPHP*RAD
   PALPHA=AU+DALPHA
   WRITE(6,52)(P(I),I=1,5),CU,CQ,VV,UV,CA,CB,L,K
   WRITE(6,52)ALPHP,DALPHA,PALPHA,OUT(1),OUT(2)
52 FORMAT(1X,11F10.5,2I5)
53 FORMAT(1H1,5X,2HP1,8X,2HP2,8X,2HP3,8X,2HP4,8X,2HP5,8X,2HCO,8X,
  *2HCQ,8X,2HVV,8X,2HUV,8X,2HCA,8X,2HCB,6X,1HL,4X,1HJ,/,5X,5HALPHP,
  *4X,6HDALPHA,4X,6HALPHAP,5X,5HALPHA,5X,4HBETA,/)
50 FORMAT(1X,9F9.5 , 3X,'ABS OF UV GT 1.0 ON SUBRUN NUMBER ',I3,)
51 FORMAT(1X,9F9.5 , 3X,'ABS OF DU GT 1.0 ON SUBRUN NUMBER ',I3,)
   RETURN
   END
```

```
      SUBROUTINE INTERGR(F,R,N,SUM)
C
C     INTERGRATE BETWEEN THE INNER RADIUS AND THE OUTER RADIUS OF
C     THE FLOW CHANNEL USING THE DATA POINT VALUE AT EACH RADIAL
C     POSITION
C
      DIMENSION F(N),R(N)
      SUM=0.0
      M=N-1
      DO 1 I=1,M
      SUM=SUM+0.5*((F(I+1)+F(I))*(R(I+1)-R(I)))
    1 CONTINUE
      RETURN
      END
```

P1 ALPHA	P2 SIGMA	P3 ALPHAP	P4 ALPHA	P5 BETA	C3	C2	VV	UV	C4	C4	I	J
[illegible]	[illegible]	.09[illegible]	.02535	.05592	.75643	.68866	-.47540	.06306	-.8[illegible]	-.12046	1	2
[illegible]	[illegible]	.04166	.03095	.06592	.75643	.68866	.43929	.06656	-.8[illegible]	-.12046	1	0
[illegible]	[illegible]	54.67[illegible]	[illegible]	.51555								
[illegible]	[illegible]	[illegible]	.04705	.07550	.13394	.61209	-.24650	.03373	-.[illegible]	-.11746	2	1
[illegible]	[illegible]	[illegible]	.07245	.07453	.13394	.61200	.11313	.00053	-.[illegible]	-.11746	2	0
[illegible]	[illegible]	[illegible]	30.47265	.05724								
[illegible]	[illegible]	[illegible]	.04415	.07139	.07392	.61191	-.11540	.02443	-.[illegible]	-.12071	3	1
[illegible]	[illegible]	[illegible]	.04419	.07139	.07092	.61191	.54524	-.00447	-.[illegible]	-.12071	3	0
[illegible]	[illegible]	51.56511	[illegible]	-.40[illegible]								
[illegible]	[illegible]	.02453	.04112	.07707	.04230	.62273	-.10469	.04211	-.26742	-.03079	4	1
[illegible]	[illegible]	.02459	.04112	.07707	.04230	.62273	.53786	.00722	-.26742	-.03079	4	0
[illegible]	[illegible]	[illegible].11416	44.90[illegible]	.41372								
[illegible]	[illegible]	.03111	.02036	.07354	.01506	.81667	-.02259	.05277	-.15[illegible]	-.04372	5	1
[illegible]	[illegible]	[illegible]	[illegible]	.07354	.01506	.81667	.56125	.02187	-.1[illegible]	-.04372	5	0
[illegible]	[illegible]	[illegible]	35.[illegible]	1.2[illegible]								
[illegible]	[illegible]	[illegible]	.01215	[illegible]	.00054	.7[illegible]	-.01[illegible]	.07417	-.1[illegible]	.01[illegible]	6	1
[illegible]	[illegible]	[illegible]	.01216	[illegible]	.00054	.7[illegible]	.01112	.03[illegible]	-.1[illegible]	.01[illegible]	6	0
[illegible]	[illegible]	[illegible]	37.[illegible]	2.2[illegible]								
[illegible]	[illegible]	.01[illegible]	.02404	.0529[illegible]	.01129	.07237	.04[illegible]	.04796	-.01[illegible]	.03637	7	1
[illegible]	[illegible]	.04251	[illegible]	.05251	.01129	.07237	.04149	.06319	-.01[illegible]	.03637	7	0
[illegible]	[illegible]	[illegible]	[illegible]	3.62271								
[illegible]	[illegible]	.02771	.01[illegible]	.05[illegible]	.01601	.59616	.05321	.10969	.03[illegible]	[illegible]	8	1
[illegible]	[illegible]	[illegible]	[illegible]	.04352	.01501	.59316	.07559	.07476	.00[illegible]	[illegible]	8	0
[illegible]	[illegible]	[illegible]	[illegible]	4.25770								
[illegible]	[illegible]	[illegible]	.03122	.05116	.00570	.4[illegible]	.02734	.12[illegible]	[illegible]	.15657	9	1
[illegible]	[illegible]	[illegible]	[illegible]	.09[illegible]	.00570	[illegible]	.72[illegible]	.06[illegible]	[illegible]	.15657	9	0
[illegible]	[illegible]	[illegible]	[illegible]	[illegible]								
[illegible]	[illegible]	.01721	[illegible]	.03305	.01275	.41955	.01[illegible]	.14223	-.01[illegible]	.22[illegible]	10	1
[illegible]	[illegible]	.31725	.03457	.03[illegible]	.01276	.41[illegible]	.77[illegible]	.10600	-.01324	.22556	10	0
[illegible]	[illegible]	[illegible].54225	21.1776[illegible]	4.20028								
[illegible]	[illegible]	.03[illegible]	[illegible]	.02146	.02394	.42076	.07173	.15174	.01135	.29323	11	1
[illegible]	[illegible]	[illegible]	[illegible]	.02446	.02394	.42076	.03308	.11715	.01135	.29323	11	0
[illegible]	[illegible]	[illegible]	[illegible]	4.72772								
[illegible]	[illegible]	.01[illegible]	[illegible]	.02416	.04633	.44466	[illegible]	.10284	-.00[illegible]	.31903	12	1
[illegible]	[illegible]	[illegible]	[illegible]	.02416	.04333	.44476	.59927	.12431	-.00[illegible]	.31903	12	0
[illegible]	[illegible]	60.7[illegible]	[illegible]	7.37192								
[illegible]	[illegible]	[illegible]	[illegible]	.01703	.02139	.41562	.06929	.14[illegible]	.01[illegible]	.24741	13	1
[illegible]	[illegible]	[illegible]	.07002	.01503	.02139	.41565	.94[illegible]	.11926	.01[illegible]	.24741	13	0
[illegible]	[illegible]	[illegible]	72.6[illegible]	5.61772								
[illegible]	[illegible]	[illegible]	-.[illegible]	.01635	.00115	.44753	.04711	.13225	.01[illegible]	.23301	14	1
[illegible]	[illegible]	[illegible]	-.[illegible]	.0[illegible]	.00115	.44753	.96[illegible]	.04756	.01127	.23301	14	0
[illegible]	[illegible]	7[illegible]	[illegible]	[illegible]								
[illegible]	[illegible]	[illegible]	.00030	.04473	.00534	.54605	.01444	.11155	.01[illegible]	.16[illegible]	15	1
[illegible]	[illegible]	[illegible]	[illegible]	.01473	.00534	.54606	.99546	.0[illegible]	.01[illegible]	.1[illegible]	15	0
[illegible]	[illegible]	33.7[illegible]	67.1[illegible]	4.64132								
[illegible]	[illegible]	[illegible]	.03021	.01366	.01130	[illegible]	.01[illegible]	.10569	-.00[illegible]	.12[illegible]	16	1
[illegible]	[illegible]	[illegible]	[illegible]	.01366	.01130	[illegible]	.99536	.07112	-.00[illegible]	.12453	16	0
[illegible]	[illegible]	[illegible]	[illegible]	[illegible]								
[illegible]	[illegible]	[illegible]	[illegible]	.01154	.01175	.6[illegible]	.64312	.0[illegible]	-.00237	.09522	17	1
[illegible]	[illegible]	[illegible]	[illegible]	.01154	.01171	.6[illegible]	.96[illegible]	.0[illegible]	-.00237	.09522	17	0
[illegible]	[illegible]	[illegible]	[illegible]	3.[illegible]								
[illegible]	[illegible]	.00766	.00026	.01062	.00603	.72779	.13[illegible]	.05[illegible]	.12292	.07746	18	1
[illegible]	[illegible]	.00250	.00026	.01062	.00603	.72779	.96693	.05556	.12292	.07746	18	0
[illegible]	[illegible]	[illegible]	105.[illegible]	[illegible].37021								
[illegible]	[illegible]	.00[illegible]	-.00531	.00724	.05565	.77196	.22560	.07432	.01[illegible]	.06376	19	1
[illegible]	[illegible]	.00461	-.00531	.00724	.05565	.77196	.92041	.06967	.01[illegible]	.06376	19	0

Table E-3 Output for Run #61

************************ INPUT DATA FOR RUN ***************************

RUN NUMBER = 61 DATE: 07 5/81

TEST CONFIG = 3 ORIFICE SIZE: 3/1 SWIRL VANE SETTING = 45
PATM = 30.00 IN HG PLINE = 500. PSIG

NO OF PRESS TAPS:	TOTAL = 68	READINGS AT:	START	END
	4 TUBE = 25	TIME	11:57	12:37
	6 TUBE = 18	ROOM TEMP	20.0	20.2 C
	8 TUBE = 25	TANK PRESS	950.	650. PSIG

OBS	TIME	PHOLE	PTANK	PLINE	FR1	FR2	TI	TO	PTI	PTO
1	1157	.07[illegible]	713.	503.	75.5	3.5	5.94	21.56	.03523	-.00303
2	1159	.0500710	744.	501.	77.9	3.4	6.10	21.34	.03456	-.00369
3	1201	.0037[illegible]	766.	500.	72.8	3.4	6.06	21.25	.03503	-.00349
4	1203	[illegible]	756.	499.	72.1	3.2	5.90	21.20	.03533	-.00245
5	1205	[illegible]	[illegible]	499.	72.6	3.1	5.74	21.14	.03497	-.00349
6	1207	[illegible]	[illegible]	498.	71.5	3.0	5.54	21.14	.03462	-.00365
7	1210	[illegible]	[illegible]	497.	71.4	3.0	5.41	21.23	.03513	-.00321
8	1212	[illegible]	687.	497.	71.4	3.0	5.23	21.12	.03426	-.00363
9	1214	[illegible]	[illegible]	496.	70.7	2.9	5.06	21.16	.03421	-.00410
10	1216	.0007773	667.	496.	71.7	2.8	4.65	21.25	.03441	-.00328
11	1218	-.0009120	619.	499.	71.7	2.9	3.65	21.56	.03544	-.00292
12	1220	.0002116	755.	501.	77.7	2.9	2.69	21.45	.03518	-.00292
13	1222	[illegible]	697.	503.	76.7	3.0	2.42	21.56	.03544	-.00200
14	1225	[illegible]	[illegible]	505.	71.5	3.3	2.27	21.46	.03605	-.00231
15	1227	[illegible]	[illegible]	504.	72.1	3.4	3.16	21.46	.03554	-.00308
16	1229	[illegible]	702.	503.	74.1	3.6	4.55	21.36	.03503	-.00297
17	1231	[illegible]	[illegible]	502.	75.7	3.7	5.29	21.22	.03492	-.00262
18	1234	-.0031972	754.	501.	77.3	3.6	5.54	21.27	.03492	-.00333
19	1236	-.00[illegible]	771.	500.	71.5	3.6	5.59	21.39	.03467	-.00226

STATIC PRESSURE VS POSITION

4 INCH TUBE Z	PRESS	6 INCH TUBE Z	THETA	PRESS	8 INCH TUBE Z	PRESS	AVG 6 IN TUBE Z	PRESS
.13	-.04623							
.25	-.04468							
.38	-.04357							
.50	-.03710							
.75	-.03909							
1.00	-.03112							
1.25	-.03033							
2.25	-.01826							
3.25	-.01655							
4.25	-.01723							
5.25	-.01469							
6.25	-.00604							
8.25	.00327							
14.25	.00747							
16.25	.00719							
18.25	.00719							
20.25	.00671							
22.25	.00654							
24.25	.00640							
26.25	.00737							
28.25	.00724							
30.25	.00721							
34.25	.00557							
36.25	.00760							
40.25	.00677							
		0	90.0	-.01346				
		-.10	70.0	-.01486				
		-.25	50.0	-.01118				
		-.50	30.0	-.01065				
		-1.00	10.0	-.01156				
		-2.00	350.0	-.01145				
		0	330.0	-.01213				
		-.10	310.0	-.01216				
		-.25	290.0	-.01029				
		-.50	270.0	-.00930				
		-1.00	250.0	-.00927				
		-2.00	230.0	-.00947				
		0	210.0	-.01276				
		-.10	190.0	-.01241				
		-.25	170.0	-.00878				
		-.50	150.0	-.01264				
		-1.00	130.0	-.00993				
		-2.00	110.0	-.00980				
							0	-.01279
							-.10	-.01326
							-.25	-.01009
							-.50	-.01046
							-1.00	-.01026
							-2.00	-.00991

****************** STATIC PRESSURE VS POSITION ********************

4 INCH TUBE Z	4 INCH TUBE PRESS	6 INCH TUBE Z	6 INCH TUBE THETA	6 INCH TUBE PRESS	8 INCH TUBE Z	8 INCH TUBE PRESS	AVG 6 IN TUBE Z	AVG 6 IN TUBE PRESS
					1.00	-.00184		
					3.00	.01610		
					5.00	.01846		
					6.25	.02252		
					6.25	.01948		
					9.38	.03356		
					11.38	.03442		
					13.38	.03524		
					15.38	.03535		
					17.38	.03514		
					19.38	.03491		
					21.38	.03459		
					23.38	.03394		
					25.38	.03368		
					27.38	.03324		
					31.38	.03289		
					33.38	.03250		
					35.38	.03163		
					37.38	.03151		
					39.38	.03094		
					41.38	.03061		
					43.38	.03019		
					45.38	.03049		
					47.38	.03008		
					49.38	.02651		

************************ OUTPUT DATA FOR RUN NO. 61 ************************

SUB RUN NO	PROBE POSITION RADIAL (INCH)	AXIAL (INCH)	VELOCITY MAGNITUDE AND DIRECTION ALPHA (DEG)	BETA (DEG)	VELOCITY (FT/SEC)	U/V	V/V	W/V	J
1	3.86	6.25	26.06	.51	72.2393	.009	.439	.898	2
2	3.79	6.25	30.87	.05	70.6470	.001	.513	.858	1
3	3.68	6.25	33.05	-.49	71.7140	-.008	.545	.838	1
4	3.58	6.25	33.91	.41	71.4945	.007	.556	.830	1
5	3.49	6.25	35.55	1.25	70.6430	.022	.581	.813	1
6	3.39	6.25	37.76	2.25	70.3434	.039	.612	.790	1
7	3.28	6.25	40.63	3.62	73.8246	.063	.642	.764	1
8	3.18	6.25	42.60	4.30	73.7455	.075	.676	.733	1
9	3.08	6.25	46.46	5.06	75.7947	.088	.722	.666	1
10	2.98	6.25	51.18	6.20	73.6856	.108	.775	.623	1
11	2.88	6.25	57.08	6.73	67.5727	.117	.834	.540	1
12	2.79	6.25	64.37	7.37	60.0601	.128	.894	.429	1
13	2.69	6.25	72.03	6.62	58.7559	.115	.945	.306	1
14	2.59	6.25	80.06	5.60	54.9526	.096	.960	.173	1
15	2.49	6.25	87.14	4.64	48.5535	.081	.995	.050	1
16	2.39	6.25	93.73	4.06	44.4620	.071	.995	-.065	1
17	2.29	6.25	99.63	3.57	41.7366	.062	.966	-.157	1
18	2.20	6.25	104.45	3.08	37.2794	.054	.967	-.249	1
19	2.12	6.25	111.70	2.26	32.9377	.039	.928	-.369	1

****************** OUTPUT DATA FOR RUN NO. 61 ********************

SUB RUN NO	PRESSURES TOTAL (PSI)	STATIC (PSI)	MOMENTUM AXIAL (PSI)	TANGTL (PSI)	FLOW RATES (LBM/SEC) DISC 1	DISC 2	URFP 1	ORFP 2	VELAVG	POAVG
1	.08819	.04352	.1156	.0353	.891	0	1.160	.245	102.93	.09077
2	.08297	.04028	.1032	.0375	.859	0	1.177	.240	102.72	.09034
3	.08121	.03721	.0990	.0402	.887	0	1.137	.239	102.53	.09003
4	.07659	.03433	.0751	.0405	.886	0	1.130	.231	102.31	.08470
5	.07421	.03146	.0580	.0404	.885	0	1.134	.227	102.12	.08941
6	.06906	.02665	.0796	.0410	.864	0	1.125	.224	101.94	.08915
7	.06328	.01652	.0711	.0459	.883	0	1.123	.224	101.78	.08892
8	.05356	.00719	.0574	.0462	.882	0	1.123	.223	101.63	.08571
9	.04530	-.00402	.0424	.0439	.881	0	1.118	.219	101.48	.08851
10	[illegible]	-.01095	.0257	.0450	.862	0	1.126	.218	101.44	.08850
11	.02[illegible]	-.01[illegible]	.0124	.0394	.866	0	1.131	.220	101.75	.08937
12	.02372	-.00750	.0045	.0280	.893	0	1.181	.221	102.02	.09017
13	.01930	-.01003	-.0050	.0173	.896	0	1.143	.227	102.35	.09069
14	.01632	-.00966	-.0083	.0089	.901	0	1.137	.236	102.68	.09154
15	.01488	-.00550	-.0054	.0020	.899	0	1.141	.240	102.75	.09136
16	.01319	-.00377	-.0036	-.0022	.894	0	1.153	.246	102.76	.09096
17	.01206	-.00238	-.0022	-.0040	.891	0	1.153	.249	102.71	.09058
18	.01004	-.00[illegible]	-.0003	-.0057	.857	0	1.173	.247	102.51	.09016
19	.00705	-.00165	.0009	-.0064	.887	0	1.127	.245	102.34	.08984

WL	WZ	XD	TI	MR	WV	VL	XI	FT	PAI	I	J
-.2094.59E-01	-.164556E-01	.200000E+01	0				0		0	1	20
.1..2.4E-02	.685442E-03	.212359E+01	-.135450E-01	-.637835E-02	-.369459E+00	.329377E+02	-.258422E+02	.764585E-02	-.197568E+00	2	19
-.750..9..E-03	-.346..0E-03	.219634E+01	-.126153E-01	-.574376E-02	-.249319E+00	.372794E+02	-.204137E+02	.100854E-01	-.205661E+00	3	18
-.49..90E-02	-.2..12..E-02	.229211E+01	-.105742E-01	-.401330E-02	-.156566E+00	.417388E+02	-.149786E+02	.120624E-01	-.180679E+00	4	17
-.[illegible]E-02	-.362290E-02	.235757E+01	-.522[illegible]E-02	-.218846E-02	-.648185E-01	.444020E+02	-.[illegible]E+01	.131947E-01	-.906726E-01	5	16
-.13..E-01	-.5..9..7E-02	.24905.E+01	.502990E-02	.201956E-02	.497659E-01	.485.35E+02	.661[illegible]E+01	.148[illegible]E-01	.8[illegible]97E-01	6	15
-.21...7E-01	-.[illegible]27E-02	.259019E+01	.230053E-01	.883187E-02	.172768E+00	.549826E+02	.246072E+02	.163590E-01	.402151E+00	7	14
-.1347.0E-01	-.[illegible]112..E-02	.266674E+01	.466640E-01	.173330E-01	.306463E+00	.567559E+02	.464147E+02	.157[illegible]E-01	.934[illegible]E+00	8	13
.111[illegible]E-01	.3969.0.E-02	.2787..E+01	.667606E-01	.239528E-01	.428957E+00	.600661E+02	.710136E+02	.2.723..E-01	.170[illegible]E+01	9	12
.3..037E-01	.1241..E-01	.286453E+01	.102214E+00	.354..3E-01	.539679E+00	.675727E+02	.105192E+03	.2..530E-01	.303.1.E+01	10	11
.766559E-01	.259929E-01	.298.3..E+01	.134389E+00	.450434E-01	.623241E+00	.736855E+02	.137016E+03	.361037E-01	.494079E+01	11	10
.13..[illegible]E+00	.423..3E-01	.308271E+01	.150665E+00	.460744E-01	.685531E+00	.757347E+02	.160255E+03	.453000E-01	.725959E+01	12	9
.1.2..9.E+00	.573..7E-01	.319345E+01	.147233E+00	.462493E-01	.733257E+00	.737455E+02	.172170E+03	.5.65.93E-01	.937294E+01	13	8
.2335..E+00	.711..6E-01	.32[illegible]E+01	.150522E+00	.45[illegible]E-01	.754159E+00	.736246E+02	.185315E+03	.6.2.3..E-01	.117237E+02	14	7
.2.9..9E+00	.7955..E-01	.335.87.E+01	.13.6.9.E+00	.410106E-01	.769784E+00	.703434E+02	.1.1161E+03	.6.9.613E-01	.129947E+02	15	6
.307...E+00	.6[illegible]E-01	.3487..E+01	.14097.E+00	.404229E-01	.815433E+00	.706430E+02	.200402E+03	.7.2.3.6E-01	.148716E+02	16	5
.3...E+00	.9.112..E-01	.3.6..3E+01	.14.245E+00	.40.1.9E-01	.829408E+00	.714946E+02	.212689E+03	.765937E-01	.1.7..60E+02	17	4
.3...5..E+00	.99.374E-01	.358230E+01	.148100E+00	.402226E-01	.858213E+00	.717140E+02	.221331E+03	.812076E-01	.179736E+02	18	3
.2901.4E+00	.103..6E+00	.378079E+01	.142168E+00	.376080E-01	.856313E+00	.706470E+02	.229256E+03	.829740E-01	.190223E+02	19	2
.44.031E+00	.1155.9E+00	.38336.E+01	.135506E+00	.352540E-01	.896303E+00	.722393E+02	.251623E+03	.851864E-01	.222074E+02	20	1
.774.73E-01	.194016E-01	.400000E+01	0				0		0	21	0

W = .27931066 T = .1643c281 S = .14713260 WAVG - 36.0461 PTM = .06651732

417

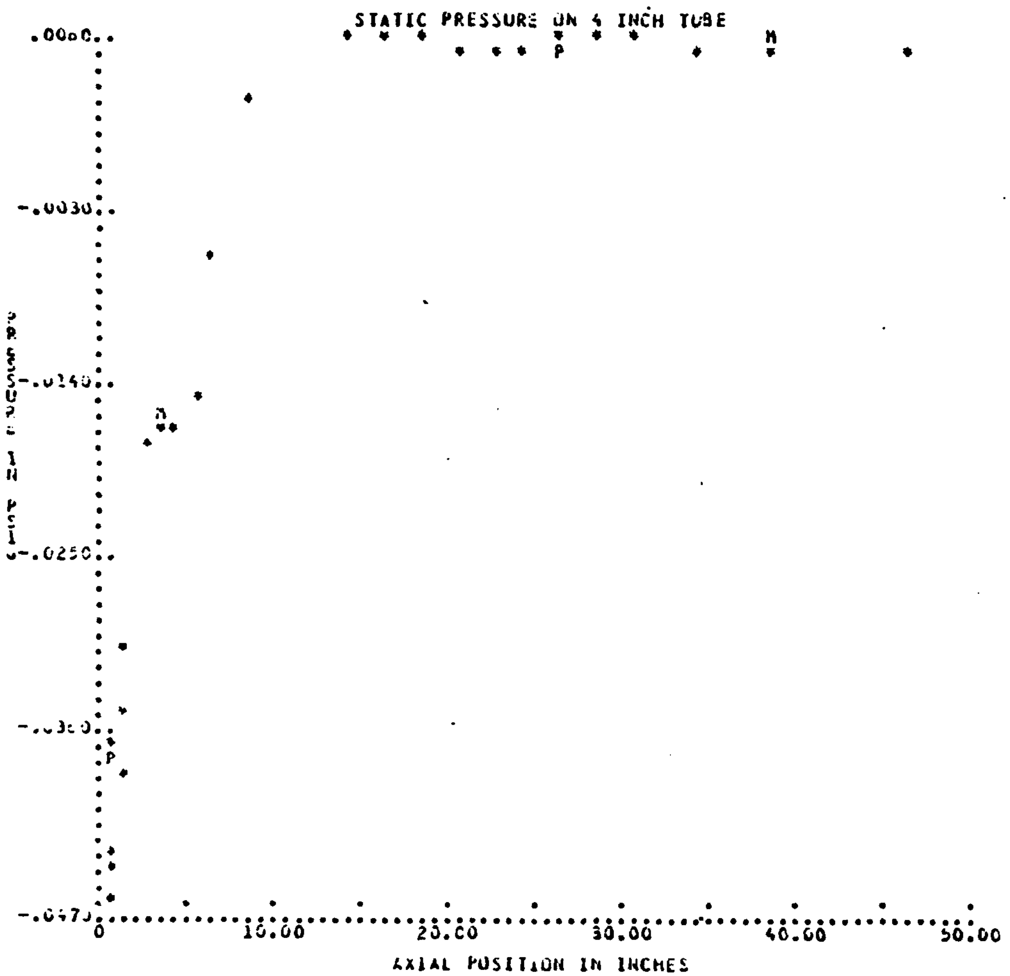
STATIC PRESSURE ON 4 INCH TUBE
PRESSURE IN PSIG
.0080
-.0030
-.0140
-.0250
-.0360
-.0470
0
10.00
20.00
30.00
40.00
50.00
AXIAL POSITION IN INCHES

STATIC PRESSURE ON 6 INCH TUBE

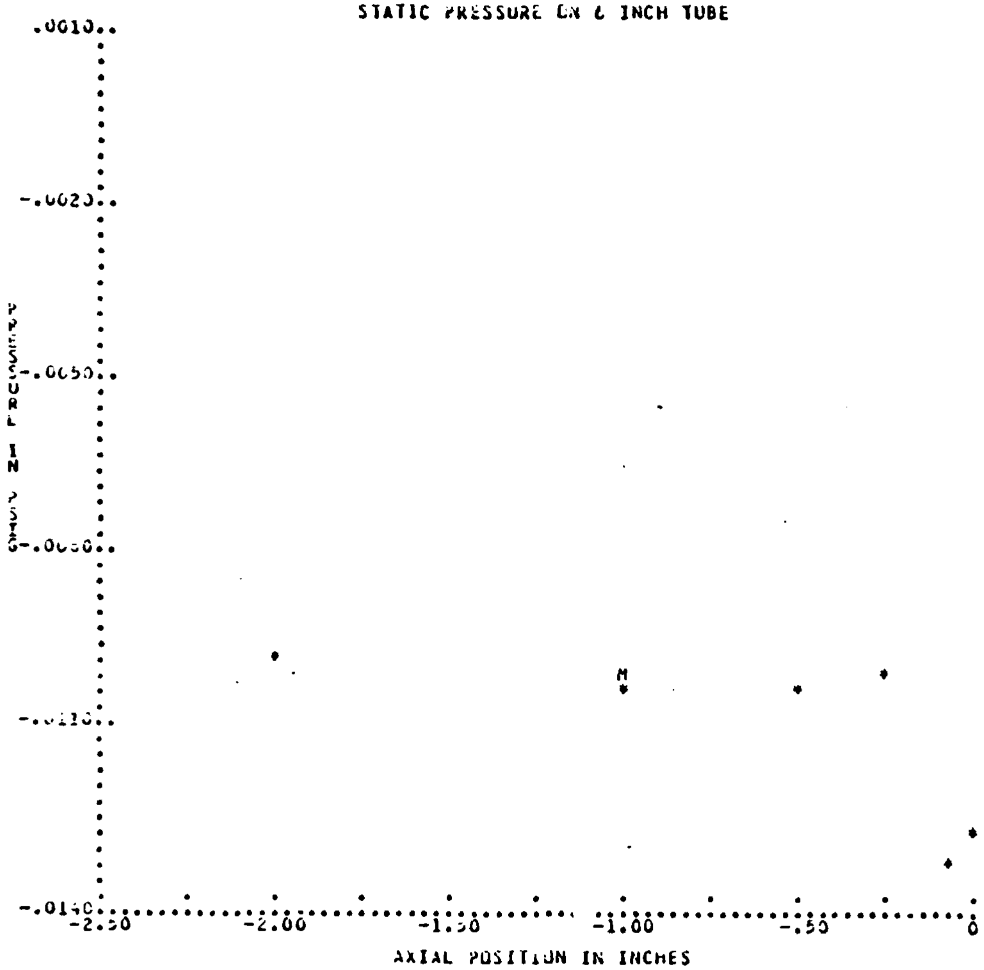

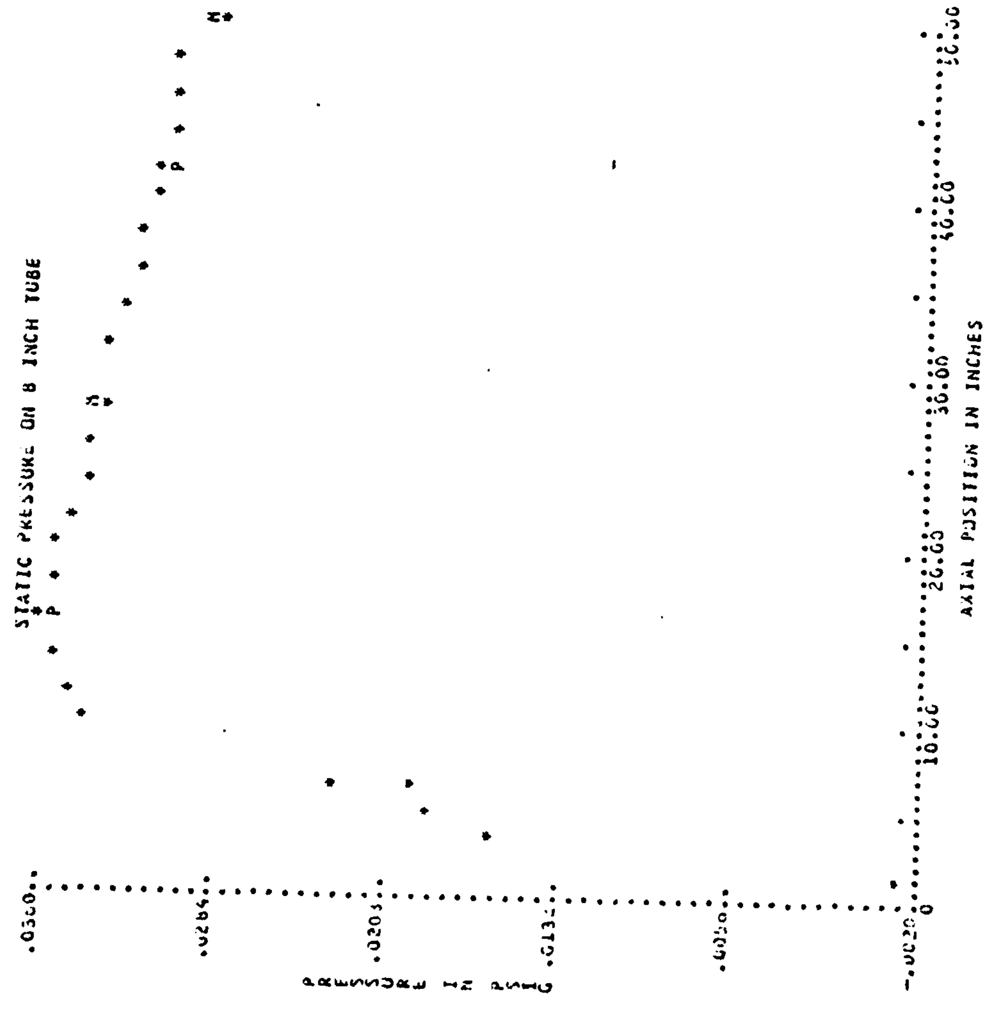
STATIC PRESSURE ON 8 INCH TUBE
AXIAL POSITION IN INCHES
10.00
20.00
30.00
40.00
50.00

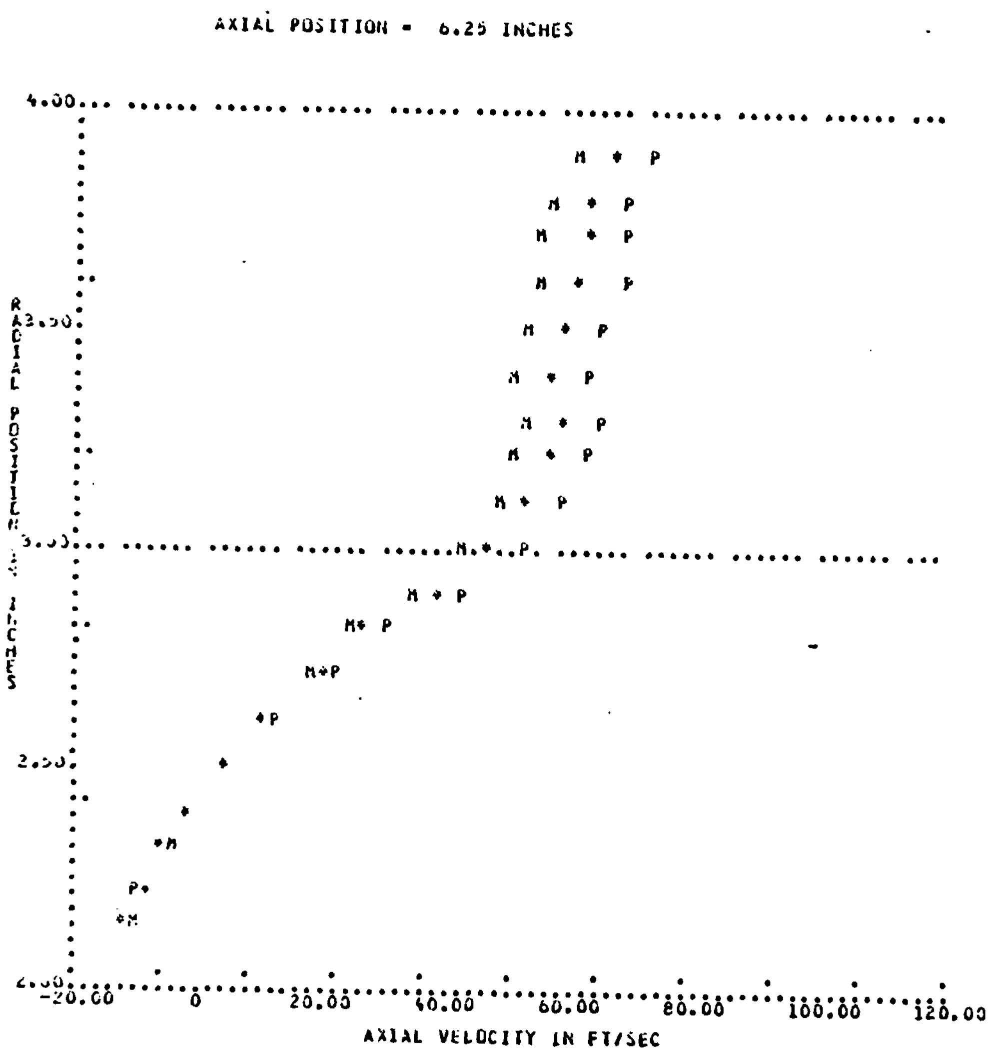
AXIAL POSITION = 6.25 INCHES
RADIAL POSITION IN INCHES
4.00
3.50
3.00
2.50
2.00
-20.00
0
20.00
40.00
60.00
80.00
100.00
120.00
AXIAL VELOCITY IN FT/SEC

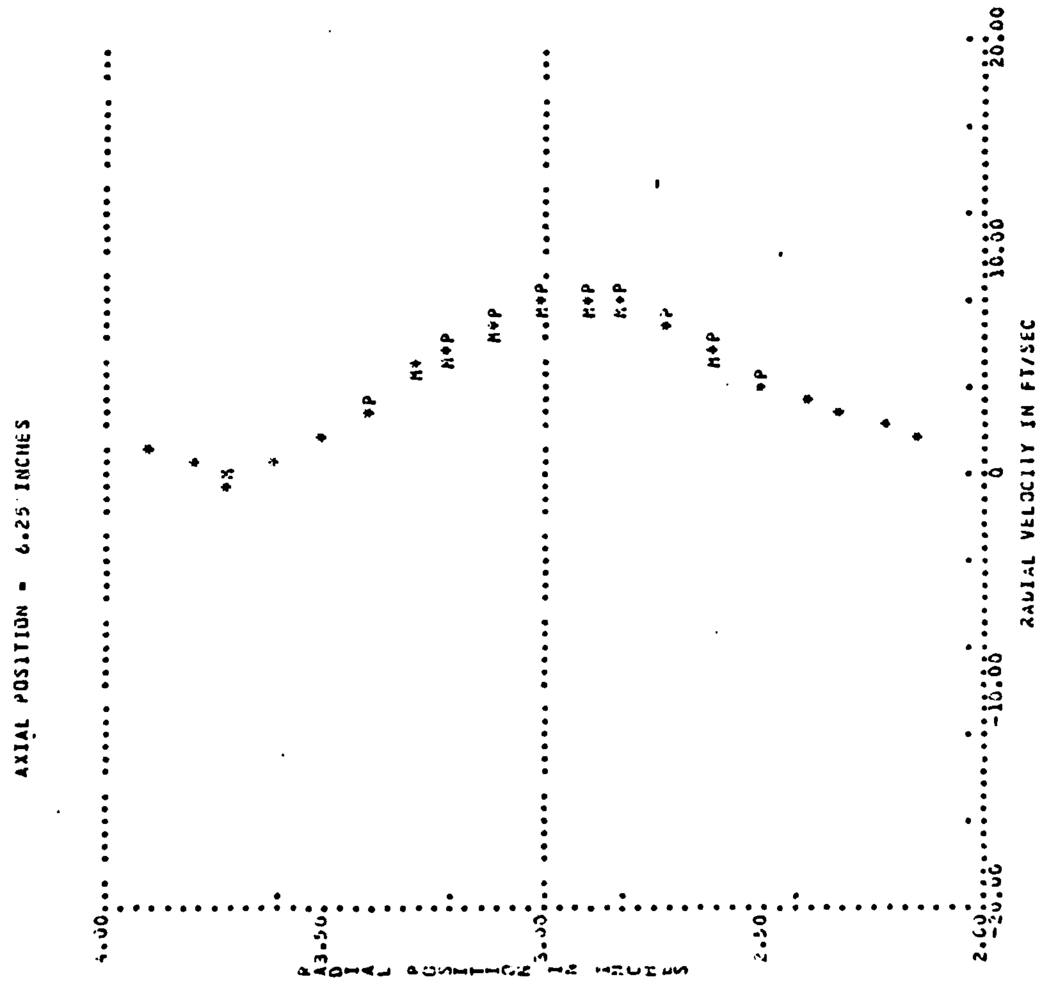
AXIAL POSITION = 6.25 INCHES
RADIAL VELOCITY IN FT/SEC
-20.00
-10.00
0
10.00
20.00
4.00
3.50
3.00
2.50
2.00

AXIAL POSITION = 6.25 INCHES

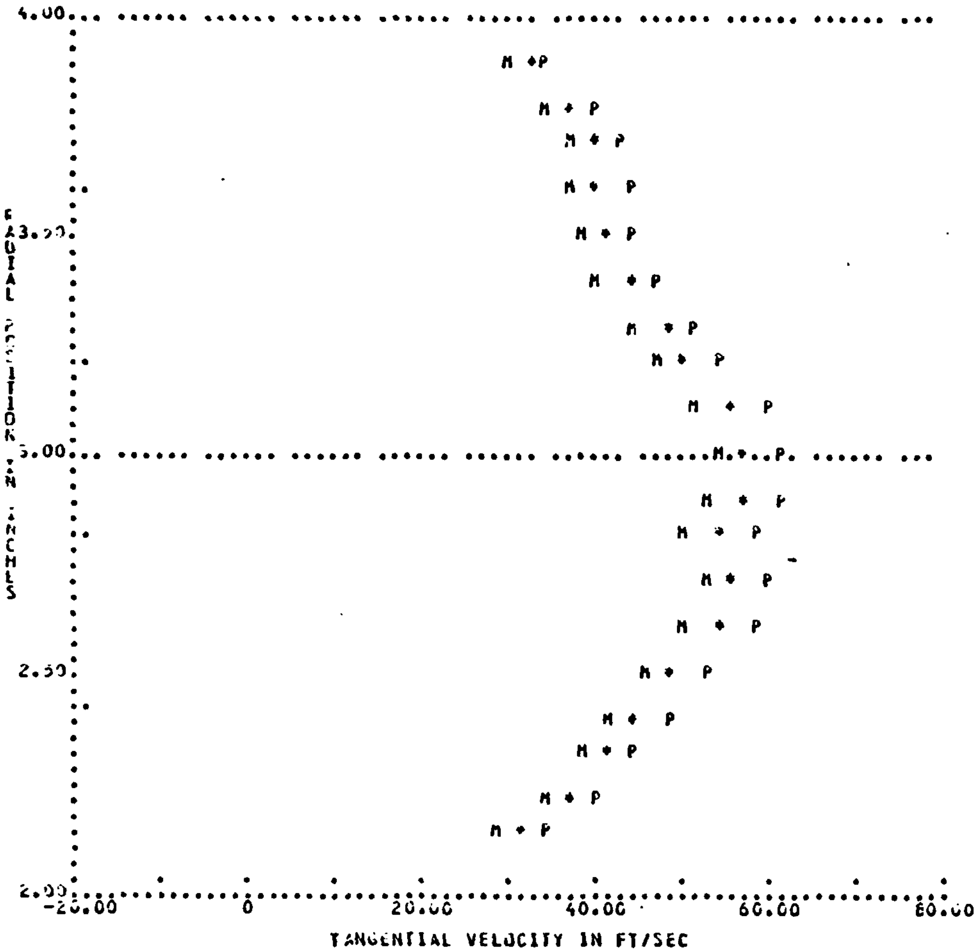

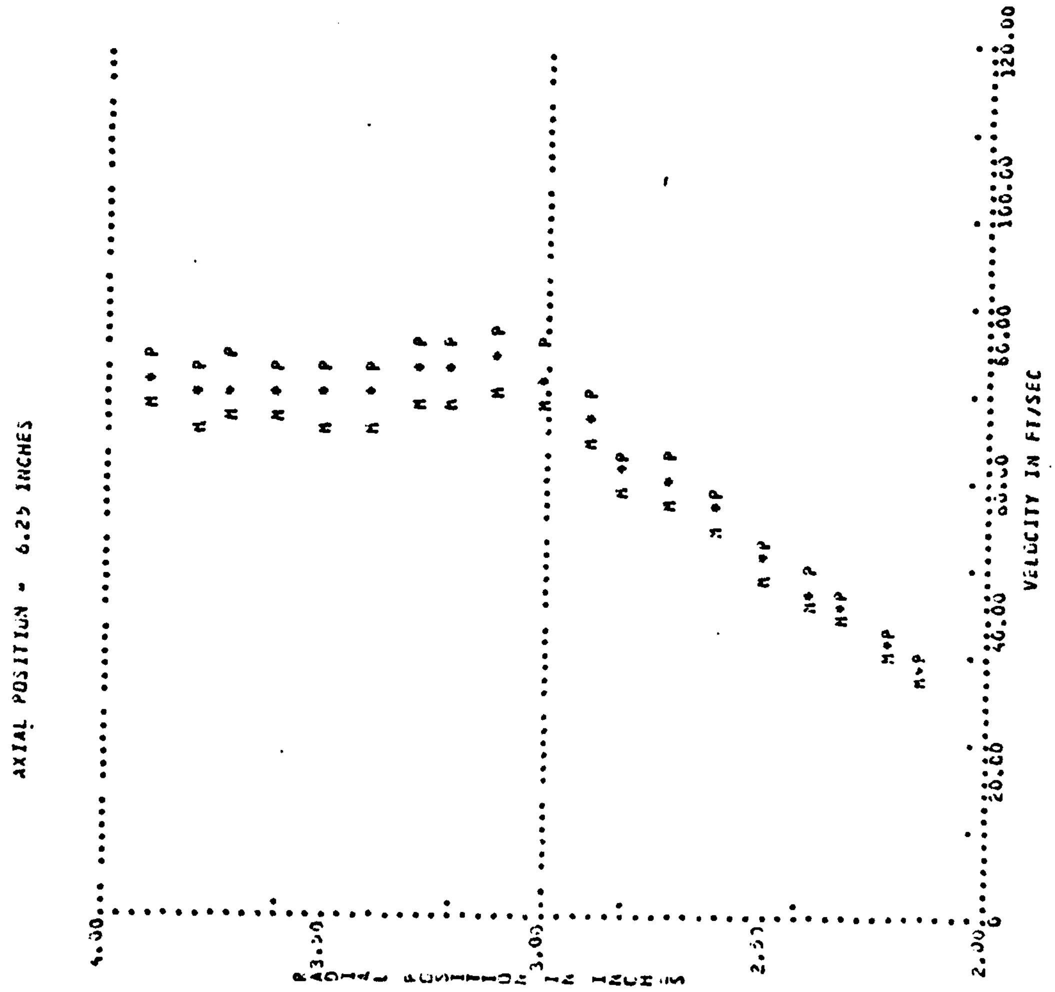
AXIAL POSITION = 6.25 INCHES
RADIAL POSITION IN INCHES
4.00
3.50
3.00
2.50
2.00
VELOCITY IN FT/SEC
0
20.00
40.00
60.00
80.00
100.00
120.00

AXIAL POSITION = 6.25 INCHES

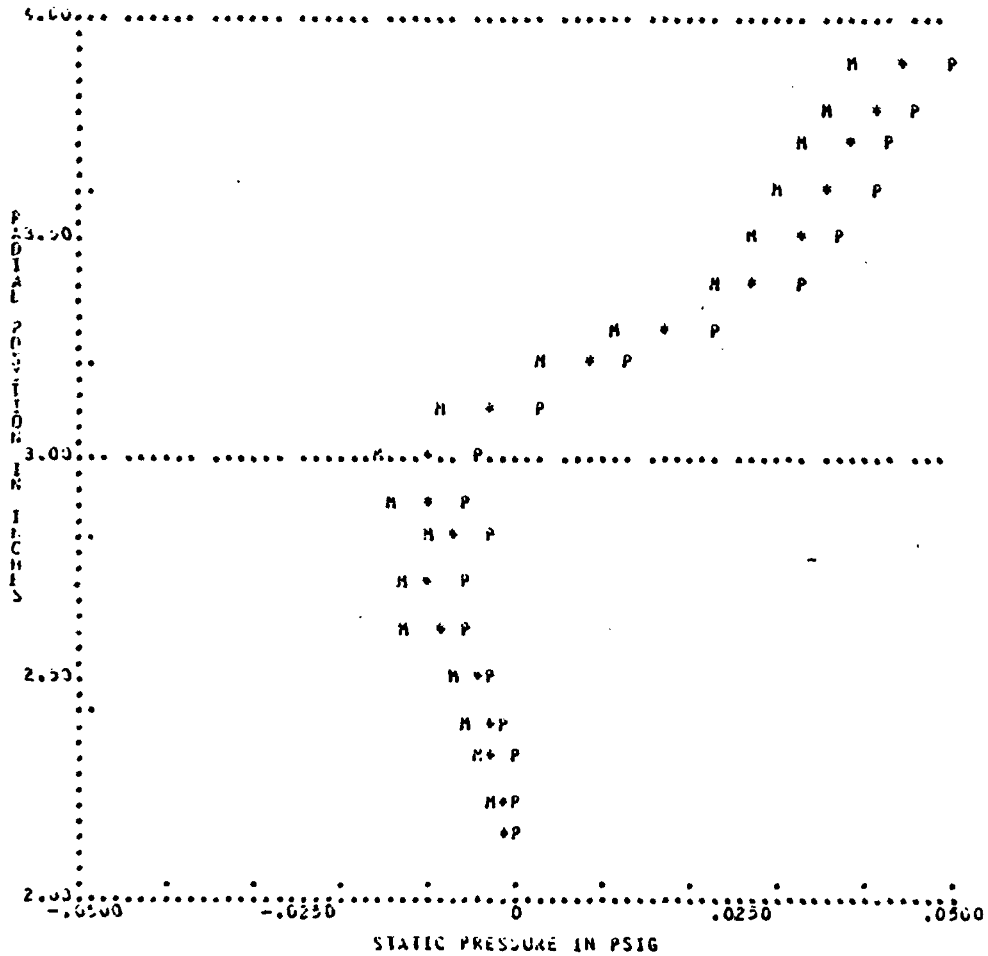

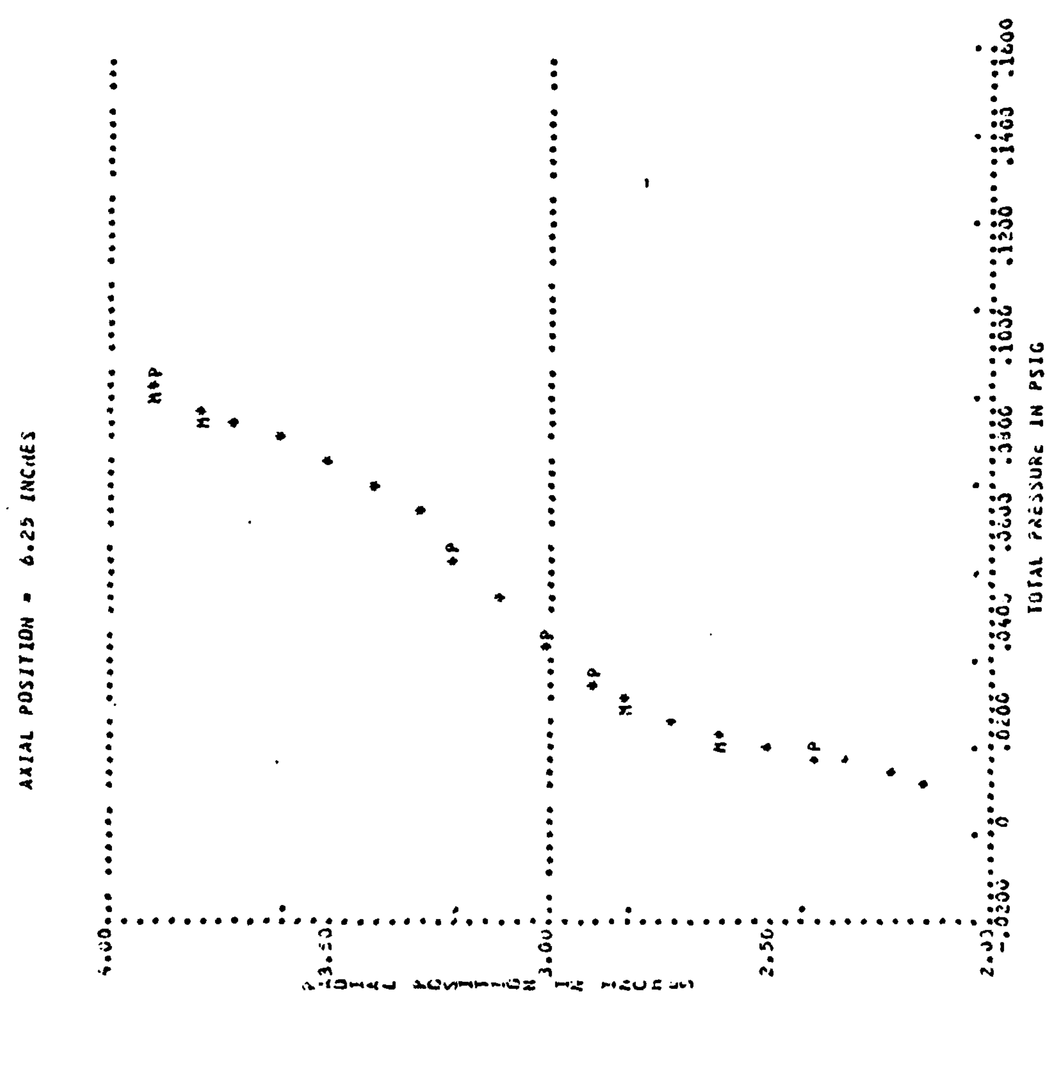
AXIAL POSITION = 6.25 INCHES
TOTAL PRESSURE IN PSIG

AXIAL POSITION = 6.25 INCHES

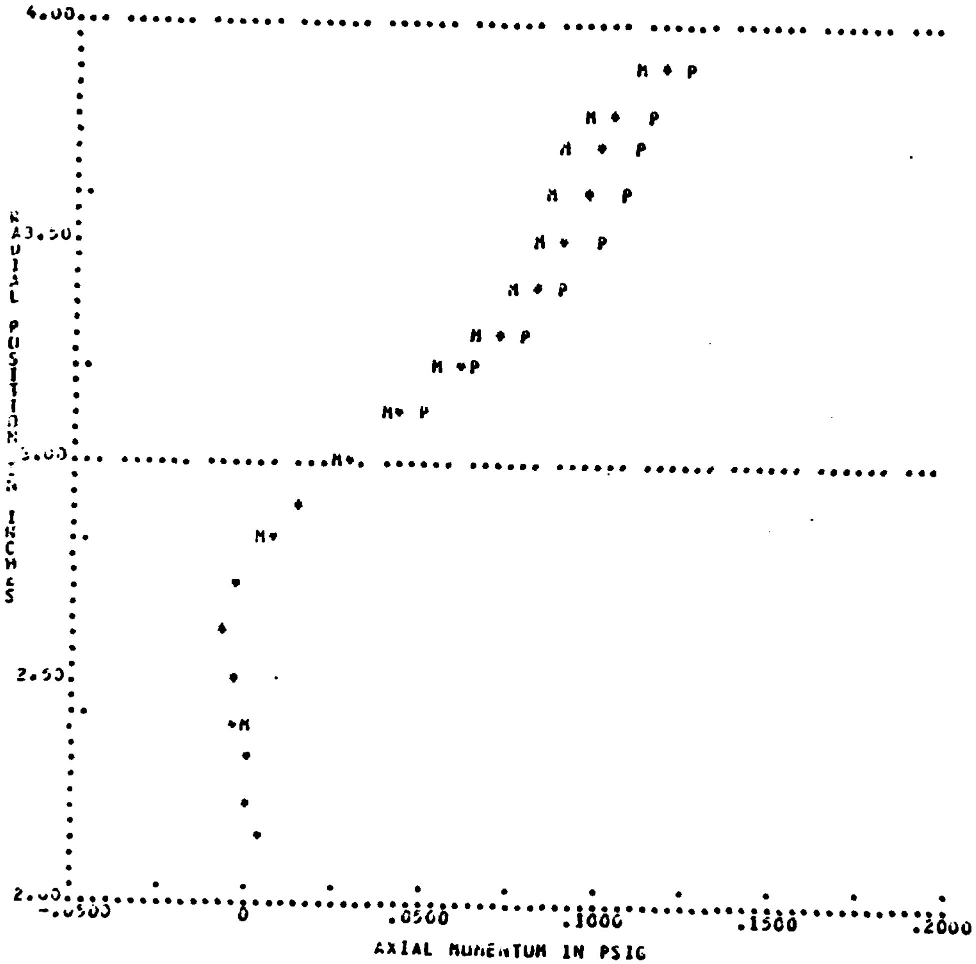

AXIAL POSITION = 6.25 INCHES

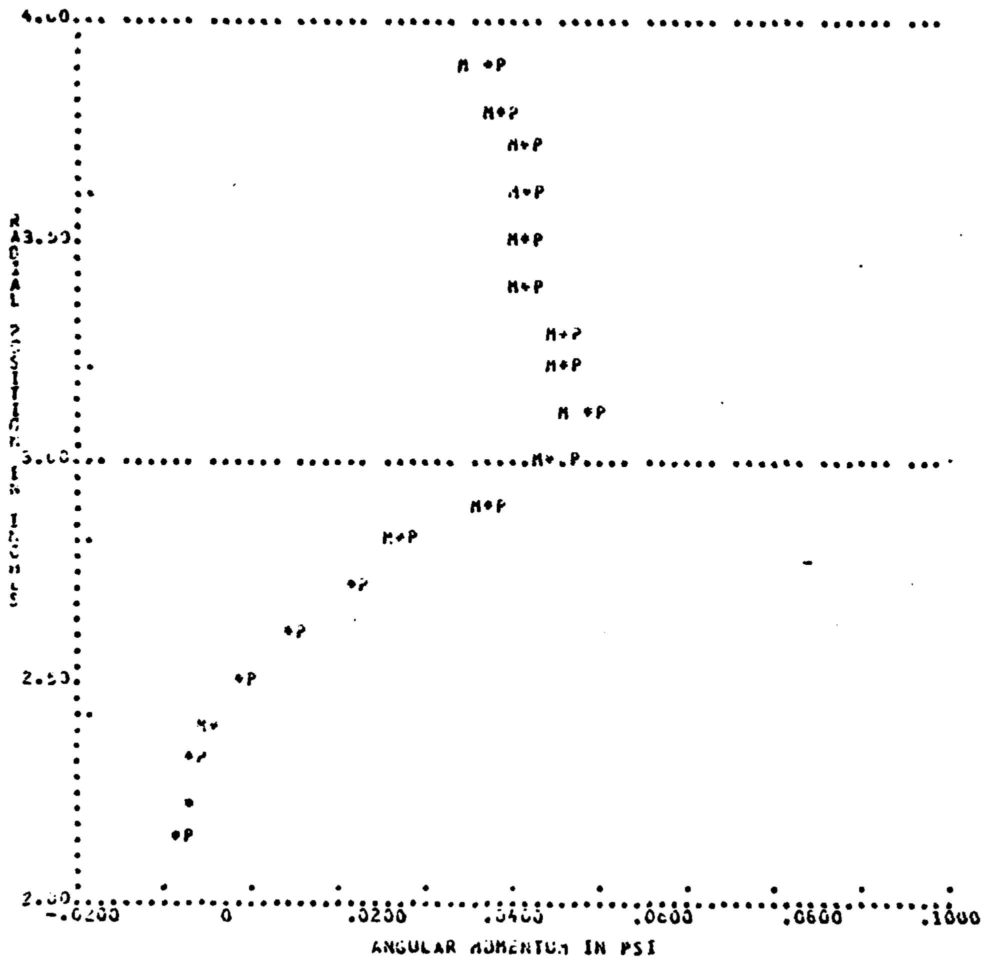

APPENDIX F

EXPERIMENTAL DATA PLOTTING PROGRAM - "PLDATA"

This appendix contains a listing of the computer program PLDATA developed to plot the results from the program DATAR4 for the thirty-six runs in the fourth set of experiments. Table F-1 is a listing of the variables used in this computer program.

TABLE F-1

Variables Used in Program "PLDATA"

A. INPUT VARIABLES

1. From File ONAME (INPXXX.DAT)

NN	- Number of input data files
FNAME	- Name of input data file (PLTXXX.DAT)
N1(I)	- Number of data files for plot I = 1, Static pressure on 4" tube I = 2, Static pressure on 6" tube I = 3, Static pressure on 8" tube I = 4, Axial velocity I = 5, Radial velocity I = 6, Tangential velocity I = 7, Total velocity I = 8, Static pressure I = 9, Total velocity I = 10, Tangential momentum I = 11, Axial momentum
N2	- Number of last plot requested, I
PLIMIT(1)	- Lower limit on X axis
PLIMIT(2)	- Upper limit on X axis
PLIMIT(3)	- Lower limit on Y axis
PLIMIT(4)	- Upper limit on Y axis
ND(1)	- Number of divisions on X axis
ND(2)	- Number of divisions on y axis

2. From File FNAME (PLTXXX.DAT)

NSRUNS(II)	- Number of subruns in file FNAME
N(II,1)	- Number of data points for static pressure on 4" tube
NPA(II)	- Number of data points for static pressure on 6" tube
N(II,3)	- Number of data points for static pressure on 8" tube
ZS4(II,J)	- Axial location on 4" tube, J = 1 to N(II,1)
PS4(II,J)	- Static pressure on 4" tube, J = 1 to N(II,1)
ZS6A(II,J)	- Axial location on 6" tube, J = 1 to NPA(II)
PS6A(II,J)	- Static pressure on 6" tube, J = 1 to NPA(II)
ZS8(II,J)	- Axial location on 8" tube, J = 1 to N(II,3)
PS8(II,J)	- Static pressure on 8" tube, J = 1 to N(II,3)

For each data point I, I = 1 to NSRUNS(II)

```
RADIAL(II,I) - Radial location
VEL(II,I)    - Total velocity
UV(II,I)     - Radial velocity
VV(II,I)     - Tangential velocity
WV(II,I)     - Axial velocity
IPOINT(II,I) - Probe calibration region
PT(II,I)     - Total pressure
PS(II,I)     - Static pressure
MZ(II,I)     - Axial momentum
MR(II,I)     - Tangential momentum
VELAVG(II,I) - Test section average axial velocity
PQAVG(II,I)  - Dynamic pressure of VELAVG(II,I)
```

B. OUTPUT VARIABLES TO SUBROUTINE "PVPLOT"

```
X(II,K)      - Value of X for data point K in run II
Y(II,K)      - Value of Y for data point K in run II
NA(II)       - Number of data points in each run,
               II = 1 to NC
IB           - Plot format, IB = 1 to 11
ERR(II,K,1)  - X lower limit for data point K
               in run II
ERR(II,K,2)  - X upper limit for data point K
               in run II
PLIMIT(J)    - Lower and upper plotting limits
               for X and Y
ND(I)        - Number of divisions on X and Y axes
NC           - Number of runs to be plotted
```

```
C     PROGRAM PLDATA - THIS PROGRAM PLOTS THE DATA THAT WAS REDUCED BY
C                        THE PROGRAM DATAR4
C
      LOGICAL*1 FNAME(10),ONAME(10)
      REAL HZ(8,35),HR(8,35)
      DIMENSION PT(8,35),PS(8,35),UV(8,35),VV(8,35),WV(8,35)
      DIMENSION RADIAL(8,35)
      DIMENSION ZS4(8,28),PS4(8,28),POAVG(8,35),VEL(8,35)
      DIMENSION ZS6A(8,6),PS6A(8,6),ZS8(8,26),PS8(8,26)
      DIMENSION PLIMIT(4),NO(2),N(8,3),NSRUNS(8),NA(8)
      DIMENSION X(8,35),Y(8,35),ERR(8,35,2),VELAVG(8,35)
      DIMENSION NI(11),NPA(8),POAA(8),IPOINT(8,35),SVEL(2),SW(2)
      DIMENSION SU(2),SV(2),SPS(2),SPT(2),SHR(2),SHZ(2)
      DATA NA/8*0/
      DATA SVEL/0.05471,0.0459/
      DATA SW/0.05518,0.04377/
      DATA SU/0.016813,0.035878/
      DATA SV/0.018912,0.028884/
      DATA SPS/0.1194,0.11615/
      DATA SPT/0.016633,0.05258/
      DATA SHR/0.04115,0.0525/
      DATA SHZ/0.09918,0.0639/
      CALL ASSIGN(5,'TI:')
      WRITE(5,111)
      READ(5,109)NOV
      WRITE(5,105)
      READ(5,109)NOP
C
C     READ THE NAME OF FILE CONTAINING THE NAMES AND PLOT
C     LIMITS OF THE DATA SETS TO BE PLOTTED
C
      WRITE(5,300)
      READ(5,302)ONAME
      CALL ASSIGN(3,ONAME,10)
```

PREVIOUS PAGE IS BLANK

```
      CALL FDBSET(3,'OLD','SHARE')
C
C     READ NAME OF EACH INPUT DATA FILE
C
      READ(3,112)NN
      DO 40 II=1,NN
      READ(3,302)FNAME
      IF(ADV.EQ.'Y')WRITE(5,115)II
      IF(ADV.EQ.'Y')READ(5,116)VAVG
  114 FORMAT(' DO YOU WANT TO SPECIFY VAVG?')
  115 FORMAT(' ENTER VAVG FOR RUN ',I2,' IN FORMAT XX.XX')
  116 FORMAT(F5.2)
      CALL ASSIGN(2,FNAME,10)
      CALL FDBSET(2,'OLD','SHARE')
      READ(2,100) NSRUNS(II),N(II,1),NPA(II),N(II,3)
      IF(N(II,1).EQ.0) GO TO 57
      K=N(II,1)
      DO 7 J=1,K
      READ(2,213) ZS4(II,J),DUMB,PS4(II,J)
    7 CONTINUE
   57 IF(NPA(II).EQ.0) GO TO 59
      K=NPA(II)
      DO 9 J=1,K
      READ(2,215) ZS6A(II,J),DUMB,PS6A(II,J)
    9 CONTINUE
   59 IF(N(II,3).EQ.0) GO TO 60
      K=N(II,3)
      DO 10 J=1,K
      READ(2,216) ZS8(II,J),DUMB,PS8(II,J)
   10 CONTINUE
   60 CONTINUE
      K=NSRUNS(II)
      DO 11 I=1,K
      READ(2,218) 18,RADIAL(II,I),DUM1,DUM1,DUM1,VEL(II,I),
```

```
     *UV(II,I),VV(II,I),UV(II,I),IPOINT(II,I)
 11  CONTINUE
     SUM=0.0
     DO 15 I=1,K
     READ(2,231)IB,PT(II,I),PS(II,I),MZ(II,I),MR(II,I),DUM1,DUM1,
     *DUM1,DUM1,VELAVG(II,I),PQAVG(II,I)
     SUM=SUM+PQAVG(II,I)
     IF(ADV.EQ.'Y')VELAVG(II,I)=VAVG
 15  CONTINUE
     RN=NSRUNS(II)
     PQAA(II)=SUM/RN
     CALL CLOSE(2)
 10  CONTINUE
C
C    CODE FOR REQUESTING PLOTS
C
C    N1(1).NE.0 - PLOT OF STATIC PRESSURE ON 4 INCH TUBE
C    N1(2).NE.0 - PLOT OF STATIC PRESSURE ON 6 INCH TUBE
C    N1(3).NE.0 - PLOT OF STATIC PRESSURE ON 8 INCH TUBE
C    N1(4).NE.0 - PLOT OF AXIAL VELOCITY
C    N1(5).NE.0 - PLOT OF RADIAL VELOCITY
C    N1(6).NE.0 - PLOT OF TANGENTIAL VELOCITY
C    N1(7).NE.0 - PLOT OF VELOCITY
C    N1(8).NE.0 - PLOT OF STATIC PRESSURE
C    N1(9).NE.0 - PLOT OF TOTAL PRESSURE
C    N1(10).NE.0- PLOT OF ANGULAR MOMENTUM
C    N1(11).NE.0- PLOT OF AXIAL MOMENTUM
C    N2 - NUMBER OF LAST PLOT REQUESTED
C
     READ(3,112)(N1(I),I=1,11),N2
     DO 32 II=1,NN
     DO 31 I=1,35
     DO 30 J=1,2
     ERR(II,I,J)=0.0
```

```
      CONTINUE
   41 CONTINUE
   42 CONTINUE
C
C     PERFORM PLOT AFTER READING SCALING REQUIRED
C
      CALL INITT(2400)
      IF(N1(1).EQ.0) GO TO 61
      DO 64 II=1,N1(1)
      NA(II)=N(II,1)
   64 CONTINUE
      IA=1
      READ(3,113)(FLIMIT(KA),KA=1,4),ND(1),ND(2)
      WRITE(5,106)
      WRITE(5,102)
      READ(5,109)AOK
      IF(AOK.EQ.'Q')GO TO 29
      WRITE(5,104)
      NC=N1(1)
      CALL PVPLOT(ZS1,ZS4,NA,IA,ERR,FLIMIT,ND,NC)
      CALL ANMODE
      READ(5,109)AOK
   61 IF(N1(2).EQ.0) GO TO 62
      DO 66 II=1,N1(2)
      NA(II)=NPA(II)
   66 CONTINUE
      IA=2
      READ(3,113)(FLIMIT(KA),KA=1,4),ND(1),ND(2)
      WRITE(5,106)
      WRITE(5,102)
      READ(5,109)AOK
      IF(AOK.EQ.'Q')GO TO 29
      WRITE(5,104)
      NC=N1(2)
```

```
      CALL FVPLOT(ZS6A,PS6A,NA,IA,ERR,PLIM T,ND,NC)
      CALL ANNODE
      READ(5,109)AOK
   62 IF(N1(3).EQ.0) GO TO 63
      DO 65 II=1,N1(3)
      NA(II) N(II,3)
   65 CONTINUE
      IA=3
      READ(3,113)(PLIMIT(KA),KA=1,4),ND(1),ND(2)
      WRITE(5,106)
      WRITE(5,102)
      READ(5,109)AOK
      IF(AOK.EQ.'0')GO TO 29
      WRITE(5,104)
      NC=N1(3)
      CALL FVPLOT(ZS8,PS8,NA,IA,ERR,PLIMIT,ND,NC)
      CALL ANNODE
      READ(5,109)AOK
   63 CONTINUE
      DO 19 IA=4,11
      DO 13 II=1,NN
      IF=NSRUNS(II)
      DO 14 I=1,IF
      K=I
      J=IPOINT(II,I)
      IAT=IA-3
      UNCF 0.00005
      PO=(PT(II,I)-PS(II,I))/FOAA(II)
      GO TO (20,21,22,23,24,25,26,27)IAT
   20 X(II,K)=UV(II,I)*VEL(II,I)/VELAVG(II,I)
      ERR(II,K,1)=X(II,K)*(1.-SVEL(J))*(1.-SU(J))
      ERR(II,K,2)=X(II,K)*(1.+SVEL(J))*(1.+SU(J))
      GO TO 28
   21 X(II,K)=-1.0*UV(II,I)*VEL(II,I)/VELAVG(II,I)
```

```
      ERR(II,K,1)=X(II,K)*(1.-SVEL(J))*(1.-SU(J))
      ERR(II,K,2)=X(II,K)*(1.+SVEL(J))*(1.+SU(J))
      GO TO 28
   22 X(II,K)=UV(II,I)*VEL(II,I)/VELAVG(II,I)
      ERR(II,K,1)=X(II,K)*(1.-SVEL(J))*(1.-SV(J))
      ERR(II,K,2)=X(II,K)*(1.+SVEL(J))*(1.+SV(J))
      GO TO 28
   23 X(II,K)=VEL(II,I)/VELAVG(II,I)
      ERR(II,K,1)=X(II,K)*(1.-SVEL(J))
      ERR(II,K,2)=X(II,K)*(1.+SVEL(J))
      GO TO 28
   24 X(II,K)=PS(II,I)/PQAVG(II,I)
      ERR(II,K,1)=X(II,K)-SPS(J)*PQ-UNCP/PQAA(II)
      ERR(II,K,2)=X(II,K)+SPS(J)*PQ+UNCP/PQAA(II)
      GO TO 28
   25 X(II,K)=PT(II,I)/PQAVG(II,I)
      ERR(II,K,1)=X(II,K)-SPT(J)*PQ-UNCP/PQAA(II)
      ERR(II,K,2)=X(II,K)+SPT(J)*PQ+UNCP/PQAA(II)
      GO TO 28
   26 X(II,K)=MR(II,I)/PQAVG(II,I)
      ERR(II,K,1)=X(II,K)-SMR(J)*PQ-UNCP/PQAA(II)
      ERR(II,K,2)=X(II,K)+SMR(J)*PQ+UNCP/PQAA(II)
      GO TO 28
   27 X(II,K)=MZ(II,I)/PQAVG(II,I)
      ERR(II,K,1)=X(II,K)*(1.-SMZ(J))-UNCP/PQAA(II)
      ERR(II,K,2)=X(II,K)*(1.+SMZ(J))+UNCP/PQAA(II)
   28 Y(II,K)=RADIAL(II,I)
   14 CONTINUE
      NA(II)=NSRUNS(II)
   13 CONTINUE
      IF(NI(IA).EQ.0) GO TO 19
      IB=IA
      READ(3,113)(FLIGHT(KA),KA=1,4),ND(1),ND(2)
      WRITE(5,103)
```

```
      WRITE(5,102)
      READ(5,109)AOK
      IF(AOK.EQ.'Q') GO TO 29
      WRITE(5,104)
      NC=N1(IA)
      CALL PVPLOT(X,Y,NA,IB,ERR,PLIMIT,ND,NC)
      CALL ANMODE
      READ(5,109)AOK
      IF(IA.EQ.N2) GO TO 29
   19 CONTINUE
  100 FORMAT(5I5)
  101 FORMAT(I1)
  102 FORMAT(/////,' HIT 'RETURN' TO PLOT NEXT GRAPH')
  104 FORMAT(' AFTER GRAPH IS COMPLETE, HIT 'RETURN' TO CONTINUE')
  105 FORMAT(' TURN OFF 'COMMAND LOCK OUT' LIGHT',/,' HIT 'RETURN'',
     *' WHEN READY')
  106 FORMAT('  !WOR 33 H!GRA 1,35!SHR')
  107 FORMAT('  !MON 35 H K!WOR 0')
  109 FORMAT(A1)
  112 FORMAT(12I2)
  113 FORMAT(4F5.2,2I2)
  213 FORMAT( 1X,F5.2,1X,F8.5,5X,F8.5)
  215 FORMAT(52X,F5.2,1X,F8.5,5X,F8.5)
  216 FORMAT(37X,F5.2,1X,F8.5,5X,F8.5)
  218 FORMAT(2X,I3,5X,F5.2,4X,F5.2,1X,F6.2,1X,F6.2,1X,F8.4,3F7.3,I3)
  231 FORMAT(1X,I3,1X,2(1X,F8.5),2(1X,F7.4),2(1X,2F5.2),F8.2,F8.5)
  300 FORMAT(//,' ENTER THE NAME OF INPUT DATA FILE IN FORMAT ',
     *'INPXXX.DAT')
  302 FORMAT(10A)
   29 CALL FINITT(0,0)
      WRITE(5,107)
      STOP
      END
```

```
      SUBROUTINE PVFLOT(X,Y,NPT,NUMP,ERR,PLIMIT,ND,NN)
      LOGICAL*1 NADE(4)
      DIMENSION X(8,35),Y(8,35),ERR(8,35,2),XF(35),XH(35),NSYM(8)
      DIMENSION ND(2),PLIMIT(4),XX(35),YY(35),NPT(8)
      DIMENSION ISTR01(13),ISTR02(15),ISTR03(14),ISTR04(14),ISTR05(14)
      DIMENSION ISTR06(15),ISTR07(19),ISTR08(19),ISTR09(24),ISTR11(6)
      DIMENSION ISTR12(9),ISTR13(9),ISTR14(9),ISTR15(9),ISTR16(9)
      DIMENSION ISTR17(9),ISTR18(9),ISTR19(9),ISTR20(30),ISTR21(30)
      DIMENSION ISTR22(30),ISTR23(22),ISTR24(24),ISTR25(18),ISTR26(3)
      DIMENSION LPXL(4),LPXU(4),LPYL(2),LPYU(2),LABELS(4),ISTR27(6)
      DATA NSYM/8,2,5,6,7,1,3,4/
      DATA LPXL/150,325,500,676/
      DATA LPXU/322,497,672,850/
      DATA LPYL/500,175/
      DATA LPYU/675,350/
      DATA ISTR01/68,73,77,69,78,83,73,79,78,76,69,83,83/
C     LABEL    01  D  I  M  E  N  S  I  O  N  L  E  S  S
      DATA ISTR02/83,84,65,84,73,67,32,80,82,69,83,83,85,82,69/
C     LABEL    02  S  T  A  T  I  C     P  R  E  S  S  U  R  E
      DATA ISTR03/84,79,84,65,76,32,80,82,69,83,83,85,82,69/
C     LABEL    03  T  O  T  A  L     P  R  E  S  S  U  R  E
      DATA ISTR04/84,79,84,65,76,32,86,69,76,79,67,73,84,89/
C     LABEL    04  T  O  T  A  L     V  E  L  O  C  I  T  Y
      DATA ISTR05/65,88,73,65,76,32,86,69,76,79,67,73,84,89/
C     LABEL    05  A  X  I  A  L     V  E  L  O  C  I  T  Y
      DATA ISTR06/82,65,68,73,65,76,32,86,69,76,79,67,73,84,89/
C     LABEL    06  R  A  D  I  A  L     V  E  L  O  C  I  T  Y
      DATA ISTR07/84,65,78,71,69,78,84,73,65,76,32,86,69,76,79,67,
C     LABEL    07  T  A  N  G  E  N  T  I  A  L     V  E  L  O  C
     &73,84,89/
C      I  T  Y
      DATA ISTR08/65,88,73,65,76,32,77,79,77,69,78,84,85,77,32,70,
C     LABEL    08  A  X  I  A  L     M  O  M  E  N  T  U  M     F
     &76,85,88/
```

```
C       L  U  X
      DATA ISTR09/34,65,78,71,69,78,84,73,65,76,32,77,79,77,69,78,
C     LABEL    09  T  A  N  G  E  N  T  I  A  L     M  O  M  E  N
     *84,85,77,32,70,76,85,88/
C       T  U  M     F  L  U  X
      DATA ISTR11/82,65,68,73,85,83/
C     LABEL    11  R  A  D  I  U  S
      DATA ISTR12/90,32,61,32,48,46,50,53,32/
C     LABEL    12  Z     =     0  .  2  5
      DATA ISTR13/90,32,61,32,50,46,50,53,32/
C     LABEL    13  Z     =     2  .  2  5
      DATA ISTR14/90,32,61,32,52,46,50,53,32/
C     LABEL    14  Z     =     4  .  2  5
      DATA ISTR15/90,32,61,32,54,46,50,53,32/
C     LABEL    15  Z     =     6  .  2  5
      DATA ISTR16/90,32,61,32,56,46,50,53,32/
C     LABEL    16  Z     =     8  .  2  5
      DATA ISTR17/90,32,61,32,49,50,46,50,53/
C     LABEL    17  Z     =     1  2  .  2  5
      DATA ISTR18/90,32,61,32,49,56,46,50,53/
C     LABEL    18  Z     =     1  8  .  2  5
      DATA ISTR19/90,32,61,32,50,52,46,50,53/
C     LABEL    19  Z     =     2  4  .  2  5
      DATA ISTR20/83,84,65,84,73,67,32,80,82,69,83,83,85,82,69,32,
C     LABEL    20  S  T  A  T  I  C     P  R  E  S  S  U  R  E
     *79,78,32,52,32,73,78,67,72,32,84,85,66,69/
C       O  N     4     I  N  C  H     T  U  B  E
      DATA ISTR21/83,84,65,84,73,67,32,80,82,69,83,83,85,82,69,32,
C     LABEL    21  S  T  A  T  I  C     P  R  E  S  S  U  R  E
     *79,78,32,54,32,73,78,67,72,32,84,85,66,69/
C       O  N     6     I  N  C  H     T  U  B  E
      DATA ISTR22/83,84,65,84,73,67,32,80,82,69,83,83,85,82,69,32,
C     LABEL    22  S  T  A  T  I  C     P  R  E  S  S  U  R  E
     *79,78,32,56,32,73,78,67,72,32,84,85,66,69/
```

```
C       O  N      8      I  N  C  H     T  U  B  E
        DATA ISTR23/68,73,77,69,78,83,73,79,78,76,69,83,83,32,
C       LABEL    23  D  I  M  E  N  S  I  O  N  L  E  S  S
       $80,82,69,83,83,85,82,69/
C       P  R  E  S  S  U  R  E
        DATA ISTR24/65,88,73,65,76,32,80,79,83,73,84,73,79,78,32,73,78,
C       LABEL    24  A  X  I  A  L     P  O  S  I  T  I  O  N     I  N
       $32,73,78,67,72,69,83/
C          I  N  C  H  E  S
        DATA ISTR25/68,65,84,65,32,80,79,73,78,84,32,83,89,77,66,79,76,83/
C       LABEL    25  D  A  T  A     P  O  I  N  T     S  Y  M  B  O  L  S
        DATA ISTR26/50,51,52/
C       LABEL    26  2  3  4
        DATA ISTR27/70,73,71,85,82,69/
C       LABEL    27  F  I  G  U  R  E
        XMIN=PLIMIT(1)
        XMAX=PLIMIT(2)
        YMIN=PLIMIT(3)
        YMAX=PLIMIT(4)
        NDX=NB(1)
        NDY=NB(2)
        XINC=(XMAX-XMIN)/FLOAT(NDX)
        YINC=(YMAX-YMIN)/FLOAT(NDY)
        IF(NUMP.LE.3)WRITE(5,200)
   200 FORMAT(' ENTER LOCATION OF TABLE OF SYMBOLS:',/,4X,'"U" FOR UPPER
       1 AND "L" FOR LOWER')
        IF(NUMP.LE.3)READ(5,198)AOK
        CALL ERASE
        CALL NEWPAG
        IF(NUMP.GT.3) GO TO 46
C
C
C       PLOTS OF STATIC PRESSURE ON 4, 6 AND 8 INCH TUBES
C
```

441

```
C
      CALL SWINDO(0,1000,0,650)
      CALL VWINDO(-1.5,10.5,-1.,6.)
      DO 19 II=1,NN
      NPS=NPT(II)
      DO 18 I=1,NPS
      YY(I)=Y(II,I)
      XX(I)=X(II,I)
      IF(YY(I).GT.YMAX)YY(I)=YMAX
      IF(YY(I).LT.YMIN)YY(I)=YMIN
   18 CONTINUE
      CALL SCALE(NPS,XX,XMIN,XMAX,0.,8.)
      CALL SCALE(NPS,YY,YMIN,YMAX,0.,5.)
      NSY=NSYM(II)
      CALL MOVEA(XX(1),YY(1))
      CALL SYMBLS(NPS,XX,YY,NSY)
      IF(II.NE.NN)GO TO 19
      CALL GRID(0.,8.,0.,5.,XMIN,XINC,NDX,YMIN,YINC,NDY,1)
   19 CONTINUE
C
C     LABEL X-AXIS
C
      CALL MOVEA(2.4,-.5)
      CALL ANSTR(24,ISTR24)
C
C     LABEL Y-AXIS
C
      CALL MOVEA(-1.2,4.5)
      DO 16 I=1,23
      ICHAR=ISTR23(I)
      CALL ANSTR(1,ICHAR)
      CALL LINEF
      CALL BAKSP
   16 CONTINUE
```


PREVIOUS PAGE IS BLANK

```
C
C     WRITE TITLE
C
      CALL MOVABS(300,550)
      IF(NUMP.EQ.1) CALL ANSTR(30,ISTR20)
      IF(NUMP.EQ.2) CALL ANSTR(30,ISTR21)
      IF(NUMP.EQ.3) CALL ANSTR(30,ISTR22)
      CALL MOVEA(3.0,-0.8)
      CALL ANSTR(6,ISTR27)
C
C     WRITE TABLE OF SYMBOLS
C
      XI=4.9
      IF(AOK.EQ.'L')YI=2.0
      IF(AOK.EQ.'U') YI=4.0
      IF(NUMP.EQ.2)XI=1.8
      CALL MOVEA(XI,YI)
      CALL ANSTR(18,ISTR25)
      ZI=XI+.3
      YI=YI-0.20
      DO 15 I=1,NN
      NSY=NSYM(I)
      CALL MOVEA(XI,YI)
      YX=YI+.03
      CALL SYMBLS(1,XI,YX,NSY)
      CALL MOVEA(ZI,YI)
      IF(I.EQ.1) CALL ANSTR(9,ISTR12)
      IF(I.EQ.2) CALL ANSTR(9,ISTR13)
      IF(I.EQ.3) CALL ANSTR(9,ISTR14)
      IF(I.EQ.4) CALL ANSTR(9,ISTR15)
      J=I
      IF(NN.EQ.8) J=I-1
      IF((I.EQ.5).AND.(J.EQ.4)) CALL ANSTR(9,ISTR16)
      IF(J.EQ.5) CALL ANSTR(9,ISTR17)
```

```
      IF(J.EQ.6) CALL ANSTR(9,ISTF18)
      IF(J.EQ.7) CALL ANSTR(9,ISTF19)
      YI=YI-0.2
   15 CONTINUE
      GO TO 50
C
C
C     PLOTS OF VELOCITIES, PRESSURES AND MOMENTUMS
C     VERSUS RADIUS
C
C
   50 CONTINUE
      CALL MOVABS(0,0)
  179 FORMAT(A1)
      DO 30 II=1,[illegible]
      NPS=NPT(II)
      NST=NSTR(II)
      DO 40 J=1,NPS
      XP(J)=[illegible](II,J,1)
      XN(J)=EFR(II,J,[illegible])
      [illegible](J)=[illegible](II,J)
      Y[illegible](J)=Y(II,[illegible]
      IF([illegible](J).GT.[illegible]
      IF([illegible](J).LT.[illegible]
   40 CONTINUE
      IF(II.GT.4)GO TO [illegible]
      LXL=LPXL(II)
      LXU=LPXU(I[illegible])
      LYL=LPYL(I[illegible])
      LYU=LPYU[illegible]
      GO TO [illegible]
   31 IJ=II-[illegible]
      LXL=LPXL(IJ)
      LXU=LPXU(IJ)
```

444

```
      LYL=LPYL(2)
      LYU=LPYU(2)
   32 CONTINUE
      CALL TWINDO(LXL,LXU,LYL,LYU)
      CALL DWINDO(0.,8.,0.,5.)
      CALL SCALE(NPS,X,XMIN,XMAX,0.,8.)
      CALL SCALE(NPS,Y,YMIN,YMAX,0.,5.)
      CALL SYMBLS(NPS,X,Y,1)
      CALL GRID(0.,8.,0.,5.,XMIN,XINC,NDX,YMIN,YINC,NDY,0)
C
C     LABEL TOP OF GRAPH
C
      LTX=LXL+30
      LTY=LYU+10
      CALL MOVABS(LTX,LTY)
      IF(II.EQ.1) CALL ANSTR(9,ISTR12)
      IF(II.EQ.2) CALL ANSTR(9,ISTR13)
      IF(II.EQ.3) CALL ANSTR(9,ISTR14)
      IF(II.EQ.4) CALL ANSTR(9,ISTR15)
      J=II
      IF(NN.EQ.8)J=II-1
      IF((II.EQ.5).AND.(J.EQ.4)) CALL ANSTR(9,ISTR16)
      IF(J.EQ.5) CALL ANSTR(9,ISTR17)
      IF(J.EQ.6) CALL ANSTR(9,ISTR18)
      IF(J.EQ.7) CALL ANSTR(9,ISTR19)
C
C     LABEL SIDES OF GRAPH
C
      IF((II.EQ.5).OR.(J.EQ.7)) GO TO 35
      GO TO 36
   35 DO 31 KI=1,2
      IF(II.EQ.5)LVX=LPXL(1)-60
      IF((J.EQ.7).AND.(KI.EQ.1))LVX=LPXU(4)+60
      IF((J.EQ.7).AND.(KI.EQ.2))LVX=LPXU(II)+60
```

```
      IF(KI.EQ.1)LVY=LFYU(1)-40
      IF(KI.EQ.2)LVY=LFYU(2)-40
      CALL MOVABS(LVX,LVY)
      DO 33 I=1,4
      ICHAR=ISTR11(I)
      CALL ANSTR(1,ICHAR)
      CALL LINEF
      CALL BAKSP
   33 CONTINUE
   31 CONTINUE
C
C     NUMBER SIDES OF GRAPH
C
      DO 39 KI=1,2
      IF(IT.EQ.5)LVX=LFXL(1)-50
      IF((J.EQ.7).AND.(KI.EQ.1))LVX=LFXU(4)+10
      IF((J.EQ.7).AND.(KI.EQ.2))LVX=LFXU(I)+10
      LVY=LFYU(KI)
      CALL MOVABS(LVX,LVY)
      ICHAR=ISTR26(5)
      CALL ANSTR(1,ICHAR)
      LYM=LFYU(KI)+LFYL(KI)
      RLVY=FLOAT(LYM)/2.
      LVY=IFIX(RLVY)
      CALL MOVABS(LVX,LVY)
      ICHAR=ISTR26(3)
      CALL ANSTR(1,ICHAR)
      LVY=LFYL(KI)
      CALL MOVABS(LVX,LVY)
      ICHAR=ISTR26(1)
      CALL ANSTR(1,ICHAR)
   39 CONTINUE
C
C     NUMBER BOTTOM OF GRAPH
```

```
C
36 GOTO(37,36,37,30,37,36,37,36)II
37 LHX=LXL-30
   LHY=LYL-75
   ENCODE(4,139,NADE)XLL
139 FORMAT(F4.1)
   LABELS(1)=NADE(1)
   LABELS(2)=NADE(2)
   LABELS(3)=NADE(3)
   LABELS(4)=NADE(4)
   CALL MOVABS(LHX,LHY)
   CALL ANSTR(4,LABELS)
   LHX=LXU-35
   ENCODE(4,139,NADE)XUL
   LABELS(1)=NADE(1)
   LABELS(2)=NADE(2)
   LABELS(3)=NADE(3)
   LABELS(4)=NADE(4)
   CALL MOVABS(LHX,LHY)
   CALL ANSTR(4,LABELS)
C
C     LABEL BOTTOM OF GRAPH
C
   LHX=LXL
   LHY=LYL-50
   CALL MOVABS(LHX,LHY)
   CALL ANSTR(13,ISTR)
   LHY1=LYL-75
   CALL MOVABS(LHX,LHY1)
66 IF(NUMF.EQ.4) CALL ANSTR(14,ISTR05)
   IF(NUMF.EQ.5) CALL ANSTR(15,ISTR06)
   IF(NUMF.EQ.6) CALL ANSTR(19,ISTR07)
   IF(NUMF.EQ.7) CALL ANSTR(11,ISTR08)
   IF(NUMF.EQ.8) CALL ANSTR(15,ISTR09)
```

```
      IF(NUMF.EQ.9) CALL ANSTR(11,ISTR08)
      IF(NUMF.EQ.10)CALL ANSTR(21,ISTR09)
      IF(NUMF.EQ.11)CALL ANSTR(1 ,ISTR08)
   38 CONTINUE
   30 CONTINUE
      CALL MOVABS(400,25)
      CALL ANSTR(6,ISTR27)
      CALL ANMODE
   50 RETURN
      END
```

```
      SUBROUTINE GRID(SXMIN,SXMAX,SYMIN,SYMAX,XMIN,XINC,IXCNT,
     *YMIN,YINC,IYCNT,ILBL)
C
C     THIS SUBROUTINE IS DESIGNED TO DRAW AND LABEL A GRID IN
C     TWO DIMENSIONS.
C
C     SXMIN     SCALE X MIN
C     SXMAX     SCALE X MAX
C     SYMIN     SCALE Y MIN
C     SYMAX     SCALE Y MAX
C     XMIN      DATA  X MIN
C     XMAX      DATA  X MAX
C     YMIN      DATA  Y MIN
C     YMAX      DATA  Y MAX
C     IXCNT     NUMBER OF INCREMENTS IN X GRID
C     IYCNT     NUMBER OF INCREMENTS IN Y GRID
C     ILBL      IF = 0, DO NOT LABEL GRID
C               IF = 1, LABEL "X" AND "Y" AXIS
C
      DIMENSION LABELS(5)
      LOGICAL*1 NADE(5)
      CALL MOVEA(SXMIN,SYMIN)
      CALL DRAWA(SXMIN,SYMAX)
      CALL DRAWA(SXMAX,SYMAX)
      CALL DRAWA(SXMAX,SYMIN)
      CALL DRAWA(SXMIN,SYMIN)
      SXINC=(SXMAX-SXMIN)/FLOAT(IXCNT)
      SYINC=(SYMAX-SYMIN)/FLOAT(IYCNT)
      DO 100 I=1,IXCNT-1
      XLOC=SXMIN+FLOAT(I)*SXINC
      CALL MOVEA(XLOC,SYMIN)
      CALL DRAWA(XLOC,SYMAX)
  100 CONTINUE
      DO 200 I=1,IYCNT-1
```

PREVIOUS PAGE IS BLANK

```
      YLOC=SYMIN+FLOAT(I)*SYINC
      CALL MOVEA(SXMIN,YLOC)
      CALL DRAWA(SXMAX,YLOC)
  200 CONTINUE
      IF(ILBL.EQ.0) GO TO 500
C     LABEL BOTTOM OF GRAPH
      DO 300 I=0,IXCNT
      XLOC=SXMIN+FLOAT(I)*SXINC-.35
      VALUE=XMIN+XINC*FLOAT(I)
      ENCODE(5,299,NADE)VALUE
      DO 250 J=1,5
      LABELS(J)=NADE(J)
  250 CONTINUE
      CALL MOVEA(XLOC,SYMIN-.25)
      CALL ANSTR(5,LABELS)
  299 FORMAT(F5.2)
  300 CONTINUE
C     LABEL SIDE OF GRAPH
      DO 400 I=0,IYCNT
      YLOC=SYMIN+FLOAT(I)*SYINC
      VALUE=YMIN+FLOAT(I)*YINC
      ENCODE(5,299,NADE)VALUE
      DO 350 J=1,5
      LABELS(J)=NADE(J)
  350 CONTINUE
      CALL MOVEA(SXMIN-.8,YLOC)
      CALL ANSTR(5,LABELS)
  400 CONTINUE
  500 CONTINUE
      RETURN
      END
```

```
      SUBROUTINE SCALE(NF,X,XMIN,XMAX,SMIN,SMAX)
C
C     THIS SUBROUTINE SCALES THE DATA FOR PLOTTING WITHIN
C     THE PLOTTING LIMITS OF SMIN AND SMAX
C
      DIMENSION X(NF)
      SFACT=(SMAX-SMIN)/(XMAX-XMIN)
      DO 1000 I=1,NF
      X(I)=(X(I)-XMIN)*SFACT+SMIN
 1000 CONTINUE
      RETURN
      END
```

```
      SUBROUTINE SYMBLS(NP,X,Y,ITYPE)
C
C     THIS SUBROUTINE DRAWS PLOTTING SYMBOLS AT DATA POINTS SPECIFIED
C     IN ARRAYS 'X' AND 'Y'. THE SYMBOL TYPE IS DETERMINED BY 'ITYPE'.
C     THERE ARE 'NP' DATA POINTS TO BE DRAWN.
C
C     ITYPE   SYMBOL
C       1     BOX
C       2     DIAMOND
C       3     PLUS(CROSS)
C       4     'X'
C       5     TRIANGLE
C       6     PENTAGON
C       7     STAR
C       8     INVERTED TRIANGLE
C       9     OCTAGON
C      10     VERTICAL BAR
C      11     SMALL CIRCLE
C
      DIMENSION X(NP),Y(NP)
      DO 1010 I=1,NP
      CALL MOVEA(X(I),Y(I))
      GOTO(10,20,30,40,50,60)ITYPE
      GOTO(70,80,90,100,110)ITYPE-6
C     DRAW A BOX
   10 CONTINUE
      CALL PNTREL(0,0)
      CALL MOVREL(-4,4)
      CALL DRWREL(8,0)
      CALL DRWREL(0,-8)
      CALL DRWREL(-8,0)
      CALL DRWREL(0,8)
      GO TO 1000
C     DRAW A DIAMOND
```

```
   20 CONTINUE
      CALL PNTREL(0,0)
      CALL MOVREL(0,7)
      CALL DRWREL(4,-7)
      CALL DRWREL(-4,-7)
      CALL DRWREL(-4,7)
      CALL DRWREL(4,7)
      GO TO 1000
C     DRAW A PLUS(CROSS)
   30 CONTINUE
      CALL MOVREL(0,5)
      CALL DRWREL(0,-10)
      CALL MOVREL(-5,5)
      CALL DRWREL(10,0)
      GO TO 1000
C     DRAW AN 'X'
   40 CONTINUE
      CALL MOVREL(-4,4)
      CALL DRWREL(8,-8)
      CALL MOVREL(-8,0)
      CALL DRWREL(8,8)
      GO TO 1000
C     DRAW A TRIANGLE
   50 CONTINUE
      CALL PNTREL(0,0)
      CALL MOVREL(0,6)
      CALL DRWREL(5,-10)
      CALL DRWREL(-10,0)
      CALL DRWREL(5,10)
      GO TO 1000
C     DRAW A PENTAGON
   60 CONTINUE
      CALL PNTREL(0,0)
      CALL MOVREL(-3,-4)
```

```
      CALL DRWREL(6,0)
      CALL DRWREL(2,5)
      CALL DRWREL(-5,4)
      CALL DRWREL(-5,-4)
      CALL DRWREL(2,-5)
      GO TO 1000
C     DRAW A STAR
   70 CONTINUE
      CALL PNTREL(0,0)
      CALL MOVREL(-5,1)
      CALL DRWREL(10,0)
      CALL DRWREL(-8,-5)
      CALL DRWREL(3,9)
      CALL DRWREL(3,-9)
      CALL DRWREL(-8,5)
      GO TO 1000
C     DRAW AN INVERTED TRIANGLE
   80 CONTINUE
      CALL PNTREL(0,0)
      CALL MOVREL(0,-6)
      CALL DRWREL(5,10)
      CALL DRWREL(-10,0)
      CALL DRWREL(5,-10)
      GO TO 1000
C     DRAW AN OCTAGON
   90 CONTINUE
      CALL PNTREL(0,0)
      CALL MOVREL(-5,0)
      CALL DRWREL(1,-4)
      CALL DRWREL(4,-1)
      CALL DRWREL(4,1)
      CALL DRWREL(1,4)
      CALL DRWREL(-1,4)
      CALL DRWREL(-4,1)
```

```
      CALL DRWREL(-4,-1)
      CALL DRWREL(-1,-4)
      GO TO 1000
C     DRAW VERTICAL BAR
  100 CONTINUE
      CALL MOVREL(0,-2)
      CALL DRWREL(0,4)
      GO TO 1000
C     DRAW A SMALL CIRCLE
  110 CONTINUE
      CALL PNTREL(0,0)
      CALL MOVREL(-4,0)
      CALL DRWREL(1,-3)
      CALL DRWREL(3,-1)
      CALL DRWREL(3,1)
      CALL DRWREL(1,3)
      CALL DRWREL(-1,3)
      CALL DRWREL(-3,1)
      CALL DRWREL(-3,-1)
      CALL DRWREL(-1,-3)
 1000 CONTINUE
      CALL MOVEA(X(I),Y(I))
 1010 CONTINUE
      RETURN
      END
```

APPENDIX G

DEVELOPMENT OF INTEGRAL RELATIONSHIPS FOR AXISYMMETRIC FLOW WITH SWIRL IN AN ANNULAR CHANNEL FORMED BETWEEN CONCENTRIC CONSTANT AREA CYLINDERS

I. INTRODUCTION

The annualr channel of interest and nomenclature for axisymmetric flow are shown in Figure 1. Integral relationships for momentum of the mean velocities in turbulent flow within this channel are developed for use in analysis of experimental data obtained for this flow configuration.

II. DEVELOPMENT OF INTEGRAL MOMENTUM EQUATIONS

For circular jets with or without swirl, the mean axial velocity (w) is much greater than the mean radialm velocity (u) and gradients in the radial direction are much larger than those in the axial direction. Becuase the flow of interest is for a nozzle Reynolds number greater than a few thousand, the viscous stresses are assumed to be much smaller than the corresponding turbulent shear stresses. Under the above conditions, the

time averaged Navier Stokes equations yield the following relationships for incompressible flow:

$$-\frac{v^2}{r} = -\frac{\partial P}{\partial r} - \frac{1}{r}\frac{\partial}{\partial r}[r\,\overline{u'^2}] + \frac{\overline{v'^2}}{r} \qquad \text{(G-1)}$$

$$u\frac{\partial v}{\partial r} + \frac{uv}{r} + w\frac{\partial v}{\partial z} = -\frac{\partial}{\partial r}(\overline{u'v'}) - 2\frac{\overline{u'v'}}{r} - \frac{\partial}{\partial z}(\overline{v'w'}) \qquad \text{(G-2)}$$

$$u\frac{\partial w}{\partial r} + w\frac{\partial w}{\partial z} = -\frac{\partial P}{\partial z} - \frac{1}{r}\frac{\partial}{\partial r}(r\overline{u'v'}) - \frac{\partial}{\partial z}(\overline{w'^2}) \qquad \text{(G-3)}$$

where the prime (') denotes the turbulent fluctuation and the overbar denotes the time average of the quantity.

Because $\partial(\overline{v'w'})/\partial z$ is very small in comparison with $\partial(\overline{u'v'})/\partial r$, it can be neglected in Equation G-2 above. Neglecting the turbulent normal stresses ($\overline{u'^2}$, $\overline{v'^2}$ and $\overline{w'^2}$) and denoting the turbulent shear stresses as

$$\tau_z = -\rho\,\overline{u'w'} \qquad \text{(G-4)}$$

$$\tau_\theta = -\rho\,\overline{u'v'} \qquad \text{(G-5)}$$

then Equations G-1 through G-3 become

$$\frac{v^2}{r} = \frac{1}{\rho}\frac{\partial P}{\partial r} \qquad \text{(G-6)}$$

$$u\frac{\partial u}{\partial r} + \frac{uv}{r} + w\frac{\partial v}{\partial z} = \frac{1}{\rho}\frac{\partial \tau_\theta}{\partial r} + \frac{2}{\rho}\frac{\tau_\theta}{r} \qquad \text{(G-7)}$$

$$u\frac{\partial w}{\partial r} + w\frac{\partial w}{\partial z} = -\frac{1}{\rho}\frac{\partial P}{\partial z} + \frac{1}{\rho r}\frac{\partial}{\partial r}(r\tau_z) \qquad \text{(G-8)}$$

Integration of Equation G-6 with respect to the radius from the inner radius (r_i) to a radius (r) in the flow yields

$$P(r,z) - P(r_i,z) = \rho\int_{r_i}^{r}(v^2/r)\,dr \qquad \text{(G-9)}$$

Multiplying Equation G-7 by ρr^2 and integrating with respect to the radius from the inner radius (r_i) to the outer radius (r_o) yields

$$\frac{d}{dz}\left[\rho\int_{r_i}^{r_o} r^2 wv\,dr\right] = (r^2\tau_\theta)\Big|_{r_i}^{r_o} \qquad \text{(G-10)}$$

Multiplying Equation G-8 by ρr and integrating with respect to the radius from the inner radius (r_i) to the outer (r_o) yields

$$\frac{d}{dz}\left[\int_{r_i}^{r_o}(P + \rho w^2)r\,dr\right] = (r\tau_z)\Big|_{r_i}^{r_o} \qquad \text{(G-11)}$$

Equations G-10 and G-11 can be simplified further by

defining the terms within each integral as follows

$$G_\theta = \int_{r_i}^{r_o} \rho r^2 wv \; dr \;\; = \int_{r_i}^{r_o} M_\theta r \; dr \qquad \text{(G-12)}$$

$$W = \int_{r_i}^{r_o} (P - P_o + \rho w^2) r \; dr \;\; = \int_{r_i}^{r_o} M_z r \; dr \qquad \text{(G-13)}$$

where P_o is a refèrence pressure

Using the above definitions of G_θ and W, Equations C-1Ø and G-11 simplify to

$$\frac{dG_\theta}{dz} = (r^2 \tau_\theta) \Big|_{r_i}^{r_o} \qquad \text{(G-14)}$$

$$\frac{dW}{dz} = (r \tau_z) \Big|_{r_i}^{r_o} \qquad \text{(G-15)}$$

Equations G-14 and G-15 give the familiar relationships that can also be obtained by control volume analysis (Reference 1) between the change in the axial direction of the radially integrated angular momentum to the tangential shear stress at the walls and the change in the axial direction of the radially integrated pressure plus axial momentum (total "stream thrust") to the axial shear stress at the walls.

III. SWIRL NUMBER

The swirl number for a flow is the ratio of the angular momentum to the total "stream thrust" times an appropriate radius. It is a simensionless number that is used to characterize flows containing swirl. The exact form of the equation used to calculate the swirl number varies between references (see References 2 and 3). The swirl number (S) can be defined as

$$S = G_\theta / (r_o W) \qquad \text{(G-16)}$$

where G_θ and W are defined by Equations G-12 and G-13, respectively, and r_o is the outer radius of the annular channel. As defined above, the swirl number is constant in the axial direction when the shear stresses at the wall are negligible.

An alternate definition of the swirl number (S) can be obtained by noting that Equation G-13 can be integrated by parts to give

$$W = \int_{r_i}^{r_o} (P - P_o + \rho w^2)\ r\ dr$$

$$W = \left. \frac{(P - P_o)\, r^2}{2} \right|_{r_i}^{r_o} + \int_{r_i}^{r_o} \rho (w^2 - v^2/2)\ r\ dr \qquad \text{(G-17)}$$

Defining the axial momentum flux, G_z, as

$$G_z = \int_{r_i}^{r_o} \rho(w^2 - v^2/2)\ r\ dr = \int_{r_i}^{r_o} M_z' r\ dr \qquad \text{(G-18)}$$

then Equation G-17 becomes

$$W = G_z + \left.\frac{(P - P_o)\, r^2}{2}\right|_{r_i}^{r_o} \qquad \text{(G-19)}$$

The swirl number (S) can then be defined as follows

$$S = \frac{G_\theta}{r_o G_z + (r_o/2)\left[(P_{r_o} - P_o)\, r_o^2 - (P_{r_i} - P_o)\, r_i^2\right]} \qquad \text{(G-20)}$$

where G_θ and G_z are defined by Equations G-12 and G-18, respectively. P_{r_o} and P_r are the wall static pressures at $r=r_o$ and $r=r_i$, respectively, P_o is a constant reference pressure, and r_i and r_o are the inner radius and the outer radius of the annular channel, respectively.

Equation G-20 for the swirl number (S) is more desirable to work with than Equation G-16 because the intergrals for determining G_θ and G_z contain only the axial velocity, w, and the tangential velocity, v. Whereas Equation G-16 for the swirl number (S) requires that the static pressure (P) in the flow be integrated between the inner and outer wall for the calculation of W (Equation

G-13). Since present measurement methods permit a more accurate measurement of the wall static pressure than the static pressure in the flow, Equation G-2Ø yields a more accurate value of the swirl number (S).

Equation G-2Ø for the swirl number (S) can be simplified for the cases of a swirling stream flowing into a space of uniform pressure, P_o , where a centerbody exists (Figure 3-3) and where a centerbody does not exist (Figures 3-1 and 3-2). The swirl number for the case when a centerbody does exist is given by

$$S = \frac{G_\theta}{r_o G_z + (r_o/2)(P_o - P_{r_i}) r_i} \qquad \text{(G-21)}$$

where r_o is the outer radius of the stream at its exit, r_i is the radius of the centerbody, P_o is the ambient pressure, and P_{r_i} is the wall static pressure on the centerbody. The swirl number for the case when no centerbody exists is given by

$$S = G_\theta/(r_o G_z) \qquad \text{(G-22)}$$

where r_o is the outer radius of the stream at its exit.

REFERENCES

1. Bird, R. B., Stewart, W. E., and Lightfoot, E. N., Transport Phenomena, Wiley, 1960.

2. Schetz, J. A., Injection and Mixing in Turbulent Flow, Progress in Astronautics and Aeronautics, Volume 68, AIAA, 1980.

3. Ribeiro, M. M., and Whitelaw, J. H., "Coaxial Jets With and Without Swirl," J. Fluid Mech, 1980, Volume 96, Part 4, pp. 769-795.

VITA

Name: JACK DENTON MATTINGLY

Date of Birth: December 8, 1943

Place of Birth: Zanesville, Ohio

Education - High School: Bishop Rosecrans H. S.
Zanesville, Ohio
Graduated in June 1961

College: University of Notre Dame
Notre Dame, Indiana
BSME in June 1965
MSME in January 1967

Military Service -

Branch: UNITED STATES AIR FORCE

Dates: January 1969 to Present

Present Rank: Major

Present Unit: UNITED STATES AIR FORCE ACADEMY

Title: Assistant Professor
of Aeronautics